

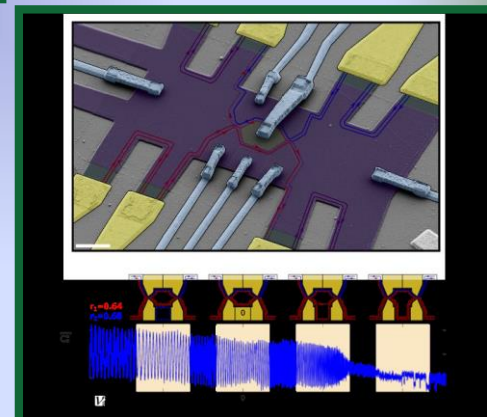
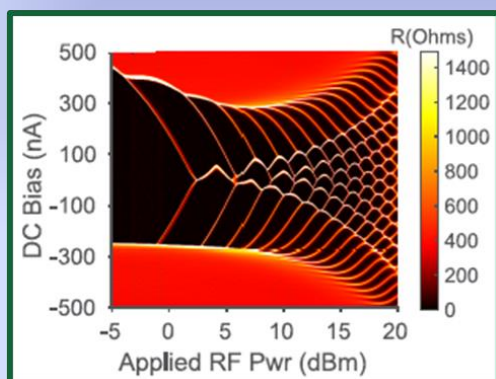
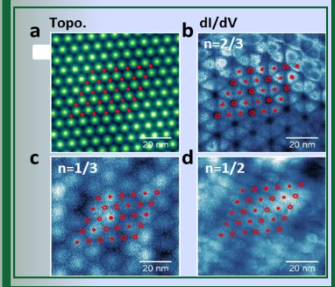
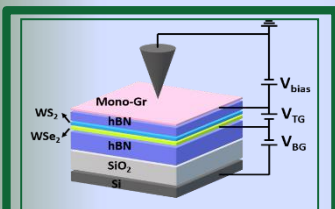
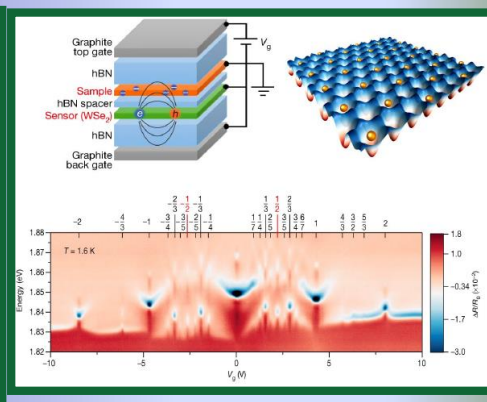
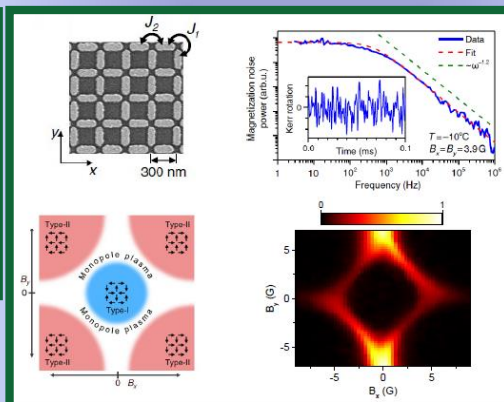
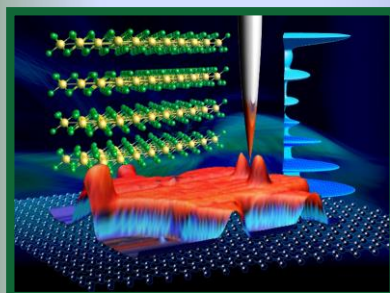
Experimental Condensed Matter Physics

Principal Investigators' Meeting–2021

Virtual Meeting, September 20–22, 2021

Program and Abstracts

Co-chairs: Jeanie Lau (OSU) and Ian Fisher (SLAC)



On the Cover

1	2	3
4	5	6

Figures are from selected highlight slides submitted to the ECMP PI Meeting.

1. Small Energy Gap in the Mott Ferromagnet-CrBr₃. TeYu Chien, University of Wyoming.
2. Field-Induced Plasma of Magnetic Monopoles in Artificial Spin Ice. Peter Schiffer, Yale University.
3. Electron Crystals in Moiré Lattices. Jie Shan, Cornell University.
4. Imaging Two-Dimensional Generalized Wigner Crystals. Feng Wang, Lawrence Berkeley National Lab.
5. Anomalous Shapiro Steps in Graphene Josephson Junctions. Gleb Finkelstein, Duke University.
6. Aharonov-Bohm Effect in Graphene-Based Fabry-Pérot Quantum Hall Interferometers. Philip Kim, Harvard University.

This document was produced under contract number DE-SC0014664 between the U.S. Department of Energy and Oak Ridge Associated Universities.

The research grants and contracts described in this document are supported by the U.S. DOE Office of Science, Office of Basic Energy Sciences, Materials Sciences and Engineering Division.

Foreword

This book contains abstracts for presentations made at the 2021 Experimental Condensed Matter Physics (ECMP) Principal Investigators' Meeting sponsored by the Materials Sciences and Engineering Division of the US Department of Energy, Office of Basic Energy Sciences (DOE-BES). The meeting convenes scientists supported within ECMP by the DOE-BES to present the most exciting, new research accomplishments and proposed future research directions in their BES supported projects. The meeting also affords PIs in the program an opportunity to see the full range of research currently being supported. We hope the meeting fostered a collegial environment to 1) stimulate the discussion of new ideas and 2) provide unique opportunities to develop or strengthen collaborations among PIs. In addition, the meeting provides valuable feedback to DOE-BES in its assessment of the state of the program and in identifying future programmatic directions. The meeting was attended by approximately 100 ECMP supported scientists.

The Experimental Condensed Matter Physics program supports research that will advance our fundamental understanding of the relationships between intrinsic electronic structure and properties of complex materials. Research supported by the program focuses on systems whose behavior derives from strong electron correlation, competing or coherent quantum interactions, topology, and effects of interfaces, defects, spin-orbit coupling, and reduced dimensionality. Scientific themes include charge, spin, and orbit degrees of freedom that result in phenomena such as superconductivity, magnetism, and topological protection, and the interactions of these in bulk and reduced-dimensional systems. The program supports synthesis and characterization of new material systems required to explore the central scientific themes. This includes development of experimental techniques that enable such research. Growth areas include emergent quantum phenomena in topological materials, low-dimensional materials, van der Waals materials, and materials with targeted clean energy-relevant and next-generation quantum information and microelectronics functionality.

The meeting was held in a virtual format and organized into six oral and six poster sessions covering the range of activities supported by the program. This structure attempts to capture in a virtual setting a change instituted in 2019, featuring fewer oral and more poster sessions, with the intent to provide enhanced PI interaction. Co-chairs for the meeting were Jeanie Lau (Ohio State) and Ian Fisher (SLAC). To these two we express our sincere appreciation for their invaluable help in organizing the meeting. We also want to gratefully acknowledge the excellent support provided by Ms. Linda Severs and Ms. Tia Moua of the Oak Ridge Institute for Science and Education and by Ms. Teresa Crockett of BES, for their efforts in organizing the meeting.

Drs. Claudia Cantoni and Mick Pechan
Program Managers, Condensed Matter and Materials Physics
Division of Materials Sciences and Engineering
Basic Energy Sciences

Experimental Condensed Matter Physics Principal Investigators' Meeting Agenda

Monday, September 20, 2021

Opening Session

11:00–11:15 **Mick Pechan and Claudia Cantoni**, Department of Energy
Welcome and Introductory Remarks

11:15–11:30 **Andy Schwartz**, Department of Energy
Remarks from BES

Oral Session 1

Chair: **Mick Pechan**

11:30–11:45 **Danna Freedman**, Northwestern University
Creating and Interfacing Designer Chemical Qubits

11:45–12:00 **Mike Manfra**, Purdue University
Direct Observation of Fractional Quantum Hall Quasiparticle Braiding Statistics via Interferometry

12:00–12:15 **Ilias Perakis**, University of Alabama–Birmingham
Ultrafast Spectroscopy of Pnictides in High Magnetic Field: Strongly Nonequilibrium Physics in the 25 Tesla Split Florida-Helix Magnet

12:15–12:30 **Tom Rosenbaum**, California Institute of Technology
Quantum Order and Disorder in Magnetic Materials

12:30–12:50 **20-Minute Break**

12:50–1:00 **Poster Introductions**

1:00–2:30 **Poster Session 1**

2:30–2:40 **10-Minute Break**

Oral Session 2

Chair: **Claudia Cantoni**

2:40–2:55 **Andrea Young**, UC-Santa Barbara
Magneto-thermal Imaging of Correlated Electrons in Moiré Heterostructures

2:55–3:10 **Eva Andrei**, Rutgers University
An Experimental Study of Flat Bands and Correlated Phases in Twisted Carbon Layers

3:10–3:25	Jim Hone , Columbia University <i>Quantum Transport in 2D Semiconductors</i>
3:25–3:40	Kin Fai Mak , Cornell University <i>Exciton Condensation in Atomic Double Layers</i>
3:40–4:00	20-Minute Break
4:00–4:10	Poster Introductions
4:10–5:40	Poster Session 2

Tuesday, September 21, 2021

11:00–11:05	Welcome to Day Two
Oral Session 3	Chair: Mick Pechan
11:05–11:20	Charles Ahn , Yale University <i>Control of Antiferromagnetic Domain Dynamics in Oxide Heterostructures</i>
11:20–11:35	Frances Hellman , Lawrence Berkeley National Laboratory <i>Non-equilibrium Magnetism: Materials and Phenomena</i>
11:35–11:50	Haidong Zhou , University of Tennessee <i>Heterostructures of Quantum Spin Liquid and Quantum Electronic Liquid for Electrically Sensing Entangled Excitations</i>
11:50–12:05	Dan Dessau , University of Colorado <i>Dynamics of Electronic Interactions in Superconductors and Related Materials</i>
12:05–12:20	Emilia Morosan , Rice University <i>Frustration as Tuning Parameter for Quantum Criticality</i>
12:20–12:40	20-Minute Break
12:40–12:50	Poster Introductions
12:50–2:20	Poster Session 3
2:20–2:30	10-Minute Break

Oral Session 4Chair: **Claudia Cantoni**

- 2:30–2:45 **Monica Plisch**, American Physical Society
APS CUWiP: Supporting the Success of All Undergraduate Women in Physics
- 2:45–3:00 **Brad Ramshaw**, Cornell University
Ultrasonic Determination of Electron Viscosity and Hydrodynamics in Metals
- 3:00–3:15 **Johnpierre Paglione**, University of Maryland
Topological Superconductivity in Strong Spin-Orbit Materials
- 3:15–3:30 **Harold Hwang**, SLAC National Accelerator Laboratory
Atomic Engineering Oxide Heterostructures: Materials by Design
- 3:30–3:45 **Anand Bhattacharya**, Argonne National Laboratory
Digital Synthesis – A Pathway to Create and Control Novel States of Condensed Matter
- 3:45–4:05 **20-Minute Break**
- 4:05–4:15 **Poster Introductions**
- 4:15–5:45 **Poster Session 4**

Wednesday, September 22, 202111:00–11:05 **Welcome to Day Three****Oral Session 5**Chair: **Mick Pechan**

- 11:05–11:20 **Rob McQueeney**, Ames Laboratory
Magnetic Interactions and Excitations in Quantum Materials
- 11:20–11:35 **Mike McGuire**, Oak Ridge National Laboratory
Correlated and Complex Materials
- 11:35–11:50 **Dan Phelan**, Argonne National Laboratory
Emerging Materials
- 11:50–12:05 **Ming Yi**, Rice University
Deciphering and Manipulating Low Dimensional Magnetism
- 12:05–12:20 **TeYu Chien**, University of Wyoming
Investigation of Topologically Trivial and Non-trivial Spin Textures and Their Relationships with the Topological Hall Effect
- 12:20–12:40 **20-Minute Break**

12:40–12:50 **Poster Introductions**

12:50–2:20 **Poster Session 5**

2:20–2:30 **10-Minute Break**

Oral Session 6 Chair: **Claudia Cantoni**

2:30–2:45 **Dave Hsieh**, California Institute of Technology
Search for 3D Topological Superconductors Using Laser-Based Spectroscopy

2:45–3:00 **Qiang Li**, Brookhaven National Laboratory
Chiral Materials and Unconventional Superconductivity

3:00–3:15 **Lu Li**, University of Michigan
Magnetometry Studies of Quantum Correlated Topological Materials in Intense Magnetic Fields

3:15–3:30 **Phuan Ong**, Princeton University
Charge and Thermal Transport Experiments on Topological Quantum Materials

3:30–3:45 **Alex Zettl**, Lawrence Berkeley National Laboratory
Novel sp^2 -Bonded Materials and Related Nanostructures

3:45–4:05 **20-Minute Break**

4:05–4:15 **Poster Introductions**

4:15–5:35 **Poster Session 6**

Closing Session

5:35–5:50 **Mick Pechan and Claudia Cantoni**, Department of Energy
Concluding Remarks

5:50 **Meeting Adjourns**

Table of Contents

Foreword	i
Agenda	iii
Session 1	
Creating and Interfacing Designer Chemical Qubits <i>Danna Freedman, David Awschalom, Mark Hersam, Jeffrey Long, James Rondinelli, and Michael Wasielewski</i>	3
Direct Observation of Fractional Quantum Hall Quasiparticle Braiding Statistics via Interferometry <i>Michael Manfra</i>	10
Ultrafast Spectroscopy of Pnictides in High Magnetic Field: Strongly Nonequilibrium Physics in the 25 Tesla Split Florida-Helix Magnet <i>Ilias E. Perakis and David J. Hilton</i>	13
Dynamics and Driven States in Quantum Magnets <i>Thomas F. Rosenbaum</i>	19
Session 2	
Magnetothermal Imaging of Correlated Electrons in Moiré Heterostructures <i>Andrea Young</i>	25
An Experimental Study of Flat Bands and Correlated Phases in Twisted Carbon Layers <i>Eva Y. Andrei</i>	29
Quantum Transport in 2D Semiconductors <i>James Hone and Cory Dean</i>	34
Strongly Correlated Excitonic Insulator in Coulomb-Coupled Bilayers <i>Kin Fai Mak</i>	38
Session 3	
Control of Antiferromagnetic Domain Dynamics in Oxide Heterostructures <i>Charles H. Ahn and Fred J. Walker</i>	43

Non-equilibrium Magnetism: Materials and Phenomena <i>Frances Hellman, Jeff Bokor, Peter Fischer, Steve Kevan, Sujoy Roy, Sayeef Salahuddin, and Lin-Wang Wang</i>	48
Heterostructures of Quantum Spin Liquid and Quantum Electronic Liquid for Electrically Sensing Entangled Excitations <i>Haidong Zhou and Jian Liu</i>	55
Massive Electron Correlations in Planar Trilayer Nickelate Pr₄Ni₃O₈ <i>Dan Dessau</i>	61
Topological Non-collinear Spin Texture in the Square-Net Centrosymmetric EuGa₂Al₂ <i>Emilia Morosan</i>	63
Session 4	
APS CUWiP: Supporting the Success of All Undergraduate Women in Physics <i>Monica Plisch</i>	69
Ultrasonic Determination of Electron Viscosity and Hydrodynamics in Metals <i>Brad Ramshaw</i>	70
Topological Superconductivity in Strong Spin-Orbit Materials <i>Johnpierre Paglione</i>	73
Atomic Engineering Oxide Heterostructures: Materials by Design <i>Harold Y. Hwang and S. Raghu</i>	78
Digital Synthesis: A Pathway to Create and Control Novel States of Condensed Matter <i>Anand Bhattacharya, Dillon D. Fong, and Sam Jiang</i>	82
Session 5	
Magnetic Interactions and Excitations in Quantum Materials <i>David C. Johnston, Liqin Ke, Robert McQueeney, Peter P. Orth, Ben G. Ueland, and David Vaknin</i>	91
Correlated Quantum Materials <i>Michael A. McGuire, Brian C. Sales, Jiaqiang Yan, Andrew F. May, and David Mandrus</i>	98
Emerging Materials <i>John F. Mitchell, Daniel Phelan, and Nirmal Ghimire</i>	104

Local and Itinerant Magnetism in 2D van der Waals Materials <i>Ming Yi</i>	108
--	-----

Investigation of Topologically Trivial and Nontrivial Spin Textures and Their Relationships with the Topological Hall Effect <i>TeYu Chien, Yuri Dahnovsky, Jinke Tang, and Jifa Tian</i>	111
---	-----

Session 6

Search for 3D Topological Superconductors using Laser-Based Spectroscopy <i>David Hsieh</i>	119
---	-----

Chiral Materials and Unconventional Superconductivity <i>Qiang Li, Mengkun Liu, Weiguo Yin, Genda Gu, and Tonica Valla</i>	122
--	-----

Magnetometry Studies of Quantum Correlated Topological Materials in Intense Magnetic Fields <i>Lu Li</i>	128
--	-----

Transport Experiments on Quantum Spin Liquids <i>N. Phuan Ong</i>	133
---	-----

Novel sp^2-Bonded Materials and Related Nanostructures <i>Alex Zettl, Marvin Cohen, Michael Crommie, Alessandra Lanzara, Steven Louie, and Feng Wang</i>	136
---	-----

Poster Session Lists

Poster Session I	143
Poster Session II	144
Poster Session III	145
Poster Session IV	146
Poster Session V	147
Poster Session VI	148

Poster Abstracts

Quantum Materials

James Analytis, Robert Birgeneau, Alessandra Lanzara, Dunghai Lee, Joel Moore, Joseph Orenstein, and R. Ramesh..... 151

Novel Temperature Limited Spectroscopy of Quantum Hall Systems

Raymond Ashoori..... 157

Creating and Probing Large Gap 2D Topological Insulators for Quantum Computing

Ray Ashoori, Joseph Checkelsky, Liang Fu, Nuh Gedik, and Pablo Jarillo-Herrero..... 161

Transport through Fermi Arcs, Unveiling Electronic Topology and a Quest for Topological Superconductivity in Bulk and Layered Materials

Luis Balicas 166

Electronic and Photonic Phenomena of Graphene-Based Heterostructures

Dimitri N. Basov 173

Revealing Collective Spin Dynamics Under Device-Operating Conditions to Enhance Tomorrow's Electronics

Valentina Bisogni..... 177

Workshop on Energy Research Opportunities for Physics Graduate Students and Postdocs

Cortney Bougher 182

Cold Exciton Gases in Semiconductor Heterostructures

Leonid Butov..... 184

Complex States, Emergent Phenomena, and Superconductivity in Intermetallic and Metal-Like Compounds

Paul Canfield, Sergey Bud'ko, Yuji Furukawa, Adam Kaminski, Makariy Tanatar, Ruslan Prozorov, and Linlin Wang..... 189

One-Dimensional Topological Nanomaterials and Superconductivity

Judy J. Cha 195

Weyl Electrons in New Frustrated Magnets

Jak Chakhalian 200

Exploring Quantized Axion Electrodynamics in Magnetic Topological Insulator Multilayer Heterostructures

Moses H. W. Chan, Chao-Xing Liu, and Cui-Zu Chang 204

New Interfaces in Intercalated Structures <i>Joseph Checkelsky</i>	209
Microwave Spectroscopy of Correlated 2D Electron Systems in Semiconductors and Graphene <i>Lloyd W. Engel and Cory Dean</i>	213
Novel Synthesis of Quantum Epitaxial Heterostructures by Design <i>Chang-Beom Eom</i>	217
Symmetries, Interactions and Correlation Effects in Carbon Nanostructures <i>Gleb Finkelstein</i>	223
Correlated Materials: Synthesis and Physical Properties <i>Ian R. Fisher, Theodore H. Geballe, Aharon Kapitulnik, Steven A. Kivelson, and Kathryn A. Moler</i>	228
Definitive Majorana Zero Modes in Optimized Hybrid Nanowires <i>Sergey M. Frolov</i>	234
Antiferromagnetism and Superconductivity <i>W. P. Halperin</i>	238
Science of 100 Tesla <i>Neil Harrison, Mun Chan, John Singleton, Marcelo Jaime, Priscila Rosa, and Scott Crooker</i>	242
Hybrid-Magnon Quantum Devices <i>Axel Hoffmann, Yi Li, Valentine Novosad, Wolfgang Pfaff, Andre Schleife, and Jian-Min Zuo</i>	248
Symmetry Engineering of Topological Quantum States <i>Jin Hu</i>	252
Proximity Effects and Topological Spin Currents in van der Waals Heterostructures <i>Benjamin Hunt</i>	258
Electronic Growth of Metals on 2D Semiconductors <i>T. Kidd, A. Stollenwerk, P. Shand, L. Strauss, and P. Lukashev</i>	263
Correlated Many-Body Quantum States in Graphene Heterostructure <i>Philip Kim</i>	267
Spectroscopy of Degenerate One-Dimensional Electrons in Carbon Nanotubes <i>Junichiro Kono</i>	272

Superconductivity and Magnetism <i>W.-K. Kwok, U. Welp, V. Novosad, A. E. Koshelev, V. Vlasko-Vlasov, and Z.-L. Xiao</i>	278
Symmetry Breaking in Two-Dimensional Flat-Band Systems for Spin and Charge Transport <i>Chun Ning (Jeanie) Lau and Marc Bockrath</i>	284
Oxide Quantum Heterostructures <i>Ho Nyung Lee, Matthew Brahlek, Gyula Eres, Hu Miao, and T. Zac Ward</i>	289
Investigating New Routes to Quantum Disordered States <i>Minhyea Lee</i>	295
Investigating New Routes to Quantum Disordered States <i>Qi Li</i>	298
Identifying the Signatures of Topological Superconductivity and Fractional Excitations in Bulk Crystals and Thin Films <i>Vidya Madhavan</i>	302
Superconductivity and Magnetism in <i>d</i>- and <i>f</i>-Electron Quantum Materials <i>M. Brian Maple</i>	303
Spectroscopic Investigations of Electronic and Magnetic Materials <i>Janice L. Musfeldt</i>	310
Nanostructure Studies of Correlated Quantum Materials <i>Douglas Natelson</i>	314
Probing the Interplay of Topology, Magnetism and Superconductivity in Intrinsic Magnetic and Superconducting Topologic Materials <i>Ni Ni</i>	318
Nonlinear Charge-Spin Conversion Phenomena in Topological Insulator/Ferromagnet Heterostructures <i>Branislav K. Nikolić, Matt F. Doty, Stephanie A. Law, and John Q. Xiao</i>	322
Probing novel Phenomena in Strongly Correlated Layered Materials through van der Waals Heterostructures <i>Claudia Ojeda-Aristizabal</i>	327
Understanding A Few Spin-Based Fundamental Interactions in Colloidal Organic-Inorganic Hybrid Perovskite Nanostructures by Ultrafast Optical Spectroscopy <i>Min Ouyang</i>	331

Synthesis and Observation of Emergent Phenomena in Heusler Compound Heterostructures <i>Christopher J. Palmstrøm and Anderson Janotti</i>	334
Broken Symmetries for Control of Spin Currents and Spin-Orbit Torques <i>Daniel C. Ralph</i>	339
Quantum Fluctuations in Narrow Band Systems <i>Filip Ronning, Eric Bauer, Michihiro Hirata, Roman Movshovich, Priscila Rosa, and Sean Thomas</i>	344
Novel Topological Josephson Junctions Architectures for Fault-Tolerant Qubits and Advanced Sensing <i>Enrico Rossi, Javad Shabani, and Wei Pan</i>	350
Exotic Frustration-Induced Phenomena in Artificial Spin Ice <i>Peter Schiffer</i>	354
Nanostructured Materials: From Superlattices to Quantum Dots <i>Ivan K. Schuller</i>	358
Planar Systems for Quantum Information <i>Jie Shan, Cory R. Dean, James Hone, Allan H. MacDonald, Kin Fai Mak, and Tony F. Heinz</i>	363
Correlated States of Two-dimensional Electron Systems in AlAs Quantum Wells <i>Monsour Shayegan</i>	367
Magneto-optical Study of Correlated Electron Materials in High Magnetic Fields <i>Dmitry Smirnov and Zhigang Jiang</i>	372
Spin-Polarized Scanning Tunneling Microscopy Studies of Magnetic, Electronic, and Spintronic Phenomena in Nitride Systems <i>Arthur R. Smith</i>	377
Exploring Nontrivial Topological Superconductivity in 2M WS₂ for Topological Quantum Computation <i>Jifa Tian, John Ackerman, TeYu Chien, Brian Leonard, and Jinke Tang</i>	381
Magneto-electronic Phenomena due to Quantum Magnetization Fluctuations <i>Sergei Urazhdin</i>	385

Van der Waals Heterostructures: Novel Materials and Emerging Phenomena <i>Feng Wang, Michael Crommie, Steven G. Louie, Zi Q. Qiu, Mike Zaletel, and Alex Zettl</i>	390
Designing Metastability: Coercing Materials to Phase Boundaries <i>T. Zac Ward</i>	397
Topological Surface and Bulk States in Dirac Semimetal α-Sn Thin Films <i>Mingzhong Wu</i>	402
Nonvolatile Active Control of Spin Transport using Interfaces with Molecular Ferroelectrics <i>Xiaoshan Xu</i>	406
Sub-Nanosecond Switching of Antiferromagnets Driven by Interfacial Spin-Orbit Torque <i>Fengyuan Yang</i>	411
Quantum Hall Systems In and Out of Equilibrium <i>Michael Zudov</i>	417
Author Index	425
Participant List	429

Session I

Creating and Interfacing Designer Chemical Qubits

Principal Investigator: Danna Freedman | Northwestern University
Co-Investigators: David Awschalom | University of Chicago; Mark Hersam | Northwestern; Jeffrey Long | University of California Berkeley James Rondinelli | Northwestern; Michael Wasielewski | Northwestern

Program Scope

Chemical control enables the creation of systems for quantum information science featuring *the unprecedented combination of atomic structural control and tunability*. This atomistic control is especially powerful for the creation of designer systems, capable of functioning as sensors that can be programmed and tuned for specific environments or analytes. Our team will harness these design attributes of molecular-based materials to create the first generation of designer molecules for quantum sensing applications. Synthesis, measurement, and theory will cooperate to create a rapid measurement feedback cycle for evaluation of the coherence properties of molecules for quantum information science. We will synthesize molecular candidates (**Freedman, Long, Wasielewski**), probe their coherence properties (**Awschalom, Freedman, Wasielewski**), and evaluate whether they integrate with sensing targets (**Hersam, Long**) developed by our team.

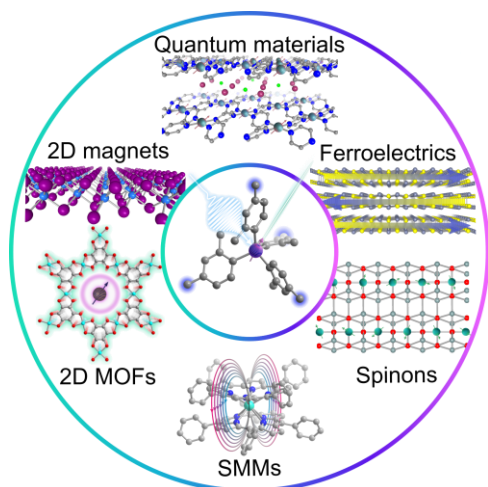


Figure 1 | Tunable optically addressable quantum sensors (center) offer integration with and nanoscale characterization of quantum materials such as 2D magnetic materials and ferroelectrics, 1D spin chains, and single-molecule magnets.

We will then execute sensing measurements on the specific target systems. Through these studies and based on a tight integration with theory (**Rondinelli**), we will develop molecular sensors. The main objectives are to: (a) develop a new class of quantum sensors tuned for magnetic field sensing; (b) develop a new class of molecular quantum sensors tuned for electric field sensing; (c) modulate the structures for integration with specific targets; and (d) execute measurements of magnetic and electric fields in target quantum materials designed by our team.

Recent Progress

The goals of DE-SC0019356 were to create and interface chemically derived qubits. Through this multi-scale study, we developed key insights into the role of spin–spin and spin–phonon interactions on qubit coherence. For instance, within the single-qubit systems, we found that systematically depleting phonon modes through chemical synthesis extends measurable coherence times (T_2) to room temperature (**Freedman, Rondinelli, Hersam**).¹ We complemented this work with a study on the fundamental impact of electronic spin–spin interactions on coherence properties in two-qubit systems at various distances. Scaling up to 3D, we created *an array of*

qubits precisely spaced 18 Å apart (Freedman, Dichtel, Wasielewski).² By attenuating relaxation-inducing spin–spin interactions through this expanded qubit distance, we were able to use a combination of computations and synthetic modulation of the phonon modes to attribute spin–lattice relaxation to chemical moieties within the extended array (Rondinelli). In a separate approach, we distilled the electronic structures of optically addressable defect-based qubit “color centers” down to their essential features and replicated these within a modular platform, producing the *first molecular color centers* (Freedman, Awschalom).³ We further showed that these design principles can be generalized to create a diverse range of molecular structures (Freedman, Awschalom, Wasielewski). This work led to 21 publications, with another four under review, including high impact publications in *J. Am. Chem. Soc.* and *Science*.¹⁻⁵ During the project period, we trained over 22 students and postdocs, developing a future quantum workforce comprised of students with highly interdisciplinary backgrounds, spanning chemistry to materials science and physics.

Area of Talk: Molecular Color Centers

To design molecular analogues of optically addressable defect sites, we demonstrated several different molecular architectures and transition metal systems are capable of optical spin initialization and readout. Freedman designed an $S = 1$ V^{3+} complex, $(\text{ArFtren})\text{V}(\text{CN}^t\text{Bu})$ ($\text{H}_3\text{ArFtren} = 2,2',2''\text{-tris}((\text{pentafluorophenyl})\text{amino})\text{triethylamine}$).⁶ The trivalent oxidation state and trigonal bipyramidal geometry give rise to the targeted $S = 1$ ground state as well as the requisite excited state structure for optical addressability. To understand the ground state spin dynamics, we turned to free-electron laser-powered high-field, high-frequency electron paramagnetic resonance (EPR) spectroscopy. We measured the coherent lifetime of the ground state spin, overcoming an inherent challenge for $S = 1$ transition metal systems that are often not measurable on conventional EPR spectrometers. Freedman, Wasielewski, and Awschalom then performed a series of time-resolved transient absorption and photoluminescence spectroscopies to characterize the excited state dynamics of this compound. The team identified emission arises from an intermediate $S = 0$ excited state with suitable dynamics for optical spin initialization and readout. The combination of excited state structure, the spin-triplet ground state and emission from an intermediate spin-singlet excited state prompted us to investigate the variable field photoluminescence spectra. With this experiment, we visualized the Zeeman splitting of the ground state *via* emission from the spin-singlet excited state to the spin-triplet ground state (Figure 2). The variable-field photoluminescence experiment indicated that, with direct excitation from the spin-triplet ground state into the spin-singlet excited state, we could optically readout variations

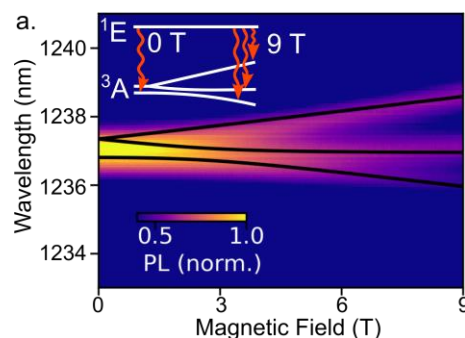


Figure 2 | Variable-field PL spectra with simulated Zeeman splitting (black) collected on a single crystal of $(\text{ArFtren})\text{V}(\text{CN}^t\text{Bu})$ (~2% in $(\text{ArFtren})\text{Ga}(\text{CN}^t\text{Bu})$). White schematic illustrates variable-field splitting of the emission.

in the magnetic field environment. In ongoing collaborative work between **Freedman**, **Awschalom** and **Hersam**, we are now pursuing investigation of low dimensional magnetic materials to probe their magnetic behavior with unprecedentedly high spatial resolution through well-controlled deposition of these materials guided by spatial dependencies predicted by **Rondinelli**. We are also expanding into other transition metals; for example, **Freedman** designed and synthesized a set of $S = 1$ Ni^{2+} electronic spin qubits that meet the requirements for optical addressability.⁷

In a separate collaboration between **Freedman** and **Awschalom**, we focused on highly symmetric, tetravalent chromium compounds.³ We outlined the requisite criteria for these systems to achieve optical spin initialization and readout, including an emissive spin-singlet excited state with narrow photoluminescence, a ground state spin-triplet, and a ground-state spin lifetime (T_1) that is longer than the excited-state lifetime. To achieve the desired excited-state structure, we synthesized a series of Cr^{4+} complexes with strongly donating aryl ligands, generating $\text{Cr}(\text{aryl})_4$ compounds where aryl = *o*-tolyl, 2,3-dimethylphenyl, 2,4-dimethylphenyl (**Figure 3**). These systems all exhibit suitably narrow emission from an $S = 0$ excited state in the range of 1010–1025 nm at 4–5 K. The high symmetry and strong ligand field result in an inherently small ground state splitting, known as zero field splitting (ZFS), for each of these complexes. The combination of the emissive spin-singlet state and small ZFS allowed us to *optically initialize, coherently manipulate and optically readout the ground state spin*. The highly collaborative nature of this work allowed us to demonstrate optical initialization and readout of the ground state spin of three unique molecular systems for the first time. This work represents an important first step towards addressing individual molecular spin centers, a critical barrier that must be overcome to integrate molecular spins with existing and future quantum technologies.

Future Plans

This progress has laid the foundation for our team to now address grand challenges in quantum sensing. Sensing relies on separating analyte signal from background noise, necessitating the design of quantum sensors that respond specifically and selectively to targeted stimuli. Having demonstrated optical read-out of molecular qubits and creation of atomically precise qubit arrays, we propose to design and synthesize the first generation of designer molecular sensors targeted to probe quantum phenomena in correlated materials. Key applications include sensing the orientation of the magnetic field in 2D magnets with high spatial precision, sensing the electric field of ferroelectrics, and the high-risk target of combining magnetic and electric field sensors to search for quasiparticle such as spinons.

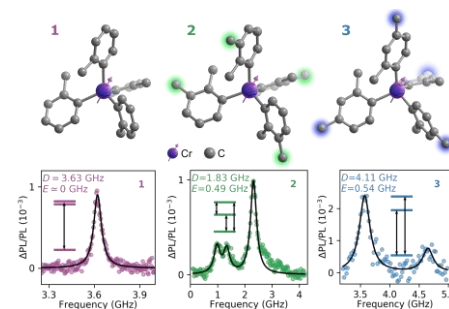


Figure 3 | Molecular structures (upper) of $\text{Cr}(\textit{o}\text{-tolyl})_4$, $\text{Cr}(\text{2,3-dimethylphenyl})_4$, and $\text{Cr}(\text{2,4-dimethylphenyl})_4$ and corresponding ODMR spectra (lower).

The initial focus of the proposal will be designing and modifying molecular quantum sensors for integration with material targets. Here we will modulate charge, surface compatibility, read-out, and sensitivity through chemical synthesis. We then will interrogate the coherence properties of these molecules. Molecules will be refined based on these outputs guided by computations. Candidate molecular sensors will be tested in several proof-of-concept applications with state-of-the-art quantum materials. Read-out of sensor information will be accomplished primarily with optically detected magnetic resonance. This project will be guided by electronic structure theory computations. Our scientific approach exploits a feedback cycle enabling the synthesis and measurement of quantum properties of materials.

References

1. Amdur, M. J.; Mullin, K. R.; Waters, M. J.; Puggioni, D.; Wojnar, M. K.; Gu, M.; Sun, L.; Oyala, P. H.; Rondinelli, J. M.; Freedman, D. E. Chemical Control of Spin-Lattice Relaxation to Create Room Temperature Molecular Qubit Candidates. **2021**, *Submitted*.
2. Yu, C.-J.; von Kugelgen, S.; Krzyaniak, M. D.; Ji, W.; Dichtel, W. R.; Wasielewski, M. R.; Freedman, D. E. Spin and Phonon Design in Modular Arrays of Molecular Qubits. *Chem. Mater.* **2020**, *32* (23), 10200–10206. <https://doi.org/10.1021/acs.chemmater.0c03718>.
3. Bayliss, S. L.; Laorenza, D. W.; Mintun, P. J.; Kivos, B. D.; Freedman, D. E.; Awschalom, D. D. Optically Addressable Molecular Spins for Quantum Information Processing. *Science* **2020**, *370* (6522), 1309–1312. <https://doi.org/10.1126/science.abb9352>.
4. Jiao, T.; Cai, K.; Nelson, J. N.; Jiao, Y.; Qiu, Y.; Wu, G.; Zhou, J.; Cheng, C.; Shen, D.; Feng, Y.; Liu, Z.; Wasielewski, M. R.; Stoddart, J. F.; Li, H. Stabilizing the Naphthalenediimide Radical within a Tetracationic Cyclophane. *J. Am. Chem. Soc.* **2019**, *141* (42), 16915–16922. <https://doi.org/10.1021/jacs.9b08926>.
5. La Porte, N. T.; Christensen, J. A.; Krzyaniak, M. D.; Rugg, B. K.; Wasielewski, M. R. Spin-Selective Photoinduced Electron Transfer within Naphthalenediimide Diradicals. *J. Phys. Chem. B* **2019**, *123* (36), 7731–7739. <https://doi.org/10.1021/acs.jpcc.9b06303>.
6. Fataftah, M. S.; Bayliss, S. L.; Laorenza, D. W.; Wang, X.; Phelan, B. T.; Wilson, C. B.; Mintun, P. J.; Kivos, B. D.; Wasielewski, M. R.; Han, S.; Sherwin, M. S.; Awschalom, D. D.; Freedman, D. E. Trigonal Bipyramidal V^{3+} Complex as an Optically Addressable Molecular Qubit Candidate. *J. Am. Chem. Soc.* **2020**, *142* (48), 20400–20408. <https://doi.org/10.1021/jacs.0c08986>.
7. Wojnar, M. K.; Laorenza, D. W.; Schaller, R. D.; Freedman, D. E. Nickel(II) Metal Complexes as Optically Addressable Qubit Candidates. *J. Am. Chem. Soc.* **2020**, *142* (35), 14826–14830. <https://doi.org/10.1021/jacs.0c06909>.

Publications for 2 year period

Under review

1. Amdur, M. J.; Mullin, K. R.; Waters, M. J.; Puggioni, D.; Wojnar, M. K.; Gu, M.; Sun, L.; Oyala, P. H.; Rondinelli, J. M.; Freedman, D. E., Chemical Control of Spin-Lattice Relaxation to Create Room Temperature Molecular Qubit Candidates *Submitted*.
2. Wang, Y.; Ziebel, M. E.; Sun, L.; Gish, J. T.; Pearson, T. J.; Lu, X.-E.; Thorarinsdottir, A. E.; Hersam, M. C.; Long, J. R.; Freedman, D. E.; Rondinelli, J. M.; Puggioni, D.; Harris, T. D. J., Strong Magnetocrystalline Anisotropy Arising from Metal–Ligand Covalency in a Metal–Organic Candidate for 2D Magnetic Order" *Submitted*.
3. Gish, J.T; Lebedev, D.; Stanev, T.K.; Jiang, S.; Georgopoulos, L.; Song, T.W.; Lim, G.H.; Garvey, E.S.; Valdman, L.; Balogun, O.; Sofer, Z.; Sangwan, V.K; Stern, N.P.; Hersam, M.C., Ambient-stable Two-dimensional CrI₃ via Organic-inorganic Encapsulation, *Submitted*.

In press

4. Murphy, R. A.; Long, J. R.; Harris, T. D., A Hard Permanent Magnet through Molecular Design, *Commun. Chem.* **2021**, *in press*.
5. Evans, A.F.; Giri, A.; Sangwan, V.K.; Xun, S.; Bartnof, M.; Torres-Castanedo, C.G.; Balch, H.B.; Rahn, M.S.; Bradshaw, N.P.; Vitaku, E.; Li, H.; Bedzyk, M.J.; Wang, F.; Bredas, J.-L.; Malen, J.A.; McGaughey, A.J.; Hersam, M.C.; Dichtel, W.R.; Hopkins, P.E., Thermally Conductive, Ultra-low-k Dielectric Layers Based on Two-dimensional Covalent Organic Frameworks," *Nature Materials*, **2021** DOI: 10.1038/s41563-021-00934-3.
6. Murphy, R.A.; Darago, L.E.; Ziebel, M.E.; Peterson, E.A.; Zaia, E.W.; Mara, M.W.; Lussier, D.; Shuh, D.K.; Urban, J.J.; Neaton, J.B.; Long, J.R., **2020**, ChemRxiv. Preprint. <https://doi.org/10.26434/chemrxiv.13473099.v1>.

Published

7. Yu, C.-J.; von Kugelgen, S. W.; Freedman, D. E., A Molecular Approach to Quantum Sensing *ACS Cent. Sci.* **2021**, *7*, **712–723**.
8. von Kugelgen, S. W.; Krzyaniak, M. D.; Gu, M.; Puggioni, D.; Rondinelli, J. M.; Wasielewski, M. R.; Freedman, D. E., Spectral Addressability in a Modular Two Qubit System *J. Am. Chem Soc.* **2021**, *143*, 8069–8077.
9. Anamimoghadam, O.; Jones, L. O.; Cooper, J. A.; Beldjoudi, Y.; Nguyen, M. T.; Liu, W. Q.; Krzyaniak, M. D.; Pezzato, C.; Stern, C. L.; Patel, H. A.; Wasielewski, M. R.; Schatz, G. C.; Stoddart, J. F., Discrete Open-Shell Tris(bipyridinium radical cationic) Inclusion Complexes in the Solid State. *Journal of the American Chemical Society* **2021**, *143* (1), 163-175 DOI: 10.1021/jacs.0c07148.

10. Ziebel, M. E.; Ondry, J. C.; Long, J. R., Two-dimensional, conductive niobium and molybdenum metal-organic frameworks. *Chemical Science* **2020**, *11* (26), 6690-6700, DOI: 10.1039/d0sc02515a.
11. Yu, C. J.; von Kugelgen, S.; Krzyaniak, M. D.; Ji, W.; Dichtel, W. R.; Wasielewski, M. R.; Freedman, D. E., Spin and Phonon Design in Modular Arrays of Molecular Qubits. *Chemistry of Materials* **2020**, *32* (23), 10200-10206. DOI: 10.1021/acs.chemmater.0c03718
12. Wojnar, M. K.; Laorenza, D. W.; Schaller, R. D.; Freedman, D. E., Nickel(II) Metal Complexes as Optically Addressable Qubit Candidates. *Journal of the American Chemical Society* **2020**, *142* (35), 14826-14830, DOI: 10.1021/jacs.0c06909.
13. Wasson, M. C.; Zhang, X.; Otake, K. I.; Rosen, A. S.; Alayoglu, S.; Krzyaniak, M. D.; Chen, Z. J.; Redfern, L. R.; Robison, L.; Son, F. A.; Chen, Y. W.; Islamoglu, T.; Notestein, J. M.; Snurr, R. Q.; Wasielewski, M. R.; Farha, O. K., Supramolecular Porous Assemblies of Atomically Precise Catalytically Active Cerium-Based Clusters. *Chemistry of Materials* **2020**, *32* (19), 8522-8529, DOI: 10.1021/acs.chemmater.0c02740.
14. Thorarinsdottir, A. E.; Harris, T. D., Metal-Organic Framework Magnets. *Chemical Reviews* **2020**, *120* (16), 8716-8789, DOI: 10.1021/acs.chemrev.9b00666.
15. Thorarinsdottir, A. E.; Bjornsson, R.; Harris, T. D., Insensitivity of Magnetic Coupling to Ligand Substitution in a Series of Tetraoxolene Radical-Bridged Fe-2 Complexes. *Inorganic Chemistry* **2020**, *59* (7), 4634-4649, DOI: 10.1021/acs.inorgchem.9b03736.
16. Lin, Y.; Wood, M.; Imasato, K.; Kuo, J. J. H.; Lam, D.; Mortazavi, A. N.; Slade, T. J.; Hodge, S. A.; Xi, K.; Kanatzidis, M. G.; Clarke, D. R.; Hersam, M. C.; Snyder, G. J., Expression of interfacial Seebeck coefficient through grain boundary engineering with multi-layer graphene nanoplatelets. *Energy & Environmental Science* **2020**, *13* (11), 4114-4121, DOI: 10.1039/d0ee02490b.
17. Jhulki, S.; Evans, A. M.; Hao, X. L.; Cooper, M. W.; Feriante, C. H.; Leisen, J.; Li, H.; Lam, D.; Hersam, M. C.; Barlow, S.; Bredas, J. L.; Dichtel, W. R.; Marder, S. R., Humidity Sensing through Reversible Isomerization of a Covalent Organic Framework. *Journal of the American Chemical Society* **2020**, *142* (2), 783-791, DOI: 10.1021/jacs.9b08628.
18. Fataftah, M. S.; Bayliss, S. L.; Laorenza, D. W.; Wang, X. L.; Phelan, B. T.; Wilson, C. B.; Mintun, P. J.; Kovos, B. D.; Wasielewski, M. R.; Han, S.; Sherwin, M. S.; Awschalom, D. D.; Freedman, D. E., Trigonal Bipyramidal V³⁺ Complex as an Optically Addressable Molecular Qubit Candidate. *Journal of the American Chemical Society* **2020**, *142* (48), 20400-20408 DOI: 10.1021/jacs.0c08986.
19. Evans, A. M.; Bradshaw, N. P.; Litchfield, B.; Strauss, M. J.; Seckman, B.; Ryder, M. R.; Castano, I.; Gilmore, C.; Gianneschi, N. C.; Mulzer, C. R.; Hersam, M. C.; Dichtel, W. R., High-Sensitivity Acoustic Molecular Sensors Based on Large-Area, Spray-Coated 2D Covalent Organic Frameworks. *Advanced Materials* **2020**, *32* (42) DOI: 10.1002/adma.202004205.

20. Bayliss, S. L.; Laurenza, D. W.; Mintun, P. J.; Kovos, B. D.; Freedman, D. E.; Awschalom, D. D., Optically addressable molecular spins for quantum information processing. *Science* **2020**, *370* (6522), 1309-+.
21. "Exchange Biased Anomalous Hall Effect Driven by Frustration in a Magnetic Kagome Lattice." Lachman, E.; Murphy, R. A.; Maksimovic, N.; Kealhofer, R.; Haley, S.; McDonald, R. D.; Long, J. R.; Analytis, J. G. *Nat. Commun.* 2020, 11, 560.
22. von Kugelgen, S.; Freedman, D. E., A chemical path to quantum information. *Science* **2019**, *366* (6469), 1070-1071, DOI: 10.1126/science.aaz4044.
23. Valdez-Moreira, J. A.; Thorarinsdottir, A. E.; DeGayner, J. A.; Lutz, S. A.; Chen, C. H.; Losovyj, Y.; Pink, M.; Harris, T. D.; Smith, J. M., Strong pi-Backbonding Enables Record Magnetic Exchange Coupling Through Cyanide. *Journal of the American Chemical Society* **2019**, *141* (43), 17092-17097, DOI: 10.1021/jacs.9b09445.
24. La Porte, N. T.; Christensen, J. A.; Krzyaniak, M. D.; Rugg, B. K.; Wasielewski, M. R., Spin-Selective Photoinduced Electron Transfer within Naphthalenediimide Diradicals. *Journal of Physical Chemistry B* **2019**, *123* (36), 7731-7739, DOI: 10.1021/acs.jpcc.9b06303
25. Jiao, T. Y.; Cai, K.; Nelson, J. N.; Jiao, Y.; Qiu, Y. Y.; Wu, G. C.; Zhou, J. W.; Cheng, C. Y.; Shen, D. K.; Feng, Y. N.; Liu, Z. C.; Wasielewski, M. R.; Stoddart, J. F.; Li, H., Stabilizing the Naphthalene Diimide Radical within a Tetracationic Cyclophane. *Journal of the American Chemical Society* **2019**, *141* (42), 16915-16922, DOI: 10.1021/jacs.9b08926.

Direct Observation of Fractional Quantum Hall Quasiparticle Braiding Statistics via Interferometry

Michael J. Manfra

Department of Physics and Astronomy

Purdue University, West Lafayette IN, 47907

Program Scope

Decoherence through sensitivity to local perturbations is a key impediment to many current generation quantum technologies. The topological properties of emergent non-local degrees of freedom in condensed matter systems are conjectured to protect quantum states from environmental noise. While numerous material systems are now under investigation to explore topological properties, perhaps the best controlled topological phase is the quantum Hall effect in AlGaAs/GaAs heterostructures. Here the notion of dissipationless edge modes and Abelian and non-Abelian braiding statistics, now central to many proposals for quantum information processing, were first theoretically developed and can be systematically studied in experiments.

Utilizing a breakthrough in AlGaAs/GaAs heterostructure design developed in our group that allows for operation of electronic Fabry-Perot interferometers with reduction of quantum dot-like charging effects while simultaneously generating sharper edge potential profiles, we have recently demonstrated Aharonov-Bohm (AB) interference of fractional quantum Hall effect edge modes. Clear demonstration of AB interference of fractional edge modes is a vital step towards demonstration Abelian and non-Abelian braiding statistics. Utilizing in-house capabilities in semiconductor growth, device fabrication, and low temperature transport, we propose a series of interferometry experiments aimed at answering the most important questions surrounding quantum coherence and braiding statistics in quantum Hall systems. Fine control of device parameters in this system facilitates systematic investigation of quantum coherence, edge state reconstruction, and braiding statistics. Our project tasks include:

- Measurement of the Abelian phase for the fractional quantum Hall state at $\nu=1/3$
- Exploration of the limit of interferometer size reduction while maintaining operation in Aharonov-Bohm regime
- Quantification of quantum coherency of fractional edge modes via measurement of the temperature dependence of AB oscillation amplitude and dependence on interferometer size
- Design of heterostructures and measurement of interferometers to probe non-Abelian braiding statistics at $\nu=5/2$

- Measurement of interferometers in which the edge potential profile is systematically modified through variation of screening well - quantum well separation to study impact on edge mode reconstruction

Our work will inform investigations of other topological material systems where systematic control of epitaxial growth, device fabrication and operation are currently in more nascent stages. We hope our work may serve as a blueprint for interrogation of other topological phases needed to support next generation quantum systems.

Recent Progress

Anyons are quasiparticles that may exist in two-dimensional interacting systems that, unlike fermions and bosons, show fractional statistics when two of them are braided. Here we describe our experimental observation of anyonic braiding statistics for quasiparticles of the $\nu=1/3$ fractional quantum Hall state using an electronic Fabry-Perot interferometer. Utilizing a purpose-designed GaAs/AlGaAs heterostructure hosting a high mobility two-dimensional electron gas, we demonstrate strong Aharonov-Bohm interference of the $\nu=1/3$ edge mode [1] that is punctuated by discrete phase slips that indicate an anyonic phase $\vartheta_{\text{anyon}}=2\pi/3$ at filling factor $1/3$ [2]. Our results are consistent with theoretical predictions for anyonic phase at $\nu=1/3$ made nearly 40 years ago. Our results are also consistent with recent theoretical models that describes operation of a Fabry-Perot interferometer in a regime in which device charging energy is small compared to the energy of formation of charged quasiparticles, which further substantiates that we have observed anyonic braiding in our experiments. Newer experimental results [3] demonstrate fine control of interferometer couplings that facilitates quantitative analysis of the impact of anyonic statistics in several regimes of device operation.

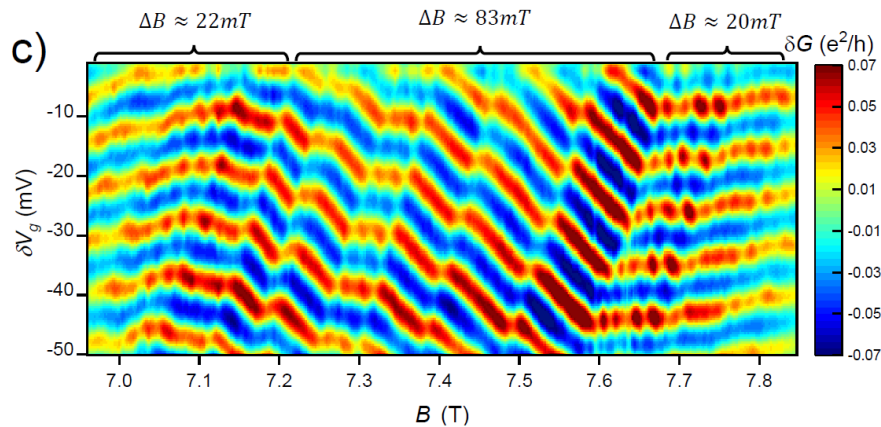


Fig. 1: Map of the conductance (color scale) versus magnetic field (B) and gate voltage in a 2D electronic interferometer. Each phase slip in conductance denotes a jump in the phase of the quantum-mechanical wave of the system, corresponding to a rotation by $-2\pi/3$. These phase jumps are the tell-tale sign of particles with fractional statistics – anyons. Data collected at $T=10\text{mK}$.

Future Plans

New experiments are focused on exploration of interference at $\nu=2/3$ and $\nu=2/5$. We are also designing and testing heterostructures for experiments at $\nu=5/2$.

References

- [1] J. Nakamura, et al., *Nature Physics* **15**, 563-569 (2019)
- [2] J. Nakamura, et al., *Nature Physics* **16**, 931-936 (2020)
- [3] J. Nakamura, et al., arXiv:2107.02136v1

Publications

- [1] J. Nakamura, et al., *Nature Physics* **16**, 931-936 (2020)
- [2] J. Nakamura, et al., arXiv:2107.02136v1

ULTRAFAST SPECTROSCOPY OF Pnictides in High Magnetic Field: Strongly Nonequilibrium Physics in the 25 Tesla Split Florida-Helix Magnet

Ilias E. Perakis and David J. Hilton

Department of Physics, University of Alabama at Birmingham

Email: iperakis@uab.edu

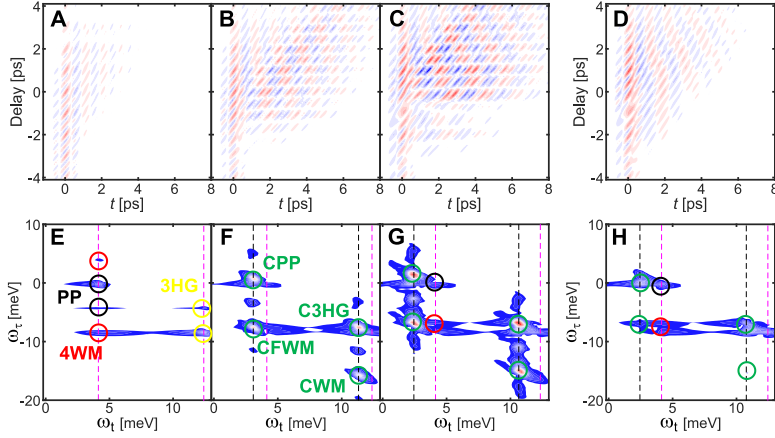
Program Scope

This program develops theory and simulations that guide new *Multi-dimensional Phase Coherent Nonlinear Terahertz Spectroscopy* (MDC-THz) experiments in superconductors (SC). These experiments use two phase-locked, intense, THz laser pulses to enable dissipationless light-wave quantum electronics and super-resolution imaging of non-equilibrium quantum states. They introduce an extra control knob: the relative phase accumulation between two phase-locked THz laser fields. Our objectives are (1) coherently control *Dissipationless Photocurrents* and *THz Dynamical Symmetry Breaking* during oscillation cycles of THz light-waves to steer quantum materials into non-equilibrium phases prior to thermalization, and (2) super-resolution imaging of THz-time-periodic-driven states in iron-pnictide and BCS superconductors. In this way, we will make progress towards dynamical sensing and coherent control of light-induced higher correlation and quantum entanglement. A grand challenge facing implementation of such an approach is how to establish a reliable and systematic universal quantum control principle for manipulating emergent orders. By combining MDC-THz experiments with simulations of THz-time-periodic driven quantum states, this project lays the groundwork for a quantum tomography technique that can impact the entire field of emergent materials phase discovery, across superconductivity, correlated electron matter, topological matter, and quantum magnetism. We envision using light-wave acceleration of Cooper pairs and electrons forming robust collective states and both the amplitude and the phase of THz laser fields in order to steer non-equilibrium quantum materials phases at faster-than-terahertz clock rates with nearly zero-heat. Successful demonstration of (1) quantum control, during THz light-wave oscillation cycles, of long-lived (100^2 ps to 10^2 ns) non-thermal states, and (2) MDC-THz super-resolution imaging of iron-based and BCS superconductors and their collective modes, can open a new path for rational design and dynamical sensing of non-equilibrium materials properties for quantum science applications.

Recent Progress

We have developed a gauge invariant, non-perturbative, quantum kinetic theory of the ultrafast coherent nonlinear response of superconductors to THz electromagnetic fields. Our theory treats nonlinear quantum transport, condensate acceleration, spatial variations, and pseudospin nonperturbative nonlinearities directly in the time domain, thus modelling directly the experimental measurement of THz transients. We take into account both the amplitude and the phase of electromagnetic excitations to guide phase coherent nonlinear spectroscopy experiments. Our simulations calculate the dependence on multiple times (real time and phase coherence times) of a gauge-invariant density matrix [1] defined on a momentum grid. This density matrix characterizes the time-evolution of the quantum state in response to two (or more) phase-locked THz pulses. After two-dimensional Fourier transformation and after extracting the correlated part

of the signal [2], we calculate the MDC-THz spectra of superconductors and guide their experimental measurement. The calculated gauge-invariant signal vanishes in the case of single laser pulse excitation. It depends on quantum interference between two excitations created by time-overlapping pulses, in addition to standard pump-probe contributions. Super-resolution is achieved by separating, along the new axis corresponding to the coherence time, spectral contributions that cannot be distinguished in traditional one-dimensional spectroscopies, static or ultrafast pump-probe. So far, we have used two THz multi-cycle laser pulses to achieve non-perturbative THz-time-periodic driving of (1) one-band BCS, and (2) coupled-band iron pnictide SC states. By simulating nonlinear photocurrents, we develop a *THz dynamical symmetry breaking* principle for coherent manipulation of quantum materials phases. Parallel experiments at Ames Lab have tested the theoretical predictions, which allowed the development of a predictive computational tool. In this project, we focus on Inversion Symmetry (IS) breaking occurring during THz oscillation cycles, prior to the establishment of quasi-stationary states [1,3,4]. Pump-probe experiments provide higher resolution to observe IS symmetry-forbidden harmonics above critical field driving [3,4]. We have also demonstrated coherent steering of a SC state into long-lived (100's ps to ~10ns) accelerated condensate current-carrying and pre-thermalized metastable quantum states, which are tuned by the THz multi-cycle driving pulse shape [3]. This year, our emphasis has been on how to achieve quantum sensing of collective modes [5] and how to measure light-driven entanglement by using the super-resolution offered by 2D frequency space. We have discovered a



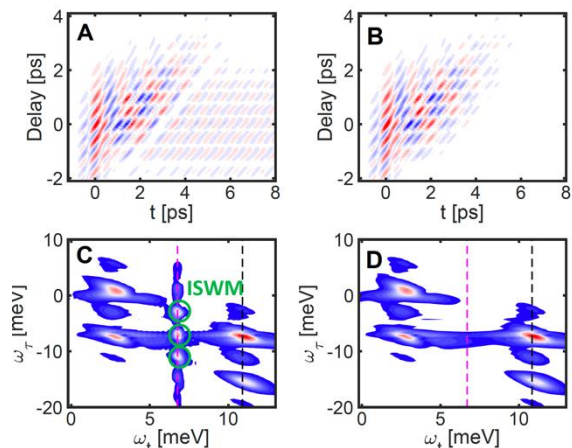
MDC-THz Coherent Spectroscopy (A-D): Correlated 2D signal as a function of sampling time t (real time) and pump-probe delay (coherence time) for low (40.0 kV/cm), intermediate (100.0 kV/cm), and high (160.0 kV/cm) pump driving field. **(E-G):** Calculated 2D Fourier transform of (A-C). Labels and circles indicate spectral positions of conventional coherent pump-probe (PP, black), four-wave-mixing (FWM, red), and third harmonic generation (3HG, yellow) peaks. New correlated wave-mixing (CPP, CFWM, C3HG, and CWM, green) peaks emerge above critical driving and signify light-induced entanglement. Vertical magenta (black) dashed lines indicate peaks splitting from conventional peaks along the new vertical axis corresponding to the coherence time. Our predicted signatures of light-induced correlation are consistent with the first experimental measurement of MDC-THz in iron pnictides. **(D and H):** results for the highest pump field of 160.0 kV/cm are calculated by ignoring order parameter pump-probe coherent modulation. They agree with the lineshapes of third-order responses and measurements in semiconductors. The new CWM peak in the right-bottom corner of 2D space (F and G) presents the most dramatic smoking-gun signature of light-driven pseudospin entanglement mediated by higher-correlation

Hybrid-Higgs collective mode and described the signatures of light-induced interactions between SC excitations leading to transient quantum entanglement [2]. Importantly, we have identified smoking gun MDC-THz features displaying anomalous temperature and field dependencies [2].

In summary, our main results are:

- MDC-THz spectra of BCS and Fe-based SCs [1-9]:** We have simulated and analyzed MDC-THz multi-dimensional datasets to guide experiment for (1) super-resolution visualization of light-induced quantum entanglement in SC systems, (2) coherent control of symmetry-breaking, dissipation-less photocurrent flow and quantum interference of pump and probe excitations during THz oscillation cycles. By tuning the relative phase between pump and probe excitations, we have revealed a

photogenerated, time-dependent interaction between *two elementary excitations*, which leads to light-induced quantum entanglement of Anderson pseudospins far from equilibrium [2]. We have predicted smoking-gun experimental signatures of THz-time-periodically-driven SC states in both one-band and two-band superconductors [2]: new Correlated Wave-Mixing (CWM) and THz Inversion Symmetry breaking Wave Mixing (ISWM) forbidden peaks, separated along the vertical frequency axis associated with the relative phase accumulation (coherence time). Above critical driving of SCs, these new MDC-THz peaks split from the conventional pump-probe (PP), four-wave mixing (FWM), and high harmonic generation (3HG) peaks. We have identified their dependencies on inter-band Coulomb coupling, driving



THz Dynamical Symmetry Breaking: By comparing our calculations with (A, C) or without (B, D) electromagnetic propagation effects, we demonstrate the emergence of new Inversion Symmetry Breaking Wave Mixing (ISWM) MDC-THz peaks at the Higgs mode frequency, with Higgs sidebands separated along the coherence time axis of two SC excitations. We have analyzed MDC-THz experimental datasets in iron pnictide high temperature superconductors to identify the predicted peaks arising from the above effects. Our ultimate goal is to use MDC-THz to achieve quantum tomography of higher correlation and entanglement across quantum systems.

field, and temperature. We attribute them to higher order nonlinear responses (7th order or higher) and IS breaking by the strong driving field. In particular, coherent pump-probe modulation of the SC order parameter parametrically drives pseudospin Rabi oscillators to give experimentally-observable higher-order nonlinear signals with distinct temperature and field dependencies. To understand the new aspects, we note that, spectroscopically, correlations are typically measured experimentally through allowed single-quanta elementary excitations. In SCs, the properties of single excitations are measured by third-order nonlinear susceptibilities. For strong fields, however, these conventional paradigms can break down. Our theoretical results stem from coherent nonlinear dynamics

2. **Discovery of Hybrid-Higgs Mode [5-6]:** Our prediction of a new controllable Hybrid-Higgs collective mode in multi-band iron pnictide superconductors was confirmed by four-wave-mixing phase-coherent experiments performed by our Ames Lab partner. A conceptually distinct Higgs amplitude mode arises in the limit of strong inter-band Coulomb interaction. We have demonstrated nonlinear quantum control of the Hybrid-Higgs coherence: strong THz driving leads to non-monotonic, nonlinear spectral changes displaying unconventional temperature and electric field dependencies. Unlike for single-band SCs, a large reversible modulation of the Hybrid-Higgs resonance strength is observed despite a persisting mode frequency. We provide compelling evidence for light-controlled coherent coupling between electron and hole amplitude collective modes enabled by inter-band quantum entanglement.
3. **Light-wave control by using quantum femtosecond magnetism and time-periodic modulation of coherent transport [10]:** A strong oscillating MIR laser electric field can enable light-wave quantum electronics by accelerating electrons back and forth during

oscillation cycles. However, without a direct interaction between photons and spins, magnetic properties can only be affected indirectly during such sub-cycle non-thermal timescales. We demonstrate that quantum fluctuations of magnetic moments responding to light-driven quantum transport of electron-magnon quasi-particles can provide new non-thermal pathways to steer antiferromagnetic states towards non-equilibrium metallic states with transient magnetization. In this way, we can influence magnetic moments in sync with electronic motion. Such light-engineering of quantum states at the ultimate speed limit provides new perspectives into quantum attosecond/femtosecond magnetism, while breaking ground for controlling correlated magnetic phases. A metastable non-equilibrium phase is established within a couple of oscillation cycles, while a light-induced softening of the phonon and transient changes in the total energy landscape open a new non-thermal pathway to an insulator-to-metal phase transition that is distinct from previously studied Mott transitions.

- 4. Dissipationless Chiral Photocurrent [11-16]:** Our Ames Lab, Brookhaven National Lab and UAB collaboration reported chiral anomaly and circular photogalvanic photocurrent in Dirac/Weyl semimetals. Nearly non-dissipative photocurrents are capable of transferring and modulating the chirality from an electromagnetic field with net helicity, and vice versa. We also reported THz-periodic driving of topological phase transitions in ZrTe₅. Our results propose a coherent light-induced phononic symmetry switch without application of static electric or magnetic fields. *First*, by selectively driving coherent Raman phonons, we demonstrated topological switching at THz speed during periodic lattice driving by a few-cycle THz pulse in ZrTe₅. Experimental results combined with first-principles modeling showed that the system transitions from a strong to a weak topological insulator state. A Dirac semimetal phase is realized in-between. *Second*, coherent pumping of symmetry-breaking infrared (IR) phonons dynamically generates Weyl points. Using circularly-polarized ultrafast excitation, we generated a chiral imbalance between right- and left-handed fermions in ZrTe₅ to obtain a giant anisotropic terahertz nonlinear current. The Berry curvature dominance marks a sharp suppression of impurity scattering due to chiral protection, which, together with a large Fermi velocity, leads to remarkably long ballistic mean free paths, $\sim 10 \mu\text{m}$, for the photocurrent.

Future Plans

This is the last year of this DOE grant. The theoretical results obtained so far in superconductors open new ways to address a non-equilibrium problem that spans across several fields, from light-induced superconductivity to parametric driving of metastable phases to quantum entanglement of supercurrent qubits to coherent control of dissipationless current flow. We have obtained coherently controlled and “symmetry-protected” superfluid and topological dissipationless photocurrents that can be immune to noise. These photocurrents enable switching by quantum coherent motion with minimal energy loss. Our analysis of MDC-THz multi-dimensional datasets can extract new information on chiral charge transport, fractionalized spin phases, quantum spin liquids, and Majorana fermions. Light-induced high temperature superconductivity might be characterized by MDC-THz peaks that reflect transient quantum entanglement. Our results point to a new phononic symmetry switch enabled by THz light control and twisting of the crystal lattice of a Dirac material. We broke ground for coherent manipulation of Weyl nodes and robust quantum transport without application of static electric or magnetic fields. The discovery of quantum chiral anomaly with a nearly dissipationless photocurrent opens new opportunities for developing *chiral qubits*, in analogy to superconducting qubits, that can be controlled all-optically.

Publications

- 1. Lightwave terahertz quantum control and sensing of non-equilibrium phases and their collective modes in superconductors**, M. Mootz, J. Wang, and I. E. Perakis, *Physical Review B* 102, 054517 (2020) <https://doi.org/10.1103/PhysRevB.102.054517>
- 2. Visualization and Light-Driven Entanglement of Quantum Systems using Terahertz Multi-Dimensional Coherent Spectroscopy**, M. Mootz, L. Luo, J. Wang, and I. E. Perakis, *Communications Physics*, 2021
- 3. Lightwave-Driven Gapless Superconductivity and Forbidden Quantum Beats by Terahertz Symmetry Breaking**, X. Yang, C. Vaswani, C. Sundahl, M. Mootz, L. Luo, J. H. Kang, I. E. Perakis, C. B. Eom and J. Wang, *Nature Photonics* 13, 707 (2019) <https://doi.org/10.1038/s41566-019-0470-y>
- 4. Terahertz Second-Harmonic Generation from Lightwave Acceleration of Symmetry-Breaking Nonlinear Supercurrents**, C. Vaswani, M. Mootz, C. Sundahl, D. H. Mudiyansele, J. H. Kang, X. Yang, D. Cheng, C. Huang, R. H. J. Kim, Z. Liu, L. Luo, I. E. Perakis, C. B. Eom, and J. Wang, *Physical Review Letters* 124, 207003 <https://doi.org/10.1103/PhysRevLett.124.207003> (2020)
- 5. Light quantum control of persisting Higgs modes in iron-based superconductors**, C Vaswani, JH Kang, M Mootz, Liang Luo, X Yang, C Sundahl, Di Cheng, Chuankun Huang, Richard HJ Kim, Zhiyan Liu, YG Collantes, EE Hellstrom, IE Perakis, CB Eom, Jing Wang, *Nature Communications* 12, 258 (2021) <https://doi.org/10.1038/s41467-020-20350-6>
- 6. Terahertz lightwave control of non-equilibrium phases and collective modes in multi-band superconductors**, Martin Mootz, Ilias E Perakis, Chirag Vaswani, Din H Mudiyansele, Xu Yang, Jigang Wang, *Proceedings of Ultrafast Phenomena and Nanophotonics XXIV 11278*, 112780F, 2020
- 7. Ultrafast nonthermal terahertz electrodynamic and possible quantum energy transfer in the Nb₃Sn Superconductor**, Yang, X., Zhao, X., Vaswani, C., Sundahl, C., Song, B., Yao, Y., Cheng, D., Liu, Z., Orth, P.P., Mootz, M., Kang, J.H, Perakis, I.E, Wang, C.-Z, Ho, K.-M, Eom, C.B, Wang, J, *Physical Review B* 99, 094504 (2019) <https://doi.org/10.1103/PhysRevB.99.094504>
- 8. Discovery of Light-induced Metastable Martensitic Anomaly Controlled by Single-Cycle Terahertz Pulses**, X. Yang , B. Song , C. Vaswani , L. Luo , C. Sundahl, M. Mootz , J-H. Kang , Y. Yao, K-M Ho , I. E. Perakis , C. B. Eom and J. Wang [arXiv:2008.08732](https://arxiv.org/abs/2008.08732) (2021)
- 9. Nonequilibrium Pair Breaking in Ba(Fe_{1-x}Co_x)₂As₂ Superconductors: Evidence for Formation of a Photoinduced Excitonic State**, X. Yang, L. Luo, M. Mootz, A. Patz, S. L. Bud'ko, P. C. Canfield, I. E. Perakis, and J. Wang, *Phys. Rev. Lett.* **121**, 267001 <https://doi.org/10.1103/PhysRevLett.121.267001> (2018)
- 10. Light-wave control of non-equilibrium correlated states using quantum femtosecond magnetism and timeperiodic modulation of coherent transport**, P. C. Lingos, M. D. Kapetanakis, J. Wang, and I. E. Perakis, *Communications Physics* 4, 60 <https://doi.org/10.1038/s42005-021-00561-z> (2021)
- 11. A light-induced phononic symmetry switch and giant dissipationless topological photocurrent in ZrTe₅**, Liang Luo, Di Cheng, Boqun Song, Lin-Lin Wang, Chirag Vaswani, PM Lozano, G Gu, Chuankun Huang, Richard HJ Kim, Zhaoyu Liu, Joong-Mok Park, Yongxin Yao, Kaiming Ho, Ilias E Perakis, Qiang Li, Jigang Wang, *Nature Materials* 20, 329 (2021). <https://doi.org/10.1038/s41563-020-00882-4> News and Views article on our work: Sirica,

- N.S., Prasankumar, R.P. Shaking up topology with light, *Nature Materials* **20**, 283–284
<https://doi.org/10.1038/s41563-021-00938-z> (2021)
12. **Ultrafast bipolar conductivity driven by intense single-cycle terahertz pulses in a topological insulator Bi₂Se₃**, Luo Liang, Xu Yang, Chirag Vaswani, Xinyu Liu, Ilias E Perakis, Margaret Dobrowolska, Jacek Furdyna, Jigang Wang, *Journal of Optics*,
<https://doi.org/10.1088/2040-8986/ac0316> (2021)
 13. **Terahertz Nano-Imaging of Electronic Strip Heterogeneity in a Dirac Semimetal**, Richard HJ Kim, Chuankun Huang, Yilong Luan, Lin-Lin Wang, Zhaoyu Liu, Joong-Mok Park, Liang Luo, Pedro M Lozano, Genda Gu, Deniz Turan, Nezih T Yardimci, Mona Jarrahi, Ilias E Perakis, Zhe Fei, Qiang Li, Jigang Wang, *ACS Photonics (published online)*
<https://doi.org/10.1021/acsp Photonics.1c00216> (2021)
 14. **Light-Driven Raman Coherence as a Nonthermal Route to Ultrafast Topology Switching in a Dirac Semimetal**, C. Vaswani, L.-L. Wang, D. H. Mudiyansele, Q. Li, P. M. Lozano, G. D. Gu, D. Cheng, B. Song, L. Luo, R. H. J. Kim, C. Huang, Z. Liu, M. Mootz, I. E. Perakis, Y. Yao, K. M. Ho, and J. Wang, *Physical Review X* **10**, 021013
<https://doi.org/10.1103/PhysRevX.10.021013> (2020)
 15. **Light control of surface–bulk coupling by terahertz vibrational coherence in a topological insulator**, Xu Yang, ..., I. E Perakis, ...J. Wang, *npj Quantum Materials* **5**, 13
<https://doi.org/10.1038/s41535-020-0215-7> (2020)
 16. **Ultrafast manipulation of topologically enhanced surface transport driven by mid-infrared and terahertz pulses in Bi₂Se₃**, Luo, L., Yang, X., Liu, X., Liu, Z., Vaswani, C., Cheng, D., Mootz, M., Zhao, X., Yao, Y., Wang, C.-Z., Ho, K.-M., Perakis, I.E., Dobrowolska, M., Furdyna, J.K., Wang, J, *Nature Communications* **10**, 607 (2019)
<https://doi.org/10.1038/s41467-019-08559-6>

Program Title: Dynamics and Driven States in Quantum Magnets

Principal Investigator: Thomas F. Rosenbaum, California Institute of Technology

Program Scope

The order-disorder transition at a quantum phase transition intertwines the static and dynamical response of the material changing state, introducing new universality classes, amplifying the effects of disorder, and etching in high relief the role of quantum fluctuations. There are ample questions remaining about the character of such transitions and the nature of the competing quantum states. There are also opportunities to drive quantum materials out of equilibrium, with the possibility of new types of correlated and coherent order, and new ways to access the dynamical evolution of ground and excited states. We seek here to probe the critical modes at a quantum phase transition in both pure and disordered ferromagnets, to quench the systems across their quantum critical points to reveal the means by which order grows, and to compare the fluctuation spectra after quantum and classical annealing protocols in both ferromagnets and spin glasses. Moreover, by tuning the disorder and the quantum tunneling probability, it should be possible to study the competition between quantum entanglement and random field effects. We hope to elucidate the fundamental quantum physics as well as addressing the question of how best to use complex systems, such as magnetic solids, to process quantum information.

Recent Progress

(A) Soft Mode Driving a Quantum Phase Transition. Quantum phase transitions have come to occupy a central place in thermodynamics and statistical mechanics. The quantum Ising model, the simplest example of a quantum phase transition, finds its clearest natural realization in the LiHoF_4 rare earth magnet, and experiments in this system (and in the associated diluted magnet $\text{LiHo}_x\text{Y}_{1-x}\text{F}_4$) over the years have probed quantum criticality in great detail. However, a key feature has been missing in experiments on this and other Ising systems. The low-energy excitation spectrum of the system must, if there is a quantum phase transition, contain a “soft mode” that drives the transition and whose energy goes to zero precisely at the critical point. Previous neutron scattering experiments have only seen gapped modes, leading to the speculation that the coupling of the electronic Ising spins to nuclear spins may have transformed the soft mode into this gapped mode. Such a scenario would imply a major change in our understanding of real-world quantum phase transitions, since spin bath modes—like nuclear spins, defects, or paramagnetic impurities—exist in any solid-state system. We directly measure the low-lying excitation modes using microwave spectroscopy at energies well below those achievable in neutron experiments and observe directly the soft mode at the quantum ferromagnetic critical point in LiHoF_4 (Publication 5).

Instead of the single low-energy excitation expected for a simple quantum Ising system, we find and characterize a remarkable array of modes arising from coupling of the spin-1/2 Ising electronic spins to a bath of spin-7/2 Ho nuclear spins. We plot in Fig. 1 the measured transmission of single-crystal LiHoF_4 in a loop-gap resonator tuned to two different frequencies at $T = 55$ mK. The loop-gap resonator permits focused magnetic fields at GigaHertz frequencies with high quality factors Q at physical dimensions compatible with mounting on the cold finger of a helium dilution refrigerator.

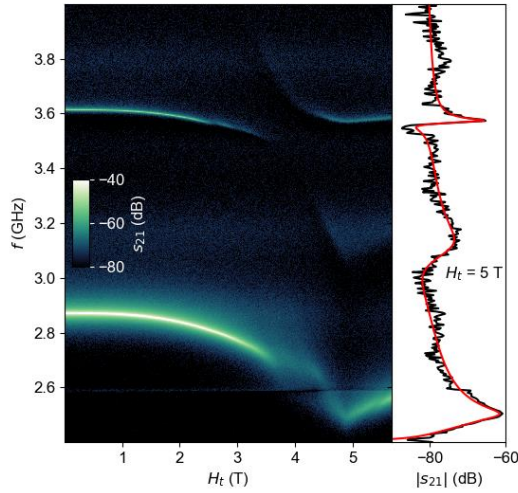
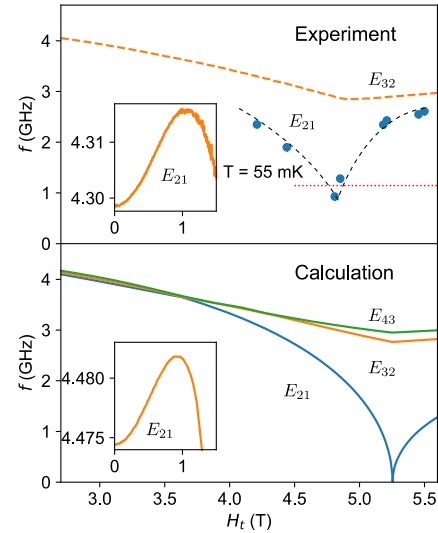


Fig. 1: Resonant absorption. Main panel: Transmission magnitude $|s_{21}|^2$ vs. frequency and transverse magnetic field for a bimodal loop-gap resonator with zero-field tuning of 2.9 and 3.6 GHz. Multiple avoided level crossings indicate points where excitation modes in LiHoF₄ cross the resonant frequencies of the loop gap resonator. For this resonator tuning, the soft mode absorption is seen at 4.5 T and 2.6 GHz. Right: Frequency spectrum at $H_t=5$ T (black) and multiple-Lorentzian fit (red).

Strong coupling is observed between the cavity photons and various excitations in the LiHoF₄ sample due to the high Q and filling factors. By repeating this process in multiple resonant cavities, we are able to map out the behavior of the lowest-lying electronuclear mode and observe its softening from above and below as it approaches the critical transverse field that defines the quantum phase transition. We compare the experimental results to Random Phase Approximation (RPA) calculations in Fig. 2.

Fig. 2: Measured and calculated excitation spectra. Top: Measured field dependence of soft mode (E_{21}) and excited state (E_{32}) spectra, as determined by on-resonance (blue points) and off-resonance (orange curve) responses, respectively. The dashed-line curve through the E_{21} points is a guide to the eye. Horizontal dashed line indicates frequency corresponding to the 55 mK measurement temperature. Bottom: Three lowest transition energies, calculated using a finite-temperature Random Phase Approximation (RPA) method. The mode structure and energy scale of the measurement and the model are in close agreement. The field scale for the QPT differs by approximately 8%. Insets: Measured and calculated frequency evolution at low field, where the three lowest modes are effectively degenerate.



Finally, we suppress the soft mode with a longitudinal magnetic field (Fig. 3), a critical test of the theory. Characterizing and experimentally manipulating these collective modes in a variety of magnetic quantum Ising systems is important because our results show that, as one approaches the quantum critical point, adiabatic quantum computing no longer can be regarded as a simple two-level avoidance process. One must consider all of the collective modes for any material that is a candidate for solid-state qubit realizations.

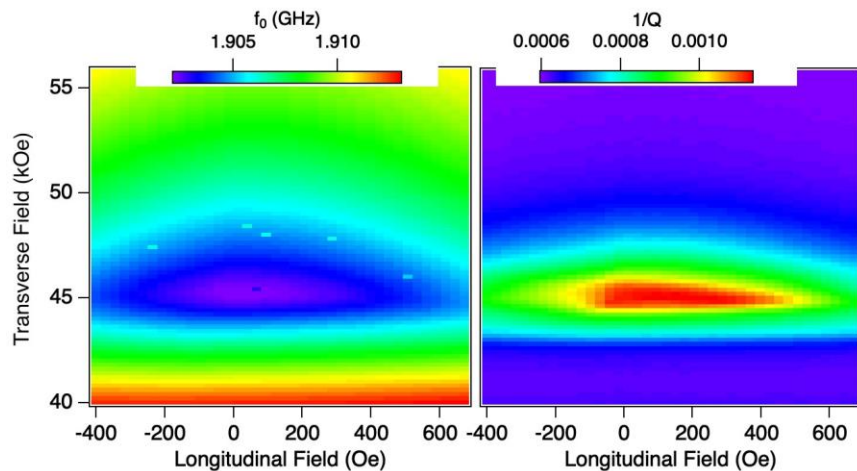


Fig. 3: Response of the real (left) and imaginary/dissipative (right) parts of the susceptibility to a longitudinal magnetic field in a 1.9 GHz resonant cavity. The field suppresses the dissipation, indicating that the soft mode no longer plunges to zero at the critical transverse field for the quantum phase transition.

(B) Quantum Dynamics in the Strongly-Driven Spin Liquid. At small Ho concentrations of a few percent, the $\text{Li}(\text{Ho},\text{Y})\text{F}_4$ system enters a strongly frustrated, spin liquid state. In this regime, the magnetic moments experience small quantum corrections to the common Ising approximation, which lead to small, degeneracy breaking energy shifts between different eigenstates. We have shown (Publication 3) that destructive interference between two almost degenerate excitation pathways burns spectral holes in the magnetic susceptibility, microscopically described in terms of Fano resonances. These already can occur in setups of only two or three frustrated moments, for which the driven level scheme has the paradigmatic L shape. For larger clusters of magnetic moments, the corresponding level schemes separate into almost isolated many-body schemes, in the sense that either the transition matrix elements between them are negligibly small or the energy difference of the transitions is strongly off-resonant to the drive. This enables the observation of Fano resonances, caused by many-body quantum corrections to the common Ising approximation. We have measured the dependence of the resonances on the driving strength and frequency as well as the crucial role that is played by lattice dissipation (Publication 2).

Future Plans

1. We propose to investigate the effects of disorder on the quantum phase transition. The critical exponents and scaling of the critical transverse field in the quantum limit are different for $\text{LiHo}_x\text{Y}_{1-x}\text{F}_4$ in the presence of disorder due to the introduction of local random fields. We plan to employ microwave spectroscopy to reveal the nature of the soft mode at the quantum phase transition as well as the critical excitations with increasing amounts of disorder. We also propose to characterize the soft mode in the x-y quantum antiferromagnet, LiErF_4 .

2. A wide range of systems, from hard magnets to soft matter, from fluids to power grids, exhibit avalanche behavior when driven out of equilibrium. The statistics and form of these avalanches can be used to reveal the nature of the underlying energy landscape and dynamics. Barkhausen noise, driven by avalanches of ferromagnetic domain motion, is perhaps the best studied realization of this general phenomenon. In conventional metallic ferromagnets, drag effects arising from eddy-current back action dominate the dynamics, but realizing either a drag-free response or alternative drag mechanisms remains an important avenue for investigation. We have measured Barkhausen noise in an insulating Ising ferromagnet, $\text{LiHo}_{0.44}\text{Y}_{0.56}\text{F}_4$. An insulator cannot support eddy currents, and, indeed, we find that the ensemble average over long-duration avalanche events just below the Curie temperature approaches a symmetric lineshape, as

expected for a drag-free response (Publication 1). This limit has not been observed previously in metallic ferromagnets. At lower temperatures and for short duration events, we do observe clear drag effects, which cannot arise from eddy currents. By studying the temperature dependence in different time regimes and comparing to the well-understood microscopic Hamiltonian of this model Ising magnet, we are able to propose the presence of two coexisting drag mechanisms: one arising from quantum-fluctuation-induced domain wall broadening and the other from random-field-induced domain wall pinning.

It is not possible yet to definitively ascribe a quantum origin to the lowest temperature noise features, but we should be able to distinguish classical and quantum effects through the application of a transverse magnetic field. At small magnitudes, a transverse magnetic field primarily creates a site-random magnetic field that pins the domain walls, creating barriers to motion that increase with random field amplitude. The rising barrier height decreases the probability of reversal at a given applied field, and the pinning potential effectively can be increased or decreased on demand and, importantly, in a temperature-independent manner. As the magnitude of the transverse field is increased, one crosses into a quantum speedup regime, where the primary effect of the transverse field is to increase the tunneling probability of the domain walls by creating an admixture of “up” and “down” Ising spins. This effect is most pronounced at the lowest temperatures.

Systems near criticality exhibit scaling relations and power-law behavior between various quantities in each system, and the exponents corresponding to these scaling relations help elucidate the underlying mechanisms and universality class for a particular system. We will examine histograms of the duration vs. event probability, area vs. event probability, energy vs. event probability, and, finally, the voltage power-spectral-density. Classically, we would expect a Gaussian distribution of event sizes, while quantum mechanically we might expect to see quantization of event sizes or, at a minimum, non-Gaussian distributions.

Publications

1. “Magnetic Domain Dynamics in an Insulating Quantum Ferromagnet,” D.M. Silevitch, J. Xu, C. Tang, K.A. Dahmen, and T.F. Rosenbaum, *Phys. Rev. B* **100**, 134405 (2019).
2. “Tuning High-Q Nonlinear Dynamics in a Disordered Quantum Magnet,” D.M. Silevitch, C. Tang, G. Aeppli, and T.F. Rosenbaum, *Nature Commun.* DOI: 10.1038/s41467-019-11985-1 (2019).
3. “Quantum Dynamics in Strongly-driven Random Dipolar Magnets,” M. Buchhold, C.S. Tang, D.M. Silevitch, T.F. Rosenbaum, and G. Refael, *Phys. Rev. B* **101**, 214201 (2020).
4. "Supercapacitance and Superinductance of TiN and NbTiN Films in the Vicinity of the Superconductor-Insulator Transition," A.Yu. Mironov, D.M Silevitch, S.V. Postolova, M.V. Burdastyh, T. Proslir, T.I. Baturina, T.F. Rosenbaum, and V.M. Vinokur, *Scientific Reports* DOI: 10.1038/s41598-021-95530-5 (2021).
5. “Direct Observation of Electronuclear Modes about a Quantum Critical Point,” M. Libersky, R.D. McKenzie, D.M. Silevitch, P.C.E. Stamp, and T.F. Rosenbaum, *Phys. Rev. Lett.*, under review.
6. “Phase Diagram of the Shastry-Sutherland Compound $\text{SrCu}_2(\text{BO}_3)_2$ under Extreme Combined Conditions of Field and Pressure,” Z. Shi, S. Dissanayake, P. Corboz, W. Steinhardt, D. Graf, D.M. Silevitch, H. Dabkowska, T.F. Rosenbaum, F. Mila, and S. Haravifard, submitted to *Nature Commun.*

Session II

Magnetothermal imaging of correlated electrons in moire heterostructures

Andrea Young, University of California, Santa Barbara

Program Scope

Our program seeks to understand the interplay between magnetism and superconductivity in correlated two dimensional materials using scanned probe microscopy based on nanoscale superconducting quantum interference devices. Our sensors are nanoscale SQUIDs fabricated at the apex of a quartz tube, and can be made as small as 30nm in diameter; moreover, they boast flux sensitivities near the quantum limit enabling, in principle, single spin detection. We have built up one working instrument, and are working on several more, to bring this technique to bear on a wide range of heterostructures over a large range of temperatures and magnetic fields. In the first year of this program, we applied this technique to directly image orbital magnetism in twisted bilayer graphene (see Fig. 1), resulting in one publication [1].

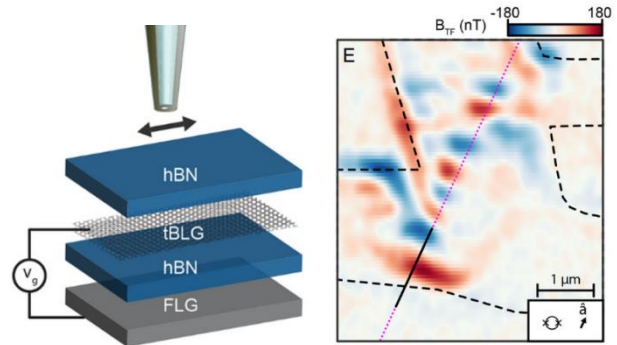


Figure 1: Left: nanoSQUID on tip microscopy schematic on a twisted bilayer. Right: gradient magnetometry of a twisted bilayer device. Both panels adapted from Tschirhart et al., Science 10.1126/science.abd3190 (2021).

Recent Progress

Originally conceived of as targeting moire materials, where flat bands may be engineered through interlayer lattice mismatch, we have recently changed this focus based on our accidental discovery of magnetism[2] and, under this award, superconductivity[3] in simpler pure graphene devices. Specifically, we have found that in rhombohedral trilayer graphene superconductivity appears at a variety of gate voltages, which tune both the carrier density and the band structure through the applied electric field. Importantly, ABC trilayer is structurally metastable, allowing highly uniform low-disorder systems to be experimentally created. Our findings point towards a broad class of previously unknown graphene superconductors based on gate-induced van Hove singularities in ultra-low disorder systems.

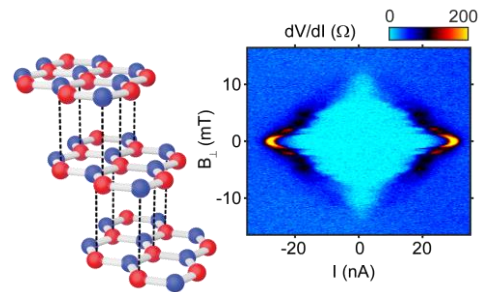


Figure 2: Crystal structure of rhombohedral trilayer graphene (left) and nonlinear resistivity in one of the superconducting states (right)

Accessing superconductivity via the electric field-effect in a clean, two-dimensional device is a central goal of nanoelectronics. While superconductivity has been realized in graphene moiré

heterostructures many of these structures are not mechanically stable, and experiments show signatures of strong disorder. Here we report the observation of superconductivity—manifesting as low- or vanishing resistivity at sub-kelvin temperatures—in crystalline rhombohedral trilayer graphene, a structurally metastable carbon allotrope. We observed superconductivity in *two* distinct gate-tuned regions (SC1 and SC2). Importantly, we find superconductivity to be deep in the clean limit defined by the ratio of mean free path and superconducting coherence length. The exceptionally high quality of the samples allows high resolution mapping of the normal state Fermi surfaces by quantum oscillations. These measurements, shown in Figure 3, reveal that both superconductors emerge from an annular Fermi sea, and are proximal carrier density to an isospin symmetry-breaking transition where the Fermi surface degeneracy changes. Whereas SC1 emerges from a paramagnetic normal state, SC2 emerges from a spin-polarized, valley-unpolarized half-metal and violates the Pauli limit for in-plane magnetic fields by at least one order of magnitude.

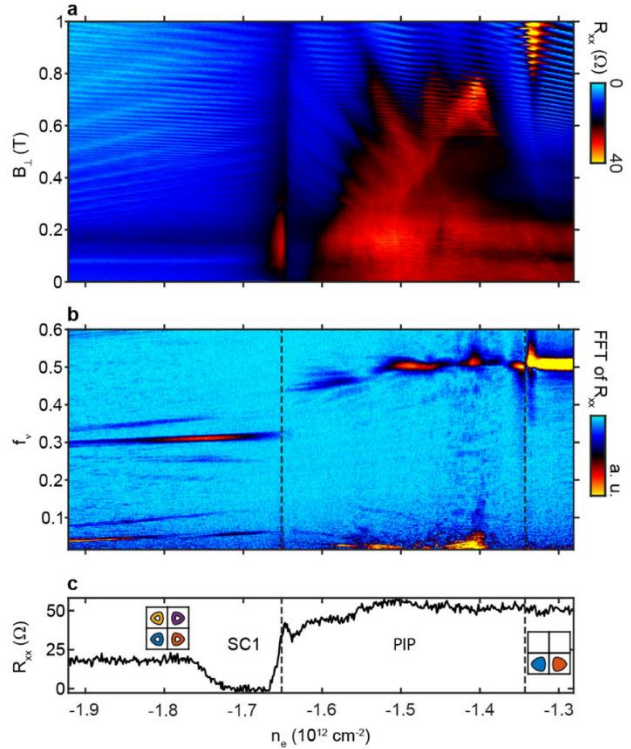
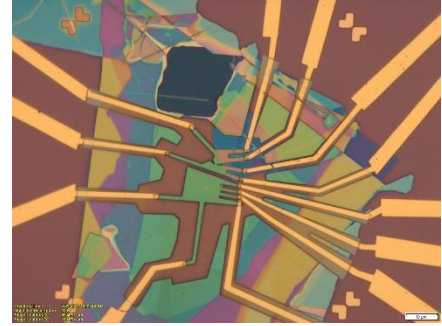


Figure 3: (a) Quantum oscillations in ABC trilayer graphene in the vicinity of the superconducting state. (b) Fourier transform of the quantum oscillation data, normalized to the total Luttinger volume. In these units, f_{ν} denotes the total fraction of the Fermi surface enclosed by a given phase coherent orbit. (c) Base temperature resistivity, showing the regime of superconductivity and the adjacent partially isospin polarized state (PIP). Superconductivity arises within the annular Fermi sea with unbroken spin- and valley degeneracy.

While the phenomenology of the superconductivity is clear, theoretically it is uncertain what the underlying mechanism is. In particular, our results may be understood in light of several proposals including both conventional phonon-mediated pairing and pairing due to intrinsic fluctuations of the Fermi sea. Most obviously, the appearance of superconductivity near symmetry breaking phase transitions suggests that fluctuations of the proximal ordered state may play a role in pairing. The plausibility of this picture hinges on the nature of the transition. Experimentally, the sudden jump in quantum oscillation spectra observed near the superconductors is suggestive of a first order transition. In this case, fluctuations might be suppressed. However, the resistivity of the normal state changes only gradually across the transition, contrasting with other isospin transitions studied in the same sample that are strongly first order. Measurements of the thermodynamic compressibility similarly do not show strong negative compressibility where superconductivity is observed, allowing for the possibility of a continuous transition.

Future Plans

The exceptionally uniformity of ABC trilayer graphene allows a new generation of experiments on ultra-clean and gate tunable superconducting and magnetic states. In the immediate term, we plan to apply magnetic- and thermal imaging to rhombohedral trilayers. These experiments will allow us to directly determine the magnetic moment of the magnetic and superconducting states. In particular, the presence of both spin- and valley- degrees of freedom allow for a wide variety of magnetic states, whose nature has significant implications for the nature of the observed superconductivity. In particular, the rapidly evolving theoretical picture for superconducting mechanisms in this system [4-12] features at least some suggestions that valley-coherent order may play a key role in all-electronic superconducting mechanisms. Direct measurements of the magnetic moment will go a long way towards constraining the symmetry breaking in different realized phases. In addition, some theoretical treatments have raised the possibility that topological superconductivity might be natural in this system [7-8]. Direct magnetic and thermal imaging may distinguish such states from more conventional symmetries, which have also been proposed to emerge from both conventional electron phonon as well as all-electronic mechanisms [4-6]. Devices for this measurement have already been fabricated, and are awaiting measurement as we write this report.



IN an alternative direction, the discovery of superconductivity where it was not expected always begs the question of where else superconductivity may appear. We speculate that ABC trilayer graphene is *not* unique; rather, all graphite allotropes likely host similar phase diagrams near van Hove singularities. In this picture, twisted bilayer and other moire systems are simply one route to generate this van Hove singularity, while ABC is another but the phenomena themselves may be ubiquitous. A major goal is thus to identify clean superconductivity in allotropes that are absolutely stable, in contrast to twisted systems which are mechanically unstable and the ABC trilayer which is only metastable. Bernal stacked bi- and multilayers are the first candidates we plan to explore in this regard.

References

1. C. L. Tschirhart, M. Serlin, H. Polshyn, A. Shragai, Z. Xia, J. Zhu, Y. Zhang, K. Watanabe, T. Taniguchi, M. E. Huber, A. F. Young. “Imaging orbital ferromagnetism in a moiré Chern insulator.” *Science*, 372:1323-1327 (2021).
2. H. Zhou, T. Xie, A. Ghazaryan, T. Holder, J. R. Ehrets, E. M. Spanton, T. Taniguchi, K. Watanabe, E. Berg, M. Serbyn, and A. F. Young, *Nature*, (2021).
3. H. Zhou, T. Xie, T. Taniguchi, K. Watanabe, and A. F. Young, *Nature*, (2021).
4. T. Lothman and A. M. Black-Schaffer, *Physical Review B* 96, 064505 (2017)

5. R. Ojajarvi, T. Hyart, M. A. Silaev, and T. T. Heikkilä, *Physical Review B* 98, 054515 (2018).
6. Y.-Z. Chou, F. Wu, J. D. Sau, and S. D. Sarma, arXiv:2106.13231 [cond-mat] (2021).
7. A. Ghazaryan, T. Holder, M. Serbyn, and E. Berg, arXiv:2109.00011.
8. S. Chatterjee, T. Wang, E. Berg, and M. P. Zaletel, arXiv:2109.00002.
9. Z. Dong and L. Levitov, arXiv:2109.01133.
10. T. Cea, P. A. Pantaleon, V. T. Phong, and F. Guinea, arXiv:2109.04345.
11. A. Szabo and B. Roy, arXiv:2109.04466.
12. Y.-Z. You and A. Vishwanath, arXiv:2109.04669

Publications

- C. L. Tschirhart, M. Serlin, H. Polshyn, A. Shragai, Z. Xia, J. Zhu, Y. Zhang, K. Watanabe, T. Taniguchi, M. E. Huber, A. F. Young. “Imaging orbital ferromagnetism in a moire Chern insulator.” *Science* **372**: 1323-1327 (2021).
- H. Zhou, T. Xie, T. Taniguchi, K. Watanabe, A. F. Young. “Superconductivity in rhombohedral trilayer graphene.” *Nature* (2021).

An experimental study of flat bands and correlated phases in twisted Carbon layers.

Eva Y. Andrei, Department of Physics, Rutgers University, 136 Frelinghuysen Rd, Piscataway, NJ 08904

Program Scope

The discovery of atomic layers and their stacking into van-der Waals heterostructures has led to the emergence of new material properties that could not have been achieved by standard chemical synthesis. In particular, superstructures created by stacking atomic layers with a twist between their crystallographic orientations introduces a periodically modulated moiré potential which can dramatically alter the electronic properties of a material, as first demonstrated by the STM/STS studies in my group.[1] In this work we discovered that the moiré potential in twisted bilayer graphene (TBG) produced two van Hove singularities where the density-of-states (DOS) is dramatically enhanced, at the same time slowing down the electron velocity. At a twist angle of $\sim 1.1^\circ$, later dubbed “magic angle”, these van-Hove-singularities merged producing an almost flat-band, where a gap that emerged at partial filling of the band indicated the emergence of a correlated-electron phase.[1] With the recent discovery of superconductivity, uncommon insulating states and magnetism, magic angle TBG has joined the realm of strongly correlated materials. Remarkably, the phenomenology of magic angle TBG is similar to that of high- T_c superconductors, a central mystery in condensed matter physics, but their behavior is richer. Transport measurements have shown that, similar to high- T_c superconductors, superconductivity in TBG emerges near the insulating phases observed at integer fillings of the moiré unit cell and exhibits a dome-like doping dependence of T_c . Further similarities include the linear in temperature resistivity, and the large ratio of T_c to the Fermi energy. Because TBLG is cleaner and its properties easily tuned by gating, as opposed to chemical doping in the case of the high- T_c superconductors, it could provide crucial insights into the underlying physics. To make further progress, detailed experimental studies that constrain the theoretical models are needed.

Recent Progress

Our recent work addressed questions concerning correlated phases in van der Waals heterostructures using techniques developed or refined in our group, including Hall density measurements, scanning tunneling microscopy and spectroscopy, Landau level spectroscopy, scanning charge spectroscopy, Kelvin force microscopy and atomic force microscopy. In addition to TBLG we have also studied the electronic properties of the layered transition metal dichalcogenide TaS_2 which exhibits a successive array of temperature-driven phase transitions into three types of charge density wave (CDW) states. Below is a brief summary of results pertaining to flat band in MA-TBG.

- *Flat bands through strain induced superstructures.*[2] Interactions between stacked atomic crystals can radically change their properties, leading to essentially new materials in terms of the electronic structure. A striking example is the emergence of flat-bands in magic angle TBG where the quenched kinetic-energy promotes electron-electron interactions and facilitates the appearance of strongly-correlated phases. Flat-bands however are rarely found in nature. In the case of magic angle TBG, their appearance requires exquisite fine-tuning of the interlayer twist-angle, posing challenges to fabrication and scalability. We have discovered an alternative route to creating flat-bands that does not involve fine tuning, by taking advantage of the fact that monolayers placed on an atomically-flat substrate can be forced to undergo a buckling-transition which results in periodically strained superlattices. Examples of graphene membranes that have undergone a

buckling transition are seen in the scanning tunneling topography images shown in Fig.1. The buckling transitions were observed upon cooling the device from 200C⁰ to 4K and were attributed to the difference in thermal expansion coefficients of the two materials. An STM height profile of a 2D triangular buckling lattice observed in graphene on NbSe₂ is shown in Fig. 2.

It is known from both theory and experiment that non-uniform strain in graphene produces a pseudo-magnetic field (PMF) with opposite signs in the K and K' valley, thus not breaking time reversal symmetry. This reconstructs the band into a sequence of flat pseudo-Landau levels (PLL), whose spacing is determined by the value of the PMF. Furthermore, owing to the peculiar valley-sublattice locking of Dirac fermions in both a real magnetic field and PMF, the K and K' electronic wave functions are constrained to reside on opposite sublattices. In other words, electrons in states corresponding to the K valley reside on one sublattice, say A, while K' valley electrons reside on the B sublattice. This provides a direct method to verify the presence of PMF through atomic resolution STM.

STS measurements on such a periodically buckled graphene layer revealed a PLL sequence corresponding to large periodically modulated pseudo-magnetic fields which reached 120T on the crests of the buckled structure (Fig. 3 left) and changed sign in the troughs where the PMF reached ~-80T. Atomic resolution topography (Fig. 3 center top and bottom insets) reveals triangular

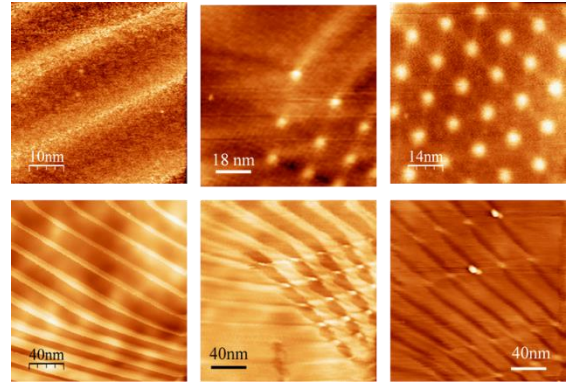


Figure 1. Buckled graphene membranes. Top row: graphene on NbSe₂. Bottom row: graphene on hBN. Buckling patterns range from 1D (left panels) to 2D (right panels).

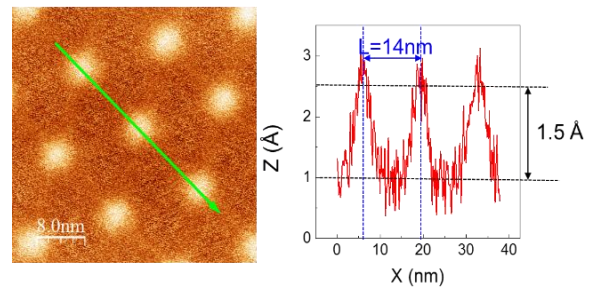


Figure 2. Buckled graphene membrane. Left: Topography map of buckled graphene on NbSe₂ showing a triangular pattern of crests (yellow) surrounded by troughs (brown). Right: height profile taken along the green line in the left panel.

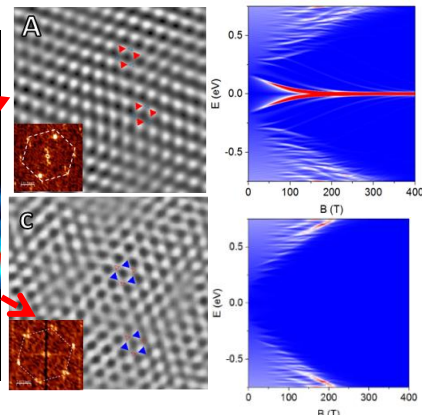
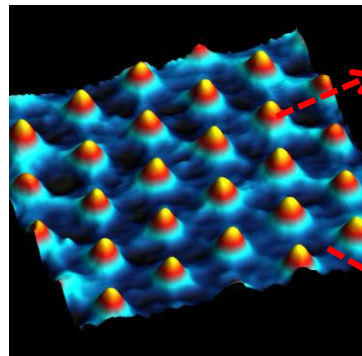
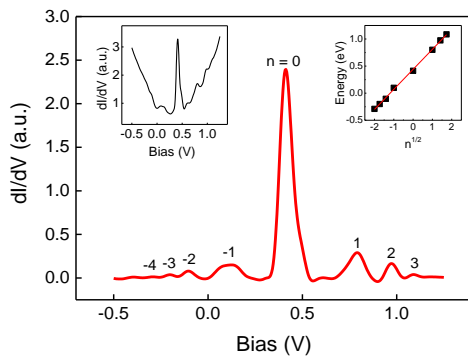


Figure 3. Pseudo Landau levels and pseudo magnetic fields in strain superlattice. Left: STS in crest regions shows a PLL sequence corresponding to a PMF of ~120T (right inset). Center: STM topography map of buckled graphene on NbSe₂ shows a strain induced buckling super-structure with period 10nm. Atomically resolved STM shows wavefunction localized on the A sublattice on the crests (top inset) and on the B sublattice in the troughs (bottom inset) (right). Right: Simulated PLL spectrum vs PMF on the crests and sublattice A (top) and B (bottom).

structures, with opposite orientations in the crests and trough regions, confirming the valley-sublattice locking expected in the presence of a PMF. This locking is similarly observed in the simulations, (Fig.3 right panels) where we plot the PMF dependence of the DOS in the K valley for the A and B sublattices (top and bottom respectively). We note that while the A sublattice hosts a low energy state, none is present on the B sublattice. This polarization is reversed in the troughs (not shown). In Fig. 4a we show the calculated band structure for the buckled G/NbSe₂ sample discussed above. Panels b & c show the experimental and theoretical DOS maps in each of the flat bands.

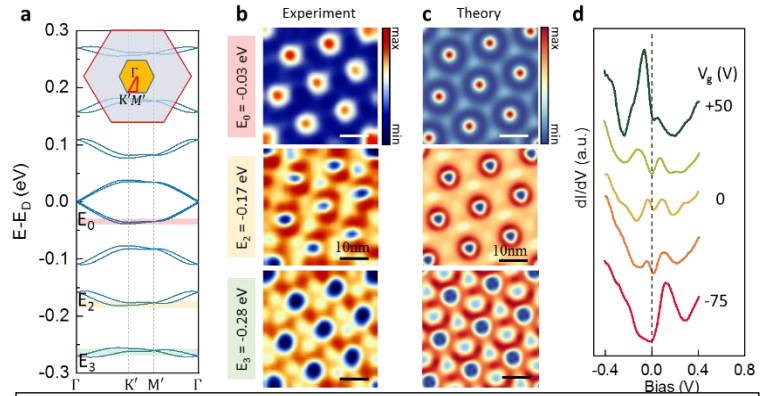


Figure 4. Flat-bands and LDOS maps. **a**, Calculated band structure for a buckled graphene superlattice with period $a_b = 14$ nm and PMF amplitude ($B = 120$ T). Inset: Superlattice mini-BZ, nested within the original BZ. **b**, **c**, Calculated LDOS contours (**b**) and measured dI/dV maps (**c**) for the three energies (E_0-E_D , E_1-E_D , E_2-E_D) that correspond to the flat-band regions in (a). **d**, Evolution of DOS with gate voltage shows pseudogap opening when Fermi level is brought into the flat band.

In the presence of a periodic strain field with period of order 10nm, theory predicts the emergence of very flat bands. Bringing the Fermi energy into such a flat band, and adding a small attractive interaction between the electrons, is expected to produce a superconducting state with a periodic gap whose amplitude is comparable to room temperature. Importantly, these parameters are achievable in buckled graphene membranes.

Because of the finite conductance of the NbSe₂ substrate it is not possible in the buckled G/NbSe₂ samples to bring the Fermi level within one of the flat-bands. Therefore, in order to access correlation effects, we used G/hBN samples. In this case, applying a gate voltage across the insulating hBN layer allowed us to bring the Fermi level within the flat-band. Utilizing the same sample preparation process as for G/NbSe₂, we again obtain buckling superlattices as illustrated in Fig. 1. Tuning the gate-voltage allowed us to gradually move the charge neutrality point from the hole-doped to the electron-doped sector. In Fig. 4d we show the evolution of the dI/dV spectra in the crest regions. The spectrum features a prominent peak that we identify with the strain-induced $N=0$ PLL. Doping the sample to partially fill the $N=0$ PLL band, the peak splits indicating the appearance of a correlation induced pseudo-gap at the Fermi level.

These results demonstrate that buckling-induced periodic strain patterns offer a new experimental strategy for the creation of flat-bands and for inducing correlated states with exceptional flexibility. The shape, period and symmetry of the buckled structures can be controlled by experimentally adjustable parameters, such as boundary geometry and strain distribution, enabling the realization of flat-bands with prescribed geometry.

- *Chern Insulators, van Hove singularities and Topological Flat-bands in Magic-angle Twisted Bilayer Graphene.*[3] In this work (Fig. 5) we reported on the discovery of surprising band-structure pliability in MA-TBG, providing direct access to the Fermi surface topology. Using Hall density measurements we found that in response to partial band-filling by electrostatic doping, the band structure transforms its topology, resulting in the emergence of van Hove singularities

(VHS) and correlation-induced gaps. The gaps generate mini-bands, which host new VHSs, leading to new correlation induced gaps, and so on. This produces a cascade of correlated phases, resulting in the first observation in this system of Chern insulating states characterized by precisely quantized Hall plateaus. Surprisingly, for magnetic fields exceeding 5T we observe a VHS at a filling of 3.5, suggesting the possibility of a fractional Chern insulator. This VHS is accompanied by a crossover from low-temperature metallic, to high-temperature insulating behavior, which suggests an entropically driven Pomeranchuk-like transitions. This work not only reveals the

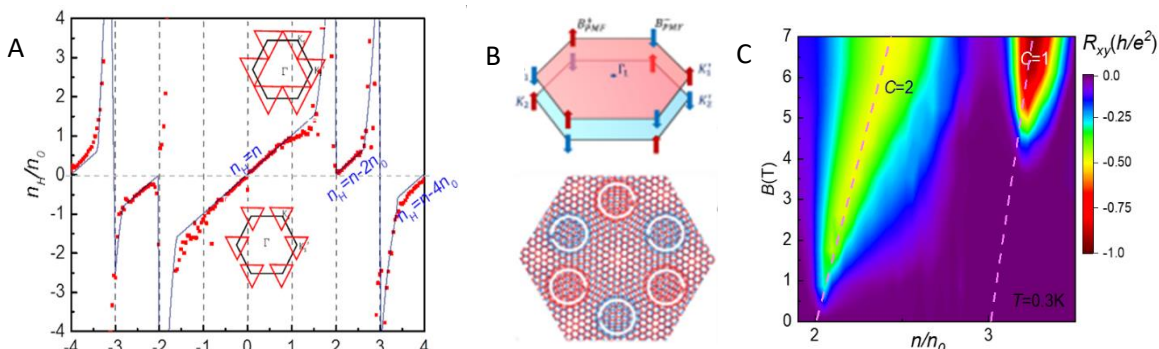


Figure 5. Low temperature Hall density and Hall resistance in MA-TBG. A) The are revealed by the VHS the doping divergence of the Hall density near integer moiré fillings. Inset, schematic evolution of the Fermi-surface (red triangles) from separate hole pockets for low doping (bottom) into a VHS (top) close to $|n/n_0| = 2$. B) Top: schematics of the opposite sign pseudo magnetic fields (red and blue arrows) at opposite corners of the BZ. Pink and cyan hexagons represent the BZs of the top and bottom layers of MA-TBG. Bottom: current density distribution in the K valley within a moiré-cell forms six circularly polarized orbital current loops with opposite chirality. C) Evolution of the Hall resistance with magnetic field shows well-quantized Hall plateaus with Chern-numbers $C = -2, -1, +2, +3$ on branches $s = 2, 3, -2, -1$ respectively (only electron branch shown).

existence of Chern insulators in this system, but also offers a new platform for inducing and understanding correlated states in MA-TBG. Furthermore, it introduces a new experimental tool for probing the Fermi surface topology in MA-TBG.

Future Plans

Future research will be guided by two experimental thrusts. (i) Elucidate the nature of the superconducting, insulating and magnetic states in TBLG. Using ultra-low temperature tunneling and transport measurements we will study the band structure reconstruction in the correlated electron states and their evolution with temperature, magnetic field, strain and carrier density. We will study the pseudogap phase in magic-angle TBLG and its relation to charge order and to the emergence of the superconducting phase, aiming to understand the pairing mechanism, the symmetry of the wave function and the low energy excitations. (ii) Devise new methods for creating flat bands and for inducing robust correlated electron states. This thrust will aim to create flat bands with non-twist induced superstructures such as strain-induced periodic pseudo-magnetic fields through thermal cycling of superposed layers with different expansion coefficients or by suspending atomic layers on nanometer-scale periodic structures.

References

- [1] G. Li, A. Luican, J.M.B. Lopes dos Santos, A.H. Castro Neto, A. Reina, J. Kong, E.Y. Andrei, Observation of Van Hove singularities in twisted graphene layers, **Nature Physics**, 6 (2010) 109
- [2] J. Mao, et al., Evidence of flat bands and correlated states in buckled graphene superlattices, **Nature**, 584 (2020) 215
- [3] S. Wu et al., Chern insulators van-Hove singularities and topological flat bands in MA-TBG **Nature Materials**, 20 (2021) 488

Recent Publications acknowledging DOE support

[2] J. Mao, S.P. Milovanović, M. Anđelković, X. Lai, Y. Cao, K. Watanabe, T. Taniguchi, L. Covaci, F.M. Peeters, A.K. Geim, Y. Jiang, E.Y. Andrei, Evidence of flat bands and correlated states in buckled graphene superlattices, **Nature**, 584 (2020) 215-220.

[3] S. Wu, Z. Zhang, K. Watanabe, T. Taniguchi, E.Y. Andrei, Chern insulators, van Hove singularities and topological flat bands in magic-angle twisted bilayer graphene, **Nature Materials**, 20 (2021) 488-494.

[3] N. Tilak, X. Lai, S. Wu, Z. Zhang, M. Xu, R.d.A. Ribeiro, P.C. Canfield, E.Y. Andrei, Flat band carrier confinement in magic-angle twisted bilayer graphene, **Nature Communications**, 12 (2021) 4180.

[4] M.A. Altvater, N. Tilak, S. Rao, G. Li, C.-J. Won, S.-W. Cheong, E.Y. Andrei, Charge Density Wave Vortex Lattice Observed in Graphene-Passivated 1T-TaS₂ by Ambient Scanning Tunneling Microscopy, **Nano Letters**, 21 (2021) 6132-6138.

[5] Y. Jiang, X. Lai, K. Watanabe, T. Taniguchi, K. Haule, J. Mao, E.Y. Andrei, Charge order and broken rotational symmetry in magic-angle twisted bilayer graphene, **Nature**, 573 (2019) 91-95.

[6]Eva Y. Andrei, Dmitri K. Efetov, Pablo Jarillo-Herrero, Allan H. MacDonald, Kin Fai Mak, T. Senthil, Emanuel Tutuc, Ali Yazdani, Andrea F. Young The marvels of moiré materials , **Nature Reviews Materials** 6, 201 (2021)

[7] Eva Y. Andrei and Allan H. MacDonald, Graphene Bilayers with a Twist, **Nature Materials** 19, 1265–1275 (2020)

[8] Michael A. Altvater, Shuang Wu, Zhenyuan Zhang, Tianhui Zhu, Guohong Li, Kenji Watanabe, Takashi Taniguchi, Eva Y. Andrei, Imaging of encapsulated graphene, **2D Materials** 6, (2019) 045034

[9] Jed H. Pixley and Eva Y. Andrei, Ferromagnetism in magic-angle graphene, **Science** 365, (2019) 543

[10] Michael A. Altvater, Nikhil Tilak, Skandaprasad Rao, Guohong Li, Choong-Jae Won, Sang-Wook Cheong and Eva Y. Andrei, Observation of a Topological Defect Lattice in the Charge Density Wave of 1T-TaS₂, To appear in Special issue of **Advanced Physics Letters** (2021).

Quantum Transport in 2D Semiconductors

James Hone, Cory Dean, Columbia University

Program Scope

The goal of this project is to perform pioneering studies of quantum transport in two-dimensional transition metal dichalcogenides (TMDs) and their related heterostructures. This work builds on advances in materials synthesis, development of new contact techniques, and implementation of new techniques for electrical transport and compressibility measurements. The specific goals include: understanding transport properties at high magnetic fields; detailed mapping of the Landau Level spectrum in TMDs with different bandstructure (e.g. bandgap) and spin-orbit coupling; studies of exciton condensate phases; and detailed studies of many body quantum states that appear in the fractional quantum Hall regime.

Recent Progress

1. Interlayer exciton condensate in bilayer transition metal dichalcogenides (TMD)

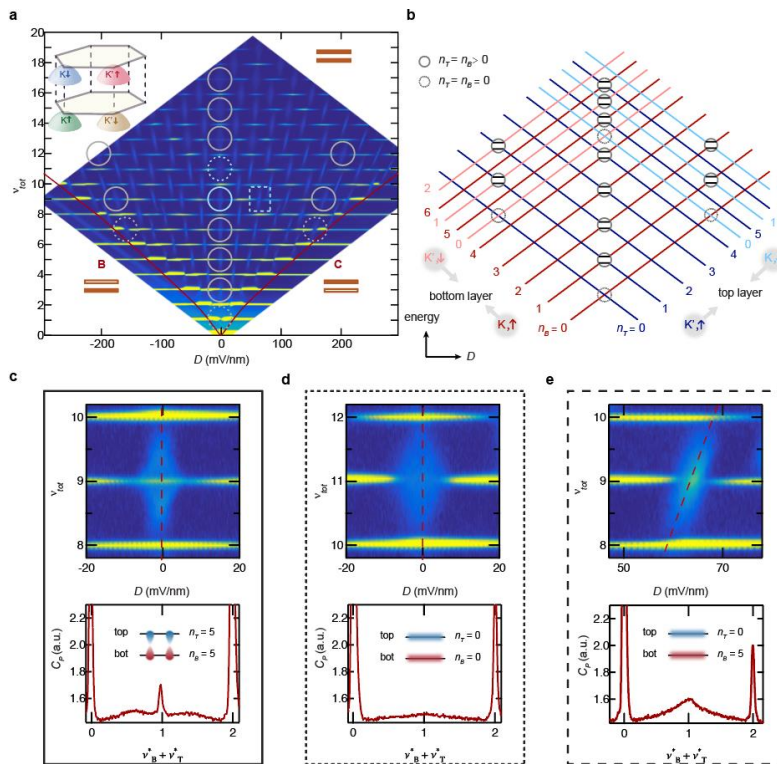


Fig 1: (a) Penetration capacitance as a function of the total filling factor ν_{tot} and displacement field D in bilayer WSe₂ at $B = 15$ T. Inset shows the band structure of bilayer WSe₂ with 4 relevant flavors as marked. (b) Schematic LL diagram. As D is varied, LLs from the two layers cross. The crossings for LLs of the same orbital number are marked by circles, with solid (dashed) circles for gapped (ungapped) cases. The gap formation at interlayer LL crossing represents easy-plane pseudospin ferromagnets, also known as exciton condensates. The top panel of (c) (d) (e) are zoom-in's of (a), focusing on the blue solid, dotted circles and dashed rectangular, respectively. The bottom panel are linecut along the red dashed line in the top panel. A gap is observed in (c) when $\nu_B^* + \nu_T^* = 1$ (total filling is integer) but not in (d) (e).

We have identified 2H-stacked bilayer WSe_2 as a natural platform for interlayer exciton condensates (EC) in the strong coupling limit. The intrinsic spin-valley structure in bilayer WSe_2 suppresses interlayer tunneling even when the separation is reduced to the atomic limit, providing access to a previously unattainable regime of strong interlayer coupling. Using capacitance spectroscopy, we investigate magneto-EC, formed when partially filled Landau levels (LL) couple between the layers. We identify that EC only forms when the relevant LLs have the same orbital number, while the spin and valley plays a minor role (see Fig.1). Remarkably, we observe for the first time EC in LLs with orbital number other than $n = 0$ (up to orbital number $n = 6$). Surprisingly, we find that in the strong coupling regime the EC can be more robust in higher LLs than in the lowest one (see Fig.2b). Comparison with theoretical calculations (Fig.2c) suggests that this is due to the crossover between two types of charge excitations – one involves layer pseudospin texture (known as meron-antimeron pairs) while the other one does not. In addition, we have observed that, for the two types of excitations, the charge gap has a different dependence on interlayer charge imbalance (Fig.2d).

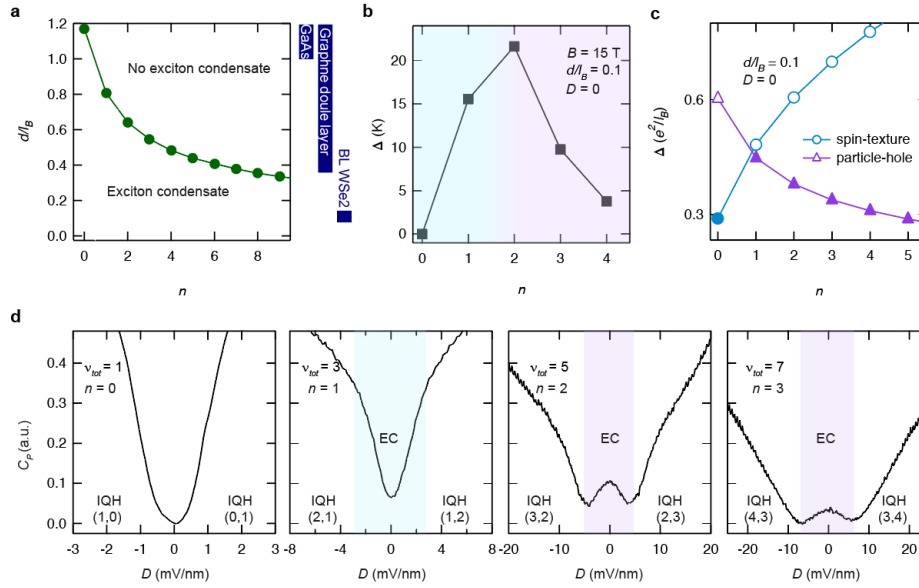


Fig. 2 (a) Numerically calculated upper limit d/l_B for EC formation (d is the interlayer spacing and l_B is the magnetic length). Experimentally accessible ranges of d/l_B for different systems are marked on the right. (b) Measured excitation gap when the layers are balanced ($D = 0$ and $\nu_B^* = \nu_T^* = 1/2$), at $B = 15$ T which corresponds to $d/l_B = 0.1$. (c) Numerically calculated charge gap values for layer balanced condition, for two types of excitations, at $d/l_B = 0.1$. The excitation energy of layer-pseudospin texture increases with n , while those for particle-hole excitations decreases with n . The filled markers stand for the lowest-energy excitations, which changes from one type to the other as n varies. (d) Penetration capacitance as a function of D , at constant total filling factor $\nu_{\text{tot}} = 1, 3, 5, 7$, as marked, while the topmost LLs has orbital numbers $n = 0, 1, 2, 3$, respectively. The shades highlight the D -range where the both layers are partially filled and charge is being transferred interlayer, while in the unshaded regions both layers are at integer fillings as marked and the system exhibits an integer quantum Hall gap. Apparently, in the partially filled regime, the gap increases with D for $n = 1$ while decreases with D for $n = 2$ and 3 .

2. Isospin-dependent transport in TMD

We have studied transport in WSe_2 in the quantum Hall regime and have identified that transport behavior is extremely sensitive to the spin and isospin flavor. In Fig. 3 (a) we plot the longitudinal and Hall resistance as a function of B , showing wide quantum Hall plateaus at high magnetic fields.

A density sweep at constant B is shown in Fig.3 (b). The resistance remains zero while the Fermi level stays in the first LL of spin down ($5 < \nu < 6$). This is in sharp contrast to the transport behavior when the Fermi level is in spin up LLs. At the same time, the Hall resistance shows a wide plateau. Further, LLs of different spin also host opposite temperature dependence in conductance (Fig.3c&d): the conductance decreases with decreasing temperature when the Fermi level is in a spin down LL. All the above observations suggest that the electrons are localized in the bulk when the Fermi level is in a spin down LL.

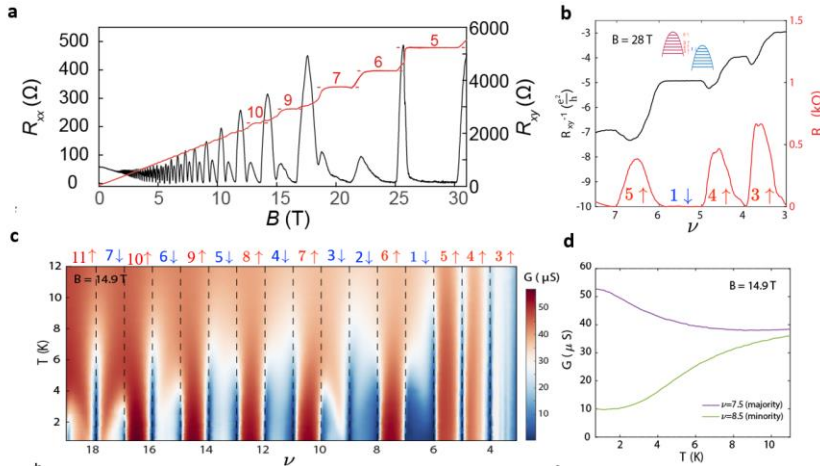


Fig. 3 (a) Longitudinal and Hall resistance in regime with only one layer populated as a function of B . (b) Longitudinal and Hall resistance as a function of filling factor at $B = 28$ T. The orbital and spin indices are marked. (c) Conductance as a function of filling factor and temperature at $B = 14.9$ T. (d) Two representative T-dependence curves at $B = 14.9$ T and $\nu = 7.5$ and 8.5 , as marked.

We further identify that the spin-sensitivity in transport results from the distinction of majority versus minority population of the isospin flavors. Indeed, even when the Fermi level always stays in spin up LLs, the transport varies sensitively as we vary the layer/valley index of the topmost LL. This is demonstrated in Fig.4(a) where we plot the resistance as a function of the total filling factor, and displacement field, which shifts the Fermi level between different layers (valleys). For example, the resistance at $\nu = 5.5$ as a function of the displacement field oscillates between high and low values (Fig.4b): when the Fermi level is in the layer whose population is the majority (minority), the resistance is high (low). Our observations demonstrate isospin-dependent transport behavior that cannot be explained by present theoretical models and calls for further studies.

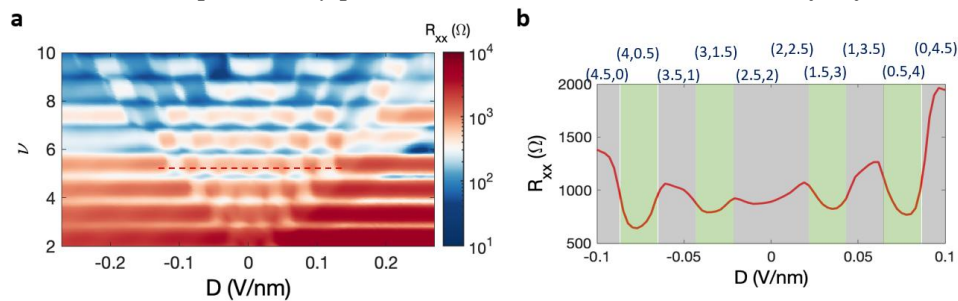


Fig. 4 (a) Resistance as a function of the total filling factor ν and displacement field D in bilayer WSe_2 at $B = 15$ T. The checkerboard region is the regime where both layers are populated. (b) Resistance as a function of D at $\nu = 5.5$. The filling factors are marked on the top as (ν_B, ν_T) .

Future Plans

1. Fractional quantum Hall interferometry in TMD monolayers

The excitations of fractional quantum Hall states (FQHS) are theoretically fractionally charged quasiparticles that obey anyonic statistics. Electron beam interferometers exploiting 1D edge states has been the most promising protocol to probe the nature of the quasiparticles. A particularly exciting species is non-Abelian anyons hosted in even-denominator FQHS, which can be the foundation for quantum computing. 2D TMD semiconductors have several advantages in engineering mesoscopic structures such as interferometers. On one hand, compared to classical semiconductors such as GaAs, the small thickness between the 2D channel and gate could reduce the fringe field effect and edge reconstruction. On the other hand, TMD semiconductors have a robust band gap which makes it easier to realize gate-tunable transmission of an electrostatically defined quantum point contacts. This is a critical technical requirement necessary to fine tune the response of an edge-state interferometer, and represents a big advantage over for example graphene, which is a semimetal with no band gap. The successful observation of FQHS including even-denominator ones and fabrication of quantum point contact suggests TMD monolayers are promising platforms for FQHS interferometry.

2. Wigner Crystals in the low density regime

Wigner crystals are predicted to form spontaneously in low density 2D electron systems, when the Coulomb interaction between the electrons overwhelms the kinetic energy. Atomically-thin TMD host high effective mass and weak screening and thus are natural platforms to pursue Wigner crystals. Recently, signatures of Wigner crystals have been reported from optical measurements on TMD monolayers and bilayers. On the other hand, the further advancement of TMD crystal quality allows the low density regime to be accessible by capacitance and transport measurements. We plan to perform systematic studies in the low density regime, in search of Wigner crystals.

Publications

1. Cao, Y., Assefa, T., Banerjee, S., Wieteska, A., Wang, D. Z. R., Pasupathy, A., Tong, X., Liu, Y., Lu, W. J., Sun, Y. P., He, Y., Huang, X. J., Yan, H. F., Chu, Y. S., Billinge, S. J. L. & Robinson, I. K. Complete Strain Mapping of Nanosheets of Tantalum Disulfide. *ACS Applied Materials & Interfaces* **12**, 43173-43179, (2020).
2. Shi, Q. H., Shih, E. M., Gustafsson, M. V., Rhodes, D. A., Kim, B., Watanabe, K., Taniguchi, T., Papic, Z., Hone, J. & Dean, C. R. Odd- and even-denominator fractional quantum Hall states in monolayer WSe₂. *Nature Nanotechnology* **15**, 569-572, (2020).
3. Q. Shi, E. Shih, D. Rhodes, B. Kim, K. Barmak, K. Watanabe, T. Taniguchi, Zlatko Papic, Dmitry A. Abanin, J. Hone, and C.R. Dean. Bilayer WSe₂ as a natural platform for interlayer exciton condensates in the strong coupling limit. Submitted.

Strongly correlated excitonic insulator in Coulomb-coupled bilayers

Kin Fai Mak

Cornell University

Program Scope

An exciton condensate is a state of matter with macroscopic quantum coherence. The concept of exciton condensation is of fundamental importance in condensed matter physics. The phenomenon may also have implications in condensate-based optoelectronics applications and exciton-mediated high-temperature superconductivity. The emergence of two-dimensional (2D) layered semiconductors with large exciton binding energy and flexibility in forming van der Waals heterostructures opens an exciting opportunity to explore high-temperature exciton condensation and other emergent quantum many-body ground states.

In this project, we will combine advanced device fabrication and tunneling, capacitance, and optical spectroscopy and imaging measurements to investigate interlayer exciton condensation in transition metal dichalcogenide (TMD) atomic double layers. Building on recent breakthrough of the PI's group on interlayer exciton condensation in MoSe₂-WSe₂ double layers, the research aims to address two open questions. The first is to understand and achieve high condensation temperature in the atomic double layer systems. The second concerns experimental signatures of exciton superfluidity and long-range spatial phase coherence. The specific objectives are:

- Determine the interlayer exciton binding energy and its dependence on interlayer separation, dielectric screening and relative orientations of the TMD materials;
- Quantify the exciton-exciton interactions, both the Hartree and the exchange correlations, and their effects on exciton condensation;
- Probe exciton superfluidity by tunneling measurements and long-range spatial phase coherence by correlation measurements of the interlayer exciton emission.

The proposed research is of fundamental importance since high-temperature exciton condensation presents one of the grand scientific challenges in condensed matter physics. The research also has the potential to impact technology including a new type of high-temperature superconductors and condensate-based superradiant light sources. Both are well aligned with the DOE missions.

Recent Progress

Excitonic insulators (EIs) arise from the formation of bound electron-hole pairs (excitons) in semiconductors and provide a solid-state platform for quantum many-boson physics. Strong exciton-exciton repulsion is expected to stabilize condensed superfluid and crystalline phases by suppressing both density and phase fluctuations. Although spectroscopic signatures of EIs have been reported, conclusive evidence for strongly correlated EI states has remained elusive. Recently, we have realized strongly correlated EIs in Coulomb-coupled bilayers of 2D semiconductors by direct thermodynamic measurements. We have also mapped the exciton phase diagram that reveals both the Mott transition and interaction-enhanced quasi-condensation.

Future Plans

The next step is to fabricate multi-exciton-terminal devices based on Coulomb-coupled bilayer systems and search for experimental signatures of exciton superfluidity.

References

L. Ma, P. X. Nguyen, Z. Wang, Y. Zeng, K. Watanabe, T. Taniguchi, A. H. MacDonald, K. F. Mak, & J. Shan, “Strongly correlated excitonic insulator in atomic double layers,” arXiv:2104.05066.

Publications

1. L. Ma, P. X. Nguyen, Z. Wang, Y. Zeng, K. Watanabe, T. Taniguchi, A. H. MacDonald, K. F. Mak, & J. Shan, “Strongly correlated excitonic insulator in atomic double layers,” *Nature* (2021) arXiv:2104.05066.
2. T. Li, S. Jiang, T. Li, Y. Zhang, K. Kang, J. Zhu, K. Watanabe, T. Taniguchi, D. Chowdhury, L. Fu, J. Shan, & K. F. Mak, “Continuous Mott transition in semiconductor moiré superlattices,” *Nature* (2021) arXiv:2103.09779.
3. T. Li, J. Zhu, Y. Tang, K. Watanabe, T. Taniguchi, V. Elser, J. Shan, & K. F. Mak, “Charge-order-enhanced capacitance in semiconductor moiré superlattices,” *Nature Nanotech.* (2021).
4. C. Jin, Z. Tao, T. Li, Y. Xu, Y. Tang, J. Zhu, S. Liu, K. Watanabe, T. Taniguchi, J. C. Hone, L. Fu, J. Shan, & K. F. Mak, “Stripe phases in WSe₂/WS₂ moiré superlattices,” *Nature Mater.* **20**, 940-944 (2021).
5. Y. Xu, C. Horn, J. Zhu, Y. Tang, L. Ma, L. Li, S. Liu, K. Watanabe, T. Taniguchi, J. C. Hone, J. Shan, & K. F. Mak, “Creation of moiré bands in a monolayer semiconductor by spatially periodic dielectric screening,” *Nature Mater.* **20**, 645-649 (2021).

6. H. Xie, S. Jiang, D. A. Rhodes, J. C. Hone, J. Shan, & K. F. Mak, “Tunable exciton-optomechanical coupling in suspended monolayer MoSe₂,” *Nano Lett.* **21**, 2538-2543 (2021).
7. Y. Tang, J. Gu, S. Liu, K. Watanabe, T. Taniguchi, J. C. Hone, K. F. Mak, & J. Shan, “Tuning layer-hybridized moiré excitons by the quantum-confined Stark effect,” *Nature Nanotech.* **16**, 52-57 (2021).
8. Y. Xu, S. Liu, D. A. Rhodes, K. Watanabe, T. Taniguchi, J. C. Hone, V. Elser, K. F. Mak, & J. Shan, “Correlated insulating states at fractional fillings of moiré superlattices,” *Nature* **587**, 214-218 (2020).
9. A. Mukherjee, K. Shayan, L. Li, J. Shan, K. F. Mak, & A. N. Vamivakas, “Observation of site-controlled localized charged excitons in CrI₃/WSe₂ heterostructures,” *Nature Commun.* **11**, 5502 (2020).
10. Y. Tang, L. Li, T. Li, Y. Xu, S. Liu, K. Barmak, K. Watanabe, T. Taniguchi, A. H. MacDonald, J. Shan, & K. F. Mak, “Simulation of Hubbard model physics in WSe₂/WS₂ moiré superlattices,” *Nature* **579**, 353-358 (2020).
11. Z. Wang, D. A. Rhodes, K. Watanabe, T. Taniguchi, J. C. Hone, J. Shan, & K. F. Mak, “Evidence of high-temperature exciton condensation in 2D atomic double layers,” *Nature* **574**, 76-80 (2019).
12. Y. Tang, K. F. Mak, & J. Shan, “Long valley lifetime of dark excitons in single-layer WSe₂,” *Nature Commun.* **10**, 4047 (2019).
13. K. Kang, T. Li, E. Sohn, J. Shan, & K. F. Mak, “Nonlinear anomalous Hall effect in few-layer WTe₂,” *Nature Mater.* **18**, 324-328 (2019).
14. D. V. Tuan, B. Scharf, Z. Wang, J. Shan, K. F. Mak, I. Zutic, & H. Dery, “Probing many-body interactions in monolayer transition-metal dichalcogenides,” *Phys. Rev. B* **99**, 085301 (2019).

Session III

Control of antiferromagnetic domain dynamics in oxide heterostructures

Charles Ahn (PI) and Fred Walker, Yale University

Program Scope

Transition-metal oxides (TMOs), such as nickelates and titanates, form an attractive platform that display a wide range of physical properties arising from strong electron correlations, including colossal magnetoresistance, metal-insulator transitions, multiferroicity, high-Tc superconductivity, and ferromagnetism. Often accompanying this behavior is an interplay between lattice, spin, charge, and orbital degrees of freedom. Understanding how the internal structural and electronic degrees of freedom are coupled in TMOs is crucial not only from the viewpoint of fundamental condensed matter physics, but also how they directly impact novel electronic phenomena relevant to basic energy sciences. Recently, intense research efforts are being focused on manipulating spin transport properties and ground state magnetism in the search for novel spintronic phenomena. Especially, exploiting antiferromagnetic (AF) materials as active constituents lays the groundwork for faster and more energy-efficient magnetic processes. Research for this project involves the synthesis and microscopic characterization of deliberately designed AF TMO-based heterostructures. The energetics and dynamics of collective magnetic excitations are tuned by changing composition and structure at interfaces and using effects due to dimensional confinement. A key ingredient for this project is the ability to grow crystalline thin film heterostructures with atomic precision using molecular beam epitaxy (MBE) comprised of alternating AF and tunable non-magnetic (NM) layers. Long-range electronic and magnetic ordering in strongly correlated oxides is intimately tied to short-range spin exchange patterns. Collective excitations in transition metal oxides can be effectively controlled by dimensional confinement via adjusting the local exchange interactions. These adjustments can realize substantial modifications to the energetics and dynamics of the collective excitations and long-range orders, opening a pathway to achieve unique behaviors that can advance quantum information and storage technologies based on collective electronic excitations.

Recent Progress

Our recent results show how we can assess the collective magnetic dynamics using x-ray photon correlation spectroscopy and control the dynamics in antiferromagnetic $(\text{NdNiO}_3)_m/(\text{NdAlO}_3)_n$ superlattices. We observe a dramatic change in the fluctuations of antiferromagnetic (AF) domain boundaries as we change the thickness of the NdNiO_3 (NNO) and NdAlO_3 (NAO) layers, the latter of which functions as a non-magnetic (NM) spacer (Panels a and b of Fig. 1). Reducing the NdNiO_3 layer thickness to approach the 2D limit inherently reduces the dimension of the AF domains, lowering the energy cost to create collective states, which is reflected as an enhancement of fluctuations at the AF domain boundaries. The collective dynamics can be further tuned by strengthening the inter-layer coupling (shown in panels c and d of Fig. 1) between separate NdNiO_3 blocks, as we reduce the NdAlO_3 layer thickness to a single unit cell. The analysis of the

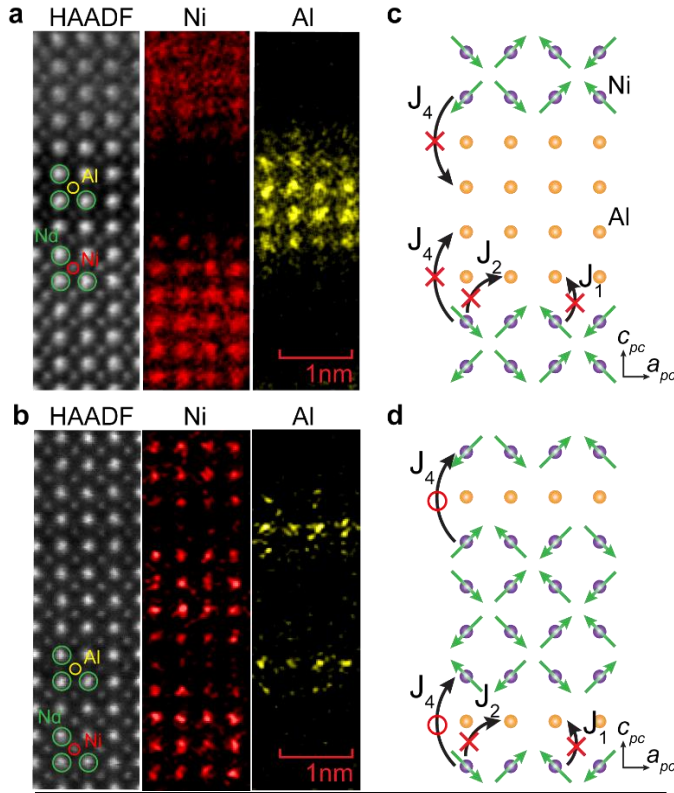


Figure 1. Real space structure and spin configurations in NNO-NAO superlattices. (a, b) High-angle annular dark field (HAADF) scanning transmission electron microscopy (STEM) images and energy-dispersive x-ray spectroscopy (EDS) maps of Ni and Al for $(\text{NdNiO}_3)_6/(\text{NdAlO}_3)_4$ and $(\text{NdNiO}_3)_4/(\text{NdAlO}_3)_1$ heterostructures, respectively. (c, d) Schematic of spin interaction in heterostructures with four NdAlO_3 layers and single NdAlO_3 layer, respectively. J_1, J_2, J_4 are double-exchange and superexchange interactions that are needed to induce the AF order observed in NdNiO_3 .

temperature dependent dynamics allows us to extract the energetics of the collective domain motion, which could be understood in terms of local exchange interactions.[1] The results demonstrate a path to control the fluctuations of antiferromagnetic domain walls in oxide heterostructures by fully exploiting the motifs of dimensional confinement and interfacial coupling. This approach is applicable to a broad class of materials to achieve unique behaviors and to advance quantum information and storage technologies based on collective electronic excitations.

NNO thin films and heterostructures are grown on LaAlO_3 (001) substrates using molecular beam epitaxy. SLs with varying NNO, NAO layer thicknesses are fabricated. X-ray diffraction and scanning transmission electron microscopy (STEM) show high crystallinity and atomically abrupt interfaces in both macroscopic and microscopic regimes (Figure 1). We perform resonant coherent soft x-ray scattering at $q_{AF} = \left(\frac{1}{4} \frac{1}{4} \frac{1}{4}\right)_{pc}$ to measure the AF ground state.

The AF domain texture in NNO arises from boundaries between domains with

dissimilar ordering wavevectors: $\mathbf{q}_1 = (1/4 \ 1/4 \ 1/4)_{pc}$, $\mathbf{q}_2 = (-1/4 \ 1/4 \ 1/4)_{pc}$, $\mathbf{q}_3 = (1/4 \ -1/4 \ 1/4)_{pc}$, $\mathbf{q}_4 = (1/4 \ 1/4 \ -1/4)_{pc}$, as well as anti-phase boundaries within a single wavevector domain. We are only sensitive to one of the four domains allowed by the fourfold surface symmetry. Coherent x-ray scattering from spatial disorder or microstructures, such as the above-described magnetic domains, results in a complicated interference pattern, known as a “speckle” pattern.

The dynamics of the speckle pattern can be quantified using an autocorrelation function, $g_2(t)$, which correlates pixel intensities I at particular regions at time separations, t . The dynamics of the AF domain wall motion can be deduced by exploring the time evolution of the speckle pattern, as the speckles are sensitive to the microscopic domain configuration. To quantify the observed dynamics, the square of the ISF is fitted with a stretched exponential:

$$|F(t)|^2 = e^{-2(t/\tau)^\beta}, \quad (1)$$

where τ is the decay constant, and β is the stretching exponent. The fit to the exponential function is shown as solid lines in Fig. 2(a). The extracted decay constants and stretching exponents at different temperatures are plotted in Fig. 2(b, c) for the $(\text{NNO})_4/(\text{NAO})_1$ superlattice. This superlattice has a dramatically different domain dynamic than thick NNO, with a decay constant measured in 10's of minutes below the Neel temperature of $\sim 150\text{K}$ and $(\text{NNO})_4/(\text{NAO})_4$ superlattices, with decay constants measured in tenths of a second.

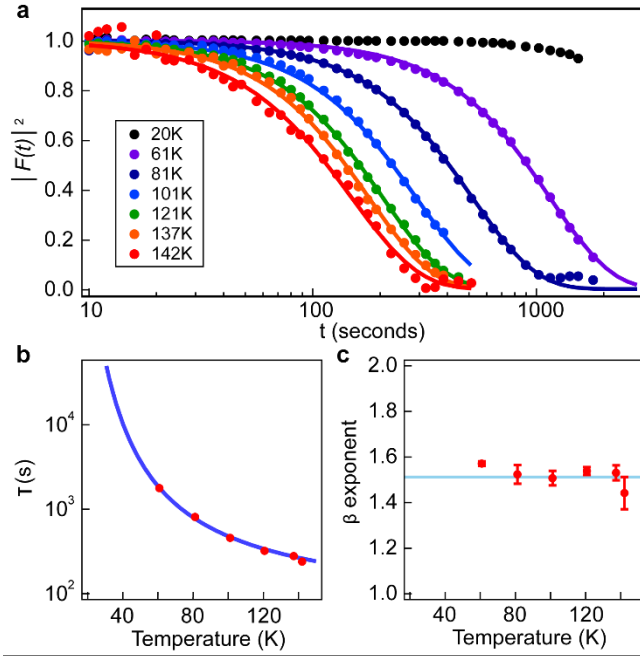


Figure 2. *Controlled domain dynamics using a non-magnetic spacer. (a) Normalized autocorrelation function for $(\text{NdNiO}_3)_4/(\text{NdAlO}_3)_1$ measured at various temperatures below T_N . Solid lines are stretched exponential fits to the data as described in the text, for temperatures above 60K. (b) τ extracted from the stretched exponential fit as a function of temperature. The blue line is an Arrhenius fit to the data. (c) β exponent extracted from the stretched exponential fit. Blue line indicates $\beta=1.5$.*

By limiting the spacer layer thickness to a single unit cell, the domains in adjacent layers are weakly pinned to one another, resulting in an intermediate domain dynamic with a decay constant that is strongly temperature dependent as the Neel temperature is approached, (Fig. 2a). The non-zero coupling across the NAO layer also suggests a microscopic model for the Arrhenius behavior observed in the $m=4$, $n=1$ SL. A thermally activated mechanism initiates the motion of a domain wall in a single layer, which, when decoupled from neighboring NNO planes, is observed to have fast dynamics. When the layers are coupled across a single NAO layer, there is an energy cost for moving the domain boundary in a single layer. After this first step, the domains of the neighboring layers can move to restore the ground state to account for the thermally activated domain motion. In this situation, the energy cost of moving the domain wall in a single layer represents the activation barrier associated with moving a domain wall in each layer by one lattice site. The measured activation

barrier of 17.6 meV is larger than predicted by theory and may reflect more than one domain being involved in the domain wall motion.

Future Plans

Perovskite nickelates and chromates are candidates for the AF active layers, as they exhibit a remarkable tunability across their rich phase diagrams. A non-magnetic isolation layer adjusts

the geometrically complex local exchange interaction patterns, which are tied to long-range magnetic ordering. The change in chemical composition and the thickness of the NM layer can modify the interfacial crystal and electronic structures of AFs to generate pronounced effects on the magnetic ground states. X-ray photon correlation spectroscopy (XPCS) of resonant diffraction peaks will allow measurement of the temperature- and length scale-dependent dynamics of the collective magnetic excitations to determine the energetics of AF domain configurations. Resonant inelastic x-ray scattering[2], angle-resolved photoemission spectroscopy[3], and crystal truncation rod measurements[4] will also be employed to provide a detailed understanding of the role of lattice, charge, orbital, and spin degrees of freedom on the collective magnetic behavior.

A key ingredient behind our approach to control the spin dynamics in oxide heterostructures is tuning the effective exchange coupling,[5] as illustrated in Figure 1c and 1d. The exchange interaction between separate magnetic layers can act across a nonmagnetic isolation layer if the thickness of the spacer layer is thin enough. The strength of the inter-layer exchange coupling can be tuned by adjusting either the thickness or the chemical composition of the insulating nonmagnetic layer. The strength of the coupling will depend on thickness, strain, and octahedral rotations of the perovskite oxygen sublattice. We will also control AF domains by using a spacer layer that is magnetic. The perovskite LaCoO_3 is such a spacer layer, with spin states and exchange interactions that can be altered with thickness, crystal structure, and strain state. Rare-earth chromates are a less studied system, and we will use the strong link between their AFM ground state and structural properties to achieve unique control of their collective magnetic behavior. LaCrO_3 (LCO) and SrCrO_3 (SCO) are AFM building blocks, insulating and metallic, respectively, for the proposed bi-layer heterostructures. In contrast to the nickelates, their AFM ground state mainly is governed by the superexchange interaction, resulting in a G-type AFM ground state, whose energetics depend strongly on the Cr-O-Cr bond angles and bond length.

References

- [1] Y. Lu *et al.*, *Physical Review X* **8**, 031014 (2018).
- [2] A. S. Disa, D. P. Kumah, J. H. Ngai, E. D. Specht, D. A. Arena, F. J. Walker, and C. H. Ahn, *Apl Mater* **1**, 032110 (2013).
- [3] J. Jiang, S. Lee, F. C. Fei, F. Q. Song, L. Vescovo, K. Kaznatcheev, F. J. Walker, and C. H. Ahn, *Apl Mater* **8**, 061106 (2020).
- [4] A. S. Disa, F. J. Walker, and C. H. Ahn, *Adv Mater Interfaces* **7**, 1901772 (2020).
- [5] S. Lee *et al.*, *Physical Review Letters* **123**, 117201 (2019).

Publications

Jiang, J., A. T. Lee, S. Lee, C. Lau, M. Li, T. M. Pedersen, C. Liu, S. Gorovikov, S. Zhdanovich, A. Damascelli, K. Zou, F. J. Walker, S. Ismail-Beigi, C. H. Ahn, *Electronic properties of epitaxial $La_{1-x}Sr_xRhO_3$ thin films*, Phys Rev B **103**, 195153 (2021). DOI: [10.1103/PhysRevB.103.195153](https://doi.org/10.1103/PhysRevB.103.195153)

Charles Ahn, Andrea Cavalleri, Antoine Georges, Sohrab Ismail-Beigi, Andrew J. Millis, Jean-Marc Triscone, *Designing, Controlling and Computing the Properties of Transition Metal Oxide Quantum Materials*, Nature Materials (2021) DOI: [10.1038/s41563-021-00989-02](https://doi.org/10.1038/s41563-021-00989-02)

Jonathan Pelliciari, Sangjae Lee, Keith Gilmore, Jiemin Li, Yanhong Gu, Andi Barbour, Ignace Jarrige, Charles H Ahn, Frederick J. Walker, Valentina Bisogni, *Tuning spin excitations in magnetic films by confinement*, Nature Materials **20**, 188 (2021). DOI: [10.1038/s41563-020-00878-0](https://doi.org/10.1038/s41563-020-00878-0)

Juan Jiang, Sangjae Lee, Fucong Fei, Fengqi Song, Elio Vescovo, Konstantine Kaznatcheev, Frederick J. Walker, Charles H. Ahn, *A comprehensive ARPES study of the type-II Dirac semimetal candidate $Ir_{1-x}Pt_xTe_2$* , APL Mater. **8**, 061106 (2020) DOI: [10.1063/5.0011549](https://doi.org/10.1063/5.0011549)

Ankit S. Disa, Frederick J. Walker, and Charles H. Ahn, *High-Resolution Crystal Truncation Rod Scattering: Application to Ultrathin Layers and Buried Interfaces*, Adv. Mat. Interfaces **7**, 1901772 (2020) DOI: [10.1002/admi.201901772](https://doi.org/10.1002/admi.201901772)

Q. Y. Chen, X. B. Luo, E. Vescovo, K. Kaznatcheev, F. J. Walker, C. H. Ahn, Z. F. Ding, Z. H. Zhu, L. Shu, Y. B. Huang, and J. Jiang, *Electronic structure study of $LaCoIn_5$ and its comparison with $CeCoIn_5$* , Physical Review B **100**, 035117 (2019). DOI: [10.1103/PhysRevB.100.035117](https://doi.org/10.1103/PhysRevB.100.035117)

Program Title: Non-Equilibrium Magnetism: Materials and Phenomena

Principle Investigator: Frances Hellman; Co-PIs Jeff Bokor, Peter Fischer, Steve Kevan, Sujoy Roy, Sayeef Salahuddin, Lin-Wang Wang; Materials Sciences Division, LBNL

Program Scope: This program focuses on the fundamental science of non-equilibrium magnetic materials and phenomena in films with strong spin-orbit interactions in the presence of interfacially-induced inversion symmetry breaking. It encompasses design, fabrication, measurement, and modeling of static and dynamic magnetic properties of these systems (Fig. 1). We focus on thermodynamic and dynamic control of magnetization, spin accumulation, and topological spin textures, addressing three interrelated thrusts: i) understand and control the free energy landscape of chiral spin textures; ii) design ferromagnet/non-magnet heterostructures with strong spin-orbit coupling that exhibit strong spin accumulation and associated switching; iii) produce highly non-equilibrium magnetic phases in these structures by fsec external excitation. Optical, electron, and x-ray techniques provide nanoscale resolution and msec-fsec time scales.

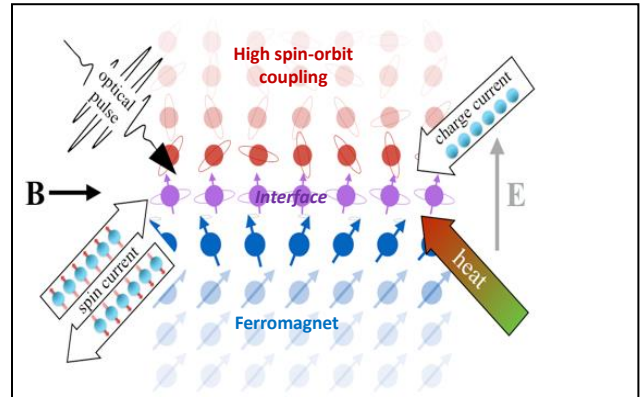


Fig. 1 Interface between ferromagnet (or other magnet) and high spin orbit coupling material, subject to optical, electrical, or heat pulses, and E or B fields. [Hellman et al. RMP, 2019]

Recent Progress (select results)

1) Stable 3D Chiral Spin Textures found in amorphous $a\text{-Fe}_x\text{Ge}_{1-x}$ by Lorentz TEM, x-ray microscopy, and coherent x-ray scattering [2].

- Data show a rich x, H, T phase diagram of helical and skyrmion phases, with a transition at low T to a state with rapid spin fluctuations. Vector spin exchange known as the Dzyaloshinskii–Moriya interaction (DMI), introduces spin chirality without global symmetry. DMI competes with exchange interaction to produce chiral spin structures. Lower x has higher DMI/exchange ratio, and shorter length scale spin structures. Structurally and chemically disordered materials with random DMI produce inversion symmetry broken topological textures, and offer flexibility in materials synthesis. [2]
- L-TEM images of the temporal evolution of skyrmions in $a\text{-Fe}_x\text{Ge}_{1-x}$ at 110K for $x=0.52$ show location dependent fluctuation rates ranging from 10 Hz to 10 mHz (Fig. 3).[2]

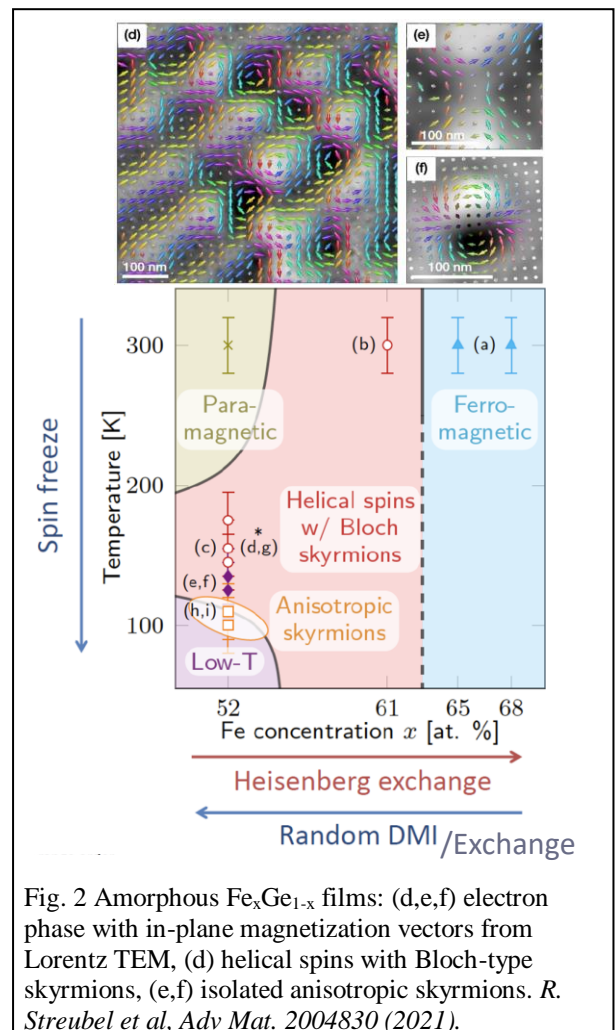


Fig. 2 Amorphous $\text{Fe}_x\text{Ge}_{1-x}$ films: (d,e,f) electron phase with in-plane magnetization vectors from Lorentz TEM, (d) helical spins with Bloch-type skyrmions, (e,f) isolated anisotropic skyrmions. R. Streubel et al, Adv Mat. 2004830 (2021).

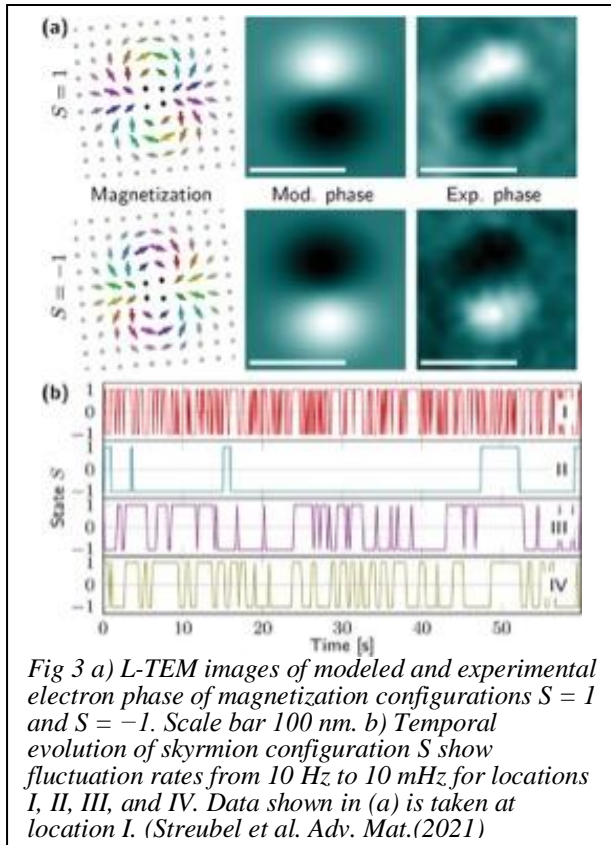


Fig 3 a) L-TEM images of modeled and experimental electron phase of magnetization configurations $S = 1$ and $S = -1$. Scale bar 100 nm. b) Temporal evolution of skyrmion configuration S show fluctuation rates from 10 Hz to 10 mHz for locations I, II, III, and IV. Data shown in (a) is taken at location I. (Streubel et al. Adv. Mat.(2021))

- Resonant magnetic soft X-ray scattering and coherent X-ray scattering studies (Fig. 4) on a - $\text{Fe}_x\text{Ge}_{1-x}$ as a function of temperature and applied magnetic field also shows these two transitions; high temperature paramagnetic to magnetic state and a lower temperature state which is not yet understood. A novel 4-fold symmetric phase was revealed, still under investigation.
- X-ray Photon Correlation spectroscopy (XPCS) shows glassy dynamics at low temperatures.
- Sub-nanosecond XPCS measurements recently performed at LCLS; data is still being analyzed

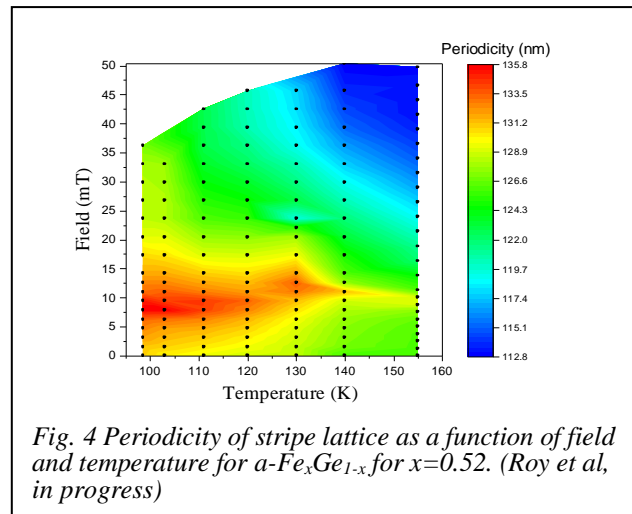


Fig. 4 Periodicity of stripe lattice as a function of field and temperature for a - $\text{Fe}_x\text{Ge}_{1-x}$ for $x=0.52$. (Roy et al, in progress)

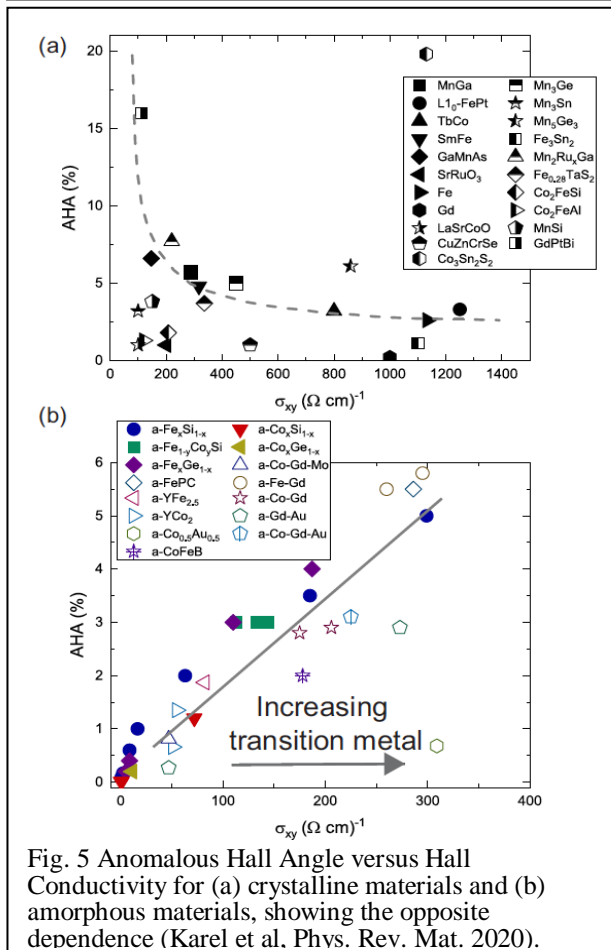


Fig. 5 Anomalous Hall Angle versus Hall Conductivity for (a) crystalline materials and (b) amorphous materials, showing the opposite dependence (Karel et al. Phys. Rev. Mat. 2020).

2) Large intrinsic anomalous Hall effect and spin orbit torques in and by amorphous TM-Si and TM-Ge alloys e.g. a - $\text{Fe}_x\text{Ge}_{1-x}$ for x from 0.4 to 0.7; in a typical crystalline ferromagnet the Hall conductivity (σ_{xy}) and conductivity σ_{xx} are correlated and usually either both large or both small, resulting in the anomalous Hall angle (AHA) ($= \sigma_{xy}/\sigma_{xx}$) decreasing with increasing σ_{xy} . By contrast, AHA *increases* with increasing σ_{xy} in amorphous systems (Fig. 5, [3]). This trend is attributed to generally low σ_{xx} , while σ_{xy} varies and can be large. Since in the amorphous systems, σ_{xx} and σ_{xy} are not coupled, there exists potential to further increase AHA by increasing σ_{xy} . Large Spin Orbit torques are also found for amorphous Fe-Si alloys (non-ferromagnets $x < 0.45$) used as spin injectors [4].

3) Designed, synthesized and experimentally verified stable hopfion spin textures via magnetic x-ray spectromicroscopies on designed Co/Pt/Ir multilayer structures.

Micromagnetic simulation of field dependent dynamics of magnetic hopfions show a transition from hopfions to torons, and identifying signatures in x-ray correlation plots that help experimentally distinguish hopfions from target skyrmions. [5]

4) Real-time TDDFT simulation of spin transport after femtosecond laser excitation for ferromagnetic metal/semiconductor, and ferromagnetic metal/diamagnetic metal heterostructures, reveal the role of exchange interaction for the spin flow. [6]

5) Amorphous heavy element Topological Insulators: Measured spin polarized surface states via spin-resolved angle resolved photoemission spectroscopy, characteristic magnetotransport measurements, and DFT in amorphous Bi₂Se₃ [7]. Theoretically discovered the transition from “trivial” (Rashba) insulator to topological insulator with increasing disorder in BiTeI; expt in progress. [8]

6) Helicity-independent all-optical switching (HI-AOS) measured in designed rare-earth transition metal ferromagnetic alloys: Observation and theoretical understanding of ultrafast helicity-independent all-optical switching (HI-AOS) in rare-earth transition metal ferromagnetic alloys incorporating both Gd and Tb as the rare earth element, elucidated the conditions required to observe HI-AOS, and showed that accounting for element-specific damping is crucial. [9]

Future Plans:

1. ***Intrinsic Anomalous Hall effect, Spin Hall effect and SOT in amorphous TM-Si, Ge:*** The high anomalous Hall effect associated with density of curvature suggests a large intrinsic spin Hall effect and SOT in related alloys. We will measure and calculate *spin Hall effect* in and *spin-orbit torque* by *a*-TM-Ge and *a*-TM-Si through second harmonic measurements.

2. ***Spin textures in amorphous TM-Si, Ge alloys:*** We will continue to explore the role of spin-orbit coupling in the evolution of helical and topological phases in *a*-TM-Ge, Si alloys as a function of magnetic field and temperature. All magnetic interactions can be tuned over a wide range by varying composition; we are specifically interested in phases where exchange, dipole, anisotropy, and thermal energies compete. Entropy stored in the resulting thermal fluctuations can stabilize new phases and textures. Resonantly tuned coherent soft X-ray scattering, LTEM, and PEEM are powerful tools to probe static textures and their spontaneous fluctuations. We will use coherent X-ray scattering on *a*-Fe-Ge films to understand the low temperature state and an unusual rotation observed in the diffraction pattern, and will continue our analysis of the LCLS data.

3. ***Three dimensional (3D) magnetic structures:*** There is strong evidence that for a deep understanding of even traditional skyrmions, the full three-dimensional configuration has to be taken into account e.g. chiral bobbars, skyrmion tubes, hybrid Bloch/Néel domain wall, Bloch points and lines. We will continue to develop and utilize advanced X-ray spectromicroscopy techniques, as well as state-of-the-art Lorentz TEM at the MF/NCEM to obtain all 3 spatial components of spin, with nanoscale spatial resolution.

4. ***Further studies of higher order spin structures:*** Fabrication of patterned magnetic multilayers (Pt/Co/Ir) and *a*-Fe-Ge alloy thin films onto co-planar waveguides will enable time-resolved X-ray microscopy to investigate field and current induced dynamics of hopfions, target skyrmions, and other topological spin structures.

5. **Manipulation of SOT by symmetry breaking:** Spin currents and torques depend on both the crystal space group of the high spin-orbit material as well as the atomic point group *local* to heavy atoms (high SOC) within the unit cell. For epitaxial heavy metal/FM systems, the spin-torques on the FM depends not only on anti-damping torques created by spin-current generated via the spin Hall effect but also from inverse spin galvanic effects (ISGE) sensitive to changes in the crystal space group and local point group symmetries. Examples where symmetry-breaking may lead to unconventional torques is metallic pyrochlore iridates $\text{Bi}_2\text{Ir}_2\text{O}_6$ and $\text{Pb}_2\text{Ir}_2\text{O}_6$.
6. **Ultrafast Optical Switching:** Upcoming BESSY-II x-ray femtoslicing beamtime will allow us to measure element specific dynamics of the amorphous Gd-Tb-Co alloys described above.
7. **Ultrafast Dynamics of antiferromagnets:** We will use novel fsec laser pump-probe methods to characterize ultrafast dynamics of antiferromagnets in response to ultrafast laser and electrical excitation. To pump the AFM-heterostructures with THz electrical fields and currents, we will embed AF heterostructures into coplanar waveguide structures with integrated ultrafast photoconductive switches. We will study the ultrafast dynamics of AF heterostructures with heavy metals. By passing THz electrical currents through a heterostructure that contains a strong SOC metal, we can generate THz spin-currents and SOTs, while transiently “softening” the AF order via ultrafast non-equilibrium excitation.
8. **Amorphous magnetic topological materials:** We will use the flexibility of the amorphous structure to allow us to create and study magnetic topological materials, for example to study the Anomalous Quantum Hall effect at higher temperature than has been yet possible in crystalline materials (e.g. amorphous MnBiTeI and related)
9. **Combine *ab initio* methods with phenomenological modelling to understand and predict out-of-equilibrium magnetic phases.** Explore the role of disorder on the emergence of topological and Rashba phases, examine the appearance of topological structures in real space (e.g. domain walls and magnetic skyrmions) and how their properties relate to the underlying chemical and structural details of these materials, build up predictive models, and understand and design functional real-space topological phenomena in magnetic materials.

References

1. F. Hellman *et al*, "Interface-Induced Phenomena in Magnetism", invited review article, Rev. Mod. Phys. **89**, 025006 (2017).
2. R. Streubel *et al*, "Chiral Spin Textures in Amorphous Iron–Germanium Thick Films", Adv. Mat. Comm. 2004830 (2021). *Selected for back cover.*
3. J. Karel *et al*, "Unexpected dependence of the anomalous Hall angle on the Hall conductivity in amorphous transition metal thin films", Phys. Rev. Mat. **4**, 114405 (2020).
4. Cheng-Hsiang Hsu *et al*, "Spin-orbit torque generated by amorphous $\text{Fe}_x\text{Si}_{1-x}$ ", arXiv:2006.07786v1 [cond-mat.mes-hall] 14 Jun 2020.
5. N. Kent *et al*, Creation and observation of Hopfions in magnetic multilayer systems, Nature Communications **12** 1562 (2021).
6. Z. Chen, J.W. Luo, L.W. Wang, "Light-induced ultrafast spin transport from ferromagnetic metals to semiconductor", (under review in Nano. Lett. 2021).
7. P. Corbae *et al*, "Evidence for topological surface states in amorphous Bi_2Se_3 ", ArXiv 1910.13412 and under review at Nat Mat.
8. P. Corbae *et al*, "Structural disorder-driven topological phase transition in noncentrosymmetric BiTeI", Phys. Rev. B **103**, 214203 (2021).
9. Alejandro Ceballos *et al*, "Role of element-specific damping on the ultrafast, helicity-independent all-optical switching dynamics in amorphous (Gd,Tb)Co thin films", Phys. Rev. B **103**, 024438 (2021).

Publications since last ECMP (Oct 2019-Sept 2021):

A. Publications primarily supported and intellectually driven by this FWP

1. N. Roschewsky, E. S. Walker, P. Gowtham, S. Muschinske, **F. Hellman**, S. R. Bank and **S. Salahuddin**, “*Spin-orbit torque and Nernst effect in Bi-Sb/Co heterostructures*,” Physical Review B **99**, 195103 (2019).
2. D. S. Bouma, Z. Chen, B. Zhang, F. Bruni, M. E. Flatte, R. Streubel, **L.-W. Wang**, R. Q. Wu, and **F. Hellman**, “*Itinerant ferromagnetism and intrinsic anomalous Hall effect in amorphous iron-germanium*”, Phys. Rev. B **101**, 014402 (2020).
3. J. Karel, D.S. Bouma, C. Fuchs, S. Bennett, P. Corbae, S.B. Song, B.H. Zhang, R.Q. Wu, **F. Hellman**, “*Unexpected dependence of the anomalous Hall angle on the Hall conductivity in amorphous transition metal thin films*”, Phys. Rev. Mat. **4**, 114405 (2020).
4. **P. Fischer**, D. Sanz-Hernández, R. Streubel, A. Fernández-Pacheco, *Research update: Launching a new dimension with 3D magnetic nanostructures*, APL Materials **8** 010701 (2020) (INVITED ARTICLE)
5. A. El-Ghazaly, J. Gorchon, R. B. Wilson, A. Pattabi, and **J. Bokor**, "Progress towards ultrafast spintronics applications," J. Magn. Magn. Mater., vol. 502, p. 166478, 2020.
6. Alejandro Ceballos, Akshay Pattabi, Amal El-Ghazaly, Sergiu Ruta, Christian P Simon, Richard F L Evans, Thomas Ostler, Roy W Chantrell, Ellis Kennedy, Mary Scott, **Jeffrey Bokor**, and **Frances Hellman**, “*Role of element-specific damping on the ultrafast, helicity-independent all-optical switching dynamics in amorphous (Gd,Tb)Co thin films*”, Phys. Rev. B **103**, 024438 (2021).
7. R. Streubel,* D. S. Bouma, F. Bruni, X. Chen, P. Ercius, J. Ciston, A. T. N’Diaye, **S. Roy**, **S. D. Kevan**, **P. Fischer**, **F. Hellman**, “*Chiral Spin Textures in Amorphous Iron–Germanium Thick Films*”, Adv. Mat. Comm. 2004830 (2021). *Selected for back cover.*
8. Cheng-Hsiang Hsu, Julie Karel, Niklas Roschewsky, Suraj Cheema, Dinah Simone Bouma, Shehrin Sayed, **Frances Hellman**, **Sayeeff Salahuddin**, Spin-orbit torque generated by amorphous Fe_xSi_{1-x}, arXiv:2006.07786v1 [cond-mat.mes-hall] 14 Jun 2020s
9. R. Streubel, A.T. N’Diaye, K. Srinivasan, A. Kalitsov, S. Jain, A. Ajan, **P. Fischer**, *The effect of Cu additions in FePt-BN-SiO₂) heat-assisted magnetic recording media*, Journal of Physics: Condensed Matter **33** 104003 (2021)
10. N. Kent, N. Reynolds, D. Raftrey, I.T.G. Campbell, S. Virasawmy, S. Dhuey, R. V. Chopdekar, A. Hierro-Rodriguez, A. Sorrentino, E. Pereiro, S. Ferrer, **F. Hellman**, P. Sutcliffe, **P. Fischer**, *Creation and observation of Hopfions in magnetic multilayer systems*, Nature Communications **12** 1562 (2021)
11. J. Chatterjee, D. Polley, A. Pattabi, H. Jang, **S. Salahuddin** and **J. Bokor**, “*RKKY exchange bias mediated ultrafast all-optical switching of a ferromagnet*,” Adv. Functional Mat. (in press).
12. A. Singh, M.K. Sanyal, J.C.T. Lee, S.A. Montoya, R.S. Streubel, J.J. Chess, M.K. Mukhopadhyay, B.J. McMorrin, E.E. Fullerton, **P. Fischer**, **S.D. Kevan**, **S. Roy**, *Evidence of Discretized Soliton-Spin-Stripes in Dipolar Magnetic Thin-Film*, Phys Rev Lett (2020) submitted

13. D. Raftrey, **P. Fischer**, *Field-driven dynamics of magnetic Hopfions*, Phys Rev Lett (2021) submitted
14. D. Raftrey, **P. Fischer**, *Advanced magnetic x-ray spectro-microscopies to characterize mesoscopic magnetic materials*, JMMM Special Issue on Mesoscopic magnetic materials and their application in information technology & biomedicine on the occasion of the 65th birthday of Prof. Kannan Krishnan, (2021) submitted.
15. Paul Corbae, Samuel Ciocys, Daniel Varjas, Steven Zeltmann, Conrad Stansbury, Manel Molina-Ruiz, Chris Jozwiak, Zhanghui Chen, **Lin-Wang Wang**, Andrew Minor, Adolfo Grushin, Alessandra Lanzara, **Frances Hellman**, “*Evidence for topological surface states in amorphous Bi₂Se₃*”, ArXiv 1910.13412 and under review at Nat Mat.
16. Z. Chen, J.W. Luo, **L.W. Wang**, "Light-induced ultrafast spin transport from ferromagnetic metals to semiconductor", (under review at Nano. Lett. 2021).

B. Collaborative publications:

1. Matthieu Amor, Alejandro Ceballos, Juan Wan, Christian Simon, Allegra Aron, Christopher Chang, **Frances Hellman**, and Arash Komeili. “*Magnetotactic bacteria accumulate a large pool of iron distinct from their magnetite crystals*”, Appl. Environ. Microbiol. 86, e01278-20 (2020). <https://doi.org/10.1128/AEM.01278-20>.
2. S.A. Morley, J.M. Porro, A. Hrabec, M.C. Rosamond, D.A. Venero, E.H. Linfield, G. Burnell, M.-Y. Im, **P.J. Fischer**, S. Langridge, C.H. Marrows, *Thermally and field-driven mobility of emergent magnetic charges in square artificial spin ice*, Sci Rep 9 15989 (2019)
3. V. Esposito, X. Y. Zheng, M. H. Seaberg, S. A. Montoya, B. Holladay, A.H. Reid, R. Streubel, J. C. T. Lee, L. Shen, J. D. Koralek, G. Coslovich, P. Walter, S. Zohar, V. Thampy, M. F. Lin, P. Hart, K. Nakahara, **P. Fischer**, W. Colocho, A. Lutman, F.-J. Decker, S. K. Sinha, E. E. Fullerton, **S. D. Kevan**, **S. Roy**, M. Dunne, J. J. Turner, *Skyrmion fluctuations at a first-order phase transition boundary*, Appl Phys Lett 116, 181901 (2020)
4. D. Sanz-Hernández, A. Hierro-Rodríguez, C. Donnelly, J. Pablo-Navarro, A. Sorrentino, E. Pereiro, C. Magén, S. McVitie, J. M. de Teresa, S. Ferrer, **P. Fischer**, A. Fernández-Pacheco *Artificial double-helix for geometrical control of magnetic chirality*, ACS Nano 14, 7, 8084 (2020)
5. X.P. Ma, J. Zheng, H.G. Piao, D.-H. Kim, **P. Fischer**, *Cherenkov-type three-dimensional breakdown behavior of the Bloch-point domain wall motion in the cylindrical nanowire*, Appl Phys Lett 117, 062402 (2020).
6. K. Jhuria, J. Hohlfeld, A. Pattabi, E. Martin, A. Y. Arriola Córdova, X. Shi, R. Lo Conte, S. Petit-Watelot, J. C. Rojas-Sanchez, G. Malinowski, S. Mangin, A. Lemaître, M. Hehn, **J. Bokor**, R. B. Wilson, and J. Gorchon, “*Spin-orbit torque switching of a ferromagnet with picosecond electrical pulses*,” Nature Electronics, vol. 3, pp. 680-686, 2020.
7. Ellis Kennedy, Neal Reynolds, Luis Rangel DaCosta, **Frances Hellman**, Colin Ophus, and M.C. Scott, “*Tilted fluctuation electron microscopy*,” Appl. Phys. Lett. **117**, 2020; DOI: 10.1063/5.0015532.
8. Paul Corbae, **Frances Hellman**, Sinéad M. Griffin, “*Structural disorder-driven topological phase transition in noncentrosymmetric BiTeI*”, Phys. Rev. B 103, 214203 (2021).

9. M. Goiriena-Goikoetxea, Z. Xiao, A. El-Ghazaly, C. V. Stan, J. Chatterjee, A. Ceballos, A. Pattabi, N. Tamura, R. Lo Conte, **F. Hellman**, R. Candler and **J. Bokor**, “*Influence of dislocations and twin walls in BaTiO₃ on the voltage-controlled switching of perpendicular magnetization*”, Phys. Rev. Mat. 5, 024401 (2021).
10. M. H. Seaberg, B. Holladay, S. A. Montoya, X.Y. Zheng, J. C. T. Lee, A. H. Reid, J. D. Koralek, L. Shen, V. Esposito, G. Coslovich, P. Walter, S. Zohar, V. Thampy, M.F. Lin, P. Hart, K. Nakahara, R. Streubel, **S. D. Kevan**, **P. Fischer**, W. Colocho, A. Lutman, F.-J. Decker, E. E. Fullerton, M. Dunne, S. Roy, S. K. Sinha, J. J. Turner, *Spontaneous fluctuations in a magnetic Fe/Gd skyrmion lattice* (2021) Physical Review Research, accepted
11. E. Josten, D. Raftrey, A. Hierro-Rodriguez, A. Sorrentino, L. Aballe, M. Lipińska-Chwałek, T. Jansen, K. Höflich, H. Kröncke, C. Dubourdieu, D. E. Bürgler, J. Mayer, **P. Fischer**, *Curvature-mediated spin textures in magnetic multi-layered nanotubes*, Nature Communications (2021) submitted.
12. S.-F. Wang, K. Chorazewicz, S. Lamichhane, R.A. Parrott, S. Cabrini, **P. Fischer**, N. Kent, J.H. Turner, T. Ishibashi, Z.P. Frohock, J. Wisser, P. Li, R. Zielinski, B. Herrington, Y. Suzuki, M. Wu, K. Munechika, C. Pina-Hernandez, R. Streubel, A.A. Sweet, *Ferromagnetic Resonances in Single-Crystal Yttrium Iron Garnet Nanofilms Fabricated By Metal-Organic Decomposition*, Appl Phys Lett (2021) submitted

Project Title: Heterostructures of quantum spin liquid and quantum electronic liquid for electrically sensing entangled excitations

PIs: Haidong Zhou (University of Tennessee), Jian Liu (University of Tennessee)

Program Scope

The overarching goal of our project is to address the grand challenge of “metallizing quantum magnets”, where emergent electronic phenomena arise as quantum mechanical consequences of exotic magnet states and excitations. Our approach in this investigation focuses on (i) materials synthesis by both single crystal and epitaxial growth, and (ii) transport characterizations complemented by other necessary analysis. The specific directions include (1) synthesizing geometrically frustrated quantum magnets (GFQMs) with unusual field-dependent magnetic structures, (2) exploring the response of correlated pseudospin-half electrons to the field-induced transitions.

Recent Progress

Anomalous magnetoresistance upon breaking the ice rule in pyrochlore heterostructures. The so-called dipolar spin ice is one of the most important representatives of frustrated magnets first discovered on pyrochlore lattice of Ising spins constrained along the local [111] direction, such as $Dy_2Ti_2O_7$ (DTO). Due to geometric frustration, the ground state of each tetrahedron settles in one of the six-fold degenerate 2-in-2-out configurations, forming a spin ice network following the ice rule in analog with water ice [1, 2]. Breaking the ice rule could lead to rich spin dynamics. For instance, applying a magnetic field along a [111] direction in DTO turns the three-

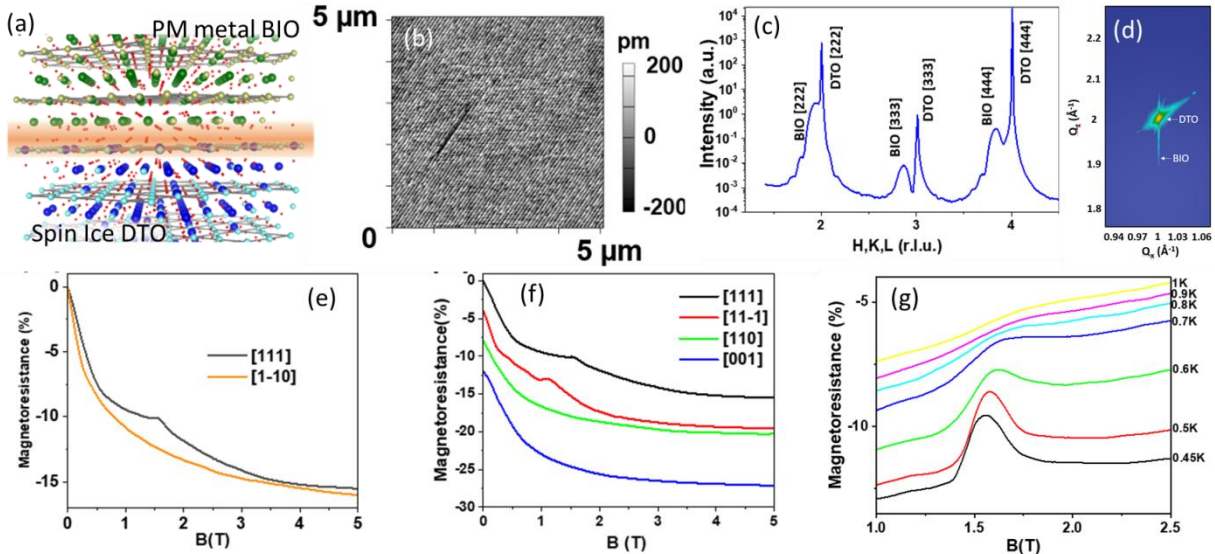


Figure 1 (a) Schematic of the BIO/DTO interface along the (111) plane. (b) A typical AFM image of DTO substrate surface. (c) A specular x-ray diffraction scan. (d) Reciprocal Space Mapping of a 4nm BIO grown on DTO single crystal near the [240] reflection. (e) MR for the BIO/DTO heterostructure at 0.03K with $H//[111]$ and $H//[1-10]$. (f) MR at 0.03K with field along different principle axes in the (1-10) plane. (g) Temperature dependence of the MR anomaly.

dimensional spin ice into a Kagome spin ice, and eventually stabilizes the 3-in-1-out or 1-in-3-out configuration [3, 4]. The spin-ice behaviors have however been only observed in highly

insulating compounds where the spins are carried by highly localized electrons, such as the f -electrons of Ho^{3+} or Dy^{3+} ions. It is an interesting open question to see whether and how the spin ice state would interact with itinerant carriers and introduce any novel electronic behaviors.

In our recent work, we observed an anomalous magnetoresistance (MR) in epitaxial pyrochlore heterostructures of $\text{Bi}_2\text{Ir}_2\text{O}_7/\text{Dy}_2\text{Ti}_2\text{O}_7$ (BIO/DTO), where DTO hosts the spin ice state and BIO is a nonmagnetic correlated metal providing charge carriers. We directly grow ultrathin films of BIO on DTO single crystals that are synthesized by the floating zone method and prepared with atomically flat (111) surfaces. Figure 1b shows a typical atomic force microscope image of the DTO single crystal substrate surface with a surface roughness of 1.21 Å. A thin layer of 3 - 5 nm BIO was epitaxially deposited on the DTO substrate by pulsed laser deposition, which is confirmed by the specular x-ray diffraction (Fig.1c). Reciprocal space mapping (Fig.1d) shows that the BIO film is in a fully strained state. The MR of BIO is known to be highly isotropic when the field is applied along different crystallographic axes. However, an emergent anisotropic feature of the MR was observed in the BIO/DTO heterostructure at 0.03 K and 1.5T (Fig.1e), when comparing MR with the field \mathbf{H} along the [111] and [1-10] directions. Our AC susceptibility measurement shows the field of this anomaly corresponds to the well-established transition from the Kagome spin ice to the 3-in-1-out state of DTO when $\mathbf{H}//[111]$.

To gain more insights, we further rotated the applied field in the (1-10) plane, where it crosses not only [111] but also [110], [11-1], and [100]. Figure 1f clearly shows that, while the MR with $\mathbf{H}//[110]$ and $\mathbf{H}//[001]$ appears to be featureless and similar to that of $\mathbf{H}//[1-10]$, the MR with $\mathbf{H}//[11-1]$ possesses a similar anomaly to the case of $\mathbf{H}//[111]$, albeit at a slightly lower field around 1.1 T due to the different demagnetization factors from the DTO substrate shape. This result confirms that the anomaly is associated with the ice-rule-breaking. We further studied the thermal evolution of this anomaly between 0.45 K and 1 K with $\mathbf{H}//[111]$. The obtained result in Fig.1g shows that the anomaly weakens with increasing temperature and starts to vanish at 0.9 K, consistent with the reported melting temperature of the spin ice state in DTO due to thermal fluctuation. We confirmed this conclusion by performing the same series of experiments on a reference sample where an $\text{Y}_2\text{Ti}_2\text{O}_7$ crystal is used as the substrate instead of DTO, and the anomaly is absent. These results demonstrate that epitaxial interface is an effective approach to induce interactions between charge carriers and exotic spin states in insulating frustrated magnets.

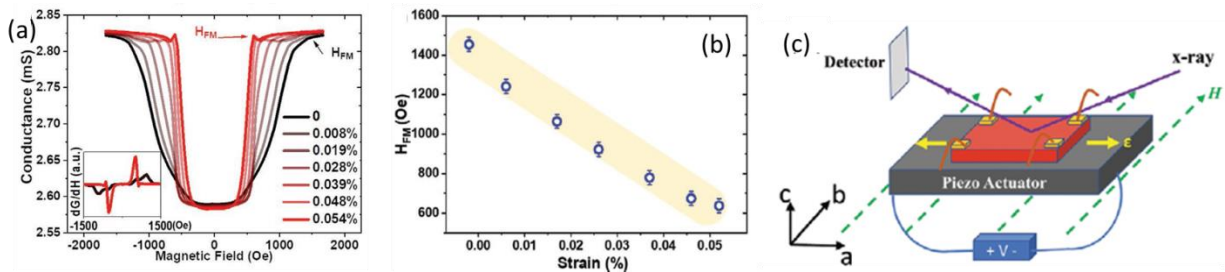


Figure 2 (a) MC under various anisotropic strains. (inset) first derivative of MC under 0.008% anisotropic strain. (b) Shift of the transition field H_{TM} as a function of in situ strain. (c) Schematic setup of the measurement.

Giant metamagnetic response of pseudospin-half electrons controlled by in-situ strain. The unusual electronic sensitivity of pseudospin-half electrons of the Ir^{4+} state to magnetic modulation could also lie in their wave function that fully preserves the spin-orbit-entanglement

of the atomic limit in a solid state environment [5]. Recently we achieve control of the entanglement by applying *in situ* strain to Sr_2IrO_4 , which is one of the most important representatives of correlated pseudospin-half electrons. Specifically, we found that an *in situ* strain of only 0.05% delivered by a piezo-actuator is able to shift the metamagnetic transition field of by almost 300% (Fig.2a&b), enabling electrical switch and electronic detection of the transition. Moreover, we performed a simultaneous measurement of conductance and magnetic scattering under concurrent controls of *in situ* strain, magnetic field, and temperature (Fig.2c). The results reveal that such a giant response is not a simple shift of the transition but a complete tuning of the transition between the spin-flip and spin-flop limits due to the so-called pseudo-Jahn-Teller effect, where modulation of the spin-orbital-entanglement is coupled to the lattice and affords a remarkably efficient magnetoelastic control. This complete control also allows us to establish the strain-magnetic field phase diagram of this system.

Anomalous magnetoresistance of frustration-driven skyrmion crystal. A new emerging field of quantum magnets centered on realization of skyrmion lattice without breaking inversion symmetry (Fig.3a) has risen recently [6]. Conventional skyrmion crystals are necessarily non-centrosymmetric because twisting the neighboring spins requires Dzyaloshinskii-Moriya interactions (DMI) to compete with Heisenberg interactions. Centrosymmetric Skyrmion crystals thus must have fundamentally different origin. The formation of charge carrier-mediated skyrmion lattice could in turn induce novel electronic behaviors, such as giant topological Hall effect. We have leveraged with our strong capabilities of materials synthesis to successfully grow single crystals of Gd_2PdSi_3 . This allows us to identify transport signatures of the underlying spin fluctuations and found that the longitudinal resistivity exhibits a rich anomalous behavior within the complex temperature-magnetic field phase diagram (Fig.3b). In particular, we observe magnetic field drastically changes the resistivity minimum from U-shape to V-shape right above the Néel temperature (Fig.3c). Our results reveal that such MR response is due to strong FM fluctuations hidden above the Néel temperature (Fig.3d), indicative of competing magnetic interactions presumably due to the frustration.

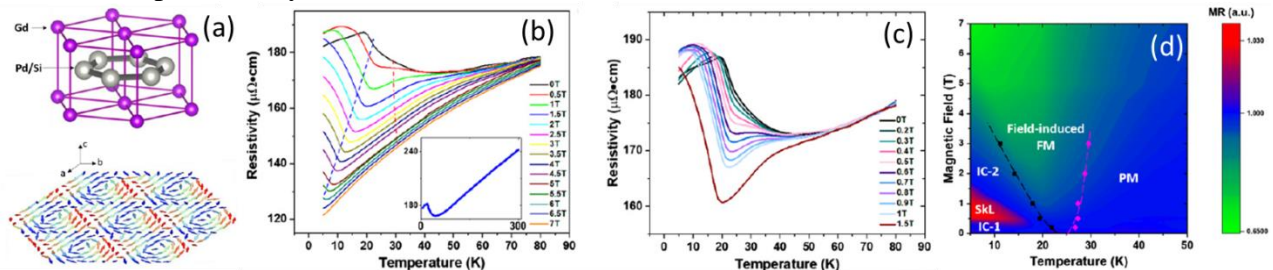


Figure 3 (a) Crystal structure of Gd_2PdSi_3 is shown on the top with the skyrmion lattice formed on the Gd atom sites at the bottom. (b) Resistivity of Gd_2PdSi_3 measured between 5 K and 80 K under external magnetic field between 0 T and 7 T, inset shows the resistivity between 5 K and 300 K under ambient magnetic field; The blue and red dashed lines shows the evolution of minimum/maximum of its 1st derivative curve with increasing magnetic field. (c) Resistivity under external magnetic field between 0 T and 1.5 T. (d) H-T phase diagram acquired from MR curves.

Other collaborative work. We actively collaborate with other PIs within the ECMP program and other DOE programs, mainly by providing high quality single crystals, performing low temperature and high field measurements, and conceiving scientific ideas. The collaboration resulted 9 publications (see publication list), including 1 Nature Physics, 3 Physical Review Letters.

Future Plans

Our work on the correlated metal/spin ice heterostructures has demonstrated the feasibility of a new interface method by depositing correlated metal ultrathin films on GFQM single crystals. This approach preserves the exotic spin state in GFQMs and enables anomalous transport behavior of the correlated charge carriers when magnetic field and temperature are varied. While this opens up many new opportunities, we plan to pursue several areas that are complementary in extending this method further. (i) We will investigate heterostructures where DTO is also grown as an epitaxial film and subject to epitaxial strain. Strain engineering has been widely used to tune properties of quantum materials and understand the underlying physics. Measuring ultrathin insulating GFQMs has however been challenging. We will take the BIO/DTO heterostructure as a representative system to turn the interface approach around for detecting any significant change DTO exhibits in a strained thin film form. (ii) We will investigate heterostructures, where the classical spin of the Dy ion in $\text{Dy}_2\text{Ti}_2\text{O}_7$ is replaced by quantum spin, such as that of Yb and Tb ions. The enhanced quantum fluctuations are known to drastically modify the ground state to quantum spin ice or quantum spin liquid. Such a state is also often subject to field-induced spin state transition and/or competing states of long-range order. We will look for corresponding transport signatures in the $\text{Bi}_2\text{Ir}_2\text{O}_7$ films. (iii) We will extend the method to GFQMs where the magnon excitation has nontrivial topology or Berry phases. This will allow us to investigate whether the charge carriers on the other side of the interface is sensitive to the Berry phase of the spin excitations. We will perform transport measurements, particularly measurement of the transverse channel, to resolve the interplay between Berry-phase-carrying spin fluctuations and Berry-phase-carrying correlated electrons. (iv) We will search for epitaxy-compatible honeycomb quantum magnets, which is also an important class of GFQMs. This will allow us to extend the interface method in the future to other lattice geometries. For instance, single crystals of $\text{Ba}_2\text{Co}(\text{PO}_4)_2$ and $\text{Ba}_8\text{Co}_{4/3}\text{Ta}_{5.8}\text{O}_{24}$ both host Co^{2+} -honeycomb lattice, as new candidates of the Kitaev model. We will establish magnetic properties of such systems by using complimentary low temperature and high field measurements, including AC, DC magnetic susceptibility, magnetic torque, specific heat, and thermal conductivity, and neutron scattering.

References

1. Gardner, J. S., Gingras, M. J. P. & Greedan, J. E. *Rev. Mod. Phys.* **82**, 53-107 (2010).
2. Bramwell, S. T. *Science* **294**, 1495-1501 (2001).
3. Tabata, Y., Kadowaki, H., Matsuhira, K., Hiroi, Z., Aso, N., Ressouche, E. & Fak, B. *Phys. Rev. Lett.* **97**, 257205 (2006).
4. Sakakibara, T., Tayama, T., Hiroi, Z., Matsuhira, K. & Takagi, S. *Phys. Rev. Lett.* **90**, 207205 (2003).
5. Kim, B. J., Jin, H., Moon, S. J., Kim, J. Y., Park, B. G., Leem, C. S., Yu, J., Noh, T. W., Kim, C., Oh, S. J., Park, J. H., Durairaj, V., Cao, G. & Rotenberg, E. *Phys. Rev. Lett.* **101**, 076402 (2008).
6. Kurumaji, T., Nakajima, T., Hirschberger, M., Kikkawa, A., Yamasaki, Y., Sagayama, H., Nakao, H., Taguchi, Y., Arima, T. hisa & Tokura, Y. *Science* **365**, 914-918 (2019).

Publications

- (1) H. Zhang, K. Noordhoek, C. K. Xing, Q. Huang, L. Hao, J. Yang, S. Pandey, T. H. Zhao, E. Dagotto, Z. G. Jiang, E. S. Choi, H. D. Zhou and J. Liu, *Anomalous Magnetoresistance by Breaking Ice Rule in $\text{Bi}_2\text{Ir}_2\text{O}_7/\text{Dy}_2\text{Ti}_2\text{O}_7$ Heterostructure*, arXiv:2011.09048.
- (2) H. Zhang, L. Hao, J. Yang, J. Mutch, Z. Liu, Q. Huang, K. Noordhoek, Andrew F. May, J. Chu, J. Kim, Philio J. Ryan, H. D. Zhou, and J. Liu, *Comprehensive electric control of metamagnetic transition of a quasi-2D antiferromagnet by in situ anisotropic strain*, *Advanced Materials* 2002451 (2020).
- (3) H. Zhang, Q. Huang, L. Hao, J. Yang, K. Noordhoek, S. Pandey, H. D. Zhou, and J. Liu, *Anomalous magnetoresistance in centrosymmetric skyrmion-lattice magnet Gd_2PdSi_3* , *New Journal of Physics* **22**, 083056 (2020).
- (4) Xiaojian Bai, Shang-Shun Zhang, Zhiling Dun, Hao Zhang, Qing Huang, Haidong Zhou, Matthew B. Stone, Alexander I. Kolesnikov, Feng Ye, Cristian D. Batista², Martin Mourigal, *Hybridized quadrupolar excitations in the spin-anisotropic frustrated magnet FeI_2* , *Nature Physics* **17**, 467 (2021).
- (5) Y. Jiang, J. Wang, T. Zhao, Z. L. Dun, Q. Huang, X. S. Wu, M. Mourigal, H. D. Zhou, W. Pan, M. Ozerov, D. Smirnov, and Z. Jiang, *Unraveling the topological phase of ZrTe_5 via magneto-infrared spectroscopy*, *Physical Review Letters* **125**, 046403 (2020).
- (6) R. J. Koch, R. Sinclair, M. T. McDonnell, R. Yu, M. Abeykoon, M. G. Tucker, A. M. Tsvetik, S. J. L. Billinge, H. D. Zhou, W. G. Yin, and E. S. Bozin, *Dual orbital degeneracy lifting in a strongly correlated electron system*, *Physical Review Letters* **126**, 186402 (2021).
- (7) X. Hu, Daniel M. Pajerowski, D. Zhang, Andrey A. Podlesnyak, Y. Qiu, Q. Huang, H. D. Zhou, I. Klich, Alexander I. Kolesnikov, Matthew B. Stone, and S. H. Lee, *Freezing of a disorder induced spin liquid with strong quantum fluctuations*, *Physical Review Letters* **127**, 017201 (2021).
- (8) L. Ding, M. Lee, E. S. Choi, J. Zhang, Y. Wu, R. Sinclair, Bryan C. Chakoumakos, Y. Chai, H. D. Zhou, and H. Cao, *Large spin-driven dielectric response and magnetoelectric coupling in the buckled honeycomb $\text{Fe}_4\text{Nb}_2\text{O}_9$* , *Physical Review Materials* **4**, 084403 (2020).
- (9) C. Kinsler-Fedon, Q. Zhang, Q. Huang, E. S. Choi, J. Q. Yan, H. D. Zhou, D. Mandrus, and V. Keppens, *Synthesis, characterization, and single crystal growth of a high entropy rare earth pyrochlore oxide*, *Physical Review Materials* **4**, 104411 (2020).
- (10) Lei Ding, Minseong Lee, Tao Hong, Zhiling Dun, Ryan Sinclair, Songxue Chi, Harish K. Agrawal, Eun Sang Choi, Bryan C. Chakoumakos, Haidong Zhou, and Huibo Cao, *Noncollinear magnetic structure and magnetoelectric coupling in buckled honeycomb $\text{Co}_4\text{Nb}_2\text{O}_9$: A single crystal neutron diffraction study*, *Physical Review B* **102**, 174443 (2020).

(11) T. Basu, T. Zou, Z. Dun, C. Q. Xu, C.R. Dela Cruz, Tao Hong, H.B. Cao, K.M. Taddei, H.D. Zhou, and X. Ke, *Magnetic Field Induced Phase Transition in Spinel $GeNi_2O_4$* , Physical Review B **102**, 134421 (2020).

(12) Zhiling Dun, Xiaojian Bai, Matthew B. Stone, Haidong Zhou, and Martin Mourigal, *Effective point-charge fit to crystal electric field— application to rare earth pyrochlores, and tripod kagome magnets $R_3Mg_2Sb_3O_{14}$* , Physical Review Research **3**, 023012 (2021).

Massive electron correlations in planar trilayer nickelate $\text{Pr}_4\text{Ni}_3\text{O}_8$

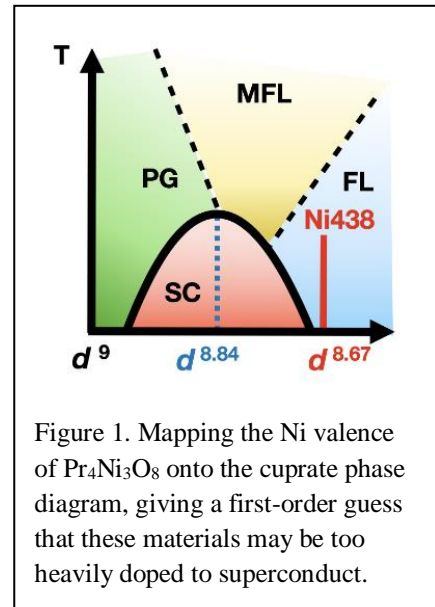
PI: Dan Dessau, University of Colorado, Boulder

Program Scope

This program focusses on high resolution ARPES studies of a variety of correlated electron systems, particularly superconductors or “failed” superconductors. The goal of the studies is to elucidate the electronic structure and the electronic interactions that give rise to the unusual behavior of these novel materials.

Recent Progress

The recent discovery of superconductivity in the “infinite layer” hole-doped square planar nickelates $\text{R}_{1-x}\text{SrNiO}_2$ ($\text{R}=\text{Pr},\text{Nd}$) raises the key questions of the similarities and differences in the electronic structure and interactions between the superconducting nickelates and cuprates, in the hopes of learning the driving forces behind the superconductivity in both classes of materials. ARPES is the most direct method to experimentally probe the k -dependent electronic structure and electronic interactions, though it is not yet been successfully demonstrated in $\text{R}_{1-x}\text{SrNiO}_2$ due to surface and cleavage issues. Instead, we study the closely-related planar trilayer nickelate $\text{Pr}_4\text{Ni}_3\text{O}_8$, which has been produced in cleavable single crystals by the Mitchell group from Argonne. Charge counting using a standard ionic model indicates that the nickel in this compound should be in a $d^{8.67}$ state, or 0.33 holes per transition-metal away from the d^9 half-filled state that is generally considered the “parent” of cuprate superconductors and presumably also the nickelate superconductors. Mapping to the doping phase diagram of the cuprates this would be very heavily hole-doped – with this potentially being the reason that this particular compound is not superconducting since it is past the superconducting dome of the cuprates (fig 1). This is one of many aspects that we can study with ARPES.



Since there are three nickel planes per unit cell, these materials have three Fermi surfaces. Our results indicate that two of the three Fermi surfaces are extremely similar to the typical Fermi surfaces observed in “properly doped” cuprates, with the third nickelate Fermi surface somewhat different from that in the cuprates and harboring the “excess” number of hole carriers (Fig 2). We thus show that based upon Fermi surface shape and topology, at least two of the three Fermi surfaces should be able to support the superconductivity.

By comparing the measured dispersion to that calculated by DFT, we can extract the electronic mass enhancements due to electronic correlations. We find this to be of order 4 for all the bands, which is about twice that observed in cuprates (Fig 3a). We nominally expect this enhancement to track across all related nickelates, including the infinite layered nickelates that exhibit superconductivity. Additionally, by studying the peak widths as a function of energy, we uncover scattering rates (imaginary self-energy) in the nickelates that linearly increase with energy (Fig 3b), similar to the linear scattering rates that have long been considered to be a key ingredient of the novel physics of those compounds. Similar to the twice-as-strong mass enhancement of the nickelates, the scattering rate growth in the nickelates is twice-as-fast as that in the cuprates.

Future Plans

Our discovery reveals a distinct strongly correlated nature of the planar trilayer nickelates that offers a new perspective on the strange metal physics and may provide clues that can help bridge the knowledge gap between the well-studied cuprates and the recently discovered nickelate superconductors. We hope to delve deeper into these similarities and differences in these and related materials.

Publication

Haoxiang Li, Peipei Hao, Junjie Zhang, Kyle Gordon, A. Garrison Linn, Hong Zheng, Xiaoqing Zhou, J.F. Mitchell, D. S. Dessau “Massive electron correlations in planar trilayer nickelate $\text{Pr}_4\text{Ni}_3\text{O}_8$ ” (under review)

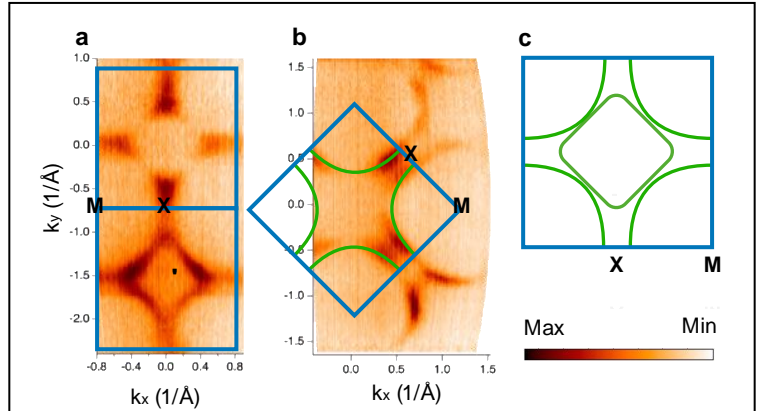


Figure 2. (a,b) Experimental Fermi surface of $\text{Pr}_4\text{Ni}_3\text{O}_8$ in two different geometries to highlight different portions of Fermi surface. (c) Combined Fermi surface of $\text{Pr}_4\text{Ni}_3\text{O}_8$ showing two hole-like pieces of Fermi surface that are in general very similar to that of cuprates, plus one smaller piece centered at Γ that is much more heavily hole doped (or lightly electron doped).

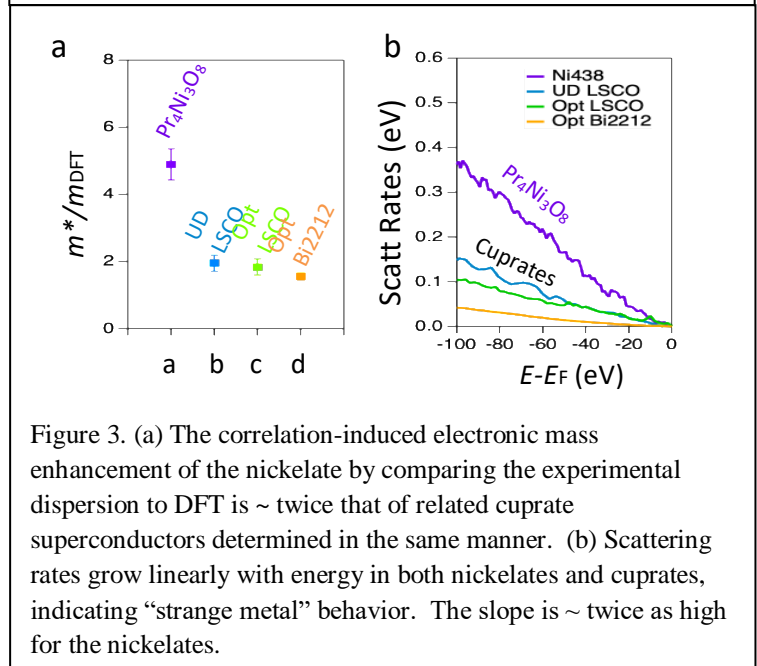


Figure 3. (a) The correlation-induced electronic mass enhancement of the nickelate by comparing the experimental dispersion to DFT is \sim twice that of related cuprate superconductors determined in the same manner. (b) Scattering rates grow linearly with energy in both nickelates and cuprates, indicating “strange metal” behavior. The slope is \sim twice as high for the nickelates.

Frustration as a tuning parameter for quantum criticality

Topological non-collinear spin texture in the square-net centrosymmetric EuGa_2Al_2

Emilia Morosan, Rice University

Program Scope

Since its discovery, normal Hall resistivity has been used to characterize the mobility and carrier concentration of metals. However, modern condensed matter physics has recognized additional contributions, such as the anomalous and topological Hall effects (AHE, THE), attributed to non-zero Berry phase accumulated when a charged carrier traverses a closed path in a material. In the former, the Berry phase arises as the integral of the Berry curvature, which can be regarded as an “effective” magnetic field in reciprocal space, and depends solely on the band structure of the material. In the latter, the Berry phase accumulation happens in real space and is generated by non-coplanar spin textures.

Our work on the square net centrosymmetric EuM_4 [1] ($M = \text{Ga}, \text{Al}$ or $\text{Ga}_{1-x}\text{Al}_x$) has revealed remarkable spin-charge entanglement, manifest in the presence of a charge density wave (CDW) in the pure Al compound as well as the ordered EuAl_2Ga_2 intermediate composition. The antiferromagnetic ground state consisted of several magnetic states, resulting in a complex H – T phase diagram for both these compounds. By contrast, the CDW was absent in the pure EuGa_4 compound at ambient pressure, where the ground state was characterized by a collinear antiferromagnetic ordered state. Therefore, a correlation appears between the spin-charge entanglement and the complex magnetism, reminiscent of some topological non-collinear spin textures (including skyrmions) in another isostructural centrosymmetric material, GdRu_2Si_2 [2].

We use detailed Hall measurements, xray and neutron diffraction on the centrosymmetric Eu based compound EuGa_2Al_2 [3], and compare with similar data on EuGa_4 and EuAl_4 . The EuGa_2Al_2 topological Hall effect (THE) reveals non-coplanar spin textures in several of the magnetic phases with a skyrmion state likely stabilized in an intermediate field phase (phase A). Furthermore, a large temperature-dependent anomalous Hall (AH) contribution is also identified, suggesting a large Berry phase accumulation, possibly explained by field-induced Weyl nodes or a CDW. While the former has been suggested in other materials, the latter is a possible new mechanism which could be used as a design principle for non-collinear topological spin states, including skyrmions, in centrosymmetric materials. A skyrmion state has also been confirmed in EuAl_4 [4], where an out-of-plane (OOP) CDW precedes the magnetic order, similar to that in EuGa_2Al_2 . Taken together with the lack of CDW, and only a simple collinear antiferromagnetic order in EuGa_4 , the picture across the Al-Ga series in this centrosymmetric class of compounds lends credence to the CDW mechanism for stabilizing a skyrmion state in particular, or, more generally, non-collinear topological spin textures.

Recent Progress

Following the discovery of complex magnetic order in EuGa_2Al_2 [1], we recently revisited the $H - T$ phase diagram [3]. A new, intermediate phase (A) was identified around 1.5 T and below ~ 7 K (Fig. 1). Zero-field neutron scattering measurements determined the magnetic structure in the AFM1 and AFM3 phases to be helical and cycloidal, respectively, both with propagation vector along a . Such non-collinear spin textures are auspicious for the formation of skyrmion states, as was the case in the isostructural square net compound GdRu_2Si_2 [2]. In this Gd centrosymmetric compound, the spin-charge entanglement was deemed responsible for stabilizing the skyrmion spin configuration, as suggested by the large THE and non-collinear spin structures bordering the skyrmion state.

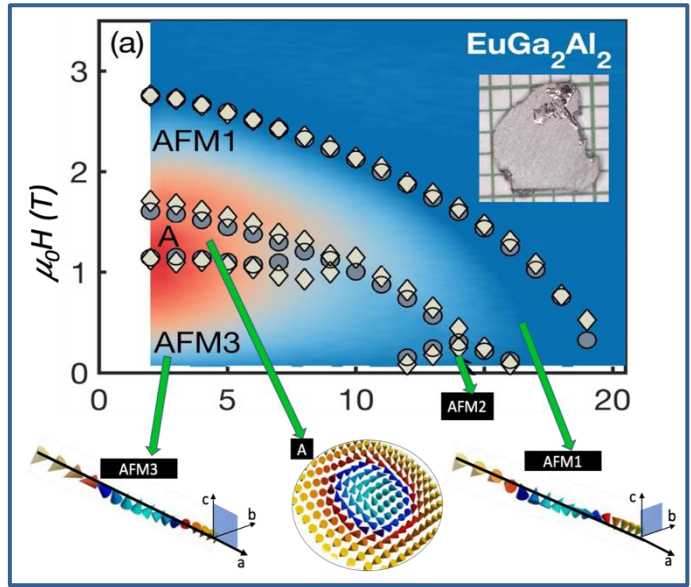


Figure 1. $H - T$ phase diagram for EuAl_2Ga_2 . Incommensurate helical spin state (AFM1) and cycloidal spin state (AFM3). Intermediate field phase A: non-coplanar spin state.

Similarly, in EuAl_2Ga_2 , Hall effect measurements reveal a large anomalous Hall contribution, and a THE which is maximized in the A phase. This indeed lends support to the skyrmion state scenario in the A phase of EuAl_2Ga_2 , a first example of a centrosymmetric compound without Gd where this spin texture is stabilized. Next, we turn to the origin of the skyrmion state in centrosymmetric square-net compounds, where the anisotropic Dzyaloshinskii-Moriya (DM) interaction (essential in non-centrosymmetric compounds) or geometric frustration (at play in triangular lattices) are both absent. Several mechanisms (based on competing multi-spin interactions) are proposed, but with no consensus on the exact path to stabilizing a skyrmion state. While the similarities between EuAl_2Ga_2 and GdRu_2Si_2 suggest like underlying mechanisms in both compounds, a further comparison, this time across the isostructural series EuGa_4 - EuAl_4 , reveals a potential novel pathway toward the observed skyrmion state in the former. The magnetic phase in EuAl_4 consists of several incommensurate states, with a confirmed skyrmion state in applied field where large THE is observed. Also, a high temperature OOP CDW precedes the magnetic order. By contrast, the magnetic ground state of EuGa_4 is a single wavevector collinear antiferromagnetic state, with no CDW at ambient pressure. The OOP CDW with $T_{\text{CDW}} > T_{\text{N}}$ (*preformed* CDW) is also present in EuAl_2Ga_2 . We propose that the preformed CDW in the Eu series produces band folding at the CDW transition that reduces the Fermi surface dimensionality. We surmise that, in turn, the low dimensional Fermi surface enhances the competition between the multi-spin energy scales (RKKY, biquadratic, compass anisotropy) and interorbital frustration in

Eu^{2+} ($4f^7$, $L = 0$) that stabilizes the skyrmion state only when the preformed CDW is present (in EuAl_4 and EuAl_2Ga_2 , but not in EuGa_4).

The preformed OOP CDW may be a new mechanism for stabilizing non-coplanar topological spin textures, in general, and magnetic skyrmions, in particular, in centrosymmetric square-net compounds.

Future Plans

We will cement the findings from the Eu-based centrosymmetric compounds by targeting multi-wavevector topological spin structures in four-fold centrosymmetric square lattice systems. The high symmetry maximizes the chance for multi-wavevector order *via* the biquadratic interaction, while the inversion center lends itself to smaller size skyrmions when compared to their non-centrosymmetric counterparts. We will tune the anisotropy and therefore the type of topological spin texture, by substituting various rare earth (*R*) elements onto the square lattice. Magnetic ions with orbital angular momentum quantum number $L = 0$ like Gd^{3+} and Eu^{2+} are expected to have low anisotropy, while Nd^{3+} , Ho^{3+} , and Er^{3+} are expected to be the most anisotropic with typically the largest value of L among the lanthanides. Intermediate anisotropy is expected in $R = \text{Pr}^{3+}$, Tb^{3+} , Tm^{3+} . This will also allow us to understand if there is a preference for skyrmion formation in easy-axis *vs* easy plane anisotropies.

Beyond the CDW centrosymmetric compounds, we will explore concurrent *real*- and *reciprocal*-space topology in Weyl semimetals, where large SOC is expected to promote spin torque transfer. This can facilitate energy-efficient manipulation of the topological spin textures. We will focus on polar square net classes of compounds which are theoretically predicted to host Weyl fermions. Both the centrosymmetric lattices and the Weyl semimetal compounds favor small skyrmion size, and thus are highly sought-after as high density non-coplanar topological spin states.

References

1. Macy Stavinoha, Joya A. Cooley, Stefan G. Minasian, Tyrel M. McQueen, Susan M. Kauzlarich, C.-L. Huang, **E. Morosan**, "Charge density wave behavior and order-disorder in the antiferromagnetic metallic series $\text{Eu}(\text{Ga}_{1-x}\text{Al}_x)_4$ " *Phys. Rev. B* **97**, 195146 (2018)
2. Y. Yasui, C. J. Butler, N. D. Khanh, S. Hayami, T. Nomoto, T. Hanaguri, Y. Motome, R. Arita, T.-h. Arima, Y. Tokura, et al., Nature communications **11**, 1 (2020)
3. Jaime M. Moya, Shiming Lei, Eleanor M. Clements, Kevin Allen, Qizhi Li, Y.Y. Peng, Matthew James Krogstad, Raymond Osborn, Douglas S. Robinson, Stella Sun, P. Abbamonte, Songxue Chi, Anand B. Puthirath, Jeffrey W. Lynn, and E. Morosan, Physical Review Letters (submitted)
4. S. Shimomura, H. Murao, S. Tsutsui, H. Nakao, A. Naka-mura, M. Hedo, T. Nakama, and Y. Onuki, Journal of the Physical Society of Japan **88**, 014602 (2019).

Publications

1. Long Qian, Shiming Lei, C.-L.Huang, Binod K., C.-L.Huang, E.Morosan, "Unconventional magnetic order emerging from competing energy scales in the new RRh_3Si_7 intermetallics (R = Gd-Yb)" *Physical Review Materials* (accepted)
2. Peng-Ling Dai, Gaoning Zhang, Yaofeng Xie, Chunruo Duan, Yonghao Gao, Zihao Zhu, Erxi Feng, Zhen Tao, Chien-Lung Huang, Huibo Cao, Andrey Podlesnyak, Garrett E. Granroth, David Voneshen, Shun Wang, Guotai Tan, Emilia Morosan, Xia Wang, Hai-Qing Lin, Lei Shu, Gang Chen, Yanfeng Guo, Xingye Lu, Pengcheng Dai, "Spinon Fermi surface spin liquid in a triangular lattice antiferromagnet NaYbSe_2 ", *Phys. Rev. X* **11**, 021044 (2021)
3. Han Wu, Alannah M. Hallas, Xiaochan Cai, Jianwei Huang, Ji Seop Oh, Vaideesh Loganathan, Ashley Weiland, Gregory T. McCandless, Julia Y. Chan, Sung-Kwan Mo, Donghui Lu, Makoto Hashimoto, Jonathan Denlinger, Robert J. Birgeneau, Andriy H. Nevidomskyy, Gang Li, Emilia Morosan, and Ming Yi, "Nonsymmorphic Symmetry-Protected Band Crossings in the Correlated Metal PtPb_4 " *npjQuantum Materials* (in review)
4. Y. Sato, S. Suetsugu, T. Tominaga, Y. Kasahara, S. Kasahara, T. Kobayashi, S. Kitagawa, K. Ishida, R. Peters, T. Shibauchi, A.H. Nevidomskyy, L. Qian, J. M. Moya, E. Morosan, and Y. Matsuda, "Charge neutral fermions and magnetic field driven instability in insulating YbIr_3Si_7 " *npjQuantum Materials* (in review)
5. Macy Stavinoha, C.-L. Huang, W. Adam Phelan, Alannah M. Hallas, V. Loganathan, Jeffrey W. Lynn, Qingzhen Huang, Franziska Weickert, Vivien Zapf, Katharine R. Larsen, Patricia D. Sparks, James C. Eckert, C. Hooley, Andriy H. Nevidomskyy, and E. Morosan, "Kondo exhaustion and conductive surface states in antiferromagnetic YbIr_3Si_7 " *Nature Commun.* (under review)
6. Bin Gao, Tong Chen, David W. Tam, Chien-Lung Huang, Kalyan Sasmal, Devashibhai T. Adroja, Feng Ye, Huibo Cao, Gabriele Sala, Matthew B. Stone, Christopher Baines, Joel A. T. Verezhak, Haoyu Hu, Jae-Ho Chung, Xianghan Xu, Sang-Wook Cheong, Manivannan Nallaiyan, Stefano Spagna, M. Brian Maple, Andriy H. Nevidomskyy, Emilia Morosan, Gang Chen and Pengcheng Dai, "Experimental signatures of a three-dimensional quantum spin liquid in effective spin-1/2 $\text{Ce}_2\text{Zr}_2\text{O}_7$ pyrochlore" *Nature Physics* **15**, 1052 (2019)

Session IV

APS CUWiP: Supporting the Success of All Undergraduate Women in Physics
Award: DE-SC0011076

Monica Plisch, American Physical Society (Principal Investigator)
Renee Michelle Goertzen, American Physical Society (Co-Investigator)

Only about 20% of undergraduate physics degrees are earned by women. Increasing the participation of women in physics is critical to addressing U.S. workforce needs in STEM. The Conferences for Undergraduate Women in Physics (CUWiP) are a collaborative effort of physicists from around the country who organize simultaneous regional conferences with support from the American Physical Society (APS). The total number of participants has increased to almost 2,000 in recent years. By comparison, nearly 2,000 women graduate with a bachelor's degree in physics each year in the U.S. The conferences provide an opportunity for women to hear inspirational talks by female physicists; participate in workshops and panel discussions on summer research, graduate school, and physics careers; learn about issues facing women and strategies to help them thrive; and develop networks and informal mentoring relationships. Evaluation results show that participants left the conferences with a heightened sense of community, elevated views of themselves as physicists, and increased feelings of being valued and respected in the physics community. All of these findings are linked to increased persistence in physics.

Ultrasonic Determination of Electron Viscosity and Hydrodynamics in Metals

Brad Ramshaw, Cornell University

Program Scope

The goal is to understand electron-electron interactions in correlated metals using ultrasonic techniques. This project was motivated by several recent claims of “electron hydrodynamics”, where the electron system in a metal interacts more strongly with itself than with impurities, leading to flow that is described by fluid dynamics rather than Boltzmann transport¹. There are two main difficulties in understanding these experiments: 1) the electron viscosities extracted from the experiments don’t match simple order-of-magnitude estimates; 2) the experiments rely on boundary conditions that are ill-defined.

Sound attenuation in a metal is dominated by electron viscosity at low temperature and this viscosity can be extracted in a model-independent way in certain ultrasonic frequency regimes. To reach this regime we require better ultrasonic techniques, including higher operating frequencies and better transducers. The ultimate goal is to measure the electron viscosity in a so-called “strange metal”, probing a conjectured quantum “bound” on viscosity². Along the way we will use ultrasound to explore other phenomena, particularly multi-component superconductivity.

Recent Progress

Our initial work focused on building a resonant ultrasound spectroscopy (RUS) apparatus that was capable of measuring sound velocity and sound attenuation down to very low temperatures (where electron viscosity dominates the attenuation.) Our ‘test’ material was the unconventional superconductor Sr_2RuO_4 , which we knew had very high electron viscosity and long elastic mean-free-paths at low temperature. We managed to overcome several technical challenges and build an RUS apparatus capable of cooling a crystal very slowly down to 1.2 K with minimal external vibration.

Upon measuring the elastic moduli and sound attenuation of Sr_2RuO_4 to low temperature, we made a remarkable discovery: one of the shear elastic moduli (c_{66}) shows a sharp discontinuity at the

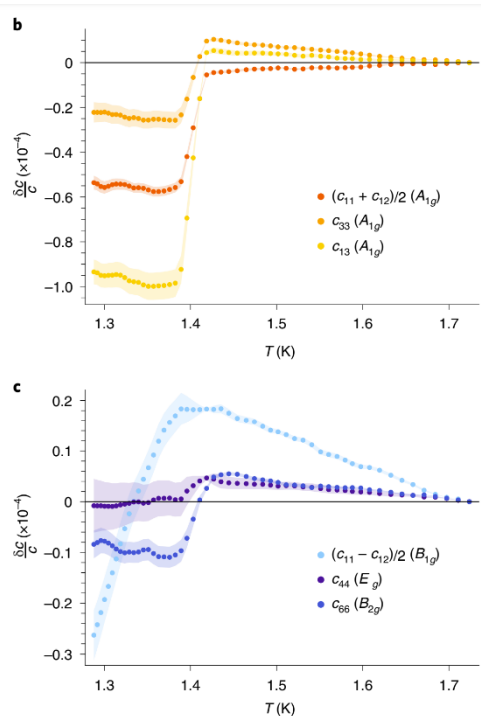


Fig. 1. Elastic moduli of Sr_2RuO_4 through the superconducting transition. Panel (b) shows the compressional moduli, which behave as expected. Panel (c) shows the shear moduli—the discontinuity in c_{66} is only possible if the superconducting order parameter has two components.

superconducting phase transition ($T_c = 1.5$ K, see Fig. 1.) This is only possible if the superconducting order parameter is of the unusual “two-component” variety, meaning it is described by 2 complex numbers rather than the usual 1. Sr_2RuO_4 was once thought to be a two-component p -wave superconductor but recent NMR experiments have shown that must have spin-singlet pairing³ (i.e. s or d -wave.) Still, there are many experiments that were thought to be understandable *only* in the context of a two-component order parameter. Our result⁴ combined with the NMR result demonstrates that Sr_2RuO_4 must be either a $d_{xz}+id_{yz}$ or a $d_{x^2-y^2}+ig_{xy(x^2-y^2)}$ superconductor: both new superconducting states that have never been seen before⁵.

Future Plans

The newly discovered superconductor UTe_2 is also thought to have two-component order parameter and there should be a very specific signature in one of the elastic moduli if this is true. Our preliminary data (Fig. 2) has found two superconducting phase transitions (expected for this crystal symmetry if there are two components to the order parameter), and our ongoing analysis should demonstrate whether these transitions are truly the result of a two-component order parameter.

Returning to the topic of electron viscosity, we have made a second discovery in Sr_2RuO_4 : the compressional viscosity increases by a factor of 7 in the superconducting state⁶. This is an unprecedented discovery in a superconductor, and strongly suggest the presence of domains in the superconducting state. Domains require a two-component superconducting order parameter, and the fact that only the compressional (and not shear) viscosity increases suggests an accidental two-component order parameter such as $d_{x^2-y^2}+ig_{xy(x^2-y^2)}$.

With our much-improved low-temperature ultrasound apparatus we are now looking into the viscosity of antimony—a fermi liquid with incredibly long mean free paths. We should be able to extract the viscosity and demonstrate the frequency-crossover regime before moving on to strange metals.

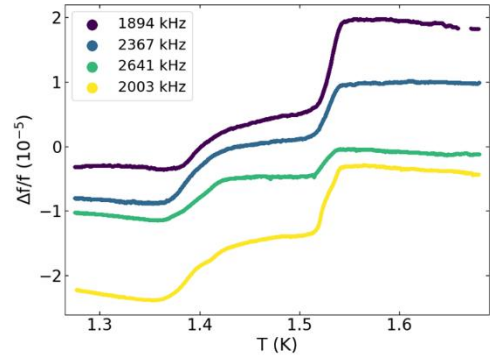


Fig. 2. Two superconducting phase transitions in UTe_2 .

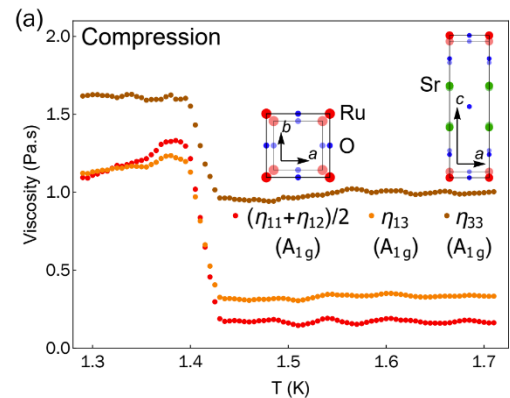


Fig 3. Compressional viscosity of $\text{Sr}_2\text{-RuO}_4$ through T_c .

References

1. Moll, P. J. W., Kushwaha, P., Nandi, N., Schmidt, B. & Mackenzie, A. P. Evidence for hydrodynamic electron flow in PdCoO₂. *Science* (80-.). **351**, 1061–1064 (2016).
2. Hartnoll, S. A. Theory of universal incoherent metallic transport. *Nat. Phys.* **11**, 54–61 (2015).
3. Pustogow, A. *et al.* Constraints on the superconducting order parameter in Sr₂RuO₄ from oxygen-17 nuclear magnetic resonance. *Nature* **574**, 72–75 (2019).
4. Ghosh, S. *et al.* Thermodynamic evidence for a two-component superconducting order parameter in Sr₂RuO₄. *Nat. Phys.* *2020 172* **17**, 199–204 (2020).
5. Kivelson, S. A., Yuan, A. C., Ramshaw, B. & Thomale, R. A proposal for reconciling diverse experiments on the superconducting state in Sr₂RuO₄. *npj Quantum Mater.* **5**, 43 (2020).
6. Ghosh, S. *et al.* Strong Increase in Ultrasound Attenuation Below T_c in Sr₂RuO₄: Possible Evidence for Domains. arXiv:2109.00041 (2021).

Publications

Ghosh, S. *et al.* Thermodynamic evidence for a two-component superconducting order parameter in Sr₂RuO₄. *Nat. Phys.* *2020 172* **17**, 199–204 (2020).

Ghosh, S. *et al.* Strong Increase in Ultrasound Attenuation Below T_c in Sr₂RuO₄: Possible Evidence for Domains. arXiv:2109.00041 (2021).

Project Title: Topological Superconductivity in Strong Spin-Orbit Materials
Principal Investigator: Johnpierre Paglione
Institution: University of Maryland
Email address: paglione@umd.edu

Project Scope

Superconductors are among the most fascinating systems for realizing topological states, either via a proximity effect, or intrinsically via an odd-parity, time-reversal-invariant pairing state. Alongside the usual signature supercurrents arising from Cooper pair coherence, a direct analogy exists between superconductors and insulators: since the Bogoliubov-de Gennes (BdG) Hamiltonian for the quasiparticles of a superconductor is essentially analogous to that of a band insulator, one can consider the interesting possibility of TI surface states arising due to a superconducting “band gap”. Similar to TI systems, a topological superconductor (TSC) thus has a fully gapped bulk band structure and gapless surface Andreev bound states. Thus the search for TSCs in materials with strong band inversion is a promising direction. In the case of time-reversal-invariant (centrosymmetric) systems, a material is a TSC if it is an odd-parity, fully gapped superconductor and its Fermi surface encloses an odd number of time-reversal-invariant momenta in the Brillouin zone [1].

This program builds on prior work on a joint experimental and theoretical effort to focus on understanding the topological superconducting state of the non-centrosymmetric material YPtBi [2], and continues to investigate the superconducting state of this material as well as related compounds such as the RPdBi (R=rare earth) and RPtSb-based compounds that contain superconducting ground states. Previous work with R. Prozorov (Iowa State University and Ames National Lab) studied the temperature variation of the London penetration depth in single crystals of YPtBi, yielding a very interesting linear temperature dependence that is indicative of the presence of line nodes in the superconducting energy gap of YPtBi with moderate impurity scattering [3]. This work has led to a new understanding of the superconductivity in this system as arising from a spin-3/2 band structure, which is the first time such physics has been considered theoretically for a superconductor. As part of this effort, the actinide superconductor UTe₂ emerged as one of the most exciting new superconductors in recent times, following the discovery of spin-triplet pairing by S. Ran together with the PI and co-workers in this nearly ferromagnetic compound [4]. Our goal is to extend previous work on YPtBi [3] and the RPdBi series [5] to fine tune magnetism, SOC and pairing interactions, utilizing both in-house and external collaborative efforts, and, for UTe₂, take advantage of both our synthesis capabilities and collaborations to elucidate topological superconductivity in this exciting material.

Recent Progress

Beyond band inversion, strong SOC has significant consequences for other physical properties both in the normal and superconducting states. SOC in the XYZ compounds separates the *p*-orbital derived 6-fold degenerate valence band into 2-fold and 4-fold degenerate bands with the latter being higher in energy. In RPtBi (R=rare earth), SOC is big enough to push the 4-fold band above the *s*-orbital derived conduction bands, i.e., band inversion of Γ_6 and Γ_8 . This band structure is identical to the first experimentally identified topological materials HgTe. In our prototypical YPtBi, the chemical potential is located in the Γ_8 band which implies *p*-like Bloch electrons occupy the low energy quasiparticle states. With a lack of inversion symmetry causing a Rasha-type

splitting of the spin-degeneracy, YPtBi exhibits phenomenal behavior such as an apparent beating of Shubnikov-de Haas (SdH) quantum oscillations from two different spin species and exotic pairing as discussed below. Generally, strong SOC introduces an extra phase factor in the Bloch wavefunction as well as Landau levels. In YPtBi, extreme SOC manifests a phase quadrature to the periodic pseudopotential of lattice, which results in the total phase difference of π . This π -phase difference causes an abrupt disappearance of SdH effect when a magnetic field is applied along crystallographic [110] direction where two quantum oscillations with the same frequency and π -phase difference. This phenomena is extremely unusual, and should be manifest in a host of XYZ compounds of interest to this project.

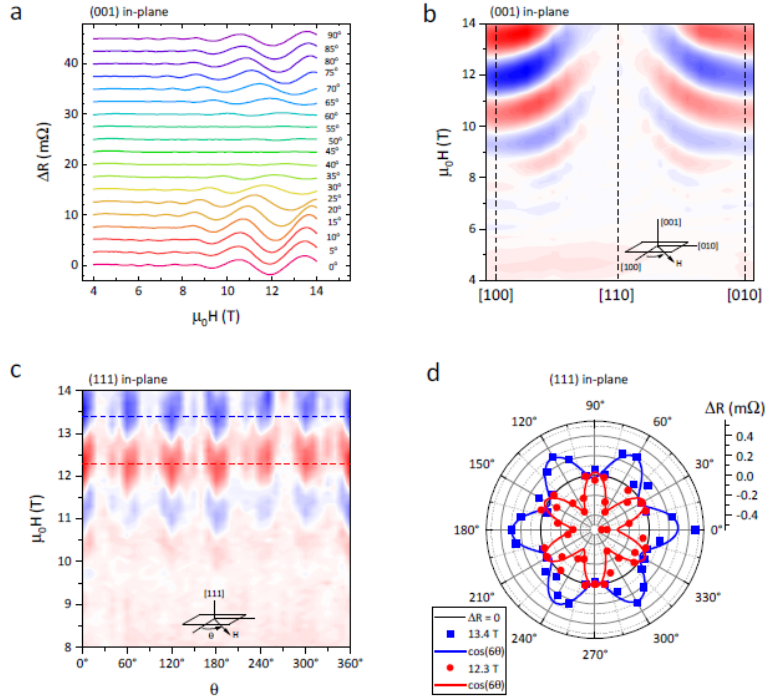


Figure 1: Angle-dependent Shubnikov-de Haas quantum oscillations at $T = 2$ K in YPtBi. (a) The oscillatory part of magnetoresistance ΔR with H rotating in the (100)-plane after subtracting smoothly varying background magnetoresistance. Contour plots of ΔR with magnetic fields rotating around [001] and [111] for (b) and (c), respectively. (d) A polar plot of ΔR shown in (c) at the fixed magnetic fields of 12.3 T and 13.4 T, shown in solid lines, which exhibit clear six-fold symmetry, and amplitude of quantum oscillation vanishes when a magnetic field is applied along the [110]-equivalent directions.

YPtBi is a perfect candidate for hosting high-spin superconductivity, and thus the understanding of its topological band structure is of utmost importance. We have recently investigated the spin-split $j = 3=2$ Fermi surface under influence of strong magnetic fields by comparing experimentally measured angle-dependent Shubnikov-de Haas (SdH) oscillations in YPtBi to a four-band $k.p$ theory in collaboration with J. Sau (UMD) examining the Zeeman gap and cyclotron orbits, providing the first direct verification of the $j = 3=2$ topological band structure of this system. To probe the $j = 3=2$ Fermi surface, we performed a complete study of SdH quantum oscillations (QOs) in YPtBi, an archtypical half-Heusler compound void of any localized magnetic moments. **Figure 1** shows magnetoresistance with SdH effect in the samples with various configurations at $T = 2$ K, which is the basis for our studying confirming the $j=3/2$ high-spin nature of electrons in this system [3].

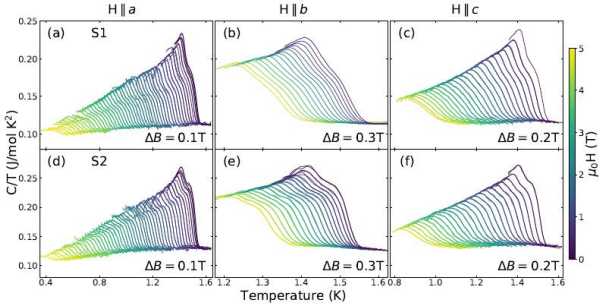


Figure 2: magnetic field evolution of the split superconducting transitions in UTe_2 [15].

the lack of magnetic order and the observation of quantum critical scaling place UTe_2 at the paramagnetic end of this ferromagnetic superconductor series. A large intrinsic zero-temperature reservoir of ungapped fermions indicates a highly unconventional type of superconducting pairing, which our thermodynamic experiments suggest forms a superconducting order parameter with a point node gap structure [7]. Most recently, together with Aharon Kapitulnik (Stanford) our team has also reported a time reversal-breaking Kerr effect (similar to that also observed in Sr_2RuO_4) and evidence of a multi-component p -wave order parameter consistent with this material hosting TSC, in particular topological Weyl superconductivity [8] with Weyl nodes in the superconducting order parameter. Together with observations of chiral edge states [9] and our report of a topological normal (Majorana) surface fluid [10], our observations suggest that UTe_2 may indeed be a realization of a chiral superconductor of the kind that has been proposed to form the basis for a topological quantum computer [11].

While all measured properties of UTe_2 point to an odd-parity, spin-triplet superconducting state, the recent measurement of time reversal symmetry breaking in our collaboration with Kapitulnik (Stanford) and Agterberg (UWM) was key to identifying a two-component order parameter [8]. However, it is highly striking that UTe_2 shows non-unitary superconductivity without the presence of inversion or time-reversal symmetry breaking in the normal state, as is the case for the other ferromagnetic U-based superconductors [12], pointing to ferromagnetically mediated pairing. To further constrain this picture, as well as definitively identify the nature of TSC in UTe_2 , it is necessary to perform more refined experiments probing the superconducting state. For example, recent follow-up work by Agterberg has suggested the location of Weyl nodes may not be fixed in high-symmetry directions, but can occur at arbitrary momenta on the Fermi surface for the two gap structures discussed above [13], calling for further refinement of the directional response of thermodynamic probes.

References

- [1] L. Fu et al., "Odd-Parity Topological Superconductors: Theory and Application to $\text{Cu}_x\text{Bi}_2\text{Se}_3$ ", *Phys. Rev. Lett.* **105**, 97001 (2010).
- [2] N. P. P. Butch et al., "Superconductivity in the topological semimetal YPtBi ", *Phys. Rev. B* **84**, 220504 (2011).
- [3] H. Kim et al., "Beyond triplet: Unconventional superconductivity in a spin-3/2 topological semimetal", *Sci. Adv.* **4**, eaao4513 (2018).
- [4] S. Ran et al., "Nearly ferromagnetic spin-triplet superconductivity", *Science* **365**, 684–687

We recently reported [4] the discovery of spin-triplet superconductivity in UTe_2 , featuring a transition temperature of 1.6 kelvin and a very large and anisotropic upper critical field exceeding 40 T and re-entrant superconducting phases at even higher fields [5]. This superconducting phase stability suggests that UTe_2 is related to ferromagnetic superconductors such as UGe_2 , URhGe , and UCoGe , but remains paramagnetic down to the lowest measured temperatures [6]. However,

- (2019).
- [5] Y. Nakajima et al., "Topological RPdBi half-Heusler semimetals: A new family of noncentrosymmetric magnetic superconductors", *Sci. Adv.* **1**, e1500242–e1500242 (2015).
 - [6] H. Kim et al., "Quantum Oscillations in a Spin-3/2 Topological Semimetal", *preprint*, arXiv:2010.12085 (2020).
 - [7] S. Ran et al., "Extreme magnetic field-boosted superconductivity", *Nat. Phys.* **15**, 1250–1254 (2019).
 - [8] S. Sundar et al., "Coexistence of ferromagnetic fluctuations and superconductivity in the actinide superconductor UTe₂", *Phys. Rev. B* **100**, 140502 (2019).
 - [9] T. Metz et al., "Point Node Gap Structure of Spin-Triplet Superconductor UTe₂", *Phys. Rev. B* **100**, 220504 (2019).
 - [10] I. M. Hayes et al., "Multicomponent superconducting order parameter in UTe₂", *Science* **373**, 797–801 (2021).
 - [11] L. Jiao et al., "Chiral superconductivity in heavy-fermion metal UTe₂", *Nature* **579**, 523–527 (2020).
 - [12] S. Bae et al., "Anomalous normal fluid response in a chiral superconductor UTe₂", *Nat. Commun.* **12**, 2644 (2021).
 - [13] S. Das Sarma et al., "Majorana zero modes and topological quantum computation", *npj Quantum Inf.* **1**, 15001 (2015).
 - [14] D. Aoki et al., "Review of U-based Ferromagnetic Superconductors: Comparison between UGe₂, URhGe, and UCoGe", *J. Phys. Soc. Japan* **88**, 022001 (2019).
 - [15] T. Shishidou et al., "Topological band and superconductivity in UTe₂", *Phys. Rev. B* **103**, 104504 (2021).

Publications

- I. M. Hayes, D.S. Wei, T. Metz, J. Zhang, Y.S. Eo, S. Ran, S.R. Saha, N.P. Butch, D.F. Agterberg, A. Kapitulnik, J. Paglione, "Multicomponent superconducting order parameter in UTe₂", *Science* **373**, 797–801 (2021).
- H. Kim, M.A. Tanatar, H. Hodovanets, K.F. Wang, J. Paglione, R. Prozorov, "Campbell penetration depth in low carrier density superconductor YPtBi", *Phys. Rev. B* **104**, 014510 (2021).
- S. Bae, H. Kim, S. Ran, Y.S. Eo, I-L. Liu, W. Fuhrman, J. Paglione, N.P. Butch, S. Anlage,, "Anomalous normal fluid response in a chiral superconductor UTe₂", *Nat. Commun.* **12**, 2644 (2021).
- I-L. Liu, C. Heikes, T. Yildirim, C. Eckberg, T. Metz, S. Ran, W. Ratcliff, J. Paglione, and N. P. Butch, "Quantum oscillations from networked topological interfaces in a Weyl semimetal," *npj Quantum Mater.* **5**, 62 (2020)
- T. Metz, S. Bae, S. Ran, I-L. Liu, Y.S. Eo, W.T. Fuhrman, D.F. Agterberg, S. Anlage, N.P. Butch, J. Paglione, "Point Node Gap Structure of Spin-Triplet Superconductor UTe₂", *Phys. Rev. B* **100**, 220504 (2019).

S. Ran, I.-L. Liu, Y. S. Eo, D. J. Campbell, P. Neves, W. T. Fuhrman, S. R. Saha, C. Eckberg, H. Kim, J. Paglione, D. Graf, J. Singleton, and N. P. Butch, “Extreme magnetic field-boosted superconductivity,” *Nat. Phys.* **15**, 1250–1254 (2019).

S. Ran, C. Eckberg, Q.-P. Ding, Y. Furukawa, T. Metz, S. R. Saha, I.-L. Liu, M. Zic, H. Kim, J. Paglione, and N. P. Butch, “Nearly ferromagnetic spin-triplet superconductivity,” *Science* **365**, 684–687 (2019).

Program Title: Atomic Engineering Oxide Heterostructures: Materials by Design

PI: H. Y. Hwang^{1,2*}; Co-PI: S. Raghu^{1,3}

¹Stanford Institute for Materials & Energy Sciences, SLAC National Accelerator Laboratory, Menlo Park, CA 94025

²Department of Applied Physics, Stanford University, Stanford, CA 94305

³Department of Physics, Stanford University, Stanford, CA 94305

**hyhwang@slac.stanford.edu*

Program Scope

A central aim of modern materials research is the control of materials and their interfaces to atomic dimensions. In the search for emergent phenomena and ever-greater functionality in devices, transition metal oxides have enormous potential. They host a vast array of properties, such as orbital-ordering, unconventional superconductivity, magnetism, and ferroelectricity, as well as quantum phase transitions and couplings between these states. Our broad objective is to develop the science and technology arising in heterostructures of these novel materials. Using atomic-scale growth techniques we explore the properties of novel interfaces and geometrically confined phases. Magnetotransport, magnetic, x-ray, and optical probes are used to determine the static and dynamic electronic and magnetic structure. Experimental efforts are guided and analyzed theoretically, particularly with respect to electronic effects arising from strong interactions, disorder, and new states of emergent order. For this we develop non-perturbative descriptions of interacting quantum systems using a broad set of analytic, numerical, and phenomenological methods. Beyond the focus of this presentation, recent topics of study include:

Correlated electron phases in two dimensions (gate-tunable superconductor-metal-insulator transitions); phase diagrams and superconductivity in infinite-layer nickelates; and stretching, bending, and breaking freestanding oxide membranes.

Recent Progress

The focus of our presentation will be regarding the long-standing mystery of the microscopic origins of superconductivity in the iconic quantum paraelectric SrTiO₃ when doped with electrons. Several striking features occur, including the occurrence of a superconducting dome in an extremely dilute limit (10^{19} - 10^{21} cm⁻³), as well as the presence of soft transverse optic (TO1) phonon modes associated with a nearly ferroelectric state. Is this a conventional BCS superconductor, or one where the phonon scale exceeds the Fermi energy (E_F), resulting in an “anti-adiabatic” regime for superconductivity? How do the soft TO1 modes couple to the conduction electrons? Symmetry dictates that in the absence of spin-orbit coupling, electrons couple to pairs of TO1 phonons, which appears to have limited phase space for superconductivity. These issues as well as the possibility of exotic unconventional superconductivity in SrTiO₃ have remained in active consideration.

We have developed planar tunneling spectroscopy to examine Nb and La doped SrTiO₃ across the superconducting dome, using atomically designed polar tunnel barriers that enable very high-resolution measurements (Fig. 1). We find that the over-doped superconducting boundary aligns, with surprising precision, to E_F crossing the Debye energy. Superconductivity emerges with decreasing density, maintaining throughout the (weak-coupling) BCS gap to transition temperature ratio – i.e. $2\Delta_0/k_B T_c = 3.53$, despite being in the anti-adiabatic regime. At lowest superconducting

densities, the lone remaining adiabatic phonon van Hove singularity is the soft TO1 mode. We suggest a scenario for pairing mediated by this mode in the presence of spin-orbit coupling, which naturally accounts for the dome and BCS ratio.

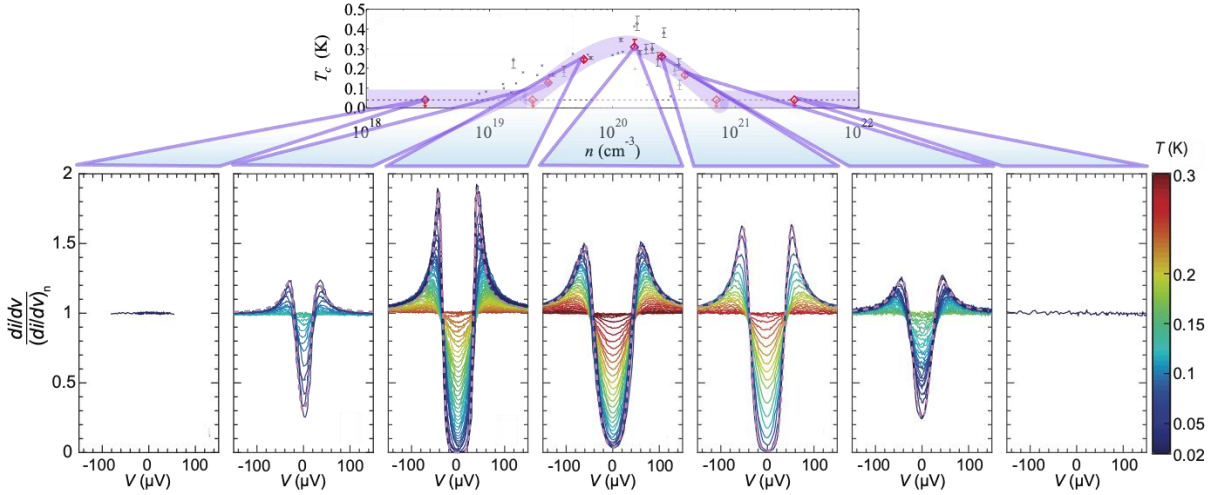


Fig. 1. Fig. 8. Superconducting gap spectra for various electron densities across the superconducting dome in doped SrTiO₃ [H. Yoon, A. G. Swartz, S. P. Harvey, H. Inoue, Y. Hikita, Y. Yu, S. B. Chung, S. Raghu, H. Y. Hwang, “Low-Density Superconductivity in SrTiO₃ Bounded by the Adiabatic Criterion,” arXiv:2106.10802].

Future Plans

In addition to continued efforts on superconductivity in 3D and 2D quantum paraelectrics, we will pursue investigations of:

- Dynamic strain control of states in oxide membranes.
- Fate of 2D electrons with interactions and disorder.
- Magnetic and electronic properties of infinite-layer nickelates.
- Interactions and coherence in 1D/mesoscopic systems.

Publications

1. Y. Yu and S. Raghu, “Effect of Strain Inhomogeneity on a Chiral p -wave Superconductor,” *Physical Review B* **100**, 094517 (2019).
2. P. Kumar, Y.-B. Kim, and S. Raghu, “Self-Duality of the Integer Quantum Hall to Insulator Transition: Composite Fermion Description,” *Physical Review B* **100**, 235124 (2019).
3. B. S. Y. Kim, Y. Hikita, T. Yajima, and H. Y. Hwang, “Heteroepitaxial Vertical Perovskite Hot-Electron Transistors Down to the Monolayer Limit,” *Nature Communications* **10**, 5312 (2019).
4. X. Wu, D. D. Sante, T. Schwemmer, W. Hanke, H. Y. Hwang, S. Raghu, and R. Thomale, “Robust dx^2-y^2 -wave Superconductivity of Infinite-Layer Nickelates,” *Physical Review B (Rapid Communications)* **101**, 060504 (2020).
5. S. S. Hong, M. Q. Gu, M. Verma, V. Harbola, B. Y. Wang, D. Lu, A. Vailionis, Y. Hikita, R. Pentcheva, J. M. Rondinelli, and H. Y. Hwang, “Extreme Tensile Strain States in La_{0.7}Ca_{0.3}MnO₃ Membranes,” *Science* **368**, 71 (2020).
6. R. J. Xu, J. W. Huang, E. Barnard, S. S. Hong, P. Singh, E. Wong, T. Jansen, V. Harbola, J. Xiao, B. Y. Wang, S. Crossley, D. Lu, S. Liu, and H. Y. Hwang, “Strain-Induced Room-

- Temperature Ferroelectricity in SrTiO₃ Membranes,” *Nature Communications* **11**, 3141 (2020).
7. D. F. Li, B. Y. Wang, K. Lee, S. P. Harvey, M. Osada, B. H. Goodge, L. F. Kourkoutis, and H. Y. Hwang, “Superconducting Dome in Nd_{1-x}Sr_xNiO₂ Infinite Layer Films,” *Physical Review Letters* **125**, 027001 (2020).
 8. Y. Yu, S. Brown, S. Raghu, and K. Yang, “Critical Temperature T_c and Pauli Limited Critical Field of Sr₂RuO₄: Uniaxial Strain Dependence,” *Physical Review B* **102**, 014509 (2020).
 9. M. Osada, B. Y. Wang, K. Lee, D. F. Li, and H. Y. Hwang, “Phase Diagram of Infinite-Layer Praseodymium Nickelate Pr_{1-x}Sr_xNiO₂ Thin Films,” *Physical Review Materials (Rapid Communications)* **4**, 121801 (2020).
 10. P. A. Nosov, I. S. Burmistrov, and S. Raghu, “Interaction-Induced Metallicity in a Two-dimensional Disordered Non-Fermi Liquid,” *Physical Review Letters* **125**, 256604 (2020).
 11. K. S. Huang, S. Raghu, and P. Kumar, “Numerical Study of a Dual Representation of the Integer Quantum Hall Transition,” *Physical Review Letters* **126**, 056802 (2021).
 12. Z. Y. Chen, B. Y. Wang, A. G. Swartz, H. Yoon, Y. Hikita, S. Raghu, and H. Y. Hwang, “Universal Behavior of the Bosonic Metallic Ground State in a Two-Dimensional Superconductor,” *npj Quantum Materials* **6**, 15 (2021).
 13. B. Y. Wang, D. F. Li, B. H. Goodge, K. Lee, M. Osada, S. P. Harvey, L. F. Kourkoutis, M. R. Beasley, and H. Y. Hwang, “Isotropic Pauli-Limited Superconductivity in the Infinite-Layer Nickelate Nd_{0.775}Sr_{0.225}NiO₂,” *Nature Physics* **17**, 473 (2021).
 14. V. Harbola, S. Crossley, S. S. Hong, D. Lu, Y. Birkhölzer, Y. Hikita, and H. Y. Hwang, “Giant Strain Gradient Elasticity in SrTiO₃ Membranes: Bending versus Stretching,” *Nano Letters* **21**, 2470 (2021).
 15. V. Harbola, R. J. Xu, S. Crossley, P. Singh, and H. Y. Hwang, “Fracture and Fatigue of Thin Crystalline SrTiO₃ Membranes,” *Applied Physics Letters* **119**, 053102 (2021).
 16. M. Osada, B. Y. Wang, B. H. Goodge, S. P. Harvey, K. Lee, D. F. Li, L. F. Kourkoutis, and H. Y. Hwang, “Nickelate Superconductivity without Rare-Earth Magnetism: (La,Sr)NiO₂,” *Advanced Materials*, in press, arXiv:2105.13494.
 17. H. Yoon, A. G. Swartz, S. P. Harvey, H. Inoue, Y. Hikita, Y. Yu, S. B. Chung, S. Raghu, and H. Y. Hwang, “Low-Density Superconductivity in SrTiO₃ Bounded by the Adiabatic Criterion,” arXiv:2106.10802.
 18. P. Kumar, P. A. Nosov, and S. Raghu, “Interaction Effects on Quantum Hall Transitions: Dynamical Scaling Laws and Superuniversality,” arXiv:2006.11862.
 19. J. H. Son and S. Raghu, “3D Network Model for Strong Topological Insulator Transitions,” arXiv: 2008.03315.
 20. Y.-T. Hsu, B. Y. Wang, M. Berben, D. F. Li, K. Lee, C. Duffy, T. Ottenbros, W. J. Kim, M. Osada, S. Wiedmann, H. Y. Hwang, and N. E. Hussey, “Insulator-to-Metal Crossover near the Edge of the Superconducting Dome in Nd_{1-x}Sr_xNiO₂,” arXiv:2105.07783.

Collaborative Publications:

21. A. Pustogow, Yongkang Luo, A. Chronister, Y.-S. Su, D. A. Sokolov, F. Jerzembeck, A. P. Mackenzie, C. W. Hicks, N. Kikugawa, S. Raghu, E. D. Bauer, and S. E. Brown, “Constraints on the Superconducting Order Parameter in Sr₂RuO₄ from Oxygen-17 Nuclear Magnetic Resonance,” *Nature* **574**, 72 (2019).
22. S. Crossley, A. G. Swartz, K. Nishio, Y. Hikita, and H. Y. Hwang, “All-Oxide Ferromagnetic Resonance and Spin Pumping with SrIrO₃,” *Physical Review B* **100**, 115163 (2019).
23. Y. Frenkel, Y. W. Xie, Y. Hikita, and B. Kalisky, “Magnetism and Conductivity Along

- Structural Domain Walls of SrTiO₃,” *Journal of Superconductivity and Novel Magnetism* **33**, 195 (2020).
24. M. Hepting, D. Li, C. J. Jia, H. Lu, E. Paris, Y. Tseng, X. Feng, M. Osada, E. Been, Y. Hikita, Y.-D. Chuang, Z. Hussain, K. J. Zhou, A. Nag, M. Garcia-Fernandez, M. Rossi, H. Y. Huang, D. J. Huang, Z. X. Shen, T. Schmitt, H. Y. Hwang, B. Moritz, J. Zaanen, T. P. Devereaux, and W. S. Lee, “Electronic Structure of the Parent Compound of Superconducting Infinite-Layer Nickelates,” *Nature Materials* **19**, 381 (2020).
 25. M. Osada, B. Y. Wang, B. H. Goodge, K. Lee, H. Yoon, K. Sakuma, D. F. Li, M. Miura, L. F. Kourkoutis, and H. Y. Hwang, “A Superconducting Praseodymium Nickelate with Infinite-Layer Structure,” *Nano Letters* **20**, 5735 (2020).
 26. P. Jaiban, M.-H. Lu, T. Ekanapakul, S. Chaiyachad, S. H. Yao, N. Pisitpipathsin, M. Unruan, S. Siriroj, R.-H. He, S.-K. Mo, A. Watcharapasorn, R. Yimnirun, Y. Tokura, Z.-X. Shen, H. Y. Hwang, S. Maensiri, and W. Meevasana, “Spectral Weight Reduction of Two-Dimensional Electron Gases at Oxide Surfaces Across the Ferroelectric Transition,” *Scientific Reports* **10**, 16834 (2020).
 27. C. W. Rischau, Y. Li, B. Fauque, H. Inoue, M. Kim, C. Bell, H. Y. Hwang, A. Kapitulnik, and K. Behnia, “Universal Bound to the Amplitude of the Vortex Nernst Signal in Superconductors,” *Physical Review Letters* **126**, 077001 (2021).
 28. E. Persky, N. Vardi, A. M. Monteiro, T. C. van Thiel, H. Yoon, Y. W. Xie, B. Fauqué, A. D. Caviglia, H. Y. Hwang, K. Behnia, J. Ruhman, and B. Kalisky, “Non-Universal Current Flow Near the Metal-Insulator Transition in an Oxide Interface,” *Nature Communications* **12**, 3311 (2021).
 29. I. El Baggari, D. J. Baek, M. J. Zachman, D. Lu, Y. Hikita, H. Y. Hwang, E. A. Nowadnick, and L. F. Kourkoutis, “Charge Order Textures Induced by Non-Linear Couplings in a Half-Doped Manganite,” *Nature Communications* **12**, 3747 (2021).
 30. H. Lu, M. Rossi, A. Nag, M. Osada, D. F. Li, K. Lee, B. Y. Wang, M. Garcia-Fernandez, S. Agrestini, Z. X. Shen, E. M. Been, B. Moritz, T. P. Devereaux, J. Zaanen, H. Y. Hwang, K. J. Zhou, and W. S. Lee, “Magnetic Excitations in Infinite-Layer Nickelates,” *Science* **373**, 213 (2021).
 31. D. P. Arovas, E. Berg, S. A. Kivelson, and S. Raghu, “The Hubbard Model,” *Annual Reviews of Condensed Matter Physics*, in press, arXiv: 2103.12097.
 32. M. Rossi, H. Lu, A. Nag, D. Li, M. Osada, K. Lee, B. Y. Wang, S. Agrestini, M. Garcia-Fernandez, Y.-D. Chuang, Z. X. Shen, H. Y. Hwang, B. Moritz, K. J. Zhou, T. P. Devereaux, and W. S. Lee, “Orbital and Spin Character of Doped Carriers in Infinite-Layer Nickelates,” arXiv:2011.00595.
 33. Z. Y. Chen, M. Osada, D. F. Li, E. M. Been, S.-D. Chen, M. Hashimoto, D. H. Lu, S. K. Mo, K. Lee, B. Y. Wang, F. Rodolakis, J. L. McChesney, C. J. Jia, B. Moritz, T. P. Devereaux, H. Y. Hwang, and Z.-X. Shen, “Electronic Structure of Superconducting Nickelates Probed by Resonant Photoemission Spectroscopy,” arXiv: 2106.03963.

Digital Synthesis: A pathway to create and control novel states of condensed matter

Anand Bhattacharya, Dillon Fong, Sam Jiang (Materials Science Division, Argonne National Laboratory)

Program Scope: ‘Digital Synthesis’ is a strategy for realizing novel states of condensed matter by creating materials in an atomic layer-by-layer fashion. With this approach, we are able to create artificial crystals, including cation-ordered and delta-doped analogs of known materials, and control charge transfer and band lineup in heterostructures. Thus, our program seeks to create new materials out of known ingredients to yield novel properties. We manipulate these properties with external fields and currents, and to develop new insights about how we might realize these properties ‘by design’. Our program focuses on correlated materials, which are mostly complex oxides, and topological semimetals and insulators, that are mostly intermetallics. The areas that we will explore include (i) a new interfacial superconductor that we discovered at the (111) interface of KTaO_3 , (ii) a new class of superconductors in the nickelates, (iii) using the spin Seebeck effect to probe the magnetic excitations in novel quantum magnets and (iv) creating and exploring epitaxial films of non-magnetic topological semimetals and insulators.

We synthesize our materials using molecular beam epitaxy (MBE), multi-target sputtering and pulsed laser deposition (PLD) techniques, and characterize them with tools that probe structural, electronic and magnetic degrees of freedom, including their spin and charge transport properties.

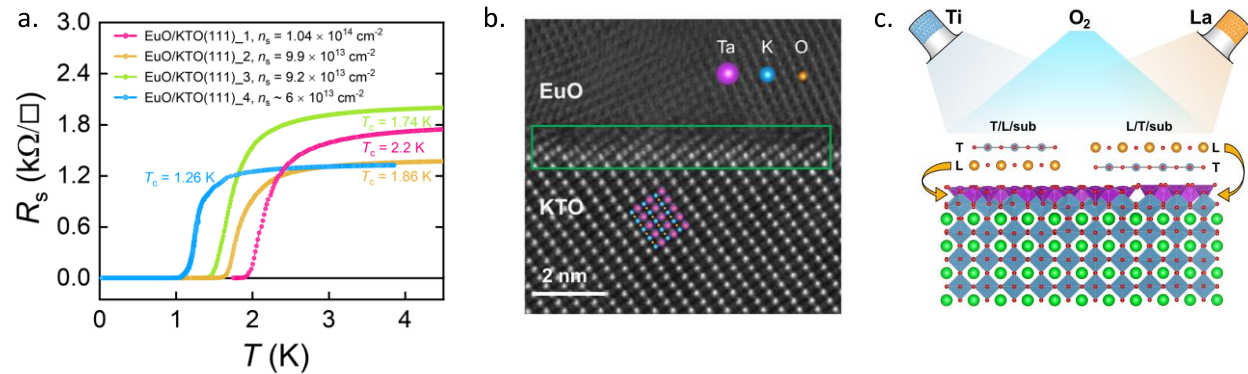


Fig.1 a. Superconducting transitions in EuO/KTO (111) interfaces. **b.** Scanning transmission electron microscopy image of a EuO/KTO (111) interface. **c.** Schematic of atomic layer by layer deposition of LaTiO_3 in a sequence of TiO_2 - LaO -.../ SrTiO_3 showing how a TiO_2 layer always floats to the top, as determined by in-situ x-ray scattering during MBE growth. Going forward, we will use this approach to tailor interfaces with KTO substrates.

Recent Progress

In this extended abstract, we describe progress and future plans related to objectives (i) and (ii) stated above, regarding superconductivity in oxide interfaces and thin films. Here we highlight a few significant developments that motivate our work, and seed our future plans:

(i) Discovery of Superconductivity in KTaO_3 (Science 2021): In recent work¹, we have discovered that a metallic electron gas formed at interfaces between (111) oriented KTaO_3 (KTO) and polycrystalline EuO (**Fig. 1b.**) or amorphous LaAlO_3 capping layers becomes superconducting with a transition temperature T_c as high as 2.2 K (**Fig. 1a.**) — far in excess of the 2DEG formed at $\text{LaAlO}_3/\text{SrTiO}_3$ interfaces, where T_c is limited to ~ 200 mK. Surprisingly, interfacial states on the

(001) surface of KTaO_3 at similar carrier densities remained normal down to 25 mK. The occurrence of superconductivity in the (111) orientation also occurs for an amorphous LaAlO_3 capping layer.

The two-dimensionality of the superconductivity is verified in the out-of-plane and in-plane upper critical field, where the extracted values of the thickness of the superconducting layer is smaller than the Ginzburg-Landau coherence length. Current-voltage measurements in the superconducting state are also found to be consistent with 2D superconductivity. We note that $B_{c\parallel}(0)$ is substantially larger than the paramagnetic pair-breaking field, which could be due to disorder but may also occur due to more intrinsic reasons, for example unconventional triplet pairing may be energetically stabilized in a magnetic field, as has been observed in bulk non-centrosymmetricⁱⁱ superconductors. Furthermore, in samples prepared with lower carrier concentrations and higher mobility, we observe a strong *in-plane* anisotropy in resistance (“stripe” phase) that forms spontaneously at $T \leq 2.2$ K. The behavior of the observed nematicity and its relation to superconductivity bears some similarity to those found in the cuprate and iron-based high-temperature superconductors and more recently in doped Bi_2Se_3 .ⁱⁱⁱ The orientational selective superconductivity and tunable electronic phases on the KTO (111) surface therefore provide a new platform for investigating unconventional superconductivity, which has long been a central theme in condensed matter physics. We should note that several groups have now confirmed that the KTO (111) interfaces superconduct^{iv}, and have found that the KTO (110) interface^v is also superconducting, though with a lower T_c .

(ii) *Understanding layer by layer growth of interfaces on SrTiO_3* (*Sci. Adv.* 2019): One of our goals is to tailor interfaces of KTaO_3 and similar oxides to create interfacial electron gases. The states found at these interfaces depend critically upon the first few layers in the immediate vicinity of the interface. In this light, we present recent results on another well studied and related d^0 oxide – SrTiO_3 .

In traditional models of heteroepitaxy, the substrate serves mainly as a crystalline template for the thin-film lattice, dictating the initial roughness of the film and the degree of coherency strain. The most common substrate used in the growth of complex oxide heterostructures is strontium titanate (SrTiO_3) partly due to the ability to consistently produce an atomically smooth, TiO_2 -terminated (001) surface. The atomic force microscopy image shows that the steps are approximate 0.4-nm-high. Since this is the size of one unit cell, researchers assume that the $\text{SrO}/\text{TiO}_2 \dots$ stacking sequence continues to the surface. However, using the molecular beam epitaxy (MBE) growth chamber we helped construct at Advanced Photon Source (APS)^{vi}, we find that the surface is not stoichiometric, regardless of how carefully the substrate is prepared. It instead exhibits excess TiO_2 such that the SrTiO_3 surface is terminated by a TiO_2 double layer.

In recent work^{vii}, we studied the implications of the TiO_2 double layer on heteroepitaxial growth. We deposited LaTiO_3 (LTO) on SrTiO_3 (001) in a layer-by-layer fashion, i.e., alternating between one monolayer of LaO and one monolayer of TiO_2 (**Fig. 1 c**). We show that the traditional model of layer-by-layer growth on SrTiO_3 should be replaced with a dynamic model in which the TiO_2 adlayer from the substrate continuously “floats” to the surface of the growing film much like a surfactant, so that while the perovskite stacking sequence is maintained at the heterointerface, the TiO_2 adlayer is also maintained at the film surface. Aside from providing a better understanding of heteroepitaxial growth, our work shows that the ultrathin films are likely to be terminated by TiO_2 regardless of the nature of the film. Similar studies are planned for growth of LTO on KTO.

(iii) *LaNiO₃ is a quantum critical metal* (*Nat. Commun.* 2020): The nature of the electronic and magnetic properties of LaNiO₃ has been debated and studied for several decades^{viii}. It is the only member of the rare-earth perovskite nickelate *ReNiO₃* family that remains metallic, without developing long range magnetic order down to the lowest temperatures. We have discovered that LaNiO₃ is a ‘strange’ metal at low temperatures, where the resistivity as a function of temperature does not agree with Fermi liquid theory, where we expect $\rho(T) = \rho_o + aT^2$. We synthesized very high mobility epitaxial thin films of LaNiO₃ using ozone assisted MBE, where the residual resistivity $\rho_o < 4 \Omega\text{-cm}$, by careful control of cation stoichiometry and mitigation of oxygen vacancy formation. Over nearly a decade of temperature below 1.2 K, we find that $\rho(T) = \rho_o + bT$.^{ix} Upon application of magnetic fields, a quadratic dependence in $\rho(T)$ is recovered, and Fermi-liquid behavior is restored. These findings are a signature of a metal whose transport properties are governed by antiferromagnetic quantum critical fluctuations, which are suppressed by magnetic fields. Furthermore, we find that the introduction of a small concentration of magnetic impurities qualitatively changes the magnetotransport properties of LNO. The magnetoresistance as a function of temperature is found to scale in a manner strongly resembling some heavy-fermion Kondo lattice systems in the vicinity of an antiferromagnetic quantum critical point.

(iv) *Understanding layer-by-layer growth of nickelates* (*APL Mater.* 2020): Reflection High Energy Electron Diffraction (RHEED) is often used to monitor the growth process during molecular beam epitaxy, as the minima / maxima indicate the completion of each monolayer. However, given the strong interaction between electrons and the surface, quantitative analysis with RHEED is difficult; furthermore, RHEED cannot be used to probe atomic-scale processes taking place below the surface.

For this reason, we constructed a new MBE chamber at the APS that allows both RHEED and surface X-ray diffraction studies during epitaxial thin film growth. This allows us to relate the growth oscillations observed during RHEED with those observed from X-ray scattering. In recent^x work, we studied the initial case of LaNiO₃ layer-by-layer growth on (La_{0.18}Sr_{0.82})(Al_{0.59}Ta_{0.41})O₃. We found that during the earliest stages of growth, the RHEED and X-ray signals are out-of-phase with each other before gradually becoming in-phase, demonstrating that while regular RHEED oscillations may imply high quality growth, the film-substrate interface can undergo significant changes during deposition due to the occurrence of interdiffusion at the growth temperature.

Future Plans

(i) *Superconductivity and electronic nematicity at KTaO₃ interfaces*: There are several key questions and opportunities that arise in this area of research building upon our findings thus far. Our effort will fall broadly into two categories – the first being materials development and understanding how to control the properties of the interfacial electron gases at KTO interfaces, and to also find other materials where such states may be found. Thus, we seek to find other overlayers on KTO that may give rise to an interesting interfacial electron gas. As an example, LaTiO₃ (LTO) is a Mott insulator and is known to give rise to an interfacial conductor on KTO (001) interfaces^{xi}, and we have already grown LTO with MBE on STO (see Recent Progress). We would also like to find ways to pattern our samples into mesoscale structures. We are collaborating with Prof. Jeremy Levy at the University of Pittsburgh to use his approach of writing nanoscale wires using a conducting AFM tip^{xii} that has been very successful in the LaAlO₃/SrTiO₃ interface. Furthermore, we’d like to understand how vacancy formation and cation diffusion using in-situ x-rays during growth of overlayers such as EuO or LTO on KTO. Ultimately, we’d like to grow KTaO₃ films

and dope them in a controlled manner. These and other aspects of materials development are being actively pursued

The second aspect of this research is to elucidate the nature of superconductivity and also the electronic nematicity that we observe. We are currently carrying out an extensive study of electric field-effect gating of superconductivity at the KTO (111) interface. Along with magnetotransport measurements currently in progress, we hope to develop a comprehensive picture of the nematic state that will constrain future theories. In all of these aspects we are collaborating with several theorists including Mike Norman, Peter Littlewood, and Ivar Martin at Argonne and Arun Paramakanti at Toronto. Two theory papers motivated by our work have appeared.^{xiii}

(ii) *Superconductivity in nickelates*: Superconductivity in nickelates was discovered in 2019, when a group at Stanford University reported that epitaxial thin films of the infinite layer ‘112’ compound $\text{Nd}_{1-x}\text{Sr}_x\text{NiO}_2$ ($x = 0.2$), with $\text{Ni}^{(1+x)+}$ in square-planar coordination with O, is a superconductor with T_c values reported as 9-15 K^{xiv}. Several follow-up results have also been reported.^{xv} The 112 phase is obtained from the perovskite (113) $\text{Nd}_{1-x}\text{Sr}_x\text{NiO}_3$ phase via topotactic reduction. The discovery of a such a closely related superconducting analog to the cuprates has aroused great interest in the quantum materials community.

We seek too explore alternative strategies to doping, including delta doping, interfacial charge-transfer and ionic-liquid gating to realize superconducting nickelates. We also seek alternative pathways to realize square planar Ni-O coordination, in collaboration with our colleagues at Argonne (John Mitchell, Mike Norman) who are actively pursuing this direction of research. We will use magnetotransport and thermogalvanic (Nernst effect) measurements to elucidate the nature of electronic states in these materials.

References

- ⁱ C. Liu et al., *Science* **371**, 716 (2021).
- ⁱⁱ Y. Lu et al., *JPSJ* **83**, 023702 (2014).
- ⁱⁱⁱ S. Yonezawa *Condens. Matter* **4**, 2 (2019); R.M. Fernandes et al., *Nat. Phys.* **10**, 97 (2014).
- ^{iv} Y. Ma et al., *Chin. Phys. Lett.* **37**, 117401; Z. Chen et al., arXiv:2009.05689
- ^v Z. Chen et al., *Phys. Rev. Lett.* **126**, 026802 (2021).
- ^{vi} G. Eres et al., *Rev. Sci. Instrum.* **90**, 093902 (2019).
- ^{vii} S. Y. Cook et al., *Sci. Adv.* **5**, eaav0764 (2019).
- ^{viii} S. Catalano et al., *Rep. Prog. Phys.* **81**, 046501 (2018).
- ^{ix} C. Liu et al., *Nat. Commun.* **11**, 1 (2020).
- ^x Xi Yan et al., *APL Mater.* **8**, 101107 (2020).
- ^{xi} K. Zou et al., *APL Mater.* **3**, 036104 (2015).
- ^{xii} C. Cen et al., *Science* **323**, 1026 (2009).
- ^{xiii} P. V. Arribi et al., *Phys. Rev B* **103**, 035115 (2021); F. L. Buessen et al., arXiv:2101.03174.
- ^{xiv} D. Li et al., *Nature* **572**, 624 (2019).
- ^{xv} S. Zeng et al., arXiv:2004.11281; M. Osada et al., arXiv: 2006.133369.

Digital Synthesis FWP Publications, since 2019.

1. “Voltage control of magnon spin currents in antiferromagnetic Cr_2O_3 ”, Changjiang Liu, Yongming Luo, Deshun Hong, Steven S-L Zhang, Brandon Fisher, John E Pearson, J Samuel Jiang, Axel Hoffmann, Anand Bhattacharya, to appear in *Science Advances*, 2021.
2. “Distinguishing antiferromagnetic sublattices using the spin Seebeck effect”, Yongming Luo, Changjiang Liu, Hilal Saglam, Yi Li, Wei Zhang, Steven S-L Zhang, John E Pearson, Brandon Fisher, Tiejun Zhou, Anand Bhattacharya, Axel Hoffmann, *Phys. Rev. B* **103**, L020401 (2021)
3. “Breaking atomic-level ordering via biaxial strain in functional oxides: A DFT study”, K. Rawat, D. D. Fong, D. S. Aidhy to appear in *J. Appl. Phys.*
4. “Two-dimensional superconductivity and anisotropic transport at KTaO_3 (111) interfaces”, C. Liu, X. Yan, D. Jin, Y. Ma, H.-W. Hsiao, Y. Lin, T. M. Bretz-Sullivan, X. Zhou, J. Pearson, B. Fisher, J. S. Jiang, W. Han, J.-M. Zuo, J. Wen, D. D. Fong, J. Sun, H. Zhou, A. Bhattacharya, *Science* **371**, 716 (2021).
5. “Topological Hall Effect in a Topological Insulator Interfaced with a Magnetic Insulator”, Peng Li, Jinjun Ding, Steven S.-L. Zhang, James Kally, Timothy Pillsbury, Olle G. Heinonen, Gaurab Rimal, Chong Bi, August DeMann, Stuart B. Field, Weigang Wang, Jinke Tang, Jidong Samuel Jiang, Axel Hoffmann, Nitin Samarth, and Mingzhong Wu, *Nano Lett.* **21**, 84 (2021).
6. “Interface creation on a mixed-terminated perovskite surface”, Y. Li, F. Wrobel, X. Yan, A. Bhattacharya, J. Sun, H. Hong, H. Zhou, H. Wang, D. D. Fong, *Appl. Phys. Lett.* **118**, 061601 (2021).
7. “Amorphization mechanism of SrIrO_3 electrocatalyst: Amorphization mechanism of SrIrO_3 electrocatalyst: How oxygen redox initiates ionic diffusion and structural reorganization”, G. Wan, J. W. Freeland, J. Kloppenburg, G. Petretto, J. N. Nelson, D.-Y. Kuo, C.-J. Sun, J. Wen, J. T. Diulus, G. S. Herman, Y. Dong, R. Kou, J. Sun, S. Chen, K. Shen, D. Schlom, G.-M. Rignanese, G. Hautier, D. D. Fong, Z. Feng, H. Zhou, & J. Suntivich, *Science Advances* **7**, eabc7323 (2021).
8. “In situ X-ray and electron scattering studies of oxide molecular beam epitaxial growth”, Xi Yan, Friederike Wrobel, Yan Li, Hua Zhou, Huanhua Wang, Anand Bhattacharya, Jirong Sun, Hawoong Hong, and Dillon D. Fong, *APL Materials* **8**, 101107 (2020).
9. “Observation of an antiferromagnetic quantum critical point in high-purity LaNiO_3 ”, Changjiang Liu, Vincent FC Humbert, Terence M Bretz-Sullivan, Gensheng Wang, Deshun Hong, Friederike Wrobel, Jianjie Zhang, Jason D Hoffman, John E Pearson, J. Samuel Jiang, Clarence Chang, Alexey Suslov, Nadya Mason, MR Norman, Anand Bhattacharya, *Nature Communications* **11**, 1 (2020).
10. “Fermi surface topology and nontrivial Berry phase in the flat-band semimetal Pd_3Pb ”, Mojammel A Khan, Po-Hao Chang, Nirmal Ghimire, Terence M Bretz-Sullivan, Anand Bhattacharya, Jidong S. Jiang, John Singleton, John F Mitchell, *Phys. Rev. B* **101**, 245113 (2020).

11. “In situ X-ray studies of the incipient ZnO Atomic Layer Deposition on In_{0.53}Ga_{0.47}As”, E.V. Skopin, L. Rapenne, J.L. Deschanvres, E. Blanquet, G. Ciatto, L. Pithan, D. D. Fong, M.-I. Richard, and H. Renevier, *Phys. Rev. Mater.* **4**, 043403 (2020).
12. “Organismic materials for beyond von Neumann machines”, H.-T. Zhang, P. Panda, J. Lin, Y. Kalcheim, K. Wang, J. W. Freeland, D. D. Fong, S. Priya, I. K. Schuller, S. K. R. S. Sankaranarayan, K. Roy, and S. Ramanathan, *Appl. Phys. Rev.* **7**, 011309 (2020).
13. “Ferroelectric domain wall motion in freestanding single-crystal complex oxide thin film”, S. R. Bakaul, J. Kim, S. Hong, M. J. Cherukara, T. Zhou, L. Stan, C. R. Serrao, S. Salahuddin, A. K. Petford-Long, D. D. Fong, M. V. Holt, *Adv. Mater.* **3**, 19007036 (2019).
14. “Counter-thermal flow of holes in high-mobility LaNiO₃ thin films”, Chanjiang Liu, Friederike Wrobel, Jason D. Hoffman, Deshun Hong, John E. Pearson, Eva Benckiser and Anand Bhattacharya, *Phys. Rev. B (R)* **99**, 041114 (2019).
15. “Parameter transferability, self-doping, and metallicity in LaNiO₃/LaMnO₃ superlattices”, A Lopez-Bezanilla, L. F. Arsenault, A. Bhattacharya, P. B. Littlewood, A. J. Millis, *Phys. Rev. B* **99**, 035133 (2019).
16. “Beyond electrostatic modification: design and discovery of functional oxide phases via ionic-electronic doping”, H.T. Zhang, Z. Zhang, H. Zhou, H. Tanaka, D. D. Fong, and S. Ramanathan, *Advances in Physics: X*, **4** 1523686 (2019).
17. “Strongly Correlated Aromatic Molecular Conductor”, Y. Hu, G. Zhong, Y.-S. Guan, J. N. Armstrong, C. Li, C. Liu, A. N'Diaye, A. Bhattacharya, S. Ren, *Small* **15**, 1900299 (2019).
18. “Experimental setup combining in situ hard X-ray photoelectron spectroscopy and real-time surface X-ray diffraction for characterizing atomic and electronic structure evolution during complex oxide heterostructure growth”, G. Eres, C. M. Rouleau, Q. Lu, Z. Zhang, E. Benda, H. N. Lee, J. Z. Tischler, and D. D. Fong, *Rev. Sci. Instrum.* **90**, 093902 (2019).
19. “In operando studies of CO oxidation on epitaxial SrCoO_{2.5+d} thin films”, C. M. Folkman, S. H. Chang, H. Jeon, E. Perret, P. M. Baldo, Carol Thompson, J. A. Eastman, H. N. Lee and D. D. Fong, *APL Mater.* **7**, 081126 (2019).
20. “Confined polaronic transport in (LaFeO₃)_n / (SrFeO₃)₁ superlattices”, S. H. Chang, S. K. Kim, Y.-M. Kim, Y. Dong, C. M. Folkman, D. W. Jeong, W. S. Choi, A. Y. Borisevich, J. A. Eastman, A. Bhattacharya, and D. D. Fong, *APL Mater.* **7**, 071117 (2019).
21. “Interfacial Octahedral Manipulation Imparts Hysteresis-free Metal to Insulator Transition in Ultrathin Nickelate Heterostructure”, Y. Dong, Z. Ma, Z. Luo, H. Zhou, D. D. Fong, W. Wu, C. and Gao, *Adv. Mater. Inter.* **6**, 1900644 (2019).
22. “Spin Seebeck effect in insulating SrFeO_{3-d} films”, D. Hong, C. Liu, J. E. Pearson, A. Hoffmann, D. D. Fong, and A. Bhattacharya, *Appl. Phys. Lett.* **114**, 242403 (2019).
23. “Mixture domain states in PbTiO₃ film with potentials for functional application”, Han Xu, Zhan Zhang, Yongqi Dong, Changgan Zeng, Dillon D. Fong, Zhenlin Luo, *Appl. Phys. Lett.* **114**, 242901 (2019).
24. “Seeded lateral solid-phase crystallization of the perovskite oxide SrTiO₃”, Y. Chen, J. A. Tilka, Y. Ahn, J. Park, A. Pateras, T. Zhou, D. E. Savage, I. McNulty, M. V. Holt, D. M. Paskiewicz, D. D. Fong, T. F. Kuech, and P. G. Evans, *J. Phys. Chem. C* **123**, 7447 (2019).

25. “How heteroepitaxy occurs on strontium titanate”, S. Y. Cook, K. Letchworth-Weaver, I.-C. Tung, T. K. Andersen, H. Hong, L. D. Marks, D. D. Fong, *Science Advances*, 5, eaav0764 (2019).
26. Y. Zhu, J. G. Connell, S. Tepavcevic, P. Zapol, R. Garcia-Mendez, N. J. Taylor, J. Sakamoto, B. J. Ingram, L. A. Curtiss, J. W. Freeland, D. D. Fong, and N. M. Markovic, Dopant-dependent stability of garnet solid electrolyte interfaces with lithium metal, *Advanced Energy Materials* 9, 1803440 (2019).

Session V

Magnetic Interactions and Excitations in Quantum Materials

D. C. Johnston, L. Ke, R. J. McQueeney, P. P. Orth, B. G. Ueland, D. Vaknin
Ames Laboratory and Iowa State University, Ames, IA 50011

Program Scope

The ability to control the magnetic symmetry and topology of magnetic quantum materials (MQMs) promises to deliver new functionalities based on phenomena such as topological- and spin-polarized transport, quantum-critical fluctuations, and unconventional superconductivity. The development of MQMs challenges our basic understanding of the interrelationship between spin and electronic charge carriers and confronts fundamental issues, such as the microscopic origins of magnetism and the roles of covalency, itinerancy, and electron-electron interactions. We aim to understand how magnetic frustration or symmetry breaking, essential for highly functional and switchable MQMs, can result from competing magnetic phases and interactions. We focus on two materials classes of MQMs:

(1) *Flat electronic bands in itinerant magnets*. Electron-electron interactions are dramatically enhanced in electronic bands with flat dispersions, leading to correlation-driven phases such as itinerant magnetism, charge order, heavy-fermions, or unconventional superconductivity.

(2) *Magnetic topological materials*. The coupling of magnetic moments to topological fermions is the primary factor controlling the emergence of unique quantum topological phases that possess exceptional optical and magneto- and thermal-transport properties. Magnetic interactions in layered topological MQMs are dependent on electron correlations, magnetic disorder, external fields, and reduced dimensionality, outlining an immense experimental and theoretical challenge.

Our two research thrusts employ a common approach and central themes that focus on itinerant magnetism, magnetic frustration, and the coupling between magnetic moments and charge carriers.

We are motivated by three common strategic goals:

- Discover new MQMs exhibiting tunable transport phenomena associated with magnetic order and spin fluctuations.
- Employ a joint experimental and theoretical approach to understand the relation between the microscopic magnetic interactions and the phenomena in MQMs.
- Reveal the coupling between magnetism and charge carriers controlling MQM properties.

Our research thrusts and strategic goals are aligned with the DOE-BES strategic plans in quantum materials, as outlined in the *Basic Research Needs on Quantum Materials for Energy Relevant Technology*, and a BES Grand Challenge that will address the question: *How do remarkable properties of matter emerge from complex correlations of the atomic or electronic constituents and how can we control these properties?*

We address our first goal through the synthesis and discovery of novel MQMs and the experimental determination and characterization of their magnetic, structural, and transport properties. Our latter two goals require tight integration between experimental methods and theory. The characterization of static and dynamic spin correlations, utilizing neutron scattering methods at the Spallation Neutron Source and High Flux Isotope Reactor at Oak Ridge National Laboratory (ORNL), are closely aligned with first-principles electronic-structure calculations, atomistic spin dynamics simulations, and analytical and data-driven theory methods. Both Thrusts share common themes of magnetic frustration and reduced dimensionality that highlight the special importance of the spin fluctuations. Success in addressing these strategic goals will result in the discovery of new MQMs and new methods to control their quantum properties.

Recent Progress

Our oral presentation describes recent progress on our study of topological MQMs where the breaking of time-reversal symmetry (via the development of magnetic order) is essential for unlocking a variety of novel phenomena that promise to revolutionize information technology. There are two main routes for the materials design of bulk topological MQMs (see Figure). The first route consists of dilute magnetic topological insulators (TIs) where magnetic ions at concentrations of a few percent can drive ferromagnetic (FM) order and trigger the quantum anomalous Hall (QAH) effect [1,2]. The second route to topological MQMs exploits intrinsic and stoichiometric magnetic compounds. Very recently, MnBi_2Te_4 (MBT) was demonstrated as the first example of an intrinsic antiferromagnetic (AF)-TI compound [3]. Intrinsic AF-TIs are extremely exciting since the AF state and field polarized FM states host unique topological axion and Chern insulating states, respectively. We have reported seminal findings in both dilute and intrinsic magnetic TI systems by characterizing their magnetic order, key magnetic interactions, and magnetic anisotropy. These efforts have revealed unanticipated and important roles of magnetic frustration, van der Waals (vdW) metamagnetism, and magnetic disorder.

We are collaborating with Jiaqiang Yan (ORNL) to study the magnetic properties of MBT and related systems, such as MnBi_4Te_7 and MnSb_2Te_4 (MST). This collaboration has made several discoveries of the basic transport and magnetic properties of MBT [4]. Neutron diffraction data confirm that MBT is an A-type AF consisting of triangular FM Mn layers with perpendicular moments whose direction alternates layer-to-layer [see Fig. (b)]. Our inelastic neutron scattering (INS) measurements of MBT powder [P18] and single-crystal [5] samples reveal a gapped magnetic spectrum representative of A-type order. Long-range interactions within the FM layer include frustrating AF NNN intralayer coupling ($|J_2/J_1| \sim 0.25$). The interlayer interactions ($|J_{\text{inter}}/J_{\text{intra}}| \sim 0.3$) and single-ion anisotropy ($|D/J_{\text{intra}}| \sim 0.2$) are consistent with observation of a spin-flop transition in applied magnetic fields. This magnetic behavior, along with the ease of exfoliation, places MBT within the class of layered vdW metamagnets.

These discoveries have generated intense interest in all materials in the MBT family. For example, it has been suggested that MST is a robust magnetic TI that might serve as a better platform than MBT for topological devices [6]. With an eye towards tunability, our studies of $\text{Mn}(\text{Bi}_{1-x}\text{Sb}_x)_2\text{Te}_4$ reveal that Sb-substitution has several effects on magnetism and transport. Magnetotransport and ARPES measurements indicate that Sb substitution effectively adds holes, resulting in a change from n -type to p -type carriers near $x = 0.3$ [P2]. This tunability could allow charge-neutral compositions to be studied for evidence of an axion insulator. Neutron diffraction [7] and high-field magnetization [8] find that the strong reduction of the saturation magnetization in Sb-substituted samples [P2] originates from defect-driven *ferrimagnetism* caused by $\sim 15\%$ Mn/Sb antisite mixing. Smaller concentrations of antisite defects ($\sim 5\%$) have

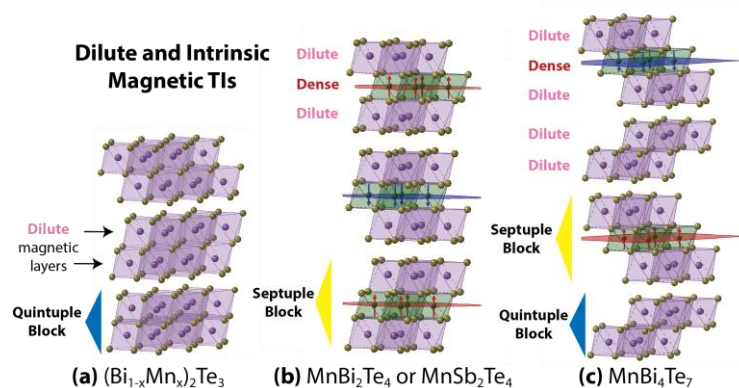


Figure. Structure and magnetism of magnetic TIs. (a) Dilute TIs based on quintuple blocks of Bi_2Te_3 with Mn substituting in the Bi layer. (b) Septuple blocks of MnBi_2Te_4 or MnSb_2Te_4 with dense AF coupled Mn layers and dilute magnetic Bi/Sb layers formed from antisite defects. (c) Alternating quintuple and septuple blocks in MnBi_4Te_7 with corresponding dense and dilute magnetic layers.

recently been observed in MBT [8]. We have performed INS investigations of the evolution of magnetic interactions in $\text{Mn}(\text{Bi}_{1-x}\text{Sb}_x)_2\text{Te}_4$ powder samples [P29]. The spin gap and spin-flop field collapse, indicating that magnetic anisotropy and interblock exchange are strongly modified by Sb substitutions. In addition to the general increase in the magnetic energy scale compared to MBT, we also observe a sharp resonant magnetic excitation in MST that is consistent with AF coupling between Mn/Sb antisite defects and the main Mn layer.

The intrinsic magnetic antisite disorder found in the MBT family generates Bi or Sb layers hosting dilute magnetism, similar to that found in dilute magnetic TI such as $(\text{Bi}_{1-x}\text{Mn}_x)_2\text{Te}_3$ (see Figure). Remarkably, INS measurements on the dilute magnetic TI $(\text{Bi}_{0.95}\text{Mn}_{0.05})_2\text{Te}_3$ observe collective FM excitations despite the low magnetic concentration [9]. Neutron-diffraction measurements reveal long-range quasi-2D FM ordering indicated by a Warren lineshape below $T_C \approx 13$ K, as expected for weak vdW magnetic coupling between Bi_2Te_3 quintuple blocks. The magnon bandwidth in this dilute TI is similar to MBT (~ 2.5 meV), suggesting that, with fewer neighbors on average, the pairwise exchange interactions between Mn spins within the dilute layers must be substantially larger than found in the dense Mn layers in MBT.

We also investigated the magnetic excitations in the cubic paramagnetic topological crystalline insulator $\text{Sn}_{0.95}\text{Mn}_{0.05}\text{Te}$ using INS. A series of sharp excitations originate from strongly coupled AF Mn-Mn dimers ($J_{\text{AF}} = 460$ μeV) comprised of *next-nearest-neighbor* (NNN) Mn pairs, in agreement with DFT calculations. This σ -bonded Mn-Te-Mn exchange path is nearly identical to that found within quintuple and septuple blocks, highlighting a key role for intrablock AF coupling in the magnetic TIs [P11].

Proposed Work

In topological MQMs, the interactions between magnetic moments set the stage for the emergence of different magnetic ground states that modify band topology and control the innate topological state. We have discovered that dilute and intrinsic magnetic TIs share many common features. For example, magnetic disorder in MBT, caused by antisite mixing of Mn and Bi ions, mimics dilute magnetic TI layers. Magnetic TIs also possess weak vdW bonding between magnetic blocks. This interblock magnetic coupling can be systematically weakened by regularly interspersing nonmagnetic blocks provided by natural single-crystal heterostructures of $(\text{MnBi}_2\text{Te}_4)(\text{Bi}_2\text{Te}_3)_n$ [10] [see Fig. (c)]. In the limit of vanishing interblock coupling (large n), the system evolves to a new state called the “single-layer magnet” [11] where the ordering is controlled by magnetic anisotropy or weaker interactions (such as dipolar). Enhanced spin fluctuations in a single-layer topological MQM may lead to exotic properties, especially at the surface. A project to study both dilute magnetic TI and MBT materials provides an ideal vantage point to understand the impacts of magnetic disorder and reduced dimensionality.

Our first objective is to understand the microscopic origins of magnetism in magnetic TIs. Our approach combines INS measurements of the magnetic excitations with bulk magnetization and transport data. Comparison of these results to *ab initio* calculations of the magnetic interactions enables an understanding of their fundamental origins, which may include long-range interactions mediated by carriers. To include the effects of magnetic disorder, atomistic spin dynamics simulations will be employed to calculate the INS spectra, magnetization, and other observables.

Continuation of our systematic studies of dilute and intrinsic magnetic TI compounds will provide important fundamental information, such as detailed spin-spin interactions, dimensionality, and single-ion anisotropy. We plan to interrogate AF-TI compounds in the MBT family, including MnBi_4Te_7 , $\text{MnBi}_6\text{Te}_{10}$, and $\text{MnBi}_8\text{Te}_{13}$ where progressively weaker interlayer interactions lead to

the crossover to the single-layer magnet. In MnBi_4Te_7 , preliminary INS data find a strongly reduced spin gap compared to MBT, consistent with weaker interblock coupling. Preliminary INS measurements on MST find much stiffer magnons than found in MBT, suggesting that key energy scales between these two compounds are very different. We also observe an additional, gapped branch in MST that is presumably caused by defect-driven ferrimagnetism.

The investigation of dilute magnetic TIs provides unique information about single-ion, dimer, and collective excitations that may not be easily accessible in dense magnetic lattices. Our current studies of $(\text{Sb}_{1-x}\text{Mn}_x)_2\text{Te}_3$ and $(\text{Bi}_{1-x}\text{Mn}_x)_2\text{Te}_3$ are addressing important questions regarding the nature of magnetic coupling and the role of magnetic disorder with application to MBT and MST. Preliminary single-crystal INS data on $(\text{Sb}_{0.97}\text{Mn}_{0.03})_2\text{Te}_3$ shows evidence for intrablock AF dimers (similar to that found in $\text{Sn}_{0.95}\text{Mn}_{0.05}\text{Te}$) that drive ferrimagnetism in MST. The nascent FM spin fluctuations in $(\text{Sb}_{0.97}\text{Mn}_{0.03})_2\text{Te}_3$ point to long-range interlayer coupling in dilute TIs.

The fundamental origin of magnetic interactions in dilute and intrinsic magnetic TIs is an open question. In dilute FM-TI, we are starting to understand how FM develops via long-range interactions between widely separated local magnetic moments that may arise from charge carriers at the Fermi surface (such as the RKKY-interaction) with applicability to MBT and MST. In the near future, we plan to study how varying the carrier concentration may influence spin excitations in dilute magnetic TIs such as $(\text{Sn}_{1-x}\text{Mn}_x)\text{Te}$ [12]. It is conceivable that INS measurements of the magnetic excitations, with control of carrier densities or using applied magnetic fields, may provide evidence for their coupling to topological fermions.

References

- [1] J. Zhang *et al.* “Topology-Driven Magnetic Quantum Phase Transition in Topological Insulators,” *Science* **339**, 1582 (2013).
- [2] C.-Z. Chang *et al.* “Experimental Observation of the Quantum Anomalous Hall Effect in a Magnetic Topological Insulator,” *Science* **340**, 167 (2013).
- [3] M. M. Otrokov *et al.* “Prediction and observation of an antiferromagnetic topological insulator,” *Nature* **576**, 416 (2019).
- [4] J. Q. Yan *et al.* “Crystal growth and magnetic structure of MnBi_2Te_4 ,” *Phys. Rev. Mater.* **3**, 064202 (2019).
- [5] B. Li *et al.* “Two-dimensional ferromagnetism with long-range interactions in the layered magnetic topological insulator MnBi_2Te_4 ,” arXiv:2007.08468 (2020).
- [6] S. Wimmer *et al.* “Ferromagnetic MnSb_2Te_4 : A topological insulator with magnetic gap closing at high Curie temperatures of 45-50 K,” arXiv:2011.07052 (2021).
- [7] T. Murakami *et al.* “Realization of interlayer ferromagnetic interaction in MnSb_2Te_4 toward the magnetic Weyl semimetal state,” *Phys. Rev. B* **100**, 195103 (2019).
- [8] Y. Lai *et al.* “Defect-driven ferrimagnetism and hidden magnetization in MnBi_2Te_4 ,” *Phys. Rev. B* **103**, 184429 (2021).
- [9] D. Vaknin *et al.* “Two-dimensional ordering and collective magnetic excitations in the dilute ferromagnetic topological insulator $(\text{Bi}_{0.95}\text{Mn}_{0.05})_2\text{Te}_3$,” *Phys. Rev. B* **99**, 220404 (2019).
- [10] I. I. Klimovskikh *et al.* “Tunable 3D/2D magnetism in the $(\text{MnBi}_2\text{Te}_4)(\text{Bi}_2\text{Te}_3)_m$ topological insulators family,” *npj Quantum Mater.* **5**, 54 (2020).
- [11] J. Wu *et al.* “Toward 2D Magnets in the $(\text{MnBi}_2\text{Te}_4)(\text{Bi}_2\text{Te}_3)_n$ Bulk Crystal,” *Adv. Mater.* **32**, 2001815 (2020).
- [12] C. W. H. M. Vennix *et al.* “Neutron-diffraction study of the carrier-concentration-induced ferromagnet-to-spin-glass transition in the diluted magnetic semiconductor $\text{Sn}_{1-x}\text{Mn}_x\text{Te}$,” *Phys. Rev. B* **48**, 3770-3782 (1993).

Publications

[P32] Santanu Pakhira, Y. Lee, Liqin Ke, V. Smetana, A.-V. Mudring, Thomas Heitmann, David Vaknin, D. C. Johnston, “Suppression of antiferromagnetic order and strong ferromagnetic spin fluctuations in $\text{Ca}(\text{Co}_{1-x}\text{Ni}_x)_2\text{-yAs}_2$ single crystals,” *Phys. Rev. B* (accepted).

<https://arxiv.org/abs/2107.02608>

[P31] D. C. Johnston, “Molecular-field-theory fits to the magnetic susceptibilities of antiferromagnetic GdCu_2Si_2 , CuO , LiCrO_2 , and $\alpha\text{-CaCo}_2\text{O}_4$ single crystals below their Néel temperatures”, *J. Magn. Magn. Mater.* **535**, 168062 (2021).

<https://doi.org/10.1016/j.jmmm.2021.168062>

[P30] Noah F. Berthussen, Yuriy Sizyuk, Mathias S. Scheurer and Peter P. Orth, “Learning crystal field parameters using convolutional neural networks,” *Sci. Post Phys.* **11**, 011 (2021).

<https://scipost.org/10.21468/SciPostPhys.11.1.011>

[P29] S. X. M. Riberolles, Q. Zhang, Elijah Gordon, N. P. Butch, Liqin Ke, J.-Q. Yan, and R. J. McQueeney, “Evolution of magnetic interactions in Sb-substituted MnBi_2Te_4 ”, *Phys. Rev. B* **104**, 064401 (2021).

<https://doi.org/10.1103/PhysRevB.104.064401>

[P28] E. Gati, J.M. Wilde, R. Khasanov, L. Xiang, S. Dissanayake, R. Gupta, M. Matsuda, F. Ye, B.Haberl, U. Kaluarachchi, R.J. McQueeney, A. Kreyssig, S.L. Bud'ko, P.C. Canfield, “Formation of short-range magnetic order and avoided ferromagnetic quantum criticality in pressurized LaCrGe_3 ,” *Phys. Rev. B*, **103** 075111 (2021).

<https://doi.org/10.1103/PhysRevB.103.075111>

[P27] S.X.M. Riberolles, T.V. Trevisan, B. Kuthanazhi, T.W. Heitmann, F. Ye, D.C. Johnston, S.L. Bud'ko, D.H. Ryan, P.C. Canfield, A. Kreyssig, A. Vishwanath, R.J. McQueeney, L.-L. Wang, P.P. Orth, B.G. Ueland, “Magnetic crystalline-symmetry-protected axion electrodynamics and field-tunable unpinned Dirac cones in EuIn_2As_2 ,” *Nat. Commun.* **12**, 999 (2021).

<https://doi.org/10.1038/s41467-021-21154-y>

[P26] S. Pakhira, T. Heitmann, S.X.M. Riberolles, B.G. Ueland, R.J. McQueeney, D.C. Johnston, D. Vaknin, “Zero-field magnetic ground state of EuMg_2Bi_2 ,” *Phys. Rev. B* **103**, 024408 (2021).

<https://doi.org/10.1103/PhysRevB.103.024408>

[P25] U.F. Kaneko, M.D. Teodoro, P.F. Gomes, N.S. Sangeetha, D.C. Johnston, “Electron-phonon coupling enhancement and displacive magnetostructural transition in SrCr_2As_2 under magneto-Raman spectroscopy,” *J. Phys.: Condens. Matter* **33**, 105401 (2020).

<https://doi.org/10.1088/1361-648X/abd0c3>

[P24] D.C. Johnston, “Noninteracting electrons in a prototypical one-dimensional sinusoidal potential,” *Am. J. Phys.* **88**, 1109 (2020).

<https://doi.org/10.1119/10.0001863>

[P23] S. Pakhira, N.S. Sangeetha, V. Smetana, A.-V. Mudring, D.C. Johnston, “Short-range ferromagnetic order due to Ir substitutions in single-crystalline $\text{Ba}(\text{Co}_{1-x}\text{Ir}_x)_2\text{As}_2$ ($0 \leq x \leq 0.25$),” *J. Physics: Condens. Matter* **33**, 115802 (2020).

<https://doi.org/10.1088/1361-648X/abd339>

[P22] D.C. Johnston, Reply to “Comment on ‘Magnetic structure and magnetization of z -axis helical Heisenberg antiferromagnets with XY anisotropy in high magnetic fields transverse to the

- helix axis at zero temperature,” *Phys. Rev. B*, **101** 026402 (2020).
<https://doi.org/10.1103/PhysRevB.101.026402>
- [P21] S. Pakhira, M. Kundu, R. Ranganathan, G. Mazumdar, “Studies on magnetocaloric effect of $\text{Tb}_2\text{Ni}_{0.90}\text{Si}_{2.94}$ compound,” *J. Phys.: Condens. Matter* **33**, 095804 (2020).
<https://doi.org/10.1088/1361-648X/abcdb2>
- [P20] Q.-P. Ding, N.S. Sangeetha, W.R. Meier, M. Xu, S.L. Bud’ko, P.C. Canfield, D.C. Johnston, Y. Furukawa, “Magnetic detwinning and biquadratic magnetic interaction in EuFe_2As_2 revealed by ^{153}Eu NMR,” *Phys. Rev. B* **102**, 180406 (2020).
<https://doi.org/10.1103/PhysRevB.102.180406>
- [P19] S. Pakhira, M.A. Tanatar, D.C. Johnston, “Magnetic, thermal, and electronic-transport properties of EuMg_2Bi_2 single crystals,” *Phys. Rev. B* **101**, 214407 (2020).
<https://doi.org/10.1103/PhysRevB.101.214407>
- [P18] B. Li, J.-Q. Yan, D. Pajerowski, E. Gordon, A.-M. Nedic, Y. Sizyuk, L. Ke, P.P. Orth, D. Vaknin, R.J. McQueeney, “Competing magnetic interactions in the antiferromagnetic topological insulator MnBi_2Te_4 ,” *Phys. Rev. Lett.* **124**, 167204 (2020).
<https://doi.org/10.1103/PhysRevLett.124.167204>
- [P17] F. Islam, R. Choudhary, Y. Liu, B.G. Ueland, D. Paudyal, T. Heitmann, R.J. McQueeney, D. Vaknin, “Controlling magnetic order, magnetic anisotropy, and band topology in semimetals $\text{Sr}(\text{Mn}_{0.9}\text{Cu}_{0.1})\text{Sb}_2$ and $\text{Sr}(\text{Mn}_{0.9}\text{Zn}_{0.1})\text{Sb}_2$,” *Phys. Rev. B* **102**, 085130 (2020).
<https://doi.org/10.1103/PhysRevB.102.085130>
- [P16] S. Pakhira, N.S. Sangeetha, V. Smetana, A.-V. Mudring, D.C. Johnston, “Ferromagnetic cluster-glass phase in $\text{Ca}(\text{Co}_{1-x}\text{Ir}_x)_{2-y}\text{As}_2$ crystals,” *Phys. Rev. B* **102**, 024410 (2020).
<https://doi.org/10.1103/PhysRevB.102.024410>
- [P15] S. Pakhira, R. Ranganathan, C. Mazumdar, “Resistivity and magnetoresistance properties of R_2NiSi_3 ($\text{R}=\text{Gd}, \text{Dy}, \text{Ho}, \text{Er}, \text{Tm}$) compounds,” *J. Magn. Magn. Mater.* **512**, 167055 (2020).
<https://doi.org/10.1016/j.jmmm.2020.167055>
- [P14] A. Pandey, A.K. Singh, S. Dan, K. Ghosh, I. Das, S. Tripathi, U. Kumar, R. Ranganathan, D.C. Johnston, C. Mazumdar, “Instability and evolution of the magnetic ground state in metallic perovskites $\text{GdRh}_3\text{C}_{1-x}\text{B}_x$,” *Phys. Rev. Mater.* **4**, 084411 (2020).
<https://doi.org/10.1103/PhysRevMaterials.4.084411>
- [P13] G.G. Kenning, D.L. Schlagel, V. Thompson, “Experimental determination of the critical spin-glass correlation length in single-crystal CuMn ,” *Phys. Rev. B*, **102**, 064427 (2020).
<https://doi.org/10.1103/PhysRevB.102.064427>
- [P12] S. Pakhira, R.N. Bhowmik, M. Avdeev, R. Ranganathan, C. Mazumdar, “Modification of magnetic ground state in $\text{TbNi}_{0.90}\text{Si}_{2.94}$ by thermal annealing,” *Intermetallics* **124**, 106874 (2020).
<https://doi.org/10.1016/j.intermet.2020.106874>
- [P11] D. Vaknin, S. Pakhira, D. Schlagel, F. Islam, J. Zhang, D. Pajerowski, C.Z. Wang, D.C. Johnston, R.J. McQueeney, “Localized singlets and ferromagnetic fluctuations in the dilute magnetic topological insulator $\text{Sn}_{0.95}\text{Mn}_{0.05}\text{Te}$,” *Phys. Rev. B* **101**, 140406 (R) (2020).
<https://doi.org/10.1103/PhysRevB.101.140406>
- [P10] N.S. Sangeetha, S. Pakhira, D.H. Ryan, V. Smetana, A.-V. Mudring, D.C. Johnston, “Magnetic phase transitions in $\text{Eu}(\text{Co}_{1-x}\text{Ni}_x)_{2-y}\text{As}_2$ single crystals,” *Phys. Rev. Mater.* **4**, 084407 (2020).
<https://doi.org/10.1103/PhysRevMaterials.4.084407>

- [P9] F. Islam, E. Gordon, P. Das, Y. Liu, L. Ke, D.L. Abernathy, R.J. McQueeney, D. Vaknin, “Spin dynamics in the antiferromagnetic oxypnictides and fluoropnictides: LaMnAsO, LaMnSbO, and BaMnAsF,” *Phys. Rev. B*, **101**, 155119 (2020).
<https://doi.org/10.1103/PhysRevB.101.155119>
- [P8] D.M. Pajerowski, D.K. Pratt, S.E. Hahn, W. Tian, G.E. Granroth, A.I. Kolesnikov, A.A. Taskin, Y. Ando, R.J. McQueeney, “Spin waves above and below the Verwey transition in TbBaFe₂O₅,” *Phys. Rev. B*, **101**, 064418 (2020).
<https://doi.org/10.1103/PhysRevB.101.064418>
- [P7] D. Rigitano, D. Vaknin, G.E. Barberis, E. Granado, “Raman scattering from one and two magnons in magnetoelectric LiNiPO₄,” *Phys. Rev. B*, **101**, 024417 (2020).
<https://doi.org/10.1103/PhysRevB.101.024417>
- [P6] N.S. Sangeetha, V. Smetana, A.V. Mudring, D.C. Johnston, “Helical antiferromagnetic ordering in EuNi_{1.95}As₂ single crystals,” *Phys. Rev. B*, **100**, 094438 (2019).
<https://doi.org/10.1103/PhysRevB.100.094438>
- [P5] J.M. Wilde, A. Kreyssig, D. Vaknin, N.S. Sangeetha, B. Li, W. Tian, P.P. Orth, A.I. Goldman, D.C. Johnston, B.G. Ueland, R.J. McQueeney, “Helical magnetic ordering in Sr(Co_{1-x}Ni_x)₂As₂,” *Phys. Rev. B*, **100**, 161113 (R) (2019).
<https://doi.org/10.1103/PhysRevB.100.161113>
- [P4] J.Q. Yan, W. Tian, H.B. Cao, S. Chi, F. Ye, A. Llobet, A. Puretzy, Q. Chen, J. Ma, Y. Ren, J.G. Cheng, J.S. Zhou, M.A. McGuire, R.J. McQueeney, “Lattice distortion in the spin-orbital entangled state in RVO₃ perovskites,” *Phys. Rev. B*, **100**, 184423 (2019).
<https://doi.org/10.1103/PhysRevB.100.184423>
- [P3] Q. Zhai, C. Martin-Mayor, D.L. Schlagel, G.G. Kenning, and R.L. Orbach, “Slowing down of spin glass correlation length growth: Simulations meet experiments,” *Phys. Rev. B*, **100**, 094202 (2019).
<https://doi.org/10.1103/PhysRevB.100.094202>
- [P2] J.Q. Yan, S. Okamoto, M.A. McGuire, A.F. May, R.J. McQueeney, B.C. Sales, “Evolution of structural, magnetic, and transport properties in MnBi_{2-x}Sb_xTe₄,” *Phys. Rev. B*, **100**, 104409 (2019).
<https://doi.org/10.1103/PhysRevB.100.104409>
- [P1] D. C. Johnston, “Cycloidal Paths in Physics as Superpositions of Translational and Rotational Motions”, *Am. J. Phys.* **87**, 802 (2019).
<https://doi.org/10.1119/1.5115340>

Correlated Quantum Materials

Michael A. McGuire, Brian C. Sales, Jiaqiang Yan, Andrew F. May, David Mandrus

Materials Science and Technology Division

Oak Ridge National Laboratory

Program Scope

Correlated quantum materials with collective emergent behavior, such as quantum transport, superconductivity, and exotic magnetism, are expected to form the basis for next-generation energy and information technologies. Magnetism underlies many of the most interesting emergent behaviors, and its understanding is built upon careful experimental studies of magnetic order and interactions in high quality crystals. For example, while theoretical treatment of topological electronic materials has become reasonably predictive without correlations, the inclusion of magnetism will require experimental data to both inform and test theoretical models. The overarching goal of this project is to advance our understanding of correlated quantum materials through discovery, development, and investigation of model materials that exhibit magnetic order, topological order, and collective phenomena. To achieve this, we have three specific aims: (1) Understand how structure and symmetry dictate magnetism and excitations in cleavable magnetic materials, (2) Control topological states in materials with intrinsic magnetism, and (3) Unlock emergent correlations in materials with flat bands. Two unifying themes are magnetism and anisotropic layered crystal structures. Our research is designed to answer key scientific questions in these specific aims through synthesis of high-quality crystals and investigation of their physical properties using electrical and thermal transport, specific heat, magnetization, and crystallographic measurements. The most interesting materials are pursued through collaborations involving theory, neutron scattering, angle resolved photoemission, and scanning tunneling microscopy. This research directly addresses the ability to control and exploit quantum mechanical behaviors targeting novel functionality, which is a priority research direction in the BES Basic Research Needs workshop report on Quantum Materials.

Recent Progress

Below we highlight examples of progress made recently in each of our specific aims

Cleavable magnetic materials. Fe_5GeTe_2 is a van der Waals layered ferromagnetic metal with a transition temperature near room temperature [1,2]. This ferromagnetism persists in exfoliated flakes at least down to a thickness of four unit cells [1], making this a particularly promising material for incorporating magnetism into functional van der Waals heterostructures. We recently found that magnetic order in this compound can be tuned dramatically by replacing some of the iron with cobalt [3]. This is illustrated in Figure 1. Low cobalt concentrations first affect the anisotropy, switching the material from an axial ferromagnet to a planar one. Larger amounts of

cobalt then change the material to an axial antiferromagnet, and change the crystallographic layer stacking sequence as well. We see evidence that cobalt prefers one specific iron site, shown in lighter orange in the figure, and through collaboration with theory confirmed that this preference and the change in layer stacking are both required to achieve the observed switching from ferro- to antiferromagnetism.

Topological magnetic materials. Magnetic fields and magnetic order play important roles in defining the global symmetry breaking in topological materials that determine the types of quantum states and responses that can be expected. Materials in which the magnetic order is realized on a separate sublattice from the topological electronic states are particularly interesting, since in principle they may allow separate chemical control of magnetism and topology within a single crystal. This has led to a great deal of interest in the series $(\text{MnTe})_n(\text{Bi}_2\text{Te}_3)_m$, which has magnetic MnTe layers and topological Bi_2Te_3 layers. These and related intrinsically magnetic topological insulators

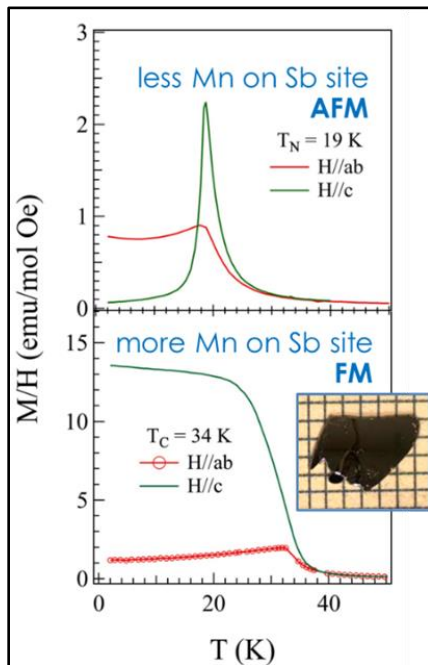


Figure 2. Magnetic susceptibility data showing the effect of Mn-Sb antisite defects on the magnetic order in MnSb_2Te_4 .

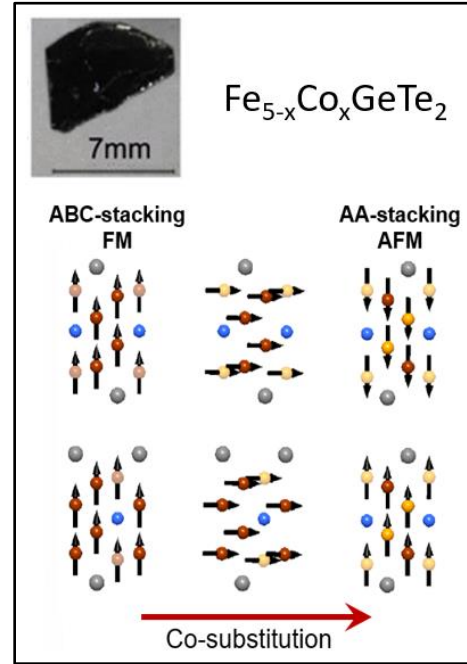


Figure 1. Partially replacing iron with cobalt in Fe_5GeTe_2 controls the magnetic ground state and layer stacking sequence.

may produce Chern insulators, axion insulators, and Weyl semimetals, and allow the observation of quantized topological phenomena.

To develop a better understanding of the physics in these materials, we initiated a collaborative effort involving careful crystal growth and characterization for the series $\text{Mn}(\text{Bi}_{1-x}\text{Sb}_x)_2\text{Te}_4$ [4-7]. One primary aim was to explain different behaviors observed in different samples of MnBi_2Te_4 that are thought to be related to defects. This led to the discovery of the key role played by Mn atoms located at the Bi or Sb site in the crystals. These antisite defects strongly affect the magnetic interactions and resulting magnetic order. This discovery was enabled by focusing on the Sb analogue, in which the antisite disorder is easier to study because it is more pronounced and can be controlled through synthesis [6]. The concentration, distribution, and effects of magnetic defects in this material were characterized using magnetic and transport measurements, neutron diffraction, scanning transmission electron microscopy, scanning tunneling microscopy, and theoretical calculations.

It was found that misplaced Mn ions, those in the Sb layer, have moments that align opposite those in the main Mn layer. This in turn affects the magnetic coupling from one slab to the next. As shown in Figure 2, this results in an overall antiferromagnetic structure when there is less Mn on the Sb site, and an overall ferromagnetic structure, and higher transition temperature, when there is more. Similar effects are expected to exist in other members of this family of intrinsically magnetic topological insulators, and likely in other families as well. This work should provide a basis for understanding similar materials and accelerate the development of new magnetic topological materials through optimizing defect configurations and concentrations.

Flat band materials. The symmetry of the kagome net generates flat electronic bands and Dirac crossings that provide opportunities to explore correlations and topology in materials starting from a relatively simple model. We are specifically interested in new sources of correlated behavior and instabilities associated with the peak in the electronic density of states related to the flat band. The CoSn structure type contains a kagome net of transition metal atoms and provides a good model system for studying these effects (Figure 3).

We have grown and studied many CoSn-type compounds as single crystals, and this has led to several interesting discoveries. For example, the paramagnetic susceptibility provides a measure of the nearness of the flat bands to the Fermi level [8], tuning the electronic structure in $\text{Fe}_{1-x}\text{Co}_x\text{Sn}$ produces a rich phase diagram of axial, canted, and planar magnetic structures with expected topological consequences [9], and electron doping the Pauli paramagnet CoSn using indium drives the material toward a magnetic instability [10]. These findings provide a foundation for pursuing new routes to correlated behaviors using flat bands enforced by lattice geometry.

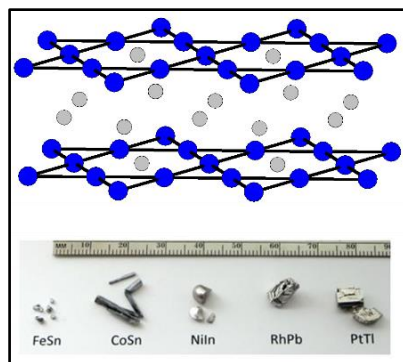


Figure 3. Kagome nets of transition metals (blue) in the CoSn structure, and crystals of several compounds in this system.

Future Plans

Building on our recent progress in these three areas, our future work will focus on the following efforts. Use neutron scattering to understand magnetic interactions in layered compounds and how they can guide development of new 2D magnetic materials. Explore layered materials with thicker magnetic slabs as a route to higher transition temperatures. Determine magnetic and topological properties of $(\text{MnTe})_n(\text{Bi}_2\text{Te}_3)_m$ compounds with multiple MnTe layers ($n > 1$). Understand the underlying physics that determines the robustness of quantization in MnBi_2Te_4 related materials. Discover new magnetic (or superconducting) instabilities in CoSn-based flat band materials. Develop new model systems for flat band physics to understand how distortion of the kagome net, spin-orbit coupling, electron count, and intrinsic magnetism affect ground states and behaviors.

References

- [1] A.F. May, D. Ovchinnikov, Q. Zheng, R. Hermann, S. Calder, B. Huang, Z. Fei, Y. Liu, X. Xu, and M.A. McGuire, *ACS Nano* 13, 4436 (2019).
- [2] A.F. May, C.A. Bridges, and M.A. McGuire, *Phys. Rev. Mater.* 3, 104401 (2019).
- [3] A.F. May, M.-H. Du, V.R. Cooper, M.A. McGuire, *Phys. Rev. Mater.* 4, 074008 (2020).
- [4] Z. Huang, M. H. Du, J.-Q. Yan, W. Wu, *Phys. Rev. Mater.* 4, 121202 (2020).
- [5] M. H. Du, J. Q. Yan, V. R. Cooper, and M. Eisenbach, *Adv. Funct. Mater.* 31, 2006516 (2021).
- [6] Yaohua Liu, Lin-Lin Wang, Qiang Zheng, Zengle Huang, Xiaoping Wang, Miaofang Chi, Yan Wu, Bryan C Chakoumakos, Michael A McGuire, Brian C Sales, Weida Wu, Jiaqiang Yan, *Phys. Rev. X* 11, 021033 (2021).
- [7] W. B. Ge, P. M. Sass, J. Q. Yan, S. H. Lee, Z. Q. Mao, and W. D. Wu, *Phys. Rev. B* 103, 134403 (2021).
- [8] W.R. Meier, M.-H. Du, S. Okamoto, N. Mohanta, A.F. May, M.A. McGuire, C.A. Bridges, G.D. Samolyuk, B.C. Sales, *Phys. Rev. B* 102, 075148 (2020).
- [9] W.R. Meier, J. Yan, M.A. McGuire, X. Wang, A.D. Christianson, B.C. Sales, *Phys. Rev. B* **100**, 184421 (2019).
- [10] B. C. Sales, W. R. Meier, A. F. May, J. Xing, J.-Q. Yan, S. Gao, Y. H. Liu, M. B. Stone, A. D. Christianson, Q. Zhang, M. A. McGuire, *Phys. Rev. Mater.* 5, 044202 (2021).

Publications supported by this project (Sept 2019-Aug 2021)

This project supported 101 publications during this period. Selected publications are listed here.

1. S. X. M. Riberolles, Q. Zhang, E. Gordon, N. P. Butch, L. Q. Ke, J. Q. Yan, R. J. McQueeney, Evolution of magnetic interactions in Sb-substituted MnBi_2Te_4 , *Phys. Rev. B.*, 104, 064401 (2021). ID 166379
2. C. Balz, L. Janssen, P. Lampen-Kelley, A. Banerjee, Y. H. Liu, J. Q. Yan, D. G. Mandrus, M. Vojta, and S. E. Nagler, Field-induced intermediate ordered phase and anisotropic interlayer interactions in $\alpha\text{-RuCl}_3$, *Phys. Rev. B* 103, 174417 (2021).
3. W. B. Ge, P. M. Sass, J. Q. Yan, S. H. Lee, Z. Q. Mao, and W. D. Wu, Direct evidence of ferromagnetism in MnSb_2Te_4 , *Phys. Rev. B* 103, 134403 (2021).
4. Q. N. Jiang, C. Wang, P. Malinowski, Z. Y. Liu, Y. Shi, Z. Lin, Z. Y. Fei, T. C. Song, D. Graf, S. Chikara, X. D. Xu, J. Q. Yan, D. Xiao, and J. H. Chu, Quantum oscillations in the field-induced ferromagnetic state of $\text{MnBi}_{2-x}\text{Sb}_x\text{Te}_4$, *Phys. Rev. B* 103, 205111 (2021).
5. Y. Lai, L. Q. Ke, J. Q. Yan, R. D. McDonald, and R. J. McQueeney, Defect-driven ferrimagnetism and hidden magnetization in MnBi_2Te_4 , *Phys. Rev. B* 103, 184429 (2021).

6. Yaohua Liu, Lin-Lin Wang, Qiang Zheng, Zengle Huang, Xiaoping Wang, Miaofang Chi, Yan Wu, Bryan C Chakoumakos, Michael A McGuire, Brian C Sales, Weida Wu, Jiaqiang Yan, Site Mixing for Engineering Magnetic Topological Insulators, *Phys. Rev. X* 11, 021033 (2021).
7. W. R. Meier, B. C. Chakoumakos, S. Okamoto, M. A. McGuire, R. P Hermann, G. D. Samolyuk, S. Gao, Q. Zhang, M. B. Stone, A. D. Christianson, B. C. Sales, A Catastrophic Charge Density Wave in BaFe_2Al_9 , *Chem. Mater.* 33, 2855 (2021).
8. D. Ovchinnikov, X. Huang, Z. Lin, Z. Y. Fei, J. Q. Cai, T. C. Song, M. H. He, Q. N. Jiang, C. Wang, H. Li, Y. Y. Wang, Y. Wu, D. Xiao, J. H. Chu, J. Q. Yan, C. Z. Chang, Y. T. Cui, and X. D. Xu, Intertwined Topological and Magnetic Orders in Atomically Thin Chern Insulator MnBi_2Te_4 , *Nano Lett.* 21 (6), 2544-2550 (2021).
9. B. C. Sales, W. R. Meier, A. F. May, J. Xing, J.-Q. Yan, S. Gao, Y. H. Liu, M. B. Stone, A. D. Christianson, Q. Zhang, M. A. McGuire, Tuning the flat bands of the kagome metal CoSn with Fe, In or Ni doping, *Phys. Rev. Mat.* 5, 044202 (2021).
10. J. Cenker, B. Huang, N. Suri, P. Thijssen, A. Miller, T. Song, T. Taniguchi, K. Watanabe, M. A. McGuire, D. Xiao, and X. Xu, Direct observation of two-dimensional magnons in atomically thin CrI_3 , *Nat. Phys.* 17, 20 (2021). ID 144840
11. M. H. Du, J. Q. Yan, V. R. Cooper, and M. Eisenbach, Tuning Fermi Levels in Intrinsic Antiferromagnetic Topological Insulators MnBi_2Te_4 and MnBi_4Te_7 by Defect Engineering and Chemical Doping, *Adv. Funct. Mater.* 31, 2006516 (2021). ID 142006
12. M. A. McGuire, Cleavable magnetic materials from van der Waals layered transition metal halides and chalcogenides, *J. Appl. Phys.* 128, 110901 (2020).
13. W. R. Meier, M. H. Du, S. Okamoto, N. Mohanta, A. F. May, M. A. McGuire, C. A. Bridges, G. D. Samolyuk, and B. C. Sales, Flat bands in the CoSn -type compounds, *Phys. Rev. B* 102, 075148 (2020).
14. B. Li, J.Q. Yan, D.M. Pajerowski, E. Gordon, A.M. Nedic, P.P. Orth, D. Vadkin, R.J. McQueeney, Competing magnetic interactions in the Antiferromagnetic Topological Insulator MnBi_2Te_4 , *Phys. Rev. Lett.* 124, 167204 (2020).
15. A.F. May, M. H. Du, V. R. Cooper, and M. A. McGuire, Tuning magnetic order in the van der Waals metal Fe_5GeTe_2 by cobalt substitution, *Phys. Rev. Mater.* 4, 074008 (2020).
16. A.F. May, J. Q. Yan, and M. A. McGuire, A practical guide for crystal growth of van der Waals layered materials, *J. Appl. Phys.* 128, 051101 (2020).
17. J. Q. Yan, Y. H. Liu, D. S. Parker, Y. Wu, A. A. Aczel, M. Matsuda, M. A. McGuire, and B. C. Sales, A-type antiferromagnetic order in MnBi_4Te_7 and $\text{MnBi}_6\text{Te}_{10}$ single crystals, *Phys. Rev. Mater.* 4, 054202 (2020).
18. B. C. Sales, V. O. Garlea, M. B. Stone, M. D. Lumsden, S. E. Nagler, D. Mandrus, and M. A. McGuire, Possible observation of Kondo screening cloud in $\text{Yb}_{14}\text{MnSb}_{11}$, *Phil. Mag.* 100, 1204 (2020).
19. B.C. Sales, J. -Q. Yan, W. R. Meier, A. D. Christianson, S. Okamoto, and M. A. McGuire, Electronic, magnetic and thermodynamic properties of the kagome layered compound FeSn , *Phys. Rev. Mater.* 3, 114203 12.

20. W. R. Meier, J.-Q. Yan, M. A. McGuire, X. P. Wang, A. D. Christianson, and B. C. Sales, Reorientation of antiferromagnetism in cobalt doped FeSn *Phys. Rev. B* 100, 184421 (2019).
21. A. F. May, C. A. Bridges, and M. A. McGuire, Physical properties and thermal stability of $\text{Fe}_{5-x}\text{GeTe}_2$ single crystals, *Phys. Rev. Mater.* 3, 104401 (2019).
22. J. Q. Yan, S. Okamoto, M. A. McGuire, A. F. May, R. J. McQueeney, and B. C. Sales, Evolution of structural, magnetic, and transport properties in $\text{MnBi}_{2-x}\text{Sb}_x\text{Te}_4$, *Phys. Rev. B* 100, 104409 (2019).
23. B. Huang, M. A. McGuire, A. F. May, D. Xiao, P. Jarillo-Herrero, and X. Xu, Emergent phenomena and proximity effects in two-dimensional magnets and heterostructures, *Nat. Mater.* 19, 1276 (2020).
24. M.-H. Du, J. Yan, V. R. Cooper, and M. Eisenbach, Tuning fermi levels in intrinsic antiferromagnetic topological insulators MnBi_2Te_4 and MnBi_4Te_7 by defect engineering and chemical doping, *Adv. Funct. Mater.* 2006516, (2020).
25. W. Ko, M. Kolmer, J. Q. Yan, A. D. Pham, M. M. Fu, F. Lupke, S. Okamoto, Z. Gai, P. Ganesh, and A. P. Li, Realizing gapped surface states in the magnetic topological insulator $\text{MnBi}_{2-x}\text{Sb}_x\text{Te}_4$, *Phys. Rev. B* 102, 115402 (2020).
26. X. Kong, G. D. Nguyen, J. Lee, C. Lee, S. Calder, A. F. May, Z. Gai, A.-P. Li, L. Liang, and T. Berlijn, Interlayer magnetism in $\text{Fe}_{3-x}\text{GeTe}_2$, *Phys. Rev. Mater.* 4, 094403 (2020).
27. P. M. Sass, J. Kim, D. Vanderbilt, J. Q. Yan, and W. D. Wu, Robust A-type order and spin-flop transition on the surface of the antiferromagnetic topological insulator MnBi_2Te_4 , *Phys. Rev. Lett.* 125, 037201 (2020).
28. P. M. Sass, W. Ge, J.-Q. Yan, D. Obeysekera, J. J. Yang, and W. D. Wu, Magnetic imaging of domain walls in the antiferromagnetic topological insulator MnBi_2Te_4 , *Nano Lett.* 20, 2609 (2020).
29. J. X. Ding, J. L. Niedziela, D. Bansal, J. L. Wang, X. He, A. F. May, G. Ehlers, D. L. Abernathy, A. Said, A. Alatas, Y. Ren, G. Arya, and O. Delaire, Anharmonic lattice dynamics and superionic transition in AgCrSe_2 , *PNAS* 117, 3930 (2020).
30. T. Song, Z. Fei, M. Yankowitz, Z. Lin, Q. Jiang, K. Hwangbo, Q. Zhang, B. Sun, T. Taniguchi, K. Watanabe, M. A. McGuire, D. Graf, T. Cao, J. H. Chu, D. H. Cobden, C. R. Dean, D. Xiao, and X. Xu, Switching 2D magnetic states via pressure tuning of layer stacking, *Nature Mater.* 18, 1298 (2019).

Emerging Materials

John F. Mitchell and Daniel Phelan (Argonne National Laboratory); Nirmal Ghimire (George Mason University)

Program Scope

Emerging Materials pursues materials synthesis and single crystal growth drivers for foundational research on newly discovered quantum materials. The program's materials focus lies primarily with correlated electron, quantum magnet, and dielectric transition metal oxides, but we have expanded recently to embrace chalcogenides, pnictides, and intermetallic compounds showing topological behavior. We concentrate along three primary research foci: (i) understanding charge and magnetic states in transition metal compounds, in particular low-dimensional materials (ii) exploring transport phenomena in low-symmetry topological quantum matter, and (iii) expanding today's framework of disorder and random fields, to more deeply understand the impact of heterogeneity and disorder on the short-range structure of matter. To enable much of this foundational science, we continue to emphasize the need to expand the boundaries of crystal synthesis and to exploit a broad range of x-ray and neutron scattering tools to understand structural and magnetic phenomena in quantum matter. Looking ahead, our research agenda is evolving to study the impact of "degeneracy breaking" on quantum materials, in particular, correlated electron nickelates, topological matter, and quantum ferroelectrics and relaxors.

Recent Progress

- *Discovered 'Chiral Nematicity' in YMn_6Sn_6* —The so-called 116 kagome lattice metals RMn_6Sn_6 are of interest due to the flat-band electronic configuration of the metal and the change in topological properties with orientation of rare earth moment.[1] We mapped out complex H-T phase diagram in this kagome lattice metal and identified that an incommensurate transverse conical magnetic structure has a topological Hall signal that increases with T. With Igor Mazin, we showed that this could be explained by the presence of a fluctuating chiral magnetic texture whose population increases with T.
- We continued our work in the trilayer nickelates, focusing on both the metallic $Pr_4Ni_3O_8$ and the charge- and spin-stripe ordered $La_4Ni_3O_8$ material. Our objective is to understand how this material relates to cuprate superconductors as well as the infinite layer nickelate superconductor, $Nd_{1-x}Sr_xNiO_2$. [2] With Dan Dessau (Colorado), measured band structure of $Pr_4Ni_3O_8$ (Pr438) showing that it may express diffusive electron transport beyond the Planckian limit, which would provide a different view on current pictures of the 'strange metal' phase in overdoped cuprates. With Mark Dean (BNL), we measured magnons in La438 and showed superexchange is comparable to cuprates.

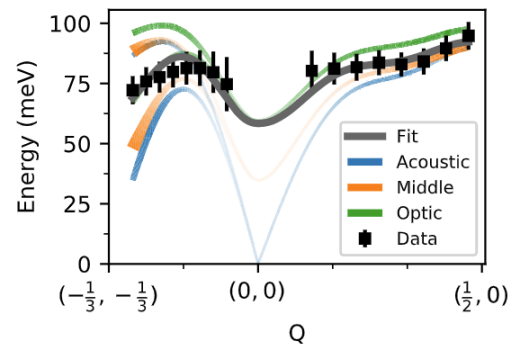


Figure 1. Magnon dispersion of $La_4Ni_3O_8$. From Ref. 3.

- *Explored Synthesis and Structure of Bulk $Nd_{1-x}Sr_xNiO_2$* —Although thin films of this series have been shown to superconduct, no bulk superconductivity has been reported. We were interested in the synthetic pathways to the bulk infinite layer materials, so we undertook a comprehensive ex situ and in situ study of the key reduction process that converts $NdNiO_3$ to $NdNiO_2$, compared several soft chemistry approaches and published the first structural study of the Sr-doped material. Importantly, we find no evidence of long range magnetic order in any of our samples.
- *Intertwined Density Waves in $R_4Ni_3O_{10}(R=La,Pr)$* —Combining scattering with theoretical modeling, we demonstrated that this layered Ruddlesden-Popper nickelate expresses an intertwined CDW-SDW state at the previously identified metal-metal transition. This is the first reported itinerant SDW in 3d transition metal oxides and it provides a conceptual bridge between the 3D $LaNiO_3$ perovskite (metallic, no order)[4] and the well-studied 2D $La_{1-x}Sr_xNiO_4$ layered perovskites (insulating, long-range ordered stripes).[5]
- *Multi-orbital degeneracy lifting in $MgTi_2O_4$* —With Simon Billinge (Columbia/BNL), we showed that the ordered $Ti^{3+}-Ti^{3+}$ dimer only partially dissociates above the insulator-metal transition. We attribute this behavior to a multi-orbital degeneracy lifted state, demonstrating the generality of the concept of an orbitally-degeneracy-lifted liquid state first seen by us in $CuIr_2S_4$.
- *Synthesis and Diffuse Scattering from $Ba_2(Nd/Pr)FeNb_4O_{15}$* —We reported the first floating-zone synthesis of the filled tetragonal tungsten bronze (TTB) relaxor ferroelectrics $Ba_2PrFeNb_4O_{15}$ and $Ba_2NdFeNb_4O_{15}$. By comparing the diffuse scattering observed from these “filled” TTB structures to that observed in “unfilled” TTB $Sr_{1-x}Ba_xNb_2O_6$, we have been able to show that common features observed in both systems are not related to the random fields generated by cation vacancies in the unfilled structures. Although dielectric properties were found to be strongly sensitive to anion (oxygen) stoichiometry, we found that the forms of local order in these systems was not.
- *Interactions and Frustration in $(Fe,Ga)_2TiO_5$* : With Art Ramirez (UCSC), we showed that the unusual anisotropic spin-glass Fe_2TiO_5 is related to the freezing of antiferromagnetic ‘surfboard-shaped’ regions via analysis of high temperature magnetometry and diffuse scattering data. Inelastic neutron scattering experiments show a shift in the spectral weight with temperature, indicating that a large percentage of the spins, but not all, are frozen in the ground-state. Crystal growth, magnetometry, and neutron scattering experiments were

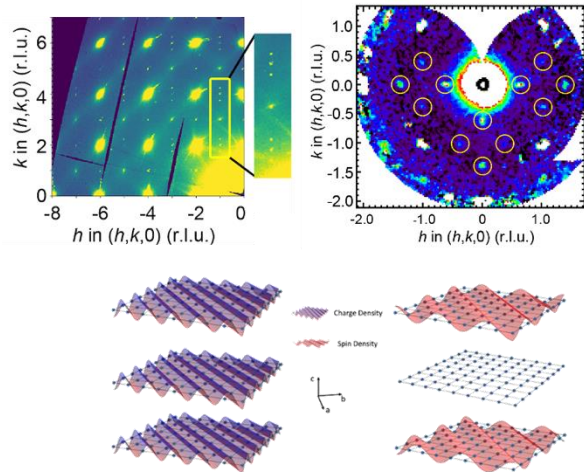


Figure 2. (top left) x-ray diffraction showing incommensurate charge superlattice. (top right) incommensurate magnetic structure revealed by neutron diffraction (bottom) schematic of density waves in a single trilayer based on analysis of scattering patterns. From Ref. 6.

performed on Ga-substituted crystals and demonstrated the reduction of exchange interactions and modification in the surfboard shape with magnetic dilution.

- *Anomalous magnetic and transport properties of EuCd_2As_2* : We have performed anisotropic transport measurements on EuCd_2As_2 to explore the Weyl and potential topological physics in collaboration with Keith Taddei (ORNL) and characterized the directionally dependent Hall effect and magnetoresistance. We are currently developing models to rationalize these transport properties with the spin structure determined by neutron scattering.
- *Magnetic interactions in the frustrated Cairo lattice*: We have grown polycrystalline and single crystal samples of the frustrated pentagonal system, $\text{Bi}_2(\text{Fe,Ga})_4\text{O}_9$. In collaboration with Art Ramirez (UCSC), the effects of magnetic dilution are being investigated using a combination of thermodynamic and magnetic measurements. The expected outcome is a testing of a recent theory proposed by Syzranov and Ramirez [7] that predicts a hidden energy scale that drives glass transitions in the presence of disorder.
- *Other research outcomes*: Mapping out full Fermi surface of the triple nodal topological metal Pd_3Pb , corroborating theory and established definitively the presence of topological electrons where band structure predicted; Measured and modeled magnons for the first time in $\alpha\text{-Li}_2\text{IrO}_3$ providing an overall energy scale for the Kitaev exchange in the iridates; demonstrated that oxygen vacancies naturally created during growth of LaNiO_3 can be reversibly healed to reveal intrinsic behavior.

Future Plans

Our future work will follow along three themes —

Quantum states and critical behavior in nickel oxides: We will explore melting of nematic stripe phases into a correlated metal and quantum critical behavior near a MIT in 3D and quasi-2D systems and investigate bulk infinite layer nickelates shown to superconduct in thin film form.

Degeneracy breaking in correlated and topological matter: We will explore frustration-driven orbital degeneracy lifting in correlated materials. We will also test the recently proposed crystal Hall effect and the role of electron-phonon coupling on topological band properties.

Ferroelectrics and relaxors in the quantum limit: We will investigate the potential for quantum criticality in these materials and its expression through static and dynamic properties.

References

1. J.-X. Yin et al., Nature 583, 533 (2020).
2. D. Li et al., Nature 572, 624 (2019).
3. J. Q. Lin et al., Phys. Rev. Lett. 126, 087001 (2021).
4. J.-S. Zhou et al., Phys Rev B 67, 020404 (2003).
5. H. Yoshizawa et al., Physical Review B 61, R854 R857 (2000).
6. J. Zhang et al., Nat Commun 11, 6003 (2020).
7. S.V. Syzranov and A.P. Ramirez, arXiv 2105.08070.

Publications

22 publications were supported by this FWP in the twenty-four months since the last ECMP PI meeting. A selection most relevant to the discussion above are listed below.

1. Wang, B.; Zheng, H.; Ren, Y.; Krogstad, M.; Mitchell, J.F.; Phelan, D. “Single Crystal Growth of Relaxor Ferroelectric $\text{Ba}_2\text{PrFeNb}_4\text{O}_{15}$ by the Optical Floating Zone Method,” *Cryst. Growth and Design* **2019**, 12,7249.
2. Khan, M.A.; Zhang, Q.; Bao, J.-K.; Fishman, R.S.; Botana, A.S.; Choi, Y.; Fabbris, G.; Haskel, D.; Singleton, J.; Mitchell, J.F. “Steplike Metamagnetic Transitions in a Honeycomb Lattice Antiferromagnet, $\text{Tb}_2\text{Ir}_3\text{Ga}_9$,” *Phys. Rev. Materials* **2019**, 3, 114411
3. Zheng, H.; Wang, B.-X., Phelan, D.; Zheng, J.; Ren, Y.; Krogstad, M.J.; Rosenkranz, R.; Osborn, R.; Mitchell, J. F. “Oxygen Inhomogeneity and Reversibility in Single Crystal $\text{LaNiO}_{3-\delta}$ ” *Crystals* **2020**, 10, 557. **Invited Article**
4. Wang, B.-X.; Zheng, H.; Krivyakina, E.; Chmaissem, O.; Papa Lopes, P.; Lynn, J.; Gallington, L.C.; Ren, Y.; Rosenkranz, S.; Mitchell, J. F.; Phelan, D. “Synthesis and characterization of bulk $\text{Nd}_{1-x}\text{Sr}_x\text{NiO}_2$ and $\text{Nd}_{1-x}\text{Sr}_x\text{NiO}_3$ ” *Phys. Rev. M* **2020**, 4, 084409. **Editor’s Suggestion**
5. Zhang, J.; Phelan, D.; Botana, A. S.; Chen, Y.-S.; Zheng, H.; Krogstad, M.; Wang, S. G.; Qiu, Y.; Rodriguez-Rivera, J. A.; Osborn, R.; Rosenkranz, S.; Norman, M. R.; Mitchell, J. F. “Intertwined Density Waves in a Metallic Nickelate.” *Nat. Commun.* **2020**, 11 (1), 6003.6.
6. Ghimire, N.J.; Dally, R.L.; Poudel, L.; Jones, D.C.; Michel, D.; Magar, N.T.; Bluel, M.; McGuire, M.A.; Jiang, J.S.; Mitchell, J.F.; Lynn, J.W.; Mazin, I.I. “Competing magnetic phases and fluctuation-driven scalar chirality in the kagome metal YMn_6Sn_6 .” *Sci. Advances* **2020**; 6:eabe2680.
7. Upton, M.; Zhang, J.; Zheng, H.; Said, A.; Mitchell, J.F. “Electronic coupling in square planar $\text{La}_4\text{Ni}_3\text{O}_8$ ” *J. Phys. Cond. Matt.* **2020**, 32, 425503.
8. Yang, L.; Koch, R. J.; Zheng, H.; Mitchell, J.F.; Yin, W.; Tucker, M. G.; Billinge, S. J. L.; Bozin, E. S. “Two-Orbital Degeneracy Lifted State as a Local Precursor to a Metal-Insulator Transition in MgTi_2O_4 .” *Phys. Rev. B* **2020**, 102, 235128.
9. Chun, S. H.; Stavropoulos, P. P.; Kee, H.-Y.; Sala, M. M.; Kim, J.; Kim, J.-W.; Kim, B. J.; Mitchell, J. F.; Kim, Y.-J. “Optical Magnons with Dominant Bond-Directional Exchange Interactions in a Honeycomb Lattice Iridate $\alpha\text{-Li}_2\text{IrO}_3$.” *Phys. Rev. B.* **2021**, 103, L020410.
10. Lopes, P.; Chung, Dong Young; Rui, Xue; Zheng, Hong; He, Haiying; Farinazzo Bergamo Dias Martins, Pedro; Strmcnik, Dusan; Stamenkovic, Vojislav; Zapol, Peter; Mitchell, J.F.; Klie, Robert; Markovic, Nenad. “Dynamically Stable Active Sites from Surface Evolution of Perovskite Materials During the Oxygen Evolution Reaction.” *J. Am. Chem. Soc.* **2021**, 143, 2741.
11. Lin, J. Q.; Arribi, P. V.; Fabbris, G.; Botana, A. S.; Meyers, D.; Miao, H.; Shen, Y.; Mazzone, D. G.; Feng, J.; Chiuzbaian, S. G.; Nag, A.; Walters, A. C.; Garcia-Fernandez, M.; Zhou, K.-J.; Pellicciari, J.; Jarrige, I.; Freeland, J. W.; Zhang, J.; Mitchell, J.F.; Bisogni, V.; Liu, X.; Norman, M. R.; Dean, M. P. M. “Strong Superexchange in a $d^{9-\delta}$ Nickelate Revealed by Resonant Inelastic X-Ray Scattering.” *Phys. Rev. Lett.* **2021**, 126, 087001.
12. LaBarre, P. G.; Phelan, D.; Xin, Y.; Ye, F.; Besara, T.; Siegrist, T.; Syzranov, S. V.; Rosenkranz, S.; Ramirez, A. P. “Fluctuation-Induced Interactions and the Spin-Glass Transition in Fe_2TiO_5 ,” *Phys. Rev. B* **2021**, 103, L220404.

Local and Itinerant Magnetism in 2D van der Waals Materials

Ming Yi, Department of Physics and Astronomy, Rice University

Program Scope

The proposed program is aimed to provide fundamental understanding of the microscopic interactions of the low dimensional magnetic systems across the semiconducting and metallic members of the two-dimensional van der Waals magnets via direct measurement of the single-particle spectral function. We specifically target two material families: the semiconducting $\text{Cr}_2(\text{Ge,Si})_2\text{Te}_6$ family and the Fe_xGeTe_2 family. Specifically, we marked out a pathway in three thrusts for both material families: i) Understand key ingredients for magnetism in 3D bulk form; ii) Understand how key ingredients evolve from 3D to 2D limit; iii) Understand how key ingredients are affected and driven by external perturbations. The goals are to be accomplished via angle-resolved photoemission spectroscopy (ARPES) measurements, first in bulk single crystal form, then on exfoliated few-layer limit, then finally understand tunable knobs including uniaxial strain, dosing, and gating.

Recent Progress

We have made progress on studying both types of proposed bulk materials: semiconducting $\text{Cr}_2(\text{Ge,Si})_2\text{Te}_6$ and metallic Fe_xGeTe_2 ($x=3,5$). In this talk, I will discuss mainly our recent ARPES work on the $\text{Fe}_{5-x}\text{GeTe}_2$ system.

Fe_xGeTe_2 ($x=3\sim 5$) (FGT) belongs to a class of van der Waals (vdW) materials that has been recently discovered to host long-range ferromagnetic order up to room temperature and beyond [1,2]. Consisting of layers of Fe-Ge sandwiched by Te, FGT can be synthesized as $\text{Fe}_{3-x}\text{GeTe}_2$, $\text{Fe}_{4-x}\text{GeTe}_2$, and $\text{Fe}_{5-x}\text{GeTe}_2$ [3]. When exfoliated down to the few-layer regime, the long-range magnetic order is sustained. Furthermore, their magnetic properties have been demonstrated to be highly tunable [2], making them prime candidates for spintronics applications. The nature of the magnetism, however, remains largely an open question. Contrary to other vdW magnets, FGT is metallic, and has been mostly claimed as an itinerant ferromagnet. However, a number of observed behaviors indicate that electronic correlations are not weak. For $\text{Fe}_{3-x}\text{GeTe}_2$, the Sommerfeld coefficient is reported to be 110mJ/mol K^2 , suggesting a mass enhancement of at least 13.3 [4]. Also, behaviors of a Kondo lattice are reported below a coherence temperature of $\sim 150\text{K}$ [1]. These indications of electronic correlations prompted us to examine the origin of magnetism in this series of materials.

We carried out ARPES measurements on the single crystals of the $\text{Fe}_{5-x}\text{GeTe}_2$ members of the material family. The material properties of the $\text{Fe}_{5-x}\text{GeTe}_2$ crystals have been known to be

sensitive to the growth method [5]. In particular, samples that are quenched from the growth temperature have been reported to exhibit distinct magnetization behaviors. In this talk, I will present our finding of two types of electronic structures in single crystals obtained via different preparation methods. Interestingly, we found the presence of a number of flatbands extending to a large portion of the momentum space. In particular, as shown in Fig. 1, we identify three flatbands in $\text{Fe}_{5-x}\text{GeTe}_2$ that hybridize with dispersive bands that form Fermi pockets. One flatband is located very close to the Fermi level, with a second near -0.25eV and a third near -0.5eV . To better understand the nature of these flatbands, we have carried out first principle calculations. From Density Function Theory calculations, no flatbands appear. However, in Dynamical Mean Field Theory calculations, flatbands at comparable energies can be identified, suggesting that correlation effects may be the origin of these flatbands. Moreover, we have carried out detailed temperature dependence measurements, from which we identify a smooth evolution of the flatbands as the Curie temperature is crossed, in contrast to an abrupt disappearance of the spin splitting for a Stoner-like itinerant ferromagnet.

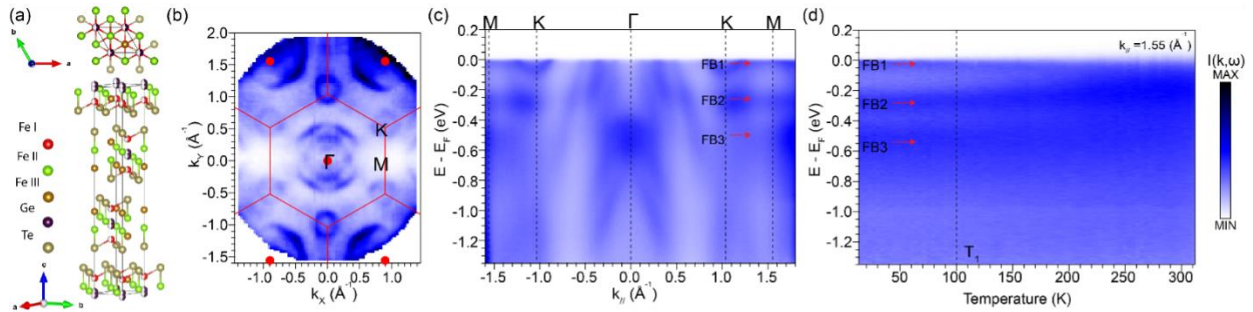


Figure 1 (a) Crystal structure of $\text{Fe}_{5-x}\text{GeTe}_2$. (b) Measured Fermi surface and (c) dispersions along the high symmetry directions. (d) Evolution of flatbands as a function of temperature.

In addition, we have also observed a nodal line along the K-H line of the Brillouin zone in the ferromagnetic phase. Since this nodal line appears in the ferromagnetic phase, the spin degree of freedom is fully quenched, hence it is a two-fold degenerate nodal line. Theoretical analysis on the related compound $\text{Fe}_{3-x}\text{GeTe}_2$ has shown that this nodal line is protected by the crystal symmetries and robust against electron correlations [6]. Therefore our findings demonstrate that this material system provides a rich platform for both experimental exploration and theoretical modeling of topology in the presence of electronic correlations and magnetism.

Future Plans

In the immediate future, we are systematically characterizing and pinning down the electronic structure against sample variations in Fe vacancy, crystal structure and magnetization to fully understand the contribution of the flatbands and dispersive bands to the long-range magnetic order in this material family. We also aim to systematically understand the effect on the

electronic structure by the layer dependence between $\text{Fe}_{3-x}\text{GeTe}_2$, $\text{Fe}_{4-x}\text{GeTe}_2$, and $\text{Fe}_{5-x}\text{GeTe}_2$ to understand the rise in T_C as the number of layers increases.

The next step on understanding the magnetism of bulk crystals is to study the effect of uniaxial strain on both the magnetic and electronic properties. To this end, we have developed various types of sample devices that are compatible with our ARPES system. The effect of uniaxial strain on the electronic structure will be examined in detail.

References

- [1] Y. Zhang, *et al.*, *Sci. Adv.* 4, eaao6791 (2018).
- [2] Y. Deng, *et al.*, *Nature* 563, 94-99 (2018).
- [3] J. Seo, *et al.*, *Sci. Adv.* 6, eaay8912 (2020).
- [4] J. Zhu, *et al.*, *Phys. Rev. B* 14, 144404 (2016).
- [5] A. May, C. Bridges, M. McGuire, *Phys. Rev. M* 3, 104401 (2019).
- [6] K. Kim, *et al.*, *Nat. Mat.* 17, 794 (2018).

Publications

(a number of manuscripts are under review or in preparations)

Investigation of topologically trivial and non-trivial spin textures and their relationships with the topological Hall effect

PI: TeYu Chien

Co-PIs: Yuri Dahnovsky, Jinke Tang, and Jifa Tian

University of Wyoming

Program Scope

The goals of the project are (1) to investigate methods to create a variety of spin textures, both topologically trivial and non-trivial, and (2) to establish the relationships between the created spin textures and the topological Hall effect (THE) signals. These goals will be achieved by utilizing the van der Waals (vdW) two-dimensional (2D) magnetic materials, such as CrX_3 ($X = \text{I, Br, and Cl}$) and Fe_3GeTe_2 , transferred onto various substrates with different interactions to create a wide range of spin textures. The created spin textures will be characterized by spin-polarized scanning tunneling microscopy (SPSTM) and the Hall resistivity measurements will be conducted through Hall bar devices. The relationship between the THE signal and the created spin textures will be established.

Recent Progress: Small Energy Gap Revealed in Exfoliated CrBr_3 Flakes

Since the graphene was exfoliated from graphite, two-dimensional (2D) materials quickly become one of the main stream research directions. It is not until 2017, the 2D ferromagnets were first reported [1,2]. These newly confirmed materials opened new research directions of fundamental understanding of the magnetic interactions at 2D limit and potential 2D spintronic devices. The electronic properties of these materials are relatively unexplored. By using scanning tunneling microscopy and spectroscopy, we revealed that the energy gap of exfoliated CrBr_3 , one of the 2D magnets, has much smaller value than thought [3]. This finding paves a solid foundation for further utilization of this materials.

CrBr_3 is one of the target 2D magnetic materials for this project. It has been studied more than a half century. Despite the plenty literature, the energy gap value and the nature of it are still not clear. It is argued to be a Mott insulator while the optical measurements exhibit ~ 1.7 eV absorption onset and is argued to be charge transfer nature [4]. A recent PL data reported 1.35 eV energy associated with $d-d$ transitions, indicating smaller gap with Mott nature is possible [5]. The theoretical calculation reported a range of energy gap from 1.15-2.95 eV [6–12]. It is known that the DFT calculations require a reliable experimental value to compare for determining the semi-empirical on-site Coulomb repulsion, U . Here we provide a high quality dI/dV measurement on exfoliated CrBr_3 flakes to reveal a reliable energy gap value.

We utilized STM/S to study the exfoliated CrBr_3 flakes. Figure 1b shows the atomic resolution STM topography images of exfoliated CrBr_3 flakes. It is consistent with the known

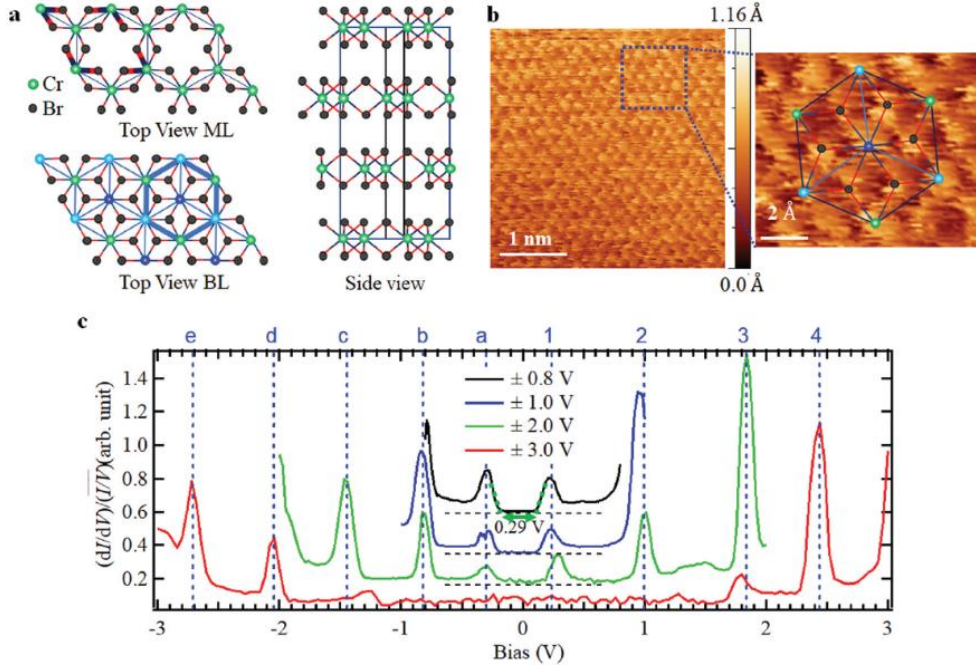


Figure 1. **a** Atomic structure of CrBr_3 . **b** Atomic resolution STM topography images, which are consistent with the known crystal structure. **c** High quality dI/dV spectra taken with various bias range to reveal detail features in the spectra.

crystal structure (Fig. 1a). Multiple peak features are observed in dI/dV spectra with various bias ranges. The peak features in conduction bands are labeled with numbers (1-4) and the peak features in the valence bands are labeled with letters (*a-e*). These labels are used in Table 1 below for comparison with reported optical measurements. Detail analysis with the assistance of DFT+U calculations allow us to conclude that the energy gap is ~ 0.6 eV with Mott nature. Our density functional theory calculations, with agreement with our experimental data, suggests a set of on-site exchange interaction, $J = 3$ eV, and on-site Coulomb repulsion energy, $U = 5$ eV, should be used in calculations for CrBr_3 .

Table 1 shows the comparison of the energy values of the reported optical measurements in found literature and the matched valence-conduction band peak pairs (Fig. 1c). All the reported optical transitions can be matched to one or two conduction-valence band peak pairs revealed in our dI/dV spectra (Fig. 1c). The excellent agreement between our dI/dV data with reported optical measurements provide the strong confidence on the revealed peak features in the dI/dV spectra. This includes the peak *a* and peak 1. Note that without these two peaks, the optical absorption transition (~ 1.68 eV) and the PL transition (~ 1.35 eV) cannot be matched to any other peak pairs. This indicates that the energy gap of CrBr_3 should be determined by peaks 1 and *a*, which leads to ~ 0.6 eV. Furthermore, if one would consider the signal onset bias in Fig. 1c, the onset energy gap is determined to be ~ 0.29 eV. Based on our DFT+U calculations, the CrBr_3 is gapless when $U = 0$ eV and it opens up upon having a non-zero U . This is a signature of Mott insulator in which peaks 1 and *a* are the upper Hubbard band and lower Hubbard band, respectively.

Table 1. Comparison between the energy values of the reported optical measurements and the energy values of valence-conduction band peak pairs (Fig. 1c). The references at the right-end of the table are cited in Ref. [3].

Measurement	Measurement temperature	Assigned transition	Reported energy gap	Corresponding energy gap (eV)	Peak pair	Peak pair energy (eV)	Ref.
PL	2.7 K		1.35 eV	1.35	2-a	1.27 ± 0.05	26
Abs.	4.2 K	4T_2	$13\,500\text{ cm}^{-1}$	1.68	1-c	1.68 ± 0.04	23,24
Abs.	4.2 K	2T_1	$14\,400\text{ cm}^{-1}$	1.79	2-b	1.78 ± 0.07	23,24
Abs.	4.2 K	4T_1	$17\,500\text{ cm}^{-1}$	2.17	3-a	2.14 ± 0.04	23,24
Abs.	4.2 K	2T_2	$18\,900\text{ cm}^{-1}$	2.36	2-c or 1-d	2.38 ± 0.05 or 2.31 ± 0.04	24
Abs.	4.2 K		$19\,200\text{ cm}^{-1}$	2.38			23
Kerr (+max)	1.5 K	$t_{1u}^n \rightarrow e_g^*$	$23\,500\text{ cm}^{-1}$	2.92	1-e or 2-d	2.97 ± 0.04 or 3.01 ± 0.05	14,15,31
Abs.	1.5 K	$t_{1u} \rightarrow e_g^*$	$24\,500\text{ cm}^{-1}$	3.04			15
Abs.	1.5 K		$24\,310\text{ cm}^{-1}$	3.02			14
Refl.	30 K		3.1 eV	3.1			25
Dielectric	1.5 K		$25\,000\text{ cm}^{-1}$	3.1			14
Kerr (-max)	1.5 K	$t_{2u}^n \rightarrow e_g^*$	$26\,700\text{ cm}^{-1}$	3.29	3-c or 4-b	3.25 ± 0.04 or 3.21 ± 0.09	14,31
Abs.	1.5 K		$29\,500\text{ cm}^{-1}$	3.66	2-e	3.67 ± 0.05	15
Abs.	1.5 K		$29\,580\text{ cm}^{-1}$	3.67			14
Refl.	30 K		3.8 eV	3.8	4-c or 3-d	3.81 ± 0.08 or 3.88 ± 0.04	25

In addition to the energy gap measurements, we have also observed a 2-nm edge degradation of a monolayer CrBr₃ flake due to ~15 min of air exposure during sample transfer into STM chamber. Figure 2a and b are the topography and dI/dV images of a monolayer CrBr₃ flake transferred on HOPG substrate. dI/dV spectrum (Fig. 2c) exhibits combined features of CrBr₃ (three labeled humps are consistent with peak 1-3 in Fig. 1c) and HOPG (overall gapless spectrum). Bright contrast in dI/dV mapping (Fig. 2b) and round topography edge indicates the sample degradation.

This edge degradation is also observed in the observed second layer CrBr₃. It is determined that the edge degradation is around 2 nm for the ~15 min of air exposure.

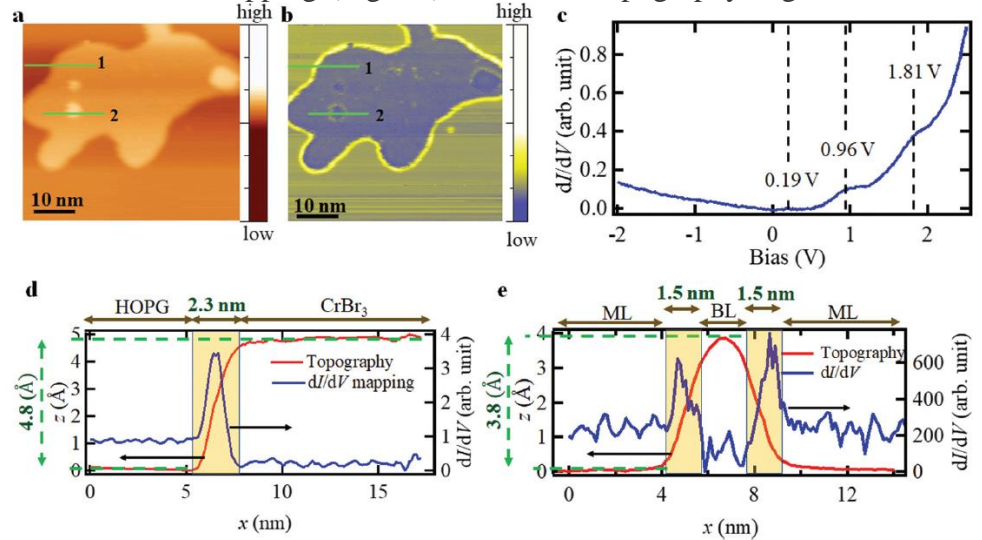


Figure 2. **a** Topography image and **b** dI/dV mapping of monolayer CrBr₃ flake. **c** dI/dV spectrum taken on the monolayer CrBr₃ flake. **d** and **e** Line profiles of the topography images and dI/dV mappings across HOPG/ML CrBr₃ boundary (line 1) and ML/BL CrBr₃ boundary (line 2).

Future Plans

Next, we plan to place CrBr₃ or other 2D magnets onto various substrates, such as WTe₂, EuO_{1-x}, 2M WS₂, Fe₃GeTe₂, and CrX₃, to generate spin textures due to the interfacial interactions. By applying spin polarized STM technique, we anticipate to reveal images of the

spin textures. We also plan to fabricate Hall bar devices using these heterostructures. The Hall measurement results will be combined with SPSTM results to gain insights on their relationships.

References

- [1] B.Huang, G.Clark, E. E.Navarro-Moratalla, D. R.Klein, R.Cheng, K. L.Seyler, Di.Zhong, E.Schmidgall, M. A.McGuire, D. H.Cobden, W.Yao, D.Xiao, P.Jarillo-Herrero, andX.Xu, *Nature* **546**, 270 (2017).
- [2] C.Gong, L.Li, Z.Li, H.Ji, A.Stern, Y.Xia, T.Cao, W.Bao, C.Wang, Y.Wang, Z. Q.Qiu, R. J.Cava, S. G.Louie, J.Xia, andX.Zhang, *Nature* **546**, 265 (2017).
- [3] D.Baral, Z.Fu, A. S.Zadorozhnyi, R.Dulal, A.Wang, N.Shrestha, U.Erugu, J.Tang, Y.Dahnovsky, J.Tian, andT.Chien, *Phys. Chem. Chem. Phys.* **23**, 3225 (2021).
- [4] J. F.Dillon, H.Kamimura, andJ. P.Remeika, *J. Appl. Phys.* **34**, 1240 (1963).
- [5] Z.Zhang, J.Shang, C.Jiang, A.Rasmita, W.Gao, andT.Yu, *Nano Lett.* **19**, 3138 (2019).
- [6] H.Li, Y.-K.Xu, K.Lai, andW.-B.Zhang, *Phys. Chem. Chem. Phys.* **21**, 11949 (2019).
- [7] W.Zhang, Q.Qu, P.Zhu, andC.Lam, *J. Mater. Chem. C* **3**, 12457 (2015).
- [8] J.Liu, Q.Sun, Y.Kawazoe, andP.Jena, *Phys. Chem. Chem. Phys.* **18**, 8777 (2016).
- [9] C.Huang, Y.Du, H.Wu, H.Xiang, K.Deng, andE.Kan, *Phys. Rev. Lett.* **120**, 147601 (2018).
- [10] A. O.Fumega, S.Blanco-Canosa, H.Babu-Vasili, P.Gargiani, H.Li, J.-S.Zhou, F.Rivadulla, andV.Pardo, *J. Mater. Chem. C* doi. org/10.1039/D0TC02003F (2020).
- [11] K.Shinagawa, T.Suzuki, T.Saito, andT.Tsushima, *J. Magn. Magn. Mater.* **140–144**, 171 (1995).
- [12] H.Wang, V.Eyert, andU.Schwingenschlög, *J. Phys. Condens. Matter* **23**, 116003 (2011).

Publications

- [1] A.Zadorozhnyi andY.Dahnovsky, *J. Magn. Magn. Mater.* **518**, 167367 (2021).
- [2] A.Zadorozhnyi andY.Dahnovsky, *J. Phys. Condens. Matter* **32**, 405803 (2020).
- [3] P.Li, J.Ding, S. S. L.Zhang, J.Kally, T.Pillsbury, O. G.Heinonen, G.Rimal, C.Bi, A.DeMann, S. B.Field, W.Wang, J.Tang, J. S.Jiang, A.Hoffmann, N.Samarth, andM.Wu, *Nano Lett.* **21**, 84 (2021).
- [4] P.Samarawickrama, R.Dulal, Z.Fu, U.Erugu, W.Wang, J.Ackerman, B.Leonard, J.Tang, T.Chien, andJ.Tian, *ACS Omega* **6**, 2966 (2021).

- [5] D.Baral, Z.Fu, A. S.Zadorozhnyi, R.Dulal, A.Wang, N.Shrestha, U.Erugu, J.Tang, Y.Dahnovsky, J.Tian, andT.Chien, *Phys. Chem. Chem. Phys.* **23**, 3225 (2021).
- [6] J.Tian, C.Şahin, I.Miotkowski, M. E.Flatté, andY. P.Chen, *Phys. Rev. B* **103**, 035412 (2021).
- [7] J. W.Hill, Z.Fu, J.Tian, andC. M.Hill, *J. Phys. Chem. C* **124**, 17141 (2020).
- [8] S.Kattel, J. R.Murphy, D.Ellsworth, J.Ding, T.Liu, P.Li, M.Wu, andW. D.Rice, *Phys. Rev. Appl.* **12**, 034047 (2019).

Session VI

Search for 3D Topological Superconductors using Laser-Based Spectroscopy

Principal Investigator: David Hsieh

Mailing Address: 1200 E. California Blvd., MC 149-33, California Institute of Technology, Pasadena, CA 91125

E-mail: dhsieh@caltech.edu

(i) Program Scope

The goal of this program is to develop a rational route to realizing the elusive three-dimensional topological superconducting (3D TSC) state by identifying its precursor phases. It is theoretically proposed that the critical fluctuations of certain inversion symmetry breaking electronic phases^{1,2} can mediate Cooper pairing in odd-parity channels and lead to topological superconductivity^{3,4}. Therefore 3D TSCs may potentially emerge upon suppressing these ordered phases to a critical point with external perturbations such as pressure. We seek to test this hypothesis by deploying a suite of optical probes including second harmonic generation, time-resolved coherent phonon spectroscopy and terahertz emission spectroscopy to identify and to characterize the predicted precursor phases in candidate materials. These techniques will be integrated with diamond anvil cells to study the pressure evolution of the precursor phases and their potential interaction with proximate superconducting states.

(ii) Recent Progress

We have succeeded in integrating optical second harmonic generation rotational anisotropy (SHG-RA) with a custom membrane-driven diamond anvil cell (DAC) and cryostat system (Fig. 1a). By using high purity diamond, we were able to greatly reduce the background SHG produced by diamond defect centers and thereby resolve the SHG-RA signal from a sample loaded inside the DAC. The material that we chose to study first was the topological Weyl

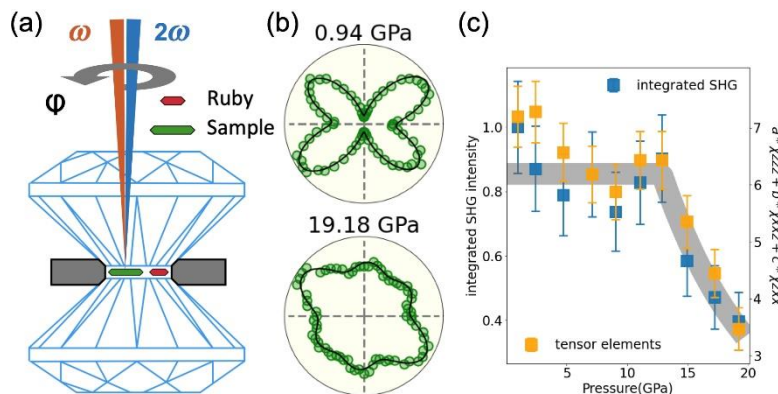


Fig 1: (a) Schematic of the high pressure SHG-RA setup. (b) SHG-RA data from TaAs below and above P_c , showing a loss of horizontal and vertical mirror symmetries. Back lines are symmetry based fits. (c) Pressure dependence of the ϕ -integrated SHG intensity (blue symbols). The magnitude of the SHG susceptibility tensor element associated with the polar axis is overlaid (orange symbols).

semimetal TaAs, which has recently been shown to exhibit a giant second-order nonlinear optical response⁵. Upon application of hydrostatic pressure above a critical value $P_c \approx 14$ GPa, x-ray

diffraction measurements show that TaAs undergoes a structural phase transition from the tetragonal space group $I4_1md$ to the hexagonal space group $P-6m2$ ⁶. Therefore there is interest to understand whether pressure may be able to tune its nonlinear optical properties. Moreover, although no superconductivity above 1.8 K has been reported in TaAs under pressure, studying TaAs could help to understand the isostructural Weyl semimetal TaP, which undergoes an analogous pressure-induced phase transition at $P_c \approx 71$ GPa concomitant with the emergence of superconductivity⁷. We performed pressure-dependent SHG-RA measurements on naturally grown (112) surfaces of TaAs single crystals and identified a clear symmetry lowering across $P_c \approx 12$ GPa consistent with a $I4_1md \rightarrow P-6m2$ transition (Fig. 1b). Despite the fact that both structures are non-centrosymmetric and are thus SHG active in the electric-dipole channel, we observed a significant drop in SHG conversion efficiency above P_c (Fig. 1c). Using a symmetry based analysis, we find that this drop is primarily attributed to the loss of a polar axis in the high pressure structure (Fig. 1c). Our results show that pressure is a means to control the second-order nonlinear response in TaAs and, more generally, demonstrate SHG-RA as a method to resolve crystallographic symmetry changes under pressure.

(iii) Future Plans

We previously discovered that the strongly spin-orbit coupled metal $Cd_2Re_2O_7$ hosts an inversion breaking multipolar nematic phase at ambient pressure¹, which is predicted to be a precursor to a 3D TSC. Our next step is to perform pressure-dependent SHG-RA measurements on $Cd_2Re_2O_7$ to study the interplay between the multipolar nematic phase and the superconducting dome that is reported to emerge under pressure⁸. We will also extend these studies to bulk $MoTe_2$, which similarly undergoes structural inversion symmetry breaking below $T \approx 250$ K under ambient conditions and becomes superconducting upon pressurization⁹.

To obtain information about the momentum-space spin texture in candidate 3D TSC precursors, we will perform contact-free photocurrent measurements using rotational anisotropy THz emission spectroscopy. As part of this award, we have recently developed a pump wavelength tunable (1200 – 2200 nm) THz emission spectrometer and demonstrated its efficacy using a Sr_2IrO_4 test sample (Fig. 2). But we plan to perform two upgrades. First, to improve the signal-to-noise ratio, we will modify the setup to be compatible with a different laser system operating at 100x higher repetition rate. Second, to improve the THz collection efficiency, we will reconfigure the experimental geometry so that the emitted THz radiation is collected normal to the sample using a wide numerical aperture off-axis parabolic mirror. Following these upgrades, we will perform measurements on TaAs, $Cd_2Re_2O_7$ and $MoTe_2$.

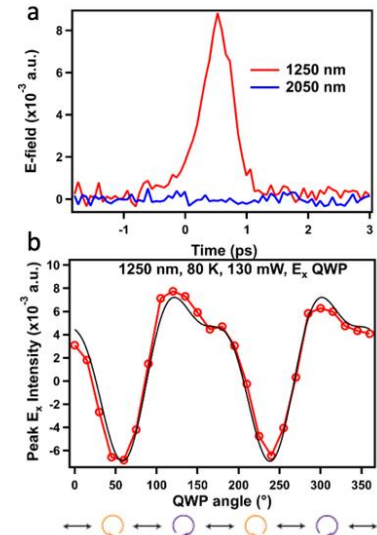


Fig 2: (a) THz emission signal from Sr_2IrO_4 for different pump wavelengths. (b) Signal maximum as a function of pump polarization modulated by a quarter waveplate (QWP).

(iv) References

1. Harter, J. W., Zhao, Z. Y., Yan, J.-Q., Mandrus, D. G. & Hsieh, D. A parity-breaking electronic nematic phase transition in the spin-orbit coupled metal $\text{Cd}_2\text{Re}_2\text{O}_7$. *Science* **356**, 295–299 (2017).
2. Fu, L. Parity-Breaking Phases of Spin-Orbit-Coupled Metals with Gyrotropic, Ferroelectric, and Multipolar Orders. *Phys. Rev. Lett.* **115**, 026401 (2015).
3. Kozii, V. & Fu, L. Odd-Parity Superconductivity in the Vicinity of Inversion Symmetry Breaking in Spin-Orbit-Coupled Systems. *Phys. Rev. Lett.* **115**, 207002 (2015).
4. Wang, Y., Cho, G. Y., Hughes, T. L. & Fradkin, E. Topological superconducting phases from inversion symmetry breaking order in spin-orbit-coupled systems. *Phys. Rev. B* **93**, 134512 (2016).
5. Wu, L. *et al.* Giant anisotropic nonlinear optical response in transition metal monpnictide Weyl semimetals. *Nat. Phys.* **13**, 350–355 (2017).
6. Zhou, Y. *et al.* Pressure-Induced New Topological Weyl Semimetal Phase in TaAs. *Phys. Rev. Lett.* **117**, 146402 (2016).
7. Li, Y. *et al.* Concurrence of superconductivity and structure transition in Weyl semimetal TaP under pressure. *Npj Quantum Mater.* **2**, 1–7 (2017).
8. Malavi, P. S., Karmakar, S. & Sharma, S. M. $\text{Cd}_2\text{Re}_2\text{O}_7$ under high pressure: Pyrochlore lattice distortion-driven metal-to-nonmetal transition. *Phys. Rev. B* **93**, 035139 (2016).
9. Qi, Y. *et al.* Superconductivity in Weyl semimetal candidate MoTe_2 . *Nat. Commun.* **7**, 11038 (2016).

(v) Publications supported by BES

1. J. Orenstein, J. E. Moore, T. Morimoto, D. H. Torchinsky, J. W. Harter & D. Hsieh. Topology and symmetry of quantum materials via nonlinear optical responses. *Annu. Rev. Condens. Matter Phys.* **12**, 247 (2021).
2. Jun-Yi Shan, A. de la Torre, N. J. Laurita, L. Zhao, C. D. Dashwood, D. Puggioni, C. X. Wang, K. Yamaura, Y. Shi, J. M. Rondinelli & D. Hsieh. Evidence for an extended critical fluctuation region above the polar ordering transition in LiOsO_3 . *Phys. Rev. Research* **2**, 033174 (2020).

Chiral Materials and Unconventional Superconductivity

Lead PI: Qiang Li

Co-PIs: Mengkun Liu, Weiguo Yin, Genda Gu and Tonica Valla

Condensed Matter Physics & Materials Science Division, Brookhaven National Laboratory

e-mail: qiangli@bnl.gov

Program Scope

This program studies topological phases and transport properties of chiral materials and unconventional superconductors. A unique feature of chiral materials is that their low-energy quasi-particles possess an additional quantum number that goes by the name of handedness or chirality. The powerful notion of chirality underpins a wide palette of new and useful phenomena, including chiral anomaly^{1,2} Recently, we proposed that the chirality may be utilized to construct a new type of qubit – the chiral qubit – potentially capable of operating at THz frequency and at room temperature.³ To this end, the program aims at providing the basic understanding of topological phase transition and chiral fermions transport process under various stimulus in chiral materials. Unconventional superconductivity arises in superconductors having, for example, order parameter with a non-zero angular momentum. To this end, the focus of the program is to look for the exotic states of matter, including pair density waves and topological superconductors. Our approach has been developed through synthesizing chiral materials and unconventional superconductors in both single crystals and thin film forms, and subsequently characterizing them using a range of techniques including transport, electron and optical spectroscopy. Experimental activities are strongly coupled with a collaborative effort on theory and computation, providing new strategies for designing robust electronic materials for energy applications and quantum computing.

Recent Progress

Topological states and phase transition explored by ARPES – Angle-resolved photoemission spectroscopy (ARPES) is a powerful technique to probe the electronic structure of topological materials. We have been using synchrotron and laser-based APRES to investigate the topological states and phases transition in semimetal ZrTe₅ and iron chalcogenide superconductors, such as FeTe_{1-x}Se_x. The laser based ARPES at BNL provides ~ 30 fs ultrafast temporal and 20 nm spatial

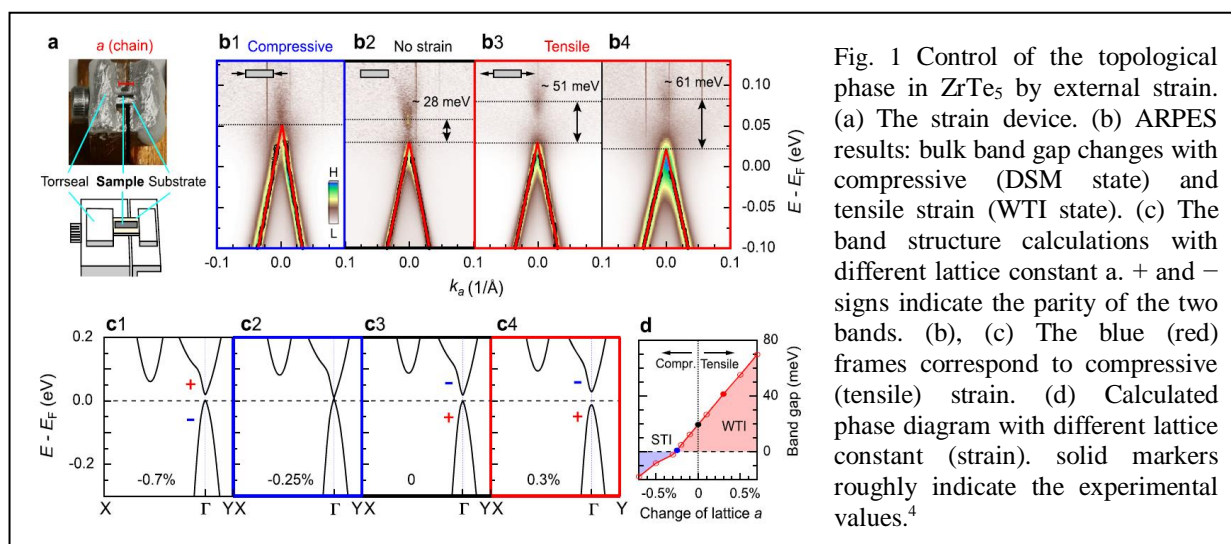


Fig. 1 Control of the topological phase in ZrTe₅ by external strain. (a) The strain device. (b) ARPES results: bulk band gap changes with compressive (DSM state) and tensile strain (WTI state). (c) The band structure calculations with different lattice constant a . + and - signs indicate the parity of the two bands. (b), (c) The blue (red) frames correspond to compressive (tensile) strain. (d) Calculated phase diagram with different lattice constant (strain). solid markers roughly indicate the experimental values.⁴

resolution. An example of visualization of the topological states in ZrTe_5 under external strain is shown in Fig. 1. A screw was used to compress or stretch the substrate on which the single crystal sample is glued to provide the uniaxial strain along the high conducting Te-chain direction. With compressive strain (Fig. 1b1), the gap was (nearly) closed, reaching a Dirac semimetal (DSM) state. With tensile strain (Fig. 1b3–1b4), the band gap became larger, stabilizing the weak topological insulator (WTI) state.⁴ In progress are the time-resolved ARPES studies of the dynamic behavior of topological fermions and electron-phonon coupling in these materials.

Topological states and time-reversal symmetry breaking in Fe-chalcogenide superconductors – In the Fe-chalcogenide superconductors, topology and superconductivity can interact to give topological superconductivity capable of supporting Majorana zero mode that could prove to be the basis of future qubit technology. Using our high resolution ARPES, we provided evidence of time-reversal symmetry breaking and associated mass acquisition in a topological surface state at the superconducting transition, an observation highly suggestive of the formation of surface ferromagnetism.⁵ Furthermore, we combined neutron scattering, laser-based scanning ARPES, and microprobe composition and resistivity measurements to characterize the electronic state of $\text{Fe}_{1+y}\text{Te}_{1-x}\text{Se}_x$. We establish a phase diagram in which the superconductivity is observed only at sufficiently low Fe concentration, in association with distinct antiferromagnetic correlations, whereas the coexisting topological surface state occurs only at sufficiently high Te concentration.⁶ In progress is the growth of Fe-chalcogenide superconductors with magnetic ion substitutions. We hope this series of substitutions will provide an avenue to disentangle the relative roles of magnetism and spin-orbit interaction in determining the topological properties in iron-based superconductors.

Theory of topological phase transition and phonon-space Dirac topology surfaces in ZrTe_5 – We use first-principles methods to demonstrate that in ZrTe_5 atomic displacements corresponding to five of the six zone-center A_g (symmetry-preserving) phonon modes can drive a topological phase transition from strong topological insulator (STI) to WTI with a DSM state emerging at the transition. This implies that the topological phase transition in ZrTe_5 can be realized with many different settings of external stimuli that are capable of penetrating through the phonon-space Dirac surface without breaking the crystallographic symmetry.⁷ Currently, we employ first-principles and effective Hamiltonian methods, and find that in ZrTe_5 that all zone-centered infra-red (IR) phonon modes can drive the system dynamically from a STI to a WSI by breaking the global inversion symmetry that leads to the formation of Weyl semimetal phase.

THz Light driven topological phase transition in Dirac semimetals – In a collaboration with J. Wang’s group at Ames Lab, we demonstrated a few-cycle THz-pulse-induced phase transition in ZrTe_5 driven by the lowest Raman active mode A_{1g} . Above a critical THz-pump field threshold, there emerged a long-lived metastable phase, of approximately 100 ps. These results, together with first-principles modeling, identified a mode-selective Raman coupling that drives the system from STI to WTI with a DSM phase established at a critical atomic displacement controlled by the phonon coherent pumping.⁸ Harnessing of vibrational coherence is now extended to steer symmetry-breaking transitions, with implications for THz topological quantum gate and error correction applications for quantum information science.

Light induced giant anisotropic THz photocurrents have been studied using femtosecond laser induced coherent phonons to break inversion symmetry (IS) in the centrosymmetric DSM ZrTe_5 .

This light-induced phononic symmetry switching leads to Weyl point (WP) formation, whose chirality manifests in a transverse, helicity-dependent current, orthogonal to the broken IS axis, via the circular photogalvanic effect (CPGE) (Fig. 2). The topological photocurrent has two distinct temperature-dependent features: i) Berry curvature creation by the separated Weyl nodes and strongly-suppressed scattering, resembling the anomalous Hall magneto-resistivity, and ii) particle-hole reversal near the Lifshitz transition. These results, together with first-principles modeling, identify two pairs of WPs dynamically created by broken IS phonons of the B_{1u} mode, which are driven by the photoexcited non-equilibrium population of spatially separated charges between the inverted bands of the Te pair. In addition to revealing dissipationless photocurrents with remarkable ballistic lengths of ~ 10 μm , the phononic symmetry switching principle breaks grounds for coherent manipulation of Weyl states without application of any static electric or magnetic fields.⁹ Currently, we are investigating the light induced photocurrent under magnetic field and external strain, as well as the planar Hall effect induced by the Berry curvature.

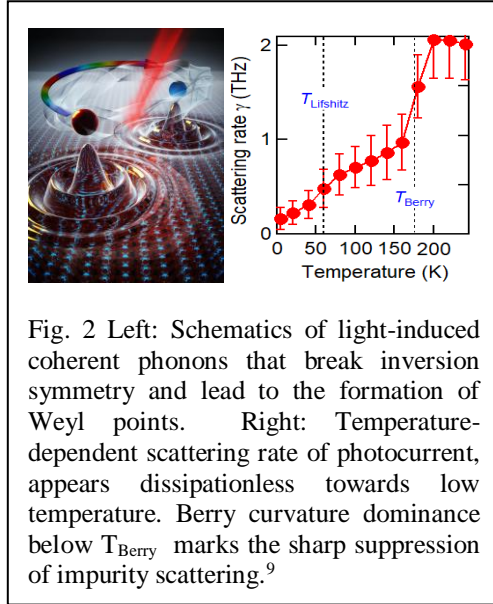


Fig. 2 Left: Schematics of light-induced coherent phonons that break inversion symmetry and lead to the formation of Weyl points. Right: Temperature-dependent scattering rate of photocurrent, appears dissipationless towards low temperature. Berry curvature dominance below T_{Berry} marks the sharp suppression of impurity scattering.⁹

Quantum Hall effect in Dirac semimetals – In earlier 2019, we reported the observation of 3D quantum Hall effect (QHE) in ZrTe_5 at the extreme quantum limit, and attributed this 3D QHE to Fermi-surface instability.¹⁰ The understanding of the origin of the quantized Hall effect in 3D electronic systems is incomplete. In collaboration with an MPI-Dresden group (J. Gooth, C. Felser), we have performed additional thermodynamic and charge transport measurements in ZrTe_5 and HfTe_5 in the quantum Hall regime. The measured thermodynamic properties, magnetization and ultrasound propagation, showed no indications of a Fermi surface instability, consistent with our recent high resolution X-ray diffraction investigation carried out at BNL’s National Synchrotron Light Source II (NSLS II). Surprisingly, in the high field quantum limit, HfTe_5 exhibits an additional peak in $\rho_{xx}(\text{B})$, accompanied by a plateau-like feature in $\rho_{xy}(\text{B})$. This is in sharp contrast to ZrTe_5 , in which $\rho_{xx}(\text{B})$ and $\rho_{xy}(\text{B})$ increase smoothly. We found that the additional peak in $\rho_{xx}(\text{B})$, in the quantum limit of HfTe_5 , is situated at $N = 3/5$, where N is the index number of the Landau level. Our observations appear to be consistent with the presence of strong electron-electron interactions.¹¹ Now we are investigating 2D QHE and a bulk gap related zero energy states in mono and few layer ZrTe_5 .

Pair density wave (PDW) in stripe ordered superconductors – PDW is a proposed topological superconducting state in high temperature cuprates, for example $\text{La}_{2-x}\text{Ba}_x\text{CuO}_4$ with $x = 1/8$.¹² In this case, the coexistence of 2D superconductivity with charge and spin stripe order was observed at temperatures below 40 K.¹² Both Zn-doping and c-axis magnetic fields have been observed to increase the spin stripe order in $\text{La}_{2-x}\text{Ba}_x\text{CuO}_4$ with x close to $1/8$. For $x = 0.095$, we showed that introducing 1% Zn also led to an initial onset of 2D superconductivity, followed by 3D superconductivity at lower temperatures, even in zero field. Application of a c-axis magnetic field caused both transitions to decrease substantially, while remaining distinct. We inferred that the Zn pins pair-density-wave order locally.¹⁴ This finding has important implications for the

analysis of the superconducting gap function in scanning tunneling microscopy studies in which quasiparticle interference is induced by Zn impurities. Thus far, there has been no direct evidence for the PDW. To this end, we have performed phase-sensitive measurements aimed at providing such direct evidence. The results will put strong constraints on the theory of electron-pairing underlying superconductivity in cuprates. The concept we are formulating now could lead to a resolution of the intense debate over the mechanism of cuprate superconductivity.

Future Plans

Relationship between topology, strain, and transport properties of chiral materials is a key research direction of this program. To this end, we will properly engineer, characterize, and understand strain-induced pseudo-magnetic fields and associated topological states in quantum materials. We will explore how pseudo-magnetic fields behave differently from real magnetic fields in topological materials. In addition, dynamic methods of topological controls using various coherent phonons will be investigated.

Interplay of topological orders, magnetism, and superconductivity is a planned study focused on the design, growth, and characterization of time reversal symmetry breaking topological materials and candidates for bulk topological superconductors. Our theoretical/computational effort will provide guiding principles for the selection of the most interesting material systems for crystal and thin film growth. A coordinated experimental effort is planned using combined ARPES + STM + IR/THz spectroscopy approach for investigating the magnetic doping effect on band structure, topological orders and superconductivity.

Ultrafast control of topological phase transitions is another planned study to exploit the unprecedented chiral response in topological materials to both internal and external stimuli at vastly different time scales from steady-state to ultrafast. We aimed at using this response to design new materials and establish new topological control principles. To this end, we will characterize the photo-excited states and topological currents under various external and internal stimuli using combined time-resolved- (tr-) IR/THz and tr-ARPES, complemented by studies using time-dependent density function theory and dynamic method.

References

1. Q. Li, G. Gu, T. Valla et al. arXiv:1412.6542 (2014), *Nature Physics* **12** 550 (2016).
2. J. Xiong, N. P. Ong, et al *Science* 350 413 (2015).
3. D. Kharzeev and Q. Li, “Quantum computing using chiral qubits” *US Patent* #10657456 (2020).
4. P. Zhang, Q. Li, G. Gu et al *Nature Communications* 12 406 (2021).
5. N. Zaki, G. Gu et al *PNAS* 118 e2007241118 (2021).
6. Y. Li, G. Gu et al *Nature Materials* 20, 1221 (2021).
7. N. Aryal, X. Jin, A. Tsvelik, Q. Li, and W. Yin, *Phys. Rev. Lett.* 126, 016401 (2021).
8. C Vaswani, Q. Li, J. Wang et al *Physical Review X* 10, 021013 (2020).
9. L. Luo, Q. Li, J. Wang et al *Nature Materials* 20 329 (2021).
10. F. Tang, G. Gu et al *Nature* 569, 537 (2019).
11. G. Galeski, G. Gu, Q. Li, et al *Nature Communications* 11, 5926 (2020).
12. Q. Li, et al *Phys. Rev. Lett.* 99, 067001 (2007).
13. E. Berg et al *Phys. Rev. Lett.* 99, 127003 (2007).
14. P. M. Lozano, G. Gu, J. M. Tranquada, and Q. Li, *Phys. Rev. B* 103, L020502 (2021).

Publications (September 2019 – Aug. 2021)

1. N. Aryal, et al “Topological phase transition and phonon-space Dirac topology surfaces in ZrTe₅” *Phys. Rev. Lett.* 126, 016401 (2021). doi: 10.1103/physrevlett.126.016401
2. L. Luo, et al “A Light-induced Phononic Symmetry Switch and Giant Dissipationless Topological Photocurrent in ZrTe₅” *Nature Materials* 10.1038/s41563-020-00882-4 (2021). doi: 10.1038/s41563-020-00882-4
3. P. M. Lozano, et al “Experimental Evidence that Zn Impurities Pin Pair-Density-Wave Order in La_{2-x}Ba_xCuO₄” *Phys. Rev. B* 103, L020502 (2021). doi: 10.1103/physrevb.103.l020502
4. J. M. Tranquada, M. Dean, and Q. Li “Superconductivity from charge order in cuprates” *Journal of the Physical Society of Japan* 90, 111002 (2021). doi: 10.7566/JPSJ.90.111002
5. S Galeski, et al “Origin of the quasi-quantized Hall effect in ZrTe₅” *Nature communications* 12, 3197 (2021). doi: 10.1038/s41467-021-23435-y
6. F Tang, et al “Two-Dimensional Quantum Hall Effect and Zero Energy State in Few-Layer ZrTe₅” *Nano Letters* 21, 5998 (2021). doi: 10.1021/acs.nanolett.1c00958
7. P. Zhang, et al “Observation and control of the weak topological insulator state in ZrTe₅” *Nature Communications* 12 406 (2021). doi: 10.1038/s41467-020-20564-8.
8. A. Sapkota, et al "Reinvestigation of crystal symmetry and fluctuations in La₂CuO₄” *Phys. Rev. B* 104, 014304 (2021). doi: 10.1103/PhysRevB.104.014304
9. Y. Li, et al "Electronic properties of the bulk and surface states of Fe_{1+y}Te_{1-x}Se_x” *Nature Materials* 20, 1221 (2021). doi: 10.1038/s41563-021-00984-7
10. N. Zaki, et al “Time-Reversal Symmetry Breaking in the Fe-Chalcogenide Superconductors” *Proceedings of National Academy of Sciences* 118 (3) e2007241118 (2021) doi: 10.1073/pnas.2007241118.
11. Z. Xie, et al “Electron-electron interactions and weak antilocalization in few-layer ZrTe₅ devices” *Phys. Rev. B* 103, 155408 (2021). doi: 10.1103/PhysRevB.103.155408
12. R. Kim, et al “Terahertz Nano-Imaging of Electronic Strip Heterogeneity in a Dirac Semimetal” *ACS Photonics* 8, 1873 (2021). doi: 10.1021/acsp Photonics.1c00216.
13. C Vaswani, et al “Light-Driven Raman Coherence as a Nonthermal Route to Ultrafast Topology Switching in a Dirac Semimetal” *Physical Review X* 10, 021013 (2020). doi: 10.1038/s41563-020-00882-4
14. S. Galeski, et al “Unconventional Hall response in the quantum limit of HfTe₅” *Nature Communications* 11, 5926 (2020). doi: 10.1038/s41467-020-19773-y

15. A. Sapkota, et al “Electron-phonon coupling and superconductivity in the doped topological crystalline insulator $(\text{Pb}_{0.5}\text{Sn}_{0.5})_{1-x}\text{In}_x\text{Te}$ ” *Phys. Rev. B* 102, 104511 (2020). doi: 10.1103/PhysRevB.102.104511
16. B. Salzmänn, et al “Nature of native atomic defects in ZrTe_5 and their impact on the low-energy electronic structure” *Phys. Rev. Materials* 4, 114201 (2020). doi: 10.1103/PhysRevMaterials.4.114201
17. T. Konstantinova, et al “Photoinduced Dirac semimetal in ZrTe_5 ” *npj Quantum Materials* 5:80 (Nov. 4 2020). doi: 10.1038/s41535-020-00280-8
18. D. Santos-Cottin, et al “Probing intraband excitations in ZrTe_5 : A high-pressure infrared and transport study” *Phys. Rev. B* 101 125205 (2020). doi: 10.1103/PhysRevB.101.125205
19. W. Zhang, et al “Negative longitudinal magnetothermopower in the topological semimetal ZrTe_5 ” *Phys. Rev. B* 102 115147 (2020). doi: 10.1103/PhysRevB.102.115147
20. W. Zhang, P. Wang, B. Skinner, R. Bi, V. Kozii, C. Cho, R. Zhong, J. Schneeloch, D. Yu, G. Gu, L. Fu, X. Wu, and L. Zhang, “Observation of a thermoelectric Hall plateau in the extreme quantum limit” *Nature Communications*, 11, 1046 (2020). doi: 10.1038/s41467-020-14819-7
21. D. Kharzeev and Q. Li, “Quantum computing using chiral qubits” US Patent #10657456 (2020)
22. T. Ozaki, et al “Ion irradiation of iron chalcogenide superconducting films” *Superconductor Science and Technology* 33, 094008 (2020). doi: 10.1088/1361-6668/ab9f66
23. Q. Li “Thermoelectrics with a twist” *Nature Materials* 18, 1267 (2019). doi: 10.1038/s41563-019-0523-0
24. Y. Zhang, et al. “Dynamic behavior of reversible oxygen migration in irradiated-annealed high temperature superconducting wires” *Scientific Reports* 10, 14848 (2020). doi: 10.1038/s41598-020-70663-1

Magnetometry Studies of Quantum Correlated Topological Materials in Intense Magnetic Fields

Lu Li, University of Michigan

Program Scope

This proposal investigates the fundamental nature of quantum correlated topological materials by torque magnetometry in intense magnetic fields. The proposal aims to answer this question: does strong electronic interaction lead to novel topological quantum states? In particular, our proposal will address the following three questions:

1. Does strong electronic correlation help make a topological material?
2. Do topological insulators stay insulating or become semimetals under magnetic fields?
3. Does strong electronic correlation lead to new electronic and magnetic states?

These questions test the *hypothesis* that, in quantum material, the strong electronic interaction creates unique topological quantum states.

This proposal aims to use advanced experimental torque magnetometry techniques to give conclusive evidence in the novel electronic and magnetic states in quantum correlated topological materials. Our research starts with magnetic torque and resistance measurements in intense magnetic fields to explore the magnetic response of quantum correlated topological material. With these efforts, we hope to carry out these following tasks:

- 1: Detecting quantum oscillations of the bulk and the surface states in quantum correlated topological materials;
- 2: Revealing the origin of quantum oscillations in quantum correlated topological materials;
- 3: Searching for novel electronic and magnetic ground states in quantum correlated topological materials.

Answering all the three key questions, the proposed research lays the foundation for the understanding of the novel electronic state in the correlated topological quantum materials. Topological materials host peculiar physical properties that particularly suited for future low-dissipation electronics [1, 2]. The highly conductive surface states are topologically protected against impurity scattering. As a result, electronic devices based on topological phases have the potential to exceed the performance of conventional silicon-based field-effect transistors, with faster operation speed, lower power consumption, and higher integration density. Furthermore, in the rare earth compounds and transition metal oxides, the enhanced electronic interaction may lead to novel phases of matter and new multi-functionalities. The interaction-driven topological phases combine the beauty of symmetry protected topological states with potentially strong electronic correlation. Many new topological phases are predicted in correlated systems, such as Weyl-Kondo semimetal, quantum anomalous Hall system, topological Mott insulator, and topological superconductor. Uncovering these effects will lead to a great advance in fundamental research of correlated quantum materials and lay the material foundation for quantum information science.

Recent Progress

(1). Unusual high-field metal in a Kondo insulator (Nature Physics 2021 [3])

The search for novel Strong electronic interactions in condensed-matter systems often leads to unusual quantum phases. One such phase occurs in the Kondo insulator YbB_{12} , the insulating state of which exhibits phenomena that are characteristic of metals, such as magnetic quantum oscillations [1], a gapless fermionic contribution to heat capacity and itinerant-fermion thermal

transport [2]. To understand these phenomena, it is informative to study their evolution as the energy gap of the Kondo insulator state is closed by a large magnetic field. Here we show that clear quantum oscillations are observed in the resulting high-field metallic state in YbB_{12} ; this is despite it possessing relatively high resistivity, large effective masses, and a huge Kadowaki–Woods ratio, a combination that usually precludes quantum oscillations. Both quantum oscillation frequency and cyclotron mass display a strong field dependence. In the attached image, Fig. 1(a) shows the quantum oscillations in the high field (above 45 T) Kondo metallic phase, observed by the AC conductivity and magnetometry (PDO) measurements. In contrast, the insert of Fig. 1(b) shows the quantum oscillations in the intense field (32 T - 45 T) Kondo insulator phase, observed by resistivity. Figure 1(b) compares the Landau Level indexing plots of these two different phases: those in the insulating phase are linear as expected for a normal metal, whereas those in the metallic phase are strongly nonlinear and are very different from a normal metal.

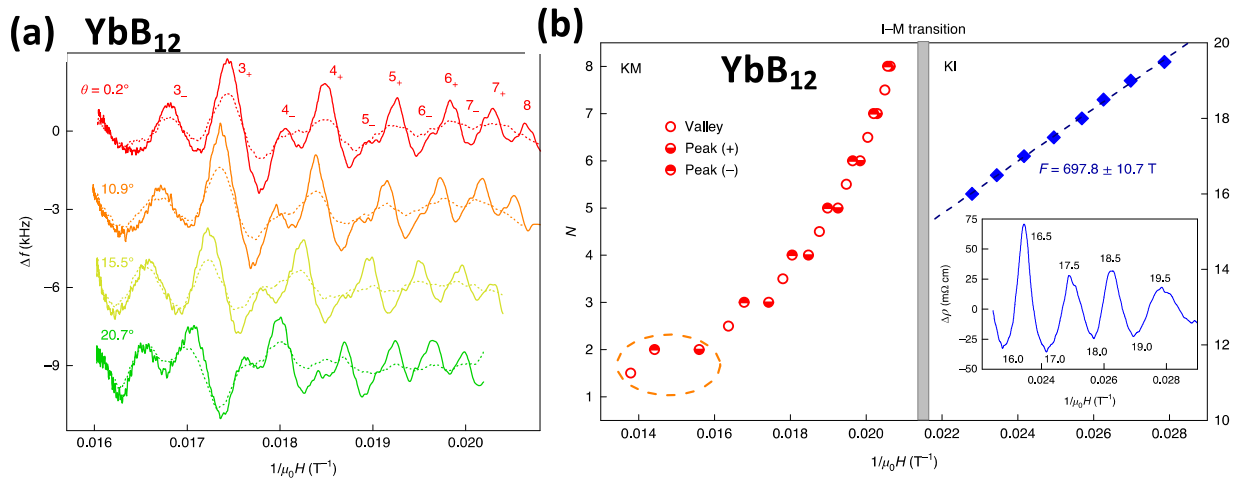


Figure 1. (a): Quantum Oscillations observe on the surface penetration depth measurement through the Polar Diode Oscillator (PDO) resonance) in YbB_{12} taken at 500 mK at various magnetic field orientations. (b): The Landau Level indexing plot in both the high field metallic state and the low field insulating state of YbB_{12} . The insert shows the original oscillation in the electrical resistivity. The Landau level indexing plot shows a standard linear trend in the insulating state. In contrast, the Landau level indexing is strongly nonlinear in the high field metallic state. Taken from Ref. [3].

By tracking the Fermi surface area, we conclude that the same quasiparticle band gives rise to quantum oscillations in both insulating and metallic states. These data are understood most simply by using a two-fluid picture in which neutral quasiparticles—contributing little or nothing to charge transport—coexist with charged fermions. Our observations of the complex field-dependent behavior of the fermion ensemble inhabiting YbB_{12} provide strong constraints for existing theoretical models.

(b) Topological surface conduction in Kondo insulator YbB_{12} (Journal of Physics D [4])

To further investigate the surface electronic state of a prototype Kondo insulator YbB_{12} , we further measured the transport properties of single crystals and microstructures. In all samples, the temperature dependence of the electrical resistivity is insulating at high temperatures, and the resistivity exhibits a plateau at low temperatures. Similar to the observation in Kondo insulator

SmB₆ [5], the magnitude of the plateau value decreases with reducing sample thickness, which is quantitatively consistent with the surface electronic conduction in bulk insulating YbB₁₂. Moreover, the magnetoresistance of the microstructures exhibits a weak-antilocalization effect at low fields. These results are consistent with the presence of a topologically protected surface state, suggesting that YbB₁₂ is a candidate material for a topological Kondo insulator. The high field resistivity measurements up to $B = 50$ T of the microstructures provide supporting evidence that the quantum oscillations of the resistivity in YbB₁₂ occur in the insulating bulk [4].

(c). Magnetometry Study of Quantum Spin Liquid materials on the interface or bulk crystals (Nano Letters 2021[6], Nature Communications 2021 [7])

Our torque magnetometry provides a powerful tool to probe the magnetic susceptibility at extreme conditions: temperatures as low as 20 mK and magnetic field as high as 65 T. We applied this technique to study the magnetic susceptibilities of quantum spin liquid candidates in both oxide interfaces and transition oxide oxides at extremely low temperatures.

We first studied a series of interface samples of a designer lattice with extremely high magnetic frustration. The work demonstrates the possible realization of a quantum spin liquid state from both experiments and theoretical calculations. In an ultrathin (111) CoCr₂O₄ slice composed of three triangular and one Kagome cation planes, the absence of a spin ordering or freezing transition is demonstrated down to 0.03 K, in the presence of strong antiferromagnetic correlations in the energy scale of 30 K between Co and Cr sublattices, leading to the frustration factor of ~ 1000 . Persisting spin fluctuations are observed at low temperatures via low-energy muon spin relaxation. Our calculations further demonstrate the emergence of highly degenerate magnetic ground states at the 0 K limit due to the competition among multiply altered exchange interactions. The results indicate the realization of a proximate quantum spin liquid state on the synthetic lattice [6].

Furthermore, our torque magnetometry is applied to answer a fundamental question on quantum spin liquid candidates: how disorder/randomness in a quantum spin liquid candidate affects its true magnetic ground state. The ultimate question is whether the quantum spin liquid survives disorder, or the disorder leads to a “spin-liquid-like” state, such as the proposed random-singlet (RS) state. Since the disorder is a standard feature of most quantum spin liquid candidates, this question represents a major challenge for quantum spin liquid candidates. YbMgGaO₄, a triangular lattice antiferromagnet with effective spin - 1/2 Yb³⁺ ions, is ideal for addressing this question since it shows no long-range magnetic ordering with Mg/Ga site disorder. However, despite the intensive study, it remains unresolved as to whether YbMgGaO₄ is a quantum spin liquid or in the RS state. Here, through ultralow-temperature thermal conductivity and magnetic torque measurements, plus specific heat and DC magnetization data, we observed a residual κ_0/T term and series of quantum spin state transitions in the zero temperature limit for YbMgGaO₄. These observations strongly suggest that a quantum spin liquid state with itinerant excitations and quantum spin fluctuations survives disorder in YbMgGaO₄ [7].

Future Plans

(a). Develop a current-driven-magnetization technique for quantum materials.

We aim to invent a new experimental technique to detect the current-driven-magnetization for quantum materials. Current-driven magnetization provides direct access to Berry curvature dipole,

the critical quantity underlying the intrinsic nonlinear Hall effect, and other responses. Driving the sample with electrical currents leads to a displaced Fermi surface in momentum space with asymmetric electron distribution. For example, in Weyl Semimetals with Berry curvature dipole, the charge current will generate a measurable spin/orbital magnetization that is intimately related to the nonlinear Hall effect.

(b). Resolving the quantum oscillations in magnetization using resonant torque differential magnetometry for pulsed magnetic fields up to 65 T and 100 T.

The quantum oscillation pattern in the ultrahigh magnetic field has only been observed in the conduction channels. For a different comparison, we would need to resolve the oscillations in magnetization (the dHvA effect) using sensitive torque differential magnetometry [8] under pulsed magnets. Quantum oscillations in magnetic susceptibility create small oscillatory forces. Therefore, the magnetic force acting on a sample glued to a resonating cantilever will shift the resonating frequencies or broaden the resonance. We choose to use quartz tuning forks for the resonating cantilevers. Our preliminary experiment succeeded in running 192 kHz tuning forks to detect the M-H hysteresis loop of underdoped YBa₂Cu₃O_{6.56} (YBCO). A tuning fork is glued to the heavy block (“qPlus” mode named for Atomic Force Microscopy), and a small AC voltage is applied to drive it to resonance. As the impedance changes, the resonance is observed in the current of the device.

The technical challenge still exists to resolve the quantum oscillations when the resonant frequency is too low and the frequency resolution in sliding FFT is about 10 Hz. And this resolution is still too large to determine quantum oscillations. To solve the problem, we have tested a range of quartz resonators with resonance frequencies in the 1.5-4 MHz range. In addition, we have built a current-voltage converter to detect excitation signals. Moreover, the tuning fork resonance is significantly damped by liquid Helium 3 when we tried to cool down samples to 0.4 K. This cold temperature is needed to resolve the dHvA effect for many materials. Therefore, we will build vacuum cells for tuning forks.

References

- [1] Z. Xiang, *et al.* “Quantum Oscillations of Electrical Resistivity in an Insulator”, *Science*, 362, 65 (2018)
- [2] Y. Sato, *et al.* “Unconventional thermal metallic state of charge-neutral fermions in an insulator”, *Nature Physics*, 15, 954 (2019)
- [3] Z. Xiang, *et al.* “Unusual high-field metal in a Kondo insulator” *Nature Physics* 17, 788 (2021)
- [4] Y. Sato, *et al.* “Topological surface conduction in Kondo insulator YbB₁₂” *Journal of Physics D* 54, 404002 (2021)
- [5] Lu Li, Kai Sun, Cagliyan Kurdak, and J. W. Aleen, “Emergent mystery in the Kondo insulator samarium hexaboride” *Nature Reviews Physics*, 2, 463 (2020).
- [6] X. Liu, *et al.* “Proximate Quantum Spin Liquid on Designer Lattice” *Nano Letters* 21, 2010 (2021)
- [7] X. Rao, *et al.* “Survival of itinerant excitations and quantum spin state transitions in YbMgGaO₄ with chemical disorder” *Nature Communications* 12, 4949 (2021)
- [8] Lu Chen, *et al.* “Torque Differential Magnetometry Using the qPlus Mode of a Quartz Tuning Fork,” *Physical Review Applied* 9, 024005 (2018).

Publications

1. Lu Chen, Ziji Xiang, Colin Tinsman, Bin Lei, Xianhui Chen, G. D. Gu, and Lu Li, “Spontaneous Nernst effect in the iron-based superconductor $\text{Fe}_{1+y}\text{Te}_{1-x}\text{Se}_x$ ” *Physical Review B* 102, 054503 (2020).
2. Lu Li, Kai Sun, Cagliyan Kurdak, and J. W. Aleen, “Emergent mystery in the Kondo insulator samarium hexaboride” *Nature Reviews Physics*, 2, 463 (2020).
3. Ziji Xiang, Lu Chen, Kuan-Wen Chen, Colin Tinsman, Yuki Sato, Tomoya Asaba, Helen Lu, Yuichi Kasahara, Marcelo Jaime, Fedor Balakirev, Fumitoshi Iga, Yuji Matsuda, John Singleton, and Lu Li “Unusual high-field metal in a Kondo insulator” *Nature Physics* 17, 788 (2021).
4. Y Sato, Z Xiang, Y Kasahara, S Kasahara, Lu Chen, C Tinsman, F Iga, J Singleton, NL Nair, N Maksimovic, JG Analytis, Lu Li, and Y Matsuda “Topological surface conduction in Kondo insulator YbB_{12} ” *Journal of Physics D* 54, 404002 (2021)
5. Xiaoran Liu, Sobhit Singh, Victor Drouin-Touchette, Tomoya Asaba, Jess Brewer, Qinghua Zhang, Yanwei Cao, Banabir Pal, Srimanta Middey, PS Anil Kumar, Mikhail Kareev, Lin Gu, DD Sarma, Padraic Shafer, Elke Arenholz, John W Freeland, Lu Li, David Vanderbilt, Jak Chakhalian “Proximate Quantum Spin Liquid on Designer Lattice” *Nano Letters* 21, 2100 (2021)
6. X Rao, G Hussain, Q Huang, WJ Chu, N Li, X Zhao, Z Dun, ES Choi, T Asaba, L Chen, L Li, XY Yue, NN Wang, J-G Cheng, YH Gao, Y Shen, J Zhao, G Chen, HD Zhou, and XF Sun “Survival of itinerant excitations and quantum spin state transitions in YbMgGaO_4 with chemical disorder” *Nature Communications* 12, 4949 (2021)

Transport experiments on quantum spin liquids

N. P. Ong, Princeton University

Program Scope

The program's focus is on the transport properties of quantum topological matter, especially thermal transport in spin liquids [1] and superconductivity in topological superconductors. In the first subtask, we employ the thermal conductivity and thermal Hall conductivity to probe the spin liquid state at temperatures down to 0.3 K. The second subtask explores signatures of topological superconductors such as the edge supercurrent in MoTe_2 recently uncovered by our group using techniques based on the proximity effect and Andreev reflections.

Recent Progress

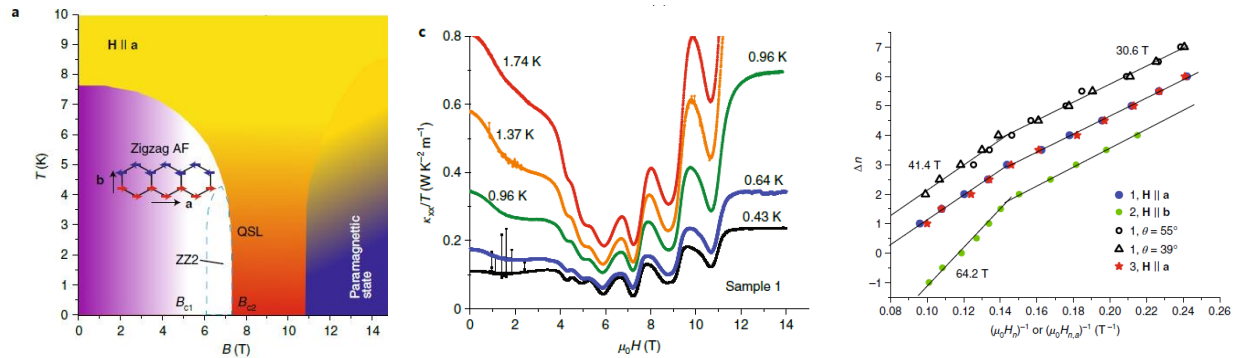


Figure 1 (Left panel) The phase diagram of $\alpha\text{-RuCl}_3$ in the B vs. T plane with $\mathbf{H} \parallel \mathbf{a}$. The antiferromagnetic zigzag state (purple) and the polarized state (deep blue) are stable below 7 T and above 11.5 T, respectively. They sandwich a spin-liquid state (orange). The middle panel shows the observed quantum oscillations in the thermal conductivity κ_{xx}/T at T from 0.43 to 1.74 K. The amplitudes are largest in the QSL state. The right panel shows the index plot of $1/H$ (or $1/H_a$) vs. integer increments Δn . The slope of the straight lines gives the “Fermi surface” area. Data from 3 samples (staggered for clarity) are shown. Czajka et al. *Nat. Phys.* 2021.

The layered quantum magnet $\alpha\text{-RuCl}_3$ is comprised of local moments in Ru arrayed on a honeycomb lattice. It is the closest proximate to the famous Kitaev honeycomb model [2] described by an Ising Hamiltonian with bond-specific (red, green and blue) exchange between nearest-neighbor spins. The ground state of the model is a spin liquid that features Majorana excitations and vortices. In $\alpha\text{-RuCl}_3$, other terms in its Hamiltonian stabilize long-range antiferromagnetic zig-zag order below 7 K in zero H . However, application of an in-plane magnetic field $\mathbf{H} \parallel \mathbf{a}$ (zigzag axis) destroys the zigzag order above 7 T, leaving a spin liquid in the field interval 7—11.5 Tesla (Fig. 1).

We performed detailed measurements of the thermal resistivity matrix λ_{ij} at temperatures T down to 0.3 K [3]. Remarkably, below 4 K, strong oscillations in the thermal conductivity κ_{xx} (measured in direction of \mathbf{H}) emerge (Fig. 1, middle panel). They resemble quantum oscillations observed in semimetals [3]. The oscillations are periodic in $1/H$ as in Shubnikov de Haas oscillations with \mathbf{H} in plane (Fig. 1, right panel). However, the material is an excellent insulator

with a charge gap of 2 eV. The oscillations suggest spin excitations that occupy a Fermi surface. From measurements over a broad interval of H and T , we find that the amplitude is largest within the spin liquid state (7 to 11.5 T). Above 12 T, the amplitude abruptly vanishes whereas below 7 Tesla, it extends as a weak tail into the zigzag phase. The experiment raises a host of interesting questions and possibilities. If the neutral fermion interpretation is correct, the results imply spinons in the spin liquid state [4].

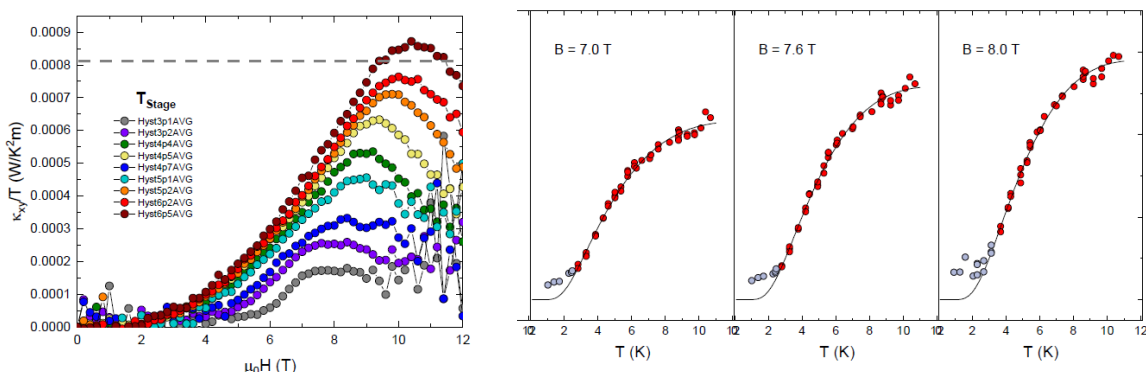


Figure 2 (Left panel) The planar thermal Hall conductivity κ_{xy}/T vs. H measured with in-plane field $\mathbf{H}||\mathbf{a}$ from $T = 3.1$ K (lowest curve, grey) to 6.5 K (uppermost, crimson). The 3 right panels display curves of κ_{xy}/T (vertical axis) versus T with B fixed at 7.0, 7.6 and 8.0 T. Solid curves are fits to Murakami's equation. Deviations below 3 K may indicate emergence of a new mode. Czajka et al. *unpublished* [6].

Concurrently with the oscillations in κ_{xx} , we have also investigated the planar thermal Hall conductivity κ_{xy} . The planar thermal Hall effect describes the appearance of a transverse heat current when \mathbf{H} is applied in the plane containing \mathbf{H} , the heat current \mathbf{J}_Q and all temperature sensors. In α - RuCl_3 , its existence was first reported by Matsuda's group (Kyoto) [5], in measurements restricted to above 3.8 K. The extended phase space we explored provides a broad perspective on how κ_{xy} varies with both T (0.3 to 10 K) and H (Fig. 2, left panel). An important characteristic of the planar κ_{xy} is its steep decrease to zero as T decreases below 4 K. At fixed H , κ_{xy}/T displays a specific T profile (Fig. 2, right panels) that fits very well to an expression (Murakami) for κ_{xy} produced by topological edge modes conveying bosonic excitations in the presence of the Berry curvature $\mathbf{\Omega}$. From the fits [6], we infer an energy scale for the excitations that agrees well with the spin gap measured by electron spin resonance (ESR) in α - RuCl_3 . Moreover, the Chern number which dictates the overall magnitude of κ_{xy}/T is found to be 1 (within our uncertainty). These results are qualitatively in conflict with the claim by the Kyoto group that κ_{xy}/T is half-quantized and carried by fermionic excitations (in that case, κ_{xy}/T should be strictly T independent, rather than strongly T dependent as observed in our experiment). The distinction between bosonic and fermionic edge modes in our experiment provides a sharp test for the validity of the half-quantization of κ_{xy} .

Future Plans

We plan to perform more measurements of κ_{xx} with \mathbf{H} rotated in the a - b (honeycomb) plane of the lattice to see how the amplitudes vary with azimuthal angle. In addition, we plan to search for the oscillations and planar Hall effect in a new spin-liquid candidate $\text{BaCo}_2(\text{AsO}_4)_2$.

References

1. Savary, L. and Balents, L., Quantum spin liquids: a review, *Rep. Prog. Phys.* **80**, 106502 (2017).
2. Kitaev, A., Anyons in an exactly solved model and beyond, *Ann. Phys.* **321**, 2-111 (2006).
3. Peter Czajka *et al.*, “Oscillations of the thermal conductivity in the spin liquid state of α - RuCl_3 ,” *Nature Physics*, **17**(8), 915–919 (2021). doi.org/10.1038/s41567-021-01243-x
4. Sodemann, I., Chowdhury, D. and Senthil, T., Quantum oscillations in insulators with neutral Fermi surfaces, *Phys. Rev. B* **97**, 045152 (2018). DOI: 10.1103/PhysRevB.97.045152
5. Kasahara, Y. et al., Majorana quantization and half-integer thermal quantum hall effect in a Kitaev spin liquid. *Nature* **559**, 227-231 (2018).
6. P. Czajka *et al.*, unpublished.

Publications

1. Sihang Liang, Satya Kushwaha, Tong Gao, Max Hirschberger, Jian Li, Zhijun Wang, Karoline Stolze, Brian Skinner, B. A. Bernevig, R. J. Cava and N. P. Ong, “A gap-protected zero-Hall effect state in the quantum limit of the non-symmorphic metal KHgSb ,” *Nature Materials* **18**, 443 (2019); doi.org/10.1038/s41563-019-0303-x
2. Ruidan Zhong, Tong Gao, N. P. Ong, R. J. Cava, “Weak-field induced nonmagnetic state in a Co-based honeycomb,” *Science Advances* **6**, eaay6953 (2020), DOI: 10.1126/sciadv.aay6953
3. Shiming Lei, Jingjing Lin, Yanyu Jia, Mason Gray, Andreas Topp, Gelareh Farahi, Sebastian Klemenz, Tong Gao, Fanny Rodolakis, Jessica L. McChesney, Christian R. Ast, Ali Yazdani, Kenneth S. Burch, Sanfeng Wu, N. Phuan Ong, Leslie M. Schoop, “High mobility in a van der Waals layered antiferromagnetic metal,” *Science Advances* **6**, eaay6407, DOI: 10.1126/sciadv.aay6407.
4. Wudi Wang, Stephan Kim, Minhao Liu, F. A. Cevallos, R. J. Cava, and N. P. Ong, “Evidence for an edge supercurrent in the Weyl superconductor MoTe_2 ,” *Science* **368**, 534-537 (2020). 10.1126/science.aaw9270
5. Peter Czajka, Tong Gao, Max Hirschberger, Paige Lampen-Kelley, Arnab Banajee, Jiaqiang Yan, David Mandrus, Stephen E. Nagler, N. P. Ong, “Oscillations of the thermal conductivity in the spin liquid state of α - RuCl_3 ,” *Nature Physics*, **17**(8), 915–919 (2021). doi.org/10.1038/s41567-021-01243-x

Novel SP2-bonded Materials and Related Nanostructures

PI: Alex Zettl, Lawrence Berkeley National Laboratory and UC Berkeley. Co PI's: Marvin Cohen, Lawrence Berkeley National Laboratory and UC Berkeley; Michael Crommie, Lawrence Berkeley National Laboratory and UC Berkeley; Alessandra Lanzara, Lawrence Berkeley National Laboratory and UC Berkeley; Steven Louie, Lawrence Berkeley National Laboratory and UC Berkeley; Feng Wang, Lawrence Berkeley National Laboratory and UC Berkeley

Program Scope

The sp² program studies, both theoretically and experimentally, sp²-bonded structures such as carbon and boron nitride nanotubes, graphene, planar h-BN, nanowires, onions, fullerenes, nanocrystals, and hybrid structures. The primary focus is on the design, synthesis, characterization, and application of low-dimensional sp²-bonded materials whose dimensions range from 1-500 nm. The program has three major thrusts: 1) Fundamentals: focus is placed on theoretical predictions of new stable structures, theoretical and experimental examinations of intrinsic electronic, magnetic, and mechanical responses, transport measurements (optical response, electrical resistivity, thermal conductivity, including suitable isotope effects), and mechanical properties and tensile strength. 2) Functionalized nanosystems: where two or more distinct nanostructures are brought together and allowed to interact. Here the emphasis is on methodologies to integrate nanosystems comprised of nanotubes and other nanoparticles interfaced with complementary nanostructures. 3) Directed growth of nanostructures: where novel synthesis and assembly methods are explored for creation of sp²-based and other nanoscale materials. Experimental approaches encompass synthesis, and characterization utilizing STM, AFM, ARPES, TEM, optics, transport, and

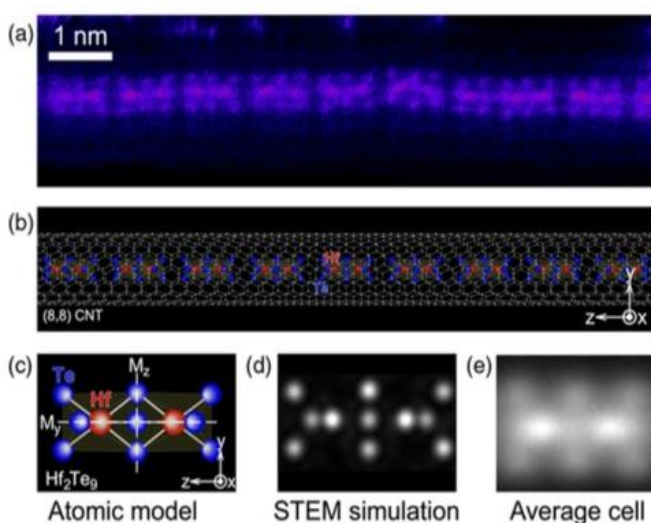


FIG. 1. Corrected HAADF STEM image of a segmented chain of Hf₂Te₉ encapsulated within a double-walled CNT. A false color is applied to visually aid the analysis. The structure consists of regularly spaced segments of Hf₂Te₉ (or Te₃-Hf-Te₃-Hf-Te₃). (b),(c) Atomic structure of the linear segmented chain of Hf₂Te₉ obtained from DFT calculations. (b) The obtained atomic structure of the segmented chain inside an (8,8) single-wall CNT is shown, where Hf and Te atoms are represented as red and blue spheres, respectively, and the chain direction is set to the z direction. (c) The building block of a Hf₂Te₉ unit is shown without a CNT for clearer presentation of the atomic structure, in which the mirror planes perpendicular to y and z axes are represented by white dashed lines and denoted as M_y and M_z, respectively. (d) Multislice simulated STEM image of a segment using the proposed atomic structure. (e) A composite STEM image generated from averaging experimentally collected 227 images. From ref. 3.

mechanical properties. Theory includes ab-initio approaches. This program also develops specialized synthesis/characterization instrumentation.

Recent Progress

The synthesis of new materials with novel or useful properties is one of the most important drivers in the fields of condensed matter physics and materials science. Such discoveries are especially significant when they point to promising future basic research and applications. van der Waals bonded materials comprised of lower-dimensional building blocks have been shown to exhibit emergent properties when isolated in an atomically thin two-dimensional form [1]. Of particular interest is the possibility of creating van der Waals bonded linear chain (one-dimensional) materials, in the single or few chain limit, encapsulated within sp^2 -bonded carbon or BN nanotubes. This program has had recent success in achieving such constructs and understanding their electronic and structural properties theoretically [2]. I shall describe the recent discovery [3] of a transition metal chalcogenide (hafnium telluride) in a heretofore unknown segmented linear chain form, where basic building blocks each consisting of two hafnium atoms and nine tellurium atoms (Hf_2Te_9) are van der Waals bonded end to end. First-principle calculations based on density functional theory reveal striking crystal-symmetry-related features in the electronic structure of the encapsulated segmented chain, including giant spin splitting and nontrivial topological phases of selected energy band states. Atomic-resolution scanning transmission electron microscopy reveals single segmented Hf_2Te_9 chains isolated within the hollow cores of carbon nanotubes, with a structure consistent with theoretical predictions. van der Waals bonded segmented linear chain transition metal chalcogenide materials could open up new opportunities in low-dimensional, gate-tunable, magnetic, and topological crystalline systems.

Future Plans

Expand characterization of new nanotube/encapsulated 1D structures to include optical response, STM spectroscopy, ARPES, and mechanical/magnetic response. Explore possible helical structures based on phosphorus and various transition metal chalcogenides. Identify mechanism for quantum emission in BN-based structures.

References

1. K. I. Bolotin, F. Ghahari, M. D. Shulman, H. L. Stormer, and P. Kim, *Nature* (London) 462, 196 (2009)
2. T. Pham, S. Oh, P. Stetz, S. Onishi, C. Kisielowski, M. L. Cohen, and A. Zettl, *Science* 361, 263 (2018)
3. Thang Pham, Sehoon Oh, Scott Stonemeyer, Brian Shevitski, Jeffery D. Cain, Chengyu Song, Peter Ercius, Marvin L. Cohen, and Alex Zettl. Emergence of Topologically Nontrivial Spin-Polarized States in a Segmented Linear Chain. *Phys. Rev. Lett.* (2020) 124, 206403 doi: 10.1103/PhysRevLett.124.206403

Publications

Category A

1. Sally Turner, Brian Shevitski, Hu Long, Maydelle Lorenzo, James Marquez, Shaul Aloni, Virginia Altoe, Marcus A. Worsley, Alex Zettl “Self-Assembly and Metal-Directed Assembly of Organic Semiconductor Aerogels and Conductive Carbon Nanofiber Aerogels with Controllable Nanoscale Morphologies” *Carbon* 153, pp 648-656 (2019)
2. Brian Shevitski, S. Matt Gilbert, Christopher T. Chen, Christoph Kastl, Edward S. Barnard, Ed Wong, D. Frank Ogletree, Kenji Watanabe, Takashi Taniguchi, Alex Zettl, and Shaul Aloni “Blue-light-emitting color centers in high-quality hexagonal boron nitride.” *Phys. Rev. B* 100, 155419 (2019)
3. Hu Long, Sally Turner, Aiming Yan, Hongmei Xu, Moonsuk Jang, Carlo Carrarod, Roya Maboudian, Alex Zettl “Plasma assisted formation of 3D highly porous nanostructured metal oxide network on microheater platform for Low power gas sensing” *Sensors and Actuators B: Chemical* 301, 127067 (2019)
4. Thang Pham, Sehoon Oh, Scott Stonemeyer, Brian Shevitski, Jeff Cain, Chengyu Song, Peter Ercius, Marvin L. Cohen, and Alex Zettl “Emergence of Topologically Non-trivial Spin-polarized States in a Segmented Linear Chain” *Phys. Rev Lett.* 124, 206403 (2020)
5. Yichuan Wu, Nirav Joshi, Shilong Zhao, Hu Long, Liujiang Zhou, Ge Ma, Bei Peng, Osvaldo N Oliveira Jr, Alex Zettl, and Liwei Lin “NO₂ gas sensors based on CVD tungsten diselenide monolayer” *Applied Surface Science* 529, 147110
6. Mehmet Dogan, S. Matt Gilbert, Thang Pham, Brian Shevitski, Peter Ercius, Shaul Aloni, Alex Zettl, and Marvin Cohen “Electron beam-induced nanopores in Bernal-stacked hexagonal boron nitride” *App. Phys. Lett.* 117, 023102 (2020)
7. Brian Shevitski, Christopher T. Chen, Christoph Kastl, Tevye Kuykendall, Adam Schwartzberg, Shaul Aloni, & Alex Zettl “Characterizing Transition-Metal Dichalcogenide Thin-Films using Hyperspectral Imaging and Machine Learning” *Scientific Reports* 10, 11602 (2020)
8. Amin Azizi, Mehmet Dogan, Hu Long, Jeffrey D. Cain, Kyunghoon Lee, Rahmatollah Eskandari, Alessandro Varieschi, Emily C. Glazer, Marvin L. Cohen, and Alex Zettl “High-Performance Atomically-Thin Room-Temperature NO₂ Sensor” *Nano Lett.* 20 6120-6127 (2020)
9. Jeffrey D. Cain, Amin Azizi, Matthias Conrad, Sinéad M. Griffin, and Alex Zettl “Layer-dependent topological phase in a two-dimensional quasicrystal and approximant” *PNAS* 117 (42) 26135-26140 (2020)
10. Scott Stonemeyer, Jeffrey D. Cain, Sehoon Oh, Amin Azizi, Malik Elasha, Markus Thiel, Chengyu Song, Peter Ercius, Marvin L. Cohen, and Alex Zettl “Stabilization of

- NbTe₃, VTe₃, and TiTe₃ via Nanotube Encapsulation” *J. Am. Chem. Soc.* 143, 12, 4563–4568 (2020)
11. Kyunghoon Lee, M. Iqbal Bakti Utama, Salman Kahn, Appalakondaiah Samudrala, Nicolas Leconte, Birui Yang, Shuopei Wang, Kenji Watanabe, Takashi Taniguchi, M. Virginia P. Altoé, Guangyu Zhang, Alexander Weber-Bargioni, Michael Crommie, Paul D. Ashby, Jeil Jung, Feng Wang, Alex Zettl “Ultra-high-resolution scanning microwave impedance microscopy of moiré lattices and superstructures” *Science Advances* 6, No. 50 eabd1919 (2020)
 12. Wenyu Zhao, Hongyuan Li, Xiao Xiao, Yue Jiang, Kenji Watanabe, Takashi Taniguchi, Alex Zettl, and Feng Wang “Nanoimaging of Low-Loss Plasmonic Waveguide Modes in a Graphene Nanoribbon” *Nano Lett.*, 21, 7, 3106–3111 (2021)
 13. Thang Pham, Scott Stonemeyer, James Marquez, Hu Long, S. Matt Gilbert, Marcus Worsley, and Alex Zettl “One-Step Conversion of Graphite to Crinkled Boron Nitride Nanofoams for Hydrophobic Liquid Absorption” *ACS Appl. Nano Mater.* (2021)
 14. Canxun Zhang, Tiancong Zhu, Salman Kahn, Shaowei Li, Birui Yang, Charlotte Herbig, Xuehao Wu, Hongyuan Li, Kenji Watanabe, Takashi Taniguchi, Stefano Cabrini, Alex Zettl, Michael P. Zaletel, Feng Wang, & Michael F. Crommie “Visualizing delocalized correlated electronic states in twisted double bilayer graphene” *Nat. Comm.* 12, 2516 (2021)
 15. Wenyu Zhao, Sihan Zhao, Hongyuan Li, Sheng Wang, Shaoxin Wang, M. Iqbal Bakti Utama, Salman Kahn, Yue Jiang, Xiao Xiao, SeokJae Yoo, Kenji Watanabe, Takashi Taniguchi, Alex Zettl & Feng Wang “Efficient Fizeau drag from Dirac electrons in monolayer graphene” *Nature* 594 pp. 517-521 (2021)

Category B

1. Thang Pham, Alex Zettl “Electrically Driven Dynamics of Few-Chain NbSe₃” *Physica Status Solidi B* 1900241 (2019)
2. S. Matt Gilbert, Adam Molnar, Donez Horton-Bailey, Helen Y. Yao, and Alex Zettl “Strain-Controlled Graphene-Polymer Angular Actuator” *MRS Advances* 4, pp 2161–2167 (2019)
3. Jeffrey D. Cain, Amin Azizi, Kathleen Maleski, Babak Anasori, Emily C. Glazer, Paul Y. Kim, Yury Gogotsi, Brett A. Helms, Thomas P. Russell, Alex Zettl “Sculpting Liquids with Two-Dimensional Materials: The Assembly of Ti₃C₂T_x MXene Sheets at Liquid–Liquid Interfaces” *ACS Nano* (2019)
4. Wu Shi, Salman Kahn, Lili Jiang, Sheng-Yu Wang, Hsin-Zon Tsai, Dillon Wong, Takashi Taniguchi, Kenji Watanabe, Feng Wang, Michael F. Crommie & Alex Zettl “Reversible writing of high-mobility and high-carrier-density doping patterns in two-dimensional van der Waals heterostructures” *Nature Electronics* (2020)

5. Amin Azizi, Mehmet Dogan, Jeffrey D. Cain, Rahmatollah Eskandari, Xuanze Yu, Emily C. Glazer, Marvin L. Cohen, and Alex Zettl “Frustration and Atomic Ordering in a Monolayer Semiconductor Alloy” *Phys. Rev. Lett.* 124, 096101 (2020)
6. Hongyuan Li, M Iqbal Bakti Utama, Sheng Wang, Wenyu Zhao, Sihan Zhao, Xiao Xiao, Yue Jiang, Lili Jiang, Takashi Taniguchi, Kenji Watanabe, Alexander Weber-Bargioni, Alex Zettl, Feng Wang “Global control of stacking order phase transition by doping and electrical field in few-layer graphene” *NanoLetters* 20, 3106-3112 (2020)
7. M. Iqbal Bakti Utama, Roland J. Koch, Kyunghoon Lee, Nicolas Leconte, Hongyuan Li, Sihan Zhao, Lili Jiang, Jiayi Zhu, Kenji Watanabe, Takashi Taniguchi, Paul D. Ashby, Alexander Weber-Bargioni, Alex Zettl, Chris Jozwiak, Jeil Jung, Eli Rotenberg, Aaron Bostwick & Feng Wang “Visualization of the flat electronic band in twisted bilayer graphene near the magic angle twist” *Nat. Phys.* 17, 184-188 (2020)
8. Chiara Trovatiello, Florian Katsch, Nicholas J. Borys, Malte Selig, Kaiyuan Yao, Rocio Borrego-Varillas, Francesco Scotognella, Ilka Kriegel, Aiming Yan, Alex Zettl, P. James Schuck, Andreas Knorr, Giulio Cerullo & Stefano Dal Conte “The ultrafast onset of exciton formation in 2D semiconductors” *Nat. Comm.* 11 5277 (2020)
9. Ziheng Yao, Xinzhong Chen, Lukas Wehmeier, Suheng Xu, Yinming Shao, Zimeng Zeng, Fanwei Liu, Alexander S. Mcleod, Stephanie N. Gilbert Corder, Makoto Tsuneto, Wu Shi, Zihang Wang, Wenjun Zheng, Hans A. Bechtel, G. L. Carr, Michael C. Martin, Alex Zettl, D. N. Basov, Xi Chen, Lukas M. Eng, Susanne C. Kehr & Mengkun Liu “Probing subwavelength in-plane anisotropy with antenna-assisted infrared nano-spectroscopy” *Nat. Comm.* 12, 2649 (2021)
10. Pin-Chun Shen, Cong Su, Yuxuan Lin, Ang-Sheng Chou, Chao-Ching Cheng, Ji-Hoon Park, Ming-Hui Chiu, Ang-Yu Lu, Hao-Ling Tang, Mohammad Mahdi Tavakoli, Gregory Pitner, Xiang Ji, Zhengyang Cai, Nannan Mao, Jiangtao Wang, Vincent Tung, Ju Li, Jeffrey Bokor, Alex Zettl, Chih-I Wu, Tomás Palacios, Lain-Jong Li, & Jing Kong “Ultralow contact resistance between semimetal and monolayer semiconductors” *Nature* 593 pp. 211-217 (2021)
11. Philipp M. Pelz, Hamish G. Brown, Scott Stonemeyer, Scott D. Findlay, Alex Zettl, Peter Ercius, Yaqian Zhang, Jim Ciston, M. C. Scott, and Colin Ophus “Phase-contrast imaging of multiply-scattering extended objects at atomic resolution by reconstruction of the scattering matrix” *Phys. Rev. Research* 3, 023159 (2021)

Poster Session Lists

Experimental Condensed Matter Physics Principal Investigators' Meeting

POSTER SESSION I Monday Morning, September 20, 2021

1. *Probing the interplay of topology, magnetism and superconductivity in intrinsic magnetic and superconducting topological materials*
Ni Ni, University of California, Los Angeles
2. *Study of topological and unconventional low-dimensional superconductors*
Qi Li, Pennsylvania State University
3. *Emergent phenomena in quantum Hall systems far from equilibrium*
Michael Zudov, University of Minnesota
4. *Toward a quantum spin liquid – materials and measurement*
Arthur Ramirez, University of California, Santa Cruz
5. *Definitive Majorana zero modes in optimized hybrid nanowires*
Sergey Frolov, University of Pittsburgh
6. *Proximity effects and topological spin currents in van der Waals heterostructures*
Ben Hunt, Carnegie Mellon
7. *Exotic quasiparticles in the fractional quantum Hall regime*
Gabor Csathy, Purdue University
8. *Broken symmetries for control of spin currents and spin-orbit torques*
Dan Ralph, Cornell University
9. *Probing novel phenomena in strongly correlated layered materials through van der Waals heterostructures*
Claudia Ojeda-Aristizabal, California State University, Long Beach
10. *Identifying the signatures of topological superconductivity and fractional excitations in bulk crystals and thin films*
Vidya Madhavan, University of Illinois

POSTER SESSION II
Monday Afternoon, September 20, 2021

1. *Science of 100 Tesla*
Neil Harrison, Los Alamos National Laboratory
2. *Van der Waals heterostructures. Novel materials and emerging phenomena*
Feng Wang, Lawrence Berkeley National Laboratory
3. *Novel synthesis of epitaxial thin films of quantum materials*
Chang-Beom Eom, University of Wisconsin, Madison
4. *Magnetoelectronic phenomena due to quantum magnetization fluctuations*
Sergei Urazhdin, Emory University
5. *Spin-polarized scanning tunneling microscopy studies of magnetic, electronic, and spintronic phenomena in nitride systems*
Arthur Smith, Ohio University
6. *Non-volatile active control of spin transport using interfaces with molecular ferroelectrics*
Xiaoshan Xu, University of Nebraska
7. *Correlated materials: Synthesis and physical properties*
Ian Fisher, SLAC National Accelerator Laboratory
8. *Superconductivity, magnetism and correlated electron phenomena in quantum materials*
Brian Maple, University of California, San Diego
9. *Novel topological Josephson junctions architectures for fault-tolerant qubits and advanced sensing*
Enrico Rossi, College of William and Mary
10. *Exploring nontrivial topological superconductivity in 2M WS₂ for topological quantum computation*
Jifa Tian, University of Wyoming

POSTER SESSION III
Tuesday Morning, September 21, 2021

1. *Antiferromagnetism and superconductivity*
Bill Halperin, Northwestern University
2. *Revealing collective spin dynamics under device-operating conditions to enhance tomorrow's electronics*
Valentina Bisogni, Brookhaven National Laboratory
3. *Spectroscopy of degenerate one-dimensional electrons in carbon nanotubes*
Junichiro Kono, Rice University
4. *Creating and probing large gap 2D topological insulators for quantum computing*
Raymond Ashoori, Massachusetts Institute of Technology
5. *Novel topological states in oriented thin films of pyrochlore iridates*
Jak Chakhalian, Rutgers University
6. *Spectroscopic investigations of novel electronic and magnetic materials*
Janice Musfeldt, University of Tennessee
7. *Planar systems for quantum information*
Jie Shan, Cornell University
8. *Symmetry engineering of topological quantum states*
Jin Hu, University of Arkansas–Fayetteville
9. *Incommensurate interfaces in intercalated quantum materials*
Joe Checkelsky, Massachusetts Institute of Technology
10. *Quantum materials*
Joseph Orenstein, Lawrence Berkeley National Laboratory

POSTER SESSION IV
Tuesday Afternoon, September 21, 2021

1. *Complex states, emergent phenomena, and superconductivity in intermetallic and metal-like compounds*
Sergey Bud'ko, Ames Laboratory
2. *Symmetries, interactions and correlation effects in carbon nanostructures*
Gleb Finkelstein, Duke University
3. *Correlated many-body quantum states in graphene heterostructures*
Philip Kim, Harvard University
4. *Quantum fluctuations in narrow band systems*
Filip Ronning, Los Alamos National Laboratory
5. *Understanding a few spin-based fundamental interactions in colloidal organic-inorganic hybrid perovskite nanostructures by ultrafast optical spectroscopy*
Min Ouyang, University of Maryland
6. *Workshop on energy research opportunities for physics graduate students and postdocs*
Cortney Bougher, American Physical Society
7. *Cold exciton gases in semiconductor heterostructures*
Leonid Butov, University of California, San Diego
8. *Symmetry breaking in two-dimensional flat-band systems for spin, charge and Cooper pair transport*
Jeanie Lau, Ohio State University
9. *Spin orbit torque in ferromagnet/topological-quantum-matter heterostructures*
John Xiao, University of Delaware
10. *Topological surface and bulk states in Dirac semimetal α -Sn thin films*
Mingzhong Wu, Colorado State University

POSTER SESSION V
Wednesday Morning, September 22, 2021

1. *Nanostructure studies of correlated quantum materials*
Doug Natelson, Rice University
2. *Correlated states of two-dimensional electron systems in AIAs quantum wells*
Mansour Shayegan, Princeton University
3. *Microwave spectroscopy of correlated 2D electron systems in semiconductors and graphene*
Lloyd Engel, Florida State University
4. *Novel temperature limited spectroscopy of quantum Hall systems*
Raymond Ashoori, Massachusetts Institute of Technology
5. *Synthesis and observation of emergent phenomena in Heusler compound heterostructures*
Chris Palmstrøm, University of California, Santa Barbara
6. *Exploring quantized axion electrodynamics in magnetic topological insulator multilayer heterostructures*
Moses Chan, Pennsylvania State University
7. *Exotic frustration-induced phenomena in artificial spin ice*
Peter Schiffer, Yale University
8. *Influence of dimensional confinement at the metal-layered crystal interface*
Timothy Kidd, University of Northern Iowa
9. *Electronic and photonic phenomena in graphene-based heterostructures*
Dmitri Basov, Columbia University
10. *Magneto-optical study of correlated electron materials in high magnetic fields*
Dmitry Smirnov, Florida State University

POSTER SESSION VI
Wednesday Afternoon, September 22, 2021

1. *Sub-nanosecond switching of antiferromagnets driven by interfacial spin-orbit torque*
Fengyuan Yang, Ohio State University
2. *One-dimensional topological nanomaterials and superconductivity*
Judy Cha, Yale University
3. *Exposing the electronic properties of topologically non-trivial and correlated compounds: A quest for topological superconductivity*
Luis Balicas, Florida State University
4. *Interfaces in epitaxial complex oxides*
Ho Nyung Lee, Oak Ridge National Laboratory
5. *Nanostructured materials: From superlattices to quantum dots*
Ivan Schuller, University of California, San Diego
6. *Superconductivity and magnetism*
Wai-Kwong Kwok, Argonne National Laboratory
7. *Hybrid-magnon quantum devices*
Axel Hoffmann, University of Illinois, Urbana-Champaign
8. *Investigation new routes to quantum disordered states*
Minhyea Lee, University of Colorado, Boulder
9. *Designing metastability: Coercing materials to phase boundaries*
Zac Ward, Oak Ridge National Laboratory

Poster Abstracts

Project Title: Quantum Materials

Principal Investigators: James Analytis, Robert Birgeneau, Edith Bourret-Courchesne, Alessandra Lanzara, Dunghai Lee, Joel Moore, Joseph Orenstein, and R. Ramesh

Affiliations: Lawrence Berkeley National Lab and University of California, Berkeley

Program Scope: This program focuses on condensed matter systems in which quantum mechanics plays a key role in determining the nature of ordered phases and the transitions between them. Our current research addresses two main themes:

Theme I: How does topology provide pathways to control transport, magnetic, and optical properties? Research in Theme I focuses on time-reversal and inversion-symmetry broken quantum materials: Weyl semimetals, transition metal dichalcogenides intercalated with magnetic ions, and skyrmion and vortex structures in polar materials.

Theme II: How do interactions among the structural, charge, orbital, and magnetic degrees of freedom generate high-T_c superconductivity? How do defects, impurities, and other forms of inhomogeneity affect these interactions? Research in Theme II seeks to disentangle the roles played by magnetic, orbital, and nematic fluctuations in generating Cooper pairing in Fe- and Cu-based superconductors, with emphasis on local probes of frustration and disorder.

Both themes are pursued with a team-oriented approach that combines bulk crystal growth and thin-film heterostructure synthesis with advanced characterization that includes: spin- and time-resolved ARPES; a suite of optical probes spanning terahertz to visible wavelengths; X-ray and neutron scattering; transport, thermodynamic, and scanning microscopy probes; and fundamental and phenomenological theoretical methods.

Recent Progress

Nonlinear electrostatics in topological semimetals: Our group is among the leaders in research whose goal is to identify and exploit the emergent properties of topological matter. Currently we are studying the two classes of Weyl semimetals (WSMs); those that break inversion and those that break time reversal symmetry. Breaking inversion symmetry allows 2nd order nonlinear electric-dipole interactions, whereby electric fields at frequency ω generate currents at 2ω and at $\omega = 0$ (phenomena known as photogalvanism and 2nd harmonic generation, respectively).

In pursuit of a clear signature of Weyl monopole singularities, we tested the prediction that the circular photogalvanic effect (CPGE) acquires a universal, quantized value in WSMs that exhibit structural chirality (de Juan et al. 2017). The CPGE is the component of photogalvanic current whose direction switches with reversal of photon helicity; uniquely, it is an emergent property

whose amplitude can be directly linked to the quantization of topological charge in a Weyl material. Using far-field coherent THz detection, we performed the first measurements of the spectrum of CPGE in the chiral Weyl semimetal, RhSi (Rees et al. 2020). The spectra display a sharp cutoff above 0.7 eV that agrees with theoretical predictions for the energy separation of Weyl nodes in RhSi. The results confirmed the topological origin of the photocurrent and showed that precise quantization was unobservable because of the presence of non-topological bands.

Direct Measurement of Helicoid Surface States in RhSi using Nonlinear Optics: In spite of the central role of Fermi arcs as a defining characteristic of topological semimetals, probing their electronic and optical properties has posed an experimental challenge, as these responses are easily overwhelmed by the contribution from the conducting bulk material. In an important theoretical proposal Chang et al. (Chang et al. 2020) showed that nonlinear optical methods could be used to directly probe Fermi arc surface states of Weyl semimetals. Taking the lead from this work, we developed a technical approach to measure the Fermi arc response, thereby opening a door to further study of the edge states of 3D topological materials (Rees et al. 2021). Our measurements of the nonlinear optical photogalvanic effect response of RhSi over a wide range of photon energies confirm important aspects of the theory [(Chang et al. 2020)].

Local optical probes of rotational and time-reversal symmetry breaking: This work is performed using an ultra-sensitive scanning polarimetric microscope developed by our group that enables mapping of local rotation-symmetry breaking. In Fe-intercalated NbS₂ we discovered that the transition to antiferromagnetic order on the triangular lattice is accompanied by local breaking of 3-fold rotational symmetry, an effect that had not been detected by X-ray and neutron scattering. Our microscope yielded striking images of domains of coupled antiferromagnetic/nematic order with relative orientation. This 3-fold (Z₃) nematic order is qualitatively different from Ising nematicity in Fe-pnictide crystals, as the global anisotropy of nematics can be continuously reoriented by external perturbations. Probing the local dynamics of nematic reorientation and domain wall propagation is a major goal of future research.

In our most recent project (Lee et al. 2021), we have measured the dynamics of magnetic domain wall motion in the WSM CoSn₂S₂. Detection of DWs in the Weyl semimetal Co₃Sn₂S₂ was performed using a scanning MOKE microscope. To measure local DW mobility the sample was placed in a coil producing H_{ac} of 30 Oe at 3 kHz. The ac MOKE signal synchronous with H_{ac} yields a signal proportional to the DW displacement, with nm sensitivity. With the local domain wall (DW) mobility as a proxy for the order parameter, we have discovered a 2D Ising phase transition that takes place *within the 2D manifold of a DW* embedded in a 3D magnetic system. This work broadens the horizon of the conventional binary classification of DWs into Bloch and Néel walls, and suggests new strategies for manipulation of DWs and their role in electron and spin transport.

Progress in superconductivity: In the Fe-based superconductors, both electronic and magnetic order play prominent roles, including possibly underlying the pairing mechanism. However, there is little quantitative information available on the nematic and magnetic correlations. We have made two important advances on these issues. First, via ARPES, we have characterized quantitatively the electronic order in the model material FeSe (Yi et al. 2019). Second, we have shown that measurements of the softening of the acoustic phonon dispersion relations as a function of temperature can yield exact information on the nematic correlation length (Wu et al. 2021). We have demonstrated this in both electron and hole doped superconductors.

In the last year, in collaboration with Bob Birgeneau and Z-X Shen's group, as well as Steven Kivelson, we examined the cause of superconductor to metal phase transition (He et al. 2020; Li, Kivelson, and Lee 2021) in overdoped cuprates. We identified the proximity to the van Hove singularity as a key player in suppressing the superfluid density hence T_c (Li, Kivelson, and Lee 2021). We identified the following as the central players in suppressing the superfluid density in over-doped cuprates: (1) the van Hove singularity enhances the anti-node to anti-node quasiparticle scattering in the presence of disorder; (2) d-wave pairing renders the above scattering pair-breaking; (3) under (1) and (2) the superconducting state spontaneously generates granularity which suppresses the superfluid density.

Future Plans:

1) Nonlinear electrodynamic of topological materials and selective probing of surface states: As described above nonlinear optics can overcome a seemingly intractable problem: detecting the electrodynamic response of topologically protected metallic surface states, despite "short-circuiting" by the metallic state that lies below. Isolating the response of the surface becomes possible in crystals with nonsymmorphic space group operations, such as screw symmetries. This provides a unique and powerful approach to probing the electrodynamic of the helicoidal surface bands predicted to occur in Weyl semimetals.

2) Dynamics of topological defects and domain walls: Topological defects (TDs) are characterized by an invariant topological charge that is resilient to local perturbations. TDs form naturally at symmetry-breaking phase transitions and can appear at the boundary between topologically distinct states of matter. Rather than obscuring intrinsic phenomena, TDs are central to the behavior of systems in which they occur. We propose to use advances in optical techniques to probe the dynamics of topological defects in quantum materials.

References

Chang, Guoqing, Jia-Xin Yin, Titus Neupert, Daniel S. Sanchez, Ilya Belopolski, Songtian S. Zhang, Tyler A. Cochran, et al. 2020. "Unconventional Photocurrents from Surface Fermi Arcs in Topological Chiral Semimetals." *Physical Review Letters* 124 (16): 166404.
He, Yu, Su-Di Chen, Zi-Xiang Li, Dan Zhao, Dongjoon Song, Yoshiyuki Yoshida, Hiroshi

- Eisaki, et al. 2020. “Superconducting Fluctuations in Overdoped $\text{Bi}_2\text{Sr}_2\text{CaCu}_2\text{O}_{8+\delta}$.” *arXiv [cond-Mat.supr-Con]*. arXiv. <http://arxiv.org/abs/2009.10932>.
- Juan, Fernando de, Adolfo G. Grushin, Takahiro Morimoto, and Joel E. Moore. 2017. “Quantized Circular Photogalvanic Effect in Weyl Semimetals.” *Nature Communications* 8 (July): 15995.
- Lee, Changmin, Praveen Vir, Kaustuv Manna, Chandra Shekhar, J. E. Moore, M. A. Kastner, Claudia Felser, and Joseph Orenstein. 2021. “Observation of a Phase Transition within the Domain Walls of the Magnetic Weyl Semimetal $\text{Co}_3\text{Sn}_2\text{S}_2$.” *arXiv [cond-Mat.mes-Hall]*. arXiv. <http://arxiv.org/abs/2104.13381>.
- Li, Zi-Xiang, Steven A. Kivelson, and Dung-Hai Lee. 2021. “Superconductor-to-Metal Transition in Overdoped Cuprates.” *Npj Quantum Materials* 6 (1): 1–7.
- Rees, Dylan, Baozhu Lu, Yue Sun, Kaustuv Manna, Rustem Ozgur, Sujan Subedi, Claudia Felser, Joseph Orenstein, and Darius H. Torchinsky. 2021. “Direct Measurement of Helicoid Surface States in RhSi Using Nonlinear Optics.” *arXiv [cond-Mat.mes-Hall]*. arXiv. <http://arxiv.org/abs/2103.09293>.
- Rees, Dylan, Kaustuv Manna, Baozhu Lu, Takahiro Morimoto, Horst Borrmann, Claudia Felser, J. E. Moore, Darius H. Torchinsky, and J. Orenstein. 2020. “Helicity-Dependent Photocurrents in the Chiral Weyl Semimetal RhSi.” *Science Advances* 6 (29): eaba0509.
- Wu, Shan, Yu Song, Yu He, Alex Frano, Ming Yi, Xiang Chen, Hiroshi Uchiyama, et al. 2021. “Short-Range Nematic Fluctuations in $\text{Sr}_{1-x}\text{NaxFe}_2\text{As}_2$ Superconductors.” *Physical Review Letters* 126 (10). <https://doi.org/10.1103/physrevlett.126.107001>.
- Yi, M., H. Pfau, Y. Zhang, Y. He, H. Wu, T. Chen, Z. R. Ye, et al. 2019. “Nematic Energy Scale and the Missing Electron Pocket in FeSe.” *Physical Review X* 9 (4): 041049.

Publications

1. Lee, Seng Huat, David Graf, Lujin Min, Yanglin Zhu, Hemian Yi, Samuel Ciocys, Yuanxi Wang, et al. 2021. “Evidence for a Magnetic-Field-Induced Ideal Type-II Weyl State in Antiferromagnetic Topological Insulator $\text{Mn}(\text{Bi}_{1-x}\text{Sbx})_2\text{Te}_4$.” *Physical Review X* 11 (3). <https://doi.org/10.1103/physrevx.11.031032>.
2. Ma, Jonathan, Ming Yi, Gregory Affeldt, Ian Hayes, Chris Jozwiak, Aaron Bostwick, Eli Rotenberg, James Analytis, Robert Birgeneau, and Alessandra Lanzara. 2020. “Spatial Nematic Fluctuation in $\text{BaFe}_2(\text{As}_{1-x}\text{Px})_2$ Revealed by Spatially and Angle-Resolved Photoemission Spectroscopy.” *Physical Review B, Condensed Matter* 101 (9). <https://doi.org/10.1103/physrevb.101.094515>.
3. Rodriguez, Josue, Gilbert Lopez, Francisco Ramirez, Nicholas P. Breznay, Robert Kealhofer, Vikram Nagarajan, Drew Latzke, et al. 2020. “Competition between Magnetic Order and Charge Localization in Na_2IrO_3 Thin Crystal Devices.” *Physical Review B, Condensed Matter* 101 (23). <https://doi.org/10.1103/physrevb.101.235415>.
4. Chen, Xiang, Yu He, Shan Wu, Yu Song, Dongsheng Yuan, Edith Bourret-Courchesne, Jacob P. C. Ruff, Zahirul Islam, Alex Frano, and Robert J. Birgeneau. 2021. “Structural and Magnetic Transitions in the Planar Antiferromagnet $\text{Ba}_4\text{Ir}_3\text{O}_{10}$.” *Physical Review B, Condensed Matter* 103 (22). <https://doi.org/10.1103/physrevb.103.224420>.

5. Huang, Jianwei, Sheng Li, Chiho Yoon, Ji Seop Oh, Han Wu, Xiaoyuan Liu, Nikhil Dhale, et al. 2021. "Room-Temperature Topological Phase Transition in Quasi-One-Dimensional Material Bi4I4." arXiv [cond-Mat.mtrl-Sci]. arXiv. <http://arxiv.org/abs/2105.13516>.
6. Huang, Jianwei, Zhicai Wang, Hongsheng Pang, Han Wu, Huibo Cao, Sung-Kwan Mo, Avinash Rustagi, et al. 2021. "Flat-Band-Induced Itinerant Ferromagnetism in RbCo2Se2." *Physical Review. B, Condensed Matter* 103 (16). <https://doi.org/10.1103/physrevb.103.165105>.
7. Song, Yu, Weiyi Wang, Eugenio Paris, Xingye Lu, Jonathan Pelliciari, Yi Tseng, Yaobo Huang, et al. 2021. "Spin Dynamics in NaFeAs and NaFe0.53Cu0.47As Probed by Resonant Inelastic X-Ray Scattering." *Physical Review. B, Condensed Matter* 103 (7). <https://doi.org/10.1103/physrevb.103.075112>.
8. Wu, Shan, Yu Song, Yu He, Alex Frano, Ming Yi, Xiang Chen, Hiroshi Uchiyama, et al. 2021. "Short-Range Nematic Fluctuations in Sr1-xNaxFe2As2 Superconductors." *Physical Review Letters* 126 (10). <https://doi.org/10.1103/physrevlett.126.107001>.
9. Wu, Shan, Junjie Yin, Thomas Smart, Arani Acharya, Craig L. Bull, Nicholas P. Funnell, Thomas R. Forrest, et al. 2019. "Robust Block Magnetism in the Spin Ladder Compound BaFe2Se3 under Hydrostatic Pressure." *Physical Review. B, Condensed Matter* 100 (21). <https://doi.org/10.1103/physrevb.100.214511>.
10. Jia, Tao, Zhuoyu Chen, Slavko N. Rebec, Makoto Hashimoto, Donghui Lu, Thomas P. Devereaux, Dung-Hai Lee, Robert G. Moore, and Zhi-Xun Shen. 2021. "Magic Doping and Robust Superconductivity in Monolayer FeSe on Titanates." *Advancement of Science* 8 (9): 2003454.
11. Li, Zi-Xiang, Steven A. Kivelson, and Dung-Hai Lee. 2021. "Superconductor-to-Metal Transition in Overdoped Cuprates." *Npj Quantum Materials* 6 (1): 1–7.
12. Song, Yu, Dongsheng Yuan, Xingye Lu, Zhijun Xu, Edith Bourret-Courchesne, and Robert J. Birgeneau. 2019. "Strain-Induced Spin-Nematic State and Nematic Susceptibility Arising from 2×2 Fe Clusters in KFe_{0.8}Ag_{1.2}Te_{2}." *Physical Review Letters* 123 (24): 247205.
13. Kozii, Vladyslav, Alexander Avdoshkin, Shudan Zhong, and Joel E. Moore. 2021. "Intrinsic Anomalous Hall Conductivity in a Nonuniform Electric Field." *Physical Review Letters* 126 (15): 156602.
14. Orenstein, J., J. E. Moore, T. Morimoto, D. H. Torchinsky, J. W. Harter, and D. Hsieh. 2021. "Topology and Symmetry of Quantum Materials via Nonlinear Optical Responses." *Annual Review of Condensed Matter Physics* 12 (1): 247–72.
15. Rees, Dylan, Kaustuv Manna, Baozhu Lu, Takahiro Morimoto, Horst Borrmann, Claudia Felser, J. E. Moore, Darius H. Torchinsky, and J. Orenstein. 2020. "Helicity-Dependent Photocurrents in the Chiral Weyl Semimetal RhSi." *Science Advances* 6 (29): eaba0509.

16. Avdoshkin, Alexander, Vladyslav Kozii, and Joel E. Moore. 2020. “Interactions Remove the Quantization of the Chiral Photocurrent at Weyl Points.” *Physical Review Letters* 124 (19): 196603.
17. Das, S., Z. Hong, V. A. Stoica, M. A. P. Gonçalves, Y. T. Shao, E. Parsonnet, E. J. Marksz, et al. 2021. “Local Negative Permittivity and Topological Phase Transition in Polar Skyrmions.” *Nature Materials* 20 (2): 194–201.
18. Das, S., Y. L. Tang, Z. Hong, M. A. P. Gonçalves, M. R. McCarter, C. Klewe, K. X. Nguyen, et al. 2019. “Observation of Room-Temperature Polar Skyrmions.” *Nature* 568 (7752): 368–72.
19. Li, Qian, Vladimir A. Stoica, Marek Paściak, Yi Zhu, Yakun Yuan, Tiannan Yang, Margaret R. McCarter, et al. 2021. “Subterahertz Collective Dynamics of Polar Vortices.” *Nature* 592 (7854): 376–80.
20. Stoica, V. A., N. Laanait, C. Dai, Z. Hong, Y. Yuan, Z. Zhang, S. Lei, et al. 2019. “Optical Creation of a Supercrystal with Three-Dimensional Nanoscale Periodicity.” *Nature Materials* 18 (4): 377–83.
21. Yadav, Ajay K., Kayla X. Nguyen, Zijian Hong, Pablo García-Fernández, Pablo Aguado-Puente, Christopher T. Nelson, Sujit Das, et al. 2019. “Spatially Resolved Steady-State Negative Capacitance.” *Nature* 565 (7740): 468–71.
22. Zhang, Hongrui, Rui Chen, Kun Zhai, Xiang Chen, Lucas Caretta, Xiaoxi Huang, Rajesh V. Chopdekar, et al. 2020. “Itinerant Ferromagnetism in van Der Waals Fe₅-xGeTe₂ Crystals above Room Temperature.” *Physical Review. B, Condensed Matter* 102 (6). <https://doi.org/10.1103/physrevb.102.064417>.
23. Little, Arielle, Changmin Lee, Caolan John, Spencer Doyle, Eran Maniv, Nityan L. Nair, Wenqin Chen, et al. 2020. “Three-State Nematicity in the Triangular Lattice Antiferromagnet Fe 1/3 NbS 2.” *Nature Materials* 19 (10): 1062–67.
24. Parker, Daniel E., Takahiro Morimoto, Joseph Orenstein, and Joel E. Moore. 2019. “Diagrammatic Approach to Nonlinear Optical Response with Application to Weyl Semimetals.” *Physical Review. B, Condensed Matter* 99 (4): 045121.
25. Rees, Dylan, Baozhu Lu, Yue Sun, Kaustuv Manna, Rustem Ozgur, Sujan Subedi, Claudia Felser, Joseph Orenstein, and Darius H. Torchinsky. 2021. “Direct Measurement of Helicoid Surface States in RhSi Using Nonlinear Optics.” Accepted for *Phys. Rev. Lett.* arXiv [cond-Mat.mes-Hall]. arXiv. <http://arxiv.org/abs/2103.09293>.

Novel Temperature Limited Spectroscopy of Quantum Hall Systems

Raymond Ashoori, Massachusetts Institute of Technology

Project Scope:

Low-dimensional electronic systems in semiconductors and in graphene have proven to be a remarkable testing ground for the physics of highly correlated states, such as the quantum Hall effect, edge states, Coulomb Blockade, and Wigner Crystallization, all of which have been extensively studied through transport measurements. However, most transport measurements are only sensitive to the structure of the system near the Fermi energy. This has driven experimentalists to search for means of measurement that provide another dimension of information beyond what is accessible by transport; that of energy level spectroscopy.

Although there is a rich body of both theoretical and experimental understanding of the quantum Hall system in semiconductors, there is study and debate about the energy scales, the transport mechanisms, and the nature of the ground state for many quantum Hall features. Many of these questions could be resolved through accurate low energy measurements of the single particle spectrum.

A traditional technique such as photoemission locally ejects a single electron from within the system under study and yields direct information about band structure, electron-electron interactions, and the resulting correlations in electron motion. The results of photoemission studies yield the “single particle density of states” otherwise known as the “single particle Green’s function”. This is a fundamental and often calculable property that forms the basis of many theoretical descriptions of interacting systems. Unfortunately, there are significant problems that hamper the use of photoemission to study low dimensional electronic systems in semiconductors and in graphene. We call our basic method “Contactless Pulsed Tunneling Spectroscopy” (CPTS).[8–11] While lacking the momentum selectivity of photoemission, CPTS has dramatically finer energy resolution. A related technique allows both momentum and energy selectivity. We call it “Momentum and Energy Resolved Tunneling Spectroscopy”, or MERTS.[12] In contrast to ARPES and STM, both CPTS and MERTS can work on insulating samples and even samples with zero electron density. They also function in high-magnetic fields. Our main aim in this work is to advance and extend these methods and to apply them to a variety of quantum Hall systems.

Recent Progress: Time, momentum, energy resolved pump-probe pulsed tunneling spectroscopy

Spectroscopy of nonequilibrium systems can uncover intricate relaxation mechanisms and short-lived metastable states that are hidden in strongly correlated materials. In a standard optical pump probe experiment, a strong laser pulse (pump pulse) is used to induce a nonequilibrium state in a sample and a weaker pulse (probe pulse) measures the changes of the physical properties (e.g. the relaxation of charge carriers and the electronic structure) of the sample on an ultrashort timescale. However, there are several limitations in applying optical pump probe techniques to low-dimensional correlated systems. First, a high intensity laser heats up the sample and forbids the study of temporal dynamics at low temperatures where many correlated electronic phases,

including superconductivity recently discovered in twisted graphene, emerge. In addition, an optical technique does not allow a precision control of the photo-excited carriers and has a difficulty in pumping the carriers into a specific energy state because the laser pulse excites the carriers into any available states that have a transition energy equal to photon energy.

We have developed a powerful new method, “time, momentum, and energy resolved pump-probe pulsed tunneling spectroscopy (Tr-MERTS)” that allows visualization of nonequilibrium states in a two-dimensional electronic system (2DES). First, Tr-MERTS can easily function in the millikelvin temperature range that has been inaccessible to standard optical pump-probe spectroscopy as the pulsed tunneling technique employs the short duty cycle measurements. Second, electrical pump pulses used in Tr-MERTS are easily tunable and permit a precision control of the pumping electron density. Finally, the electrons can be pumped into a specific energy state even for a system with equidistant energy levels (see Fig. 1b and c).

The basic Tr-MERTS measurement on a 2D-2D tunnel device proceeds as follows (Fig. 1a and b). First, we apply a “pump” pulse to eject electrons from one of the two layers (source) and pump these electrons into the other layer (target). During pumping, the energy of the pumped states in the target can be tuned by the pump pulse height. Immediately after the pump pulse, we apply a second “delay” pulse to induce an out-of-resonance condition where the pumped states in the target and the available states in the source are misaligned in energy. The pumped electrons thus cannot flow back to the source and remain in the target during the delay pulse. Finally, after the delay pulse, we apply an extremely short “probe” pulse and determine tunneling current I by measuring an initial rise of the charge dQ/dt detected at charge sensor. By controlling time delay t between the pump and probe pulses, we can identify time-dependent changes of tunneling current flowing into a nonequilibrium state. Momentum space information can be also simultaneously acquired by applying an in-plane magnetic field B_{\parallel} that shifts the momentum $\Delta k = eB_{\parallel}d/\hbar$ of the tunneling electrons, where d is the

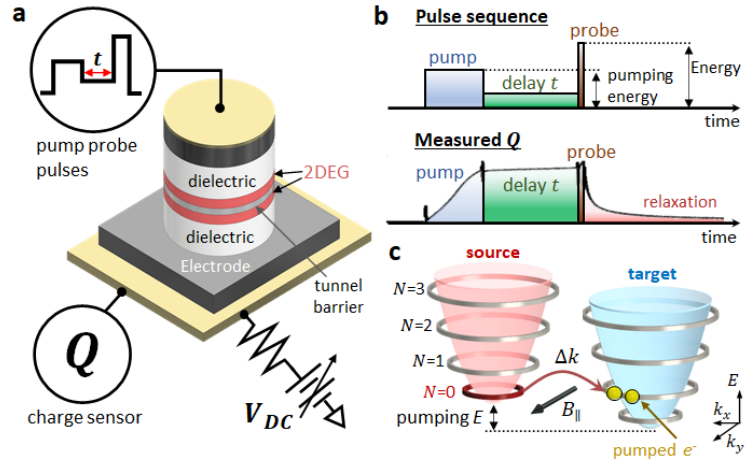


Fig.1 a, Schematic of a tunnel device and Tr-MERTS setup. The tunnel device consists of two 2DEGs separated by a thin tunnel barrier. A sequence of electrical pulses is applied at the top electrode, and the image charge Q of the tunneled electrons is detected at the bottom electrode. **b**, Pulse sequence (top) and measured Q (bottom). The first “pump” pulse ejects electrons from the source and pumps these electrons into the target. The second “delay” pulse turns off tunneling between the source and target during time delay (t). The last “probe” pulse detects tunneling current dQ/dt flowing into the target in an extremely short period of time. Momentum space information can be simultaneously acquired by applying B_{\parallel} that shifts the momentum of the tunneling electrons. **c**, A cartoon depicting the pumping process between the Landau levels in the source and target. During the pump pulse, electrons in the $N=0$ Landau level in the source are pumped into the Landau level in the target. The height of the pump pulse selects the Landau level that is being pumped.

physical separation between the target and the source. Therefore, we can map out the full transient electronic structure by tuning both t and Δk .

Fig. 2 shows a sequence of Tr-MERTS spectra measured as a function of time before ($t < 0$) and after ($t \geq 0$) pumping the target in an applied perpendicular magnetic field $B_{\perp} = 5.1$ T. The filling factors of the source and target are 0.36 and 1, respectively. Before

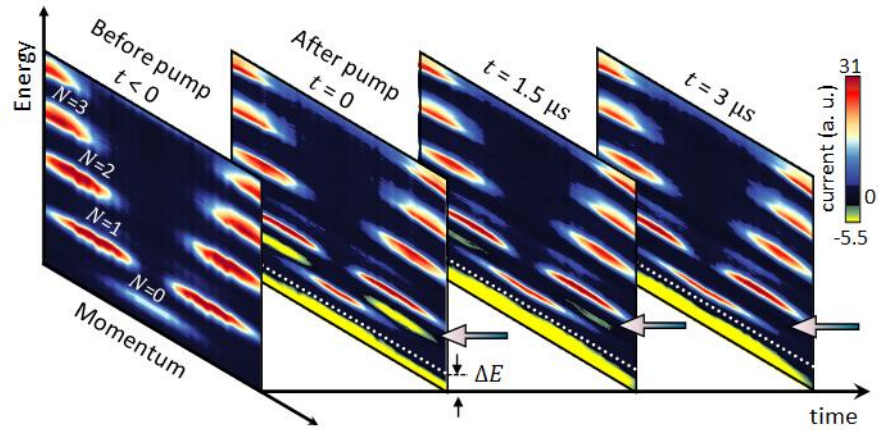


Fig. 2 A sequence of Tr-MERTS spectra measured as a function of t before or after pumping the target at $B_{\perp} = 5.1$ T and $T = 50$ mK. Arrows indicate transient features that appear immediately after pumping the $N = 1$ Landau level. The energy shift ΔE arises from a charging effect that is proportional to the density of pumped electrons.

pumping the target, the spectra show quantized Landau levels in energy and momentum space. After pumping the $N = 1$ Landau level in the target, the upward energy shift ΔE that arises from the charging energy of the pumped electrons appears in the tunneling spectra. The magnitude of ΔE is proportional to the density of the pumped electrons in the target and the constant ΔE observed in all of the spectra measured at $t \geq 0$ indicates that the pumped electrons do not leak out during the delay pulse. In addition to ΔE , the spectra at $t = 0$ show transient features at the energy slightly below the $N = 1$ Landau level (see yellow regions marked by colored arrows in Fig. 2). This transient current arises from the pumped electrons flowing back to the source under a specific condition: When the pumped energy level in the target matches the available energy states in the source, the pumped electrons can tunnel back to the source (see Fig. 3a). In such a case, the spectral weight of tunneling current is proportional to the number of the pumped electrons in the $N = 1$ Landau level. At large t , the transient current disappears as the pumped electrons in the $N = 1$ Landau level decay to a lower Landau level (see Fig. 2).

In order to study the relaxation dynamics of the electrons pumped into a higher Landau level, we measured the target filling factor ν dependence of the spectra. Fig. 3b and c show the tunneling spectra measured as a function of E and ν before and after pumping the $N = 1$ Landau level a fixed $\Delta k = 0.014 \text{ \AA}^{-1}$. The filling factor of the source is fixed at 0.36 and the source is nearly spin polarized. Before pumping the target, the tunneling spectrum shows a chemical potential jump and a sharp change of tunneling current at $\nu = 1$ (Fig. 3b) as the 2D system forms an incompressible spin-polarized state. Immediately after pumping, transient negative current (see yellow features indicated by colored arrows in Fig. 3c) that arises from the pumped electrons appear near $\nu = 1$ and at $\nu \geq 1.5$. At other filling factors, these transient features are absent because the relaxation rates of the pumped electrons are faster than the pumping rate which is set by the RC time constant (10 ~ 100 ns) of the tunnel device used in the study.

Currently, we are planning to extend our Tr-MERTS measurement on crystalline states and unconventional FQH states such as $\nu = 5/2$. We believe that further study on these quantum Hall states will reveal their unique temporal dynamics and provide better insight into the strongly correlated quantum Hall phases.

Publications

1. Ahmet Demir, Neal Staley, Samuel Aronson, Spencer Tomarken, Ken West, Kirk Baldwin, Loren Pfeiffer, Raymond Ashoori, “Correlated double-electron additions at the edge of a two-dimensional electronic system” *Physical Review Letters*, 126, 256802, June 23, 2021
2. Joonho Jang, Heun Mo Yoo, Loren N Pfeiffer, Kenneth W West, KW Baldwin, Raymond C Ashoori, “Strong interlayer charge transfer due to exciton condensation in an electrically isolated GaAs quantum well bilayer”, *Applied Physics Letters*, 118, 202110, May 17, 2021
3. HM Yoo, KW Baldwin, K West, L Pfeiffer, RC Ashoori, “Spin phase diagram of the interacting quantum Hall liquid”, *Nature Physics*, 16, 1022-1027, October 2020

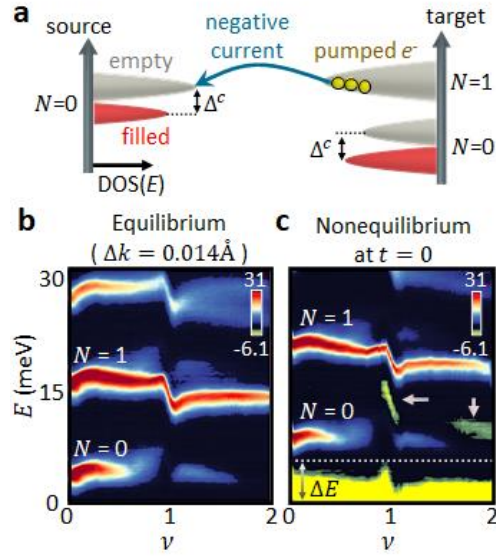


Fig. 3 a, A cartoon explaining the origin of the negative tunneling current. When the pumped electron energy aligns with the empty states in the source, the pumped electrons can tunnel back to the source. Δ^c is a Coulomb energy gap between the filled and empty states in the lowest Landau level. **b and c**, The tunneling current measured before (left) and immediately after pumping the $N = 1$ Landau level (right) at $B_{\perp} = 6.5T$ and $\Delta k = 0.014\text{\AA}^{-1}$. The vertical axis is the tunneling energy tuned by the height probe pulse (see Fig. 1b). The horizontal axis is ν proportional to the electron density of the target. The filling factor of the source is fixed at 0.35. The colored arrows indicate a negative tunneling current that arises from nonequilibrium electrons in the target.

Creating and Probing Large Gap 2D Topological Insulators for Quantum Computing

Ray Ashoori (PI), Joseph Checkelsky (Co-PI), Liang Fu (Co-PI), Nuh Gedik (Co-PI), and Pablo Jarillo-Herrero (Co-PI) Massachusetts Institute of Technology.

Program Scope: The investigation of new candidate materials for quantum computing is an essential and urgent task since the current generation of quantum computing devices are highly susceptible to errors that arise from unwanted interactions between the qubits and a noisy environment. For reducing this error sensitivity, materials that permit the realization of topological superconductors are of particular interest. The main motivation of the present QIS project is to identify new, improved platforms suitable for quantum computing, with a particular focus towards the Majorana bound states in topological superconductors.

Initially, the platform with the biggest appeal were the nanowires (which were heavily invested in by Microsoft), but after a lot of materials science research with a goal of improving that system, there are still doubts about what the experiments actually see and whether the zero bias peaks are Majorana or merely Andreev bound states. It is thus important to find alternatives to nanowires. In our proposal, we listed two main classes of setups: one based on interfaces between quantum spin Hall insulators (QSHI) and superconductors, and superconducting vortex core states. The first one relies on the identification of a high quality QSHI platform, which supports helical edge states which retain their properties over longer edge lengths and that can either be proximitized by an s-wave superconductor or can host superconductivity by itself under some conditions (for example WTe₂, which is both a two-dimensional topological insulator and a superconductor after doping). However, the present material candidates for high quality TIs are quite limited, the only experimental verified examples are HgTe and 1T' WTe₂. These have small topological gaps that likely would not lead to room temperature operation.

To broaden the candidate material platforms, we are using specialized materials growth methods to generate new TIs. Moreover, because it has proven difficult to make contacts to many of these materials, we utilizing contactless methods to screen materials for desirable TI properties such as (1) low disorder to preserve the integrity of topological edge states; (2) a large topologically non-trivial band gap to allow for high temperature operation; and (3) either intrinsic superconductivity or the capacity to develop it via proximity from an adjacent layer. The main aims of our work involve developing and improving means of growth for layered TI systems and then utilizing new contactless probes such as electronic methods such as pulsed tunneling and capacitance along with optical techniques such as laser ARPES and second harmonic generation to determine the electronic properties of these materials. We also rely heavily on theoretical guidance from Liang Fu's group in determining which materials systems to study and that could be useful for new means of quantum computing.

Recent Progress: There are three basic areas of work being done under our QIS grant. First, we are working to expand the list of topological materials and to create new functionality in these materials. Second, we are developing methods for identifying and growing new topological materials. Third, we are developing novel means for measuring these materials.

We have worked in two realms to broaden the scope of potentially topological materials. In one effort, we have focused on growing TMDs with potentially topological properties, while in the other we have worked on creating new “twistronic” materials functionality by creating layer-by-layer stacks with a twist between the layers. In this regard, the Jarillo-Herrero group and the Fu groups (with primary funding from our QIS grant) have produced a breakthrough in ferroelectricity in twisted TMD layers. Ultrathin semiconducting transition metal dichalcogenides (TMDs) such as MoSe₂ hold promise for next generation electric and optoelectronic devices thanks to their extremely rich properties such as thickness dependent band gap, strong Coulomb interactions and spin-valley locking. These properties are further enriched by employing unique degrees of freedom in van der Waals (vdW) heterostructures with non-equilibrium stacking configurations. For example, varieties of emergent phenomena such as interlayer excitons, moiré excitons, and correlated insulating states have been recently discovered in heterobilayers of TMDs. Jarillo-Herrero and Fu have discovered a new emergent property in semiconducting rhombohedral-stacked bilayer TMDs: ferroelectricity. The exfoliated bilayer TMD is non-ferroelectric because the adjacent layers are stacked antiparallel to each other.

Jarillo-Herrero and Fu’s idea utilizes vdW assembly to stack the two monolayers in parallel configuration to achieve a different crystal structure (see Figure 1). The synthetic bilayer takes rhombohedral-stacking configuration, with out-of-plane ferroelectric polarization which is flipped by in-plane sliding motion. They visualize the moiré ferroelectric domains and directly demonstrate and visualize electric-field-induced domain wall motion with piezoelectric force microscopy (PFM). The ferroelectric switching of TMDs is further confirmed using a nearby graphene electronic sensor in a ferroelectric field-effect transistor geometry. The experimentally-obtained magnitude of polarization is shown to be in excellent agreement with our first-principles calculations.

These results have some profound implications. First, the results not only introduce a new family of ferroelectric materials, but actually nearly double the number of existing room-temperature out-of-plane 2D ferroelectrics. Despite the technological importance of such 2D ferroelectric materials as ultrathin nonvolatile memory, only five of them have been identified so far. Their findings add four new nanometer-thick ferroelectrics to this series, namely rhombohedral-stacked bilayer WSe₂, MoSe₂, MoS₂, and WS₂. Second, the ferroelectric properties can be used to control the rich electric and optical properties of TMDs in a nonvolatile manner. They can obtain rare ferroelectric semiconductors by gating the TMDs, where electronic conduction is switched on and off by the polarization direction. The ferroelectric polarization is also coupled to the excitonic

properties of TMDs, enabling non-volatile electrical control of the optical response. Third, beyond the parallel-stacked systems, the layer polarized nature of TMDs demonstrated in this study will serve as fundamental building blocks of twisted homo-bilayer TMDs, and will cause dramatic electric field response both in real and momentum spaces.

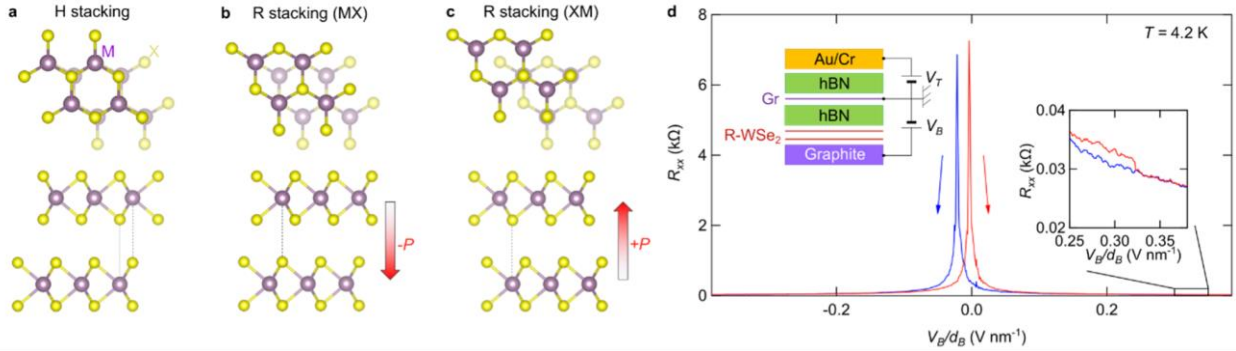


Figure 1: Ferroelectricity in R-stacked TMDs. a, H-stacked bilayer TMD. The bulk crystal form of 2H-TMD crystals. Two layers are stacked in antiparallel, and the inversion symmetry is restored as a whole. b, c, MX (b), and XM (c) stacking forms of R-stacked bilayer TMD. Two layers are stacked in parallel, and the out-of-polarization exists due to the vertical alignment of different atoms. d, The resistance of graphene in R-stacked bilayer WSe₂ devices as a function of the bottom gate in the forward and backward scan directions. Notable hysteresis is observed due to the ferroelectric nature of WSe₂.

Liang Fu's group, working together with the group of Prof. Marin Soljacic at MIT, has also made a substantial advance that we believe will greatly simplify and speed the process of finding new topological materials. Theorists have been using machine learning to find TI candidates, but the machine learning has basically acted as a black box with it being extremely difficult to tease out reductionist principles that humans can understand to give an intuition about what materials will behave as useful topological insulators. Liang and colleagues came up with a simple rule based on the chemical formula for a new material. They trained a neural net with a subset of known topological materials and determined chemical rules that are very simple. They came up with a quantity that they call the "topogivity", a number that every chemical element will have assigned to it. Using simple rules, they get a verified success rate of 70-80% in predicting topological materials. The learned topogivities are consistent with our human intuition, and moreover provide new chemical insights for understanding topological materials. Fu and collaborators apply this chemical rule to predict candidate topological materials beyond those diagnosable by symmetry indicators, and then perform DFT calculations on the candidates to determine which are truly topological. The DFT identifies a variety of topological materials, including Weyl semimetals, nodal line semimetals, and topological crystalline insulators. Many of these identified materials were not previously known in the literature and thus represent newly-discovered topological materials, including several high-quality Weyl semimetals that are promising for experimental observation. The concept of topogivity represents a fundamentally new approach to the study of topological materials, and opens up new directions of research at the intersection of chemistry, machine learning, and band topology.

Checkelsky’s group has performed synthesis and characterization of quantum materials that are potential platforms for 2D TI phases as well as materials that may be useful to probe them in heterostructures. Continuing efforts from year 1, Checkelsky’s group has improved the synthesis of both WTe_2 and ZrTe_5 (platforms for 2D TI systems). They have fine tuned Te annealing conditions to improve these materials in terms of electronic quality and filling. For ZrTe_5 in particular we have combined this with flux growth to realize high quality bulk crystals that can reach the quantum limit with fields below 1 T, allowing their characterization in the extreme quantum limit. See Fig. 2 for magnetotransport results from this material. Checkelsky’s group used similar methods to realize HfTe_5 with similar quantum limit behavior. Checkelsky and Gedik are writing a manuscript in collaboration with Gedik that combines time-resolved ARPES measurements and electric/thermoelectric characterization of vapor transport grown materials.

Future Plans: Checkelsky’s group has also used a Se flux method to synthesize WSe_2 with varying degrees of Se vacancy. These materials are potentially useful for barrier layers for tunneling. A partly QIS funded postdoc working with Jarillo-Herrero and a recently hired junior faculty member in the MIT Physics Dept. (Prof. Long Ju) to characterize their quality using a novel Fourier transform infrared photoconductivity spectroscopy experiment. The Checkelsky group has identified two new material systems in the past year and started to develop their synthesis. One is Bi_2TeI , which is comprised of 2D layers of buckled bismuthene between semiconducting BiTeI layers. Here, the structure is proposed to stabilize the long-predicted 2D TI bismuthene. Checkelsky has started to synthesize these materials using a self-flux technique.

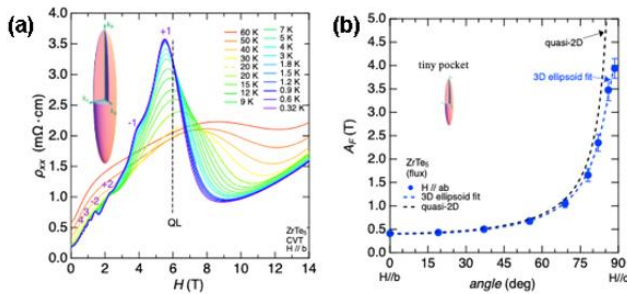


Figure 2: (a) Magnetotransport and Fermi surface in CVT grown ZrTe_5 . (b) Fermi surface cross section with low quantum limit in flux grown and annealed ZrTe_5 .

Monolayer WTe_2 has drawn significant interest as a 2D topological insulator with a relatively large bandgap that supports a quantum spin Hall state. Though the bandgap has been observed in low temperature transport, ARPES, and STM experiments, a gap was not initially expected and the origin of the gap remains an open question. Recently, transport and dc tunneling experiments have revealed two new, striking signatures of the insulating ground state in high-quality monolayers of WTe_2 : (1) quantum oscillations in the resistance of the insulating state (see Wang et al., Landau quantization and highly mobile fermions in an insulator, *Nature* **589**, 225 (2021)), and (2) spectroscopic evidence of a correlation-driven gap, possibly due to an excitonic insulator ground state (see Jia et al., Evidence for a Monolayer Excitonic Insulator, arXiv:2010.05390). Each of these phenomena is potentially groundbreaking on its own, however, neither case can be

conclusively determined by transport or dc tunneling alone. To support this point, the Ashoori and Jarillo-Herrero groups have measured transport of a 4-terminal dual-gated monolayer WTe_2 device. However, proper probing of the gap and any excitations that occur in the gap, necessitates a probe that does not require non-zero conductivity of the system under study. Tunnel capacitance and contactless pulsed tunneling spectroscopy (CPTS) are two related techniques that satisfy this requirement and allow a reliable measurement of energy gaps and excited states in the energy spectrum. Both methods are achievable in the same device geometry. To this end, we have fabricated a tunnel capacitance device and are currently measuring it. We are also working to (soon) validate the use of CPTS using WSe_2 samples that should show evidence of clear Landau level structure.

Topological insulators are characterized by insulating bulk states and conducting edge states. The Gedik group aims to use the pump-probe high-harmonic generation (HHG) ARPES to directly visualize the bulk band structure of several large-gap TI candidates. To access the band structure at a wide energy and momentum range and to map out the band structure before the sample aging, a high-repetition-rate HHG light source is crucial. Hence, the Gedik group is upgrading their HHG light source. By employing an advanced Yb-fiber laser system and gas-jet design, the Gedik group succeeded in generating sufficiently strong and stable high harmonics at a repetition rate of up to 500 kHz, a remarkable improvement compared to most HHG setups in the world. The new HHG setup will enable screening the band structure of proposed 2D TI candidates with higher efficiency and quality.

Publications

- 1. Zhang, Yang, Trithap Devakul, and Liang Fu. "Spin-textured Chern bands in AB-stacked transition metal dichalcogenide bilayers." *Proceedings of the National Academy of Sciences* 118, no. 36 (2021).**
- 2. Yang Zhang, Noah F. Q. Yuan, Liang Fu, "Moiré quantum chemistry: charge transfer in transition metal dichalcogenide superlattices", *Physical Review B, Rapid Communications*, Volume 102, 201115, 2020.**
- 3. Devakul, T., Crépel, V., Zhang, Y. and Fu, L., 2021. Magic in twisted transition metal dichalcogenide bilayers. *arXiv preprint arXiv:2106.11954***
- 4. Xirui Wang, Kenji Yasuda, Yang Zhang, Song Liu, Kenji Watanabe, Takashi Taniguchi, James Hone, Liang Fu, and Pablo Jarillo-Herrero, "Interfacial ferroelectricity in rhombohedral-stacked bilayer transition metal dichalcogenides", *arXiv:2108.07659***

Transport through Fermi arcs, unveiling electronic topology and a quest for topological superconductivity in bulk and layered materials

Luis Balicas – National High Magnetic Field Lab- Florida State University

Program Scope

Here, we proposed an effort focused on the physical properties of topological compounds, including those displaying Dirac like dispersions. For instance, we propose to explore the electrical transport properties associated with the extended Fermi arcs observed in multifold Weyl Fermions. The intent is to evaluate their surface conductivity and expose novel physical phenomena associate with the cyclotron orbits (Weyl orbits) exploring these arcs. This study should clarify if such compounds might have potential as low dissipation interconnects for Si based electronics. Compounds crystallizing in the T_d orthorhombic structure, (i.e. WTe_2 , $NbIrTe_4$ etc.) are claimed to be Weyl semimetals in the bulk and characterized by a non-trivial Z_2 topological invariant. Monolayer (1L) T_d - $MoTe_2$ displays a relatively high superconducting transition temperature, with 1L- WTe_2 seemingly displaying topological insulating behavior. We propose to explore the nature of the superconducting state resulting from the stacking of monolayers of each compound, explore the role of gating and the fabrication of moiré patterns with the hope of stabilizing triplet superconductivity with a relatively high transition temperature. The triplet nature of the pairing could be exposed through, for example, the Little-Parks effect, or the behavior of the superconducting transition temperature as a function of magnetic fields applied along a planar direction.

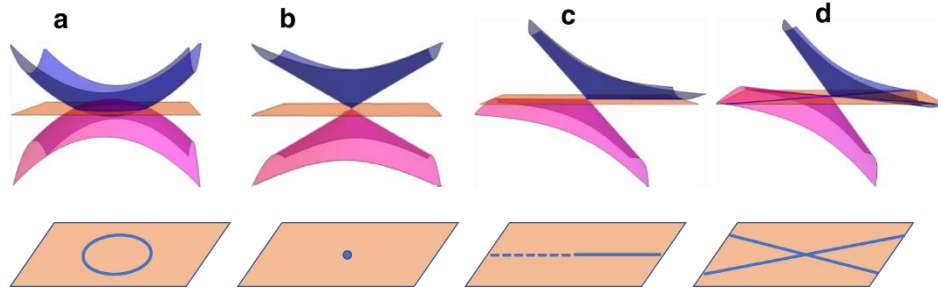


Fig. 1. (a) Bands dispersing quadratically can intersect, leading to a nodal ring when this crossing coincides with the Fermi level ε_F (depicted by the orange plane). (b) Linearly dispersing bands may meet at a point, forming a Dirac type-I node. (c) This Dirac dispersion can be tilted with respect to ε_F , leading, at a critical tilting angle, to a flat band at ε_F (forming a Dirac line [1]), characterized by highly anisotropic effective masses. The Dirac line is associated to a non-trivial topological Z_2 invariant [1]. The associated Dirac node is classified as Dirac type-III. (d) When the tilting exceeds this critical value, conduction (blue) and valence (magenta) bands would intersect at ε_F , originating electron and hole Fermi surface pockets that touch at a Dirac type-II node. From Ref. [2].

Among compounds displaying linearly dispersing bands, we realized that those belonging to the Ir_3Ge_7 family tend to display a rich Dirac structure near the Fermi level, that is displaying several Dirac nodes, i.e. Dirac type-I, tilted type-I, type-II, and even type-III nodes (Fig. 1). Dirac type-III nodes have been discussed in the context of artificial

photonic structures but have yet to be reported for any material. Given the chemical malleability of the 37 structure we propose to synthesize a number of these compounds, to expose the true nature of their electrical transport and its anisotropy.

Recent Progress

Recently, we reported the synthesis *via* an indium flux method of a novel single-crystalline compound $\text{Rh}_3\text{In}_{3.4}\text{Ge}_{3.6}$ (see Fig. 2) that belongs to the cubic Ir_3Ge_7 structure type [1]. In $\text{Rh}_3\text{In}_{3.4}\text{Ge}_{3.6}$, the In and Ge atoms choose to preferentially occupy, respectively, the $12d$ and $16f$ sites of the $Im\bar{3}m$ space group, thus creating a colored version of the Ir_3Ge_7 structure. Like the

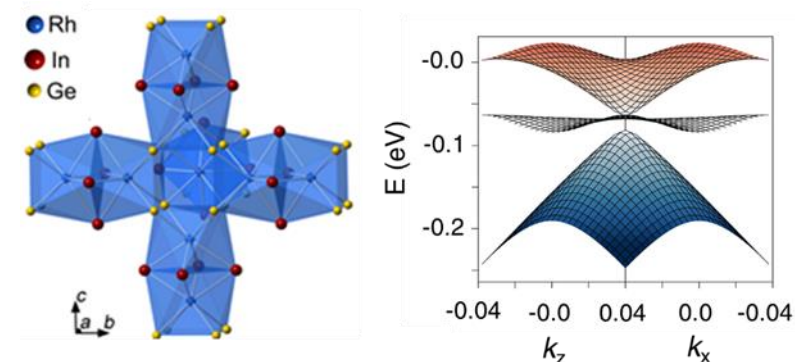


Fig. 2. Left: The crystal structure of $\text{Rh}_3\text{In}_3\text{Ge}_4$. Face-sharing dimers of Rh-centered In_4Ge_4 antiprisms are connected via edge-sharing into a framework; two such frameworks interpenetrate to form the three-dimensional Ir_3Ge_7 -type structure. Right: Electronic band dispersion around the valence band k_{h1} point showing a lateral perspective of the electronic dispersion as a function of k_x and k_y , with the bands plotted as 3D surfaces. Following the standard definition, the intersection of a Dirac node with a flat band is classified as a Dirac type-III node. Our preliminary calculations suggest that the 37 family of compounds exhibit a rich Dirac structure relatively close to the Fermi level that remains to be exposed. From Ref. [2].

other compounds of the Ir_3Ge_7 family, $\text{Rh}_3\text{In}_{3.4}\text{Ge}_{3.6}$ shows potential as a thermoelectric displaying a relatively large power factor, $PF \sim 2 \text{ mW/cmK}^2$, at a temperature $T \sim 225 \text{ K}$ albeit showing a modest figure of merit, $ZT = 8 \times 10^{-4}$, due to the lack of a finite band gap. These figures might improve through a use of chemical substitution strategies to achieve band gap opening. Remarkably, band structure calculations reveal that this compound displays a complex Dirac-like electronic structure relatively close to the Fermi level (Fig. 3). The electronic structure is composed of several Dirac type-I and type-

II nodes, and even Dirac type-III nodes that result from the crossing between a flat band and a linearly dispersing band. Our calculations indicate the presence of hitherto unreported structures

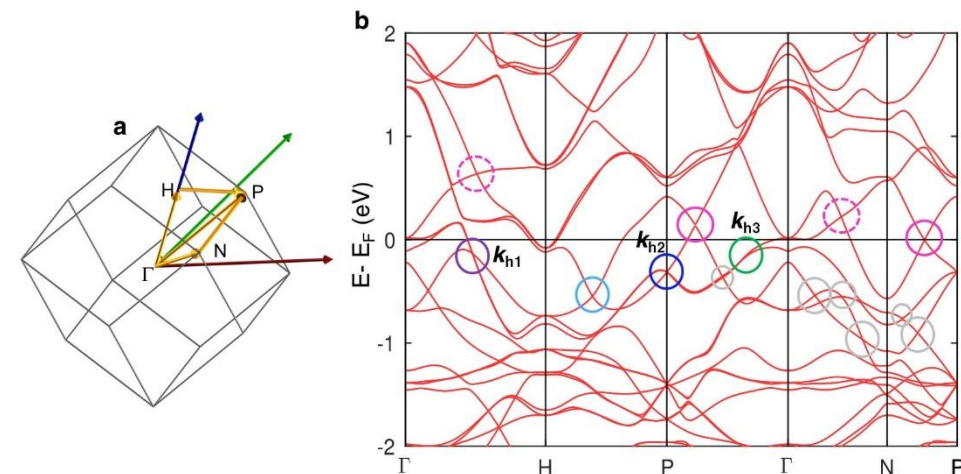


Fig. 3. (a) First Brillouin zone (BZ) for $\text{Rh}_3\text{In}_3\text{Ge}_4$ indicating its high symmetry points within its 1st BZ. (b) Electronic band structure for stoichiometric $\text{Rh}_3\text{In}_3\text{Ge}_4$. A series of band crossings leading to Dirac nodes are observed. Magenta circles and dashed magenta circles indicate Dirac type-I and tilted Dirac type-I nodes observed in the conduction band. As discussed in the main text, purple circle around k_{h1} , blue around k_{h2} and green circle surrounding k_{h3} indicates the location in the valence bands of a Dirac type-III, yet another type of Dirac type-III, and a Dirac type-II node, respectively. Clear blue and grey circles indicate the existence of other Dirac like crossings observed at lower energies.

like triple degenerate nodes where a Dirac node intersects a flat band to form a type-III node. This rich Dirac-like electronic dispersion offers the possibility to observe Dirac type-III nodes and study

their role in the physical properties of $\text{Rh}_3\text{In}_{3.4}\text{Ge}_{3.6}$ and related Ir_3Ge_7 -type materials.

We have also measured the anomalous Hall, Nernst, and thermal Hall coefficients of the itinerant ferromagnet Fe_3GeTe_2 (see, **Fig. 4**) finding that it displays several features upon cooling, like a reversal in the Nernst signal below $T = 50$ K pointing to a topological transition possibly associated to the development of bulk magnetic spin textures [3]. Since the anomalous transport variables are directly related to the texture of the Berry curvature, a possible topological transition might imply deviations from the Wiedemann-Franz (WF) law. This law has not yet been validated for the anomalous transport variables given that recent experimental studies yield contradictory, material-dependent results. Despite these features, the anomalous Hall and thermal Hall coefficients of Fe_3GeTe_2 are found, within our experimental accuracy, to satisfy the WF law for magnetic fields $\mu_0 H$ applied along its inter-layer direction.

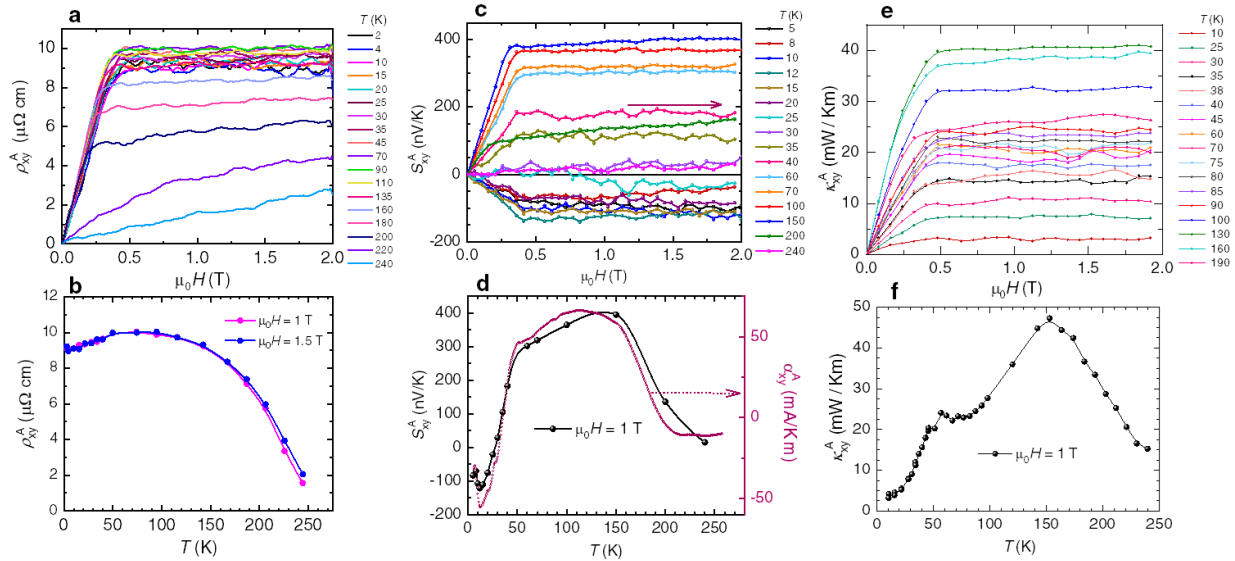


Fig.4. Anomalous transport variables for magnetic fields along the inter-layer direction. (a) Anomalous Hall resistivity $\rho_{xy}^A = R_H \cdot t$, where $R_H = V_H / I$ is the Hall resistance, t the sample thickness and I the electrical current respectively, for a $\text{Fe}_{3-x}\text{GeTe}_2$ crystal as a function of $\mu_0 H \parallel c$ -axis and for several T s. We have not subtracted the comparatively small conventional Hall signal which would add a slope superimposed onto the Hall like plateau. (b) ρ_{xy}^A under $\mu_0 H = 1$ T (magenta) and 1.5 T (blue) as a function of T . In contrast to M , ρ_{xy}^A decreases slightly below $T \leq 50$ K. (c) Anomalous Nernst effect S_{xy}^A as a function of $\mu_0 H$ for several T s. (d) S_{xy}^A as a function T collected under $\mu_0 H = 1$ T applied along the c -axis. Notice how S_{xy}^A changes sign upon cooling below ≤ 50 K after reaching a maximum at ~ 150 K. (e) Anomalous thermal Hall conductivity κ_{xy}^A as a function of $\mu_0 H \parallel c$ -axis for several T s. (f) κ_{xy}^A under $\mu_0 H = 1$ T as a function of T . Both κ_{xy}^A and S_{xy}^A display anomalies at ~ 50 and ~ 150 K. These data were collected on the same single crystal using the same electrodes, while Nernst and thermal Hall were measured simultaneously. From Ref. [3].

Surprisingly, large anomalous transport coefficients are also observed for $\mu_0 H$ applied along the planar a -axis as well as along the gradient of the chemical potential generated by thermal gradients or electrical currents, a configuration that should not lead to their observation due to the absence of Lorentz force. However, as $\mu_0 H \parallel a$ -axis is increased, magnetization and neutron scattering indicate just the progressive canting of the magnetic moments towards the planes followed by their saturation. These anomalous planar quantities are found to not scale with the component of the planar magnetization (M_{\parallel}), showing instead a sharp decrease beyond $\mu_0 H \parallel a = 4$

T which is the field required to align the magnetic moments along $\mu_0 H \parallel$. We argue that spin-canting leads to a field dependent spin chirality among non-coplanar spins in the two inequivalent Fe sites and to a novel type of topological anomalous transport in the absence of interaction between the magnetic field and electrical or thermal currents. These observations reveal not only a new way to detect and expose topological excitations, but also a new configuration for heat conversion that expands the current technological horizon for thermoelectric energy conversion.

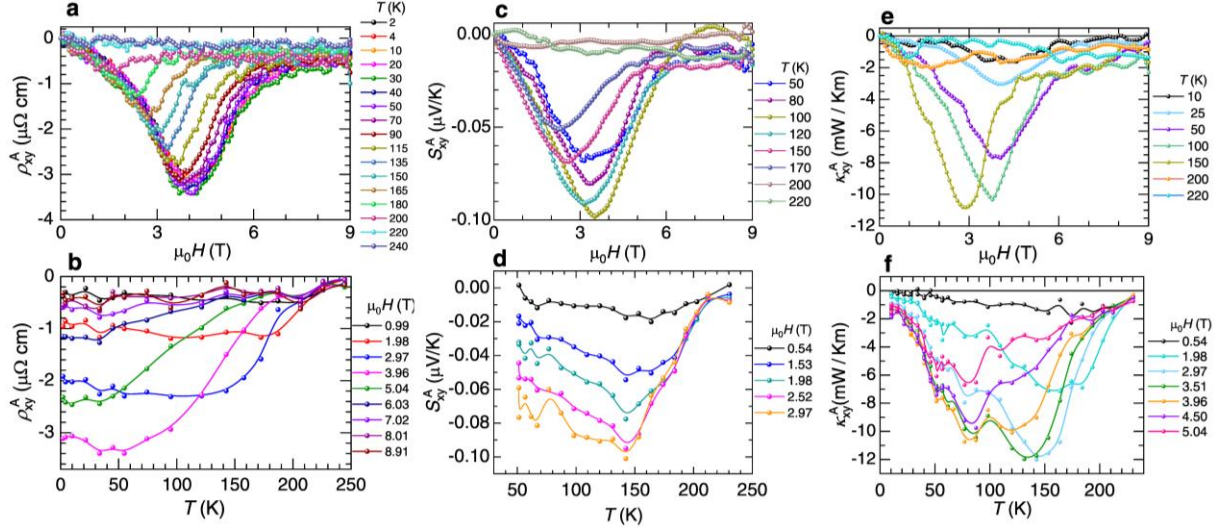


Fig. 5. Field-induced maxima in the anomalous transport variables for currents and thermal gradients aligned along $\mu_0 H \parallel$ to the a -axis. **a**, Anomalous Hall resistivity ρ_{xy}^A for a $\text{Fe}_{3-x}\text{GeTe}_2$ crystal as a function of $\mu_0 H$ applied along the a -axis and for several T s. ρ_{xy}^A displays a peak as a function of $\mu_0 H$ whose position is T -dependent. **b**, ρ_{xy}^A as a function of T for several values of $\mu_0 H$ applied along a planar direction. **c**, Anomalous Nernst effect S_{xy}^A as a function of $\mu_0 H$ along a planar direction for several T s. **d**, S_{xy}^A as a function T collected under several values of the field applied along a planar direction. **e**, Anomalous thermal Hall conductivity κ_{xy}^A as a function of $\mu_0 H$ applied along a planar direction and for several values of T . **f**, κ_{xy}^A as a function of T and for several values of $\mu_0 H$ applied along a planar direction. The anomalous transport variables follow a similar dependence on magnetic field which, contrasts with the one followed by the magnetization. From Ref. [3]

Future Plans

- 1) We are fabricating microstructures of PdGa or RhSn (space group 198, multifold Weyl fermions), to expose the so-called Weyl orbits, or cyclotron orbits involving solely the Fermi arcs.
- 2) We are finalizing measurements in $\text{Fe}_{5-x}\text{GeTe}_2$, that displays a higher Curie temperature than $\text{Fe}_{3-x}\text{GeTe}_2$ and somewhat similar anomalous topological transport up to room temperature.
- 3) We are fabricating heterostructures composed of twisted bilayer $2H\text{-NbSe}_2$ to evaluate the possible role of the moiré periodicity on its superconducting properties.
- 4) To attempt the stabilization of superconductivity in heterostructures composed of $2H\text{-NbSe}_2$ and $\text{Fe}(n-x)\text{GeTe}_2$ with goal of stabilizing a possible triplet component.
- 5) To work on the possible topological superconductivity of 1L- and 3L- $T_d\text{-MoTe}_2$, in collaboration with Columbia U. and U. of Wisconsin. Exploration of moirés, including combinations with $T_d\text{-WTe}_2$.
- 6) We are also exploring novel heterostructures of semiconducting compounds to stabilize superconductivity and correlated phases upon doping.

References

- [1] *Black-hole horizon in the Dirac semimetal $Zn_2In_2S_5$* . Huang, H. Q.; Jin, Y. W.; Liu, F., Phys. Rev. B **98**, 121110(R) (2018).
- [2] *Complex Dirac-like Electronic Structure in Atomic Site Ordered $Rh_3In_{3.4}Ge_{3.6}$* , A. F. Savvidou, J. K. Clark, H. Wang, K. Wei, E. S. Choi, S. Mozaffari, X. Qian, Michael Shatruk, L. Balicas, Chem. Mater. **33**, 1218-1227 (2021).
- [3] *Magnetic field-induced non-trivial electronic topology in $Fe_{3-x}GeTe_2$* . J. Macy, D. Ratkovski, P. P. Balakrishnan, M. Strungaru, Y.-C. Chiu, A. Flessa, A. Moon, W. Zheng, A. Weiland, G. T. McCandless, J. Y. Chan, G. S. Kumar, M. Shatruk, A. J. Grutter, J. A. Borchers, W. D. Ratcliff, E. S. Choi, E. J. G. Santos, L. Balicas, arXiv:2106.09861 (Under review at Applied Physics Reviews).

Publications

- High-temperature superconductivity on the verge of a structural instability in lanthanum superhydride*
Sun, D., Minkov, V. S., Mozaffari, S., Sun, Y., Ma, Y., Chariton, S., Prakapenka, V. B., Eremets, M. I., Balicas, L., and Balakirev, F. F. Nat. Commun. **12** (in press)
- Evidence of a coupled electron-phonon liquid in $NbGe_2$* . H.-Y. Yang, X. Yao, V. Plisson, S. Mozaffari, Scheifers, J. P., Savvidou, A. F., Choi, E. S., McCandless, G. T., Padlewski, M. F., Putzke, C., Moll, P. J. W., Chan, J. Y., Balicas, L., Burch, K. S., and Tafti, F. Nat. Commun. **12**, ? (2021): DOI:10.1038/s41467-021-25547-x.
- Superconductivity up to 243K in the yttrium-hydrogen system under high pressure*. Kong, P., Minkov, V. S., Kuzovnikov, M. A., Drozdov, A. P., Besedin, S. P., Mozaffari, S., Balicas, L., Balakirev, F. F., Prakapenka, V. B., Chariton, S., Knyazev, D. A.; Greenberg, E., Eremets, M. I. Nat. Commun. **12**, 5075 (2021).
- Paramagnetic Molecular Semiconductors Combining Anisotropic Magnetic*. Ungor, O., Burrows, M., Liu, T. H., Bodensteiner, M., Adhikari, Y., Hua, Z. Q., Casas, B., Balicas, L., Xiong, P., Shatruk, M., Inorg. Chem. **60**, 10502-10512 (2021).
- Experimental Observation and Spin Texture of Dirac Node Arcs in Tetradymite Topological Metals*. Dai, J., Frantzeskakis, E., Aryal, N., Chen, K. W., Fortuna, F., Rault, J. E., Le Fevre, P., Balicas, L., Miyamoto, K., Okuda, T. Manousakis, E., Baumbach, R. E., Santander-Syro, A. F. Phys. Rev. Lett. **126**, 196407 (2021).

7. *Complex Dirac-like Electronic Structure in Atomic Site Ordered $Rh_3In_{3.4}Ge_{3.6}$* , A. F. Savvidou, J. K. Clark, H. Wang, K. Wei, E. S. Choi, S. Mozaffari, X. Qian, Michael Shatruk, L. Balicas, Chem. Mater. **33**, 1218-1227 (2021).
8. *Giant and Reversible Barocaloric Effect in Trinuclear Spin-Crossover Complex $Fe_3(bntrz)_6(tcnsct)_6$* , M. Romanini, Y. Wang, K. Gürpınar, G. Ornelas, P. Lloveras, Y. Zhang, W. Zheng, M. Barrio, A. Aznar, A. Gràcia-Condal, B. Emre, O. Atakol, C. Popescu, H. Zhang, Y. Long, L. Balicas, J. L. Tamarit, A. Planes, M. Shatruk, L. Mañosa, Adv. Mater. **33**, 2008076 (2021).
9. *Bulk Fermi surface of the Weyl type-II semimetallic candidate $NbIrTe_4$* . R. Schönemann, Y.-C. Chiu, W. Zheng, V. L. Quito, S. Sur, G. T. McCandless, J. Y. Chan, and L. Balicas, Phys. Rev. B **99**, 195128 (2019).
10. *Kondo behavior in $IT-VTe_2$ single crystals*, X. Ding, J. Xing, G. Li, L. Balicas, K. Gofryk, and H.-H. Wen, Phys. Rev. B **103**, 125115 (2021).
11. *Bulk Fermi surfaces of the Dirac type-II semimetallic candidate $NiTe_2$* , W. Zheng, R. Schönemann, S. Mozaffari, Y.-C. Chiu, Z. Bryce Goraum, N. Aryal, E. Manousakis, T. M. Siegrist, K. Wei, and L. Balicas, Phys. Rev. B **102**, 125103 (2020).
12. *Multiple Dirac Nodes and Symmetry Protected Dirac Nodal Line in Orthorhombic α - $RhSi$* , S. Mozaffari, N. Aryal, R. Schönemann, K.-W. Chen, W. Zheng, G. T. McCandless, J. Y. Chan, E. Manousakis, and L. Balicas, Phys. Rev. B **102**, 115131 (2020).
13. *Superconductivity in single crystals of $ZrP_{1.27}Se_{0.73}$* , K.-W. Chen, G. Chappell, S. Zhang, W. Lan, T. Besara, K. Huang, D. Graf, L. Balicas, A. P. Reyes, and R. E. Baumbach, Phys. Rev. B **102**, 144522 (2020).
14. *Fermi surface of $PtCoO_2$ from quantum oscillations and electronic structure calculations*, F. Arnold, M. Naumann, H. Rosner, N. Kikugawa, D. Graf, L. Balicas, T. Terashima, S. Uji, H. Takatsu, S. Khim, A. P. Mackenzie, and E. Hassinger, Phys. Rev. B **101**, 195101 (2020).
15. *Thermal transport in yttrium iron garnet at very high magnetic fields*, D. R. Ratkovski, L. Balicas*, A. Bangura, F. L. A. Machado, and S. M. Rezende, Phys. Rev. B **101**, 174442 (2020).
16. *Origin of the butterfly magnetoresistance in a Dirac nodal-line system*, Y. -C. Chiu, K. -W. Chen, R. Schönemann, V. L. Quito, S. Sur, Q. Zhou, D. Graf, E. Kampert, T. Förster, K. Yang, G. T. McCandless, Julia Y. Chan, R. E. Baumbach, M. D. Johannes, and L. Balicas, Phys. Rev. B **100**, 125112 (2019).
17. *Possible manifestations of the chiral anomaly and evidence for a magnetic field induced topological phase transition in the type-I Weyl semimetal $TaAs$* , Q. R. Zhang, B. Zeng, Y. C. Chiu, R. Schönemann, S. Memaran, W. Zheng, D. Rhodes, K.-W. Chen, T. Besara, R. Sankar, F. Chou,

G. T. McCandless, J. Y. Chan, N. Alidoust, S.-Y. Xu, I. Belopolski, M. Z. Hasan, F. F. Balakirev, and L. Balicas, *Phys. Rev. B* **100**, 115138 (2019).

18. *Antiferroelectric Phase Transition in a Proton-Transfer Salt of Squaric Acid and 2,3-Dimethylpyrazine*, J. Lengyel, X. Wang, E. S. Choi, T. Besara, R. U. Schönemann, S. K. Ramakrishna, J. Holleman, A. L. Blockmon, K. D. Hughey, T. Liu, J. Hudis, D. Beery, L. Balicas, S. A. McGill, K. Hanson, J. L. Musfeldt, T. Siegrist, N. Dalal, M. Shatruk, *JACS* **141**, 41, 16279 (2019). DOI: 10.1021/jacs.9b04473.

Electronic and photonic phenomena in graphene-based heterostructures

D.N. Basov, Columbia University

Program Scope

The PI investigates two new classes of physical phenomena in graphene-based van der Waals (vdW) heterostructures:

Thrust 1. The PI proposed to study surface plasmon polariton (SPP) propagation in current-carrying graphene devices. Recently published work [1] uncovered the effect of plasmonic drag by electrical currents. These findings pave the way for the systematic imaging of the current flow patterns in graphene in both ohmic and hydrodynamic regimes.

Thrust 2. The PI proposed to harness surface plasmon polaritons to quantify charge transfer across graphene/RuCl₃ interfaces. RuCl₃ is interesting in its own right: the Mott insulator and quantum spin liquid candidate material. The PI plans to visualize the spatial inhomogeneity associated with the charge transfer and will probe the dynamics in the top atomic layers on the RuCl₃ side of the interface proximal to graphene.

Recent Progress

The PI discovered polaritonic drag in current carrying graphene reminiscent of the Fizeau effect for light in moving water. Fizeau's momentous discovery is among the experimental cornerstones of Einstein's special relativity theory and is well understood in the context of relativistic kinematics. In contrast, experiments on dragging photons by an electron flow in solids are riddled with inconsistencies and have so far eluded agreement with the theory. The PI reported on the electron flow dragging surface plasmon polaritons: hybrid quasiparticles of infrared photons and electrons in graphene. The drag is visualized directly through infrared nano-imaging of propagating plasmonic waves in the presence of a high-density current. The polaritons in graphene shorten their wavelength when propagating against the drifting carriers. Unlike the Fizeau effect for light, the SPP drag by electrical currents defies explanation by simple kinematics and is linked to the nonlinear electrodynamics of Dirac electrons in graphene. The observed plasmonic Fizeau drag enables breaking of time-reversal symmetry and reciprocity at infrared frequencies without resorting to magnetic fields or chiral optical pumping. The Fizeau drag also provides a tool with which to study interactions and nonequilibrium effects in electron liquids.

The PI has established that graphene offers an ideal medium for observing the plasmonic Fizeau drag as it supports the propagation of highly-confined, long-lived and electrically tunable

surface plasmon polaritons. Crucially, graphene also withstands ultra-high current densities so that the carrier drift velocity u can be comparable with the SPP group velocity. In the absence of current, the SPP dispersion follows $\omega(-q) = \omega(q) \sim \sqrt{q}$ (Fig. 1a), where ω and q are the frequency and wavevector of SPPs, respectively. Under applied current, the dispersion can be expected to depend on the relative orientation of SPP propagation and carrier flow, generating the plasmonic Fizeau effect that breaks the reciprocity of the system: $\omega(-q) \neq \omega(q)$. The PI exploited the unique attributes of graphene to demonstrate the physics of the plasmonic Fizeau effect where SPPs are dragged by drifting Dirac electrons.

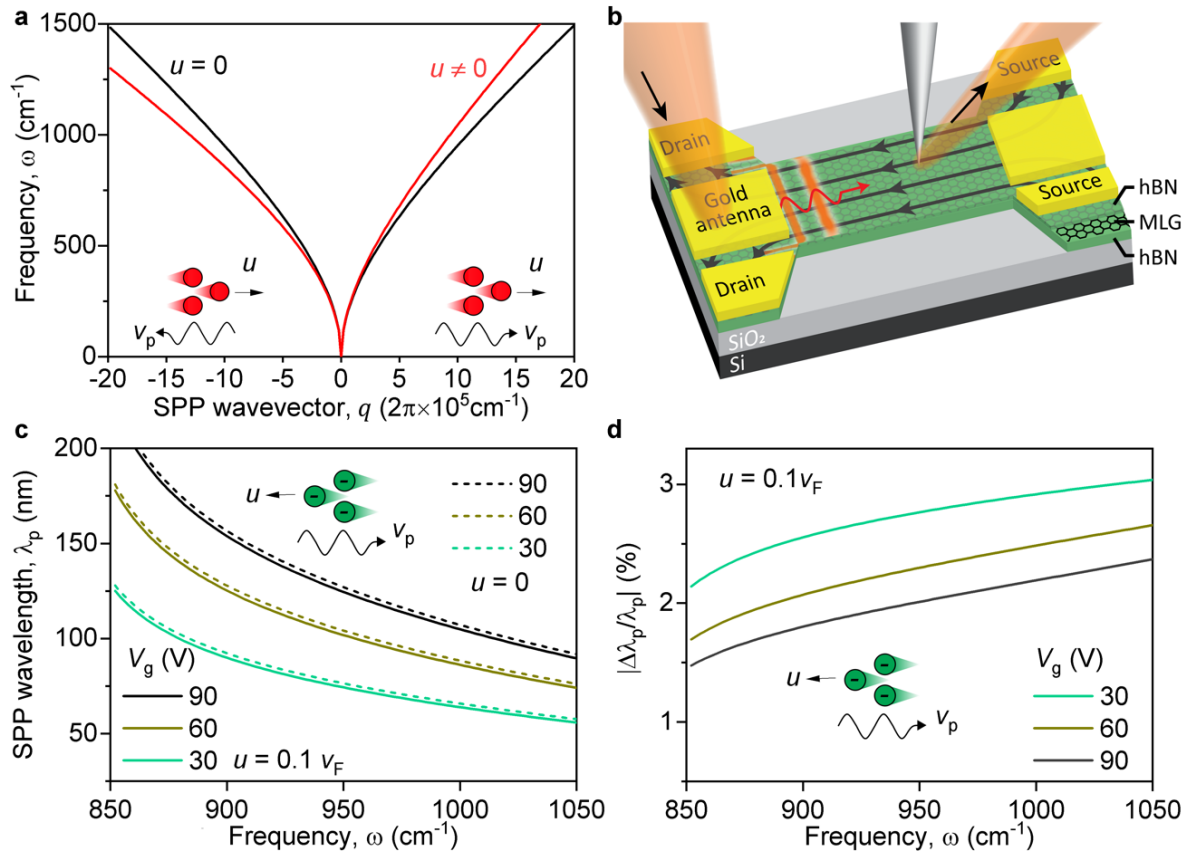


Fig. 1. Plasmonic Fizeau drag in graphene: theory and modeling. **a**, theoretically predicted SPP dispersion with (red line) and without (black line) drifting carriers. Carrier density is $n = 1 \times 10^{11}$ cm⁻² and the non-zero drift velocity is $u=0.7v_p$, with $+u$ along $+q$ direction. Wavy black arrows indicate SPP propagating direction and straight black arrows represents carrier drift direction. **b**, schematic of a graphene device with a constricted channel. Under the illumination of an IR laser, gold antennas launched propagating SPPs, which were visualized by near-field tip-based imaging. Black streamlines represent carrier drift directions. **c**, the SPP wavelength plotted as a function of the laser frequency with (solid lines) and without (dashed lines) current at different gate voltages V_g . The SPP wavelength is diminished under drifting current. **d**, the Fizeau shift $|\Delta\lambda_p/\lambda_p|$ as a function of the laser frequency ω at different gate voltages V_g for a typical drift velocity $u = 0.1v_F$. Adapted from Ref.[1].

The current-induced Fizeau drag of plasmons discovered by the PI reveals novel aspects of interactions between infrared photons and Dirac electrons in graphene. Commonly, drag effects are understood as friction-like momentum transfer between two coupled sub-systems. Examples include Coulomb drag between spatially separated conductors, or drag effects between electrons and phonons in a crystal. New data generated by the PI show that the notion of drag need to be extended to the two constituents of a polaritonic quasiparticle: a superposition of IR photons and Dirac electrons. By ramping up the current in our platform (Figure 1), the PI solely perturbed the electronic constituent of the quasiparticles. The photonic component reacts by abiding to the rules of quasi-relativistic theory.

Future Plans

Thrust 1. The PI plans to continue systematic studies of plasmonic drag in graphene-based heterostructure. The in-depth theoretical analysis and modeling revealed that the observed plasmonic drag is not a mere consequence of relativistic kinematics. The plasmonic Fizeau drag in graphene is inherently a non-equilibrium and nonlinear phenomenon whose magnitude depends on dynamics of electron-electron, electron-phonon, and electron-photon interactions of the Dirac electrons. A task for future experiments is to map the Fizeau drag for the entire dispersion in order to optimize the infrared nonreciprocity for on-the-chip applications. In principle, plasmonic Fizeau drag offers means to probe the unique motional Fermi liquid effects, and can be extended to double layer graphene system. The PI plans to extend the Fizeau drag experiments to twisted bilayer graphene. These latter experiments present intriguing opportunities to probe the physics of Fermi velocity renormalization and strong correlations in the electronic system. Moreover, by further enhancing the drift velocity of carriers and approaching the plasmon velocity, plasmon instability and amplification are expected to pave the way towards realizing plasmonic emission. At the moment, it is unclear if the regime of plasmonic instabilities is attainable in realistic devices. Ongoing measurement carried out by the PI are intended to provide high-fidelity experimental answers.

Thrust 2. Using a charge-transfer heterostructure consisting of graphene on α -RuCl₃, the PI plans to conduct a proof-of-concept study demonstrating the existence of intrinsic nanoscale lateral p-n junctions in the vicinity of graphene nanobubbles. Our multi-pronged experimental approach incorporates scanning tunneling microscopy (STM) and spectroscopy (STS) in collaboration with Prof. Pasupathy and scattering-type scanning nearfield optical microscopy (*s*-SNOM) developed in the group of the PI. A combination of these two imaging modalities will simultaneously probe both the electronic and plasmonic responses of nanobubble p-n junctions.

Preliminary results obtained by the PI are exciting and encourage further pursuit. The PI focused on nanobubbles that arise spontaneously at the heterostructure interface during fabrication as a testbed for probing the in-plane and out-of-plane behavior of interlayer charge transfer. Differential conductivity maps and point spectroscopy performed at the boundary of nanobubbles reveal that highly-doped and nominally undoped graphene are separated by a lateral distance of

less than 3 nm and vertically by < 0.5 nm, generating internal fields on the order of 10^8 V/m that are largely confined to the graphene plane. At the same time, the rapid change in the graphene conductivity in the vicinity of nanobubbles acts as a hard plasmonic barrier that reflects surface plasmon polaritons generated in the course *s*-SNOM measurements. The results of STS measurements will inform the interpretation of the *s*-SNOM data and allow the PI to accurately model the complex valued nearfield signal in the vicinity of nanobubbles using a perturbative point-scatterer approach.

The PI has already developed a procedure for fabricating graphene/ α -RuCl₃ heterostructures using standard dry transfer techniques from components isolated using exfoliation from single-crystal sources. α -RuCl₃ flakes and single-layer graphene were sequentially lifted from an SiO₂ substrate using a poly(bisphenol A carbonate) (PC) coated transfer slide. The PC together with the stack were flipped over onto an SiO₂ chip such that the graphene faced upward. Using a micro soldering method, a Field's metal indium alloy is placed on the graphene flake in order to make electrical contact for STM measurements. This technique preserves sample quality compared to lithography methods. The resulting heterostructure consists of large regions of flat graphene forming a good interface with the underlying α -RuCl₃, which are occasionally interrupted by graphene nanobubbles.

In order to gain insight into the spatial dependence of interlayer charge transfer, the PI performed a series of STM and STS measurements in the vicinity of four different graphene nanobubbles (in collaboration with Prof. A.Pasupathy). Armed with the results of STM and STS experiments, the PI will thoroughly investigate *s*-SNOM images conducted on graphene nanobubbles. Preliminary data were collected on four different nanobubbles over a frequency range of 930 – 2280 cm⁻¹. These data reveal characteristic images of plasmonic waves. Immediately outside the radius of the nanobubble, radial oscillations of both nearfield channels decay as a function of distance. A closer examination of linecuts is needed to show if the spacing between fringes clearly disperses with frequency. However, it is not immediately obvious from the preliminary data whether the fringes arise from plasmons generated on and propagating away from nanobubbles or if they are the result of plasmonic generation at the AFM tip that reflect from the nanobubble boundary (or both). Ongoing experiments are aimed at resolving this uncertainty.

Publications

- [1] Y. Dong, L. Xiong, I.Y. Phinney, Z. Sun, R. Jing, A.S. McLeod, S. Zhang, S. Liu, F.L. Ruta, H. Gao, Z. Dong, R. Pan, J.H. Edgar, P. Jarillo-Herrero, L.S. Levitov, A.J. Millis, M.M. Fogler, D.A. Bandurin, and D.N. Basov, “*Fizeau drag in graphene plasmonics*,” Nature 594, 513 (2021)
- [2] Sai S. Sunku, Alexander S. McLeod, Tobias Stauber, Hyobin Yoo, Dorri Halbertal, Guangxin Ni, Aaron Sternbach, Bor-Yuan Jiang, Takashi Taniguchi, Kenji Watanabe, Philip Kim, Michael M. Fogler, and D. N. Basov “*Nano-photocurrent Mapping of Local Electronic Structure in Twisted Bilayer Graphene*” Nano Lett. 20, 2958 (2020).

Revealing Collective Spin Dynamics Under Device-Operating Conditions to Enhance Tomorrow's Electronics

Valentina Bisogni, National Synchrotron Light Source II, Brookhaven National Laboratory, USA, bisogni@bnl.gov

Program Scope

Collective spin excitations (CSE) in quantum materials provide a revolutionary alternative for devices with improved performances and energy-efficiency, as they permit the transfer of information without any movement of charge, thus eliminating the dominant source of energy dissipation. Understanding how to manipulate CSE would provide a foundation for the next generation of energy-efficient electronic devices. A promising direction is to undertake the study of the microscopic spin dynamics in technologically relevant quantum materials under device-operating conditions. This FWP focuses on utilizing soft X-ray Resonant Inelastic Scattering (RIXS) to achieve an unprecedented insight into the material properties and the behavior of the CSE when subject to device-relevant perturbations of applied current, electric-field, and temperature gradient.

Recent Progress

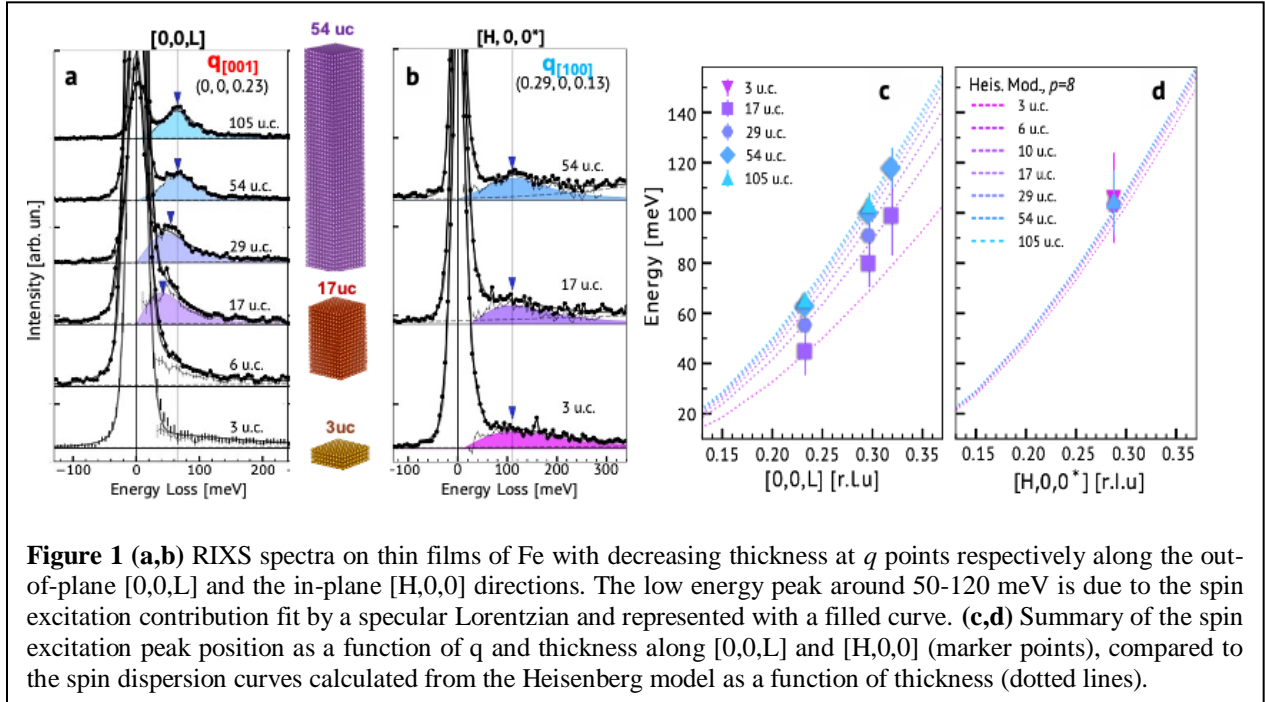
Spin excitations of magnetic thin films are the founding element for novel transport concepts in spintronics, magnonics, and magnetic devices in general. In the last two years of this FWP, we focused on 1) the evolution of the spin dynamics as a function of sample thickness, within the mesoscale range; 2) the investigation of the CSE involved in the spin transport phenomena.

Tuning Spin Excitations in Magnetic Films by Confinement

While spin dynamics have been extensively studied in bulk materials, their detection in mesoscopic films -- spanning from a few monolayers to a hundred nanometers -- has been hampered so far by experimental limitations. However, there are still many outstanding unanswered questions of how magnetic properties and excitations evolve and emerge in low dimensional systems, such as thin films. In fact, the interplay between confinement, dimensionality, interface/surface hybridization, strain, and exchange-bias, has the potential to realize an effective tuning of magnetism in thin films, ultimately leading to exquisite control of spin dynamics. Understanding how such spin dynamics unfold in low-dimensional magnetic systems is thus an essential step towards gaining control of spin wave-based transport phenomena.

To this purpose, we performed studies of the evolution of the spin dynamics in magnetic films as a function of the film thickness, and we considered a benchmark magnetic material as reference system: the ferromagnetic, bcc Iron metal. In collaboration with the group headed by Charles Ahn from University of Yale, we grew and characterized several Fe films with thicknesses of 105 u.c., 54 u.c., 29 u.c., 17 u.c., 6 u.c. and 3 u.c. (uc=unit cell). All films showed comparable magnetization curves with respect to bulk Fe.

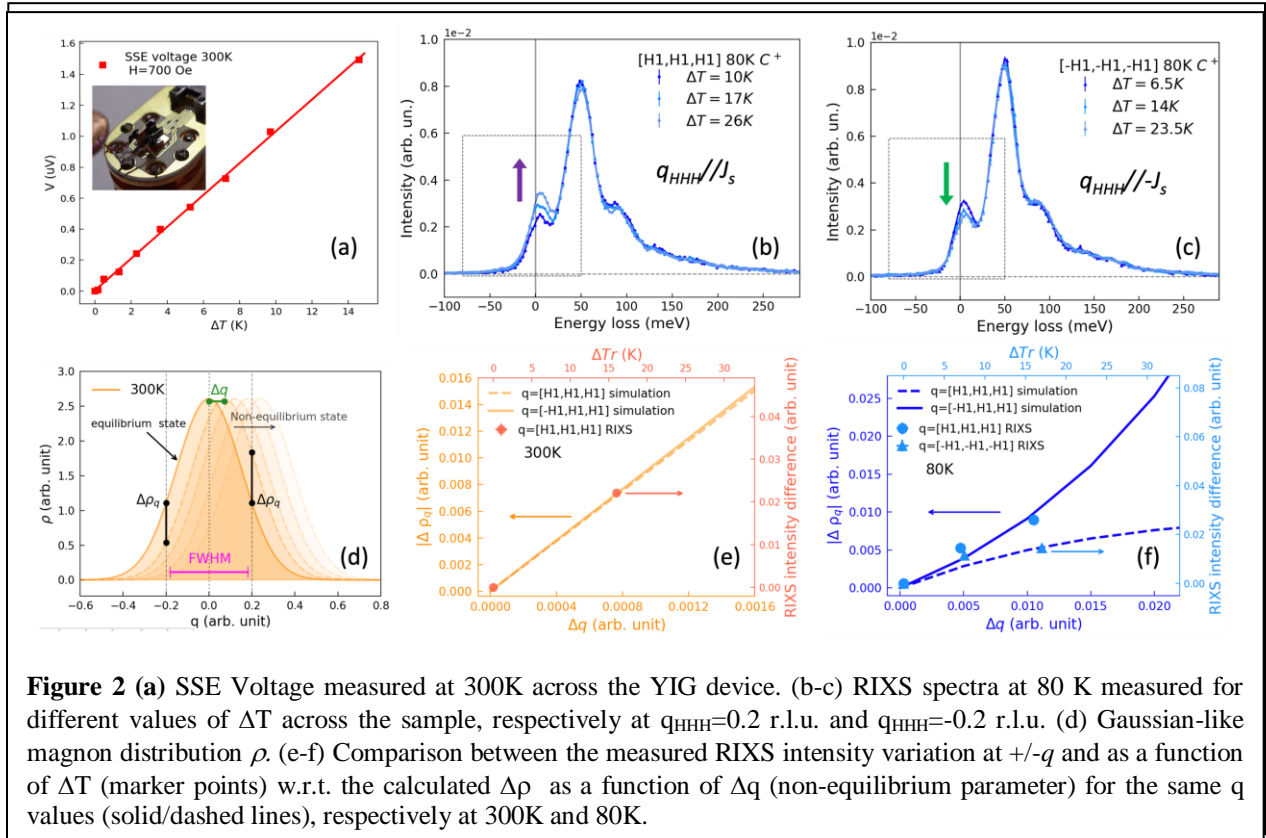
Resonant Inelastic X-ray Scattering (RIXS) at the Fe L_3 edge was utilized to probe the spin dynamics in these systems. The spin dispersion measured on a thick sample (54 u.c.) returned an isotropic ferromagnon dispersion, in agreement with previous results obtained by Inelastic Neutron Scattering on a bulk crystal [1]. The systematic investigation of the spin dynamics as a function of thickness, looking at spin dispersion both along the in-plane $[H,0,0^*]$ and the out-of-plane $[0,0,L]$ directions (see Fig. 1 (a,b)), revealed instead interesting results.



Firstly, spin excitations demonstrate to survive down to the ultra-thin film limit. Secondly, while no significant change in the spin excitation energy could be identified along the in-plane direction $[H,0,0^*]$, a gradual softening of the spin excitation energy was instead observed in the out-of-plane direction $[0,0,L]$. Such a finding, summarized in Fig. 1(c, d), is explained within a Heisenberg model based on an isotropic, effective short-range exchange interaction, at the presence of confinement. The calculated spin dispersion curves as a function of thickness are plotted in Fig. 1(c,d), as dotted lines. From the good agreement between the experimental data points and the calculated dispersions, we conclude that the effect of geometrical confinement well explain our observation as it induces an anisotropic boundary condition to the spin wave dispersion, causing the anisotropic response between the $[H,0,0^*]$ and $[0,0,L]$ directions. Furthermore, the calculations well reproduce the spin energy softening as a function of thickness along the $[0,0,L]$ direction, as a direct consequence of the reduction of Fe bonds. These results highlight the role of the film thickness as a knob to tune the spin dynamics in magnonic materials [2].

Momentum- and energy-resolved detection of magnon current in an insulating ferrimagnet

The ferrimagnetic insulator Yttrium iron garnet ($\text{Y}_3\text{Fe}_5\text{O}_{12}$, YIG) is considered a model system for novel magnonic devices thanks to its unique magnetoelastic properties, long-range spin-waves propagation, and low Gilbert damping [3]. Considering its strong magnetic moment $S=5/2$ and highly dispersive ferromagnons [4], this system is thus ideal for proofing the next goal of this research project: visualize the spin-wave current with energy and momentum resolution using RIXS, thus gaining microscopic insights about the elementary excitations leading the transport. To this purpose, we exploited the spin Seebeck effect (SSE) in $\text{Y}_3\text{Fe}_5\text{O}_{12}$ (YIG) to generate a spin-wave current J_s through the application of a temperature gradient across the sample [5]. A fully in-house made device was prepared and tested [see Fig. 2(a)], and ultimately operated inside the UHV experimental chamber of the RIXS spectrometer at 2ID Beamline of NSLSII. These measurements were realized using the unique *Opera* sample environment fully supported by this project.



By controlling the applied temperature gradient ∇T across the YIG device, we performed RIXS measurements at different momenta q and at different temperatures. Figs. 2(b-c) focus on the 80K data set, measured respectively at $q_{\text{HHH}}=0.2$ r.l.u. and at $q_{\text{HHH}}=-0.2$ r.l.u.. At each q -value, the RIXS data displays a clear change in the spectral weight around the quasi-elastic region ($< 30\text{meV}$) as a function of temperature difference ΔT . Interestingly, however, when q is parallel to the magnon current J_s [Fig. 2(b)], the spectral weight is enhanced for increasing ΔT ; instead, when q is

antiparallel to J_s [Fig. 2(c)], the spectral weight is suppressed. This opposite behaviour at opposite q directions excludes on one hand that this observation is caused by local spin accumulation or averaged thermal variation of the sample. On the other hand, this result suggests that our measurement is sensitive to a $\pm q$ symmetry breaking mechanism, i.e. the flow of the spin-wave current. With the assumption that the low-energy RIXS signal is mostly sensitive to the acoustic ferromagnon mode and its distribution - apart from some constant rescaling factors, we performed calculations based on a Gaussian-shaped magnon distribution ρ under equilibrium (distribution centered at $q=0$) and non-equilibrium (distribution shifted by Δq due the current flow) conditions. Considering the RIXS intensity variation is proportional to the magnon distribution variation $\Delta\rho$ between non-equilibrium and equilibrium conditions at a specific q , our calculations not only reproduce the sign reversal observed between by our $+q$ and $-q$ dataset, but also explain the magnitude of the RIXS intensity variation. The excellent agreement between the simulations and the experimental data displayed by Figs. 2(f-g) proof in first place that our experimental approach is capable to visualize the magnon current components with a q - and energy- resolution supporting the dominant role of the low-energy acoustic ferromagnon to the Spin Seebeck effect; secondly, it enables to quantify a SSE efficiency for the YIG material, by estimating the non-equilibrium parameter Δq for a given ΔT . This method promises to shed new light on the microscopic understanding of magnon transport in general, and can be easily extended to other systems.

Future Plans

- Complete ongoing research topics and corresponding manuscript about: 1) Fe_2O_3 – multi-magnons evidence; 2) cuprates - study of the superconducting gap in preparation of tunable superconducting devices by electric field, 3) YIG: spin Seebeck effect and high-energy spin dynamics, 4) LiCuVO_4 – presence of quadrupolar excitations.
- Prepare a Sr_2CuO_3 – based device for studying the spin Seebeck effect in the one-dimensional spin chain system and perform first RIXS experiment to unravel the collective modes behind the transport effect.
- Investigate the spin dynamics in van der Waals magnets as well as its evolution as a function of “thickness”, using single crystals and exfoliated flakes as samples. This project is in collaboration with the EFRC - Pro-QM (Programmable Quantum Materials) consortium.
- Study the spin dynamics in the multiferroic system BiFeO_3 as a function of strain and its control possibilities by applying an electric field.

References

[1] Phys. Rev. B 7, 336 (1973); [2] J. Pelliciari et al., Nature Materials 20, 188 (2021); [3] A. Chumak et al., Nat. Phys. 11, 453(2015); [4] A. J. Princep et al., NPJ Quantum Materials 2 63 (2017); [5] K. Uchida et al., Nature 455, 778 (2008).

Publications

- 1.** “Strongly Correlated Charge Density Wave in $\text{La}_{2-x}\text{SrCuO}_4$ Evidenced by Doping-Dependent Phonon Anomaly” by J.Q. Lin, H. Miao, D.G. Mazzone, G.D. Gu, A. Nag, A.C. Walters, M. García-Fernández, A. Barbour, J. Pellicciari, I. Jarrige, M. Oda, K. Kurosawa, N. Momono, K.-J. Zhou, V. Bisogni, X. Liu, M.P.M. Dean. *Physical Review Letter* 124, 207005 (2020). <https://doi.org/10.1103/PhysRevLett.124.207005>
- 2.** “Tuning spin excitations in magnetic films by confinement” by J. Pellicciari, S. Lee, K. Gilmore, J. Li, Y. Gu, A. Barbour, I. Jarrige, C. H. Ahn, F. J. Walker and V. Bisogni; *Nature Materials* 20, 188 (2021); <https://doi.org/10.1038/s41563-020-00878-0>
- 3.** “Local electronic structure of rutile RuO_2 ” by C. Occhialini, V. Bisogni, H. You, A. Barbour, I. Jarrige, J. F. Mitchell, R. Comin, and J. Pellicciari; *Physical Review Research* 3, 033214 (2021); <https://doi.org/10.1103/PhysRevResearch.3.033214>

Workshop on energy research opportunities for physics graduate students and postdocs

Cortney Bougher, American Physical Society

Program Scope

The American Physical Society (APS) holds an annual series of one-day workshops for graduate students and postdocs that highlight the contributions made by physics-related research in responsibly meeting the nation's energy needs. Approximately 80-100 graduate students and postdocs attend each workshop. The format and organization of the workshops is developed by the leadership of the APS Topical Group on Energy and Research Applications (GERA). Workshop speakers are asked to give a broad overview of their area of research before discussing more specifically their own work. Extensive time for discussion is provided to facilitate student interaction with the speakers and networking with others in the field. These presentation/interaction times are followed by a panel discussion on careers in energy research. The workshops are held immediately prior to the APS March Meeting and these activities provide a springboard into the March Meeting itself, with its many technical talks on energy-related issues.

Recent Progress

The 2019 Workshop on Energy and Research Applications was held prior to the APS March Meeting in Boston, MA. The major goals of the 2019 workshop were to bring energy experts together to describe the current landscape in energy in research, policy, and industry for the benefit of ~100 students/postdocs. The format included talks, a lunch, several coffee breaks and a reception, all intended to provide the students with maximal access to the experts to ask questions both formally during the talks and informally outside them. In this iteration of the workshop, the topics aimed to provide the students a broader view of energy by including non-scientific researchers. Our keynote speaker was from industry (Google) and policy (served in 3 separate administrations). This informed students of not only current scientific questions and endeavors, but also of how they fit into the broader picture of energy concerns in the country and the world.

Applications for the workshop exceeded 140% of the planned capacity for the workshop. Down-selection was done on the basis of abstracts, resulting in a student population that was curious about and engaged already in energy pursuits and study. This facilitated a very active discussion between the students and the experts. Several new members of GERA were gained by exposure to the group through the workshop, additionally resulting in new volunteers with GERA. The secondary goal of increasing involvement in energy research was also satisfied. Student feedback was extremely positive and indicated that the approach of a broad layout

including not only scientific research but its intersection with policy and business was very useful to them.

The 2020 Workshop was cancelled as a direct result of the cancellation of the APS March Meeting 2020 due to the COVID-19 pandemic. Many of the workshop attendees had completed travel or were en route to the meeting when the cancellation was announced. The travel funds for the 2020 workshop were still disbursed as appropriate and significantly alleviated the strain on those attendees.

Future Plans

The 2022 Workshop on Energy and Research Applications is scheduled for March 13, 2022. The workshop will be collocated with the APS March Meeting in Chicago, IL. Planning is currently underway; the workshop will tentatively focus on approaches to sustainable energy storage.

Cold Exciton Gases in Semiconductor Heterostructures

Leonid Butov, University of California San Diego

Program Scope

A spatially indirect exciton (IX) is a bound pair of an electron and a hole confined in spatially separated layers in a semiconductor heterostructure. IXs are characterized by a set of properties:

- Long lifetimes of IXs allow them to cool below the temperature of quantum degeneracy. This gives an opportunity to realize quantum excitonic systems.
- Due to IX built-in dipole moment, IX energy is effectively controlled by voltage. This gives an opportunity to create tailored potential landscapes for IXs by voltage.
- Due to their built-in dipoles, IXs form a system with strong correlations.
- Long IX lifetimes allow them to travel over large distances before recombination. This gives an opportunity to study exciton transport by imaging spectroscopy.
- The electron-hole separation in IX and the suppression of exciton scattering in IX condensate result to the suppression of spin relaxation. This allows the realization of long-range coherent spin transport.

Due to these properties, IXs are explored as a platform for basic studies of cold excitons – cold bosons in semiconductor materials and for the development of excitonic devices. The goal of this project is to explore IXs in GaAs heterostructures, which form the lowest-disorder platform for studying IXs, and in van der Waals transition-metal dichalcogenides (TMD) heterostructures, which are characterized by high IX binding energies and can bring the quantum IX phenomena to high temperatures.

Recent Progress

1. Moiré pattern of interference dislocations in condensate of IXs in GaAs

heterostructures [1]. Interference patterns provide direct measurement of coherent propagation

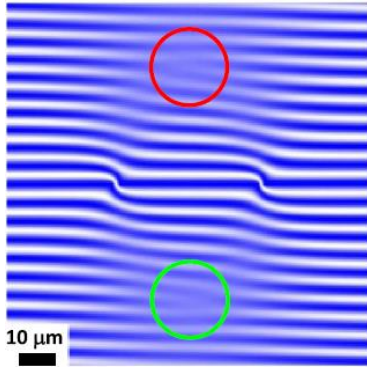


Fig. 1. Simulations: The combined interference patterns of radial IX condensate matter waves propagating from two sources produce interference dislocations due to the moiré effect. Right- and left- dislocations are marked by red and green circles.

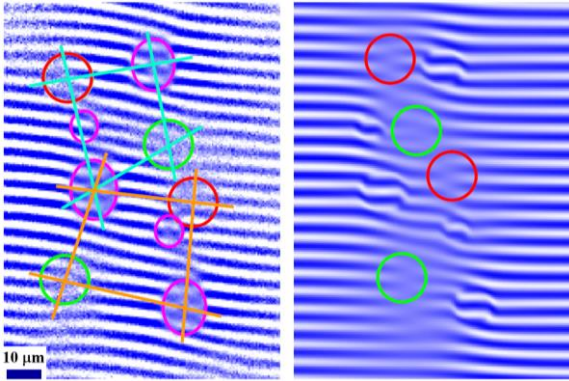


Fig. 2. Measured (left) and simulated (right) moiré patterns of interference dislocations. IX sources are embraced by magenta lines. Right- and left-dislocations are marked by red and green circles. Cyan and orange lines are drawn between the dislocations and stronger sources forming them.

of matter waves in quantum systems.

Superfluidity in Bose-Einstein condensates of excitons can enable long-range ballistic exciton propagation and can lead to emerging long-scale interference patterns. The theory predicts that the reduced IX recombination enables IX superfluid propagation over macroscopic distances. In work [1], we present dislocation-like phase singularities in interference patterns produced by condensate of IXs (Figs. 1 and 2).

The results:

- We show that the moiré effect creates dislocations in interference patterns.
- We analyze how exciton vortices and skyrmions should appear in the interference experiments and show that the observed interference dislocations are not associated with these phase defects.
- We show that the observed interference dislocations originate from the moiré effect in combined interference patterns of propagating IX condensate matter waves.
- The interference dislocations are formed by the IX matter waves ballistically propagating over macroscopic distances. The long-range ballistic IX propagation is the evidence for IX condensate superfluidity.

2. Attractive and repulsive dipolar interaction in bilayers of indirect excitons [2]. We explore attractive dipolar interaction in IXs [2]. For one layer of IXs in a single pair of coupled quantum wells (CQWs), the out-of-plane IX electric dipoles lead to repulsive dipolar interaction between IXs. The attractive dipolar interaction between IXs is realized in a two-CQW

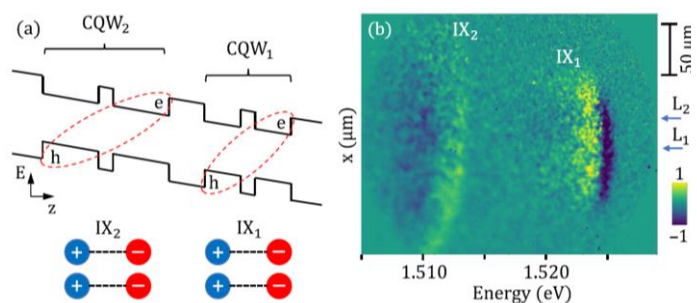


Fig. 3. (a) Diagram of the two-CQW structure. The intra-CQW interaction between IX_2 (or IX_1) side-to-side dipoles is repulsive. The inter-CQW interaction between IX_2 and IX_1 head-to-tail dipoles is attractive. (b) Differential x-energy luminescence image showing an increase in IX_2 energy, a decrease in IX_1 energy, and a spatial shift of the IX_1 cloud towards the IX_2 cloud due to the repulsive and attractive dipolar interactions.

heterostructure with two IX layers in two separated CQW pairs (Fig. 3). We found both in experimental measurements and theoretical simulations that increasing density of IXs in one layer causes a monotonic energy reduction for IXs in the other layer. We also found an in-plane shift of a cloud of IXs in one layer towards a cloud of IXs in the other layer. This behavior is qualitatively consistent with attractive dipolar interaction. The measured IX energy reduction and IX cloud shift are higher than the values given by the correlated liquid theory.

3. Indirect excitons and trions in $MoSe_2/WSe_2$ van der Waals heterostructures [3].

IX quantum Bose gases and IX devices were explored in GaAs heterostructures where an IX range of existence is limited to low temperatures due to low IX binding energies. IXs in van der TMD heterostructures are characterized by large binding energies giving the opportunity for exploring excitonic quantum gases and for creating excitonic devices at high temperatures. TMD heterostructures also offer a new platform for studying single-exciton phenomena and few-particle complexes. In work [3], we present studies of IXs in $MoSe_2/WSe_2$ heterostructures and

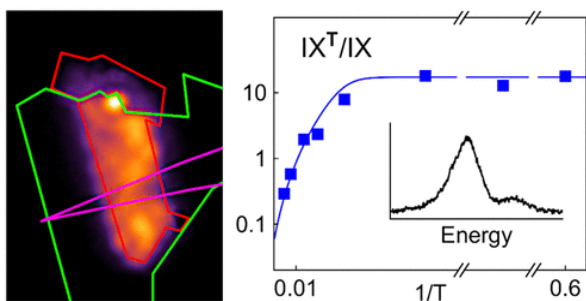


Fig. 4. (left) x-y map of indirect luminescence in $MoSe_2/WSe_2$ heterostructure. $MoSe_2$ (red), WSe_2 (green), and graphene (magenta) layer boundaries are shown. (right) Experimental (symbols) and simulated (line) luminescence intensity ratio IX^T/IX vs $1/T$. The energy splitting and temperature dependence identify the two IX lines as neutral and charged IXs.

report on two IX luminescence lines whose energy splitting and temperature dependence identify them as neutral and charged IXs. The experimentally found binding energy of the indirect charged excitons, that is, indirect trions, is close to the calculated binding energy of 28 meV for negative indirect trions in TMD heterostructures. We also report on the realization of IXs with a luminescence line width reaching 4 meV at low temperatures. An enhancement of IX luminescence intensity and the narrow line width are observed in localized spots.

4. Voltage-controlled long-range propagation of indirect excitons in van der Waals heterostructure [4]. IXs can form the medium for excitonic devices whose operation is based on controlled propagation of excitons. A proof of principle for excitonic devices was demonstrated in GaAs heterostructures where the operation of excitonic devices is limited to low temperatures. IXs in van der Waals TMD heterostructures are characterized by high binding energies making IXs robust at room temperature and offering an opportunity to create excitonic devices operating at high temperatures suitable for applications. However, a characteristic feature of TMD heterostructures is the presence of moiré superlattice potentials, which are predicted to cause strong modulations of IX energy. These in-plane energy landscapes lead to IX localization, making IX propagation fundamentally different in TMD and GaAs heterostructures and making uncertain if long-range IX propagation can be realized in TMD heterostructures. In work [4], we realize

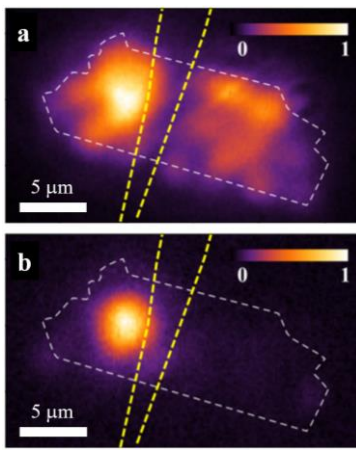


Fig. 5. Voltage-controlled long-range IX propagation in MoSe₂/WSe₂. (a) on, (b) off.

voltage-controlled long-range propagation of IXs in MoSe₂/WSe₂ (Fig. 5). The results:

- In the off regime, IXs are localized by the moiré potential.
- In the on regime, the IX 1/e luminescence decay distance reaches 13 μm, 4x the previously achieved values.
- The long-range propagation indicates the small disorder for IX transport scattering in the fabricated device.
- The control of IX propagation in TMD heterostructures is governed by new mechanism, beyond the mechanisms for controlling IX transport known since earlier studies of GaAs heterostructures.

Future Plans

GaAs heterostructures form the lowest-disorder platform for studying IXs. We plan to explore the IX superfluidity and spin transport in condensate of IXs in GaAs heterostructures. IXs in van der Waals heterostructures based on single-atomic-layers of TMD are characterized by high binding energies, significantly higher than in GaAs heterostructures. Due to this property, theoretical predictions indicate that TMD heterostructures can bring the IX quantum phenomena studied in GaAs heterostructures at low temperatures, such as condensation and superfluidity, to high temperatures. We plan to explore IX quantum phenomena in TMD heterostructures.

Publications

1. J.R. Leonard et al, Lunhui Hu, A.A. High, A.T. Hammack, Congjun Wu, L.V. Butov, K.L. Campman, A.C. Gossard, Moiré pattern of interference dislocations in condensate of indirect excitons, *Nat. Commun.* 12, 1175 (2021).
2. D.J. Choksy, Chao Xu, M.M. Fogler, L.V. Butov, J. Norman, A.C. Gossard, Attractive and repulsive dipolar interaction in bilayers of indirect excitons, *Phys. Rev. B* 103, 045126 (2021).
3. E.V. Calman, L.H. Fowler-Gerace, D.J. Choksy, L.V. Butov, D.E. Nikonov, I.A. Young, S. Hu, A. Mishchenko, A.K. Geim, Indirect Excitons and Trions in MoSe₂/WSe₂ van der Waals Heterostructures, *Nano Lett.* 20, 1869 (2020).
4. L.H. Fowler-Gerace, D.J. Choksy, L.V. Butov, Voltage-controlled long-range propagation of indirect excitons in van der Waals heterostructure, *arXiv:2101.01262* (2021).
5. L.V. Butov, Condensation of indirect excitons, *MRS Bulletin* 45, 380 (2020).

Program Title: Complex States, Emergent Phenomena, and Superconductivity in Intermetallic and Metal-Like Compounds

Principle Investigators: Paul Canfield (FWP leader), Sergey Bud'ko, Yuji Furukawa, Adam Kaminski, Makariy Tanatar, Ruslan Prozorov, Linlin Wang. Division of Materials Science and Engineering, Ames Laboratory, Iowa State University, Ames, IA 50011

Program Scope

The specific scientific question to be addressed by this FWP is: how can we develop, discover, understand, and ultimately control and predictably modify new and extreme examples of complex states, emergent phenomena, and superconductivity? We study materials manifesting specifically clear or compelling examples (or combinations) of superconductivity, strongly correlated electrons, novel electronic topology, quantum criticality, and exotic, bulk magnetism because of their potential to lead to revolutionary steps forward in our understanding of their complex, and potentially energy-relevant, properties. For example, part of our effort will focus on the understanding and control of FeAs-based superconductors, as well as searching for other examples of novel, or high-temperature, superconductivity. This work will be leveraged via highly collaborative interactions between the scientists within this FWP, as well as through extensive collaborations with other Ames Laboratory FWPs, other DOE laboratories, and other universities and labs throughout the world. Experiment and theory will be implemented synergistically. The experimental work will consist of new materials' development and crystal growth, combined with detailed and advanced measurements of microscopic, thermodynamic, transport, and spectroscopic properties, as well as electronic structure, at extremes of pressure, temperature, magnetic field and resolution. The theoretical work focuses on understanding and modeling transport, thermodynamic and spectroscopic properties using world-leading and advanced phenomenological approaches to superconductors and electronic band structure.

This work supports the DOE mission by directly addressing the Grand Challenge of understanding the Emergence of Collective Phenomena: Strongly Correlated Multiparticle Systems as well as Priority Research Directions identified in the recent Synthesis Science and Quantum Materials for Energy Relevant Technology Basic Research Needs Workshops, and is a key contributor to fulfilling the Ames Laboratory DMSE Strategic Plan. This FWP will design, discover, characterize and understand systems that shed light on how remarkable properties of matter emerge from complex correlations of the atomic or electronic constituents and, as a result, provide better control of these properties.

Recent Progress:

Studies in fragile magnetism: ferromagnetic quantum phase transitions:

We have investigated the T-P-H phase diagram of LaCrGe₃, an ambient pressure, itinerant ferromagnet (FM) [1] that has clear avoidance of a FM-quantum critical point (QCP) below 2 GPa

[2-4]. Initially it was thought that the higher pressure, low field state was a form of long-

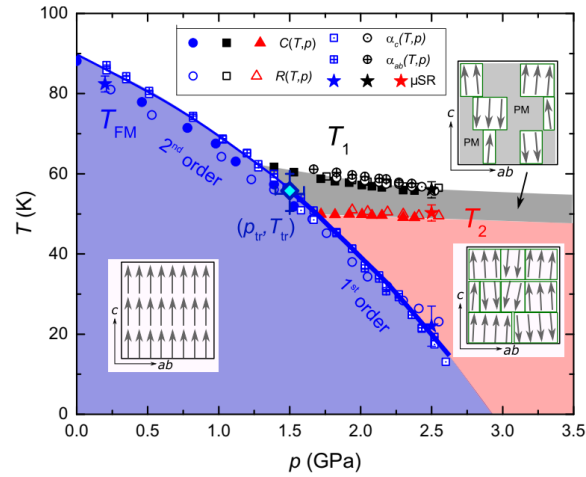


Fig. 1. Temperature – pressure phase diagram of LaCrGe₃ constructed from different measurements under pressure, shown by different symbols. Different magnetic orders are schematically depicted in the insets by arrows.

wavelength antiferromagnetic (AFM) ordering.[2] By combining thermodynamic (specific heat [5] and thermal expansion), transport, x-ray and neutron scattering as well as muon spin relaxation (μ SR) and NMR measurements new insights on the temperature-pressure phase diagram of LaCrGe₃ were revealed (Fig. 1). [6,7] The avoidance of the quantum critical point with pressure is accompanied by the formation of short-range FM-ordered clusters in LaCrGe₃. This short-range magnetically ordered cluster phase emerges as the FM transition is suppressed, suggesting that disorder is inevitably present even in stoichiometric metallic compounds.

As part of an ongoing search for fragile magnetic ordering [8,9], we recently discovered the itinerant, FM compound La₅Co₂Ge₃. [10] At ambient pressure, thermodynamic, transport, and μ SR measurements showed that La₅Co₂Ge₃ undergoes a FM transition at $T_C \sim 3.8$ K. The magnetism associated with La₅Co₂Ge₃ was found to be itinerant with a low-field saturated moment of $\sim 0.1\mu_B/\text{Co}$. These properties make La₅Co₂Ge₃ a rare, small-moment, low- T_C compound, which is a promising candidate material for tuning the FM transition towards even lower temperatures. Motivated by this discovery, we investigated the pressure-temperature phase diagram of La₅Co₂Ge₃. [11] Magnetization, resistivity, and specific heat measurements under pressure up to 5.12 GPa were performed on single-crystalline La₅Co₂Ge₃. The ambient-pressure ferromagnetic transition temperature T_C is suppressed upon increasing pressure up to ~ 1.7 GPa. Instead of T_C being suppressed further upon increasing pressure beyond 1.7 GPa, we find that La₅Co₂Ge₃ enters a different low-temperature ground state. The transition temperature T^* into the new state has a nonmonotonic dependence on pressure up to 5.12 GPa. Overall, our study shows that La₅Co₂Ge₃ manifests another example of avoided FM quantum criticality in a metallic system via the appearance of a new ordered state. Based on our transport data in zero and finite field, it seems likely that this new type of order is magnetic in nature with an AFM component.

Future Plans

A promising route to emergent quantum states, such as high temperature superconductivity, is to look in the proximity of a suppressed, competing phase transition or, in some cases, near a quantum critical point. A wide swath of phase space is opened by the idea of searching for fragile magnetic systems and tuning their transition temperatures to zero, ending in either a QPT or QCP [8,9]. We propose to study a diverse set known and promising fragile magnetic systems in search of QCPs and emergent physics.

We will continue detailed studies of avoided FM QCP in materials highlighted in research done in previous 2 years. In $\text{La}_5\text{Co}_2\text{Ge}_3$ we propose to study the new, high pressure state with pressure dependent NMR and μSR studies. In addition to working with the pure material, we also propose to study $\text{La}_5(\text{Co}_{1-x}\text{TM}_x)_2\text{Ge}_3$ (TM = Fe, Ni, Rh) to see how the FM transition can be tuned and possibly changed to an ambient pressure AFM state.

In the past we were able to employ diamond anvil cell to apply pressure up to ~ 25 GPa on $\text{YbFe}_2\text{Zn}_{20}$ and detect a discontinuous change from its low pressure, low temperature heavy fermion ground state to a high pressure, low temperature magnetically ordered state, that we identified as probably being FM [12]. We propose to study $\text{YbRh}_2\text{Zn}_{20}$, an ambient pressure HF with similar Kondo temperature, and degeneracy as $\text{YbFe}_2\text{Zn}_{20}$, as a function of pressure. Given that the $\text{RRh}_2\text{Zn}_{20}$ family appears to host AFM ground states for the trivalent rare earth members, we anticipate an AFM, QCP associated with $\text{YbRh}_2\text{Zn}_{20}$ to be revealed.

Whereas for well-ordered, stoichiometric metallic FM systems the theoretical prediction of avoided QCPs seems to be robust, with LaCrGe_3 , $\text{La}_5\text{Co}_2\text{Ge}_3$, and other compounds manifesting different versions of this basic avoidance, there are at least two predicted routes to having a FM QCP in a metal. One is via the introduction of disorder and the other is through careful attention to symmetry, magnetic anisotropy and spin-orbit coupling [13-16]. We propose to pursue both of these routes over the next review period. Taking LaCrGe_3 and $\text{La}_5\text{Co}_2\text{Ge}_3$ as two model systems, we propose to use high-energy electron and proton irradiation to systematically introduce varying degrees of disorder. We will then study the modified T-p phase diagrams to (i) see if the second order FM transition can be brought down to a QCP and (ii) correlate changes in thermodynamic and transport properties with dose, annealing and residual resistivity. Recent theoretical work has claimed “that non-centrosymmetric metals with strong spin-orbit interaction” can manifest FM-QCP in clean systems. We propose to design and discover examples of metallic FMs with non-centrosymmetric structures, determine their T-p phase diagrams, and, as necessary, try to infer the strength of the spin-orbit interaction (e.g. via comparison of measurements of anisotropic magnetization with band structure calculations). So far, through an analysis of symmetry and composition, several promising systems have been identified. If there is still avoided QCP behavior, we will be able to set limits on how strong the spin-orbit interaction needs to be.

We also propose to identify and study potentially fragile, itinerant AFM systems; empirically these are much harder to find than FM ones. Given the relative rarity of small moment, itinerant magnetic systems, we propose to use band structure analysis to help guide and focus our search for new examples of potentially fragile magnetic systems.

References

1. Xiao Lin, et al., “Suppression of ferromagnetism in the $\text{LaV}_x\text{Cr}_{1-x}\text{Ge}_3$ system,” Phys. Rev. B 88, 094405 (2013).

2. Valentin Taufour, et al., “Ferromagnetic Quantum Critical Point Avoided by the Appearance of Another Magnetic Phase in LaCrGe₃ under Pressure,” *Phys. Rev. Lett.* 117, 037207 (2016).
3. Valentin Taufour, et al., “Ferromagnetic quantum criticality: New aspects from the phase diagram of LaCrGe₃,” *Physica B* 536, 483 (2018).
4. Udhara S. Kaluarachchi, et al., “Tricritical wings and modulated magnetic phases in LaCrGe₃ under pressure,” *Nat. Comm.* 8, 546 (2017).
5. Elena Gati, et al., “Use of Cernox thermometers in AC specific heat measurements under pressure,” *Rev. Sci. Instr.* 90, 023911 (2019).
6. Elena Gati, et al., “Formation of short-range magnetic order and avoided ferromagnetic quantum criticality in pressurized LaCrGe₃,” *Phys. Rev. B* 103, 075111 (2021)
7. K. Rana, et al., “Magnetic properties of the itinerant ferromagnet LaCrGe₃ under pressure studied by ¹³⁹La NMR,” *Phys. Rev. B* 103, 174426 (2021).
8. P. C. Canfield and S. L. Bud’ko, “Preserved entropy and fragile magnetism,” *Rep. Prog. Phys.*, 79, 084506 (2016).
9. P. C. Canfield, “New Materials Physics,” *Rep. Prog. Phys.* 83, 016501 (2020).
10. S. M. Saunders, et al., “Exceedingly small moment itinerant ferromagnetism of single crystalline La₅Co₂Ge₃,” *Phys. Rev. B* 101, 214405 (2020).
11. Li Xiang, et al., “Avoided ferromagnetic quantum critical point in pressurized La₅Co₂Ge₃,” *Phys. Rev. B* 103, 054419 (2021).
12. Udhara S. Kaluarachchi, et al., “Collapse of the Kondo state and ferromagnetic quantum phase transition in YbFe₂Zn₂₀,” *Phys. Rev. B* 98, 174405 (2018).
13. M. Brando, et al., “Metallic quantum ferromagnets,” *Rev. Mod. Phys.* 88, 025006 (2016).
14. T.R. Kirkpatrick and D. Belitz, “Ferromagnetic Quantum Critical Point in Noncentrosymmetric Systems,” *Phys. Rev. Lett.* 124, 147201 (2020).
15. H. Kotegawa, et al., “Indication of ferromagnetic quantum critical point in Kondo lattice, CeRh₆Ge₄,” *J. Phys. Soc. Jpn.* 88, 093702 (2019).
16. B. Shen, et al., “Strange-metal behavior in a pure ferromagnetic Kondo lattice,” *Nature* 579, 51 (2020).

Publications

NOTE: Below we list a few, selected, papers relevant for this particular subtask published in the 2-year period.

Elena Gati, Yuji Inagaki, Tai Kong, Robert J. Cava, Yuji Furukawa, Paul C. Canfield, and Sergey L. Bud'ko, "Multiple ferromagnetic transitions and structural distortion in the van der Waals ferromagnet VI_3 at ambient and finite pressures," *Phys. Rev. B* 100, 094408 (2019)

Li Xiang, Elena Gati, Kathryn Neilson, Sergey L. Bud'ko, and Paul C. Canfield, "Physical properties of RBi_2 ($\text{R}=\text{La}, \text{Ce}$) under pressure," *Phys. Rev. Materials* 3, 095006 (2019).

Na Hyun Jo, Lin-Lin Wang, Peter P. Orth, Sergey L. Bud'ko, and Paul C. Canfield, "Magnetoelastoresistance in WTe_2 : Exploring electronic structure and extremely large magnetoresistance under strain," *PNAS* 116 (51), 25524 (2019).

P. C. Canfield, "New Materials Physics," *Rep. Prog. Phys.* 83, 016501 (2020).

Elena Gati, Li Xiang, Sergey L. Bud'ko, Paul C. Canfield, "Hydrostatic and Uniaxial Pressure Tuning of Iron-Based Superconductors: Insights into Superconductivity, Magnetism, Nematicity, and Collapsed Tetragonal Transitions," *Ann. Phys.* 532 (10), 2000248 (2020).

Na Hyun Jo, Brinda Kuthanazhi, Yun Wu, Erik Timmons, Tae-Hoon Kim, Lin Zhou, Lin-Lin Wang, Benjamin G. Ueland, Andriy Palasyuk, Dominic H. Ryan, Robert J. McQueeney, Kyungchan Lee, Benjamin Schruck, Anton A. Burkov, Ruslan Prozorov, Sergey L. Bud'ko, Adam Kaminski, and Paul C. Canfield, "Manipulating magnetism in the topological semimetal EuCd_2As_2 ," *Phys. Rev. B* 101, 140402(R) (2020).

K. Rana, L. Xiang, P. Wiecki, R. A. Ribeiro, G. G. Lesseux, A. E. Böhmer, S. L. Bud'ko, P. C. Canfield, and Y. Furukawa, "Impact of nematicity on the relationship between antiferromagnetic fluctuations and superconductivity in $\text{FeSe}_{0.91}\text{S}_{0.09}$ under pressure" *Phys. Rev. B* 101, 180503(R) (2020).

Sergey L. Bud'ko, Li Xiang, Chaowei Hu, Bing Shen, Ni Ni, and Paul C. Canfield, "Pressure tuning of structural and magnetic transitions in EuAg_4As_2 ," *Phys. Rev. B* 101, 195112 (2020).

Li Xiang, Dominic H. Ryan, Warren E. Straszheim, Paul C. Canfield, and Sergey L. Bud'ko, "Tuning of charge density wave transitions in LaAu_xSb_2 by pressure and Au stoichiometry," *Phys. Rev. B* 102, 125110 (2020).

E. I. Timmons, S. Teknowijoyo, M. Kończykowski, O. Cavani, M. A. Tanatar, Sunil Ghimire, Kyuil Cho, Yongbin Lee, Liqin Ke, Na Hyun Jo, S. L. Bud'ko, P. C. Canfield, Peter P. Orth, Mathias S. Scheurer, and R. Prozorov, "Electron irradiation effects on superconductivity in PdTe₂: An application of a generalized Anderson theorem," *Phys. Rev. Research* 2, 023140 (2020).

Elena Gati, Li Xiang, Sergey L. Bud'ko, and Paul C. Canfield, "Measurements of elastoresistance under pressure by combining in-situ tunable quasi-uniaxial stress with hydrostatic pressure," *Rev. Sci. Instr.* 91, 023904 (2020).

Li Xiang, Elena Gati, Sergey L. Bud'ko, Raquel A. Ribeiro, Arif Ata, Ulrich Tutsch, Michael Lang, and Paul C. Canfield, "Characterization of the pressure coefficient of manganin and temperature evolution of pressure in piston-cylinder cells," *Rev. Sci. Instr.* 91, 095103 (2020).

K. R. Joshi, N. M. Nusran, M. A. Tanatar, K. Cho, S. L. Bud'ko, P. C. Canfield, R. M. Fernandes, A. Levchenko, and R. Prozorov, "Quantum phase transition inside the superconducting dome of Ba(Fe_{1-x}Co_x)₂As₂ from diamond-based optical magnetometry," *New J. Phys.* 22, 053037 (2020).

S. M. Saunders, L. Xiang, R. Khasanov, T. Kong, Q. Lin, S. L. Bud'ko, and P. C. Canfield, "Exceedingly small moment itinerant ferromagnetism of single crystalline La₅Co₂Ge₃," *Phys. Rev. B* 101, 214405 (2020).

Elena Gati, John M. Wilde, Rustem Khasanov, Li Xiang, Sachith Dissanayake, Ritu Gupta, Masaaki Matsuda, Feng Ye, Bianca Haberl, Udhara Kaluarachchi, Robert J. McQueeney, Andreas Kreyssig, Sergey L. Bud'ko, and Paul C. Canfield, "Formation of short-range magnetic order and avoided ferromagnetic quantum criticality in pressurized LaCrGe₃," *Phys. Rev. B* 103, 075111 (2021).

Li Xiang, Elena Gati, Sergey L. Bud'ko, Scott M. Saunders, and Paul C. Canfield, "Avoided ferromagnetic quantum critical point in pressurized La₅Co₂Ge₃," *Phys. Rev. B* 103 054419 (2021).

K. Rana, H. Kotegawa, R. R. Ullah, E. Gati, S. L. Bud'ko, P. C. Canfield, H. Tou, V. Taufour, and Y. Furukawa, "Magnetic properties of the itinerant ferromagnet LaCrGe₃ under pressure studied by ¹³⁹La NMR," *Phys. Rev. B* 103, 174426 (2021).

Sergey L. Bud'ko, Elena Gati, Tyler J. Slade, and Paul C. Canfield, "Magnetic order in the van der Waals antiferromagnet CrPS₄: Anisotropic H-T phase diagrams and effects of pressure," *Phys. Rev. B* 103, 224407 (2021).

One-dimensional topological nanomaterials and superconductivity

Judy J. Cha, Yale University

Program Scope

The main scope of the project is 1) to synthesize and study superconducting topological crystalline insulator nanowires for the investigation of topological superconductivity and 2) to synthesize other one-dimensional (1D) topological nanomaterials for novel electronic behaviors and potential applications.

Recent Progress

Three projects were carried out last year.

1) Time-reversal symmetry broken superconductivity and Te coating in SnTe nanowires

In the last annual report (2019-2020), we reported the investigation of Josephson junction behaviors using SnTe nanowires as weak links. This on-going collaboration with James R. Williams at the University of Maryland, College Park got finally published in *npj Quantum Materials* this year [1]. The major finding of this work is an unexpected breaking of time-reversal symmetry in the SnTe nanowire Josephson junction devices, which were drawn from the observations of an asymmetric critical current in the DC Josephson effect, a prominent second harmonic in the AC Josephson effect, and a magnetic diffraction pattern with a minimum in critical current at zero magnetic field (Fig. 1a).

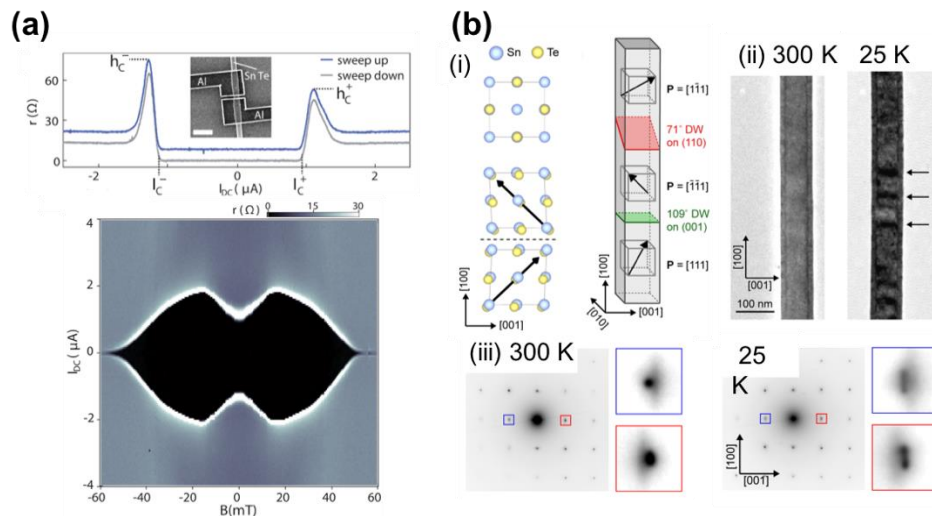


Figure 1. SnTe nanowires. (a) (top) Asymmetric critical current in DC Josephson effect and (bottom) magnetic diffraction pattern with a minimum in critical current at zero magnetic field of SnTe nanowire Josephson junctions. (b) (i) Room temperature cubic and low temperature rhombohedral crystal structure of SnTe. (ii) TEM images of SnTe nanowires at 300 K and 25 K. At 25 K, dark bands (indicated by arrows) appear. (iii) Electron diffraction patterns at 25 K show peak splitting, indicating the structural transition.

My group's contribution was to provide SnTe nanowires and characterize the structural distortion of the SnTe nanowires at low temperatures [1,2], which is responsible for ferroelectricity in SnTe, using *in situ* cryogenic transmission electron microscopy (TEM) (**Fig. 1b**).

We also have been optimizing *in situ* Te coating on our SnTe nanowires in order to prevent surface oxidation of SnTe nanowires. After growing SnTe nanowires using Sn-Au alloy nanoparticles to obtain small diameters for the nanowires [2], Te powder is heated in the tube furnace to create Te vapor. The Te vapor is carried to the growth substrates that contain SnTe nanowires and gets condensed on the surface of SnTe nanowires as an amorphous layer. Transport measurements on the Te-coated SnTe nanowires are ongoing with mixed results that suggest our *in situ* Te coating can be effective in preserving surface properties but the coating is non-uniform. One notable observation is that the ferroelectric transition temperature is distinctly lower for Te-coated SnTe nanowires than for uncoated, bare SnTe nanowires. This might suggest interfacial effects from the Te layer on the phase transition of SnTe from its room temperature rock salt structure to low temperature rhombohedral structure.

2) High conductivity of MoP nanowires for interconnect applications

Last year, we reported synthesis of topological semimetal MoP nanowires (**Fig. 2a**) [3]. Transport studies of bulk MoP single crystals show that MoP has very low resistivity and high carrier concentration, suitable for interconnect applications [4]. We have carried out transport measurements of these MoP nanowires as a function of the nanowire diameter, focusing on their potential use as low-resistance interconnects.

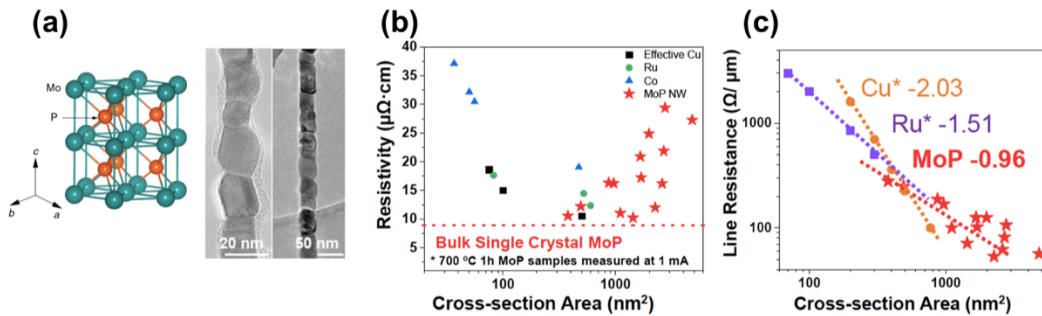


Figure 2. MoP nanowires. (a) MoP crystal structure and nanowires. (b) Resistivity of MoP nanowires measured at room temperature, benchmarked against Ru, Co, and effective Cu. (c) Line resistance of MoP nanowires compared against those of effective Cu and Ru as a function of cross-section area. Data for Cu and Ru from Ref [5].

Resistivity and line resistance of poly-crystalline MoP nanowires were measured at room temperature to prove that MoP is indeed a compelling material that can replace effective Cu (Cu with a barrier layer) or Ru at the nanoscale (**Fig. 2b, c**). The surprising trend of decrease in resistivity of MoP nanowires with decreasing diameter is attributed to the nanoscale grains present in these polycrystalline nanowires, as characterized by TEM. We found that the average grain size

does not increase as the wire diameter increases, which means that there are fewer grain boundaries for MoP wires with smaller diameters than for MoP wires with larger diameters. Thus, the resistivity would decrease for decreasing nanowire diameter due to decreasing number of grain boundaries. Moreover, we demonstrated that MoP nanowires were stable in air for up to two days with little change in their resistivity values while Cu films left in air quickly oxidized with increased resistance values. Stability in resistance in ambient or oxygen conditions is important for interconnect applications.

3) Nanoscale effects on the phase transition of MoTe₂ flakes

Weyl semimetal MoTe₂ can be in 1T' or T_d phase. Its topologically protected surface states get affected when MoTe₂ undergoes a phase transition at 240 K that changes the structure from orthorhombic (Weyl semimetal) to monoclinic (trivial metal) (**Fig. 3a**) [6]. We investigated the phase transition in mechanically exfoliated MoTe₂ flakes using *in situ* cryo-TEM and observed unexpected emergence of stacking disorder in MoTe₂ flakes at room temperature. This stacking disorder affects the phase transition as well, in which the low temperature phase was never realized even when MoTe₂ flakes were cooled to 25 K.

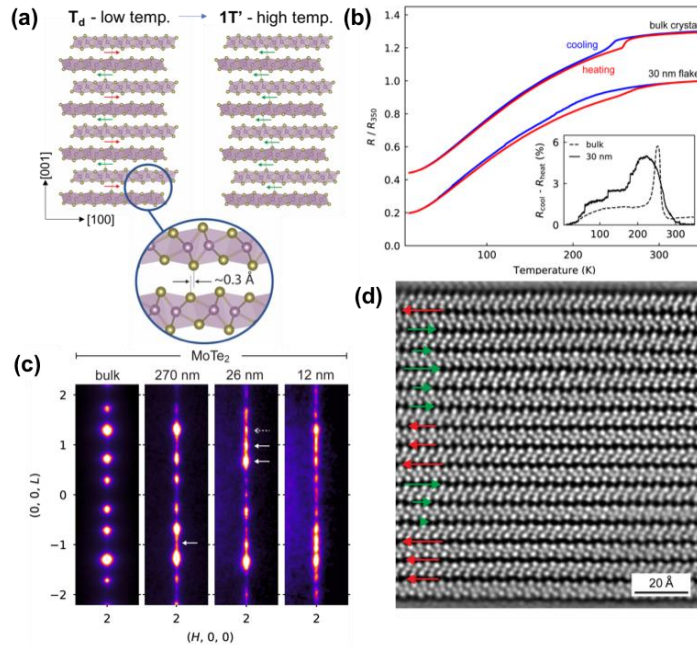


Figure 3. MoTe₂ nanoflakes. (a) Phase transition between 1T' and T_d phases of MoTe₂. (b) Resistance versus temperature curve shows a kink at the transition temperature for bulk MoTe₂. For exfoliated MoTe₂ flakes, the kink in the resistance curve is washed out. (c) Electron diffraction patterns from the cross-sections of MoTe₂ samples from bulk to 12 nm in thickness. The diffraction spots get smeared and additional spots appear when MoTe₂ gets thinned, showing disorder in layer stacking. (d) Cross-sectional scanning TEM image taken at room temperature shows clearly that the layers are not stacked according to the well-ordered 1T' phase.

Room temperature and low temperature structures of MoTe₂ flakes were examined by electron diffraction both in plan-view and in cross-sections. While bulk MoTe₂ samples show well-ordered 1T' at room temperature, exfoliated MoTe₂ flakes with thicknesses below 270 nm show clear disorder in layer stacking (**Fig. 3c**). We do not think this stacking disorder is due to strain and shear induced during the mechanical exfoliation as WTe₂ flakes exfoliated using the same method does not show stacking disorder. Cross-sectional scanning TEM images of WTe₂ flakes clearly show the stacking disorder (**Fig. 3d**).

The observed disorder in MoTe₂ flakes can explain the washed-out features of the transport measurements of MoTe₂ flakes during the phase transition where a sharp change in resistivity is not observed (**Fig. 3b**). Currently, we are trying to understand the origin for the nanoscale effects.

Future Plans

We will continue to improve Te coating in SnTe nanowires for improved transport properties and investigate the nanoscale effects on the ferroelectric transition of SnTe nanowires as a function of nanowire diameter.

For MoP nanowires, we need to improve our synthesis method to obtain single-crystalline MoP nanowires with their diameters smaller than 20 nm, and measure their resistivity. This will confirm if MoP will indeed outperform effective Cu and Ru as low-resistance interconnects below 7 nm technology node. Further, we need to understand the role of the topological protection and topological surface states on the low resistance values of polycrystalline MoP nanowires. We will conduct low temperature magneto-transport measurements to gauge the extent of electron surface scattering as a function of MoP nanowire diameter for this purpose.

We plan to extend our *in situ* cryo-TEM capabilities by integrating nanoscale devices in *in situ* TEM. The lab will move to Cornell University July next year to realize this goal. Such capability will enable structure-electronic property measurements of nanoscale topological materials.

The current funded project (DE-SC0014476) ended in August 31th of this year. A renewal proposal was not submitted because of the impending lab move to Cornell next year. I will submit a proposal next year from Cornell University to continue working on nanoscale topological materials.

References

1. C. J. Trimble, M. T. Wei, N. F. Q. Yuan, S. S. Kalantre, P. Liu, H. J. Han, M. G. Han, Y. Zhu, J. J. Cha, L. Fu, and J. R. Williams, "Josephson detection of time-reversal symmetry broken superconductivity in SnTe nanowires," *npj Quantum Materials* **2021**, 6, 61.
2. P. Liu, H. J. Han, J. Wei, D. Hynek, J. L. Hart, M. G. Han, C. J. Trimble, J. R. Williams, Y. Zhu, J. J. Cha, "Synthesis of narrow SnTe nanowires using alloy nanoparticles," *ACS Appl. Electron. Mater.* **2021**, 3, p.184-191.
3. H. J. Han, D. Hynek, Z. Wu, L. Wang, P. Liu, J. V. Pondick, S. Yazdani, J. M. Woods, M. Yarali, Y. Xie, H. Wang, J. J. Cha, "Synthesis and resistivity of topological metal MoP nanostructures," *APL Materials* **2020**, 8, 011103.
4. N. Kumar, *et. al.*, "Extremely high conductivity observed in the triple point topological metal MoP," *Nature Commun.* **2019**, 10:2475.
5. M. H. Van der Veen, *et. al.*, "Damascene benchmark of Ru, Co and Cu in scaled dimensions," *IEEE ITC* **2018**, 172-174. <https://doi.org/10.1109/IITC.2018.8430407>.
6. A. N. Berger, *et. al.*, "Temperature-driven topological transition in 1T'-MoTe₂," *npj Quantum Materials* **2018**, 3:2.

Publications resulting from work supported by DOE over the previous 2 years

1. J. L. Hart, J. J. Cha, "Seeing quantum materials with cryogenic transmission electron microscopy," *Nano Letters* **2021**, 13, p.5449-5452.
2. X. Zhang, V. Kakani, J. M. Woods, J. J. Cha, X. Shi, "Thickness dependence of magneto-transport properties in tungsten ditelluride," *arXiv:2104.14464* (2021), under review.
3. D. J. Hynek, R. M. Singhanian, J. L. Hart, B. Davis, M. Wang, N. C. Strandwitz, J. J. Cha, "Effects of growth substrate on the nucleation of monolayer MoTe₂," *CrystEngComm* **2021**, doi.org/10.1039/D1CE00275A
4. D. J. Hynek, R. M. Singhanian, S. Xu, B. Davis, L. Wang, M. Yarali, J. V. Pondick, J. M. Woods, N. C. Strandwitz, J. J. Cha, "cm²-scale synthesis of MoTe₂ thin films with large grains and layer control," *ACS Nano* **2021**, 15, p.410-418
5. C. J. Trimble, M. T. Wei, N. F. Q. Yuan, S. S. Kalantre, P. Liu, H. J. Han, M. G. Han, Y. Zhu, J. J. Cha, L. Fu, and J. R. Williams, "Josephson detection of time-reversal symmetry broken superconductivity in SnTe nanowires," *npj Quantum Materials* **2021**, 6, 61.
6. X. Zhang, J. M. Woods, J. J. Cha, X. Shi, "Crossover between weak antilocalization and weak localization in few-layer WTe₂: role of electron-electron interactions," *Phys. Rev. B* **2020**, 102, 115161.
7. N. Liu, Y. Xie, G. Liu, S. Sohn, A. Raj, G. Han, B. Wu, J. J. Cha, Z. Liu, J. Schroers, "General nanomolding of ordered phases," *Phys. Rev. Lett.* **2020**, 124, 036102.
8. P. Liu, H. J. Han, J. Wei, D. Hynek, J. L. Hart, M. G. Han, C. J. Trimble, J. R. Williams, Y. Zhu, J. J. Cha, "Synthesis of narrow SnTe nanowires using alloy nanoparticles," *ACS Appl. Electron. Mater.* **2021**, 3, p.184-191.
9. H. J. Han, D. Hynek, Z. Wu, L. Wang, P. Liu, J. V. Pondick, S. Yazdani, J. M. Woods, M. Yarali, Y. Xie, H. Wang, J. J. Cha, "Synthesis and resistivity of topological metal MoP nanostructures," *APL Materials* **2020**, 8, 011103.
10. J. M. Woods, D. Hynek, P. Liu, M. Li, J. J. Cha, "Synthesis of WTe₂ nanowires with increased electron scattering," *ACS Nano* **2019**, 13, p.6455-6460.
11. P. Liu, J. R. Williams, J. J. Cha, "Topological nanomaterials," *Nat. Rev. Mater.* **2019**, 4, p.479-496.
12. Y. Zhou, J. V. Pondick, J. L. Silva, J. M. Woods, D. J. Hynek, G. Matthews, X. Shen, Q. Feng, W. Liu, Z. Lu, Z. Liang, B. Brena, Z. Cai, M. Wu, L. Jiao, S. Hu, H. Wang, C. M. Araujo, J. J. Cha, "Unveiling the interfacial effects for enhanced hydrogen evolution reaction on MoS₂/WTe₂ hybrid structures," *Small* **2019**, 15, 1900078.
13. S. Yazdani, M. Yarali, J. J. Cha, "Recent progress on in situ characterizations of electrochemically intercalated transition metal dichalcogenides," *Nano Research* **2019**, 12, p.2126-2139.
14. P. Liu, Y. Xie, E. Miller, Y. Ebine, P. Kumaravadeivel, S. Sohn, J. J. Cha, "Dislocation-driven SnTe surface defects during chemical vapor deposition growth," *J. Phys. Chem. Solids* **2019**, 128, p.351-359.

Weyl Electrons in New Frustrated Magnets

Jak Chakhalian, Rutgers University

Program Scope

Non-trivial topological phases are well-known for non-correlated compounds, but they are still scarce in correlated electron systems. The current research scope of the project is focused on two challenges (i) creating new synthetic templates with rich many-body behavior derived from the class of rare-earth pyrochlore iridates $R_2\text{Ir}_2\text{O}_7$ or RPyIr (here $R=\text{Pr} \dots \text{Lu}$) and (ii) the initial investigation of magnetic states and magneto-transport effects including anomalous Hall effect, negative magneto-resistance and potential chiral anomaly in (111)-oriented thin films emerging from long-range anti-ferromagnetic spin order, frustrated lattice and non-trivial band topology.

Recent Progress

(111)-oriented thin film synthesis.

Challenges: Thin films of PyIr and other Pt group metals (e.g., Ir, Re, Os) are notoriously difficult to fabricate with most results remain theoretical or obtained on micron-size powder. For instance, the theory predicts that YPyIr based bi-layer and tri-layer heterostructures grown along the [111] direction are novel QAHE materials, which can be crucial for the next-generation topological spintronics. However, up until now, despite very active efforts in this direction, no group has reported on the growth of bilayer or tri-layer films of RPyIr or even on a layer-by-layer control during the film deposition. Moreover, to-date, as shown in Fig. 1 (b-d) all the reported thin films are of poor crystallinity near the interface and shows various degrees of non-stoichiometry critical for the electronic and magnetic properties of RPyIr. Here we report on the *first successful all-in-situ synthesis* of high-quality [111]-oriented epitaxial structures of YPyIr and EuPyIr (see the STEM images in Fig. 1a and Fig. 1e, unpublished) [1].

New synthesis protocol: The (111)- and (100)-oriented epitaxial PyIr thin films are grown on $5 \times 5 \text{ mm}^2$ (111) yttria-doped ZrO_2 (YSZ) substrates by pulsed laser deposition ($\lambda = 248 \text{ nm}$, energy density $J = 6 \text{ J/cm}^2$, and a laser pulse repetition rate of 10-20 Hz). The key to success is in the iridium-enriched phase-mixed multicomponent target with a cation ratio of $\text{Y}:\text{Ir} = 1:3$. The deposition process is performed at the lowest possible substrate temperature of 520-540 C under a 50-100 mTorr atmosphere of ultra-

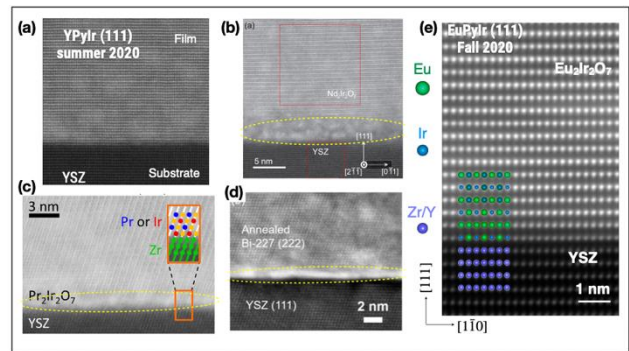


Figure 1. Representative STEM cross-section images of the PyIr epitaxial thin films fabricated via two-step solid phase epitaxy. (a) The PI's growth. (b)-(d) Film quality reported by other groups e) Our new development of all in-situ one-step solid phase epitaxy[1]

pure Ar and O₂ gas mixture with the partial pressure ratio Ar:O₂=10:1. After the deposition, the films require delicate post-annealing in-situ at 900-950 C for no longer than 8-10 min under a 620-650 Torr atmosphere of ultra-pure oxygen.[1]

Structural quality: The summary of structural characterization of the films is shown in Fig. 2. Our protocol for each sample is as follows: (1) We perform X-ray diffraction measurements to observe sharp interference fringes around the film Bragg reflection, which implies that the film has high crystallinity and well-defined layered structure akin to that shown in Fig. 2 a. Here, the control information is the value of the experimental lattice parameter to be close and ideally identical to that of the bulk. (2) Next, the rocking curve scan around a high-angle (e.g., (444)) diffraction peak yields a full-width-at-half-maximum (FWHM) of the PyIr sample. From this result, we obtain the lateral coherence length of structural domains (as an example, see Fig. 2b). (3) The film-substrate epitaxial relationship and the strain status is derived from azimuthal ϕ -scan and reciprocal space mappings (RSM). As illustrated in Fig. 2c (in blue), to confirm the expected film symmetry, we perform a ϕ -scan (e.g. on 222) which exhibits a characteristic three-fold symmetry coherent with that of the YSZ substrate's. This important measurement confirms that the film contains no misoriented domains or stacking faults.

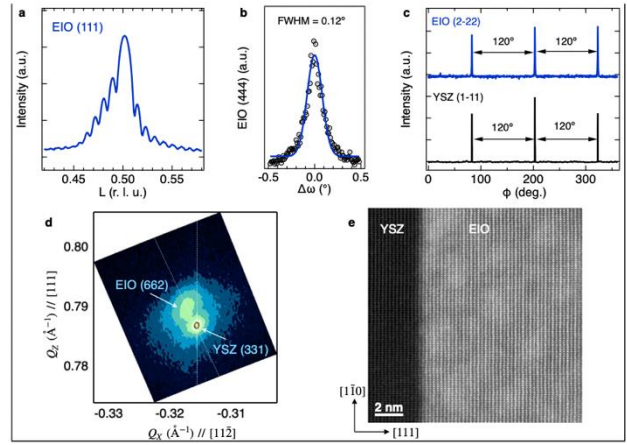


Figure 2. a. Coupled HKL-scan around the EuPyIr (111) diffraction in the reciprocal lattice unit (r.l.u.) of YSZ substrate. b. Rocking curve scan of the EuPyIr (444) diffraction. The FWHM is around 0.12°. c. Azimuthal ϕ -scans around the YSZ (1-11) and the EuPyIr (2-22) diffraction, respectively. Both peaks exhibit the three-fold symmetry. d. Reciprocal space mappings around YSZ (331) diffraction. The EuPyIr (662) diffraction is clearly observed along the radial direction in the reciprocal space. e. larger scale STEM-HAADF cross-sectional imaging of the (111) EuPyIr film on YSZ substrate.

Future Plans

Synthesis: Our current understanding of the growth and initial nucleation should allow us to identify several key challenges to overcome to reach the most desirable *atomic layer-by-layer growth*. First, Ir is a platinum group metal member and is very stable chemically. However, iridium readily oxidizes into a trioxide IrO₃ which is a *gas phase*! The major problem is that IrO₃ is highly volatile even under ambient pressure. For thin film growth in a low-pressure oxygen environment, it means that though Ir metal must be oxidized around 1000 C, and yet the RPyIr oxidation process is still accompanied by rapid evaporative losses of Ir and O due to the trioxide formation. Here we will focus on YPyIr and PrPyIr (111)-oriented thin films.

In addition to the YSZ substrate we will explore a new set of atomically polished *spin ice pyrochlores* ($R_2Ti_2O_7$) single crystals as a new candidate substrate for the RPyIr growth. These (111) oriented and polished crystals will be prepared by Jianshi Zhou, UT Austin. This approach has not been tried before.

Next, to mitigate the iridium loss due to the evaporative process, we can control it by altering growth kinetics by the ablation pulse rate; The higher laser pulse rate brings more atoms to the surface, potentially preventing the evaporation from occurring. A drawback of this rapid growth is the limited surface adatom migration, which affects the crystallinity and surface roughness of the film; thus, for the practical reason, we will limit the laser pulse-rate to about 20 Hz. Note, the relatively high roughness of about 2 nm may present an additional issue for ARPES limiting the momentum resolution of photoelectrons escaping the sample surface.

The second issue that we plan to investigate is the resputtering of the film surface during growth caused by the ionized species' high kinetic energy in the ablation plume, which set by the energy of the laser pulse. This seemingly straightforward issue is, in fact, rather hard to resolve because the reduction of laser energy causes large composition variations that occur close to the ablation energy threshold. Instead, we propose to explore *a new approach to moderate the kinetic energy* of the plume by gas-phase collisions with the *heavy process gas*. Considering the large atomic mass of Ir⁹² we will explore the growth kinetics by admixing 10%-50% of Xe¹³¹ gas into pure O¹⁶.

Magnetic state and magneto-transport.

At this point, it is important to emphasize that a very special kind of antiferromagnetic order known as all-in-all-out (AIAO) or 4-in-4-out is required for the emergence of topological states from the higher temperature nodal LAB phase (see Fig. 3). Surprisingly, despite such a crucial importance of the AIAO spin order, even for the bulk RPyIr very little direct experimental knowledge from magnetic scattering is reported to-date [2,3] *As for the thin films, no magnetic scattering demonstrating the presence of AIAO has been reported at all.*

To check the feasibility of detecting AIAO in ultra-thin films, the PI has submitted a proposal for beamline 6-ID-B and 33-BM-C of the Advanced Photon Source, ANL. We intent to carry out resonant (Ir L₃-edge at 11.215 keV) magnetic scattering measurements with the incident x-rays linearly polarized perpendicular to the scattering plane. To perform the polarization analysis, pyrolytic graphite (001) crystal will be used to analyze the polarization of the scattered x-rays. The prime reason of the polarization analysis is as follows: Both the resonant magnetic scattering and the anisotropic tensor susceptibility due to the lattice (ATS) scattering strongly contribute to YPyIr (0 0 10) reflection thus spoiling the magnetic signal. The ATS signal results from the local trigonal distortion of the IrO₆ octahedra due to the anisotropic nature of 5d orbitals

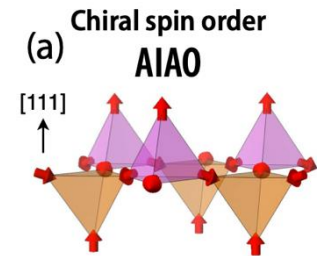


Figure 3. (a) All-in-all-out long-range AFM spin order which defines several topological states of PyIr.

and charge distribution at the Ir^{4+} sites and can be *very effectively suppressed through the polarization analysis*.

Thus, the very first demonstration of the AIAO AFM ordering in magnetic scattering accompanied by an intrinsic anomalous Hall effect in a zero external field will serve as one of the key direct pieces of evidence for the magnetic Weyl metallic phase in 111-films of PyIr [4].

References

1. Xiaoran Liu, Fangdi Wen, E. Karapetrova, J-W Kim, P. J. Ryan, J.W. Freeland, M. Terilli, T-C Wu, M. Kareev, and J. Chakhalian. In-situ fabrication and transport properties of (111) $\text{Y}_2\text{Ir}_2\text{O}_7$ epitaxial thin film. Applied Physics Letters, 117(4):041903, 2020.
2. C. Donnerer, M.C. Rahn, M Moretti Sala, J.G. Vale, D. Pincini, J. Stremper, M Krisch, D. Prabhakaran, A.T. Boothroyd, and D.F. McMorrow. All-in-all-out magnetic order and propagating spin waves in $\text{Sm}_2\text{Ir}_2\text{O}_7$. Physical Review Letters, 117(3):037201, 2016.
3. H. Sagayama, D. Uematsu, T-H Arima, K. Sugimoto, J.J. Ishikawa, E. O'Farrell, and S. Nakatsuji. Determination of long-range all-in-all-out ordering of ir $4+$ moments in a pyrochlore iridate $\text{Eu}_2\text{Ir}_2\text{O}_7$ by resonant x-ray diffraction. Physical Review B, 87(10):100403, 2013.
4. Bohm-Jung Yang and Naoto Nagaosa. Emergent topological phenomena in thin films of pyrochlore iridates. Physical review letters, 112(24):246402, 2014.

Publications

None yet, as the project just started (Sept. 2021).

Project title: Exploring quantized axion electrodynamics in magnetic topological insulator multilayer heterostructures

Moses H. W. Chan (PI)

Chao-Xing Liu (Co-PI)

Cui-Zu Chang (Co-PI)

Department of Physics, The Pennsylvania State University, University Park, PA16802

Program Scope

The current program is focusing on investigating the properties of the high Chern number quantum anomalous Hall (QAH) effect in magnetic topological insulator (TI) multilayer heterostructures and the exploration of the topological magnetoelectric effect in thick magnetic TI films/heterostructures. Our program includes both experimental and theoretical efforts on this topic.

Recent Progress

In the past 2 years, our team's efforts supported by the DOE grant (DE-SC0019064, \$749,007, 08/01/2018 ~ 07/31/2021; 1-year No Cost Extension) entitled "*Exploring quantized axion electrodynamics in magnetic topological insulator multilayer heterostructures*" have been productive. We have published 19 high-profile papers (see Publication section). Published papers include 1 in *Nature*, 1 in *Science*, 1 in *Nature Materials*, 4 in *Nature Communications*, 2 in *Physical Review Letters*, and 1 in *Science Advances*. The accomplishments with primary DOE support include the realization of the high Chern number QAH insulators in magnetic TI multilayer heterostructures (*Nature* 2020, #3 in Publication), the observation of the occurrence of the QAH effect, and the topological Hall effect in magnetic TI sandwich heterostructures (*Nature Materials* 2020, #4 in Publication), the demonstration of the interface induced Berry curvature engineering in magnetic TI bilayer heterostructures (*Nature Communications* 2021, #2 in Publication), the demonstration of the effectiveness of the gapless criterion for the noninteraction crystals from effective axion field (*Physical Review Letters* 2020, #5 in Publication), and the studies of exotic phonon dynamics induced by electronic Berry curvature in antiferromagnetic topological materials (*Physical Review Letters* 2021, accepted, #1 in Publication). In this presentation, we will focus on the realization of the high Chern number QAH insulators and tuning the Chern number in QAH insulators. We will also discuss our recent progress along this direction about the demonstration of the zero magnetic field plateau to plateau quantum transition in higher Chern number QAH insulators.

To date, the QAH effect has been realized in magnetic TI¹⁻⁷ and magic-angle twisted bilayer graphene^{8,9}. However, the QAH effect at zero magnetic fields has so far been realized only for the Chern number $C = 1$. In this work, we used molecular beam epitaxy (MBE) to fabricate magnetic TI/TI multilayers with symmetric structures, specifically $[3 \text{ QL Cr-doped (Bi, Sb)}_2\text{Te}_3/4 \text{ QL (Bi, Sb)}_2\text{Te}_3]_m/3 \text{ QL Cr-doped (Bi, Sb)}_2\text{Te}_3$ multilayer structures, where m is an integer reflecting the

number of bilayer periods. We observed a well-quantized QAH effect with tunable Chern number C of 1 to 5 (Figs. 1a to 1e). The Chern number C of the QAH insulators is determined by the number m of undoped TI layers in multilayer structures. In the same sample configuration, we found that the Chern number can be tuned by varying either the magnetic doping concentration or the thickness d of the interior magnetic TI layers. The realization of QAH insulators with high tunable Chern numbers facilitates possible applications of dissipationless chiral edge currents in energy-efficient electronic devices and opens opportunities for developing multi-channel quantum computing and higher-capacity chiral circuit interconnects.

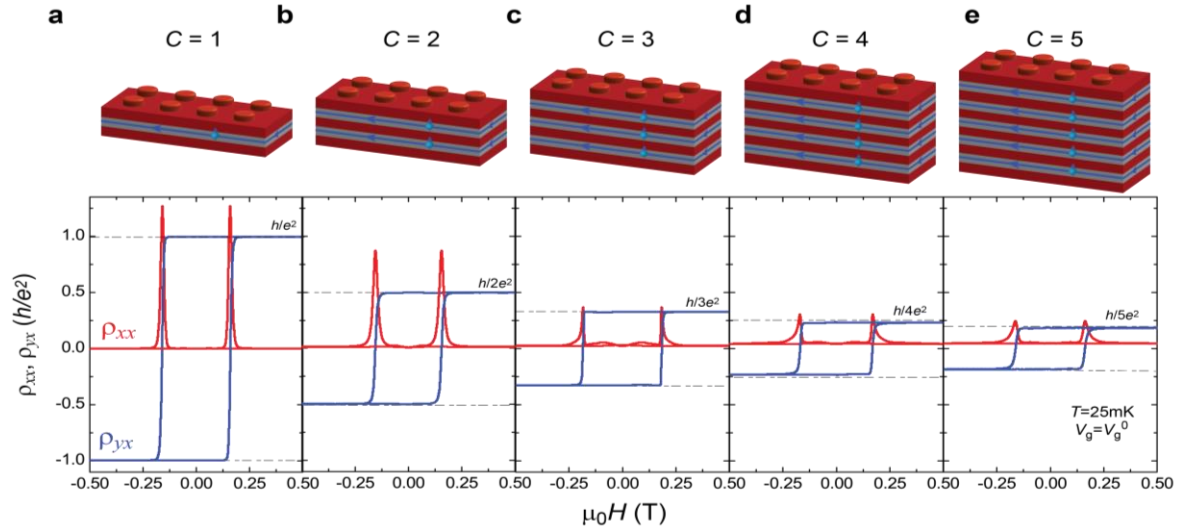


Fig. 1. High Chern number QAH effect realized in magnetic TI/TI multilayer samples. (a-e) Top: schematics (Legos) of the multilayer structures for the QAH effect with Chern number from $C = 1$ to $C = 5$. Bottom: $\mu_0 H$ dependence of the longitudinal resistance ρ_{xx} (red curve) and the Hall resistance ρ_{yx} (blue curve) measured at the charge neutral point $V_g = V_g^0$ and $T = 25$ mK.

More recently, based on the recently discovered high Chern number QAH insulators, we systematically tuned the Cr doping concentration in the middle magnetic TI layer of the magnetic TI/TI penta-layer heterostructures and found a zero magnetic field quantum phase transition between the $C = 1$ and $C = 2$ QAH insulators. During the Chern number quantum phase transition, the Hall resistance monotonically decreases from h/e^2 to $h/2e^2$, while the longitudinal resistance exhibits a maximum at the critical point. Our results show that the ratio between the Hall resistance and longitudinal resistance is greater than 1 at the critical point, which indicates that the original chiral edge channel from the $C = 1$ QAH insulator coexists with the dissipative bulk conduction channel while one more chiral edge channel is gradually formed during the phase transition. This study will motivate further investigations of the Chern number change-induced quantum phase transition under zero magnetic field and advance the development of the conceptual QAH-chiral edge current-based electronic and spintronic devices.

Future Plans

Based on our recent progress, we will pursue the following projects:

1. Explore the three-dimensional (3D) QAH effect and axion insulator states in MBE-grown magnetic TI films/heterostructures with thickness greater than 200nm.
2. Explore the topological magnetoelectric effect in the above-mentioned 3D QAH insulators and axion insulators.
3. Explore the QAH insulator with the Chern number greater than 10 and the possible Weyl semimetal phase in MBE-grown magnetic TI multilayer structures.
4. Investigate the fundamental properties of the recently discovered high Chern number QAH insulators, such as the scaling behaviors and current breakdown.

References

- 1 Chang, C. Z., Zhang, J. S., Feng, X., Shen, J., Zhang, Z. C., Guo, M. H., Li, K., Ou, Y. B., Wei, P., Wang, L. L., Ji, Z. Q., Feng, Y., Ji, S. H., Chen, X., Jia, J. F., Dai, X., Fang, Z., Zhang, S. C., He, K., Wang, Y. Y., Lu, L., Ma, X. C. & Xue, Q. K. Experimental Observation of the Quantum Anomalous Hall Effect in a Magnetic Topological Insulator. *Science* **340**, 167-170 (2013).
- 2 Chang, C. Z., Zhao, W. W., Kim, D. Y., Zhang, H. J., Assaf, B. A., Heiman, D., Zhang, S. C., Liu, C. X., Chan, M. H. W. & Moodera, J. S. High-Precision Realization of Robust Quantum Anomalous Hall State in a Hard Ferromagnetic Topological Insulator. *Nat. Mater.* **14**, 473-477 (2015).
- 3 Deng, Y., Yu, Y., Shi, M. Z., Guo, Z., Xu, Z., Wang, J., Chen, X. H. & Zhang, Y. Quantum anomalous Hall effect in intrinsic magnetic topological insulator MnBi_2Te_4 . *Science* **367**, 895-900 (2020).
- 4 Kou, X. F., Guo, S. T., Fan, Y. B., Pan, L., Lang, M. R., Jiang, Y., Shao, Q. M., Nie, T. X., Murata, K., Tang, J. S., Wang, Y., He, L., Lee, T. K., Lee, W. L. & Wang, K. L. Scale-Invariant Quantum Anomalous Hall Effect in Magnetic Topological Insulators beyond the Two-Dimensional Limit. *Phys. Rev. Lett.* **113**, 137201 (2014).
- 5 Checkelsky, J. G., Yoshimi, R., Tsukazaki, A., Takahashi, K. S., Kozuka, Y., Falson, J., Kawasaki, M. & Tokura, Y. Trajectory of the Anomalous Hall Effect towards the Quantized State in a Ferromagnetic Topological Insulator. *Nat. Phys.* **10**, 731-736 (2014).
- 6 Mogi, M., Yoshimi, R., Tsukazaki, A., Yasuda, K., Kozuka, Y., Takahashi, K. S., Kawasaki, M. & Tokura, Y. Magnetic Modulation Doping in Topological Insulators toward Higher-Temperature Quantum Anomalous Hall Effect. *Appl. Phys. Lett.* **107**, 182401 (2015).

- 7 Ou, Y., Liu, C., Jiang, G., Feng, Y., Zhao, D., Wu, W., Wang, X. X., Li, W., Song, C., Wang, L. L., Wang, W., Wu, W., Wang, Y., He, K., Ma, X. C. & Xue, Q. K. Enhancing the Quantum Anomalous Hall Effect by Magnetic Codoping in a Topological Insulator. *Adv. Mater.* **30**, 1703062 (2017).
- 8 Serlin, M., Tschirhart, C. L., Polshyn, H., Zhang, Y., Zhu, J., Watanabe, K., Taniguchi, T., Balents, L. & Young, A. F. Intrinsic quantized anomalous Hall effect in a moiré heterostructure. *Science* **367**, 900-903 (2020).
- 9 Sharpe, A. L., Fox, E. J., Barnard, A. W., Finney, J., Watanabe, K., Taniguchi, T., Kastner, M. A. & Goldhaber-Gordon, D. Emergent Ferromagnetism near Three-Quarters Filling in Twisted Bilayer Graphene. *Science* **365**, 605-608 (2019).

Publications (#1 to #5, #9, and #13 were primarily supported by the DOE grant)

1. Hu, L.-H., Yu, J., Garate, I. & Liu, C. X. Phonon helicity induced by electronic Berry curvature in Dirac materials. *Phys. Rev. Lett.* (2021, accepted; arXiv:2104.02270).
2. Wang, F., Wang, X., Zhao, Y. F., Xiao, D., Zhou, L. J., Liu, W., Zhang, Z., Zhao, W., Chan, M. H. W., Samarth, N., Liu, C., Zhang, H. & Chang, C. Z. Interface-induced sign reversal of the anomalous Hall effect in magnetic topological insulator heterostructures. *Nat. Commun.* **12**, 79 (2021).
3. Zhao, Y. F., Zhang, R., Mei, R., Zhou, L. J., Yi, H., Zhang, Y. Q., Yu, J., Xiao, R., Wang, K., Samarth, N., Chan, M. H. W., Liu, C. X. & Chang, C. Z. Tuning the Chern number in quantum anomalous Hall insulators. *Nature* **588**, 419-423 (2020).
4. Jiang, J., Xiao, D., Wang, F., Shin, J. H., Andreoli, D., Zhang, J. X., Xiao, R., Zhao, Y. F., Kayyalha, M., Zhang, L., Wang, K., Zang, J. D., Liu, C. X., Samarth, N., Chan, M. H. W. & Chang, C. Z. Concurrence of quantum anomalous Hall and topological Hall effects in magnetic topological insulator sandwich heterostructures. *Nat. Mater.* **19**, 732-737 (2020).
5. Yu, J., Song, Z. D. & Liu, C. X. Gapless Criterion for Crystals from Effective Axion Field. *Phys. Rev. Lett.* **125**, 036401 (2020).
6. Lee, S. H., Graf, D., Min, L., Zhu, Y., Yi, H., Ciocys, S., Wang, Y., Choi, E. S., Basnet, R. & Fereidouni, A. Evidence for a Magnetic-Field-Induced Ideal Type-II Weyl State in Antiferromagnetic Topological Insulator Mn(Bi_{1-x}Sb_x)₂Te₄. *Phys. Rev. X* **11**, 031032 (2021).
7. Liu, J., Yu, J., Ning, J., Yi, H., Miao, L., Min, L., Zhao, Y., Ning, W., Lopez, K. & Zhu, Y. Spin-valley locking and bulk quantum Hall effect in a noncentrosymmetric Dirac semimetal BaMnSb₂. *Nat. Commun.* **12**, 1-10 (2021).
8. Xiao, R., Xiao, D., Jiang, J., Shin, J. H., Wang, F., Zhao, Y. F., Zhang, R. X., Richardella, A., Wang, K., Kayyalha, M., Chan, M. H. W., Liu, C. X., Chang, C. Z. & Samarth, N.

- Mapping the phase diagram of the quantum anomalous Hall and topological Hall effects in a dual-gated magnetic topological insulator heterostructure. *Phys. Rev. Research* **3**, L032004 (2021).
9. Zhang, J.-X., Andreoli, D., Zang, J. & Liu, C.-X. Topological Hall effect in magnetic topological insulator films. *J. Magn. Magn. Mater.* **528**, 167700 (2021).
 10. Yan, C., Fernandez-Mulligan, S., Mei, R., Lee, S. H., Protic, N., Fukumori, R., Yan, B., Liu, C., Mao, Z. & Yang, S. Origins of electronic bands in the antiferromagnetic topological insulator MnBi₂Te₄. *Phys. Rev. B* **104**, L041102 (2021).
 11. Kayyalha, M., Xiao, D., Zhang, R. X., Shin, J., Jiang, J., Wang, F., Zhao, Y. F., Xiao, R., Zhang, L., Fijalkowski, K. M., Mandal, P., Winnerlein, M., Gould, C., Li, Q., Molenkamp, L. W., Chan, M. H. W., Samarth, N. & Chang, C. Z. Absence of evidence for chiral Majorana modes in quantum anomalous Hall-superconductor devices. *Science* **367**, 64-67 (2020).
 12. Wu, X., Xiao, D., Chen, C. Z., Sun, J., Zhang, L., Chan, M. H. W., Samarth, N., Xie, X. C., Lin, X. & Chang, C. Z. Scaling behavior of the quantum phase transition from a quantum-anomalous-Hall insulator to an axion insulator. *Nat. Commun.* **11**, 4532 (2020).
 13. Yu, J. & Liu, C. X. Piezoelectricity and topological quantum phase transitions in two-dimensional spin-orbit coupled crystals with time-reversal symmetry. *Nat. Commun.* **11**, 2290 (2020).
 14. Fu, H. X., Liu, C. X. & Yan, B. H. Exchange bias and quantum anomalous Hall effect in the MnBi₂Te₄/CrI₃ heterostructure. *Sci. Adv.* **6**, eaaz0948 (2020).
 15. Wu, X. X., Benalcazar, W. A., Li, Y. X., Thomale, R., Liu, C. X. & Hu, J. P. Boundary-Obstructed Topological High-T-c Superconductivity in Iron Pnictides. *Phys. Rev. X* **10**, 041014 (2020).
 16. Zhang, J.-X. & Liu, C.-X. Disordered quantum transport in quantum anomalous Hall insulator-superconductor junctions. *Phys. Rev. B* **102** (2020).
 17. Li, J., Leng, H.-B., Fu, H., Watanabe, K., Taniguchi, T., Liu, X., Liu, C.-X. & Zhu, J. Superconducting proximity effect in a transparent van der Waals superconductor-metal junction. *Phys. Rev. B* **101**, 195405 (2020).
 18. Yu, J. & Liu, C.-X. Surface Majorana flat bands in $j = 3/2$ superconductors with singlet-quintet mixing. *Chin. Phys. B* **29**, 017402 (2020).
 19. Pan, J., Yu, J., Zhang, Y.-F., Du, S., Janotti, A., Liu, C.-X. & Yan, Q. Quantum anomalous Hall effect in two-dimensional magnetic insulator heterojunctions. *npj Comput. Mater.* **6**, 152 (2020).

New Interfaces in Intercalated Structures

Joseph Checkelsky, Massachusetts Institute of Technology

Program Scope

The objective of this study is to realize new types of incommensurate interfaces in bulk crystals with equilibrium (via direct synthesis) and nonequilibrium (post-synthesis) intercalated structures. Opportunities for new science and device applications with these systems is a nascent area, with potential impact on new materials and devices exhibiting magnetism, topology, superconductivity, multiferroic behavior, and other emerging phenomena. This proposal examines semiconducting structures as a means to elevate the electronic quality and operating temperature of the exotica observed in purely 2D systems. This work leverages collaborative efforts in advances spectroscopy, electrochemistry, and theoretical methods. Discoveries herein could offer new platforms for energy saving technology based on incommensurate interfaces.

Recent Progress

This new project aims to study transition metal dichalcogenides and their modified structures using inorganic and organic intercalants. Combining material synthesis and a variety of intercalation strategies we will explore non-equilibrium structures and their electronic properties. New functionalities at these emergent interfaces will also be investigated. Understanding what types of new interfaces can be created in intercalated structures may enable new types of 2D materials and their layered analogs.

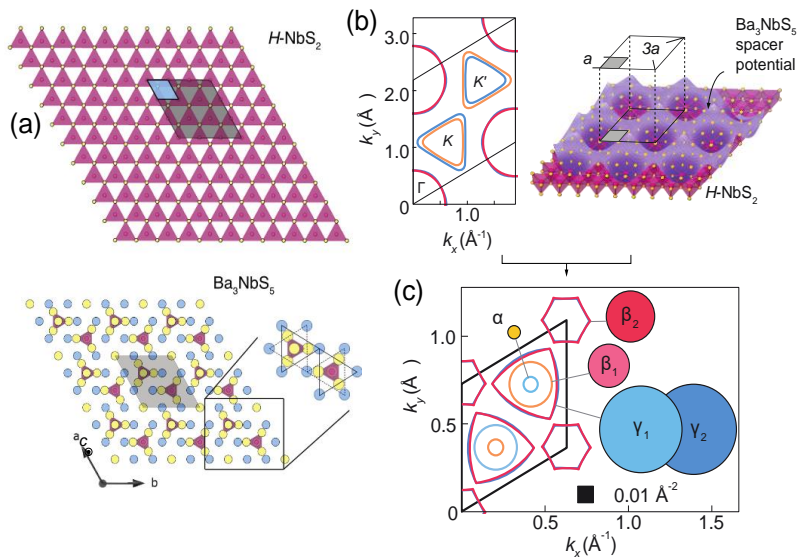


Figure 1: (a) Structure of constituent layers of $\text{NbS}_2:\text{BaNb}_3\text{S}_5$ superlattice. (b) Monolayer NbS_2 structure and zone folding leading to (c) renormalized superlattice band structure.

New types of superlattice structures have recently been reported which create novel types of interfaces between transition metal dichalcogenide (TMD) layers and inorganic buffer layers [1]. As shown in Fig. 1, combining TMD layers with disparate spacer layers (Fig. 1(a)) leads to profound changes of the electronic structure through superlattice potentials (Fig. 1(b)) that renormalize the electronic bands (Fig. 1(c)). Extending this to other materials within this class has the potential to realize a number of new electronic structures; we are investigating extending these interfaces to introduce new functionalities to the buffer layer and also stabilize otherwise metastable TMD structures.

While previously studies in the context of *2H-NbS₂*, the TMD layers themselves offer a rich variety of possible quantum ground states to manipulate by choosing the transition metal (see Fig. 2) [2]. The chalcogen layer also plays an important role in tuning the dimensionality and strength of spin-orbit interaction in the system. Complex stacking structures of the TMD layers themselves (*e.g.* *4Hb*) offer an additional design degree of freedom.

In order to navigate this large phase space, we are combining experimental synthesis campaigns with structural stability calculations to evaluate materials of greatest interest. Thus, from a pure synthesis perspective we are able to target both active layers in the system.

In terms of post synthesis creation of new interfaces, there is a long history of the intercalation of organic molecules into layered systems including TMDs [3], see for example the structure in Fig. 3. In systems which are composed of highly decoupled layers (*e.g.* graphite) this has proven to be a particularly versatile process. We are investing intercalation into new superlattice TMD systems which have enhanced decoupling

compared to transitional TMDs to investigate the role of more complex intercalation structures. The selection of the intercalant species can control the degree of layer coupling as well as carrier

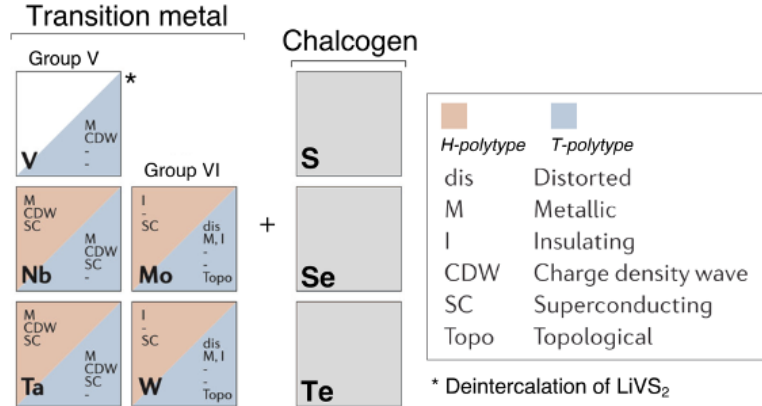


Figure 2: Overview of ground states of selected pristine TMD systems (from [2]).

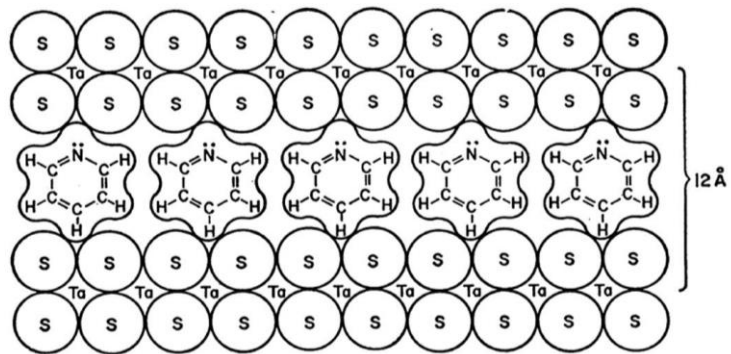


Figure 3: Depiction of organic intercalation into TMDs (from [3]).

density via charge transfer. Application of modern electron microscopy techniques to these systems will offer an unprecedented degree of characterization that may enable higher degrees of material control.

In ongoing work, we are selecting and synthesizing new candidate systems. A substantial challenge is the electronic modeling of these systems, as for example the unit cells can be very large. Previous work in misfit structures has made extensive use of approximate models [4]; we will pursue this as well as model Hamiltonian approaches to understanding the impact of supermodulations on the TMD layers. In addition, growth methods beyond traditional bulk synthesis and intercalation are being investigated in order to stabilize new building blocks for these layered systems.

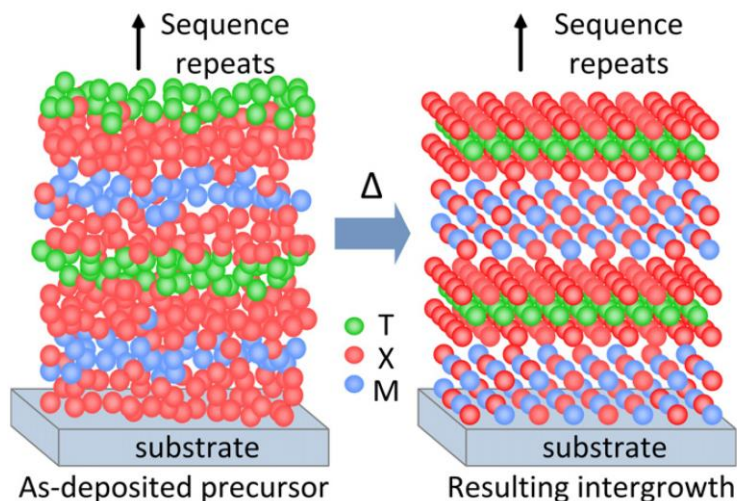


Figure 4: MER method for growth of superlattice materials (from [5]).

For example, it has previously been established that the modulated elemental reaction (MER) (see Fig. 4) is a successful pathway to enable new types of layered structures [5]. This includes with elements that are often difficult to incorporate into highly layered structures and may allow a significant expansion of material phase space. We are exploring the use of MER and related out-of-equilibrium methods to realize new types of interfaces that in particular include strong spin-orbit coupled elements.

Future Plans

We will employ the design principles outlined here to develop new interfaces in TMD systems to introduce long wavelength potentials to 2D layers. The study of their structural, electronic, and magnetic properties will be performed to evaluate the new functionalities that may arise.

References

1. Devarakonda A, Inoue H, Fang S, Ozsoy-Keskinbora C, Suzuki T, Kriener M, Fu L, Kaxiras E, Bell DC, Checkelsky JG (2020) Clean 2D superconductivity in a bulk van der Waals superlattice. *Science*, 370(6513):231–236. <https://doi.org/10.1126/science.aaz6643>
2. Manzeli S, Ovchinnikov D, Pasquier D, Yazyev OV, Kis A (2017) 2D transition metal dichalcogenides. *Nature Reviews Materials*, 2(8):17033. <https://doi.org/10.1038/natrevmats.2017.33>

3. Gamble FR, DiSalvo FJ, Klemm RA, Geballe TH (1970) Superconductivity in Layered Structure Organometallic Crystals. *Science*, 168(3931):568–570. <https://doi.org/10.1126/science.168.3931.568>
4. Cario L, Rouxel J, Meerschaut A, Moelo Y, Corraze B, Chauvet O (1999) Band structure and electronic properties of the incommensurate misfit compound. *Journal of Physics: Condensed Matter*, 11(14):2887–2900. <https://doi.org/10.1088/0953-8984/11/14/005>
5. Beekman M, Heideman CL, Johnson DC (2014) Ferecrystals: non-epitaxial layered intergrowths. *Semiconductor Science and Technology*, 29(6):064012. <https://doi.org/10.1088/0268-1242/29/6/064012>

Publications

N/A

Microwave spectroscopy of correlated 2D electron systems in semiconductors and graphene

L.W. Engel, NHMFL/FSU and Cory Dean, Columbia University

Program Scope

Two-dimensional electrons can form a wide variety of correlated states, particularly in systems for which the disorder can be kept extremely small. These systems include semiconductor heterostructures and more recently graphene, in particular when it is encapsulated in clean BN. This project is aimed at studying electron solids and other correlated states by means of broadband microwave spectroscopy. The main method of performing this spectroscopy utilizes transmission lines like that pictured in Figure 1.



Figure 1 Photomicrograph of a coplanar waveguide transmission line on top of a BN graphene stack containing twisted bilayer graphene (TBLG). The transmission line has a driven center conductor and grounded side planes, and contains an array of contacts to the graphene beneath. Light yellow areas are metal. Two leads connected to a graphite gate layer form the “v” at top. The sample was fabricated at Columbia.

A main goal of the program has been to perform this spectroscopy on various graphene systems. These include:

- 1) electron solids within integer quantum Hall states, which may exhibit a pinning or propagating hybrid transverse-longitudinal mode, as predicted for electron solids in magnetic fields
 - 2) the superconducting or correlated insulating states of twisted bilayer graphene (TBLG) [1,2],
 - 3) ordinary bilayer graphene, which can exhibit a voltage controlled cyclotron resonance in the microwave range under certain conditions [3].
- Graphene samples are to be fabricated at Columbia, and microwave experiments to be run at NHMFL/FSU.

The scope of the project also includes investigations of 2D electrons systems (2DES), hosted in semiconductors including GaAs, and also anisotropic AlAs. The semiconductor work is implemented with coplanar waveguide (CPW) transmission lines patterned onto the surface of the device, and coupled to the 2DES capacitively. The work on semiconductors is mainly focused on carriers condensed into solid phases, of which there is a wide variety.

Recent Progress

a) Novel cyclotron resonance in AIAs

We have found that when a CPW is only a few mm long, the measured transmission easily reveals cyclotron resonance, along with 2D plasmon resonances associated with the dimensions of the device. AIAs has two band masses owing to its ellipsoidal Fermi surface [4,5]; calculated heavy and light masses (m_H and m_L) are respectively 1.1 and 0.19 free electron masses. Conventional cyclotron

resonance (CR) experiments done on material with two masses show a line corresponding to the geometric mean of the masses, $\omega_c = eB(m_H m_L)^{-1/2}$. For AIAs, $(m_H m_L)^{-1/2}$ using the calculated values would result in a cyclotron frequency of 60.9 GHz/T. Figure 2 shows a color value plot of magnetic field vs microwave absorption for an AIAs sample, of a quality only recently developed [6]. The magenta dotted line has slope of 59.4 GHz/T, close to the predicted value for the geometric mean mass. At frequencies above that (lower on the graph) magnetoplasmons contribute to absorption, and the brown arcs correspond to features in the geometry of the CPW. The novel CR appears as a green dashed line, and is highlighted in one place within a magenta box; the dasheding is artifactual and would not appear if spectra were taken at more fields. The slope of the novel resonance is 27.8 GHz/T, close to the 24.4 GHz/T expected for the bare heavy mass, and no magnetoplasmons appear until the higher cyclotron frequency of the geometric-mean mass is exceeded. An interpretation for this, suggested by ref. [7], is that strongly varying microwave fields at CPW edges couple to one edge of cyclotron orbits, analogous to Azbel'-Kaner CR in metals.

b) Results in GaAs quantum wells (QWs)

This is the topic of the highlight and poster submitted for this conference.

The archetypical electron solid state is the Wigner solid (WS) [8-10] that occurs at the high magnetic field (B), low filling factor (ν) termination of the series of fractional quantum Hall effect states in GaAs. Here we present studies of that phase for a series of GaAs quantum wells (QWs) of various well thicknesses ($d=30,40,50$ and 70 nm). The samples are similar to each other in design except for their well thickness, and their residual disorder is minimized to the current state of the art. rf spectroscopy is used to study pinning modes [9,10], in which pieces of the solid oscillate within the potential of residual disorder. We have long ago found that pinning mode frequencies are sensitive to the vertical confinement of the 2DES; the series of

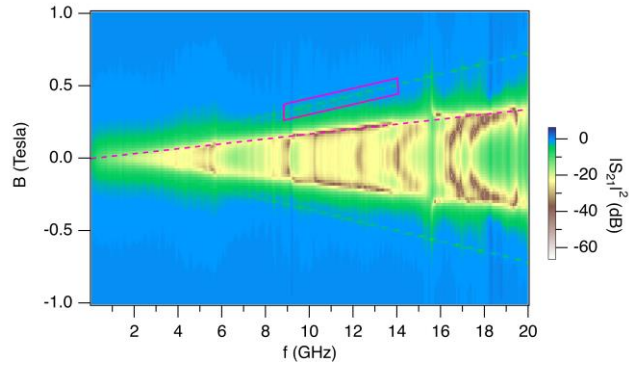


Fig. 2 : color scale plot of magnetic field vs absorption for AIAs. Magenta dotted line and box are drawn in to highlight the features of the data.

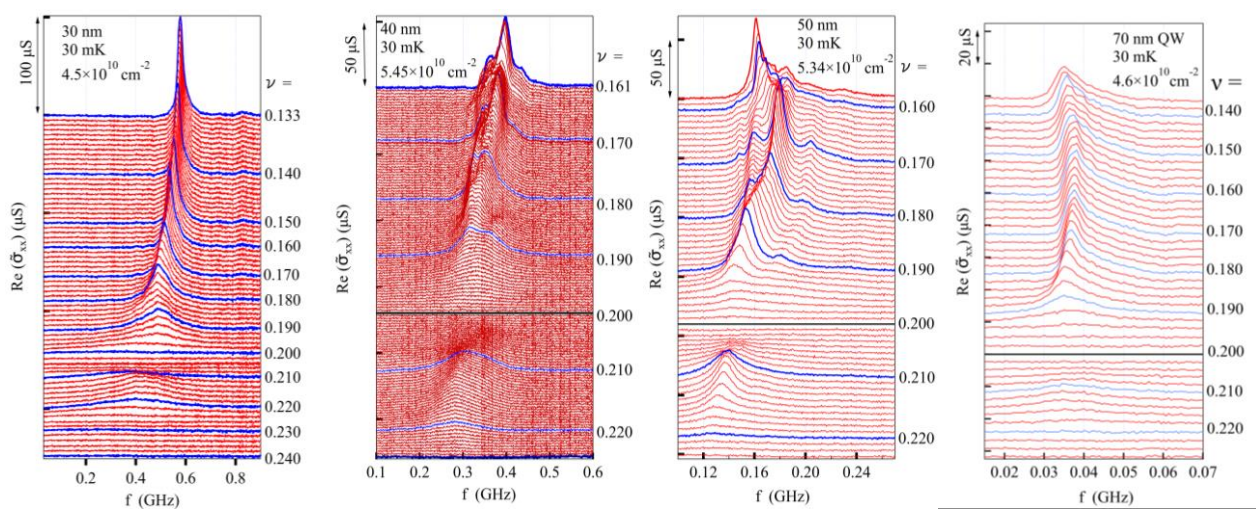


Fig. 3: Pinning mode spectra for the QWs of the series for many Landau level filling factors (ν) plotted offset downward proportional to ν . QW width d and density n are shown on each plot.

similar QWs lets us examine that effect by itself, and gives us information on what disorder is causing the pinning.

Figure 3 shows spectra from the low ν solid ranges of the samples in the QW series. The resonance appears weakly in a narrow range with ν above the range of 1/5 fractional quantum Hall effect, and becomes much sharper and stronger as n decreases below 1/5. In the $d=70$ nm QW, the pinning mode frequency (f_{pk}) is only 36 MHz, the lowest ever observed.

Figure 4 shows f_{pk} vs d for the samples of the series with, along with several calculated curves. Most sources of disorder for GaAs QWs would not show such a strong effect on changing d .

Weak-pinning theories of pinning modes [11-13] predict that f_{pk} is proportional to the square of the disorder strength. Interface roughness with infinite barriers [14] produces a variation of the subband energy which goes as d^{-3} , and hence $f_{pk} \propto d^{-6}$, which in Fig. 4 changes with d much more quickly than the data do.

One source of disorder is due to tails of the growth-direction wave function in the $Al_xGa_{1-x}As$ barriers that contain the QW. With P_B is the probability of charge being in the alloyed barrier, $f_{pk} \propto P_B^2$ is predicted. P_B^2 calculations are plotted in Fig. 4 for a simple finite square well model (labeled 0.144 eV) and for a self-consistent calculation of the charge density in the well, done by Prof. R. Winkler. The agreement of the calculations with the data is a good indication that charge within the barriers is the main type of disorder producing the pinning.

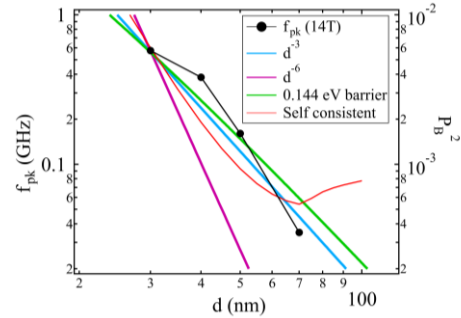


Fig. 4: f_{pk} (left axis) and P_B^2 (right axis) vs d . f_{pk} data as black dots, various calculated curves in color. The calculated curves are multiplied by arbitrary factors to make them coincide with the $d=30$ nm f_{pk} data point. The left and right axes cover the same range, on the log scales so that the relative change of predictions can be compared with the data.

c) Progress in graphene

Progress towards fabricating graphene samples optimized for the microwave experiments was delayed due to COVID-related shutdown of user facilities and travel restrictions. Regardless we have restarted these efforts and have recently completed a first attempt of the total process including both fabricating graphene coupled to waveguides in the Dean lab followed by measurement in the high frequency cryostat of the Engel lab. These first measurement sets were limited by issues related to making electrical contact to the local graphite gate in our device design. We expect to be able to resolve this in the next generation of devices and hope to have microwave data on graphene by the end of the current performance period.

Future Plans

Future plans call for Jeongmin Park, our mutual postdoc, to measure the new generation of graphene samples. These will include single layer graphene, to search for signatures of electron solids as well as TBLG samples. The QW studies are to be extended to p-type and selected samples are to be measured in higher magnetic fields at NHMFL facilities.

References

1. Y. Cao, et al., Nature **556**, 43 (2018).
2. M. Yankowitz et al., Science **363** 1059 (2019).
3. Y. Barlas et al., Phys. Rev. Lett. **101** 097601 (2008).
4. M. Shayegan et al., Physica Status Solidi (b) **243**, 3629 (2006).
5. K. Maesawa, T. Mizutani and S. Yamada, Appl. Phys. Lett. **71**, 296 (1991).
6. Y. J. Chung et al., Phys. Rev. Materials **2**, p. 071001 2018.
7. I. V. Andreev et al., Phys. Rev. B **96**, 161405 (2017).
8. Y. E. Lozovik and V. I. Yudson, JETP Lett. **22**, 11 (1975).
9. E. Y. Andrei et al., Phys. Rev. Lett. **60**, 2765 (1988).
10. P. D. Ye et al., Phys. Rev. Lett. **89**, 176802 (2002).
11. H. A. Fertig, Phys. Rev. B, **59**, 2120 (1999).
12. M. M. Fogler and D. A. Huse, Phys. Rev. B **62**, 7553 (2000).
13. R. Chitra, T. Giamarchi and P. Le Doussal, Phys. Rev. B **65**, 035312 (2001).
14. H. Sakaki, Applied Phys. Lett. **51**, 1934 (1987).

Publications

- A. T. Hatke, H. Deng, Yang Liu, L. W. Engel, L. N. Pfeiffer, K. W. West, K. W. Baldwin and M. Shayegan, "Wigner solid pinning modes tuned by fractional quantum Hall states of a nearby layer", Science Advances **5**, 2848 (2019).
- H. Deng, L. N. Pfeiffer, K. W. West, K. W. Baldwin, L. W. Engel and M. Shayegan, "Probing the melting of a two-dimensional quantum Wigner crystal via its screening efficiency", Phys. Rev. Lett. **122**, 116601 (2019).

Program Title: Novel Synthesis of Quantum Epitaxial Heterostructures by Design

Principle Investigator: Chang-Beom Eom

Mailing Address: Room 2166 ECB, 1550 Engineering Drive, University of Wisconsin-Madison, Madison, WI 53706

E-mail: eom@engr.wisc.edu

Program Scope

Quantum materials such as unconventional superconductors, interfacial two-dimensional electron gases (2DEGs), and multiferroics have been fertile ground for new discoveries. Our overarching goal is to develop novel synthesis routes that will create a new generation of epitaxial quantum thin film heterostructures for study of fundamental science and for development of new applications. These films can be of comparable or higher quality than available bulk single crystals, but more importantly film deposition conditions can be maintained far from equilibrium, so that metastable phases (nonexistent in nature) can be obtained by epitaxial stabilization of thin films. But these novel systems are usually sensitive to thin film heterostructure constraints, including interaction with the substrate, the difficulty in controlling point defects, and the challenge of forming atomically perfect interfaces.

Our hypothesis is that designing substrate interactions, controlling and identifying point defects, and working toward atomically perfect interfaces will reveal new phenomena and fundamental intrinsic properties of quantum materials arising from dimensionality, anisotropy, and electronic correlations. We have begun to implement some of these approaches. We have already demonstrated strain engineering of the Fe-based superconductor BaFe_2As_2 and made the first direct observation of the two-dimensional hole gas (2DHG) at an oxide interface. As next steps, we are developing a unique free-standing oxide stacked membrane fabrication technique to apply large dynamic strain, implementing chemical pulsed laser deposition (CPLD), and beginning to understand a route to new discoveries through control of highly perfect and defect free films and heterostructures. The **thrusts** of our proposed new work develop these advances, and expand into new materials systems:

- (1) *Novel CPLD Synthesis Route for oxide interface strain control, and oxide hole doping.*
- (2) *Interface- and Strain engineered Fe-based superconductors*

Recent Progress

Recently, a new class of “high temperature” superconductivity has been discovered in heterostructures based on KTaO_3 (KTO). Previously, superconductivity was observed in KTO only at very low temperatures (~ 50 mK) in response to electrolyte doping [1]. Recent experiments show superconducting behavior at temperatures exceeding 2 K at (111) and (110) epitaxial heterointerfaces of KTO with thin layers of LaAlO_3 or EuO [2]. The availability of a new family of superconducting semiconductor heterostructures based on KTO enables a unique “stereoscopic” view into a “high temperature” mechanism of superconductivity, one that may be important in the development of new classes of superconductors.

A striking feature of the KTO system is the large spin-orbit (SO) coupling which originates from the $5d$ electron of Ta [3]. This SO coupling an order of magnitude greater than STO enables a comparative investigation into the role of SO coupling in mediating pairing strength. Engineering of SO interactions may also enable new opportunities in heterostructure spintronics or spin current manipulation by the spin Hall effect (SHE) and inverse spin Hall effect (ISHE).

Such a novel approach requires development of a new route to epitaxial oxide thin films and interfaces clean enough to probe fundamental quantum phenomena. We have extended the use of hybrid pulsed laser deposition (HPLD) growth process. We have already demonstrated dramatically lower point defect concentration in other complex oxide thin films such as SrTiO_3 thin films. Such higher quality epitaxial films and heterostructures remove several roadblocks that

have limited the development of KTO-based systems, which have generally poorer bulk crystalline quality. The proposed research relies critically on the HPLD process to reduce point defects, primarily in strained epitaxial KTO.

But alkali *5d* metal oxides, pose great challenges for high-quality epitaxial film growth due to their extremely high vapor pressures and instabilities. At the same time, they offer new opportunities to explore emerging quantum heterostructures such as KTaO₃ (KTO). Here, we demonstrate the ability to synthesize, for the first time, high-quality epitaxial KTO thin films and tune point defects in oxide-based quantum heterostructures of LaAlO₃/KTaO₃ (LAO/KTO), using a newly developed hybrid pulsed laser deposition (HPLD) growth technique. X-ray diffraction studies show that HPLD enables the synthesis of highly perfect homo- and heteroepitaxial KTO thin films. Electrical transport measurements reveal that LAO/KTO heterostructures grown on single crystal KTO substrates (LAO/KTO/KTO) exhibit higher two-dimensional carrier densities (n_{2D}) than LAO on KTO substrates, which not only highlight the importance of controlling the point defect and interface structures in this new 2DEG system but more importantly offer a viable pathway to deterministically controlled transport properties. These enables the study of novel quantum phenomena in complex oxide heterostructures.

We choose the LAO/KTO heterostructure as a model system to demonstrate KTO point defect with the HPLD growth technique. We used K₂O as a potassium source during the laser ablation of a Ta₂O₅ target (Figure 1a). The mechanism of HPLD growth for KTO is related to that of hybrid MBE, where KO can only be adsorbed to form KTO on TaO₂-terminated surface, whereas it would be desorbed on KO-terminated one. Using this technique, we were able to achieve highly stoichiometric KTO. To find the stoichiometric growth window, thermodynamic calculations were performed in K₂O-Ta₂O₅ system. The stability regions of possible ternary compounds in the K-Ta-O system were evaluated. Such calculations reveal a wide processing window for obtaining stoichiometric KTO (Figure 1b). At the typical growth temperature of 700 °C and oxygen partial pressure of 10⁻⁵ Torr, KTO is predicted to be formed under potassium partial pressures in the range of 10⁻¹⁰ to 10⁻⁶ Torr.

To confirm these predictions, we synthesized hetero- and homoepitaxial 15 nm KTO thin films on (110) GdScO₃ (GSO) and (111) KTO single crystal substrates. Out-of-plane θ -2 θ X-ray diffraction patterns of 15 nm KTO / GSO (110) heterostructures (Figure 2a) show that the KTO films are highly crystalline and

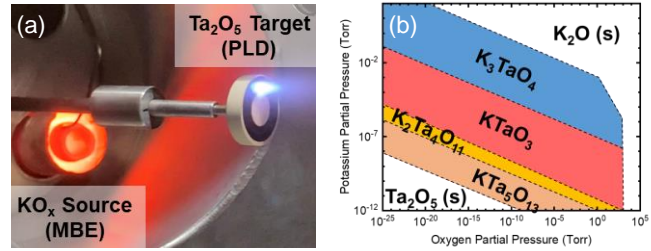


Figure 1. (a) Novel synthesis route: Hybrid PLD. (b) Calculated phase diagram showing the growth window of KTaO₃ thin film.

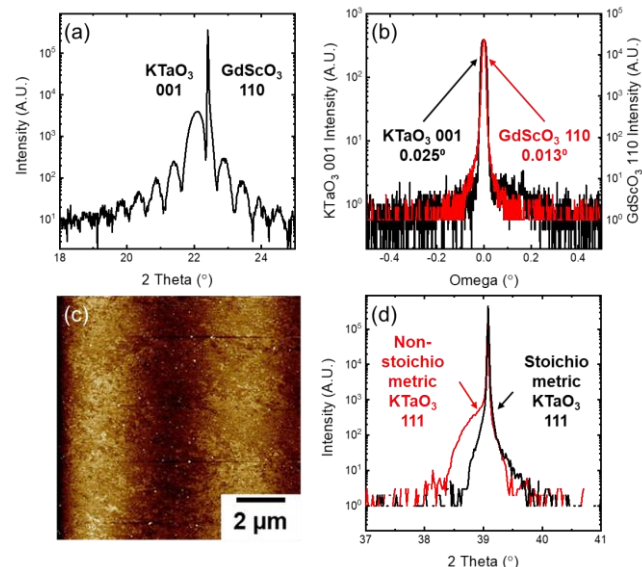


Figure 2. (a) Out-of-plane θ -2 θ X-ray diffraction patterns of KTO / GSO (110) heterostructures. (b) Rocking curves about the KTO 001- and GSO 110-diffraction conditions. (c) Topography of KTO / GSO (11) heterostructures. (d) Out-of-plane θ -2 θ X-ray diffraction patterns of KTO / KTO (111) homo structures.

single phase. Rocking curves about the 001-diffraction conditions (Figure 2b) show that the full-width-at-half-maximum values of KTO peaks are comparable to the substrate, which further confirm the high-quality epitaxial growth. Atomic force microscopy showed atomically flat surfaces (Figure 2c). Point defects in homoepitaxial KTO films can be either enhanced (non-stoichiometric, red in Figure 2d) or suppressed (stoichiometric, black in Figure 2d) by tuning growth parameters. These results demonstrate that HPLD can control KTO growth with high precision.

We investigated the electrical transport behavior of 2DEGs in homoepitaxial KTO / KTO (111) by growing *in situ* a 20 nm LAO layer. Using the KTO films as templates, amorphous LAO layers were grown on KTO by conventional PLD to investigate the effect of homoepitaxial KTO growth on 2DEG properties. In addition, LAO layers were grown without the homoepitaxial KTO layer to serve as reference. Notably, both the LAO/KTO/KTO (111) and LAO/KTO (111) heterostructures exhibit metallic behavior down to 2K, and LAO/KTO/KTO (111) heterostructures exhibit significantly higher 2D carrier concentrations ($4.38 \times 10^{14} \text{ cm}^{-2}$) compared to LAO/KTO (111) heterostructures ($4.24 \times 10^{13} \text{ cm}^{-2}$) at 300K [Figure 3]. These results demonstrate that homoepitaxially-grown KTO layers may be effective in controlling the 2DEG behavior in LAO/KTO systems.

Future Plans

(1) Novel HPLD Synthesis Route for advances in oxide films and heterostructures

We will continue development of the hybrid pulsed laser deposition (HPLD) growth process that is already showing dramatically lower concentration of point defects in complex oxide thin films. The higher quality epitaxial films and heterostructures described here remove several roadblocks that have limited the development of new science using quantum materials.

(2) Superconductivity in LAO/KTO/KTO heterostructures

We will use our HPLD synthesized heterostructures to understand the relation between point defect and electron gas properties, and to investigate high- T_c interfacial superconducting electron gases to understand the fundamental aspects of 2DEG superconductivity. We will also grow heterointerfaces between KTaO_3 and a wide variety of oxide materials including LaScO_3 and LaAlO_3 using PLD with high pressure *in situ* RHEED to investigate the effect of strain and point defects in KTO heterostructures on its superconductivity and spin manipulation properties.

(3) Strain and Interface Engineered Unconventional Superconducting Quantum Heterostructures

We will also use our new synthesis routes to explore strain- and electric-field dependent superconducting properties such as (1) strain-controlled lattice distortion and symmetries for investigation of the pnictide superconducting mechanism (2) the interaction of monolayer FeSe with strain- and interface engineered SrTiO_3 films.

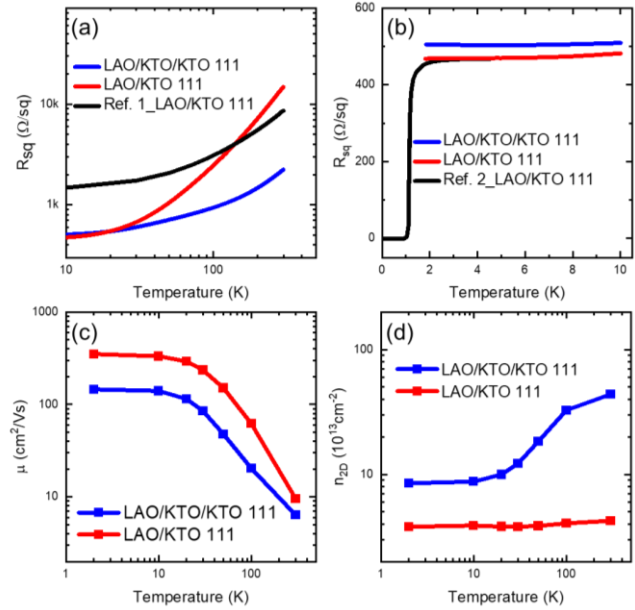


Figure 3. (a) Sheet resistance as a function of temperature down to 10K. (Ref. 1: Chen *et al.*, Science 2021) (b) Sheet resistance as a function of temperature down to 10K. (Ref. 2: Liu *et al.*, Science 2021). (c) Mobility as a function of temperature. (d) 2D carrier concentrations as a function of temperature.

References

1. Ueno K, Nakamura S, Shimotani H, Yuan HT, Kimura N, Nojima T, Aoki H, Iwasa Y, Kawasaki M (2011) Discovery of superconductivity in KTaO_3 by electrostatic carrier doping. *Nature nanotechnology*, 6(7):408–412. <https://doi.org/10.1038/nnano.2011.78>
2. Liu C, Yan X, Jin D, Ma Y, Hsiao H-W, Lin Y, Bretz-Sullivan TM, Zhou X, Pearson J, Fisher B, Samuel Jiang J, Han W, Zuo J-M, Wen J, Fong DD, Sun J, Zhou H, Bhattacharya A (2020) Discovery of two-dimensional anisotropic superconductivity at KTaO_3 (111) interfaces. *arXiv [cond-mat.supr-con]*, <http://arxiv.org/abs/2004.07416>
3. Wadehra N, Tomar R, Varma RM, Gopal RK, Singh Y, Dattagupta S, Chakraverty S (2020) Planar Hall effect and anisotropic magnetoresistance in polar-polar interface of LaVO_3 - KTaO_3 with strong spin-orbit coupling. *Nature communications*, 11(1):874. <https://doi.org/10.1038/s41467-020-14689-z>

Publications (which acknowledge DOE support)

1. “Long-Range Non-Coulombic Electron–Electron Interactions between LaAlO₃/SrTiO₃ Nanowires” Yuhe Tang, Anthony Tylan-Tyler, Hyungwoo Lee, Jung-Woo Lee, Michelle Tomczyk, Mengchen Huang, Chang-Beom Eom, Patrick Irvin, and Jeremy Levy, *Advanced Materials Interfaces* 2019, **6**, 1900301 (2019).
2. “Anisotropic spin-orbit torque generation in epitaxial SrIrO₃ by symmetry design” T. Nana, T. J. Anderson, J. Gibbons, K. Hwang, N. Campbell, H. Zhou, Y. Q. Dong, G. Y. Kim, D. F. Shao, T. R. Paudel, N. Reynolds, X. J. Wang, N. X. Sun, E. Y. Tsymbal, S. Y. Choi, M. S. Rzchowski, Yong Baek Kim, D. C. Ralph, and C. B. Eom, *PNAS*, **116**, 16186 (2019) doi/10.1073/pnas.1812822116
3. "Lightwave-Driven Gapless Superconductivity and Forbidden Quantum Beats by Terahertz Symmetry Breaking," X. Yang, C. Vaswani, C. Sundahl, M. Mootz, L. Luo, J. H. Kang, I. E. Perakis, C. B. Eom, J. Wang, *Nature Photonics*, **13**, 707 (2019) DOI: 10.1038/s41566-019-0470-y (2019).
4. “Pascal conductance series in ballistic one-dimensional LaAlO₃/SrTiO₃ channels” Megan Briggeman, Michelle Tomczyk, Binbin Tian, Hyungwoo Lee, Jung-Woo Lee, Yuchi He, Anthony Tylan-Tyler, Mengchen Huang, Chang-Beom Eom, David Pekker, Roger S. K. Mong, Patrick Irvin, and Jeremy Levy, *Science* **367**, 769 (2020) DOI:10.1126/science.aat6467
5. “Charge density wave modulation in superconducting BaPbO₃/BaBiO₃ superlattices” D. T. Harris, N. G. Campbell, C. Di, J.-M. Park, L. Luo, H. Zhou, G.-Y. Kim, K. Song, S.-Y. Choi, J. Wang, M. S. Rzchowski, and C. B. Eom, *Phys. Rev. B* **101**, 064509 (2020)
6. “Spontaneous Hall effect enhanced by local Ir moments in epitaxial Pr₂Ir₂O₇ thin films” Lu Guo, Neil Campbell, Yongseong Choi, Jong-Woo Kim, Philip J. Ryan, Huaixun Huyan, Linze Li, Tianxiang Nan, Jong-Hong Kang, Chris Sundahl, Xiaoqing Pan, M. S. Rzchowski, and Chang-Beom Eom, *Phys. Rev. B* **101**, 104405 (2020)
7. “New approaches for achieving more perfect transition metal oxide thin films” J. L. MacManus-Driscoll, Matthew P. Wells, Chao Yun, Jung-Woo Lee, Chang-Beom Eom, and Darrell G. Schlom, *APL Mater.* **8**, 040904 (2020)
8. “Terahertz Second-Harmonic Generation from Lightwave Acceleration of Symmetry-Breaking Nonlinear Supercurrents” C. Vaswani, M. Mootz, C. Sundahl, D. H. Mudiyansele, J. H. Kang, X. Yang, D. Cheng, C. Huang, R. H. J. Kim, Z. Liu, L. Luo, I. E. Perakis, C. B. Eom, and J. Wang, *Phys. Rev. Lett.* **124**, 207003 (2020)
9. “Epitaxial Antiperovskite/Perovskite Heterostructures for Materials Design” Camilo X. Quintela, Kyung Song, Ding-Fu Shao, Lin Xie, Tianxiang Nan, Tula R. Paudel, Neil Campbell, Xiaoqing Pan, Thomas Tybell, Mark S. Rzchowski, Evgeny Y. Tsymbal, Si-Young Choi, Chang-Beom Eom, *Science Advances*, **6**, eaba4017 (2020)
10. “Frictional drag between superconducting LaAlO₃/SrTiO₃ nanowires”. Yuhe Tang, Jung-Woo Lee, Anthony Tylan-Tyler, Hyungwoo Lee, Michelle Tomczyk, Mengchen Huang,

Chang-Beom Eom, Patrick Irvin and Jeremy Levy, *Semicond. Sci. Technol.* **35**, 09LT01 (2020)

11. “Superconductivity in undoped BaFe₂As₂ by tetrahedral geometry design” Jong-Hoon Kang, Jong-Woo Kim, Philip J. Ryan, Lin Xie, Lu Guo, Chris Sundahl, Jonathon Schad, Neil Campbell, Yesusa G. Collantes, Eric E. Hellstrom, Mark S. Rzchowski, Chang-Beom Eom, *PNAS* **117**, 21170 (2020)
12. “Controlling spin current polarization through non-collinear antiferromagnetism” T. Nan, C. X. Quintela, J. Irwin, G. Gurung, D. F. Shao, J. Gibbons, N. Campbell, K. Song, S.-Y. Choi, L. Guo, R. D. Johnson, P. Manuel, R. V. Chopdekar, I. Hallsteinsen, T. Tybell, P. J. Ryan, J.-W. Kim, Y. Choi, P. G. Radaelli, D. C. Ralph, E. Y. Tsymbal, M. S. Rzchowski & C. B. Eom, *Nature Comm.* **11**, 4671 (2020)
13. “Engineered spin-orbit interactions in LaAlO₃/SrTiO₃-based 1D serpentine electron waveguides” Megan Briggeman, Jianan Li, Mengchen Huang, Hyungwoo Lee, Jung-Woo Lee, Kitae Eom, Chang-Beom Eom, Patrick Irvin, and Jeremy Levy, accepted for publication in *Science Advances* **6**, eaba6337 (2020)
14. “Nanoscale control of LaAlO₃/SrTiO₃ metal–insulator transition using ultra-low-voltage electron-beam lithography” Dengyu Yang, Shan Hao, Jun Chen, Qing Guo, Muqing Yu, Yang Hu, Kitae Eom, Jung-Woo Lee, Chang-Beom Eom, Patrick Irvin, and Jeremy Levy *Appl. Phys. Lett.* **117**, 253103 (2020)
15. “Light quantum control of persisting Higgs modes in iron-based superconductors” C. Vaswani, J. H. Kang, M. Mootz, L. Luo, X. Yang, C. Sundahl, D. Cheng, C. Huang, R. H. J. Kim, Z. Liu, Y. G. Collantes, E. E. Hellstrom, I. E. Perakis, C. B. Eom & J. Wang *Nature Communications* **12**, 258 (2021)
16. “One-dimensional Kronig–Penney superlattices at the LaAlO₃/SrTiO₃ interface” Megan Briggeman, Hyungwoo Lee, Jung-Woo Lee, Kitae Eom, François Damanet, Elliott Mansfield, Jianan Li, Mengchen Huang, Andrew J. Daley, Chang-Beom Eom, Patrick Irvin and Jeremy Levy, *Nature Physics*, **17**, 782 (2021).
17. “Electronically reconfigurable complex-oxide heterostructure free-standing membranes” Kitae Eom, Muqing Yu, Jinsol Seo, Dengyu Yang, Hyungwoo Lee, Jung-Woo Lee, Patrick Irvin, Sang Ho Oh, Jeremy Levy, Chang-Beom Eom, *Science Advances*, **7**, eabh1284 (2021)
18. “Searching for a route to in situ synthesis of epitaxial Pr₂Ir₂O₇ thin films guided by thermodynamic calculations” Lu Guo, Shun-Li Shang, Neil Campbell, Mark Rzchowski, Zi-Kui Liu, and Chang-Beom Eom, *npj Computational Materials*, **7**, 144 (2021)
19. “Low-Voltage Magnetoelectric Coupling in Membrane Heterostructures” S. Lindemann, J. Irwin, G.-Y. Kim, B. Wang, K. Eom, J. J. Wang, J. M. Hu, L. Q. Chen, S. Y. Choi, C. B. Eom, M. S. Rzchowski, *Science Advances*, in press (2021)

Symmetries, Interactions and Correlation Effects in Carbon Nanostructures

Gleb Finkelstein, Physics Department, Duke University, Durham, NC 27708

Program Scope

1) The PI's group had performed some of the early studies of the superconducting proximity in graphene. The highlights include: the first detection of supercurrent through a quantum Hall (QH) region [Science 2016]; creating a QH-based SQUID [Science Advances 2019]; and most recently, the first detection of the chiral Andreev edge states and their interference [Nature Physics 2020]. Most of the group efforts continue to focus on investigating the superconductor - quantum Hall hybrid structures.

2) The PI's group has recently realized multi-terminal (MT) graphene-based Josephson junctions [Nano Letters 2019]. We achieved, for the first time, the regime in which coupling between all terminals was ballistic. It had been predicted that the Andreev bound states in such structures could emulate energy band structures of topological materials. We are working to realize these predictions.

3) We have recently studied the "Shapiro steps" in the I-V characteristics of the Josephson junctions under microwave excitation. In high quality graphene junctions, these steps are highly hysteretic, and the patterns deviate significantly from the textbook "Bessel function" regime. We are working on extending these microwave measurements to the multi-terminal junctions.

Recent Progress

1. Probing Chiral Andreev Edge States

In the QH regime, an electron propagating along the interface with the superconductor could be Andreev-reflected as a hole flowing in the same chiral direction. The hole could then be Andreev-reflected as an electron, etc. (Figure 1a). This combination of Andreev reflections with the QH chiral motion yields chiral Andreev edge states (CAES) [1, 2]. Under certain conditions, CAES could become chiral Majorana fermions – charge neutral single-particle excitations.

We have recently detected CAES in a sample that has several normal and superconducting contacts [3]. We measure the sample shown in Figure 3d at $B = 3$ T, at which field the broken symmetry states with all integer ν are well developed. We use a setup similar to that in Ref. [4] (Figure 1d): Current I is sourced from one of the normal contacts, a , and flows clockwise to a grounded superconducting contact, c . We focus on the $\nu = 2$ and $\nu = 6$ plateaus (circled in Figure 1e), which show well quantized Hall conductance G_{xy} (red curve in Figure 1e). Simultaneously, we measure the voltage V_d at the normal contact, d , located downstream from the grounded superconducting contact, c . Most noticeably, we observe pronounced and reproducible regions of negative non-local "downstream resistance" $R_d = d(V_d - V_c)/dI$: the voltage on the downstream contact d drops below that of the grounded superconducting contact. We observed similar behavior in fields from 0.5 to 5 T, a range of filling factors, and in both monolayer and bilayer graphene.

A slight increase of temperature up to ~ 2 K is enough to completely wash away the observed features. This scale is much smaller than the QH activation gaps (tens of meV), and the quantization of G_{xy} is not affected by the increased temperature. In fact, for $T \sim 3$ K we recover a conventional (non-superconducting) quantum Hall behavior: the downstream resistance vanishes, while G_{xy} stays quantized. We therefore conclude that the observed non-zero R_d originates in the superconducting properties of contact c .

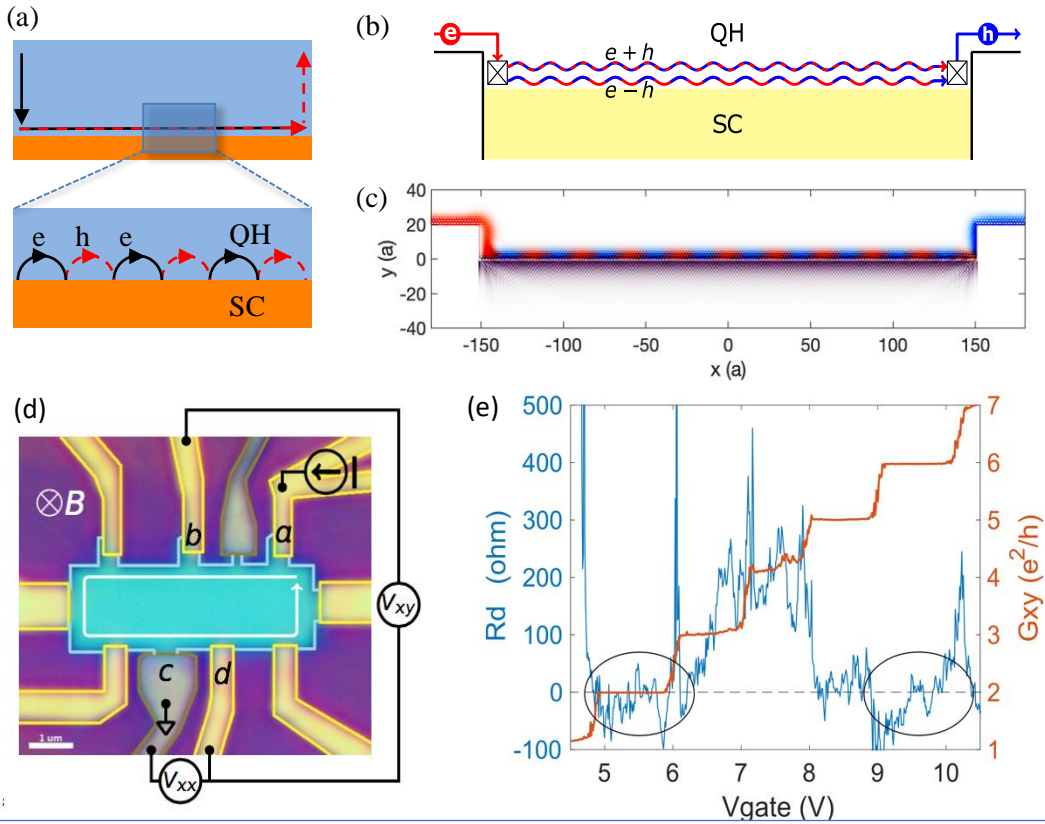


Figure 1. a) Schematic of the chiral Andreev edge state as skipping trajectory along the QH-SC interface. b) Schematic of an electron split into a linear combination of CAES, propagating along a SC interface, and turning into a hole. c) Numerical simulations of the electron (red) and hole (blue) density along a graphene-SC interface performed by our collaborators (H. Baranger) using the KWANT package. Oscillations between the electron and hole probability are visible. The length of the interface is chosen such that a hole is emitted downstream. d) Optical image of the sample and the sketch of the CAES measurement configuration. e) R_d (blue) and G_{xy} (red) measured simultaneously as a function of gate voltage at 3 Tesla. Regions of negative R_d appear on top of perfectly quantized G_{xy} plateaus.

To explain the observed behavior, we point out that when an incoming QH electron approaches the superconducting interface, it should split into two CAES. The two states then accumulate a phase difference as they propagate along the QH-SC interface with different wavevectors (Figure 1b,c). When the two CAES recombine on the other side of the interface, there is a finite probability that an electron or a hole is emitted. If a hole is emitted, the chemical potential in the downstream contact is lowered, resulting in a negative dV_d/dI . The sign of the signal is reversed for an outgoing electron.

We have collaborated with our theory colleague Harold Baranger on developing a model of the CAES in our system (see e.g. Figure 1c). The simulations qualitatively reproduce many of the observed features, for example R_d which fluctuates with mesoscopic randomness around a zero mean value as a function of the gate voltage and magnetic field, as we observe in the experiment [3]. Incidentally, the theoretical model indicates that while the CAES are on average neutral, they are *not* chiral Majorana fermions. Nonetheless the measurements discussed here could be used to detect chiral MF in systems where these excitations are expected.

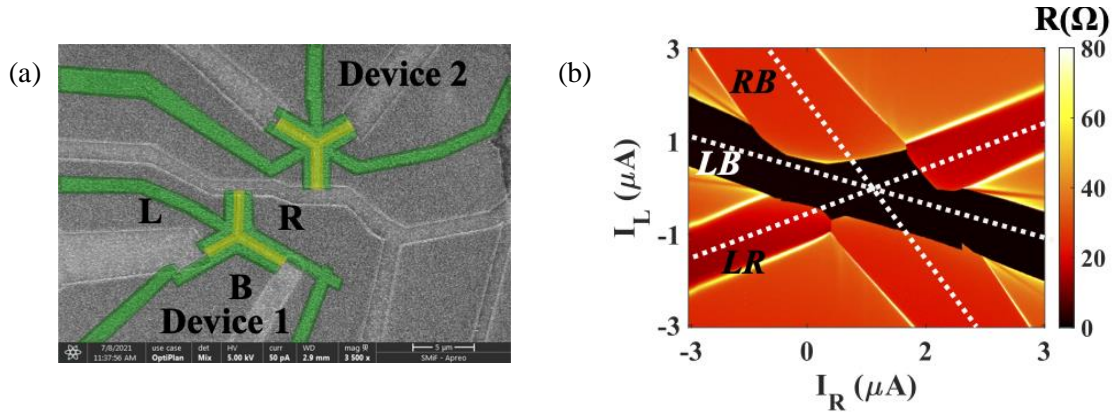


Figure 2. a) Scanning electron micrograph of two three-terminal samples. b) Differential resistance maps measured simultaneously between the left (L) and the grounded bottom (B) contacts as the function of the left/right currents. The central dark corresponds to the supercurrent coupling between all contacts. Three major resonances are observed, for which supercurrent couples only one pair of contacts. Minor “quartet” lines are also visible, corresponding to the transport of two entangled Cooper pairs.

2. Multiterminal Josephson junctions

SNS junctions with a normal region connected to several (more than two) superconducting leads were first fabricated 20 years ago. These systems have received renewed attention in the past few years, driven in part by theoretical predictions that Andreev bound states in such structures could emulate energy band structures of topological materials.

We have recently reported on the three and four-terminal graphene Josephson junctions, in which for the first time ballistic coupling between the terminals was achieved [5]. This work followed by similar reports by other groups. In a typical measurement, we apply currents from the left and right contacts to a grounded contact at the bottom (see Figure 2a), and measure voltages on the left and right contacts with respect to the ground. Figure 2b shows the resulting differential resistance map $R_L = dV_L/dI_L$ as a function of I_L and I_R . At small applied bias currents, all contacts are coupled to each other (central dark feature). From this region, three branches extend outwards corresponding to superconducting coupling between three pairs of contacts.

3. The inverse AC Josephson effect (Shapiro steps)

The I - V curves of Josephson junctions excited by a microwave radiation demonstrate the “Shapiro steps” of quantized voltage at $V = nhf / 2e$. Here, the integer n counts the number of periods by which the superconducting phase difference progressed over one period of excitation. Recently, interest to Josephson junctions made of topological materials have reinvigorated the use of the AC Josephson effect as a tool to probe the junction's current-phase relation (CPR) [6].

We have conducted a detailed investigation of Shapiro steps in graphene Josephson junctions, which are expected to be topologically trivial. We have shown that a variety of patterns can be obtained within the same junction by tuning the gate voltage and magnetic field (Figure 3) [7]. Both the Bessel function regime (panels c, d, h) and the strongly hysteretic regime with “zero crossing steps” (panels a, b, f, g) have been observed. Finally, we simulated the observed patterns using an extension of the resistively and capacitively shunted junction (RCSJ) model, which allowed us to elucidate the role of the on-chip microwave environment in the observed patterns.

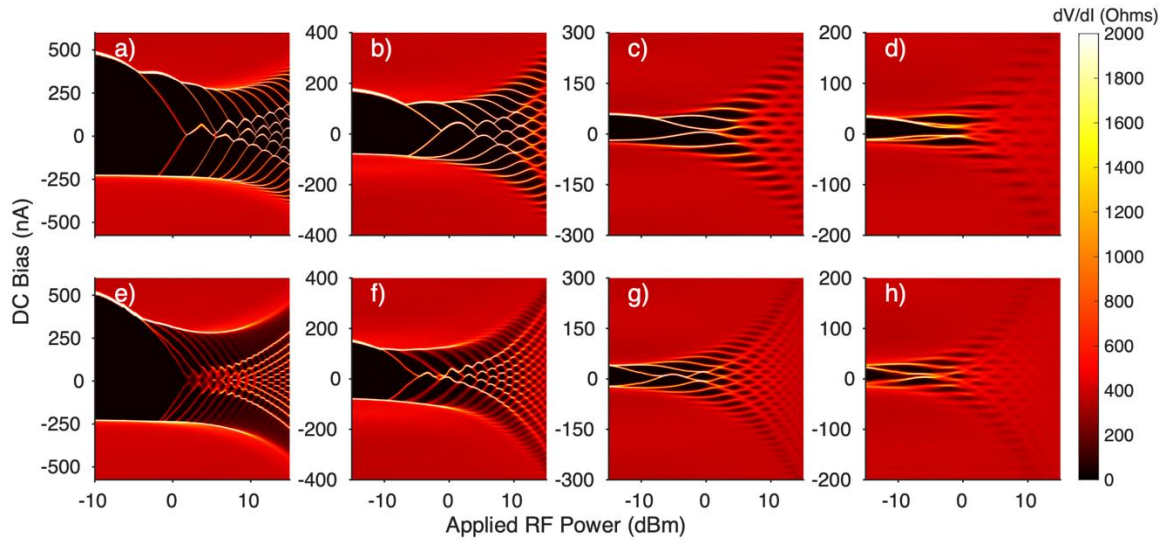


Figure 3. Differential resistance maps of an RF-irradiated junction plotted vs. DC bias current and RF power. The well-quantized Shapiro steps appear as dark regions of zero $R = dV/dI$. The maps are measured at two frequencies (top row: 5 GHz, bottom row: 3 GHz) and different switching currents (left to right: $I_s = 650, 240, 80$ and 35 nA). The value of the switching current is controlled by applying perpendicular magnetic field in the mT range, which does not change other junction parameters.

Future Plans

Building on our existing momentum in graphene-based Josephson junctions, the PI plans to concentrate on the following directions:

- 1) To further study the QH-superconductor structures, in particular to investigate the coherence properties of the CAES and their role in the supercurrent the QH regime.
- 2) To explore the phase space of the multiterminal Josephson junctions at zero magnetic field, in particular to look for the theoretically predicted regime in which the spectrum of Andreev bound states emulates the Brillouin zone of a topological material.
- 3) To investigate multiterminal junctions under microwave radiation, in particular searching for the Floquet bands in this system.

References

- 1) H. Hoppe, U. Zulicke and G. Schon, Phys Rev Lett **84**, p. 1804-7 (2000).
- 2) J.A.M. van Ostaay, A.R. Akhmerov and C.W.J. Beenakker, Phys. Rev. B **83**, p. 195441 (2011).
- 3) L. Zhao, E.G. Arnault, A. Bondarev, A. Seredinski, T.F.Q. Larson, A.W. Draelos, H. Li, K. Watanabe, T. Taniguchi, F. Amet, H.U. Baranger and G. Finkelstein, Nature Physics **16**, p. 862-867 (2020).
- 4) G.-H. Lee, K.-F. Huang, D.K. Efetov, D.S. Wei, S. Hart, T. Taniguchi, K. Watanabe, A. Yacoby and P. Kim, Nature Physics **13**, p. 693-698 (2017).
- 5) A.W. Draelos, M.T. Wei, A. Seredinski, H. Li, Y. Mehta, K. Watanabe, T. Taniguchi, I.V. Borzenets, F. Amet and G. Finkelstein, Nano Letters **19**, p. 1039-1043 (2019).
- 6) L.P. Rokhinson, X. Liu and J.K. Furdyna, Nature Physics **8**, p. 795-799 (2012).
- 7) T.F.Q. Larson, L. Zhao, E.G. Arnault, M.-T. Wei, A. Seredinski, H. Li, K. Watanabe, T. Taniguchi, F. Amet and G. Finkelstein, Nano Letters **20**, p. 6998-7003 (2020).

Publications in 2019-2021

1. *Quantum Hall-based superconducting interference device*, Andrew Seredinski, Anne W. Draelos, Ethan G. Arnault, Ming-Tso Wei, Hengming Li, Kenji Watanabe, Takashi Taniguchi, Francois Amet, and Gleb Finkelstein, **Science Advances** **5**, eaaw8693 (2019). <https://doi.org/10.1126/sciadv.aaw8693>

2. *Anomalous periodicity of magnetic interference patterns in encapsulated graphene Josephson junctions*. C.T. Ke, A.W. Draelos, A. Seredinski, M.T. Wei, H. Li, M. Hernandez-Rivera, K. Watanabe, T. Taniguchi, M. Yamamoto, S. Tarucha, Y. Bomze, I.V. Borzenets, F. Amet, G. Finkelstein, **Phys. Rev. Research** **1**, 033084 (2019). <https://doi.org/10.1103/PhysRevResearch.1.033084>

3. *Chiral quasiparticle tunneling between quantum Hall edges in proximity with a superconductor*. M.T. Wei, A.W. Draelos, A. Seredinski, C.T. Ke, H. Li, Y. Mehta, K. Watanabe, T. Taniguchi, M. Yamamoto, S. Tarucha, G. Finkelstein, F. Amet, I.V. Borzenets, **PRB** **100**, 121403 (2019). <https://doi.org/10.1103/PhysRevB.100.121403>

4. *Sub-Kelvin Lateral Thermal Transport in Diffusive Graphene*, A. W. Draelos, A. Silverman, B. Eniwaye, E. G. Arnault, C. T. Ke, M. T. Wei, I. Vlassiuk, I. V. Borzenets, F. Amet, and G. Finkelstein, **PRB** **99**, 125427 (2019). <https://doi.org/10.1103/PhysRevB.99.125427>

5. *Supercurrent Flow in Multi-Terminal Graphene Josephson Junctions*, Anne W. Draelos, Ming-Tso Wei, Andrew Seredinski, Hengming Li, Yash Mehta, Kenji Watanabe, Takashi Taniguchi, Ivan V. Borzenets, Francois Amet, and Gleb Finkelstein, **Nano Letters** **19**, 1039 (2019), <https://doi.org/10.1021/acs.nanolett.8b04330>

6. *Zero Crossing Steps and Anomalous Shapiro Maps in Graphene Josephson Junctions*, Trevyn F. Q. Larson, Lingfei Zhao, Ethan G. Arnault, Ming-Tso Wei, Andrew Seredinski, Henming Li, Kenji Watanabe, Takashi Taniguchi, Francois Amet, and Gleb Finkelstein, **Nano Letters** **20**, 6998 (2020). <https://doi.org/10.1021/acs.nanolett.0c01598>.

7. *Interference of chiral Andreev edge states*, L. Zhao, E.G. Arnault, A. Bondarev, A. Seredinski, T. Larson, A.W. Draelos, H. Li, K. Watanabe, T. Taniguchi, F. Amet, H.U. Baranger, G. Finkelstein, **Nature Physics** **16**, 862 (2020). <https://doi.org/10.1038/s41567-020-0898-5>

8. *One-Dimensional Edge Contact to Encapsulated MoS₂ with a Superconductor*. A. Seredinski, E. G. Arnault, V. Z. Costa, L. Zhao, T. F. Q. Larson, K. Watanabe, T. Taniguchi, F. Amet, A. K. M. Newaz, and G. Finkelstein, **AIP Advances** **11**, 045312 (2021). <https://doi.org/10.1063/5.0045009>

9. *Nonequilibrium Quantum Critical Steady State: Transport through a Dissipative Resonant Level*, Gu Zhang, Chung-Hou Chung, Chung-Ting Ke, Chao-Yun Lin, Henok Mebrahtu, Alex I. Smirnov, Gleb Finkelstein, and Harold U. Baranger, **Physical Review Research** **3**, 013136 (2021). <https://doi.org/10.1103/PhysRevResearch.3.013136>

Correlated Materials: Synthesis and Physical Properties

I. R. Fisher, T. H. Geballe, A. Kapitulnik, S. A. Kivelson, K. A. Moler

Stanford University and SLAC National Accelerator Laboratory

Program Scope

An enduring aim of our FWP has been to discover and understand the nature, causes and consequences of emergent behavior in quantum materials, especially in relation to the occurrence of superconductivity. We incorporate synthesis, measurement and theory to coherently address big questions at the heart of these issues. Our current work continues to focus on superconductivity, with a new emphasis on multicomponent superconductors and various types of composite order. Our current research can be loosely divided into three purposefully overlapping areas; (1) multicomponent superconductivity, (2) symmetry breaking due to vestigial order, and (3) the interplay of multiple ordering tendencies in complex materials.

Recent Progress

During the last two years we have worked on a variety of inter-related areas including charge density wave order [3,9,11,22,26,30,34], electronic nematicity [1,10,13,17,18,24,33], superconductivity [8,14,16,21,23,27,31,32,35] and transport beyond the quasiparticle paradigm [2,4,5,6,7,19,28,36]. For this ECMP PIs meeting, we will present on just one very recent exciting result: the interrelation of nematicity, broken TRS and superconductivity in an Fe based superconductor. The short statement associated with this work is that we have discovered an unanticipated multicomponent chiral superconducting state in $\text{Ba}(\text{Fe}_{1-x}\text{Co}_x)_2\text{As}_2$, a representative Fe-based superconductor. The chiral state seems to be closely associated with the electronic nematic phase transition.

The first evidence for this new superconducting state was found in elastocaloric effect (ECE) measurements. The ECE is a thermodynamic quantity, relating changes in entropy (isothermal conditions) or temperature (adiabatic conditions) to strains experienced by materials. We have recently developed a sensitive AC method to measure the ECE, and have shown that it is a very sensitive probe of subtle electronic phase transitions that can be tuned by strain [10,13,18]. Measurements of the ECE of $\text{Ba}(\text{Fe}_{1-x}\text{Co}_x)_2\text{As}_2$ for compositions close to optimal doping revealed not only the superconducting and coupled nematic/structural phase transitions (occurring with critical temperatures T_c and T_S respectively), but also an additional phase transition at a lower temperature, $T^* < T_c$. The doping dependence of T^* is striking – it rises with increasing cobalt concentration and meets T_c close to where T_S intersects T_c , at optimal doping. Motivated by these results, Kerr effect measurements were performed. These preliminary measurements (still in

progress) reveal an onset of Kerr rotation at a temperature T_K , very close to the T^* identified in the ECE measurements. It appears, then, that this representative Fe-based superconductor harbors a heretofore hidden chiral superconducting state beneath the superconducting dome.

Such a chiral state implies a multicomponent order parameter. From a theoretical perspective, two unconventional superconducting states are possible/anticipated for the material, s₊- & d-wave (corresponding to A_{1g} & B_{1g} representations of the point group) (see, for example, refs [a] & [b]). Evidence from Raman scattering for a Bardasis-Schreiffer mode implies that these are close in energy, with the d-wave state being sub-dominant (see for example ref [c]). The morphology of the phase diagram that we are uncovering is suggestive of a novel interaction between the nematic and the two superconducting order parameters [d], perhaps suggestive that nematic fluctuations play a role in producing a cooperative linkage between the s and d-wave pair-fields to obtain an s₊+id chiral state. Ongoing experimental and theoretical work in our FWP is investigating this possibility.

Commentary: It is important to note that the multicomponent superconductor does *not* appear to arise from a multidimensional irreducible representation of the point group (E_g), but rather from a near-degeneracy of two distinct singlet representations. i.e. it is not a strict consequence of symmetry, but rather appears to arise due to an apparently ‘accidental’ degeneracy. However, the fact that this second superconducting phase appears close to the point at which the nematic transition bisects the superconducting dome, suggests that the state is far from being a complete coincidence. Furthermore, this phase does not seem to arise due to a transition from s-wave to d-wave pairing, as has been discussed for (Ba,K)Fe₂As₂ (see for example ref [e] & [f]).

Significance: This result **(1)** reveals an unanticipated richness to the superconductivity in the Fe-pnictides; **(2)** demonstrates that the nematic is not a ‘side show’ in terms of determining the pairing symmetry; **(3)** potentially provides a new avenue to discover topological superconductors; and **(4)** motivates study of materials with lower point symmetries, without multidimensional irreducible representations, in search of other chiral superconductors, guided by the principles we are uncovering here.

Future Plans

Specific questions that our FWP will address in the coming years include: Which material-systems are chiral topological superconductors, and why? What roles do composite/vestigial charge order play in unconventional superconductivity? What other forms of vestigial order can be discovered/identified, including, for instance, non-superconducting states with vestigial chiral order? And looking beyond the traditional paradigms of competing and coexisting order, in what new ways can multiple types of complex electronic order inter-relate? Among other things, our research involves the study of chiral superconducting states in Fe-based superconductors, UTe₂ and related materials; possible vestigial nematic states in CePd₂Si₂ and RTe₃ (R=rare-earth); and possible vestigial chiral state in YBiPt and related materials.

References

- [a] *Near-degeneracy of several pairing channels in multiorbital models for the Fe pnictides*, S. Graser, T. A. Maier, P. J. Hirschfeld and D. J. Scalapino, *New Journal of Physics* **11**, 025016 (2009).
- [b] *Gap symmetry and structure of Fe-based superconductors*, P.J. Hirschfeld, M. M. Korshunov, I.I. Mazin, *Rep. on Prog. in Phys.* **74**, 124508 (2011).
- [c] *Raman-Scattering Detection of Nearly Degenerate s-Wave and d-Wave Pairing Channels in Iron-Based $Ba_{0.6}K_{0.4}Fe_2As_2$ and $Rb_{0.8}Fe_{1.6}Se_2$ Superconductors*, F. Kretzschmar, B. Muschler, T. Böhmer, A. Baum, R. Hackl, H.-H. Wen, V. Tsurkan, J. Deisenhofer, and A. Loidl, *Phys. Rev. Lett.* **110**, 187002 (2013).
- [d] *Nematicity as a Probe of Superconducting Pairing in Iron-Based Superconductors* Rafael M. Fernandes and Andrew J. Millis, *Phys. Rev. Lett.* **111**, 127001 (2013).
- [e] *Exotic d-Wave Superconducting State of Strongly Hole-Doped $K_xBa_{1-x}Fe_2As_2$* , R. Thomale, C. Platt, W. Hanke, JP. Hu and A. B. Bernevig, *Phys. Rev. Lett.* **107**, 117001 (2011).
- [f] *Superconductivity with broken time-reversal symmetry inside a superconducting s-wave state*, V. Grinenko, R. Sarkar, K. Kihou, C. Lee, I. Morozov, S. Aswartham, B. Buchner, P. Chekhonin, W. Skrotzki, K. Nenkov, R. Hušhne, K. Nielsch, S. L. Drechsler, V. L. Vadimov, M. A. Silaev, P. A. Volkov, I. Eremin, H. Luetkens, and H. H. Klauss, *Nature Physics* **16**, 789 (2020).

Publications (Sept 2019 – Sept 2021)

(a) Publications that were primarily supported by this FWP

- 1) *Growth of nematic susceptibility in the field-induced normal state of an iron-based superconductor revealed by elastoresistivity measurements in a 65 T pulsed magnet*, J. A. W. Straquadine, J. C. Palmstrom, P. Walmsley, A. T. Hristov, F. Weickert, F. F. Balakirev, M. Jaime, R. McDonald, and I. R. Fisher, *Phys. Rev. B.* **100**, 125147 (2019) (selected as an Editors' Suggestion)
- 2) *Thermalization and possible signatures of quantum chaos in complex crystalline materials* Jiecheng Zhang, Erik D. Kountz, Kamran Behnia, and Aharon Kapitulnik, *Proceedings of the National Academy of Sciences* **116** (40), 19869 (2019)
- 3) *Disorder-induced suppression of charge density wave order: STM study of Pd-intercalated $ErTe_3$* , Alan Fang, Joshua A. W. Straquadine, Ian R. Fisher, Steven A. Kivelson, and Aharon Kapitulnik, *Phys. Rev. B* **100**, 235446 (2019)
- 4) *Thermal Diffusivity Above Mott-Ioffe-Regel Limit*, Jiecheng Zhang, Erik D. Kountz, Eli M. Levenson-Falk, Dojoon Song, Richard L. Greene, Aharon Kapitulnik, *Phys. Rev. B* **100**, 241114(R) (2019).

- 5) *Theory of the strange metal $Sr_3Ru_2O_7$* , Connie H. Mousatov, Erez Berg, and Sean A. Hartnoll, PNAS **117** (6) 2852-2857 (2020).
- 6) *On the Planckian bound for heat diffusion in insulators*, Connie H. Mousatov and Sean A. Hartnoll, Nature Physics. **16**, 579–584 (2020).
- 7) *Enhanced Thermal Hall Effect in Nearly Ferroelectric Insulators*, Jing-Yuan Chen, Steven A. Kivelson, and Xiao-Qi Sun, Phys. Rev. Lett. **124**, 167601 (2020).
- 8) *Ferromagnetic order beyond the superconducting dome in a cuprate superconductor*, Tarapada Sarkar, D. S. Wei, J. Zhang, N. R. Poniatowski, P. R. Mandal, A. Kapitulnik, and Richard L. Greene, Science **368**, 532 (2020).
- 9) *Magnetic breakdown and charge density wave formation: A quantum oscillation study of the rare-earth tritellurides*, P. Walmsley, S. Aeschlimann, J. A. W. Straquadine, P. Giraldo-Gallo, S. C. Riggs, M. K. Chan, R. D. McDonald, and I. R. Fisher, Phys. Rev. B **102**, 045150 (2020).
- 10) *Frequency-dependent sensitivity of AC elastocaloric effect measurements explored through analytical and numerical models*, J. A. W. Straquadine, M.S. Ikeda and I. R. Fisher, Reviews of Scientific Instruments **91**, 083905 (2020).
- 11) *Robust superconductivity intertwined with charge density wave and disorder in Pd-intercalated $ErTe_3$* , Alan Fang, Anisha G. Singh, Joshua A. W. Straquadine, Ian R. Fisher, Steven A. Kivelson, and Aharon Kapitulnik, Phys. Rev. Research **2**, 043221 (2020).
- 12) *The Quantum Hall Effect in the Absence of Disorder*, Kyung-Su Kim and Steven A. Kivelson, npj Quantum Mater. **6**, 22 (2021).
- 13) *Nematic quantum criticality in an Fe-based superconductor revealed by strain-tuning* Thanapat Worasaran, Matthias S. Ikeda, Johanna C. Palmstrom, Joshua A. W. Straquadine, Steven A. Kivelson, and Ian R. Fisher, Science Vol. **372**, Issue 6545, pp. 973-977 (2021).
- 14) *Local observation of linear- T superfluid density and anomalous vortex dynamics in URu_2Si_2* , Yusuke Iguchi, Irene P. Zhang, Eric D. Bauer, Filip Ronning, John R. Kirtley, and Kathryn A. Moler, Phys. Rev. B Letter **103**, L220503 (2021).
- 15) *Nanoscale Turing patterns in a bismuth monolayer*, Yuki Fuseya, Hiroyasu Katsuno, Kamran Behnia, Aharon Kapitulnik, Nature Physics, [https://doi: 10.1038/s41567-021-01288-y](https://doi.org/10.1038/s41567-021-01288-y) (2021)
- 16) *Multicomponent superconducting order parameter in UTe_2* , Ian M. Hayes, Di S. Wei, Tristin Metz, Jian Zhang, Yun Suk Eo, Sheng Ran, Shanta R. Saha, John Collini, Nicholas P. Butch, Daniel F. Agterberg, Aharon Kapitulnik, Johnpierre Paglione Science, **373**, 6556, 797 (2021).

- 17) *Nematic antiferromagnetism and deconfined criticality from the interplay between electron-phonon and electron-electron interactions*, Chao Wang, Yoni Schattner, and Steven A. Kivelson, *Phys. Rev. B* **104**, L081110 (2021)
- 18) *Elastocaloric signature of nematic fluctuations*, Matthias S. Ikeda, Thanapat Worasaran, Elliott W. Rosenberg, Johanna C. Palmstrom, Steven A. Kivelson and Ian R. Fisher, *PNAS* **118** (37) e2105911118 (2021)

(b) Collaborative publications supported by this FWP

- 19) *Thermalization and Possible Signatures of Quantum Chaos in Complex Crystalline Materials*, Jiecheng Zhang, Erik D. Kountz, Kamran Behnia, Aharon Kapitulnik, *PNAS* **116** (40), 19869 (2019).
- 20) *Possible scale invariant linear magnetoresistance in pyrochlore iridates $Bi_2Ir_2O_7$* Jiun-Haw Chu, Jian Liu, Han Zhang, Kyle Noordhoek, Scott C Riggs, Maxwell Shapiro, Claudy Ryan Serro, Di Yi, M Mellisa, S J Suresha, C Frontera, E Arenholz, Ashvin Vishwanath, Xavi Marti, I R Fisher, R Ramesh, *New Journal of Physics* **21**, 113041 (2019)
- 21) *Anisotropic Superconducting Gap in Optimally Doped Iron-Based Material* A. Pal, M. Chinotti, J.-H. Chu, H.-H. Kuo, I. R. Fisher, L. Degiorgi, *Journal of Superconductivity and Novel Magnetism*, **33**, pages2313–2318 (2020).
- 22) *Light-induced charge density wave in $LaTe_3$* , Anshul Kogar, Alfred Zong, Pavel E. Dolgirev, Xiaozhe Shen, Joshua Straquadine, Ya-Qing Bie, Xirui Wang, Timm Rohwer, I-Cheng Tung, Yafang Yang, Renkai Li, Jie Yang, Stephen Weathersby, Suji Park, Michael E. Kozina, Edbert J. Sie, Haidan Wen, Pablo Jarillo-Herrero, Ian R. Fisher, Xijie Wang, Nuh Gedik, *Nature Physics* **16**, 159-163 (2020).
- 23) *Low work function in the 122-family of iron-based superconductors* H. Pfau, H. Soifer, J. A. Sobota, A. Gauthier, C. R. Rotundu, J. C. Palmstrom, I. R. Fisher, G.-Y. Chen, H.-H. Wen, Z.-X. Shen, and P. S. Kirchmann *Phys. Rev. Materials* **4**, 034801 (2020).
- 24) *Nematic transitions in iron pnictide superconductors imaged with a quantum gas*, Fan Yang, Stephen F. Taylor, Stephen D. Edkins, Johanna C. Palmstrom, Ian R. Fisher and Benjamin L. Lev, *Nature Physics* **16**, 514–519 (2020).
- 25) *High resolution time- and angle-resolved photoemission spectroscopy with 11 eV laser pulses*, Changmin Lee, Timm Rohwer, Edbert J. Sie, Alfred Zong, Edoardo Baldini, Joshua Straquadine, Philip Walmsley, Dillon Gardner, Young S. Lee, Ian R. Fisher and Nuh Gedik, *Reviews of Scientific Instruments* **91**, 043102 (2020).
- 26) *Interplay of charge density wave states and strain at the surface of $CeTe_2$* Bishnu Sharma, Manoj Singh, Burhan Ahmed, Boning Yu, Philip Walmsley, Ian R. Fisher, and Michael C. Boyer, *Phys. Rev. B* **101**, 245423 (2020).

- 27) *A proposal for reconciling diverse experiments on the superconducting state in Sr_2RuO_4* , S.A. Kivelson, A. C. Yuan, B.J. Bramshaw, and R. Thomale, *npj Quantum Mater.* **5**, 43 (2020).
- 28) *Sample shape and boundary dependence of measured transverse thermal properties* Samuel Mumford, Tiffany Paul, Erik Kountz, and Aharon Kapitulnik, *J. Appl. Phys.* **128**, 175105 (2020).
- 29) *Nonadiabatic coupling of the dynamical structure to the superconductivity in $YSr_2Cu_{2.75}Mo_{0.25}O_{7.54}$ and $Sr_2CuO_{3.3}$* S. D. Conradson, T. H. Geballe, C.-Q. Jin, L.-P. Cao, A. Gauzzi, M. Karppinen, G. Baldinozzi, W.-M. Li, E. Gilioli, J. M. Jiang, M. Latimer, O. Mueller, V. Nasretdinova, *Proc. Natl. Acad. Sci. USA* **117**, 330999 – Published 29 December 2020
- 30) *Ultrafast formation of domain walls of a charge density wave in $SmTe_3$* M. Trigo, P. Giraldo-Gallo, J. N. Clark, M. E. Kozina, T. Henighan, M. P. Jiang, M. Chollet, I. R. Fisher, J. M. Glowia, T. Katayama, P. S. Kirchmann, D. Leuenberger, H. Liu, D. A. Reis, Z. X. Shen, and D. Zhu, *Phys. Rev. B* **103**, 054109 (2021).
- 31) *The superconductor-to-metal transition in overdoped cuprates* Zi-Xiang Li, Steven A. Kivelson, and Dung-Hai Lee, *npj Quantum Materials* **6**, 36 (2021).
- 32) *Signatures of two-dimensional superconductivity emerging within a three-dimensional host superconductor*, Carolina Parra, Francis C. Niestemski, Alex W. Contryman, Paula Giraldo-Gallo, Theodore H. Geballe, Ian R. Fisher, and Hari C. Manoharan, *PNAS* April 20, 2021 **118** (16) e2017810118
- 33) *Anisotropic quasiparticle coherence in nematic $BaFe_2As_2$ studied with strain-dependent ARPES*, H. Pfau, S. D. Chen, M. Hashimoto, N. Gauthier, C. R. Rotundu, J. C. Palmstrom, I. R. Fisher, S.-K. Mo, Z.-X. Shen, and D. Lu, *Phys. Rev. B* **103**, 165136 (2021)
- 34) *Nonequilibrium charge-density-wave order beyond the thermal limit* J. Maklar, Y. W. Windsor, C. W. Nicholson, M. Puppini, P. Walmsley, V. Esposito, M. Porer, J. Rittmann, D. Leuenberger, M. Kubli, M. Savoini, E. Abreu, S. L. Johnson, P. Beaud, G. Ingold, U. Staub, I. R. Fisher, R. Ernstorfer, M. Wolf & L. Rettig, *Nature Communications* volume **12**, Article number: 2499 (2021).
- 35) *High Temperature superconductivity in a lightly doped quantum spin liquid*, Hong-Chen Jiang and Steven A. Kivelson, *Phys. Rev. Lett.* **127**, 097002 (2021).
- (c) Publications that were primarily supported by this FWP and currently under review**
- 36) *Anomalous thermal transport and violation of Wiedemann-Franz law in the critical regime of a charge density wave transition* Erik D. Kountz, Jiecheng Zhang, Joshua A. W. Straquadine, Anisha G. Singh, Maja D. Bachmann, Ian R. Fisher, Steven A. Kivelson, Aharon Kapitulnik, arXiv:2012.15048

Definitive Majorana Zero Modes in Optimized Hybrid Nanowires

Sergey M. Frolov, University of Pittsburgh

Program Scope

Researchers around the world have been excited about Majorana Zero Modes (MZM). There have been many promising reports. They ignited a broad materials research effort and inspired their own quantum computing paradigm. The momentum does not show signs of dissipating with new results and platforms being announced. But while encouraging experiments are abundant, and a ‘mission accomplished’ has been issued on several occasions, there has not been a definitive demonstration of MZM in any platform. The reasons for that largely fall under two categories. First, MZM and topological superconductivity put rather stringent requirements on materials in terms of crystalline defects, mean free path, and various interactions such as spin-orbit, superconductivity and magnetism – which need to coexist in just the right proportion. This in practice eliminates many approaches even if they nominally appear promising.

The second reason why MZM have not been firmly established is that we have found other excitations that look so much like MZM, but are not of a topological origin. This is a remarkable development that has little precedent in the history of science – when a phenomenon so carefully mapped out can be, in fact, due to something else. These alternative non-Majorana phenomena are all related to trivial Andreev bound states.

The goal of this project is to firmly establish Majorana Zero Modes in superconductor-semiconductor hybrid devices. We have developed an approach that includes everything that we have learned over the past 10 years. We are going to use a new hybrid superconductor-semiconductor material that addresses all major challenges experienced before. And we are going to use a recently developed three-terminal experimental measurement technique that allows to distinguish Majorana and Andreev states. Once Majorana modes are established, this opens doors to a large number of exciting and long-awaited experiments that explore and leverage all of the predicted Majorana properties, from teleportation to fractional Josephson effect and braiding.

Recent Progress

A recent success has been the PI’s work on combining InSb nanowires with Sn superconducting shells [1]. This work is the first demonstration of a hard gap induced superconductivity that also preserves charge parity outside of the well-studied aluminum. The results obtained in a broad collaboration between Pittsburgh, Eindhoven, Santa Barbara and

Grenoble opened up new possibilities for engineering topological and transmon qubits. Devices based on these nanowires demonstrate ‘hard’ superconducting gap in tunneling measurements up to fields of 4T. Hard gap, i.e. zero conductance at low bias, is an essential requirement for the demonstration control over multiple Majorana zero modes. [2]

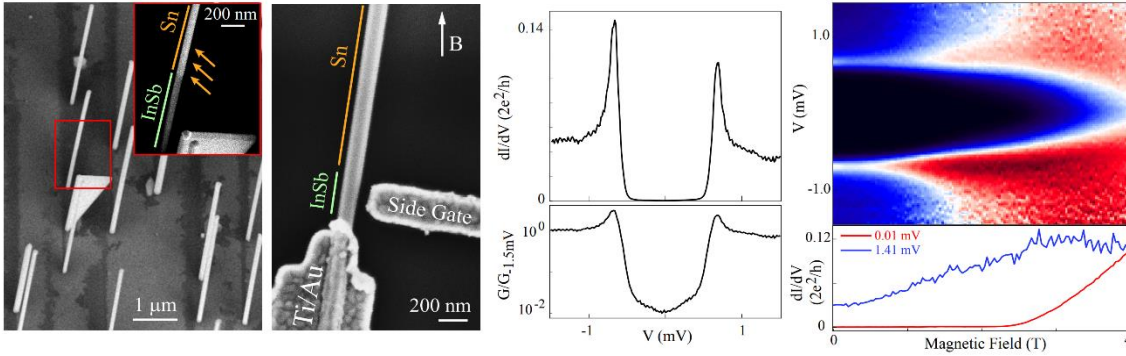


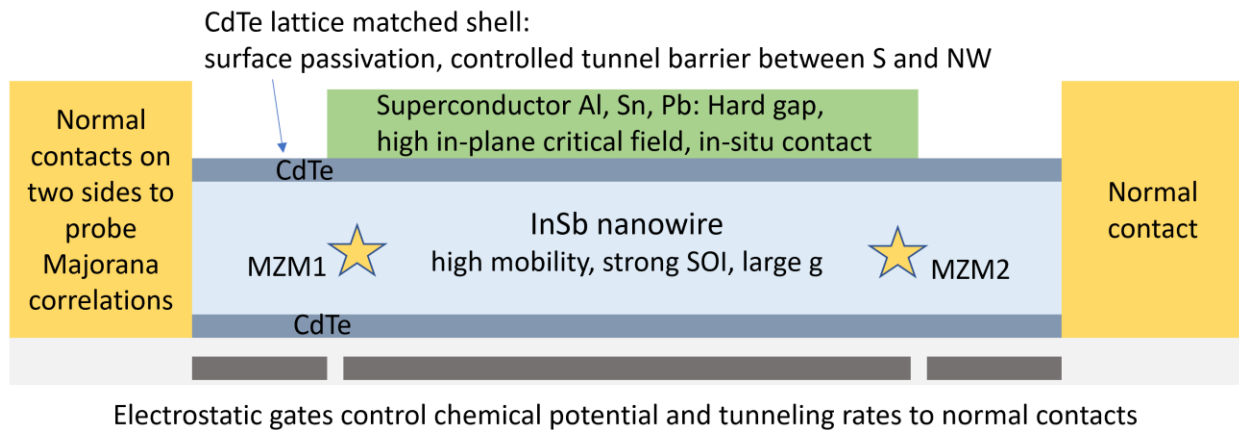
Figure 1: Left: New generation stemless InSb nanowires shadowed by flakes to form selectively deposited tin shells (Sn) and devices made using such wires. Right: tin induces hard gap superconductivity in InSb that sustains to large magnetic fields. From Ref. [1]

The PI just co-authored a Nature Physics perspective summarizing my modern view on the status of this research direction [3]. The main message is that efforts to establish Majorana states beyond any doubt are still very much ongoing. The key issue is that Majorana devices are rather complex, and thus other quantum states not of Majorana origin may exist in these devices. In particular, Andreev bound states localized on one end of the nanowire were demonstrated to also exhibit zero-bias peaks robust to changes in parameters such as magnetic field [4, 5]. The PI is carefully exploring these questions and have completed several studies explicitly highlighting zero-bias peaks of non-Majorana origin [5, 6].

Future Plans

We shall use the next generation of the nanowire platform that has the potential to solve the most important challenges that were identified so far. In these wires we aim to definitively establish Majorana modes and unlock their potential for fundamental research and technology. The new material that makes it possible is an InSb nanowire with two shells: a large bandgap semiconductor CdTe inner shell and on the outside of it a metallic superconductor such as Pb, Sn or Al (see diagram on the next page). InSb is the highest mobility and the longest mean free path semiconductor with strong spin-orbit interaction (SOI) and large g-factor. This material has already been our choice for Majorana experiments before. The new CdTe shell is from another family of materials (group II-VI rather than III-V), however it is lattice matched to InSb. It serves a dual purpose – it protects electrons in InSb from surface scattering leading to increased mean free path. And at the same time, it is a tunnel barrier between InSb and a semiconductor.

Decoupling of the super- and semi- layers has been proposed by calculations as key to realizing Majorana modes [7].



We shall perform three-terminal transport experiments on InSb-CdTe-(Al, Pb, Sn) nanowires. Correlated zero-bias resonances, as well as the observation of all other predicted Majorana signatures (quantized peak height, Majorana oscillations, topological phase diagram) simultaneously in the same nanowire will reliably exclude alternative explanations. Working with the new nanowires that feature hard gaps, high mobility and at the same time a tunnel barrier at the super-semi interface makes it possible to deliberately enter the topological regime and generate MZM. Trivial Andreev states can form in nanowire devices even when disorder is extremely low, simply due to the complex device geometry with multiple electrodes on top and around the nanowire inducing non-trivial confinement profiles. The key is then to separate trivial states from topological. As we demonstrate in a recent paper [6], this can be accomplished in the three-terminal geometry. MZM must appear in pairs, and in contrast the trivial states need not have a partner. Looking at the two ends of a nanowire and observing correlated signals is thus the most robust and straightforward way to separate topological and trivial states.

References

Put the list of references here using this font (Times New Roman 12 pt).

1. Pendharkar M, Zhang B, Wu H, Zarassi A, Zhang P, Dempsey CP, Lee JS, Harrington SD, Badawy G, Gazibegovic S, Jung J, Chen A-H, Verheijen MA, Hocevar M, Bakkers EPAM, Palmström CJ, Frolov SM (2021) Parity-preserving and magnetic field resilient superconductivity in indium antimonide nanowires with tin shells. *Science*, :508-. <http://arxiv.org/abs/1912.06071>
2. Chang W, Albrecht SM, Jespersen TS, Kuemmeth F, Krogstrup P, Nygård J, Marcus CM (2015) Hard gap in epitaxial semiconductor–superconductor nanowires. *Nature Nanotechnology*, 10(3):232–236. <https://doi.org/10.1038/nnano.2014.306>
3. Frolov SM, Manfra MJ, Sau JD (2020) Topological superconductivity in hybrid devices.

Nature Physics, 16(7):718–724. <https://doi.org/10.1038/s41567-020-0925-6>

4. Lee EJH, Jiang X, Houzet M, Aguado R, Lieber CM, Franceschi S De (2014) Spin-resolved Andreev levels and parity crossings in hybrid superconductor-semiconductor nanostructures. *Nature nanotechnology*, 9(1):79–84. <https://doi.org/10.1038/nnano.2013.267>

5. Chen J, Woods BD, Yu P, Hocevar M, Car D, Plissard SR, Bakkers EPAM, Stanescu TD, Frolov SM (2019) Ubiquitous Non-Majorana Zero-Bias Conductance Peaks in Nanowire Devices. *Physical Review Letters*, 123(10):107703. <https://doi.org/10.1103/PhysRevLett.123.107703>

6. Yu P, Chen J, Gomanko M, Badawy G, Bakkers EPAM, Zuo K, Mourik V, Frolov SM (2021) Non-Majorana states yield nearly quantized conductance in superconductor-semiconductor nanowire devices. *Nature Physics*, <https://doi.org/10.1038/s41567-020-01107-w>

7. Reeg C, Loss D, Klinovaja J (2018) Metallization of a Rashba wire by a superconducting layer in the strong-proximity regime. *Physical Review B*, 97(16):165425. <https://doi.org/10.1103/PhysRevB.97.165425>

Publications

New project started in July 2021.

Antiferromagnetism and Superconductivity

W.P. Halperin, Northwestern University

Program Scope

This project investigates the relationship between magnetism and superconductivity in high quality crystals of cuprates, pnictides, and topological superconductors, using state-of-the-art nuclear magnetic resonance (NMR) techniques extending to very high magnetic fields up to 14 T at Northwestern and $H = 30$ T at the National High Magnetic Field Laboratory (NHMFL) complemented by neutron scattering investigations of superconducting vortices. This program is especially important and relevant to understanding unconventional superconductivity, both for even-parity and odd-parity superconducting order parameters. Crystal preparation, including growth, isotope exchange and annealing are followed by characterization using Laue X-ray, electrical transport, SEM, and SQUID magnetization measurements.

Recent Progress

We measured nuclear spin coherence of ^{17}O NMR at high magnetic fields in the new world-record, all-superconducting 32 T magnet at NHMFL. NMR characterizations of chemical, physical, and biological materials, depend on coherent nuclear spin states which require the stability of a superconducting magnet. Ours are among the first results at NHMFL to measure spin-coherence in a 30 T class, high-field magnet. With high-quality single crystals of $\text{HgBa}_2\text{CuO}_4$ we have then been able to localize spin dependent vortex core excitations to be in the CuO_2 plane.

i) *Single crystal*: Our $\text{HgBa}_2\text{CuO}_4$ crystal (Hg1201) (UD81, 20 mg) was grown at Los Alamos, then isotope exchanged for ^{17}O , annealed, and characterized at Northwestern University. NMR measurements were performed at Northwestern and NHMFL. Magnetization shows a sharp onset of diamagnetism that onsets at $T_c = 81$ K for the underdoped cuprate UD81 (optimal doping is $T_c = 93$ K) with negligible inhomogeneous broadening. A clear signature of very high crystal quality is exemplified in the narrow quadrupolar satellite spectra for both planar O(1) and apical O(2) oxygen sites which we report here. Satellite spectra are well separated in frequency, red and blue arrows respectively figure 1, and are preferred for precise investigations of vortex physics, *i.e.* dynamic and static local magnetic fields. [1]

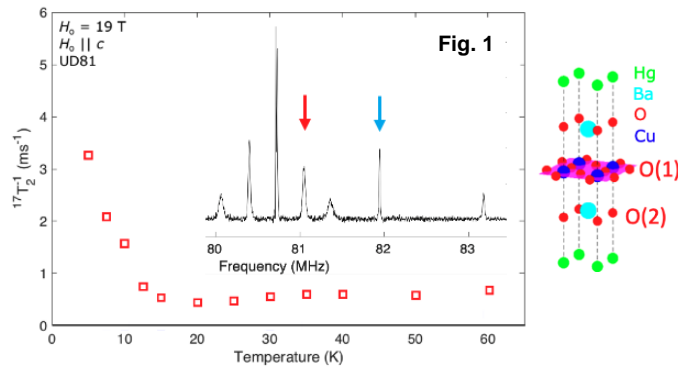


Figure 1. Spin-spin relaxation rate and spectra for ^{17}O NMR of $\text{HgBa}_2\text{CuO}_4$ single crystal $T_c = 81$ K. At right structure indicating planar O(1) and apical O(2) oxygen atom positions.

ii) *The new magnet:* "The all-superconducting magnet at NHMFL is the world's most powerful superconducting magnet. Before this magnet reached full field, the world's strongest superconducting user magnet had a field strength of $H = 23.5$ T. At 32 T it is a giant leap in technology. The 2.3-ton magnet system features about 6 miles of YBCO tape".[2] In the spring of 2021 the first external users were given access to this magnet performing remote experiments including our study. This report is the first demonstration of high field NMR phase coherence with the measurement of T_2 , a measurement that is not possible in hybrid or resistive high-field magnets.[1,2] Modern NMR technology requires phase-manipulation using RF pulse sequences which we have shown are now enabled at high magnetic field at NHMFL for the first time.

iii) *NMR spectra:* The inset in figure 1 shows ^{17}O spectra at $T = 90$ K for $c \parallel H$. Vortices freeze from their liquid state near 15 K, demonstrated in T_2 measurements, as expected theoretically based on the known penetration depth λ_{ab} , [3] and from earlier reports from our group.[4] Measurements of the spectra up to 30 T were conducted as a function of temperature and magnetic field, figures 2a, 3, and 4. We expected the inhomogeneous NMR lineshape characteristic of the local field distribution from a vortex lattice, figure 2a (blue), calculated from Ginzburg-Landau theory using Brandt's algorithm.[1,4] We observed a much narrower apical satellite spectrum O(2), shown in figure 2a (black) for comparison. Unexpectedly, there is no change in linewidth (FWHM) down to $T = 5$ K and as high as $H = 30$ T, figure 3 (green). In contrast at the planar oxygen site satellite (pink) the linewidth increases linearly with magnetic field. We infer that *there are no static vortex local fields observable at the apical site*. The planar site has a checkerboard structure which has been identified in Bi2212 by STM [5] and observed by NMR. It appears that a similar vortex-central spin-density wave is consistent with field dependence of our NMR linewidth measurements for O(1) in Hg1201.[1]

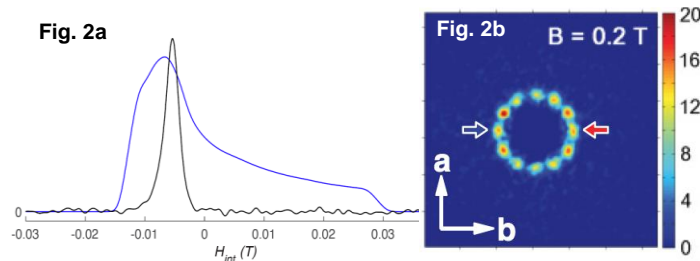


Figure 2. a) Calculated NMR spectrum from Brandt's Ginzburg-Landau theory (blue) compared to the observed spectrum (black). b) Small angle neutron scattering SANS vortex lattice only at low magnetic fields.[6]

We note that an identification of a well-formed static vortex lattice was reported from small angle neutron scattering measurements by Li *et al.*[6] on this compound at very low magnetic field. In that work, the diffraction intensity from the vortex lattice decreased with increasing magnetic field, disappearing at approximately $H = 0.35$ T attributed to c-axis disorder of vortex pancakes, figure 2b, taken from [6].

iv) *Spin-lattice relaxation rate:* Since there does not appear to be any coupling from vortex cores ^{17}O at the apical site we focus on electronic excitations associated with vortices at the planar site, O(1) NMR satellite. We have looked for spatial resolution of vortex excitations evidenced by

variation of $^{17}T_1^{-1}$ throughout the spectrum.[1] There is little variation in figure 4, indicating substantial in-plane vortex disorder.

v) *Spin coherence*: Phase coherence is determined by the spin-spin relaxation rate, $^{17}T_2^{-1}$. In all cases the time recovery was exponential. For the planar O(1) satellite the ^{17}O NMR decoherence rate $^{17}T_2^{-1}$ is shown in figure 1.[1] The increase in the rate at low temperatures signals spin dynamics in the vortex core localized in the CuO_2 plane and undetectable at the apical site. The physical origin for this relaxation has not yet been identified. Our observations were made possible using the new superconducting magnet technology at NHMFL and this phenomenon will be investigated as a function of magnetic field, temperature, and hole doping in future work.

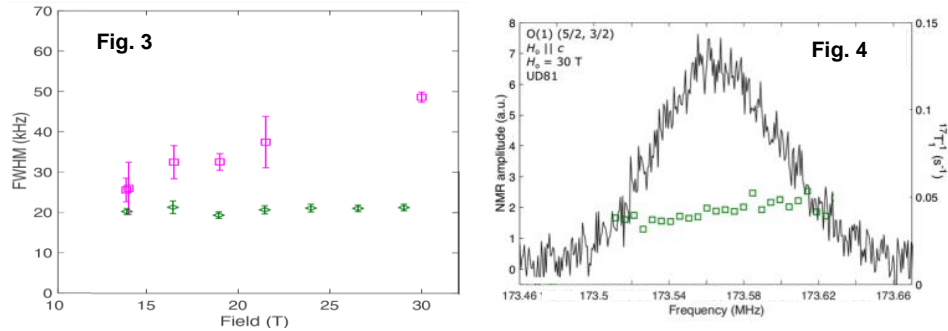


Figure 3-4. (Left side) NMR linewidth as function of magnetic field comparing planar oxygen site (pink) with apical oxygen site (green). There is no evidence of a vortex lattice manifest at the apical site. (Right side) Close investigation at $H = 30$ T was made of possible frequency-resolved vortex structure in the spin-lattice relaxation rate; this would have been correlated with spatially resolved vortex structure at the planar oxygen site. Its absence indicates a high level of in-plane vortex disorder.

vi) *Conclusions*: In contrast with NMR on aligned powders of YBCO and lesser quality single crystals of Hg1201 [4], high- T_c vortex pancakes are highly disordered with electronic core excitations isolated to the CuO_2 plane in a very high-quality crystal.

Future Plans

Our discovery of NMR phase decoherence that can be associated with the vortex core of Hg1201 using the 32 T high field magnet at NHMFL prompts our investigation as a function of field to determine their spectral density and thereby determine the physical origin of these vortex core excitations. Vortices are highly significant topological singularities in even-parity unconventional superconductors. This work will be supported by a collaboration with theory at Northwestern University and quantum materials crystal growth at Los Alamos National Laboratory. Further work on crystal growth, including annealing and oxygen isotope exchange to effect modifications of physical properties for investigation of impurity effects at Northwestern of high quality topological materials will also be part of this effort. NMR experiments will be performed up to $H = 14$ T at Northwestern University and to 30 T at NHMFL.

References

1. Ingrid Stolt, PhD thesis Northwestern University 2021; and publication in preparation.
2. NHMFL, nationalmaglab.org
3. L.I. Glazman and K.E. Kochelev Phys. Rev. B **43** 2835 (1991).
4. J.A. Lee *et al.* Phys. Rev. B **95**, 024512 (1917)
5. J.E. Hoffman *et al.* Science **294**, 466 (2002)
6. Y. Li *et al.* Phys. Rev. B **83**, 0654507 (2011)

Publications (two-year time frame)

RKKY coupled local moment magnetism in $\text{NaFe}_{1-x}\text{Cu}_x\text{As}$, Yizhou Xin, Ingrid Stolt, Yu Song, Pengcheng Dai, and W. P. Halperin, Phys. Rev. B (2021, in review).

Electron-beam Floating-zone Refined UCoGe , K. E. Avers, M. D. Nguyen, J. W. Scott, A. M. Zimmerman, S. M. Thomas, P. F. S. Rosa, E. D. Bauer, J. D. Thompson, and W. P. Halperin, Phys. Rev. Materials **5**, 054803 (2021).

Fingerprinting triangular-lattice antiferromagnet by excitation gaps, K. E. Avers, P. A. Maksimov, P. F. S. Rosa, S. M. Thomas, J. D. Thompson, W. P. Halperin, R. Movshovich, and A. L. Chernyshev, Phys. Rev. B **103**, L180406 (2021).

Broken Time-Reversal Symmetry in the Topological Superconductor UPt_3 , K. E. Avers, W. J. Gannon, S.J. Kuhn, W.P. Halperin, J.A. Sauls, L. DeBeer-Schmitt, C.D. Dewhurst, J. Gavilano, G. Nagy, U. Gasser, and M.R. Eskildsen, Nature Physics, **16**, 531 (2020).

Stripe Antiferromagnetism and Disorder in the Mott Insulator $\text{NaFe}_{1-x}\text{Cu}_x\text{As}$ ($x < 0.5$), Yizhou Xin, Ingrid Stolt, Yu Song, Pengcheng Dai, and W.P. Halperin, Phys. Rev. B **101**, 064410 (2020).

Toward the Mott State with Magnetic Cluster Formation in Heavily Cu-doped $\text{NaFe}_{1-x}\text{Cu}_x\text{As}$, Yizhou Xin, Ingrid Stolt, Jeongseop A. Lee, Yu Song, Pengcheng Dai, and W.P. Halperin, Phys. Rev. B **99**, 155114 (2019).

Science of 100 Tesla

Neil Harrison, Mun Chan, John Singleton, Marcelo Jaime, Priscila Rosa and Scott Crooker, Los Alamos National Laboratory

Program Scope

Here we are concerned with classes of layered materials in which significant scientific progress requires access to magnetic fields of order 100 T. These include (i) layered superconductors such as the cuprates [1] and iron-based superconductors [2], in which unconventional pairing predominantly takes place within isolated layers, (ii) materials in which the bonding between layers is of the van der Waals type such as graphite or (iii) systems in which the physical properties change dramatically upon exfoliation [3-5]. In the layered unconventional superconductors, strong pairing and short coherence lengths lead to very high superconducting upper critical fields that necessitate magnetic fields of order 100 T to access the physics of the normal state [1]. There is mounting evidence that superconductivity nucleates around a singular point, referred to as a quantum critical point [6-8]. One of our goals is to identify the order parameter or the change in symmetry responsible for quantum criticality in the cuprates, which remains a major milestone in quantum matter [1], and is likely to be accomplished only by the application of a very strong magnetic field.

Recent Progress

The role of the pseudogap regime of layered cuprate high- T_c superconductors remains a central unresolved problem in physics [9]. Of interest is the question whether it pertains to an unconventional order parameter, multiple order parameters or some form of pairing in advance of the superconducting state. A related question concerns whether unconventional order parameters terminate at a quantum critical point [1].

At lower temperatures, experiments in high magnetic fields, mostly in the yttrium cuprate $\text{YBa}_2\text{Cu}_3\text{O}_{6+x}$ (Y123) have previously found very clear signatures of Fermi surface reconstruction. This includes magnetic quantum oscillations and a negative Hall coefficient [10,11]. We map out the negative Hall coefficient as a function of hole doping in the mercury cuprate $\text{HgBa}_2\text{CuO}_{4+x}$ (Hg1201), finding this to span two critical points [12]. At these points where the Fermi surface reconstruction terminates is where superconductivity is found to be most robust under a magnetic field.

On comparing the two cuprates that have similarly high superconducting transition temperatures and quantum oscillations (Hg1201 and Y123) in Fig. 1, a number of similarities are found in their phase diagrams [12]. This includes the existence of two islands of residual superconductivity in strong magnetic fields, centered on two critical points. However, owing to the greater two-dimensionality of Hg1201, the superconductivity is suppressed much more rapidly in a magnetic field. From this, we are able to infer that the reconstructed Fermi surface giving rise to the negative Hall coefficient extends all the way to $p_{c2} \sim 0.2$, which is believed to be a quantum critical point. Factors that make the observations in Hg1201 more representative of CuO_2 planes include the tetragonal crystal structure, the absence of CuO chains and the absence of spurious spin glass phases.

Thus far, the largest quantum oscillations have been detected in Y123. Recently, samples significantly higher in quality were grown at the Max Planck Institute in Stuttgart. Our recent careful study of the sawtooth de Haas-van Alphen waveform reveals a striking similarity to an ideal 2D Fermi gas [13]. This indicates that the reconstructed Fermi surface pocket responsible for the negative Hall coefficient is the only section of Fermi surface present in the material in the

pseudogap regime. It therefore shows that the majority of the Fermi surface predicted by bandstructure calculations is completely gapped at low temperatures, revealing a “hard antinodal gap” in the pseudogap regime.

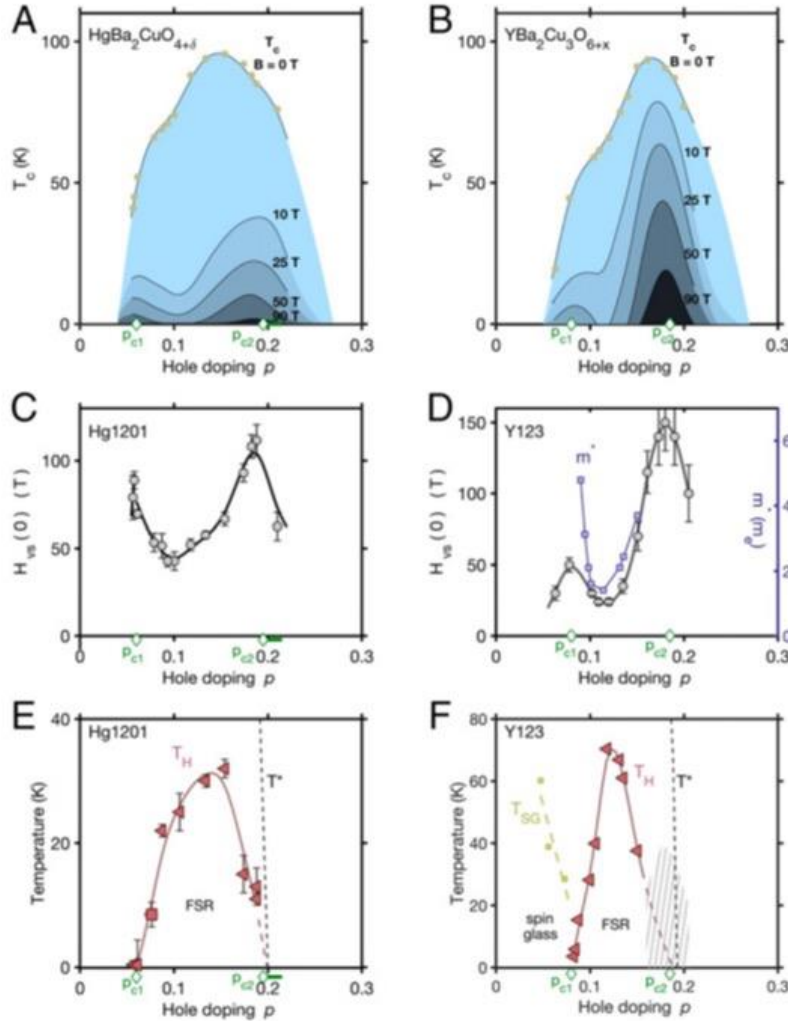


Fig. 1. Superconductivity and the boundaries of Fermi-surface reconstruction. **(A)** Magnetic-field dependence of T_c for Hg1201, defined as the temperature below which the resistivity is zero measured for samples, with zero-field T_c 's indicated by yellow circles. **(B)** T_c for Y123. **(C)** Vortex-melting field at zero temperature $H_{vs}(0)$ for Hg1201. **(D)** $H_{vs}(0)$ for Y123. Effective mass m^* from quantum oscillations (purple squares, right axes) is shown. **(E)** Characteristic temperature corresponding to the sign change of the Hall coefficient T_H in Hg1201. The pseudogap temperature T^* (dashed line) is an extrapolation from high temperature transport data. **(F)** T_H for Y123. R_H in Y123 has not been reported within the hatched gray region around p_{c2} . A glassy spin-density wave phase appears below T_{SG} in the far underdoped regime that is apparently absent in Hg1201.

One leading hypothesis for the Fermi surface reconstruction, based on prior studies and X-ray scattering, is charge density wave order of a biaxial nature, or possibly a pair density wave. This has, of course, remained controversial [10,11]. The charge ordering, negative Hall coefficient and quantum oscillations are seen to span same range of dopings and temperature, indicating a strong connection between the charge ordering and the reconstructed Fermi surface. The evidence for an ideal sawtooth de Haas-van Alphen oscillations from a single pocket (like those in GaAs heterostructures for example) includes a sawtooth waveform, an inverted U susceptibility and

Fourier peaks that decay exponentially with increasing harmonic index.

Another recent study of ours shows rather conclusively that the state exhibiting quantum oscillations, a negative Hall effect and charge ordering, is not the normal state [14]. Routine electrical transport measurements (typically performed in pulsed magnetic fields and with high currents to maximize signal-to-noise) find an electrically resistive state. However, we had long suspected, based on our prior observations of hysteresis in the magnetic torque, that the system is still in the vortex state. We confirmed this by way of electrical transport measurements. When the current is made sufficiently low, and if the temperature is lowered to dilution fridge temperatures, and if the field is swept very slowly or held constant, the resistivity falls to zero. An anomalous vortex melting transition is therefore indicated.

On plotting the vortex phase diagram, the vortex solid phase (for which the electrical resistivity is zero) extends to much higher magnetic fields than the $H_{c2} \sim 24$ T that was previously concluded from measurements made at much higher currents and in pulsed magnetic fields. A fragile high magnetic field/low temperature vortex solid state is therefore indicated within the underdoped regime of Y123. This immediately inspired a followup study that confirmed generality of this to other cuprates [15].

Consistent with a vortex solid at the lowest temperatures, we find current (j) versus voltage (V) to exhibit a non-linear behavior, which can be qualitatively understood in terms of thermally assisted flux flow (TAFF). At higher temperatures, the current-voltage behavior becomes characteristic of a metal, suggesting a vortex liquid.

Evidence for an unconventional quantum vortex solid phase is present in both the magnetic torque and electrical resistivity. In the former, the vortex solid gives rise to hysteresis resulting from trapped flux in the sample. Over this same region of the phase diagram, the electrical resistivity vanishes at low current densities. The magnetic torque exhibits magnetic quantum oscillations, as has previously been reported. However, the electrical resistivity exhibits quantum oscillations only at current densities above the critical current density j_c . The quantum oscillations are further found not to undergo any change in amplitude in crossing over into the vortex liquid phase at higher temperatures. Nor is there any characteristic magnetic field above which the quantum oscillations change. This must therefore be the case all the way at least to 100 T [16].

Indications are, therefore, that the quantum oscillations in Y123 (and probably also in Hg1201) occur in a fragile superconducting state — a state in which the superconducting gap is large but where a small current density appears to cause it to look deceptively like a metal. The region of the phase diagram exhibiting a fragile vortex solid also appears to host a charge-density wave phase. The coexistence of fragile superconductivity and a charge density wave at high magnetic fields strongly suggests the existence of a pair-density wave order parameter. At the time of publication, our publication was accompanied by a commentary by Mike Norman from Argonne NL entitled “Fragile superconductivity at high magnetic fields [17].”

Future Plans

Future plans in the cuprates include using angular magnetoresistance measurements in Hg1201 to map changes in the pseudogap regime as a function of temperature and hole doping in a system where there is no antiferromagnetism. There are ongoing quantum oscillation measurements of the effective mass as a function of doping and of the quasiparticle g -factor. Another important area of interest is distinguishing phenomena consistent with quantum criticality and the unitary regime of a Fermi gas, thereby making connections with the Bardeen-Cooper-Schrieffer to Bose-Einstein condensation crossover physics of cold atomic Fermi gases.

References

- [1] B. Keimer, S. A. Kivelson, M. R. Norman, S. Uchida & J. Zaanen, From quantum matter to high-temperature superconductivity in copper oxides. *Nature* **518**, 179 (2015).
- [2] D. C. Johnston, The puzzle of high temperature superconductivity in layered iron pnictides and chalcogenides. *Adv. Phys.* **59**, 803 (2010).
- [3] K.S. Novoselov *et al.*, Two-dimensional gas of massless Dirac fermions in graphene. *Nature* **438**, 197 (2005).
- [4] A. Splendiani *et al.*, Emerging Photoluminescence in monolayer MoS₂. *Nano. Lett.* **10**, 1271 (2010).
- [5] K. F. Mak, C. Lee, J. Hone, J. Shan, & T. F. Heinz, Atomically thin MoS₂: A new direct gap semiconductor. *Phys. Rev. Lett.* **105**, 136805 (2010).
- [6] B.J. Ramshaw *et al.*, Quasiparticle mass enhancement approaching optimal doping in a high- T_c superconductor. *Science* **348**, 317 (2015).
- [7] B. Michon *et al.*, Thermodynamic signatures of quantum criticality in cuprate superconductors. *Nature* **567**, 218 (2019).
- [8] S. Licciardello *et al.*, Electrical resistivity across a nematic quantum critical point. *Nature* **567**, 213 (2019).
- [9] T. Timusk & B. Statt, The pseudogap in high-temperature superconductors: an experimental survey. *Rep. Prog. Phys.* **62**, 61 (1999).
- [10] S. E. Sebastian, N. Harrison & G. G. Lonzarich, Towards resolution of the Fermi surface in underdoped high- T_c superconductors. *Rep. Prog. Phys.* **75**, 102501 (2012).
- [11] C. Proust & L. Taillefer, The remarkable underlying ground states of cuprate superconductors, *Annual Review of Condensed Matter Physics* **10**, 409 (2019).
- [12] M.K. Chan *et al.*, Extent of Fermi-surface reconstruction in the high-temperature superconductor HgBa₂CuO_{4+ δ} , *Proceedings of the National Academy of Science USA*. **117**, 9782 (2020).
- [13] M. Hartstein *et al.*, Hard antinodal gap revealed by quantum oscillations in the pseudogap regime of underdoped high- T_c superconductors, *Nature Physics* **16**, 841 (2020).
- [14] Y.-T. Hsu *et al.*, Unconventional quantum vortex matter state hosts quantum oscillations in the underdoped high-temperature cuprate superconductors, *Proceedings of the National Academy of Science USA* **118**, e2021216118 (2021).
- [15] Y.-T. Hsu *et al.*, Anomalous vortex liquid in charge-ordered cuprate superconductors, *Proceedings of the National Academy of Science USA* **118**, e2016275118 (2021).
- [16] S. E. Sebastian *et al.*, Quantum oscillations from nodal bilayer magnetic breakdown in the underdoped high temperature superconductor YBa₂Cu₃O_{6+x}. *Phys. Rev. Lett.* **108**, 196403 (2012).
- [17] M. R. Norman, Fragile superconductivity at high magnetic fields, *Proceedings of the National Academy of Science USA*. e2100372118; (2021).

Significant publications

1) Spin-valley locking and bulk quantum Hall effect in a noncentrosymmetric Dirac semimetal BaMnSb₂, Liu, J. Y., Ning, J. L., Yi, H. M., Miao, L., Min, L. J., Zhao, Y. F., Ning, W., Lopez, K. A., Zhu, Y. L., Pillsbury, T., Zhang, Y. B., Wang, Y., Hu, J., Cao, H. B., Chakoumakos, B. C., Balakirev, F., Weickert, F., Jaime, M., Lai, Y., Yang, K., Sun, J. W., Alem, N., Gopalan, V.,

Chang, C. Z., Samarth, N., Liu, C. X., McDonald, R. D., Mao, Z. Q., NATURE COMMUNICATIONS 12, 4062 JUL 1 2021

2) Unusual high-field metal in a Kondo insulator, Xiang, Z., Chen, L., Chen, K.-W., Tinsman, C., Sato, Y., Asaba, T., Lu, H., Kasahara, Y., Jaime, M., Balakirev, F., Iga, F., Matsuda, Y., Singleton, J., Li, L., NATURE PHYSICS 17, 788 APR 2021

3) Controlling magnetic anisotropy in a zero-dimensional $I = 1$ magnet using isotropic cation substitution, Manson, J. L., Curley, S P. M., Williams, R. C., Walker, D., Goddard, P. A., Ozarowski, A., Johnson, R. D., Vibhakar, A. M., Villa, D. Y., Rhodehouse, M. L., Birnbaum, S. M., Singleton, J., JOURNAL OF THE AMERICAN CHEMICAL SOCIETY 143, 4633 MAR 31 2021

4) Proximity to a critical point driven by electronic entropy in URu_2Si_2 , Harrison, N., Kushwaha, S. K., Chan, M. K., Jaime, M., NPJ QUANTUM MATERIALS 6, 24 MAR 5 2021

5) Unconventional quantum vortex matter state hosts quantum oscillations in the underdoped high-temperature cuprate superconductors, Hsu, Y.-T., Hartstein, M., Davies, A. J., Hickey, A. J., Chan, M. K., Porras, J., Loew, T., Taylor, S. V., Liu, H., Eaton, A. G., Le Tacon, M., Zuo, H., Wang, J., Zhu, Z., Lonzarich, G. G., Keimer, B., Harrison, N., Sebastian, S. E., PROCEEDINGS OF THE NATIONAL ACADEMY OF SCIENCES OF THE UNITED STATES OF AMERICA 118, 2021216118 FEB 16 2021

6) Scale-invariant magnetic anisotropy in $RuCl_3$ at high magnetic fields, Modic, K. A., McDonald, R. D., Ruff, J. P. C., Bachmann, M. D., Lai, Y., Palmstrom, J. C., Graf, D., Chan, M. K., Balakirev, F. F., Betts, J. B., Boebinger, G. S., Schmidt, M., Lawler, M. J., Sokolov, D. A., Moll, P. J. W., Ramshaw, B. J., Shekhter, A., NATURE PHYSICS 240 OCT 2020

7) Superconductivity and quantum criticality linked by the Hall effect in a strange metal, Hayes, I. M., Maksimovic, N., Lopez, G. N., Chan, M. K., Ramshaw, B. J., McDonald, R. D., Analytis, J. G., NATURE PHYSICS 17, AUG 2020

8) Colossal magnetoresistance in a nonsymmorphic antiferromagnetic insulator, Rosa, P., Xu, Y., Rahn, M., Souza, J., Kushwaha, S., Veiga, L., Bombardi, A., Thomas, S., Janoschek, M., Bauer, E., Chan, M., Wang, Z., Thompson, J., Harrison, N., Pagliuso, P., Bernevig, A., Ronning, F., NPJ QUANTUM MATERIALS 5, 52 JUL 24 2020

9) Non-monotonic pressure dependence of high-field nematicity and magnetism in $CeRhIn_5$, Helm, T., Grockowiak, A. D., Balakirev, F. F., Singleton, J., Betts, J. B., Shirer, K. R., Markus König, T. F., Bauer, E. D., Ronning, F., Tozer, S. W., Moll, P. J. W., NATURE COMMUNICATIONS 11, 3482 JUL 13 2020

10) Temperature scaling behavior of the linear magnetoresistance observed in high-temperature superconductors, Singleton, J., PHYSICAL REVIEW MATERIALS 4, 061801 JUN 25 2020

- 11) Hard antinodal gap revealed by quantum oscillations in the pseudogap regime of underdoped high- T_c superconductors, Hartstein, M., Hsu, Y.-T., Modic, K. A., Porras, J., Loew, T., Le Tacon, M., Zuos, H., Wang, J., Zhu, Z., Chan, M. K., McDonald, R. D., Lonzarich, G. G., Keimer, B., Sebastian, S. E., Harrison, N., NATURE PHYSICS 16, 841 MAY 2020
- 12) Extent of Fermi-surface reconstruction in the high-temperature superconductor $\text{HgBa}_2\text{CuO}_{4+\delta}$, Chan, M. K., McDonald, R. D., Ramshaw, B. J., Betts, J. B., Shekhter, A., Bauer, E. D., Harrison, N., PROCEEDINGS OF THE NATIONAL ACADEMY OF SCIENCES OF THE UNITED STATES OF AMERICA 117, 9782 MAY 5 2020
- 13) Dirac fermions and flat bands in the ideal kagome metal FeSn , Kang, M., Ye, L., Fang, S., You, J.-S., Levitan, A., Han, M., Facio, J. I., Jozwiak, C., Bostwick, A., Rotenberg, E., Chan, M. K., McDonald, R. D., Graf, D., Kaznatcheev, K., Vescovo, E., Bell, D. C., Kaxiras, E., Van den Brink, J., Richter, M., Prasad Ghimire, M., Checkelsky, J. G., Comin, R., NATURE MATERIALS 19, 163 FEB 2020
- 14) Magnetic field-tuned Fermi liquid in a Kondo insulator, Kushwaha, S. K., Chan, M. K., Park, J., Thomas, S. M., Bauer, E. D., Thompson, J. D., Ronning, F., Rosa, P. F. S., Harrison, N., NATURE COMMUNICATIONS 10, 5487 DEC 2 2019
- 15) Extreme magnetic field-boosted superconductivity, Ran, S., Liu, I.-L., Eo, Y. S., Campbell, D. J., Neves, P. M., Fuhrman, W. T., Saha, S. R., Eckberg, C., Kim, H., Graf, D., Balakirev, F., Singleton, J., Paglione, J., Butch, N. P., NATURE PHYSICS 15, 1250 DEC 2019
- 16) de Haas-van Alphen effect of correlated Dirac states in kagome metal Fe_3Sn_2 , Ye, L., Chan, M. K., McDonald, R. D., Graf, D., Kang, M., Liu, J., Suzuki, T., Comin, R., Fu, L., Checkelsky, J. G., NATURE COMMUNICATIONS 10, 4870 OCT 25 2019
- 17) Unconventional thermal metallic state of charge-neutral fermions in an insulator, Sato, Y., Xiang, Z., Kasahara, Y., Taniguchi, T., Kasahara, S., Chen, L., Asaba, T., Tinsman, C., Murayama, H., Tanaka, O., Mizukami, Y., Shibauchi, T., Iga, F., Singleton, J., Li, L., Matsuda, Y., NATURE PHYSICS 15, 954 SEP 2019
- 18) Spin-lattice and electron-phonon coupling in 3d/5d hybrid $\text{Sr}_3\text{NiIrO}_6$, O'Neal, K. R., Paul, A., Al-Wahish, A., Hughey, K. D., Blockmon, A. L., Luo, X., Cheong, S.-W., Zapf, V. S., Topping, C. V., Singleton, J., Ozerov, M., Birol, T., Musfeldt, J. L., NPJ QUANTUM MATERIALS 4, 48 AUG 21 2019
- 19) Magnetic field-temperature phase diagram of multiferroic $(\text{NH}_4)_2\text{FeCl}_5 \cdot \text{H}_2\text{O}$, Clune, A. J., Nam, J., Lee, M., Hughey, K. D., Tian, W., Fernandez-Baca, J. A., Fishman, R. S., Singleton, J., Lee, J. H., Musfeldt, J. L., NPJ QUANTUM MATERIALS 4, 44 AUG 12 2019

There are 22 additional publications, which have been omitted due to space limitations.

Hybrid-Magnon Quantum Devices

Axel Hoffmann^{1,2,3}, Yi Li⁴, Valentine Novosad⁴, Wolfgang Pfaff^{2,3}, Andre Schleife¹, and Jian-Min Zuo^{1,3}

1. Materials Science and Engineering, University of Illinois at Urbana-Champaign, Urbana, IL 61801
2. Department of Physics, University of Illinois at Urbana-Champaign, Urbana, IL 61801
3. Materials Research Laboratory, University of Illinois at Urbana-Champaign, Urbana, IL 61801
4. Materials Science Division, Argonne National Laboratory, Lemont, IL 60439

Program Scope

Magnons, the quanta of collective spin excitations in magnetically ordered media, have recently emerged as an exciting candidate for quantum information processing and quantum transduction [1]. In particular, magnons exhibit unique features for microwave quantum engineering, *i.e.*, their ultra-small wavelength down to the nanometer scale and their potential for non-reciprocity, which are highly desired for nanoscale-pitch-size quantum gates and noise-isolated qubit operations with on-chip integration. Although quantum operations of magnons have been demonstrated in bulk magnetic crystals, the quantum property of propagating magnons in magnetic films remains a fundamental challenge in both physics and materials science and is crucial for building magnon-based quantum information devices.

Our main objective is the development of a materials strategy for realizing hybrid magnonic quantum systems around magnetic materials that can be integrated into on-chip quantum systems via standard lithography. We will optimize magnon-photon coupling and test our main hypothesis that reduced magnetic damping is the key challenge, since it directly determines magnon coherence. Towards our first objective of increased magnon coherence, we will pursue a multipronged approach based on investigating low-damping metallic alloys, developing new synthesis approaches for low-damping magnetic insulators, and employing spin-orbitronics approaches for synthetically reduced damping. Our second objective is to utilize one of the unique advantages of magnetic systems, namely their inherently non-reciprocal dynamics. We will address this objective by proper engineering of hybrid magnon systems through geometric constraints as well as interfacial symmetry breaking, which both can be utilized for tuning chiral interactions in magnetic thin-film structures. Lastly, our third objective is to integrate these new

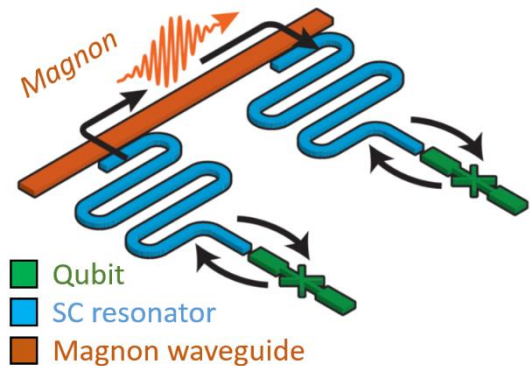


Fig. 1 Schematics of the magnon-qubit hybrid circuit with nonreciprocal magnonic conduit for on-chip quantum noise isolation and qubit dephasing improvement.

materials systems in prototypical quantum information systems with superconducting qubits with the goal to demonstrate new quantum coherent functionality, as is schematically shown in Fig. 1.

The main program scope is to demonstrate quantum coherent operation based on nonreciprocal magnon propagations for providing noise isolation in quantum information systems (Fig. 1). To achieve this goal, this program will overcome three major challenges: 1) low-damping (down to 10^{-4}) magnetic thin film and devices platform to provide efficient coherent magnonic operations with on-chip integration, 2) magnon nonreciprocity that provides sufficient isolation for coherent magnon-qubit transductions and is compatible with cryogenic environment, 3) qubit optimization to maintain state-of-the-art coherence in the presence of magnetic field

Recent Progress

This is a new project that just started in September 2021, so that there is not yet any recent progress to report.

Future Plans

In order to identify suitable magnetic materials, we will pursue a two-pronged approach. On one end we will investigate metallic alloys and their damping properties at cryogenic temperatures required for operating superconducting quantum devices, since their processing is easily compatible with lithographic approaches for their integration into hybrid structures [2,3]. We will target in particular ternary alloys based on Fe and Co, since these alloys provide some of the largest saturation magnetization and therefore are beneficial for strong coupling to microwave photons. Our starting point will be $\text{Co}_{25}\text{Fe}_{75}$, which has already been reported to have a magnetic damping close to 10^{-4} [4]. We will then systematically add elements that promote the formation of amorphous structures, such as B, C, and Si, since for the $\text{Co}_{50}\text{Fe}_{50}$ alloy it has been shown that the structural transition to amorphous films leads to a reduction of the damping by one order of magnitude [5]. The experimental work will be guided by concomitant first principles simulations. We will study the composition dependence of the density of states near the Fermi level for CoFe alloys, in particular in the vicinity of $\text{Co}_{25}\text{Fe}_{75}$. We will also account for atomic disorder, towards amorphization, in order to explore a further reduction of damping that was observed by introduction of boron or carbon. If needed, we can include boron or carbon atoms explicitly in the first-principles simulations. This will provide the composition and structural dependence of the density of states near the Fermi level, as our proxy for damping.

Alternatively, we will develop alternative approaches for integrating $\text{Y}_3\text{Fe}_5\text{O}_{12}$ (YIG) thin films with planar microwave circuitry. One of the main issues is that films grown on $\text{Gd}_3\text{Ga}_5\text{O}_{12}$ (GGG) have unacceptable high microwave losses at cryogenic temperatures due to the large magnetic susceptibility of GGG. As a first quick step, we will take our epitaxial YIG films and subsequently polish the GGG substrate down to μm thickness. At the same time, we will use advanced transmission electron microscopy (see Fig. 2) to characterize quantitatively both defects and magnetic structure and correlate them to measured damping. In addition, we will develop a

cluster expansion approach to our first principles simulations, which will lay the foundation for studying the magnon-phonon coupling in these materials. Furthermore, we will prepare simulations of magnon-phonon coupling by studying Fe vacancies in YIG, by computing relaxed geometries using sufficiently large super cells.

One of the key concepts that we want to evaluate is the possibility to use non-reciprocal phenomena for directional microwave propagation in on-chip devices. Towards this end, we will investigate nonreciprocal magnon propagation in YIG/ $\text{Ni}_{80}\text{Fe}_{20}$ (Py) synthetic antiferromagnets, which has been recently predicted in theory as induced by interlayer dipolar interaction [6]. We will achieve high-quality epitaxial growth of low-damping YIG films and efficient interlayer exchange coupling between YIG and Py, which are crucial for enabling pronounced magnon nonreciprocity. The investigation will be supported by high-resolution scanning transmission electron microscopy (STEM) and elemental resolved EDX characterization of thin-film YIG/Py samples grown on GGG substrate (Fig. 2).

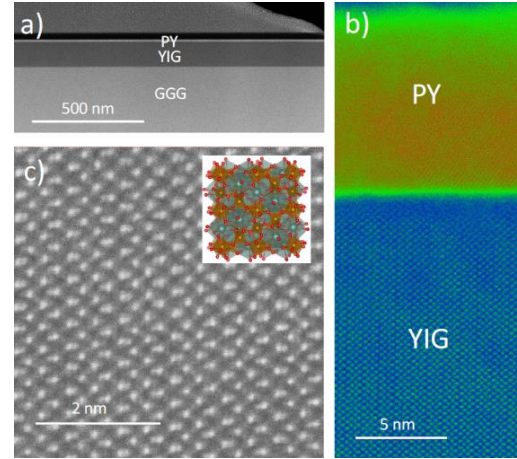


Fig. 2: Structural characterization of YIG/Py using scanning transmission electron microscopy (STEM): (a) Low magnification of Py/YIG bilayer on GGG. (b) Color coded STEM intensity at the interface. (c) Atomic resolution image of the YIG.

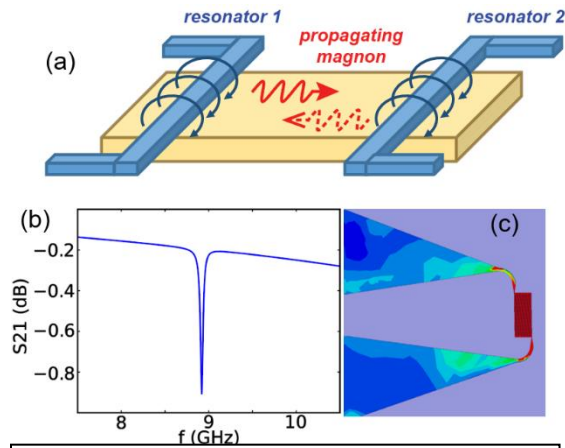


Fig. 3 (a) Schematics long distance microwave coupling in magnetic thin-film waveguide. (b) HFSS simulation results of superconducting resonators incorporating a nanowire meander line. (c) Resonant mode profile of the nanowire meander line in the superconducting resonator.

In parallel, we will also explore microwave circuit design for exciting short-wavelength propagating spin waves, which have large enough group velocity for magnon-mediated remote coupling. In particular, we will achieve this goal by embedding a nanowire meander-line antennas into high-quality-factor superconducting resonators (Fig. 3), which has optimal coupling to short-wavelength propagating magnons. We will work on electromagnetic simulation, superconducting meander nanowire fabrication, optimization of superconducting thin-film growth and cryogenic microwave characterizations. The planned work will be the first demonstration of strong coupling of *propagating* magnon modes to microwave photons.

Lastly, we will focus on optimizing superconducting quantum circuitry to compatible with the magnetic fields that we want to apply for operating the magnetic components. Therefore, an important consideration for introducing magnetic films to superconducting quantum devices is the detrimental effect of magnetic fields on

quantum coherence, in particular for conventional Al/AlO_x Josephson circuits. We will investigate how circuits can be operated at fields at which films that host magnon modes of interest show promising behavior. For one, we will study how magnetic fields impact coherence in different types of superconducting thin films, with the goal of finding an avenue toward quantum circuits that may operate at modest magnetic fields. Second, we will investigate hybrid packaging solutions in which only specific parts of the circuit are exposed to external fields, whereas other parts (such as conventional Josephson qubits) are spatially separated and shielded to retain their coherence. This will provide the foundation then for coplanar hybrid devices that combine superconducting qubits with propagating magnon waveguides, which will then be used to characterize individual magnons.

References

- [1] D. D. Awschalom, *et al.*, IEEE Trans. Quantum Engin. **2**, 5500836 (2021).
- [2] Y. Li, *et al.*, Phys. Rev. Lett. **123**, 107701 (2019).
- [3] J. T. Hou and L. Liu, Phys. Rev. Lett. **123**, 107702 (2019).
- [4] M. A. Schuen, *et al.*, Nature Phys. **12**, 839 (2016).
- [5] J. Wang, *et al.*, Phys. Rev. Appl. **12**, 034011 (2019).
- [6] R. A. Gallardo, *et al.*, Phys. Rev. Appl. **12**, 034012 (2019).

Publications

No publication to report yet.

Symmetry Engineering of Topological Quantum States

Jin Hu, University Arkansas

Program Scope

Topological band theory has bridged condensed matter and high energy physics. Dirac, Weyl, and Majorana fermions have found their counterparts in Dirac semimetals, Weyl semimetals, and topological superconductors. The topological character of the bands creates symmetry-protected band crossings with linearly dispersing electronic states, giving rise to exotic phenomena including chiral anomaly and surface Fermi arcs, as well as technologically useful properties such as high mobility and large linear magnetoresistance. The protected band crossings in topological semimetals, i.e., the Dirac or Weyl points, are guaranteed by specific crystal symmetries and/or time-reversal symmetry (TRS). Symmetry breaking is expected to create, split, and annihilate Dirac/Weyl points in topological semimetals. This project aims on probing the intimate connection between symmetry and topological electronic states in topological semimetals. We propose to pursue crystal symmetry-breaking and TRS-breaking with synergistic experimental and theoretical efforts. We expect the realization of various new topological quantum states and quantum phenomena through symmetry engineering of topological quantum states.

Recent Progress

We recently made progress on both direction of crystalline symmetry and TRS engineering study. For crystalline symmetry, we studied the quantum transport of the novel surface electronic state which arising from the breaking translation symmetry at the sample's surface [1]. For TRS, we discovered two new magnetic topological semimetal candidates [2,3].

(i) Novel surface state due to translation symmetry-breaking

In crystals processing non-symmorphic crystalline symmetry, certain electronic bands degenerate due to symmetry requirement. ZrSiS-family topological materials crystallize in a non-symmorphic $P4/nmm$ space group. The $\{M_z|1/2, 1/2, 0\}$ symmetry ensures band degeneracy at X, M, R, and A points in the Brillouin zone (BZ). At the crystals' surface where the translation symmetry along z no longer exists, early studies has predicted the lift of degeneracy at \bar{X} [4], which leads to a 2D electronic band "floating" on the surface of a crystal. Such a new state originates from the symmetry reduction at the surface, thus it is distinct from the common surface states due to surface chemistry in conventional materials, or the widely seen topological surface states arising from the bulk-boundary correspondence principle in topological materials.

The existence of such a new surface band has been demonstrated by our recent work on ZrSiSe [1], a compound belongs to the ZrSiS-family. Owing to relatively weak interlayer binding between the Zr-Se bi-layers (Fig. 1a), thin flakes of this compounds can be obtained via mechanical exfoliation (Figs. 1b-d). At low temperatures, our magnetotransport measurements revealed Shubnikov-de Haas (SdH) quantum oscillations, which show a surprising additional oscillation frequency in flakes below 60 nm thickness (Figs. 1e-f). Such additional frequency exhibits

increasing weight with reducing flake thickness (Fig. 1f), and shows 2D characters in angular dependent SdH oscillation measurements (Fig. 1g). Those findings are consistent with the transport of a surface state, which becomes substantial in thin flakes due to the enhanced surface-to-bulk ratio.

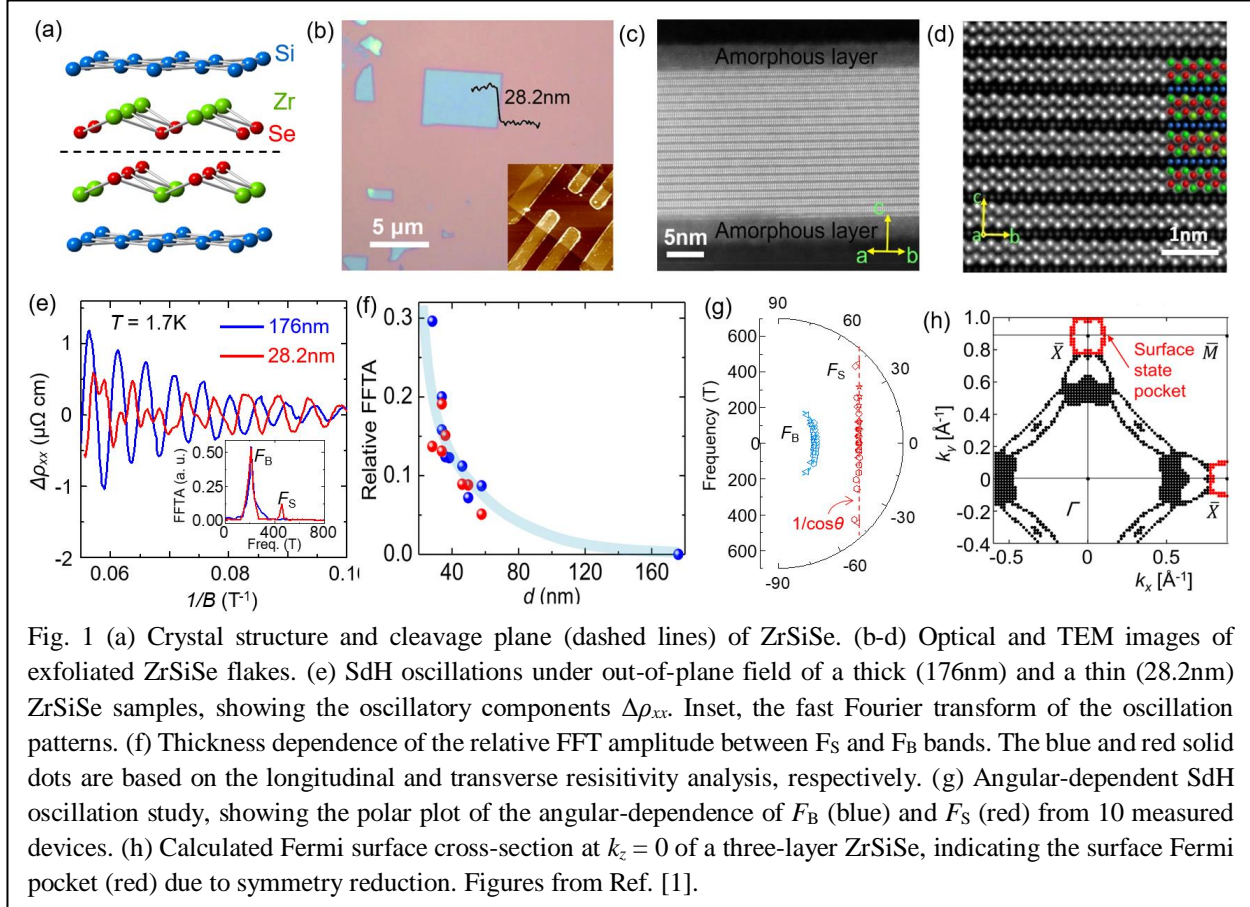


Fig. 1 (a) Crystal structure and cleavage plane (dashed lines) of ZrSiSe. (b-d) Optical and TEM images of exfoliated ZrSiSe flakes. (e) SdH oscillations under out-of-plane field of a thick (176nm) and a thin (28.2nm) ZrSiSe samples, showing the oscillatory components $\Delta\rho_{xx}$. Inset, the fast Fourier transform of the oscillation patterns. (f) Thickness dependence of the relative FFT amplitude between F_S and F_B bands. The blue and red solid dots are based on the longitudinal and transverse resistivity analysis, respectively. (g) Angular-dependent SdH oscillation study, showing the polar plot of the angular-dependence of F_B (blue) and F_S (red) from 10 measured devices. (h) Calculated Fermi surface cross-section at $k_z = 0$ of a three-layer ZrSiSe, indicating the surface Fermi pocket (red) due to symmetry reduction. Figures from Ref. [1].

The nature of the probed surface state is further clarified to be the predicted 2D floating band from symmetry reduction at surface. First, unlike the widely seen topological surface states due to the bulk-boundary correspondence principle in topological materials, the 2D floating band is predicted to be non-topological, which is consistent with the observed trivial Berry phase from the SdH oscillations. Second, the oscillation frequency of 445 T matches well the calculated Fermi pocket size of the 2D floating band (Fig. 1h).

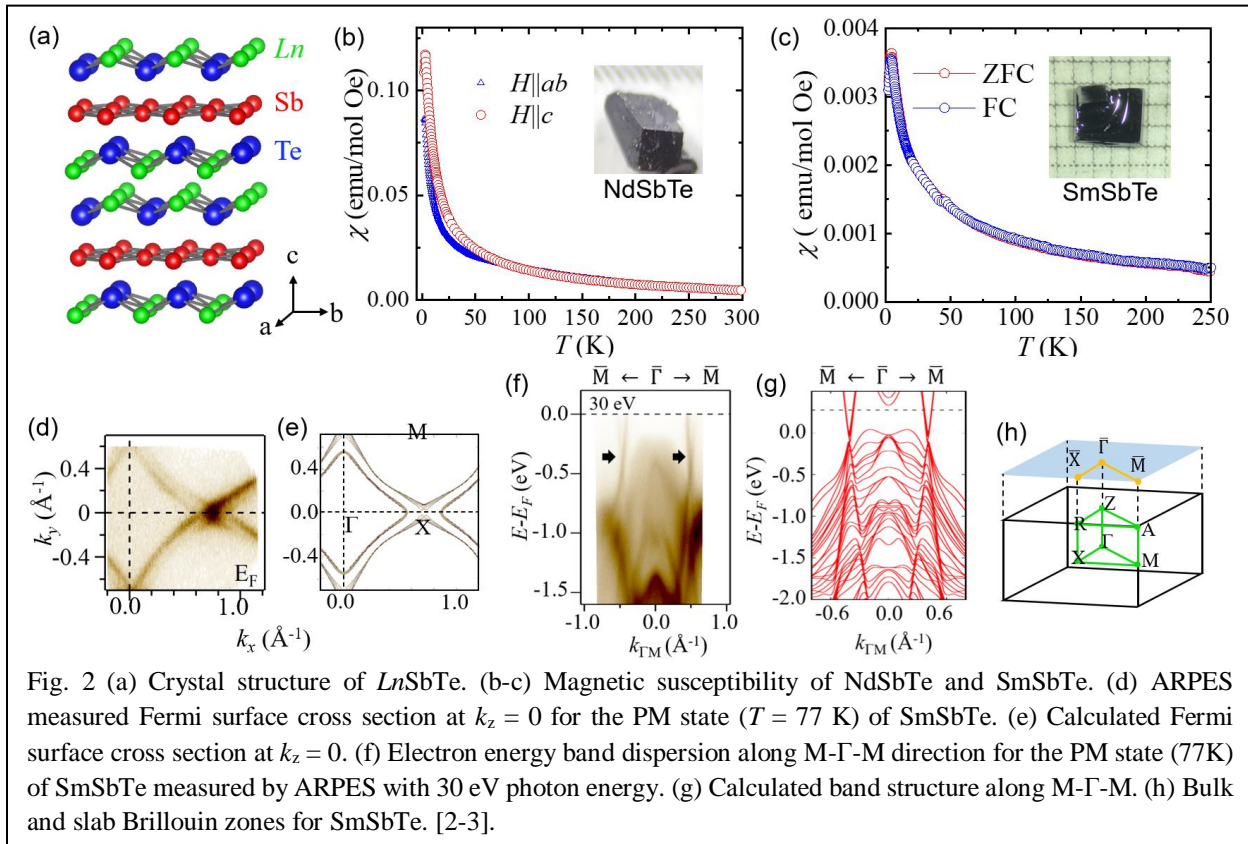
It is worth noting that this surface state is robust and display high mobility. Despite of the amorphous layers formed on the top of thin flakes as revealed by TEM observations (Fig. 1c), SdH oscillations from the surface band can be probed. Quantum oscillations from a topologically trivial surface state is rarely seen. Here, the surface band exhibits robust SdH oscillation, high quantum mobility and transport mobility, despite it is topologically trivial. Future studies to clarify the mechanism of such disorder-insensitive and high mobility bands are desired.

In summary, we probed transport of the 2D floating band, a new class of surface state. Our work provides a new arena for the study of exotic surface states in topological quantum materials,

which is an important step towards practical application in modern electronics and surface-related device such as quantum computing and spintronics.

(ii) Turn on TRS in ZrSiS-family topological semimetals

The non-magnetic ZrSiS and related compounds exhibit two types of Dirac states: (i) a gapless Dirac point state protected by nonsymmorphic symmetry, and (ii) a Dirac nodal-line generated by the glide mirror symmetry, which is gapped by spin-orbit coupling (SOC). In addition to those non-magnetic materials, the spin degree of freedom can be activated in isostructural $LnSbTe$ (Ln = magnetic lanthanide element, Fig. 2a) [5,6]. The interplay between spin and topological degrees of freedom may generate new quantum state and phenomena.



We have successfully grown large single crystals for previously unexplored NdSbTe and SmSbTe and verified the tetragonal crystal structure similar to ZrSiS. We clarified their antiferromagnetic (AFM) ground state through magnetization and heat capacity measurements (Figs. 2b-c). Belonging to the ZrSiS-topological material family, the existence of Dirac fermion has been verified by our ARPES study. ARPES observations at high temperature paramagnetic states of SmSbTe reveal a clean Fermi surface consist of Dirac bands only (Figs. 2d, f), which is consistent with our band structure calculations (Figs. 2e, g).

Our heat capacity experiments have revealed additional interesting properties. By using non-magnetic LaSbTe as a reference, we have extracted the electronic and magnetic specific heat

for NdSbTe and SmSbTe, as shown in Figs. 3a-b. Surprisingly, both compounds exhibit large Sommerfeld coefficient, reaching 115 mJ/mol K² for NdSbTe and 160 mJ/mol K² for SmSbTe. Such values are greatly larger than conventional simple metals (~1 mJ/mol K²), implying enhanced electronic effective mass and correspondingly enhanced electronic correlations. This is further supported by the calculated electronic energy bands in the AFM ground state for SmSbTe, which clearly reveals flat bands near the Fermi energy owing to the *f*-electrons of Sm.

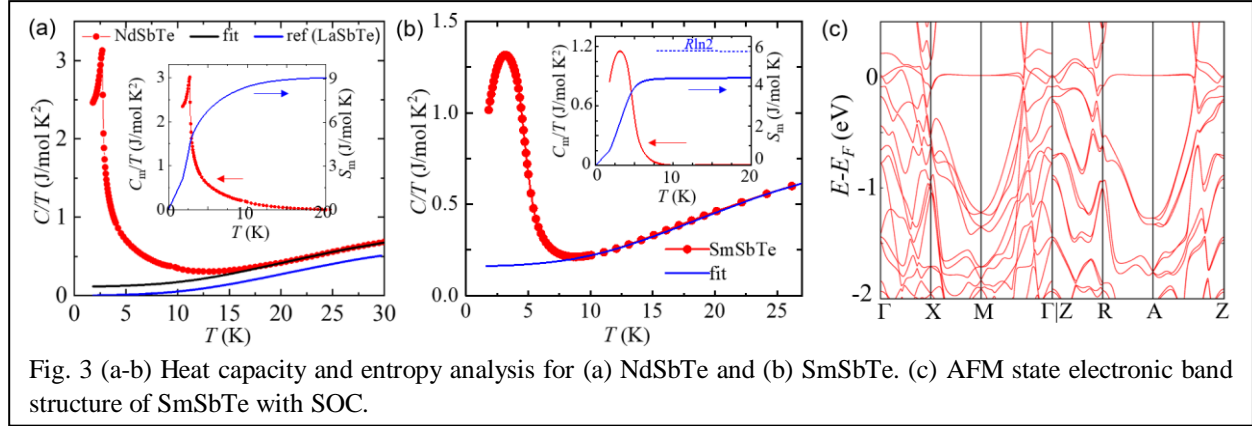


Fig. 3 (a-b) Heat capacity and entropy analysis for (a) NdSbTe and (b) SmSbTe. (c) AFM state electronic band structure of SmSbTe with SOC.

Our results indicate that *LnSbTe* materials exhibit a unique coexistence of degrees of diverse quantum freedom such as spin, topology, and charge correlations. Hence these materials provide promising platforms not only for searching new quantum states and phenomena, but also for exploring technology applications exploiting its tunable topological quantum states.

Future Plans

Our results describe above open new research directions. For novel surface state due to translation symmetry-breaking, clarifying mechanism for its robustness and high mobility would be an important direction, for which we will: (1) extend the study to various devices such as gate-modulated devices and with various surfaced treatment; (2) chemical doping to modulate the location of the Fermi energy of the crystals for device fabrication; (3) study other surfaces in addition to the (001) surface.

For magnetic *LnSbTe*, future plans include: (1) clarifying the coupling between composition stoichiometry and topological states, and investigating the possible orthorhombic distortion and charge density wave; (2) tuning magnetism by doping to better clarify the coupling between topology and TRS, based on which to (3) explore new quantum phase and quantum phenomena arising from the interplay between spin, topology, charge, lattice, and correlations.

References

- [1] X. Liu *et al.*, Nano Lett. **21**, 4887 (2021).
- [2] K. Pandey *et al.*, Phys. Rev. B **101**, 235161 (2020).
- [3] K. Pandey *et al.*, Adv. Quantum Technol., 2100063 (2021).
- [4] A. Topp *et al.*, Phys. Rev. X **7**, 041073 (2017).
- [5] L. M. Schoop *et al.*, Sci. Adv. **4**, eaar2317 (2018).
- [6] M. M. Hosen *et al.*, Sci. Rep. **8**, 13283 (2018).

Publications

11 Publications supported by DE-SC0019467 in the past two years 09/2019-09/2021

1. K. Pandey, D. Mondal, J. W. Villanova, J. Roll, R. Basnet, A. Wegner, G. Acharya, M. R. U. Nabi, B. Ghosh, Jun Fujii, J. Wang, B. Da, A. Agarwal, I. Vobornik, A. Politano, S. Barraza-Lopez, and J. Hu, “*Magnetic Topological Semimetal Phase with Electronic Correlation Enhancement in SmSbTe*”, *Advanced Quantum Technologies*, 2100063 (2021)
2. B. Ji, K. Pandey, C.P. Harmer, F. Wang, K. Wu, J. Hu, J. Wang, “*Centrosymmetric or Noncentrosymmetric? Transition Metals Talking in $K_2TGe_3S_8$ ($T=Co, Fe$)*”, *Inorganic Chemistry*, 60, 10603 (2021)
3. S. H. Lee, D. Graf, L. Min, Y. Zhu, H. Yi, S. Ciocys, Y. Wang, E. S. Choi, R. Basnet, A. Fereidouni, A. Wegner, Y.-F. Zhao, K. Verlinde, J. He, D. Graf, R. Redwing, V. Gopalan, H. O. H. Churchill, A. Lanzara, N. Samarth, C.-Z. Chang, J. Hu, and Z.Q. Mao, “*Evidence for a Magnetic-Field induced Type-II Weyl State in Antiferromagnetic Topological Insulator $Mn(Bi_{1-x}Sb_x)_2Te_4$* ”, *Physical Review X*, 11, 031032 (2021)
4. R. Basnet, A. Wegner, K. Pandey, S. Storment, J. Hu, “*Highly sensitive spin-flop transition in antiferromagnetic van-der Waals material MPS_3 ($M = Ni$ and Mn)*”, *Physical Review Materials*, 5, 064413 (2021)
5. J.Y. Liu, J.B. Yu, J.L. Ning, L.X. Miao, A. Kleysner, L.J. Min, Y.L. Zhu, H.M. Yi, T. Pillsbury, Y. B. Zhang, Y. Wang, J. Hu, H.B. Cao, F. Balakirev, F. Weickert, M. Jaime, K. Yang, J.W. Sun, N. Alem, V. Gopalan, C.Z. Chang, N. Samarth, J. Jain, C.X. Liu, R.D. McDonald and Z.Q. Mao, “*Spin-valley locking and bulk quantum Hall effect in a noncentrosymmetric Dirac semimetal $BaMnSb_2$* ”, *Nature Communications*, 12, 4062 (2021)
6. X. Liu, C. Yue, S.V. Erohin, Y. Zhu, A. Joshy, J. Liu, A. M. Sanchez, D. Graf, P.B. Sorokin, Z. Mao, J. Hu, J. Wei, “*Quantum transport of the 2D surface state in a nonsymmorphic semimetal*”, *Nano Letters*, 21, 4887 (2021)
7. Y. Wang, J. Balgley, E. Gerber, M. Gray, N. Kumar, X. Lu, J.-Q. Yan, A. Fereidouni, R. Basnet, S. J. Yun, D. Suri, H. Kitadai, T. Taniguchi, K. Watanabe, X. Ling, J. Moodera, Y. H. Lee, H. O. H. Churchill, J. Hu, L. Yang, E.-A. Kim, D. G. Mandrus, E. A. Henriksen, and K. S. Burch, “*Modulation Doping via a Two-Dimensional Atomic Crystalline Acceptor*”, *Nano Letters*, 20, 8446 (2020)
8. K. Pandey, R. Basnet, A. Wegner, G. Acharya, M. R. U. Nabi, J. Liu, J. Wang, Y. Takahashi, B. Da, and J. Hu, “*Electronic and magnetic properties of the topological semimetal candidate $NdSbTe$* ”. *Physical Review B*, 101, 235161 (2020)
9. S. Davari, J. Stacy, A. M. Mercado, J. D. Tull, R. Basnet, K. Pandey, J. Hu, and H. O. H. Churchill, “*Gate-defined, accumulation mode quantum dots in monolayer and bilayer WSe_2* ”. *Physical Review Applied*, 13, 054058 (2020)
10. Y. Zhu, X. Gui, Y. Wang, D. Graf, W. Xie, J. Hu, Z. Mao, *Evidence from transport measurements for YRh_6Ge_4 being a triply degenerate nodal semimetal*, *Physical Review B*, 101, 035133 (2020)

11. R. Basnet, M. H. Doha, T. Hironaka, K. Pandey, S. Davari, K. M. Welch, H. O. H. Churchill, J. Hu, “*Growth and Strain Engineering of Trigonal Te for Topological Quantum Phases in Nonsymmorphic Chiral Crystals*”. *Crystals*, 9, 486 (2019)

Proximity effects and topological spin currents in van der Waals heterostructures

Benjamin Hunt, Carnegie Mellon University

Program Scope

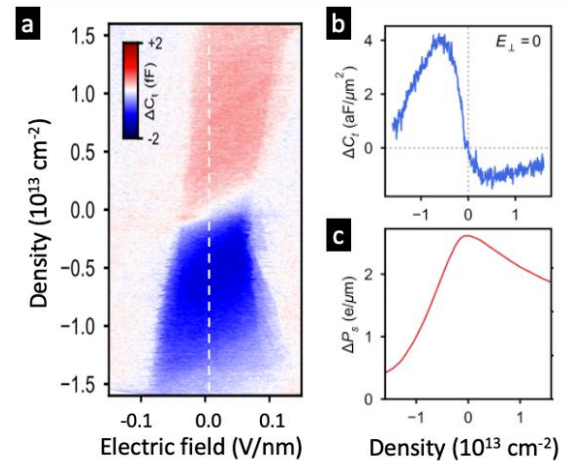
The major goals of this project are to study spin-polarized topological edge states, specifically those of the quantum anomalous Hall (QAH) effect, which has been proposed to be realizable via a (simultaneous) magnetic and spin-orbit proximity effect in graphene¹. En route to realizing the QAH effect, the goal was also to study the newly-discovered 2D van der Waals magnetic insulators, and the extent to which magnetic effects could be seen in graphene via proximity coupling. The QAH effect was initially observed in magnetic topological insulators, and since the beginning of this project has been subsequently observed in several layered materials and van der Waals heterostructures: in “magic-angle” twisted bilayer graphene aligned to boron nitride²; in MnBi_2Te_4 ³; and in a moiré heterostructure of $\text{MoTe}_2/\text{WSe}_2$ ⁴. Observation of the QAHE as a consequence of magnetic + spin-orbit proximity effects in graphene is still outstanding and would mark a significant step in our understanding of the emergence of topological states in heterostructures.

The broader scientific context of the experiments in this proposal is to understand the physical mechanisms behind proximity effects in van der Waals heterostructures. Perhaps the ultimate scientific and technological goal of realizing topological states through proximity effects is the creation of Majorana zero modes in solid-state devices, which has been identified as a major priority in condensed-matter physics because of the potential use of Majorana zero modes in topological quantum computing⁵. Van der Waals materials offer advantages in this area because of the diversity of materials that can potentially be used and the unique device architectures that are possible using the van der Waals assembly techniques. There are several possible routes to Majorana modes using topological edge states: one involves proximity-coupling the QAH edge state to a superconductor; another involves proximity-coupling the quantum spin Hall (QSH) edge state to a superconductor and interrupting it with a magnetic insulator⁵. We have expanded our investigation of spin-polarized topological states by investigating the nature of the QSH in the only 2D van der Waals material in which it is known to occur, monolayer $1\text{T}'\text{-WTe}_2$ ⁶. We have studied its energy gaps using quantum capacitance and we have coupled it to a van der Waals superconductor, NbSe_2 . We have also studied as-grown bilayer and twisted bilayer WTe_2 using capacitance and STM. The goals of this related effort in WTe_2 are (1) to understand the magnitude and mechanism of the energy gaps in WTe_2 , (2) to understand the nature of the proximity-induced superconducting gap in the QSH edge state, measured directly for the first time and presented in ref. ⁷, and (3) to understand the interplay of the QSH effect with other phenomena present in WTe_2 , such as ferroelectricity, by studying the behavior of the QSH edge states as the twist angle between the two layers is varied.

Recent Progress

Capacitance Measurements of Ferroelectric Bilayer WTe₂. Conducting bilayer WTe₂ exhibits a switchable, out-of-plane electric polarization, rendering it a rare example of a ferroelectric metal. The single previous study⁸ of the ferroelectricity in this material relied on an indirect technique for an approximate measurement of its polarization. This work used the change induced in the conductance of a proximal graphene layer by the polarization reversal in the WTe₂, a technique which does not easily permit measurement of the dependence of the polarization on WTe₂ carrier density. We used a layer-sensitive capacitance technique to directly measure the layer-specific electronic compressibility, and thus could infer the charge distribution on the two layers, as the overall carrier density is varied. Our layer-resolved capacitance measurements agree remarkably well with a model of the bilayer WTe₂ Hamiltonian, which allows us to reveal the roles of interlayer coupling and spin-orbit coupling in the layer distribution of the wavefunctions that determine the out-of-plane ferroelectric polarization. Both the capacitance-based measurement technique and the theoretical understanding are widely applicable to the emerging field of ferroelectricity in two-dimensional materials. This work is now published at *Nature Communications* **12**, 5298 (2021).

Fig. 1 (a). Capacitance C_i between WTe₂ and top gate is measured while varying electric field E and density n . Pictured here is the difference ΔC_i between up and down sweeps of E ; the red and blue regions represent the hysteretic behavior and thus the difference between the two ferroelectric polarization states. (b). Line cut of (a) at $E=0$. (c). Integration of the curve in (b) is proportional to the polarization change ΔP between the two states.



Scanning Tunneling Microscopy Studies: (1)

Quantum Spin Hall States in Twisted Bilayer WTe₂, and (2) Graphene/CrBr₃ Heterostructure.

In the first STM study, we explored the quantum spin Hall (QSH) states in twisted bilayer (tBL) WTe₂, which was a natural follow-up to our work on proximity-induced superconductivity in the QSH states of monolayer WTe₂. The latter was presented at the 2019 ECMP-PI meeting and now published in *Nature Physics* **16**, 526 (2020). We studied twisted bilayer (tBL) WTe₂ in two distinct configurations: one in which an edge of a monolayer was folded back on itself, and another in which we purposely used the “tear and stack” method to prepare the twisted bilayer. Due to the broken out-of-plane mirror symmetry, these two methods produce distinct atomic configurations for a given twist angle.

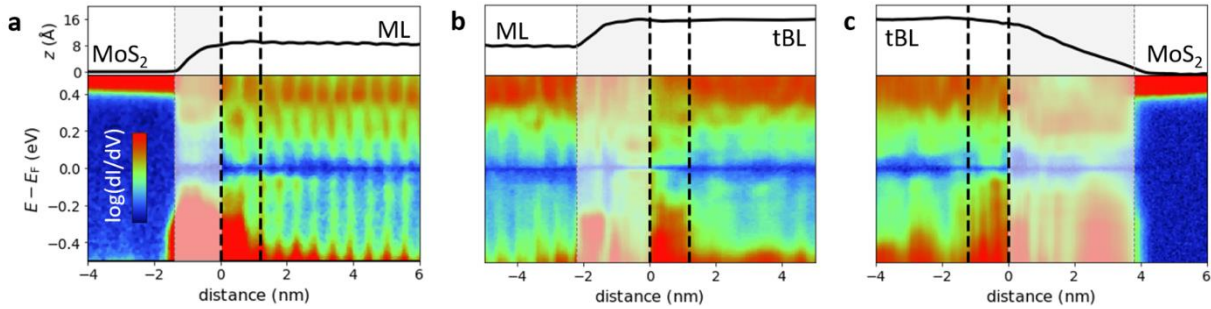


Fig. 2. STM spectra (dI/dV vs energy and position) in an MoS_2 /monolayer WTe_2 /tBL WTe_2 heterostructure, where the tBL layer is created by a naturally occurring fold of the monolayer back on itself (at an angle of 66 degrees). The enhancement of dI/dV (between the black dashed lines) for tunneling into the valence band is interpreted as evidence of QSH edge states, as for ML WTe_2 in other studies (refs. 6,7). This occurs at both the ML/tBL interface (b) and at the tBL/ MoS_2 interface (c) (i.e. along the fold).

We used scanning tunneling microscopy and spectroscopy (STM/STS) to study tBL WTe_2 with four different orientations (in the folded configuration) and one in the “tear and stack” configuration and compared it to a topologically trivial as-grown bilayer. We observed edge states in the twisted bilayers which correspond to the characteristic spectroscopic signature of the QSH edge state, namely an enhancement of the density of states at negative tunneling bias. This includes the observation of QSH edge states along a coinciding edge (i.e. along a fold) where two sets of QSH edge states sit on top of the other (Fig. 2c). By comparing our experimental observations to first-principles calculations, we concluded that the twisted bilayers are weakly coupled, preserving the topological nature of the individual layers. This work is current under review and is on at arXiv:2010.13699.

In the second study, we used STM/STS to investigate heterostructures of graphene and van der Waals magnetic insulators (specifically CrI_3 and CrBr_3), as we had proposed to do in the “Future Plans” of the 2019 ECMP-PI meeting. We prepared 10 devices of which 8 exhibited clear degradation of the magnetic insulator, particularly for G/CrI_3 devices, which was presumably due to even a short exposure to the few ppm of $\text{O}_2/\text{H}_2\text{O}$ in the glove box in which the devices were built. The remaining two devices, both G/CrBr_3 , showed that the graphene was strongly p-doped due to a large charge transfer to the CrBr_3 ; the Dirac point appeared at a tip bias of roughly +250 mV. This result is consistent with transport measurements of graphene on similar magnetic insulators⁹ and with our own (unpublished) transport measurements of G/CrI_3 . These studies are ongoing.

Future Plans

In the next year of this program, we are planning three approaches to the study of proximity effects and topological edge states in van der Waals heterostructures. First, we plan to continue to use STM to study graphene/magnetic insulator van der Waals heterostructures, extending our studies to STM in the presence of electrostatic gating and external magnetic field. Second, using our van

der Waals assembly techniques developed for QSH/superconductor (WTe₂/NbSe₂) heterostructures, we plan to investigate the QAHE edge states in MoTe₂/WSe₂ heterostructures. Finally, with the support of this DOE grant we have recently developed a new technique for *planar* tunneling into van der Waals heterostructures based on the via contact method¹⁰, which will allow us to study topological phases in regimes that have traditionally been difficult using STM, such as at dilution refrigerator temperatures and in tilted magnetic fields.

References

1. Zhang, J., Zhao, B., Yao, Y. & Yang, Z. Robust quantum anomalous Hall effect in graphene-based van der Waals heterostructures. *Phys. Rev. B* **92**, 165418 (2015).
2. Serlin, M. *et al.* Intrinsic quantized anomalous Hall effect in a moiré heterostructure. *ArXiv190700261 Cond-Mat* (2019).
3. Deng, Y. *et al.* Quantum anomalous Hall effect in intrinsic magnetic topological insulator MnBi₂Te₄. *Science* **367**, 895–900 (2020).
4. Li, T. *et al.* Quantum anomalous Hall effect from intertwined moiré bands. *ArXiv210701796 Cond-Mat* (2021).
5. Alicea, J. New directions in the pursuit of Majorana fermions in solid state systems. *Rep. Prog. Phys.* **75**, 076501 (2012).
6. Tang, S. *et al.* Quantum spin Hall state in monolayer 1T'-WTe₂. *Nat. Phys.* **13**, 683–687 (2017).
7. Lüpke, F. *et al.* Proximity-induced superconducting gap in the quantum spin Hall edge state of monolayer WTe₂. *Nat. Phys.* **16**, 526–530 (2020).
8. Fei, Z. *et al.* Ferroelectric switching of a two-dimensional metal. *Nature* **560**, 336 (2018).
9. Zhou, B. *et al.* Evidence for charge transfer and proximate magnetism in graphene-- α -RuCl₃ heterostructures. *Phys. Rev. B* **100**, 165426 (2019).
10. Telford, E. J. *et al.* Via Method for Lithography Free Contact and Preservation of 2D Materials. *Nano Lett.* **18**, 1416–1420 (2018).

Publications Acknowledging DOE Support (since Sept. 2019)

S.C. de la Barrera, Q. Cao, Ya. Gao, Yu. Gao, V. Bheemarasetty, J. Yan, D.G. Mandrus, W. Zhu, D. Xiao, and B. Hunt, “Direct Measurement of Ferroelectric Polarization in a Tunable Semimetal”, *Nature Communications* **12**, 5298 (2021). <https://doi.org/10.1038/s41467-021-25587-3>

Z. Sun, J. Beaumariage, Q. Wan, H. Alnatah, N. Houglund, J. Chisholm, Q. Cao, K. Watanabe, T. Taniguchi, B. Hunt, I.V. Bondarev, and D.W. Snoke, “Charged Bosons Made of Fermions in a Solid State System without Cooper Pairing”, *Nano Letters, advanced online publication* (Sept. 13th 2021). doi.org/10.1021/acs.nanolett.1c02422

M.R. Sinko, S.C. de la Barrera, O. Lanes, K. Watanabe, T. Taniguchi, S. Tan, D. Pekker, M. Hatridge, and B. Hunt, “Superconducting Contact and Quantum Interference Between a Two-Dimensional van der Waals Superconductor and a Conventional Metal”, *Phys. Rev. Materials* **5**, 014001 (2021). doi.org/10.1103/PhysRevMaterials.5.014001

Z. Sun, J. Beaumariage, Q. Cao, K. Watanabe, T. Taniguchi, B. Hunt, and D.W. Snoke, “Interlayer Exciton Gases in WSe₂-pWSe₂ Heterostructures”, *ACS Photonics* **7**, 1622 (2020). doi.org/10.1021/acsp Photonics.0c00476

D. Aasen, R.S.K. Mong, B. Hunt, D. Mandrus, and J. Alicea, “Electrical Probes of the Non-Abelian Spin Liquid in Kitaev Materials”, *Phys. Rev. X* **10**, 031014 (2020). doi.org/10.1103/PhysRevX.10.031014

F. Lüpke, D. Waters, S.C. de la Barrera, M. Widom, D.G. Mandrus, J. Yan, R.M. Feenstra, and B. Hunt, “Proximity-induced Superconducting Gap in the Quantum Spin Hall Edge State of Monolayer WTe₂”, *Nature Physics* **16**, 526 (2020). doi.org/10.1038/s41567-020-0816-x

J. Liang, K. Xu, M. Wu, B. Hunt, W.-H. Wang, K. Cho, and S.K. Fullerton-Shirey, “All-Solid-State Non-Volatile Two-Dimensional Crystal Memory Gated by a Monolayer Electrolyte”, *Nano Letters* **19**, 8911 (2019). doi.org/10.1021/acs.nanolett.9b03792

F. Lüpke, D. Waters, Ahn T. Pham, D.G. Mandrus, J. Yan, P. Ganesh, and B. Hunt, “Quantum Spin Hall Edge States in Twisted Bilayer 1T'-WTe₂”, arXiv:2010.13699 (2020), *in review*.

“Intrinsic Flat Bands and Magnetic Proximity in Two-Dimensional Materials”, Edward J. Seifert, Ph.D. thesis, Carnegie Mellon University (2021).

Electronic Growth of Metals on 2D Semiconductors

T. Kidd, A. Stollenwerk, P. Shand, L. Strauss, P. Lukashev

University of Northern Iowa, Cedar Falls, IA, 50614

Program Scope

The goal of this project is to investigate the novel properties which exist at the interface between van der Waals crystals and various metals grown upon their surface. Our first goal for year one was to finalize work on the Au/MoS₂ system, which exhibits quantized electronic growth at nanometer scale coverages, but evolves into epitaxial layer-by-layer growth above 10 nm thicknesses. To extend this work, we intended to explore additional noble metals on MoS₂, as well as if nickel could exhibit similar growth mechanisms to create novel magnetic properties. The abrupt interface between the metal and layered dichalcogenide could be optimal for spin injection into the metallic layers, for example. We also intended to explore different chalcogen based layered materials, starting with WSe₂, to ascertain the origins of different growth behaviors.

We also wanted to explore the use of density functional theory (DFT) calculations to explain and predict novel behaviors we have been measuring with scanning tunneling microscopy (STM). Our intent was to compare structural properties measured with STM, the Fermi surface topology of the given metal, and the DFT calculations of binding energy, diffusion energy barrier, and density of states (DOS) to try and develop a microscopic theory to explain why these systems could exhibit quantized electronic growth modes at, and even above, room temperature, when nearly all other systems exhibiting such behavior were constrained to cryogenic growth conditions.

We had also intended to explore the potential of magnetic layered crystals as substrates, but unfortunately our crystal growth program was mostly suspended owing to Covid restrictions. We also were not able to travel to DOE user facilities at Argonne or Brookhaven National Laboratory, but we were at least able to take advantage of the computational facilities at BNL. We had also intended to perform optical and Raman based measurements at Texas Tech, but these trips also had to be delayed until Covid-related restrictions are lifted. Currently, many restrictions have been lifted for travel, but there is a backlog for access. Hopefully we will be able to catch up in our work over the next year in these areas.

Recent Progress

We have greatly advanced our knowledge of the Au/MoS₂ system. While we have not developed a microscopic theory, we are now able to produce samples exhibiting either quantized nanostructures or ultra-flat surfaces using multiple deposition techniques. With regards to the ultra-flat Au surfaces, we find an RMS surface roughness with an upper limit of 50 pm and no signs of grain boundaries over scans exceeding 16 square microns. We believe these results, published in a recent issue of Langmuir, could be used for the investigation and characterizations of self-assembled monolayers (SAMS), which often utilize a thiol group to attach to gold substrates. The critical features for such gold substrates are surface uniformity (i.e. lack of granularity) and minimal surface roughness. Our results, with no signs of granularity over 16 square microns and a surface roughness of less than 50 pm, greatly exceed current technologies. Perhaps the leading manufacturer in this area, Platypus technologies, advertises ultraflat surfaces with grains spanning only a few 100 nm laterally at best, and surface roughness exceeding 1,000 pm.[1] Our samples are far more uniform, and far more atomically flat, which has led us to filing a provisional patent to protect intellectual property as we investigate the potential of this new technology.

We have made significant progress in understanding the critical features related to inducing quantized electronic growth modes at temperatures compatible with standard semiconductor device fabrication processes. We found that all noble metals tested (Pd, Ag, and Au) exhibit quantized electronic growth on MoS₂, while Ni formed clusters as seen for Volmer-Webber growth modes. This was quite interesting in that usually such clustering is seen in the growth of metals on inert surfaces, such as glasses, with weak interfacial bonding and significant surface mobility. Traditionally, when relatively unreactive metals, such as the noble metals, find it far more preferential to bond to each other rather than the substrate and so form hemispherical clusters to minimize surface free energy. Here, we are seeing the opposite effect!

Our DFT calculations show that nickel has the largest binding energy to the MoS₂ surface, yet it forms clusters. Pd has the 2nd highest bonding energy, and it shows weak electronic growth. Ag and Au have the weakest bonding to the surface, yet both exhibit the strongest electronic growth modes. Furthermore, all of the systems have lattice mismatch exceeding 8%, so any form of epitaxial growth would not be expected without cryogenic deposition temperatures. Still, Au, Ag, and Pd all form nanostructures with atomically flat surfaces and Au even shifts to fully epitaxial growth as described above. So for whatever reason, the energy savings associated with gapping the electronic structure must be relatively high in these systems. Apparently, the interfacial bonding is weak enough to minimize the impact of strain, but even so surface free energy alone would normally dominate growth processes at these temperatures.

We performed a variety of DFT calculations to assess the electronic density of states (DOS). For Ni/MoS₂, the mismatch was sufficiently large that we could perform a strain free calculation matching a 4x4 MoS₂ unit cell to a 5x5 Ni unit cell as shown in Figure 1. The Ni DOS is very

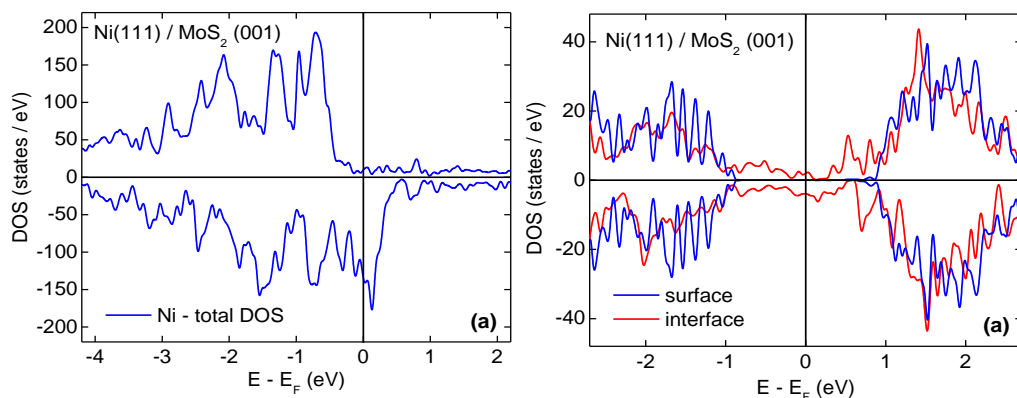


Figure 1. DFT calculations of DOS in the Ni/MoS₂ system. System is composed of a three atom thick Ni film with 5x5 Ni unit cell. Two layers of MoS₂ were used, with a 4x4 unit cell to match the two lattices for a strain-free calculation. **Left Panel:** Density of states in the Ni film. **Right Panel:** Bottom MoS₂ is gapped and bulk-like. The interfacial layer bonded to Ni is both metallic and spin polarized.

bottom layer remained semiconducting and appeared more like bulk MoS₂. This indicates that the metallic states and spin-polarization extend into the uppermost MoS₂ layer, likely due to hybridization from interfacial bonding. This could indicate the potential for novel magnetic or spintronic properties, there is no sign of discrete electronic states that would be associated with electronic growth. This would be expected given that we do not see evidence for electronic growth in the Ni/MoS₂ system from STM measurements.

The lattice mismatch in Au was too small to achieve strain free calculations with an overwhelming number of atoms to include in the calculation. Instead we used a 1x1 lattice cell with varying thicknesses of Au atop two layers of MoS₂ molecules. We calculated a number of

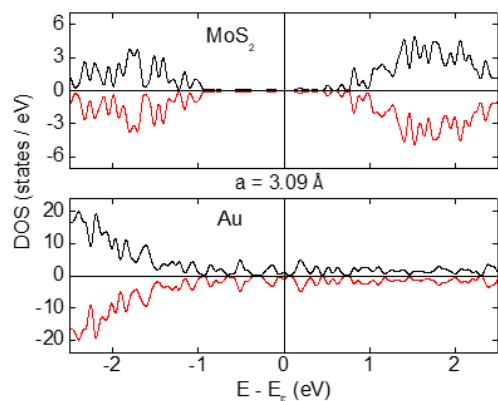


Figure 2. DFT calculations of DOS in the Au/MoS₂ system. Graphs are representative of a variety of lateral lattice constants and Au thicknesses ranging from 3 to 15 atoms. **Top Panel:** Au DOS. **Bottom Panel:** DOS in uppermost MoS₂ layer.

lateral lattice constants varying the system between pure Au and pure MoS₂ to explore the potential DOS (Fig. 2). No matter the thickness of the Au film or the value of the lateral lattice constant, the results consistently showed discrete states existed within both the Au film and the uppermost MoS₂ layer, while once again the bottom MoS₂ layer remained semiconducting and bulk-like. In addition to showing discrete states in the metallic regions of the system, the Au DOS was far smaller near the Fermi level than bulk Au. This behavior is exactly what one would expect for a system dominated by electronic growth modes, with significant energy savings seen by inducing discrete electronic states gapped (or nearly so) at the Fermi level. Another interesting feature is that the metallic states creep into the uppermost MoS₂ layer. This indicates the electronic

similar to the bulk, which was somewhat surprising given the Ni film was composed only three atoms thick. The uppermost MoS₂ layer, which was bonded to Ni, was calculated to be metallic, while the

character of the Au/MoS₂ interface is not necessarily abrupt, although it is abrupt between the two uppermost MoS₂ molecules.

We have also begun preliminary measurements in the WSe₂ system. The Ni behaves almost exactly the same, but Au behaves somewhat differently. In Au/WSe₂, we see the same type of atomically flat features, but we have not been able to find common size intervals which would indicate electronic growth. Bonding and diffusion characteristics are similar across the MoS₂ and WSe₂ systems, so we will perform additional DFT calculations to determine if there are fundamental differences in the electronics structure or confinement in the WSe₂ system.

Future Plans

Aside from catching up to our original goals, our discoveries in the past two years have given us new directions to explore. First, we intend to partner with scientists involved with SAMS research to determine the effectiveness of our ultra-flat Au/MoS₂ surfaces and see if they out-compete current substrate technologies. Second, we will performed DFT calculations on the WSe₂ system, and the remaining noble metals Ag & Pd, to determine if there are fundamental differences with regards to bonding, confinement, or other features inherent to the substrate. Third, we intend to examine alternate sulfur terminated layered semiconductors. Sulfur is one of the few elements to effectively bond to gold, meaning that there could be significant differences in the growth modes based on the chalcogen which exists at the surface layers.

References

1. **“STM microscopy of ultra-flat gold surfaces” Platypus Technologies,**
<https://www.platypustech.com/scanning-tunneling-microscopy-of-ultra-flat-gold-surfaces>

Publications

1. “First principles study of nearly strain-free Ni/WSe₂ and Ni/MoS₂ interfaces,” AJ Stollenwerk, L Stuelke, L Margaryan, TE Kidd, PV Lukashev, *Journal of Physics: Condensed Matter* **33** 425001 (2021)
2. “Preparation of Ultrathin Gold Films with Subatomic Surface Roughness,” TE Kidd, J Weber, E O’Leary, AJ Stollenwerk, *Langmuir* **37** 9472 (2021)
3. “Electronic growth of Pd(111) nanostructures on MoS₂,” TE Kidd, S Scott, S Roberts, R Carlile, PV Lukashev, AJ Stollenwerk, *Journal of Applied Physics* **129** 174303 (2021)
4. “Self-assembled Ag (111) nanostructures induced by Fermi surface nesting,” TE Kidd, E O’Leary, A Anderson, S Scott, AJ Stollenwerk, *Physical Review B* **100**, 235447 (2019)

Correlated Many-body Quantum States in Graphene Heterostructure

Philip Kim, Department of Physics, Harvard University

Program Scope

Atomically thin van der Waals (vdW) materials provide a new fundamental platform to realize novel quantum emergent phenomena. Particularly, the ability to assemble dissimilar vdW layers enables building vdW heterostructures with atomically sharp interfaces. Such a capability allows us to fabricate various vertical functional heterostructure devices, including electron double layer systems. In electronic double layer systems, unusual pairing can be created across the atomically thin vdW interface, utilizing strong Coulomb interactions. In this project, we pursue three different approaches to explore unusual many-body quantum correlations in graphene-based van der Waals heterostructures. The first approach is to create Josephson junctions in the superfluid formed by magnetoexcitons Bose-Einstein condensation (BEC) in a graphene double layer. Here, we will employ robust many-body condensation to couple quantum states across the atomically thin van der Waals interface in the quantum Hall effect regime. The second approach uses the anyonic quasiparticle excitation in the FQHE in graphene. The relatively large energy gap of FQHE in graphene allows us to build a versatile mesoscopic device where anyons can be manipulated coherently. We will create a completely gate-defined, phase-sensitive quantum Hall interferometer to probe exchange statistics of abelian and non-abelian anyons in the FQHE regime. Finally, we plan to make coupled 2D-to-1D or -0D hybrid devices to study strong correlations across dimensionality. Two different platforms will be adopted for this part of projects: 2D Dirac-Fermi (DF) liquid with 1D Luttinger liquid in graphene/nanotube; and DF liquid to a Sachdev-Ye-Kitaev (SYK) state in graphene quantum dots under high magnetic fields [23]. Here we will use a combination of electronic and thermal transport in these hybrid devices to investigate the strongly correlated nature of the couple many-body states.

Recent Progress

Emergent correlated electronic states in twisted multi-layer graphene: Engineering moire superlattices by twisting and stacking two layers of Van der Waals materials has proved to be an effective way to promote interaction effects and induce exotic phases of matter. After the discovery of superconductivity and correlated insulators in magic-angle twisted bilayer graphene (MA-TBG), several different two-dimensional materials have been utilized to create two-layer twisted systems and various novel phases [1,2]. However, superconductivity, which sparked much of the initial excitement, is still not well understood, nor has it been conclusively realized in a twisted system other than MA-TBG. Reducing the energy bandwidth of electrons in a lattice below the long-range Coulomb interaction energy promotes correlation effects. Moiré superlattices, which are created by stacking van der Waals heterostructures with a controlled twist angle, enable the engineering of electron band structure. Exotic quantum phases can emerge in an engineered moiré flat band. The recent discovery of correlated insulator states, superconductivity and the quantum

anomalous Hall effect in the flat band of magic-angle twisted bilayer graphene has sparked the exploration of correlated electron states in other moiré systems. The electronic properties of van der Waals moiré superlattices can further be tuned by adjusting the interlayer coupling or the band structure of constituent layers. Extending the recent theoretical prediction, using van der Waals heterostructures of twisted double bilayer graphene (TDBG), we demonstrate a flat electron band that is tunable by perpendicular electric fields in a range of twist angles as shown in Fig. 1. Similarly to magic-angle twisted bilayer graphene, TDBG shows energy gaps at the half- and quarter-filled flat bands, indicating the emergence of correlated insulator states. We find that the gaps of these insulator states increase with in-plane magnetic field, suggesting a ferromagnetic order. On doping the half-filled insulator, a sudden drop in resistivity is observed with decreasing temperature. This critical behaviour is confined to a small area in the density–electric-field plane, and is attributed to a phase transition from a normal metal to a spin-polarized correlated state. The discovery of spin-polarized correlated states in electric-field-tunable TDBG provides a new route to engineering interaction-driven quantum phases.

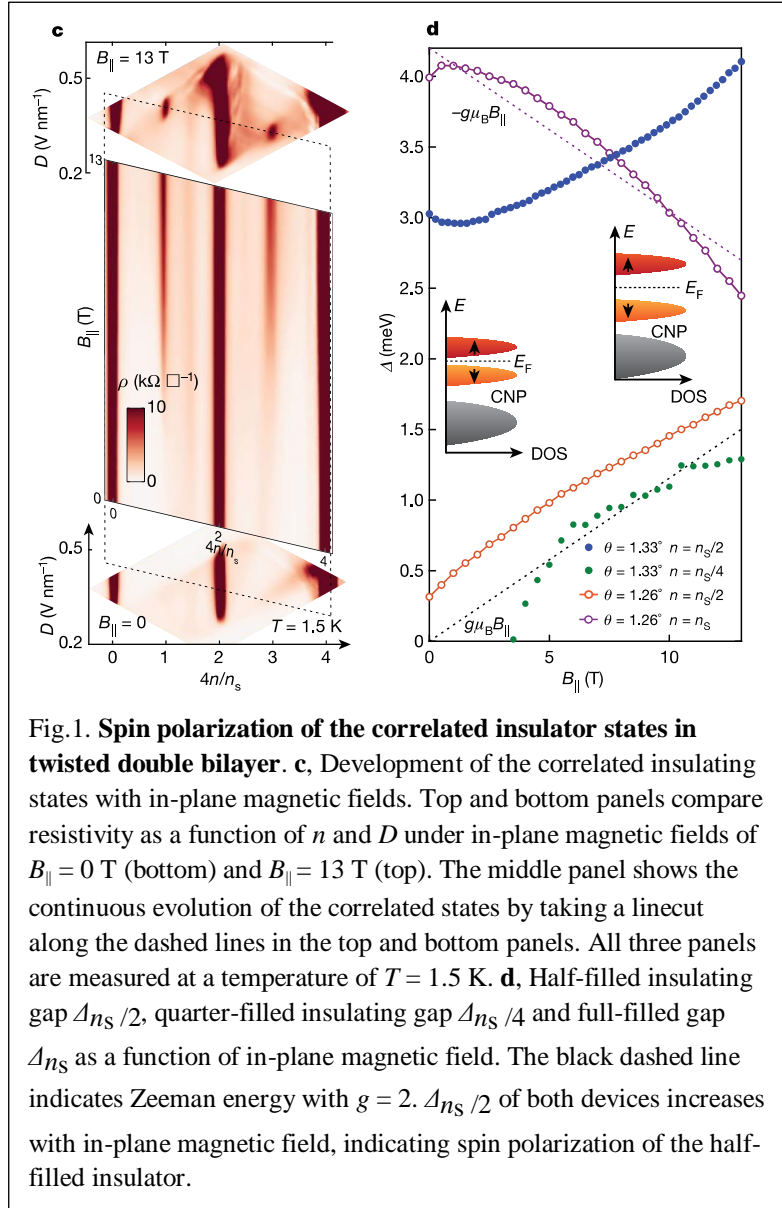


Fig. 1. Spin polarization of the correlated insulator states in twisted double bilayer. **c**, Development of the correlated insulating states with in-plane magnetic fields. Top and bottom panels compare resistivity as a function of n and D under in-plane magnetic fields of $B_{||} = 0$ T (bottom) and $B_{||} = 13$ T (top). The middle panel shows the continuous evolution of the correlated states by taking a linecut along the dashed lines in the top and bottom panels. All three panels are measured at a temperature of $T = 1.5$ K. **d**, Half-filled insulating gap $\Delta_{n_S}/2$, quarter-filled insulating gap $\Delta_{n_S}/4$ and full-filled gap Δ_{n_S} as a function of in-plane magnetic field. The black dashed line indicates Zeeman energy with $g = 2$. $\Delta_{n_S}/2$ of both devices increases with in-plane magnetic field, indicating spin polarization of the half-filled insulator.

Quantum Hall Interferometer for Fractional Quantum Hall States in graphene:

Quantum interferometers are powerful tools for probing the wave-nature and exchange statistics of indistinguishable particles. Of particular interest are interferometers formed by the chiral, one-dimensional edge channels of the quantum Hall effect (QHE) that guide electrons without dissipation. Using quantum point contacts (QPCs) as beamsplitters, these channels can be split and

recombined, enabling interference of charged particles. Such quantum Hall interferometers (QHIs) can be used for studying exchange statistics of anyonic quasiparticles in the fractional quantum Hall effect (FQHE). As shown in Fig. 2, we develop a robust fabrication technique for QHIs in van der Waals (vdW) materials and realize a highly tunable, graphene-based Fabry-Pérot (FP) QHI. Our new graphite gate architecture allows observation of FQHE as low as 3T and precise partitioning of a wide range of integer and

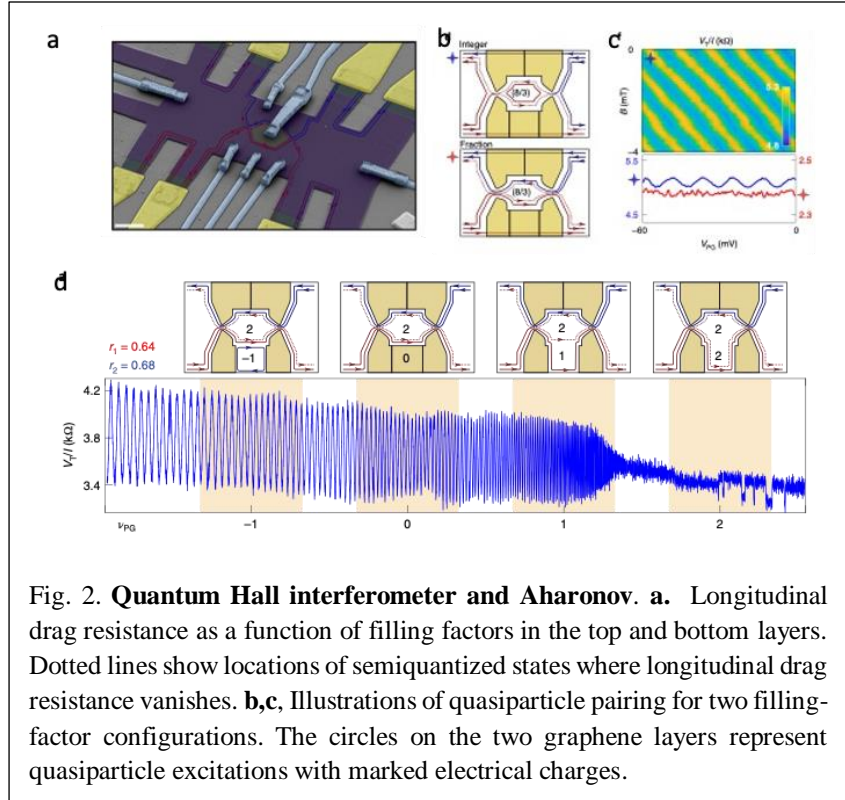


Fig. 2. **Quantum Hall interferometer and Aharonov.** **a.** Longitudinal drag resistance as a function of filling factors in the top and bottom layers. Dotted lines show locations of semi-quantized states where longitudinal drag resistance vanishes. **b,c,** Illustrations of quasiparticle pairing for two filling-factor configurations. The circles on the two graphene layers represent quasiparticle excitations with marked electrical charges.

fractional edge modes. Importantly, we measure pure Aharonov-Bohm interference in the integer QHE, a major technical challenge in finite size FP interferometers. We find that integer edge modes exhibit high visibility interference due to relatively large velocities and long phase coherence lengths. With tunable QPCs and FQHE at hand, our device provides a versatile platform for interferometer studies in vdW heterostructures and enables future experiments accessing abelian and non-abelian quasiparticles.

Previously, interlayer coupled integer quantum Hall effect has been observed in coupled GaAs quantum wells and more recently in coupled graphene double-layers under strong magnetic fields. This interlayer integer quantum Hall effect can also be viewed as exciton Bose-Einstein condensate phase (BEC). In this work, exploiting the strong Coulomb interaction across atomic thin hBN layers and drastically enhanced sample quality by dual graphite gates, we discover surprising and unexpected interlayer coupled FQH effects (Fig.2). We found that the observed interlayer FQH states can be explained by coupled composite fermions (CF). Remarkably, we also discover a BEC of CF excitonic pairs and a ‘semi-quantized’ quantum Hall state due to the pairing of anyonic quasiparticles in two layers. The newly discovered interlayer FQH in a double-layer system will open an entirely new research direction of FQH study. The properties of the discovered states await further investigation. The rich phase diagram of double-layer quantum Hall systems invites further pursuits of new topological states.

BEC-BCS Crossover in magneto-exciton condensation in graphene double layer: In fermionic systems, superconductivity and superfluidity are enabled through the condensation of fermion pairs. The nature of this condensate can be tuned by varying the pairing strength, with

weak coupling yielding a BCS-like condensate and strong coupling resulting in a BEC-like process. However, demonstration of this cross-over has remained elusive in electronic systems. Recently, we study graphene double-layers separated by an atomically thin insulator. Under applied magnetic field, electrons and holes couple across the barrier to form bound magneto-excitons whose pairing strength can be

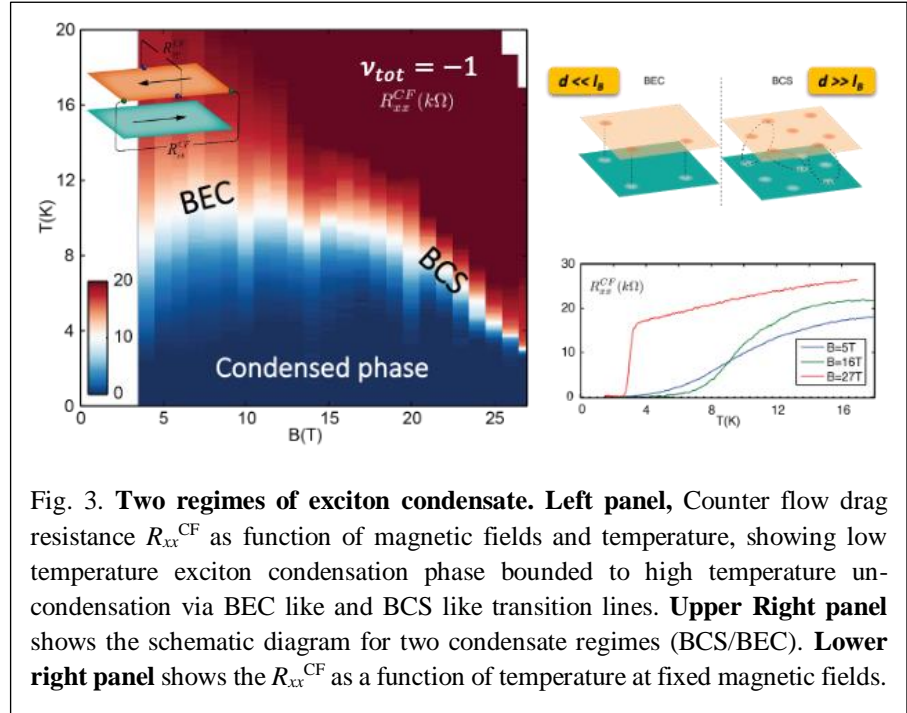


Fig. 3. **Two regimes of exciton condensate.** **Left panel,** Counter flow drag resistance R_{xx}^{CF} as function of magnetic fields and temperature, showing low temperature exciton condensation phase bounded to high temperature uncondensation via BEC like and BCS like transition lines. **Upper Right panel** shows the schematic diagram for two condensate regimes (BCS/BEC). **Lower right panel** shows the R_{xx}^{CF} as a function of temperature at fixed magnetic fields.

continuously tuned by varying the effective layer separation (Fig. 3). Using temperature-dependent Coulomb drag and counter-flow current measurements, we demonstrate the capability to tune the magneto-exciton condensate through the entire weak-coupling to strong-coupling phase diagram. Our results establish magneto-exciton condensates in graphene as a model platform to study the crossover between two Bosonic quantum condensate phases in a solid state system.

Future Plans

To extend our success beyond our ongoing work, we propose a set of research aims to explore novel physical phenomena stemming from the Correlated manybody quantum states in graphene. The near future plans include:

- Investigation of fractional quantum Hall interference with gate controlled quasi particle density control in the anti-dot geometry
- Josephson coupling between two different magneto-exciton condensation states.
- Electrical and thermoelectrical transport in strongly correlated graphene quantum structures for realization of SYK state

References

- [1] Cao, Y. et al. Unconventional superconductivity in magic-angle graphene superlattices. Nature 556, 43–50 (2018).
- [2] Cao, Y. et al. Correlated insulator behaviour at half-filling in magic-angle graphene superlattices. Nature 556, 80–84 (2018).

Publications

X. Liu, Z. Hao, E. Khalaf, J. Y. Lee, Y. Ronen, H. Yoo, D. H. Najafabadi, K. Watanabe, T. Taniguchi, A. Vishwanath, P. Kim, “Tunable Spin-polarized Correlated States in Twisted Double Bilayer Graphene,” *Nature* **583**, 221-225 (2020).

Y. Ronen, T. Werkmeister, D. Najafabadi, A. T. Pierce, L. E. Anderson, Y. J. Shin, S. Y. Lee, Y. H. Lee, B. Johnson, K. Watanabe, T. Taniguchi, A. Yacoby, P. Kim, “Aharonov Bohm Effect in Graphene Fabry Perot Quantum Hall Interferometers,” *Nature Nano*, **16**, 563-569 (2021).

X. Liu, J. I. A. Li, K. Watanabe, T. Taniguchi, J. Hone, B. I. Halperin, P. Kim, C. R. Dean, “Crossover between Strongly-coupled and Weakly-coupled Exciton Superfluids,” arXiv:2012.05916, accepted for publication in *Science*.

Spectroscopy of degenerate one-dimensional electrons in carbon nanotubes

Prof. Junichiro Kono, William Marsh Rice University, Houston, TX

Program Scope

The goal of this research program is to understand the fundamental properties of degenerate one-dimensional (1-D) electrons in single-wall carbon nanotubes (SWCNTs). SWCNTs provide an ideal 1-D environment in which to study many body physics. Semiconducting SWCNTs exhibit rich optical spectra dominated by extremely stable 1-D excitons, whereas metallic SWCNTs contain massless 1-D carriers with ultralong mean-free paths. Despite a large number of electrical, optical, and magnetic studies of SWCNTs during the last two decades, most of the predicted exotic properties of interacting 1-D electrons have yet to be observed, and some of the reported experimental results remain highly controversial.

Recent Progress

Thermoelectric (TE) materials convert heat into electricity and vice versa, offering great potential for waste heat recovery and solid-state cooling. TE materials are usually evaluated by the ZT factor, defined as $ZT = S^2\sigma T\kappa^{-1}$, where S is the Seebeck coefficient, σ is the electrical conductivity, κ is the thermal conductivity, and T is the temperature. While previous studies on thermoelectric materials have primarily focused on reducing κ to improve ZT , enhancing the power factor (PF), defined as $PF = S^2\sigma$, is more important for certain applications such as energy harvesting applications¹ and active cooling.²

In addition to the basic TE properties, practical applications require other considerations, such as toxicity, flexibility, and scalability.³ Compared to conventional inorganic (e.g., Bi_2Te_3 and its alloys⁴) and organic-like (e.g., monolayer graphene⁵ and ultrathin FeSe ⁶) TE materials, macroscopically ordered CNT assemblies with superb thermal and mechanical properties⁷ offer high TE performance, flexibility, and scalability simultaneously. However, experimentally measured PF for CNT assemblies has remained small,⁸ presumably due to low σ originating from poor sample morphology.

Here, we studied the TE properties of macroscopic weavable CNT fibers. These neat CNT fibers simultaneously possess a high degree of CNT alignment, a high density, a high CNT aspect ratio (length per diameter), and a low level of impurities, leading to ultrahigh electrical conductivity, $\sigma > 10 \text{ MS m}^{-1}$. We tuned the Fermi energy (E_F) to the vicinity of a 1-D van Hove singularity (VHS) through a chemical treatment to maximize S , obtaining PF as high as $14 \pm 5 \text{ mW m}^{-1} \text{ K}^{-2}$. This is the highest PF value achieved for any CNT system and approaching the

highest values reported for 2-D materials. We developed a theoretical model to explain the E_F dependence of PF and validated it with finer E_F tuning using electrolyte gating.⁹

CNTs used to fabricate fibers mainly contained double-wall CNTs (DWCNTs) with an average outer (inner) wall diameter of 1.8 ± 0.2 nm (0.9 ± 0.1 nm). A solution spinning method¹⁰ was used to spin CNTs into a continuous fiber. CNTs were first dissolved in chlorosulfonic acid (CSA) to create a spin dope. The dope was then filtered and extruded into a coagulant. Finally, the coagulated fiber was collected onto a rotating drum. This method produced meters (>100 m) of fiber with densely packed and highly aligned CNTs, as shown in Fig. 1a. The average diameter of the fiber was determined to be 8.9 ± 0.9 μm . The CNTs inside the solution spun fiber have a high aspect ratio, as well as a low impurity density, and are highly crystalline, leading to exceptional mechanical (tensile strength of 4.2 ± 0.2 GPa) and electrical ($\sigma > 10$ MS m^{-1}) properties while retaining flexibility.¹⁰

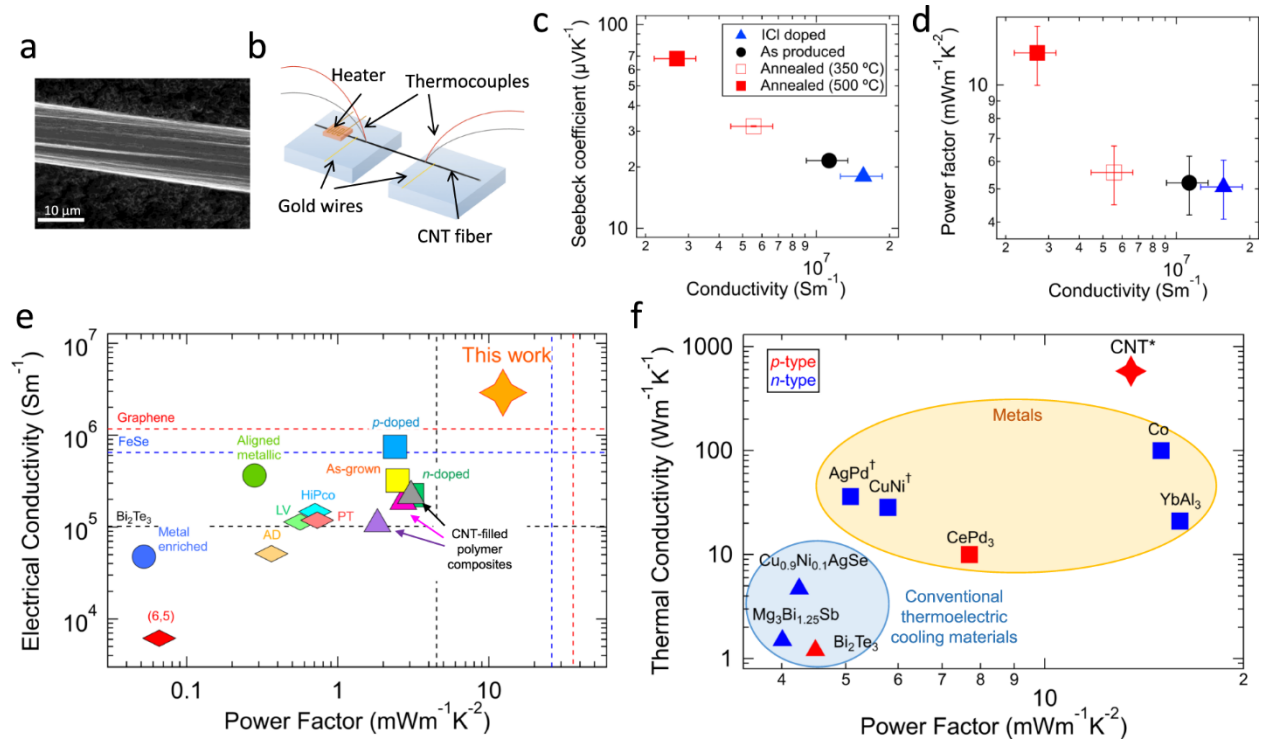


Figure 1: Thermoelectric properties of densely packed and highly aligned CNT fibers. **a** SEM image of a CNT fiber. **b** Schematic of the experimental setup used for measuring the electrical conductivity (σ) and Seebeck coefficient (S) of CNT fibers. **c** Measured S and **d** corresponding power factor ($PF = S^2\sigma$) as a function of σ for four CNT fibers that underwent different chemical treatments: Iodine monochloride (ICl) doped (solid blue triangles), as-produced (solid black circles), annealed at 350 °C (open red squares), and annealed at 500 °C (solid red squares). **e** Comparison of reported PF values for various CNT samples with σ^1 . PF values of Bi_2Te_3 alloys⁹, graphene¹⁰, and FeSe ¹¹ serve as references. **f** Comparison of reported PF values for representative materials with the thermal conductivity (κ) at 300 K with a temperature difference (ΔT) of 1 K¹.

To tune E_F , we heavily p-doped as-produced CNT fibers with CSA during the solution spinning process resulting in σ of 11 ± 2 MS m^{-1} . Doping an as-produced CNT fiber with iodine

monochloride (ICl) increased the value of σ to $16 \pm 3 \text{ MS m}^{-1}$ through further p-type doping, while annealing them at a temperature of $350 \text{ }^\circ\text{C}$ ($500 \text{ }^\circ\text{C}$) decreased σ to $5.6 \pm 1.1 \text{ MS m}^{-1}$ ($2.7 \pm 0.5 \text{ MS m}^{-1}$) through dedoping.

Figure 1b shows the schematic of the experimental setup to measure the σ and S of these CNT fibers at room temperature under vacuum. The measured S values were all positive, indicating p-type carriers. Figure 1c shows a monotonic decrease of S with increasing σ , resulting in a decrease of PF with σ (Fig. 1d). The highest S was obtained for the CNT fiber annealed at $500 \text{ }^\circ\text{C}$. The maximum PF value, $14 \pm 5 \text{ mW m}^{-1} \text{ K}^{-2}$, is the highest value ever achieved for any CNT sample. Figure 1e summarizes the room-temperature PF values reported for different CNT systems with σ . Our value is over three times larger than that of Bi_2Te_3 , the commercially used inorganic p-type TE material ($\sim 4.5 \text{ mW m}^{-1} \text{ K}^{-2}$),⁴ and is approaching the highest PF achieved at room temperature by 2-D materials: monolayer graphene ($36.6 \text{ mW m}^{-1} \text{ K}^{-2}$).⁵ It is important to note that the giant PF in this work was observed in macroscopic samples ($\sim 1 \text{ cm}$ length), whereas the highest PF reported for 2D materials has been measured in microscopic samples (typically in μm -scale).

Furthermore, the high PF observed is promising for use in active cooling, leveraging the high thermal conductivity ($580 \text{ W m}^{-1} \text{ K}^{-1}$) of the CNT fibers.¹¹ TE active cooling requires a material with large κ and large PF , simultaneously, to maximize κ_{eff} . However, no existing TE materials satisfy this requirement, as shown in Fig. 1f. Conventional TE cooling materials have relatively large PF , but small κ .

Finally, we demonstrated the weavability and scalability of the CNT fibers by fabricating a textile thermoelectric generator sewn into the fabric, capable of turn on a light-emitting diode.⁹

Future Plans

Our next steps include understanding the fundamental properties of quantum degenerate ($E_F \gg k_B T$) 1-D electrons in SWCNTs, where E_F is the Fermi energy and k_B is the Boltzmann constant. Recent advances in separation and sorting techniques have allowed researchers to prepare highly enriched, single-chirality macroscopic ensembles of SWCNTs. This impressive progress is revolutionizing the field of CNT optics, enabling detailed chirality-dependent spectroscopy studies that were previously impossible to perform. While many of the features in prior studies were obscured due to the many different chiralities present in the samples, in highly enriched samples these features are better resolved, allowing one to study the intrinsic behaviors of 1-D electrons, phonons, and excitons in far greater detail. We will be trying to fabricate single crystals of single-chirality SWCNTs. Such crystals are expected to exhibit new phenomena arising from the intrinsically 1-D nature of the interacting electrons in these systems in a chirality-specific manner. Moreover, the availability of highly purified single-chirality SWCNTs opens up new possibilities for the development of optoelectronic devices that are useful for optical communications, spectroscopy, imaging, and sensing.

References

1. Liu, W. *et al.* n-type thermoelectric material $\text{Mg}_2\text{Sn}_{0.75}\text{Ge}_{0.25}$ for high power generation. *Proc Natl Acad Sci USA* **112**, 3269–3274 (2015).
2. Zebarjadi, M. Electronic cooling using thermoelectric devices. *Appl. Phys. Lett.* **106**, 203506 (2015).
3. Russ, B., Gludell, A., Urban, J. J., Chabinyc, M. L. & Segalman, R. A. Organic thermoelectric materials for energy harvesting and temperature control. *Nat Rev Mater* **1**, 16050 (2016).
4. Poudel, B. *et al.* High-Thermoelectric Performance of Nanostructured Bismuth Antimony Telluride Bulk Alloys. *Science* **320**, 634–638 (2008).
5. Duan, J. *et al.* High thermoelectric power factor in graphene/hBN devices. *Proc Natl Acad Sci USA* **113**, 14272–14276 (2016).
6. Shimizu, S. *et al.* Giant thermoelectric power factor in ultrathin FeSe superconductor. *Nat Commun* **10**, 825 (2019).
7. Gao, W. *et al.* Macroscopically aligned carbon nanotubes for flexible and high-temperature electronics, optoelectronics, and thermoelectrics. *J. Phys. D: Appl. Phys.* **53**, 063001 (2020).
8. Blackburn, J. L., Ferguson, A. J., Cho, C. & Grunlan, J. C. Carbon-Nanotube-Based Thermoelectric Materials and Devices. *Adv. Mater.* **30**, 1704386 (2018).
9. Komatsu, N. *et al.* Macroscopic weavable fibers of carbon nanotubes with giant thermoelectric power factor. *Nat Commun* **12**, 4931 (2021).
10. Taylor, L. W. *et al.* Improved properties, increased production, and the path to broad adoption of carbon nanotube fibers. *Carbon* **171**, 689–694 (2021).
11. Behabtu, N. *et al.* Strong, Light, Multifunctional Fibers of Carbon Nanotubes with Ultrahigh Conductivity. *Science* **339**, 182–186 (2013).

Publications

1. S. Dal Forno, N. Komatsu, M. Wais, A. Mojibpour, I. Wadgaonkar, S. Ghosh, Y. Yomogida, K. Yanagi, K. Held, J. Kono, and M. Battiato, "Origin of the Background Absorption in Carbon Nanotubes: Phonon-Assisted Excitonic Continuum," arXiv:2107.08659 (2021).
2. Y. Yomogida, K. Horiuchi, R. Okada, H. Kawai, Y. Ichinose, H. Nishidome, K. Ueji, N. Komatsu, W. Gao, J. Kono, and K. Yanagi, "Hall Effect in Gated Single-Wall Carbon Nanotube Films," *Scientific Reports*, under review. DOI:10.21203/rs.3.rs-849926/v1.
3. N. Komatsu, Y. Ichinose, O. S. Dewey, L. W. Taylor, M. A. Trafford, Y. Yomogida, G. Wehmeyer, M. Pasquali, K. Yanagi, and J. Kono, "Macroscopic Weavable Fibers of Carbon Nanotubes with Giant Thermoelectric Power Factor," *Nature Communications* **12**, 4931 (2021).
4. L. W. Taylor, O. S. Dewey, R. J. Headrick, N. Komatsu, N. Marquez Peraca, G. Wehmeyer, J. Kono, and M. Pasquali, "Improved Properties, Increased Production, and the Path to Broad Adoption of Carbon Nanotube Fibers," *Carbon* **171**, 689 (2021).
5. W. Gao, D. Adinehloo, A. Mojibpour, Y. Yomogida, A. Hirano, T. Tanaka, H. Kataura, M. Zheng, V. Perebeinos, and J. Kono, "Band Structure Dependent Electronic Localization in Macroscopic Films of Single-Chirality Single-Wall Carbon Nanotubes," *Carbon* **183**, 774 (2021).
6. A. Baydin, N. Komatsu, F. Tay, S. Ghosh, T. Makihara, G. T. Noe II, and J. Kono, "Giant Terahertz Polarization Rotation in Ultrathin Films of Aligned Carbon Nanotubes," *Optica* **8**, 760 (2021).
7. A. Baydin, T. Makihara, N. Marquez Peraca, and J. Kono, "Time-Domain Terahertz Spectroscopy in High Magnetic Fields," *Frontiers of Optoelectronics* **14**, 110 (2021).
8. N. Wei, Y. Tian, Y. Liao, N. Komatsu, W. Gao, A. Lyuleeva, Q. Zhang, A. Hussain, E.-X. Ding, F. Yao, J. Halme, K. Liu, J. Kono, H. Jiang, and E. Kauppinen, "Colors of Single-Wall Carbon Nanotubes," *Advanced Materials* **33**, 2006395 (2021).
9. N. Marquez Peraca, A. Baydin, W. Gao, M. Bamba, and J. Kono, "Ultrastrong Light-Matter Coupling in Semiconductors," in: *Semiconductor Quantum Science and Technology, Semiconductors and Semimetals*, Volume **105**, edited by M. Kira and S. T. Cundiff (Elsevier, Amsterdam, 2020), pp. 89-151
10. K. Cong, W. Jiang, B. E. Anthonio, G. T. Noe II, H. Liu, H. Kataura, M. Kira, and J. Kono, "Quantum-Memory-Enabled Ultrafast Optical Switching in Carbon Nanotubes," *ACS Photonics* **7**, 1382 (2020).
11. F. R. G. Bagsican, M. Wais, N. Komatsu, W. Gao, L. W. Weber, K. Serita, H. Murakami, K. Held, F. A. Hegmann, M. Tonouchi, J. Kono, I. Kawayama, and M. Battiato, "Terahertz Excitonics in Carbon Nanotubes: Exciton Autoionization and Multiplication," *Nano Letters* **20**, 3098 (2020).

12. N. Komatsu, M. Nakamura, S. Ghosh, D. Kim, H. Chen, A. Katagiri, Y. Yomogida, W. Gao, K. Yanagi, and J. Kono, “Groove-Assisted Global Spontaneous Alignment of Carbon Nanotubes in Vacuum Filtration,” *Nano Letters* **20**, 2332 (2020).
13. W. Gao, N. Komatsu, L. Taylor, G. V. Naik, K. Yanagi, M. Pasquali, and J. Kono, “Macroscopically Aligned Carbon Nanotubes for Flexible and High-Temperature Electronics, Optoelectronics, and Thermoelectrics” (invited review article), *Journal of Physics D: Applied Physics* **53**, 063001 (2020).
14. S. Yamaguchi, I. Tsunekawa, N. Komatsu, W. Gao, T. Shiga, T. Kodama, J. Kono, and J. Shiomi, “One-Directional Thermal Transport in Densely Aligned Single-Wall Carbon Nanotube Films,” *Applied Physics Letters* **115**, 223104 (2019).
15. Y. Ichinose, A. Yoshida, K. Horiuchi, K. Fukuhara, N. Komatsu, W. Gao, Y. Yomogida, M. Matsubara, T. Yamamoto, J. Kono, and K. Yanagi, “Solving the Thermoelectric Trade-Off Problem with Metallic Carbon Nanotubes,” *Nano Letters* **19**, 7370 (2019).

Superconductivity and Magnetism

**W. –K. Kwok; Co-PIs: U. Welp, V. Novosad, A. E. Koshelev, V. Vlasko-Vlasov, Z. -L. Xiao
Materials Science Division, Argonne National Laboratory, 9700 S. Cass Ave., Lemont IL
60439**

Program Scope

This program explores novel physical phenomena associated with superconductivity, magnetism, and their interactions, determines the origins of these occurrences and designs innovative functionalities for superconductivity. The broad range of physical effects at the intersection of superconductivity and magnetism in bulk crystals, thin films and artificial hybrid heterostructures constitutes a rich platform to explore, discover and control new behaviors. Furthermore, the boundaries between superconductivity and magnetism are fluid, with thematically interconnected phenomena in magnetic superconductors, vortex matter, and superconducting/ferromagnetic hybrid heterostructures. Our current program has three main objectives: (1) explore and determine the characteristics of bulk and nanostructured topological superconductors, (2) tune the topology of magnetic high- T_c superconductors to evoke Majorana fermions. (3) pursue innovative hybrid FM/SC structures and nanostructures for microelectronics and exploit magnon-Cooper pair dynamics in search of new effects and functionalities. A major goal is to discover new topological materials/architectures that can be transformative to the current enterprise related to quantum computing and quantum information science. Below, we highlight our research area on unique architectures related to flux quantum control in hybrid FM/SC structures.

Recent Progress

The flux quanta or vortex matter in type II superconductors control the electromagnetic behavior of all applied superconductors. Mitigation of vortex liquid flow in high temperature superconductors constitutes an important scientific challenge to enhance critical currents. Furthermore, with the emergence of vortices that can harbor Majorana bound states in topological superconductors, the importance of vortex-braiding and dissipation has risen to the forefront in the race for novel quantum computers based on topological superconductors. Our current research builds upon our recent advances in controlling flux quanta in artificial spin ice (ASI) based ferromagnetic/superconducting (FM/SC) heterostructure that can in-situ reconfigure the vortex lattice structure to create electronic rectification effects and tailored geometric frustration [1, 2]. We fabricated a spatially reconfigurable magnetic potential utilizing a pinwheel ASI structure on top of a MoGe superconducting film to explore new functionalities. The pinwheel structure is comprised of an array of permalloy nano-magnetic bars [350 nm (l) x 80 nm (w) x 25 nm (d)] in two designs, one rotated at 45 degrees from the other as shown in Figure. 1 in a microbridge format for transport measurements (Fig. 1). The poles of the nanomagnets acts as an attractive/repulsive potential for the flux quanta. An in-plane magnetic field of $H_{xy} = 3$ kOe directed at different angles is used to in-situ reconstitute the magnetic charges of the nanomagnets to form a magnetic chain

structure (attractive/repulsive potential valleys/ridges). Applying an out-of-plane field induces vortices. The strong interaction between magnetic charges and superconducting vortices allows significant modification of the transport properties of the underlying superconducting thin film. For the top left pinwheel pattern shown in Fig. 1a, with the current directed along the microbridge with an applied out-of-plane field, the Lorentz force pushes the vortices along the magnetic chains and across the chains, constituting an easy and hard direction for vortex motion, depending on the in-situ configuration of the magnetic chain directions (H_y and H_z) respectively as shown in Fig. 1b. Hence by rotating the in-plane magnetic field, a switching behavior can be observed in the electronic response (Fig. 1c top panel). Furthermore, the phase of the switching behavior inverts at higher out-of-plane magnetic fields (Fig. 1c bottom panel) as the enhanced vortex-vortex interaction can squeeze vortices between the horizontal magnetic chain structures, consistent with our molecular dynamics (MD) simulations of vortex behavior.

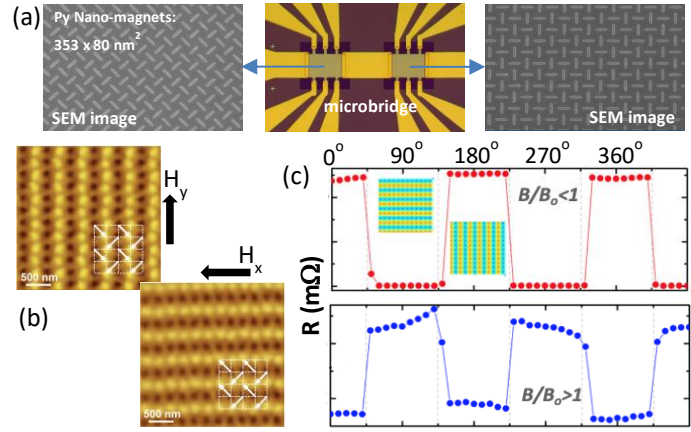


Figure 1. (a) Microbridge with two pinwheel ASI patterns deposited on top of a MoGe superconducting film. (b) MFM images of the pinwheel on the top left panel in (a) showing the magnetic chain structures induced by in-plane magnetic field in the y and x direction. The white arrows indicate the magnetization of individual permalloy elements. (c) Switching of the resistivity by in-situ reconstitution of the magnetic chain structures via field rotation. At higher magnetic fields, the switching phase inverts. $B_0=165.6$ Oe, where the density of vortices is equivalent to the density of nanomagnets.

In addition to the switching of vortex motion, the alternating row-by-row attractive potential valleys and repulsive potential ridges provide a perfect system for guided vortex motion. Since vortices are favored to move along the attractive potential valleys, we can tailor the path of moving vortices to deviate from their nominal direction given by the Lorentz force. For this purpose, we designed a vortex Hall device in which vortices could have a longitudinal component of the motion under a transverse driving force. We designed a pinwheel ASI array that is rotated by 45° from the one shown in the top left panel of Fig. 1 and shown in the top right panel. Here, the pinwheel ASI array produces diagonally oriented magnetic charge chains whose orientation can be in-situ switched between -45° and $+45^\circ$ by an in-plane field (Fig. 2a). Since the motion of vortices induces a voltage perpendicular to their moving direction, a longitudinal vortex motion results in a transverse (Hall) voltage. This allows us to detect the vortex Hall effect using the same conventional six-probe electrical contact configuration as that used for investigating the electric charge Hall effect. We measured the magnetic field (out-of-plane) and current dependences of the Hall voltages at -45° and $+45^\circ$ orientations of ASI's charge chains as shown in Fig. 2b. Clear Hall voltage signals are observed, indicating the realization of the vortex Hall effect. The Hall signal shows interesting behavior with positive and negative Hall voltage values over the magnetic field

and current maps. Here, the Lorentz force generated by horizontal electrical currents, is in the vertical direction, and the magnetic charge chains produce force with the direction perpendicular to the chains, preventing vortices from moving across the chains. The resultant force drives the vortices in a diagonal direction, which results in a horizontal vortex velocity, leading to a measurable Hall voltage signal. The horizontal components of the vortex motion are in the opposite directions for the case of -45° and $+45^\circ$ magnetic charge chains, resulting in inverted

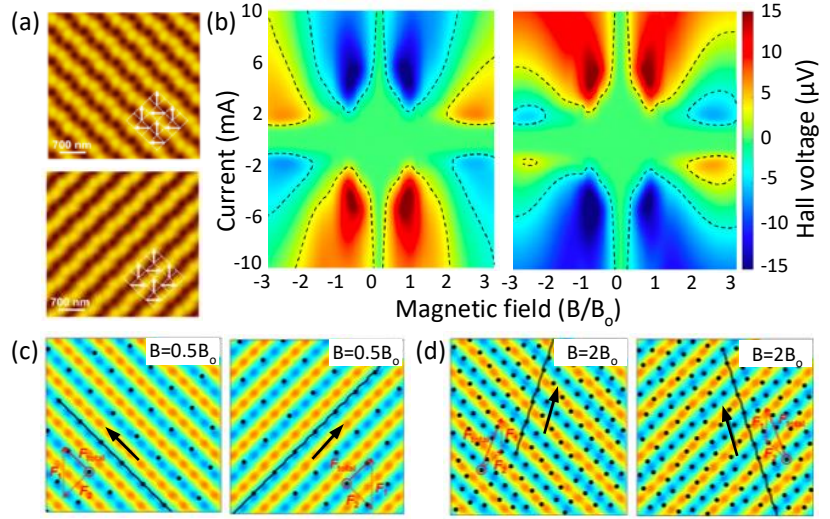


Figure 2. Reprogrammable vortex Hall effect. (a) MFM images of the $\pm 45^\circ$ magnetic charge chains. (b) Switching of the magnetic field and current dependences of the vortex Hall voltage respectively, obtained under the magnetic charge configurations shown in (a). (c) Corresponding MD simulations of vortex motion at low fields and (d) at high fields with enhanced vortex-vortex interactions. Black arrows and lines represent the direction and trajectory of vortex motion, respectively.

polarities of the Hall signals. Since the corresponding transverse components of vortex velocities are equivalent under both $\pm 45^\circ$ magnetic charge chain configurations, the longitudinal voltages are identical for the two cases. Switching of the Hall signal polarity can also be obtained by rotating the in-plane fields to change the orientation of the magnetic charge chains, similar to Fig. 1c. Furthermore, besides reversing Hall signals by tuning the ASI's states, the Hall signals can also be reversed by increasing the out-of-plane magnetic field. The sign of the Hall voltage inverts at high magnetic fields as compared to low magnetic fields, again attributed to the strong vortex-vortex interactions. Our MD simulations for low and high fields (Fig. 2 c, d) demonstrate that the horizontal component of vortex motion reverses with field. The reversal of the Hall signal with increasing magnetic fields cannot occur for electronic charges, such as electrons or holes and is a unique property of superconducting vortices. Furthermore, with superconducting vortices, reversing the magnetic field would flip their polarity and the Lorentz force acting on them, causing the vortices to move in the opposite direction along the chains. Thus, reversal of the magnetic field orientation will not change the polarity of the Hall voltage signal, giving rise to the mirror symmetry with respect to the zero magnetic field line in Fig. 2b, in contrast to the Hall effect from electronic charges, which shows a reversed Hall voltage when the magnetic field is reversed.

Future Plans

In future work, we plan to explore spin-waves in FM/SC hybrid structures with new ASI lattice structures to investigate the interaction between the spin-waves and local flux quanta. We also

plan to explore high fidelity flux quanta control in a more complex magnetic geometry as shown in Fig. 3 with a ‘T’ and ‘I’ letter-shaped permalloy structure deposited on a niobium film to create a labyrinth-like flux motion. Preliminary magneto-optical images show emergence of a complex vortex flow dynamics which can be controlled with an in-plane magnetic field to a high degree of precision. In addition to magnetic charges, we have recently demonstrated that nano-blindholes can be utilized to create novel electronic behavior such as a superconducting diode effect using conformal-mapped nanoholes [4]. By combining nanoholes with magnetic charges, we show a schematic in Fig. 3c that could potentially be used to collectively braid vortices by simply rotating an in-plane magnetic field.

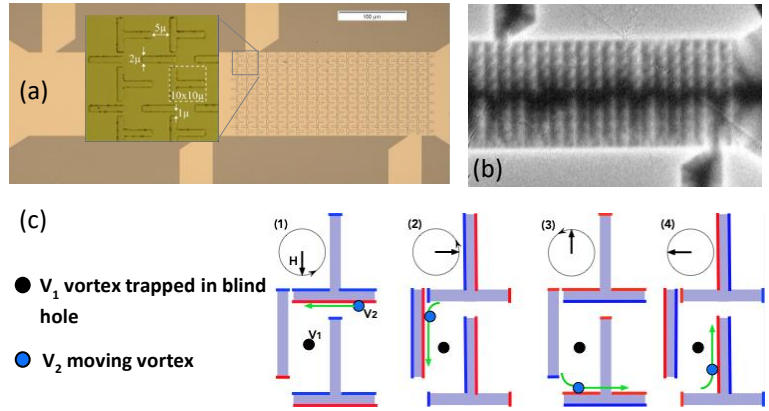


Figure 3. (a) Optical picture of a 100 nm thick niobium microbridge with 75 nm thick permalloy ‘T’ and ‘I’ letter-shaped magnetic structures. (b) Magneto-optical image of labyrinth-like flux entry. (c) Schematic for collective flux quanta braiding by incorporating blindholes into the Nb film. The red and blue lines represent the magnetic charges that attract (repel) the flux quanta.

In summary, our work on FM/SC hybrid structures could lead to novel phenomena and physics, such as reconfigurable dynamic vortex Mott transitions [5]. The method demonstrated here for tuning vortex motion could also be applied to other topological charges such as magnetic skyrmions [6], providing a universal and convenient approach to design new reprogrammable functionalities in magnetic particle systems. These heterostructures can also be incorporated into hybrid FM/SC resonators to probe magnon dynamics for quantum information processes [7, 8].

References

- [1] Y. L. Wang et al., *Rewritable Artificial Magnetic Charge Ice*, *Science* 352, 6288 (2016).
- [2] Y. L. Wang et al., *Switchable geometric frustration in an artificial-spin-ice superconductor hetero-system*, *Nature Nanotechnology* 13, 560-565 (2018).
- [3] Y. Y. Lyu et al., *Reconfigurable Pinwheel Artificial-Spin-Ice and Superconductor Hybrid Device*, *Nano Letters* 20 (12), 8933 (2020).
- [4] Y. Y. Lyu et al., *Superconducting Diode Effect via Conformal Mapped Nanoholes*, *Nature Communications* 12, 2303 (May 11, 2021)
- [5] N Poccia et al., *Critical Behavior at a dynamic vortex insulator-to-metal transition*, *Science* 349, 1202 (2015)
- [6] X. Ma et al., *Reversible Vector Ratchets for Skyrmion Systems*, *Ma, Phys. Rev. B: Condens. Matter Mater. Phys.* 95, 104401 (2017).
- [7] Y. Li et al., *Hybrid magnonics: physics, circuits and applications for coherent information processing*, *Journal of Applied Physics* 128 (13), 130902 (2020).
- [8] M. T. Kaffash et al., *Nanomagnonics with artificial spin ice*, *Phys. Letters A* 402, 127364 (2021).

Publications 10/2019 – 9/2021 (49 Publications, 20 highlighted below)

1. *Tuning edge-localized spin waves in magnetic microstripes by proximate magnetic structures* Zhizhi Zhang, Michael Vogel, M Benjamin Jungfleisch, Axel Hoffmann, Yan Nie, Valentine Novosad, Physical Review B 100(17) 174434 (Nov 2019)
2. *Magnetization-governed magnetoresistance anisotropy in the topological semimetal CeBi* Yang-Yang Lyu, Fei Han, Zhi-Li Xiao, Jing Xu, Yong-Lei Wang, Hua-Bing Wang, Jin-Ke Bao, Duck Young Chung, Mingda Li, Ivar Martin, Ulrich Welp, Mercouri G. Kanatzidis, and Wai-Kwong Kwok, Physical Review B100, 180407(R) (Nov 2019)
3. *Spin-wave frequency division multiplexing in an yttrium iron garnet microstripe magnetized by inhomogeneous field*, Zhizhi Zhang, Michael Vogel, José Holand, M. Benjamin Jungfleisch, Changjiang Liu, Yi Li, John E. Pearson, Ralu Divan, Wei Zhang, Axel Hoffmann, Yan Nie, and Valentyn Novosad, Applied Physics Letters 115, 232402 (Dec 2019)
4. *The Quest for High Critical Current in Applied High-Temperature Superconductors*, Andreas Glatz, Ivan A. Sadovskyy, Ulrich Welp, Wai-Kwong Kwok and George W. Crabtree, Journal of Superconductivity and Novel Magnetism 33 (1), pp127-141, (Jan 2020)
5. *Magnetic and superconducting anisotropy in Ni-doped RbEuFe₄As₄ single crystals*, K. Willa, M. P. Smylie, Y. Simsek, J.-K. Bao, D. Y. Chung, M. G. Kanatzidis, W.-K. Kwok, and U. Welp Physical Review B 101, 064508 (Feb 2020)
6. *Nodeless superconducting gap in the candidate topological superconductor Sn_{1-x}In_xTe for x=0.7*, M. P. Smylie, Kaya Kobayashi, T. Takahashi, C. Chaparro, A. Snezhko, W.-K. Kwok, and U. Welp, Physical Review B 101, 094513 (Mar 2020)
7. *Cooperative response of magnetism and superconductivity in the magnetic superconductor RbEuFe₄As₄*, V. K. Vlasko-Vlasov, U. Welp, A. E. Koshelev, M. Smylie, J.-K. Bao, D. Y. Chung, M. G. Kanatzidis, and W.-K. Kwok, Physical Review B 101, 104504 (Mar 2020)
8. *Temperature-dependent anisotropic magnetoresistance and spin-torque-driven vortex dynamics in a single microdisk*, S. Lendinez, T. Polakovic, J. J. Ding, M. B. Jungfleisch, J. Pearson, A. Hoffmann, V. Novosad, Journal of Applied Physics 127, 243904 (Jun 2020)
9. *Mesa-Sidewall Effect on Coherent Terahertz Radiation via Spontaneous Synchronization of Intrinsic Josephson Junctions in Bi₂Sr₂CaCu₂O_{8+d}*, G. Kuwano, M. Tsujimoto, Y. Kaneko, T. Imai, Y. Ono, S. Nakagawa, S. Kusunose, H. Minami, T. Kashiwagi, K. Kadowaki, Y. Simsek, U. Welp, and W.-K. Kwok, Physical Review Applied 13, 014035 (Jan 2020)
10. *On-Chip Sensing of Hotspots in Superconducting Terahertz Emitters*, Xianjing Zhou, Xu Han, Dieter Koelle, Reinhold Kleiner, Ulrich Welp, Xufeng Zhang, and Dafei Jin, Nano Letters 20 (6) 4197–4203 (May 2020)

11. *Charge density wave and superconductivity competition in $\text{Lu}_5\text{Ir}_4\text{Si}_{10}$: A proton irradiation study*, Maxime Leroux, Vivek Mishra, Christine Opagiste, Pierre Rodière, Asghar Kayani, Wai-Kwong Kwok and Ulrich Welp, *Physical Review B* 102, 094519, (Sept 2020)
12. *Hybrid magnonics: physics, circuits and applications for coherent information processing*, Yi Li, Wei Zhang, Vasyl Tyberkevych, Wai-Kwong Kwok, Axel Hoffmann, Valentyn Novosad, *Journal of Applied Physics* 128(13), 130902 (Oct 2020)
13. *Asymmetric crossing of the attractive and repulsive magnetic potential by Abrikosov vortices* V. Vlasko-Vlasov, A. Glatz, D. Rosenmann, R. Divan, W. K. Kwok, *Physical Review B* 102(17), 174511 (Nov 2020)
14. *Reconfigurable Pinwheel Artificial-Spin-Ice and Superconductor Hybrid Device*, Y. Y. Lyu, X. Ma, J. Xu, Y. L. Wang, Z. L. Xiao, S. N. Dong, B. Janko, H. B. Wang, R. Divan, J. E. Pearson, P. H. Wu, W. K. Kwok, *Nano Letters* 20(12), 8933 (Dec 2020)
15. *Non-Ohmic negative longitudinal magnetoresistance in two-dimensional electron gas*, Yang-Yang Lyu, Xian-Jing Zhou³, Zhi-Li Xiao, Roxanna Fotovat, Jing Xu, Gobind Basnet, Yong-Lei Wang, Dafei Jin, Ralu Divan, Hua-Bing Wang, and Wai-Kwong Kwok, *Physical Review B* 103, 035422 (Jan 2021)
16. *Switchable X-Ray Orbital Angular Momentum from an Artificial Spin Ice*, Justin Woods, Xiaoqian Chen, Rajesh V. Chopdekar, Barry Farmer, Claudio Mazzoli, Roland Koch, Anton Tremsin, Wen Hu, Andreas Scholl, Steve Kevan, Stuart Wilkins, Wai-Kwong Kwok, Lance E. De Long, Sujoy Roy, and J. Todd Hastings, *Physical Review Letters* 126, 117201 (Mar 2021)
17. *Observing the Suppression of Superconductivity in the magnetic-Superconductor $\text{RbEuFe}_4\text{As}_4$ via Quantitative Magnetic Imaging*, D. Collomb, S. J. Bending, A. E. Koshelev, M. P. Smylie, L. Farrar, J.-K. Bao, D.-Y. Chung, M. G. Kanatzidis, W.-K. Kwok, and U. Welp *Physical Review Letters* 126, 157001 (Apr 2021)
18. *Superconducting Diode Effect via Conformal Mapped Nanoholes*, Yang-Yang Lyu, Ji Jiang, Yong-Lei Wang, Zhi-Li Xiao, Sining Dong, Qing-Hu Chen, Milorad V. Milošević, Huabing Wang, Ralu Divan, John E. Pearson, Peiheng Wu, Francois M. Peeters and Wai-Kwong Kwok *Nature Communications* 12, 2303 (May 2021)
19. *Advances in Coherent Coupling Between Magnons and Acoustic Phonons (invited paper)*, Yi Li, Chenbo Zhao, Wei Zhang, Axel Hoffmann, and Valentyn Novosad, *Applied Physics Letters Materials* 9, 060902 (Jun 2021)
20. *Interface roughness governed negative magnetoresistances in two-dimensional electron gases in AlGaN/GaN heterostructures*, Ting-Ting Wang, Sining Dong, Zhi-Li Xiao, Chong Li, Wen-Cheng Yue, Bin-Xi Liang, Fei-Fan Xu, Xiao-Li Lu, Jianhua Li, Chenguang Wang, Zixiong Yuan, Yong-Lei Wang, Song-Lin Li, Guo-Zhu Sun, Bin-Liu, Hai Lu, Hua-Bing Wang, Wai-Kwong Kwok, *Physical Review Materials* 5, 064003 (June 2021)

Symmetry Breaking in Two-Dimensional Flat-band Systems for Spin and Charge Transport

PI: Chun Ning (Jeanie) Lau

co-PI: Marc Bockrath

Department of Physics, The Ohio State University, Columbus, OH 43210

Program Scope

In a flat band system, the charge carriers' energy-momentum relation is very weakly dispersive. The resultant large density of states and the dominance of Coulomb potential energy relative to the kinetic energy often favor the formation of strongly correlated electron states. Such strong electronic correlations and competition between different degrees of freedom give rise to the formation of many interesting many-body phases, such as ferromagnetism, nematicity, antiferromagnetism, superconductivity, and charge density waves.

The advent of 2D materials has enabled unprecedented engineering and exploration of flat bands via control of layer thickness, magnetic field, and twisting. Building on past accomplishments, in this program we seek to create, engineer, and control the correlated states in flat band systems in 2D materials and heterostructures, and to exploit these states for transport of spins, charges and Cooper pairs. In the first thrust, we will focus on flat bands generated by magnetic fields that quench the charge carriers' kinetic energy. We plan to investigate the transport of spin degrees of freedom through the antiferromagnetic insulating states in monolayer and bilayer graphene[1, 2], with the goal of achieving electrical control of magnetic switching. By coupling trilayer graphene to superconductors, we will also engineer devices that host the much sought-after Majorana fermions[3] and may enable fault tolerant quantum computation.

The second thrust aims at investigating the correlated insulating states in few-layer graphene and superlattices. In the single particle picture, these systems are predicted to be metals, yet they are electrical insulators due to the strong electronic interactions. Here we will investigate the quantum Hall insulator and insulator-metal transition in tetralayer graphene, and the correlated insulator state in twisted bilayer graphene[4-7]. The latter system is particularly intriguing, since, by stacking two pieces of graphene at slightly different orientation, it becomes both a superconductor and an insulator, where the transition is tunable by charge density.

We will study these systems by transport measurements of high quality devices and varying temperatures, magnetic field, electric field, bias, charge density and disorder. These experiments will provide a comprehensive investigation of the many novel phenomena produced by electron-electron interactions in these exciting materials, and harness their unique properties for quantum information applications. Successful implementation of the project will be a major step forward in our fundamental knowledge of electron correlation and many-body physics in materials, which is important for physics, material science, engineering and energy science.

Recent Progress

In the past two years, we have made significant progress in our studies of ultra-clean ultra-clean graphene devices that are either suspended or supported on hexagonal BN substrates. Some of the works are highlighted below.

1. Helical Edge States and Quantum Phase Transitions in Tetralayer Graphene

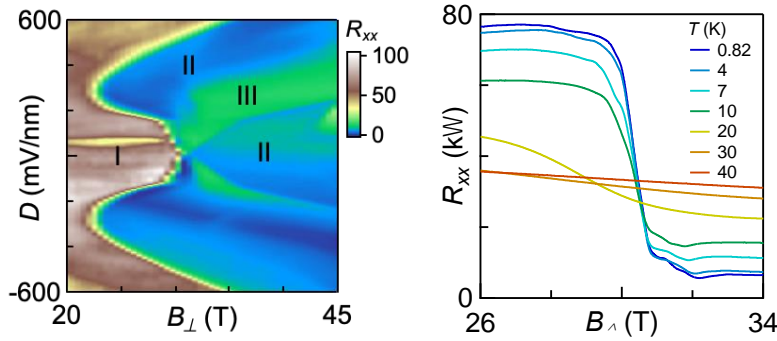


Fig. 1. (Left) Electronic phase diagram of tetralayer graphene , plotting $R_{xx}(D, B_{\perp})$ at $n=D=0$, different phases are labeled I, II and III. The unit is $k\Omega$. (Right) $R_{xx}(B_{\perp})$ at $n=D=0$ at selected temperatures.

Helical conductors with spin-momentum locking are promising platforms for Majorana fermions. Here we report observation of two topologically distinct phases supporting helical edge states in charge neutral Bernal-stacked tetralayer graphene in Hall bar and Corbino geometries. As the magnetic field B_{\perp} and out-of-plane displacement field D are varied, we observe a phase diagram consisting of an insulating phase and two metallic phases, with 0, 1 and 2 helical edge states, respectively. These phases are accounted for by a theoretical model that relates their conductance to spin-polarization plateaus. Transitions between them arise from a competition among inter-layer hopping, electrostatic and exchange interaction energies. Our work highlights the complex competing symmetries and the rich quantum phases in few-layer graphene. This work is published by *Physical Review Letters* and selected as **Editor's Suggestion**. (<https://link.aps.org/doi/10.1103/PhysRevLett.125.036803>)

2. Substrate-Dependent Band Structures in Trilayer Graphene/hBN Heterostructures

The tight-binding (TB) model has been spectacularly successful in elucidating the electronic and optical properties of a vast number of materials. Within the TB model, the hopping parameters that determine much of the band structure are often taken as constants. Here, using ABA-stacked trilayer (TLG) graphene as the model system, we show that, contrary to conventional wisdom, the hopping parameters and therefore band structures are not constants, but are systematically variable depending on their relative alignment angle between hexagonal BN (hBN). Moreover, addition or removal of the hBN substrate results in an inversion of the K and K' valley in TLG's lowest Landau level (LL). Our work illustrates the oft-ignored and rather surprising impact of the substrates on band structures of 2D materials. This work is published by *Physical Review Letters*.

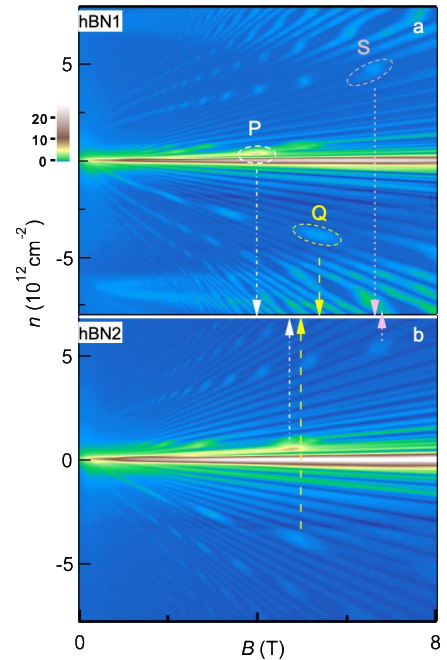


Fig. 2. Landau fan of two trilayer graphene devices showing different crossing points, indicating substrate-dependent hopping parameters.

(<https://journals.aps.org/prl/abstract/10.1103/PhysRevLett.125.246401>)

3. Strange metal behavior of the Hall angle in twisted bilayer graphene

Twisted bilayer graphene (TBG) with interlayer twist angles near the magic angle $\approx 1.08^\circ$ hosts flat bands and exhibits correlated states including Mott-like insulators, superconductivity, and magnetism. A linear-in-temperature normal state resistivity in TBG has been attributed to an exotic Planckian dissipation mechanism but can be equally well explained in terms of conventional electron-phonon scattering. To address this issue, we perform combined temperature-

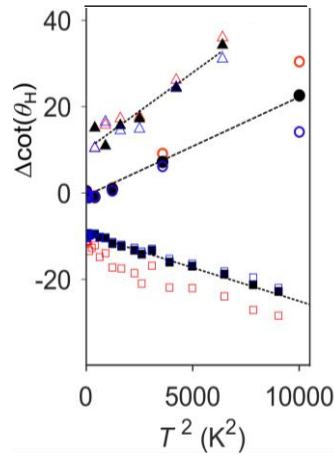


Fig. 3. $\cot \Theta_H(T)$ changes from its low temperature value versus T^2 , for three different samples (triangles, squares, and circles). Filled (open) symbols indicate data taken near (away from) half-filling. Dashed lines show linear fits to the half-filling data.

dependent transport measurements of both the longitudinal and Hall resistivities in near-magic-angle TBG. While the observed longitudinal resistivity follows linear temperature T dependence consistent with previous reports, the Hall resistance shows an anomalous T dependence with the cotangent of the Hall angle $\cot \Theta_H \propto T^2$. Boltzmann theory for quasiparticle transport predicts that both the resistivity and $\cot \Theta_H$ should have the same T dependence, contradicting the observed behavior. This failure of quasiparticle-based theories is reminiscent of other correlated strange metals such as cuprates.

4. Quantum Hall Effect Measurement of Spin–Orbit Coupling Strengths in Ultraclean Bilayer Graphene/WSe₂ Heterostructures

We study proximity-induced spin–orbit coupling (SOC) in bilayer graphene/few-layer WSe₂ heterostructure devices. Contact mode atomic force microscopy (AFM) cleaning yields ultraclean interfaces and high-mobility devices. In a perpendicular magnetic field, we measure the quantum Hall effect to determine the Landau level structure in the presence of out-of-plane Ising and in-plane Rashba SOC. A distinct Landau level crossing pattern emerges when tuning the charge density and displacement field independently with dual gates, originating from a layer-selective SOC proximity effect. Analyzing the Landau level crossings and measured inter-Landau level energy gaps yields the proximity-induced SOC energy scale. The Ising SOC is ~ 2.2 meV, 100 times higher than the intrinsic SOC in graphene, whereas its sign is consistent with theories predicting a dependence of SOC on interlayer twist angle. The Rashba SOC is ~ 15 meV. Finally, we infer the magnetic field dependence of the inter-Landau level Coulomb interactions. These ultraclean bilayer graphene/WSe₂ heterostructures provide a high mobility system with the potential to realize novel topological electronic states and manipulate spins in nanostructures. This work was published by *Nano Letters* (<https://pubs.acs.org/doi/abs/10.1021/acs.nanolett.9b02445>)

5. Correlated insulating and superconducting states in twisted bilayer graphene below the magic angle

The emergence of flat bands and correlated behaviors in “magic angle” twisted bilayer graphene (tBLG) has sparked tremendous interest, though its many aspects are under intense debate. Here

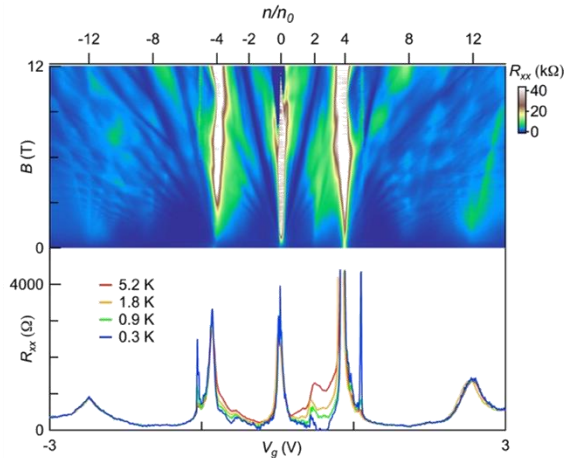


Fig. 4. Data from a twisted bilayer graphene. (Top panel): Landau fan of R_{xx} vs. magnetic field B and gate voltage V_g . The top axis labels the number of charges per superlattice cell. (Bottom panel): $R_{xx}(V_g)$ at different temperatures.

we report observation of both superconductivity and the Mott-like insulating state in a tBLG device with a twist angle of $\sim 0.93^\circ$, which is smaller than the magic angle by 15%. At an electron concentration of ± 5 electrons/moiré unit cell, we observe a narrow resistance peak with an activation energy gap ~ 0.1 meV. This indicates additional correlated insulating state, and is consistent with theory predicting a high-energy flat band. At doping of ± 12 electrons/moiré unit cell we observe resistance peaks arising from the Dirac points in the spectrum. Our results reveal that the “magic” range of tBLG is in fact larger than what is previously expected, and provide a wealth of new information to help decipher the strongly correlated phenomena observed in tBLG. This work is published by *Science Advances*.

(<https://advances.sciencemag.org/content/5/9/eaaw9770>)

Future Plans

Apart from the general direction outlined in the first section, our immediate plans for the next year include investigation of

- spin transport mechanism in graphene quantum Hall antiferromagnet
- Josephson junctions based on trilayer graphene
- superconductivity in graphene-based moiré systems

References

- [1] S. Takei *et al.*, Phys. Rev. Lett. **116**, 216801 (2016).
- [2] P. Stepanov *et al.*, Nat. Phys. **14**, 907 (2018).
- [3] P. San-Jose *et al.*, Phys. Rev. X **5**, 041042 (2015).
- [4] Y. Cao *et al.*, Nature **556**, 80 (2018).
- [5] Y. Cao *et al.*, Nature **556**, 43 (2018).
- [6] R. Bistritzer, and A. H. MacDonald, Proc. Nat. Acad. Sci. **108**, 12233 (2011).
- [7] J. M. B. Lopes dos Santos, N. M. R. Peres, and A. H. Castro Neto, Phys. Rev. Lett. **99**, 256802 (2007).

Two-year Publications Supported by BES

1. E. Codecido, Q. Wang, R. Koester, S. Che, H. Tian, R. Lv, S. Tran, K. Watanabe, T. Taniguchi, F. Zhang, M. Bockrath, and C. N. Lau, Correlated Insulating and Superconducting States in Twisted Bilayer Graphene Below the Magic Angle, *Sci. Adv.* **5**, eaaw9770 (2019).
2. D. Wang, S. Che, G. Cao, R. Lyu, K. Watanabe, T. Taniguchi, C. N. Lau, and M. Bockrath, Quantum Hall Effect Measurement of Spin–Orbit Coupling Strengths in Ultraclean Bilayer Graphene/WSe₂ Heterostructures, *Nano Lett.* **19**, 7028 (2019).
3. S. Che, Y. Shi, J. Yang, H. Tian, R. Chen, T. Taniguchi, K. Watanabe, D. Smirnov, C. N. Lau, E. Shimshoni, G. Murthy, and H. A. Fertig, Helical Edge States and Quantum Phase Transitions in Tetralayer Graphene, *Phys. Rev. Lett.* **125**, 036803 (2020). **Editor's**

Suggestion

4. S. Che, P. Stepanov, S. Ge, M. Zhu, D. Wang, Y. Lee, K. Myhro, Y. Shi, R. Chen, Z. Pi, C. Pan, B. Cheng, T. Taniguchi, K. Watanabe, Y. Barlas, R. K. Lake, M. Bockrath, J. Hwang, and C. N. Lau, Substrate-Dependent Band Structures in Trilayer Graphene Heterostructures, *Phys. Rev. Lett.* **125**, 246401 (2020).
5. C. N. Lau, F. Xia, and L. Cao, Emergent quantum materials, *MRS Bulletin* **45**, 340 (2020).
6. L. Du, T. Hasan, A. Castellanos-Gomez, G.-B. Liu, Y. Yao, C. N. Lau, and Z. Sun, Engineering symmetry breaking in 2D layered materials, *Nature Review Physics*, **3**, 193 (2021).
7. R. Lyu, Z. Tufeld, N. Verma, H. Tian, K. Watanabe, T. Taniguchi, C. N. Lau, M. Randeria, and M. Bockrath, Strange metal behavior of the Hall angle in twisted bilayer graphene, *Phys. Rev. B* **103**, 245424 (2021).

Oxide Quantum Heterostructures

Ho Nyung Lee (PI), Matt Brahlek, Gyula Eres, Hu Miao, and T. Zac Ward

Oak Ridge National Laboratory, Oak Ridge, TN 37831

Program Scope

The controlled synthesis of interfaces in oxide heterostructures with a wide variety of oxide-based quantum materials provides tremendous opportunities for producing materials with remarkable physical properties and functionalities. The overarching goal of this project is to understand, control, and exploit the electronic, magnetic, and structural interactions of oxide quantum heterostructures through interfacial coupling. To address this goal, this project focuses on the following specific aims: (1) Exploit spin orbit coupling and lattice symmetry to develop oxide heterostructures with novel quantum phenomena, (2) Create novel electronic ground states by interfacial charge transfer and orbital coupling, and (3) Understand strain coupling to develop novel ferroic quantum materials. Particular topical emphasis will be on studying the spin orbit coupling, Dzyaloshinskii-Moriya interaction, anomalous Hall states, topologically non-trivial states, and spin and charge transport. These quantum phenomena will be studied by combining the strong correlations of 3d transition metal oxides (TMOs) with the strong spin-orbit coupling of heavy elements containing 5d TMOs. Underpinning this work is a unique combination of experimental expertise, in particular, in the growth of epitaxial oxides using pulsed-laser epitaxy and detailed characterization of the physical properties by in-house equipment, neutron scattering, and optical and x-ray spectroscopy. Ultimately, the outcome of this work will result in enhanced understanding of interfacial behaviors and functionalities in oxide quantum heterostructures, providing guidance in the development of novel quantum materials for next-generation information and energy technologies.

Recent Progress

The research in this project is focused on the discovery of new materials and phenomena arising from well-controlled, functionally cross-coupled interfaces. In particular, we have focused on the development of interfacial heterostructures and their emerging electronic, ionic, magnetic, and structural properties. A combination of precision synthesis, theoretical and experimental in situ and post-growth characterization methods was used to gain insight into charge transfer, interface structure, electronic and ionic transport. The major studies include understanding the interfacial magnetism in correlated oxide heterostructures. Special emphasis was on understanding and controlling non-collinear spin structures and magnetism in *3d-5d* correlated oxide heterostructures by modifying the degree of the Dzyaloshinskii-Moriya interaction through interfacial symmetry modifications. This project also developed a novel synthesis route for growing nanobrush architectures designed to form high-density oxygen vacancies and tailoring magnetic anisotropy. The interface between magnetic materials and topological insulators in thin films grown by molecular-beam epitaxy was studied to understand the formation of exotic

phases of matter that enable functionality through manipulation of strong spin polarized transport. In the following, examples of the recent focus areas of this project on developing novel oxide quantum heterostructures are presented. The overall goal is to understand how to co-design correlated and topological states of matter by exploiting the interplay between symmetry, correlation, and topology in oxide- and chalcogenide-based quantum heterostructures.

Correlated Oxide Dirac Semimetal in the Extreme Quantum Limit

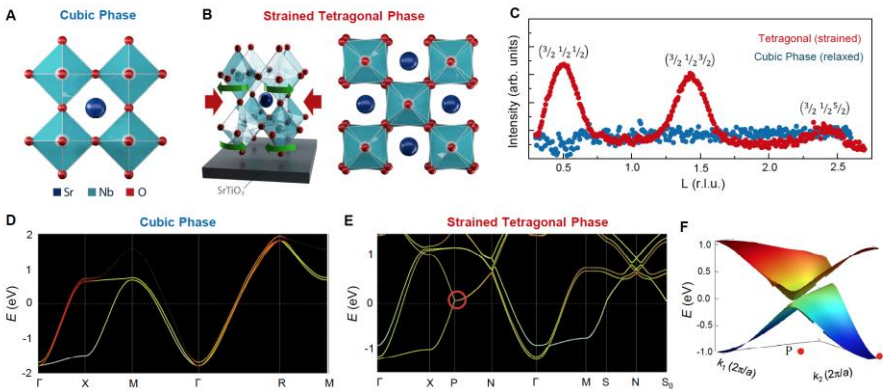


Figure 1. Strain-induced Dirac metallic state in SrNbO₃ thin films. (A–B) Octahedral distortion pattern for (A) cubic SrNbO₃ ($a^0a^0a^0$ in the Glazer notation) and (B) strained tetragonal SrNbO₃ (a^0a^0c). Epitaxial strain induces octahedral distortion. (C) Octahedral rotation-induced half-order superstructure diffraction peaks of $(3/2 \ 1/2 \ L/2)$ with $L = 1, 3, 5$ for fully strained (red, 7.2 nm, c^- rotation) and fully relaxed (blue, 130 nm, c^0 rotation) SrNbO₃ thin films. (D–E) Calculated electronic structure of (D) cubic SrNbO₃ and (E) strained tetragonal SrNbO₃. The red circle in plot (E) shows the Dirac point that appears near the Fermi level at the P point in the strained tetragonal phase. (F) Dirac dispersions near the P point within the tetragonal Brillouin zone. The larger Fermi velocity in the tetragonal phase, near the P point, would lead to higher carrier mobility and a favorable source of a non-trivial Berry phase in the presence of a magnetic field.

The combination of symmetry, correlation and topology is predicted to realize novel quantum states of matter. Despite a variety of experimental attempts to reshape the wave function topology and to induce entangled quantum states that intertwine charge, spin and orbital degrees of freedom, only a handful of materials have been identified and continue to be debated and explored as candidate correlated topological

materials. In this work, the strain-induced symmetry modification (Fig. 1) in correlated oxide SrNbO₃ thin films and their emerging topological band structure as a proof of an oxide-based Dirac semimetal is studied. A recent report on bulk $5d$ -based CaIrO₃ as an oxide Dirac semimetal is a promising discovery for the realization of oxide-based correlated topological quantum materials (CTQMs) as this bulk material revealed the hallmark signature of high mobility for the first time from any oxide-based candidates [1]. In this system, correlated electrons are reported to reach the quantum limit. However, the key signature for localization of Dirac electrons, i.e., fractional quantum states with high effective mass, has not been observed. The discovery of a material system that obeys fractional statistics, which cannot be understood from the noninteracting limit, is highly important for two reasons. It can deepen our understanding of many-body interactions and provide components relevant to quantum computing applications.

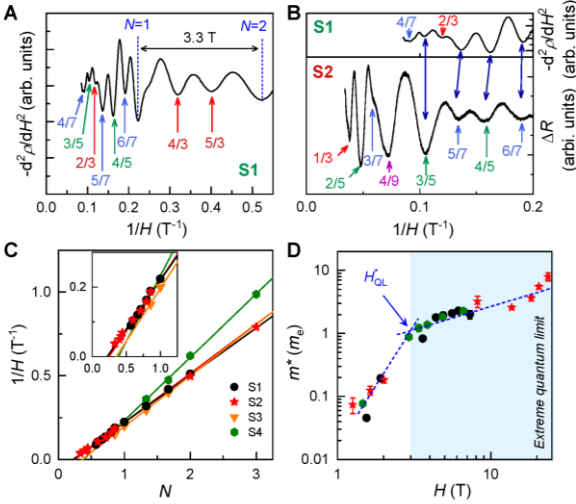


Figure 2. Anomalous quantum oscillations in the quantum limit. (A) $-d^2\rho/dH^2$ as a function of $1/H$ under a magnetic field of up to 14 T for S1. The resistivity minima are assigned as integer (fractional) Landau levels, as indicated by the arrows. (B) ΔR as a function of $1/H$ under a magnetic field of up to 30 T for S2. S1 and S2 samples show consistent behavior. (C) Landau fan diagram of the Landau level index N versus $1/H$ for four different samples. All samples clearly show linear behavior. The inset shows an enlarged view of the high-field region. All samples have a non-trivial Berry phase as predicted by the calculations. (D) Effective mass at different magnetic fields for four different samples. Strong mass enhancement is found at $H_{QL}^* \sim 3.3$ T.

rare example of correlated-oxide Dirac semimetals, in which strong correlation of Dirac electrons leads to the realization of novel correlated topological QMs.

Epitaxial growth and atomic-scale control of triangular-lattice metallic delafossites

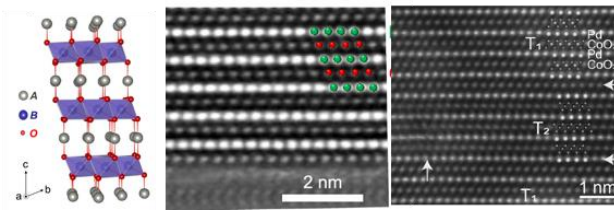


Figure 3. (left) Schematic of the delafossite structure and successful epitaxy of (middle) PdCrO_2 and (right) PdCoO_2 seen from scanning transmission electron microscopy, highlighting the layered structure composed of 2D Pd layers and edge-sharing transition metal octahedra.

Some of the fractional states, for example $5/2$ and $12/5$ fractional states, are expected to have a non-abelian quasiparticle, which is the most basic ingredient for topological quantum computing, along with Majorana fermions in topological superconductors. Since CaIrO_3 is a 5d-TMO, we presume the correlation effect may not be strong enough. Therefore, we study 4d based TMOs, which are a class of materials that have not been much explored, as they may provide a good balance between the strong correlation and SOC. In this PI meeting, strain-induced symmetry modification in correlated oxide SrNbO_3 thin films creates an emerging topological band structure will be presented. Dirac electrons in strained SrNbO_3 films revealed ultra-high mobility ($\mu_{\text{max}} \approx 100,000 \text{ cm}^2/\text{Vs}$), exceptionally small effective mass ($m^* \sim 0.04m_e$), and non-zero Berry phase [2]. More importantly, strained SrNbO_3 films reached the extreme quantum limit, exhibiting a sign of fractional occupation of Landau levels and giant mass enhancement (Fig. 2). Our results suggest that symmetry-modified SrNbO_3 is a

The epitaxial growth of metallic delafossites was achieved, (Fig. 3) where it was found that high-quality materials require a careful balance of growth conditions and interfacial symmetry control [3]. The natural layering of metallicly bonded 2D layers and edge-sharing transition metal octahedra on a triangular lattice impart intriguing physical properties, particularly extremely high conductivity, novel magnetic states, and strongly

intercoupling among the itinerate electrons and localized magnetic states. While the unique layered structure interleaving the triangular metallic A layers and the oxidized BO₂ layers is interesting, there are challenges in synthesizing high-quality materials. Particularly, for A = Pd, requires careful balance since oxidizing the Pd to the 1+ state requires high oxygen pressure, yet too high oxygen pressure (>mTorr) causes Pd-deficiency due to sublimation the PdO. Further, we have found that nearly single phase PdCrO₂ can be grown using pulsed laser deposition when a proper buffer layer was used to template the delafossite structure, which open routes to single phase materials. The ability to control these materials down to the single layer limit creates routes to addressing many fundamental questions in correlated materials.

Future Plans

The grand challenge we are facing now lies in the combination of electronic correlation and topology to realize correlated topological quantum states (CTQS). There are fundamentally two possible routes to CTQS: (1) creation of topological band structures in correlated materials and (2) realization of correlation-induced topological orders. However, there exists a significant knowledge gap in our understanding on how the electronic correlations manifest themselves in topologically protected band structures, hindering the realization of CTQS. Thus, we will focus on filling the knowledge gap on how to experimentally realize CTQMs and unveil their exotic physical properties. Thus, this project will focus on how to co-design correlated and topological states of matter by exploiting the interplay between symmetry, correlation, and topology in oxide- and chalcogenide-based quantum heterostructures. Two classes of materials systems, including transition metal oxide (TMO) based materials synthesized by pulsed-laser deposition (PLD) and intrinsic magnetic topological insulators (MTIs) grown by molecular-beam epitaxy (MBE), will be the main focus. The PLD approach will focus on gaining an understanding of how to create topological phases in correlated electron materials, including perovskites (SrNbO₃) and pyrochlores (*Re*₂Ir₂O₇, *Re*=rare earth), and delafossites (PdCoO₂ and PdCrO₂). The MBE approach will focus on identifying fundamental mechanisms to control the surface topological states in intrinsic magnetic topological materials (MnBi₂Te₄ and related heterostructures) using heterogeneities and interfacial coupling with oxide-based correlated materials. ORNL's recent investment in the unique capability of 11 eV laser-based spin-ARPES directly connected with the PLD and MBE growth systems will further enable us to investigate the topological characteristics of candidate CTQMs.

References

1. J. Fujioka, Y. Tokura et al., Strong-correlation induced high-mobility electrons in Dirac semimetal of perovskite oxide, *Nat Commun.* **10**, 362 (2019).
2. J. M. Ok, H. N. Lee et al., Correlated oxide Dirac semimetal in the extreme quantum limit arXiv:2108.08408. to appear in *Science Adv.*
3. J. M. Ok *et al.*, Pulsed-laser epitaxy of metallic delafossite PdCrO₂ films, *APL Mater.* **8**, 051104 (2020).

Publications (selected from a total of 51 publications)

1. C. Sohn, E. Skoropata, Y. Choi, X. Gao, A. Rastogi, A. Huon, M. A. McGuire, L. Nuckols, Y. Zhang, J. Freeland, D. Haskel, and H. N. Lee, Room-temperature ferromagnetic insulating state in highly cation-ordered double perovskite $\text{Sr}_2\text{Fe}_{1+x}\text{Re}_{1-x}\text{O}_6$ films, *Adv. Mater.* **31**, 1805389 (2019). (Highlighted as a cover page article)
2. E.-J. Guo, R. D. Desautels, D. Keavney, M. A. Roldan, B. J. Kirby, D. Lee, Z. Liao, T. Charlton, A. Herklotz, T. Z. Ward, M. R. Fitzsimmons, and H. N. Lee, Nanoscale ferroelastic twins formed in strained LaCoO_3 films, *Sci. Adv.* **5**, eaav5050 (2019).
3. Z. Liao, E. Skoropata, J. W. Freeland, E.-J. Guo, R. Desautels, X. Gao, C. Sohn, A. Rastogi, T. Z. Ward, T. Zhou, T. Charlton, M. R. Fitzsimmons, and H. N. Lee, Large orbital polarization in nickelate-cuprate heterostructures by dimensional control of oxygen coordination, *Nat. Commun.* **10**, 589 (2019).
4. Z. Liao, M. Brahlek, J. M. Ok, L. Nuckols, Y. Sharma, Q. Lu, Y. Zhang, and H. N. Lee, Pulsed-laser epitaxy of topological insulator Bi_2Te_3 thin films, *APL Mater.* **7**, 041101 (2019).
5. A. Rastogi, M. Brahlek, J. M. Ok, Z. Liao, C. Sohn, S. Feldman, and H. N. Lee, Metal-insulator transition in (111) SrRuO_3 ultrathin films, *APL Mater.* **7**, 091106 (2019). (Editor's pick article)
6. M. Brahlek, G. Rimal, J. M. Ok, D. Mukherjee, A. Mazza, Q. Lu, H. N. Lee, T. Z. Ward, R. R. Unocic, G. Eres, and S. Oh, Growth of metallic delafossite PdCoO_2 by molecular beam epitaxy, *Phys. Rev. Mater.* **3**, 093401 (2019).
7. E. Guo, R. Desautels, D. Lee, M. A. Roldan, Z. Liao, T. Charlton, H. Ambaye, J. Molaison, R. Boehler, D. Keavney, A. Herklotz, T. Z. Ward, H. N. Lee, and M. R. Fitzsimmons, Exploiting symmetry mismatch to control magnetism in a ferroelastic heterostructure, *Phys. Rev. Lett.* **122**, 187202 (2019).
8. E. Skoropata, J. Nichols, J. M. Ok, R. V. Chopdekar, E. S. Choi, A. Rastogi, C. Sohn, X. Gao, S. Yoon, T. Farmer, R. D. Desautels, Y. Choi, D. Haskel, J. W. Freeland, S. Okamoto, M. Brahlek, and H. N. Lee, Interfacial tuning of chiral magnetic interactions for large topological Hall effects in $\text{LaMnO}_3/\text{SrIrO}_3$ heterostructures, *Sci. Adv.* **6**, eaaz3902 (2020).
9. J. M. Ok, S. Yoon, A. Lupini, P. Ganesh, M. F. Chisholm, and H. N. Lee, Interfacial stabilization for epitaxial CuCrO_2 delafossites, *Sci. Rep.* **10**, 11375 (2020).
10. J. M. Ok, M. Brahlek, W. S. Choi, K. M. Roccapiore, M. F. Chisholm, S. Kim, C. Sohn, E. Skoropata, S. Yoon, J. S. Kim, and H. N. Lee, Pulsed-laser epitaxy of metallic delafossite PdCrO_2 films, *APL Mater.* **8**, 051104 (2020).
11. D. Lee, X. Gao, L. Sun, Y. Jee, J. Poplawsky, T. O. Farmer, L. Fan, E.-J. Guo, Q. Lu, W. T. Heller, Y. Choi, D. Haskel, M. R. Fitzsimmons, M. F. Chisholm, K. Huang, B. Yildiz, and H. N. Lee, Colossal oxygen vacancy formation at a fluorite-bixbyite interface, *Nat. Commun.* **11**, 1371 (2020).
12. M. Brahlek, A. R. Mazza, K. C. Pitike, E. Skoropata, J. Lapano, G. Eres, V. R. Cooper, and T. Z. Ward, Unexpected crystalline homogeneity from the disordered bond network in $\text{La}(\text{Cr}_{0.2}\text{Mn}_{0.2}\text{Fe}_{0.2}\text{Co}_{0.2}\text{Ni}_{0.2})\text{O}_3$ films, *Phys. Rev. Mater.* **4**, 054407 (2020). (Editor's Suggestion)

13. J. Lapano, A. R. Mazza, H. Li, D. Mukherjee, E. M. Skoropata, J. M. Ok, H. Miao, R. G. Moore, T. Z. Ward, G. Eres, H. N. Lee, and M. Brahlek, Strong spin-dephasing in a topological insulator-paramagnet heterostructure, *APL Mater.* **8**, 091113 (2020).
14. J. Lapano, L. Nuckols, A. R. Mazza, Y. Y. Pai, J. Zhang, B. Lawrie, R. G. Moore, G. Eres, H. N. Lee, M.-H. Du, T. Z. Ward, J. S. Lee, W. J. Weber, Y. Zhang, and M. Brahlek, Adsorption-controlled growth of MnTe(Bi₂Te₃)_n by molecular beam epitaxy exhibiting stoichiometry-controlled magnetism, *Phys. Rev. Mater.* **4**, 111201 (2020).
15. Q. Lu, C. Sohn, G. Hu, X. Gao, M. F. Chisholm, I. Kylanpaa, J. T. Krogel, P. R. C. Kent, O. Heinonen, and H. N. Lee, Metal-insulator transition tuned by oxygen vacancy migration across VO₂/TiO₂ interface, *Sci. Rep.* **10**, 18554 (2020).
16. D. Nevola, H. X. Li, J.-Q. Yan, R. G. Moore, H. N. Lee, H. Miao, and P. D. Johnson, Coexistence of surface ferromagnetism and gapless topological state in MnBi₂Te₄, *Phys. Rev. Lett.* **125**, 117205 (2020). Editor's suggestion and Featured in Physics
17. S. Yoon, J. M. Ok, S. A. Lee, J. Lee, A. Huon, A. R. Lupini, W. S. Choi, and H. N. Lee, Atomic structure of the initial nucleation layer in hexagonal perovskite BaRuO₃ thin films, *Adv. Mater. Interfaces* 2100023 (2021).
18. E. Skoropata, A. Mazza, A. Herklotz, J. M. Ok, G. Eres, M. Brahlek, T. R. Charlton, H. N. Lee, and T. Z. Ward, Post-synthesis control of Berry phase driven magnetotransport in SrRuO₃ films, *Phys. Rev. B* **103**, 085121 (2021).
19. H. Miao, Y. L. Wang, J.-X. Yin, J. Zhang, S. Zhang, M. Z. Hasan, R. Yang, X. C. Wang, C. Q. Jin, T. Qian, H. Ding, H. N. Lee, and G. Kotliar, Hund's superconductor Li(Fe,Co)As, *Phys. Rev. B* **103**, 054503 (2021).
20. H. Li, T. T. Zhang, A. Said, G. Fabbris, D. G. Mazzone, J. K. Keum, J. Q. Yan, D. Mandrus, S. Murakami, G. Halasz, S. Okamoto, M. P. M. Dean, H. N. Lee, and H. Miao, Giant phonon anomalies in the proximate Kitaev quantum spin liquid α -RuCl₃, *Nature Commun.* **12**, 3513 (2021).
21. H. Li, T. Zhang, A. Said, Y. Fu, G. Fabbris, D. G. Mazzone, J. Zhang, J. Lapano, H. N. Lee, H. C. Lei, M. P. M. Dean, S. Murakami, and H. Miao, Observation of a chiral wave function in twofold degenerate quadruple Weyl system BaPtGe, *Phys. Rev. B*, **103**, 184301 (2021).
22. S. Yoon, X. Gao, J. M. Ok, Z. Liao, M.-G. Han, Y. Zhu, P. Ganesh, M. F. Chisholm, W. S. Choi, H. N. Lee, Strain-induced atomic-scale building blocks for ferromagnetism in epitaxial LaCoO₃, *Nano Lett.* **21**, 4006 (2021).
23. C. Sohn, X. Gao, R. K. Vasudevan, S. M. Neumayer, N. Balke, J. M. Ok, D. Lee, E. Skoropata, H. Y. Jeong, Y.-M. Kim, and H. N. Lee, Strain-driven autonomous control of cation distribution for artificial ferroelectrics, *Sci. Adv.* **7**, eabd7394 (2021).
24. H. X. Li, T. T. Zhang, Y.-Y. Pai, C. Marvinney, A. Said, T. Yilmaz, Q. Yin, C. Gong, Z. Tu, E. Vescovo, R.G. Moore, S. Murakami, H.C. Lei, H. N. Lee, B. Lawrie, H. Miao, Observation of unconventional charge density wave without acoustic phonon anomaly in kagome superconductors AV₃Sb₅ (A= Rb, Cs), *Phys. Rev. X* **11**, 031050 (2021).

Investigating new routes to quantum disordered states

Minhyea Lee, University of Colorado Boulder

Program Scope Unconventional magnetic phases of matter lie at the forefront of advances in spintronics and quantum information processing. Applications in these fields require a complete understanding of the fundamental properties of both the ground and excited states of systems that can host one or more types of magnetic order, topological states, gapped or gapless quantum spin-liquid phases, and fractional excitations. This project aims understand both magnetically ordered states with strong magnetic anisotropy and highly entangled quantum disordered states in proximity to the ordered phase. Leveraging intense magnetic fields and inherently large magnetic anisotropies, we investigate particularly the contributions from underlying lattice (phonons) that are not system-specific in a wide range of unconventional quantum magnets. This, in turn, offers a suite of probes for pinning down entangled and unconventional magnetic states that are highly sought after.

Recent Progress We have investigated the anisotropic magnetic response of an insulating 4f electronic system by measuring two key thermodynamic quantities, the magnetic susceptibility in the low-field limit [Fig. Top left] and the magnetotropic coefficients over very wide field and temperature ranges [Fig. Top right]. We have shown that the anisotropies in both quantities can be

formulated within a set of anisotropic van Vleck (VV) coefficients, which arise as the second-order perturbative corrections of the Zeeman interaction to the zero-field crystal electric field (CEF) spectrum. This leads to the essential finding that the VV coefficients constitute independent physical quantities that describe the crucial magnetic properties of 4f spin systems across the full range of applied fields and extant anisotropies. We find that a proper account of the ground-state VV coefficients is indispensable for an accurate and unambiguous determination of the microscopic parameters governing the CEF Hamiltonian, a process for which otherwise few routes are known to date. The VV coefficients fulfill the vital function of unifying the low-field, low-temperature magnetic susceptibility with the high-field magnetotropic coefficients and CEF levels.

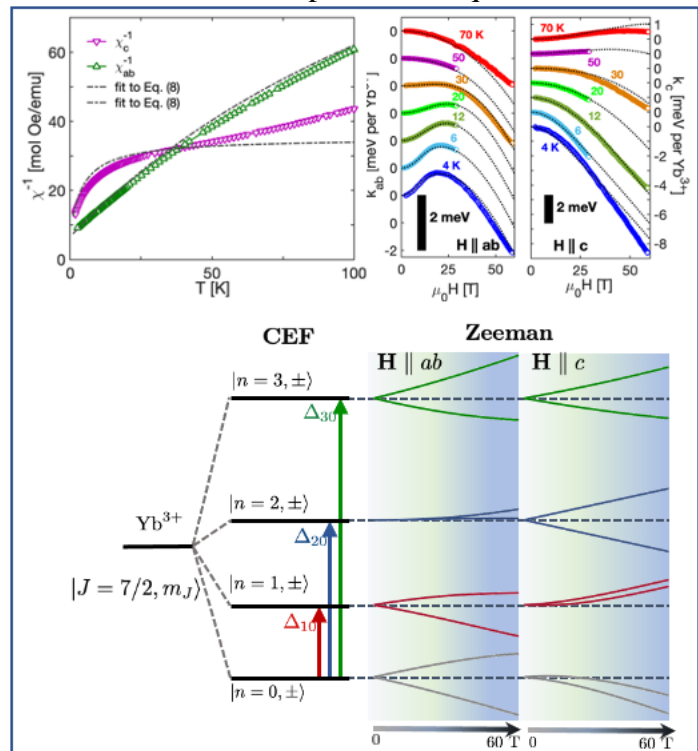


Fig. Temperature dependence of inverse magnetic susceptibility in CsYbSe₂ at taken 1 T (Top left) and magnetotropic coefficients as a function of field are shown in (Top right). Schematic energy level diagram under magnetic field is shown in Bottom.

In this sense their role as stand-alone physical quantities allowing a full interpretation of magnetic anisotropies has not been appreciated before.

Our experimental results highlight the value of the resonant torsion magnetometry (RTM) method, from which we extract the magnetotropic coefficients over these broad field and temperature ranges. They play the key role in obtaining a unique set of the coefficients of Stevens operators describing the microscopic CEF Hamiltonian with unprecedented fidelity. We reiterate that a fitting analysis must provide complete consistency from zero to high field and at all relevant temperatures, and our fits meet this challenge. With the full CEF spectrum in hand, we can examine the validity of different and popular approximations that have been applied to many materials. Specifically, we identify the limits of a Curie-Weiss fit to the temperature-dependence of the magnetic susceptibility and the boundaries of the effective pseudospin-1/2 description for systems with a ground-state Kramers doublet.

We have developed and applied our analysis for the material CsYbSe₂, which is a member of a family of Yb-delafossites displaying triangular-lattice geometry. Because the CEF levels of the Yb ion are four Kramers doublets, these compounds are leading candidates in the search for quantum spin-liquid (QSL) behavior [1, 2], and indeed the full CEF spectrum we obtain up to high fields [Fig. Bottom] reveals an intricate and anisotropic energy landscape amenable to unconventional magnetism. This spectrum allows one to construct a maximally informed pseudospin-1/2 model for the low-energy physics of the system, and within a minimal XXZ spin Hamiltonian we conclude that CsYbSe₂ is a strongly XY triangular antiferromagnet. While we await further experimental confirmation of this result, we note again that our analysis is applicable to a wide range of 4f materials with complex CEF spectra and especially with ground-state doublets allowing an effective spin-1/2 description, which should significantly expand the scope of the search for QSL phases.

Future Plans We are investigating the field dependence of thermal conductivity in CsYbSe₂ and identify a peculiar feature – a pronounced minimum in in-plane thermal conductivity as a function of field, only in temperature range of $4\text{ K} < T < \sim 30\text{ K}$. With the full CEF spectrum in hand from our RTM study, we consider a magnetoelastic coupling that enables the hybridized excitations between phonon and spin-flip of the lowest Kramers doublet under magnetic field. We find the minimum feature in the field dependence of thermal conductivity is *not* system-specific but generic for any system with 2 levels (e. g. the lowest Kramers doublet in CsYbSe₂), of which gap changes linearly to H, as long as phonon-phonon scattering is not too strong. Further investigations on other materials of the same situations and more elaborated correction based on the spin-phonon scattering model from our previous results [3] is under the way.

References

- [1] P.-D. Dai, G. Zhang, Y. Xie, et al., **Phys. Rev. X** **11**, 021044 (2021).
- [2] M. M. Bordelon, E. Kenny, C. Liu et al., **Nat. Phys.** **15**, 1058 (2019).
- [3] C. A. Pocs, I. A. Leahy, H. Zheng, et al., **Phys. Rev. Research** **2**, 013059 (2020).

Publications

- [1] Peter E. Siegfried, Mark Maus, Alexander C. Bornstein, Dirk Wulferding, Ryan E. Baumbach, Eric D. Bauer, Filip Ronning, Jeehoon Kim, and Minhyea Lee, “Hall effect, magnetic ac susceptibility and the evolution of topological magnetic bubble domains in the uniaxial-ferromagnet CeRu₂Ga₂B” (submitted)
- [2] Christopher A. Pocs, Peter E. Siegfried, Jie Xing, Athena S. Sefat, Michael Hermele, Bruce Normand, and Minhyea Lee, “Systematic fitting of crystal-field levels and accurate extraction of quantum magnetic models in Yb-based triangular-lattice delafossites” (submitted)

Study of topological and unconventional superconductors in nanoscale

Qi Li

Department of Physics, Pennsylvania State University, University Park, PA 16802

Project scope

The goal of the project is to study proximity-induced superconductivity, quantum phenomena, and unconventional superconductors in several two-dimensional (2D) and nanoscale systems. The systems studied are either known topological insulators, 2D electron systems with large Rashba spin-orbit coupling (SOC), and thin films with enhanced T_c from their bulk values. Several materials systems have been studied which include quantum transports in two-dimensional (2D) electron liquids at the SrTiO₃ (111) interfaces at high magnetic field which reaches the quantum limit; inducing superconductivity in topological insulator Bi₂Te₃ nanotubes, quantum anomalous Hall materials, and ferromagnetic metal nanowires; and superconductivity in very thin TiOx and monolayer FeSe, both of which have higher T_c in thin films than that of the corresponding bulks. Most of the materials have been demonstrated or predicted to have topological states.

Transition metal oxides in the (111) orientation have recently attracted special interest because of their hexagonal structural symmetry, similar to topological insulator Bi₂Se₃ and graphene. In addition, large SOC and strong interplay between charge, spin, and lattice degrees of freedom may result in exotic phases, such as spin liquids and Mott topological insulators.¹ We have developed a fabrication method to create 2D electron systems at the SrTiO₃ (111) interfaces with high mobility exceeding 20,000 cm²V⁻¹s⁻¹. Pronounced Shubnikov-de Haas oscillations at high magnetic fields up to 35 T and down to 300 mK have been observed, which reaches the quantum limit at field between 12-19 T. We have studied inducing superconductivity in three systems, topological Bi₂Te₃ nanotubes, quantum anomalous Hall effect thin films, and magnetic Ni nanowires, using superconducting Nb films in contact with those materials to seek signatures of topological superconductivity and Majorana fermions. We have also studied superconductivity in two thin film systems: TiOx (111) thin films and monolayer FeSe, both of which have displayed much higher T_c than that of the corresponding bulk material, highlighting the role interfaces and boundaries can play in enhancing T_c in thin films. In addition, we have also synthesized MbB₂ thin films with T_c of 40 K and high H_{c2} on SrTiO₃ (111) in preparation for further studies on inducing superconductivity with high T_c and H_{c2} superconductors.

Recent Progress

Shubnikov-de Haas Oscillations into the Quantum Limit in Two-Dimensional Electron Systems at SrTiO₃ (111) Interfaces

We have developed a fabrication method using amorphous cap layers to form high mobility 2D electron liquid at (111)-oriented SrTiO₃ interface with the mobility exceeding to 20,000 cm²V⁻¹s⁻¹. We find that amorphous insulating cap layers result in higher mobility than that of epitaxial structures, possibly due to minimum strain in the 2D electron systems. SrTiO₃ is a band insulator, but conducting interface can be formed at the interfaces with a variety of other insulators. We have studied the Shubnikov-de Haas (SdH) oscillations at National High Magnetic Field Lab up to 60 T (pulse field) and 35 T (DC field) and down to 300 mK. Owing to the high mobility of the samples, pronounced SdH oscillations can be observed from a relatively low magnetic field of ~ 2 T at low temperatures all the way to the last oscillation dip, beyond which no more oscillations exist. The last dip correspond to the quantum limit field where where all carriers are condensed in the lowest energy Landau level state. Four samples with different carrier densities have been measured. All samples reached quantum limit with the field ranging from 19.9 T to 12.6 T with reducing carrier densities. The electron system displays a single oscillation frequency as revealed by fast Fourier transformation (FFT) of the SdH oscillations. The results are shown in Fig. 1 and 2 for Sample A (see manuscript section). Further analysis of the results show the effective mass is $m^* = 1.46 \pm 0.05 m_e$. The positions of resistance dips and peaks have a linear relation with the Landau level index n and the intercepts of the linear fits are very close to -0.2 for all samples, suggesting the non-zero Berry phase in the system, which is related to the degeneracy of electron states and Rashba SOC at the interface.

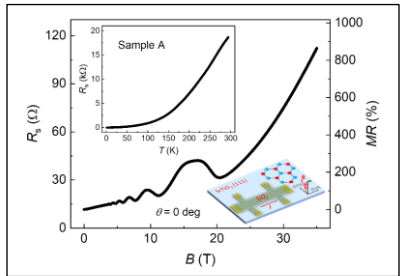


FIG. 1. Sheet resistance R_s versus magnetic field at high magnetic field up to 35 T and 320 mK in Sample A. Upper inset: R_s versus temperature.

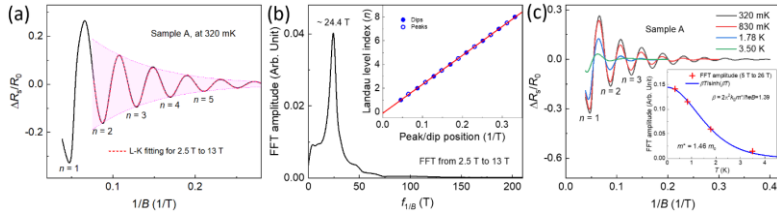


FIG. 2. (a) $\Delta R_s/R_0$ has a periodicity in $1/B$. Oscillations for Landau level $n \geq 2$ follows the trendline given by L-K formula. (b) Fast Fourier transformation of $\Delta R_s/R_0$. Inset: Landau fan diagram. The integer Landau level index (n) is assigned to the n -th oscillation dip. (c) $\Delta R_s/R_0$ ($1/B$) at different temperatures. Inset: temperature dependence of the SdH FFT amplitude.

Achieving the lowest Landau level at relatively low field enables us to study the ultra-quantum limit transport which, to the best of our knowledge, has never been reached in SrTiO₃ (111) electron systems. There are two significant effects observed in this range: (1) A clear spin splitting at the last oscillation peak which becomes more pronounced at tilted field angles. This result is fitted by a model that considers Zeeman splitting and Rashba SOC with Lande' factor g

= 0.29 and Rashba coefficient $\alpha = 0.6 \text{ meV} \cdot \text{nm}$. This yields the Rashba energy of 0.3 meV at the Fermi level. (2). The temperature dependence of the resistance changes from metallic to insulating behavior after reaching the quantum limit, indicating a metal to insulating state transition. At the same point, a significant change in the MR behavior also occurs; it undergoes a dramatic transition from a predominantly quadratic field dependence to an unsaturated linear field dependence with a very large MR exceeding 1400%. This indicates an insulating state in the quantum limit, possibly due to strong electron correlations when all carriers occupy the lowest Landau level state.

Inducing superconductivity in topological and nanoscale systems

Inducing superconductivity in Bi₂Te₃ nanotube/Nb proximity coupled structures

We studied induced superconductivity in a single Bi₂Te₃ nanotube with Nb contacts and different combinations of Nb and Au contacts by using e-beam lithography. We observed a sudden increase of the nanotube resistance when the Nb became superconducting, which disappeared when the temperature is above the T_c of Nb or the applied magnetic field is larger than the H_{c2} of Nb. This result is possibly related to the superconducting fluctuation effect (our measurements are limited to 2K and therefore cannot reach very low temperature to confirm a superconducting transition.).

We have also participated in studying two other systems with Nb hybrid devices: a quantum anomalous Hall (QAH) insulator coupled to Nb, and Ni magnetic nanowires coupled to Nb. The results have been reported in the publication list.

Superconductivity in thin films

We have synthesized and studied superconductivity in two systems: Capping layer influence and isotropic in-plane upper critical field of the superconductivity at the FeSe/SrTiO₃ interface, and synthesizing high T_c (~40K) MgB₂ thin films on SrTiO₃ (111) substrate using the Hybrid Physical and Chemical Vapor Deposition (HPCVD) technique developed previously.

Future Plans

We plan to study the nature of the insulating phases in ultra-quantum limit in SrTiO₃ (111) 2D electron liquid, such as whether it is Wigner crystal state or a nematic phase. We also plan to study quantum oscillations in other orientations and whether the quantum limit can be reached. On the superconductivity side, we plan to study superconductivity in SrTiO₃ (111) 2D electron systems and comparing the superconductivity with different orientations and the relationship between virgin carrier densities and the superconductivity. We will also seek for low temperature and high magnetic field measurements to see whether the sign of re-entrant superconductivity could be observed in the low Landau level states. We plan to complete the study of induced superconductivity and the anomalous effect observed in Bi₂Te₃ nanotubes at lower temperatures

where the resistance transition might be expected. With the establishment of growing MgB₂ thin films with high T_c and high H_{c2}, we plan to study induced superconductivity in various topological samples using the higher T_c contact with a goal to achieve topological superconductivity at higher temperatures.

Reference

1. D. Doennig, W.E. Pickett, and R. Pentcheva, “Massive symmetry breaking in LaAlO₃/SrTiO₃(111) quantum wells: a three-orbital strongly correlated generalization of graphene” *Phys. Rev. Lett.* 111, 126804 (2013).

Publications in the last two years (acknowledge DOE support)

1. C. Zhang, Y. Fan, T. Wang, X. Liu, Q. Li, Y. Yin, X. Li, “Quantum Griffiths singularity in TiO superconducting thin films with insulating normal states”. *NPG Asia Materials*, 11, 9. (2019).
2. Morteza Kayyalha, Di Xiao, Ruoxi Zhang, Jaeho Shin, Jue Jiang, Fei Wang, Yi-Fan Zhao, Run Xiao, Ling Zhang, Kajetan M. Fijalkowski, Pankaj Mandal, Martin Winnerlein, Charles Gould, Qi Li, Laurens W. Molenkamp, Moses H. W. Chan, Nitin Samarth, Cui-Zu Chang “Absence of evidence for chiral Majorana modes in quantum anomalous Hall-superconductor devices”. *Science*, 367 64-67 (2020).
3. Tej B. Limbu, Basant Chitara, Martha Garcia Cervantes, Jason D. Orlando, Shalini Kumari, Qi Li, Yongan Tang, and Fei Yan “Green synthesis of reduced Ti₃C₂T_x MXene nanosheets with enhanced conductivity, oxidation stability, and SERS activity”. *J. Mat. Chem. C* 8,4722 (2020).
4. DukSoo Kim, Renzhong Du, Shih-Ying Yu, Yuewei Yin, Sining Dong, Qi Li, Suzanne E Mohney, Xiaoguang Li, and Srinivas Tadigadapa “Enhanced thermoelectric efficiency in Nnanocrystalline bismuth telluride nanotubes” *Nanotechnology* 31, 365703 (2020).
5. Yanan Li, Ziqiao Wang, Run Xiao, Qi Li, Ke Wang, Anthony Richardella, Jian Wang, and Nitin Samarth “Capping layer influence and isotropic in-plane upper critical field of the superconductivity at the FeSe/SrTiO₃ interface”, *Phys. Rev. Materials* 5, 034802 (2021).

Manuscript submitted (selected)

6. Ziqiao Wang, Autumn Heltman, Shalini Kumari, Lunhui Hu, Zhu Lin, Lin Jiao, Shalinee Chikara, Alexey Suslov, John Singleton, Fedor Balakirev, Chaoxing Liu, and Qi Li, “Shubnikov-de Haas Oscillations into the Quantum Limit in Two-Dimensional Electron Systems at SrTiO₃ (111) Interfaces” submitted (2021).
7. Jue Jiang, Weiwei Zhao, Fei Wang, Renzhong Du, Ludi Miao, Ke Wang, Qi Li, Cui-Zu Chang, and Moses H.W. Chan, “Long-Range Superconducting Proximity Effect in Nickel Nanowires”, submitted (2021).
8. S. Kumari, D. K. Pradhan, S. Liu, M. M. Rahaman, P. Zhou, D. K. Pradhan, A. Kumar, G. Srinivasan, Qi Li, R. S. Katiyar, and J. F. Scott “Room Temperature Magnetoelectricity in Transition Metal Doped Ferroelectrics” submitted (2020).
9. Tej B. Limbu, Shalini Kumari, Ziqiao Wang, Chetan Dhital, Qi Li, Yongan Tang, and Fei Yan, “Anomalous Enhancement of Ferromagnetism in Chemically-Reduced 2D Ti₃C₂T_x MXene Nanosheets”, submitted (2021).

Identifying the signatures of topological superconductivity and fractional excitations in bulk crystals and thin films

Vidya Madhavan, University of Illinois, Urbana Champaign

Program Scope

The goal of the project is to use low temperature scanning tunneling microscopy (STM), spectroscopy (STS), and MBE thin film growth to investigate topological superconductivity in 2D and 3D materials. We will study 3D topological superconductors, as well as the effects of proximity induced superconductivity in 2D systems with both chiral and helical topological edge modes. Our goal is to interrogate and understand systems hosting fractional excitations such as Majorana fermions and understand the physics of new phases of matter such as Weyl superconductors which are predicted to host Majorana arcs at surfaces. Spectroscopic imaging - STM with its ability to obtain nanoscale, high-resolution information on electronic properties at millikelvin temperatures is one of the best experimental techniques probe these topological phases. The novel aspects of this proposal include the use of strain in combination with magnetic fields to obtain information on the order parameter of UTe_2 , the use of back-gating to probe monolayer WTe_2 and its proximitized edge states; and the MBE growth and proximitization of kagome and flat band ($Co_3Sn_2S_2$ and $FeSn$) systems which are ideal candidates to realize new kinds of fractional excitations.

Recent Progress

Uranium based heavy fermion systems that can harbor both strong correlations and magnetism are considered ideal candidate spin-triplet superconductors. Recent studies of the newly discovered heavy fermion superconductor, UTe_2 with a T_{SC} of 1.6K7 indicate that UTe_2 may be a triplet-chiral topological superconductor. Magnetic field studies reveal the existence of multiple competing phases and magnetic fluctuations. The role of these fluctuations in determining each of the low energy phases is as yet unknown. We have carried out high resolution STM measurements of UTe_2 at low temperatures to reveal a charge density wave of double the Te-periodicity along the Te chains. The order that is suppressed with magnetic field suggesting that the ordering may be accompanied by a possible spin density wave order. The observation of a new charge and potential spin density wave orders in UTe_2 provides new information to understand the phase space and possible competing orders in UTe_2

Future Plans

The next steps are to study the response of the ordering to in-plane magnetic fields and with doping.

Project Title: Superconductivity and magnetism in d - and f -electron quantum materials

Principal Investigator: M. Brian Maple

Mailing address: Department of Physics, University of California, San Diego, La Jolla, California 92093

Email: mbmaple@ucsd.edu

Program Scope

Introduction

The objectives of this research program are the experimental investigation of emergent phases and phenomena that are produced by competing interactions in strongly correlated electron quantum materials and the elucidation of the underlying physics. Emergent phenomena of interest in our research include unconventional (non BCS) types of superconductivity, magnetic and charge ordered phases, "hidden order" (HO) in URu_2Si_2 , quantum phase transitions and criticality, metal-insulator transitions, correlated electron topological insulators, Weyl semimetals, and quantum spin liquids. Competing interactions can be "tuned" by varying control parameters such as elemental substituent composition x , pressure P , and magnetic field H , leading to complex phase diagrams containing a multitude of correlated electron phases. For example, unconventional superconductivity, exotic magnetic phases and non-Fermi liquid behavior in low temperature physical properties are often found in the vicinity of a quantum critical point where a second order phase transition (usually, antiferromagnetic) is suppressed to 0 K. A combination of materials synthesis and physical properties measurements are employed to characterize these phenomena, map out the complex phase diagrams in which they reside, determine how different phases are related to one another, probe the underlying physics, and, when possible, test relevant theoretical models. We are also interested in studying quantum matter under extreme conditions of pressure P (megabar range), magnetic field H (45 T – static, 65 T – pulsed), and temperature T (mK region).

Recent Progress

Progress in two current research projects is described below. The first project involves the small gap semiconductor FeSi which has a conducting surface state below 19 K, discovered in our lab several years ago, and may be a d -electron counterpart of an f -electron topological Kondo insulator. The second project focuses on the electronic phases that emerge from "tuning" competing interactions in the "hidden order" compound URu_2Si_2 via the substitution of Fe and Os for Ru, and the application of high pressure and high magnetic fields.

FeSi – conducting surface state and possible d -electron topological Kondo insulator

Transition metal monosilicides have attracted a considerable amount of attention because of their novel magnetic, thermoelectric, and electrical conductivity properties, which are of interest for basic research and technological applications. These intermetallic compounds typically have a cubic B20 crystal structure, which is the only group in the cubic system without a center of inversion. Some widely studied examples within this class are MnSi, CoSi, and FeSi. Unlike many other transition metal monosilicides, FeSi is considered to be a strongly correlated electron semiconductor with a small energy gap of about 0.05 eV at low temperatures. One of the most intriguing physical properties of FeSi is its magnetic susceptibility that increases with temperature above 100 K, passes through a broad maximum at ~ 500 K, and then exhibits Curie-Weiss behavior at

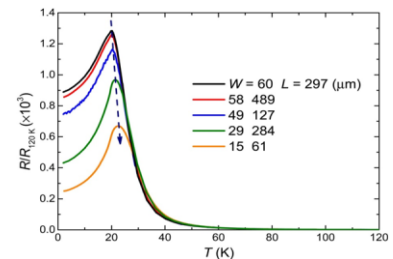


Figure 1: Normalized electrical resistance of selected FeSi samples below 120 K [1].

higher temperatures. The electrical conductivity of FeSi also rises steeply in the same temperature interval as the magnetic susceptibility. Neutron diffraction measurements have not revealed any evidence of magnetic order in FeSi. The electrical resistivity $\rho(T)$ evolves continuously with decreasing temperature from metallic behavior ($d\rho/dT > 0$) to semiconducting behavior ($d\rho/dT < 0$) at low temperatures.

During the past several years, we have been investigating the physical properties of high quality FeSi single crystals prepared in our laboratory by growth in a molten Sn flux. The FeSi single crystals prepared by this method grow along the [111] direction and form long thin bar-shaped samples. Electrical transport, thermal and magnetic measurements on the FeSi single crystals revealed a semiconducting to metallic crossover with decreasing temperature at ~ 19 K, which was not accompanied by any features in the specific heat or magnetic susceptibility [1]. The metallic conductivity below ~ 19 K is evident in the ρ vs. T data for a selection of the FeSi single crystals between 2 K and 300 K shown in Figure 1. The low temperature metallic conductivity depends strongly on the width and thickness of the samples, indicative of a conducting surface state in FeSi at low temperatures. Application of a magnetic field easily suppresses the electrical resistivity at low temperatures but has only a small effect on the temperature below which metallic conduction occurs. These experiments provide evidence for a conducting surface state in FeSi, reminiscent of the conducting surface state of a topological insulator.

Similarities in the properties of FeSi and SmB₆

The properties of FeSi are remarkably similar to those of *f*-electron Kondo insulators such as SmB₆, which has led to the speculation that FeSi may be a *d*-electron counterpart of an *f*-electron Kondo insulator. Moreover, since there is strong experimental and theoretical evidence that SmB₆ is a topological Kondo insulator, FeSi may be a topological Kondo insulator, as well. One of the objectives of our research on FeSi has been to compare the responses of the surface states of FeSi and the putative topological Kondo insulator SmB₆ to magnetic field and pressure.

Measurements of the magnetoresistance $MR = (\rho_H - \rho_{0T})/\rho_{0T}$ of FeSi in high magnetic fields up to 60 T were performed at the NHMFL at LANL. The resultant MR data for FeSi are compared to those for SmB₆ in Figure 2. The overall behavior of the MR data for the two compounds as a function of T and H are similar within and outside of the H - T region occupied by the surface state. Measurements of $\rho(T)$ were carried out at high pressures to 3.5 GPa in a piston-cylinder cell in our laboratory at UCSD and to 7.6 GPa in a diamond anvil cell at the Center for High Pressure Science and Technology Advanced Research in Shanghai. These measurements have been analyzed at temperatures above 19 K where bulk conductivity dominates and below 19 K in the region where the conducting surface state develops. The pressure dependence of $\rho(T)$ of FeSi is similar to that of the Kondo insulator SmB₆, which lends further support to the conjecture that FeSi is a *d*-electron analogue of an *f*-electron Kondo insulator. A T vs. P phase diagram for FeSi based on the $\rho(T,P)$ measurements is shown in Figure 3. The increase of the energy gaps Δ_1 and Δ_2 , extracted from

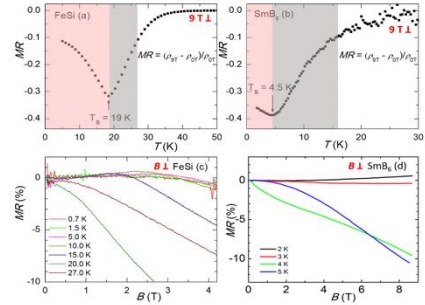


Figure 2. MR vs. T and H for FeSi and SmB₆.

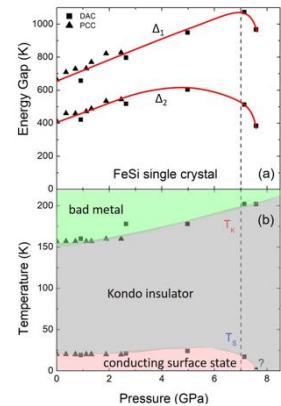


Figure 3. (a) Energy gaps Δ_1 and Δ_2 vs. P ; (b) T vs. P phase diagram for FeSi.

Arrhenius plots of $\ln\rho$ vs. $1/T$, with pressure followed by the collapse near 7 GPa are shown in part (a) of the figure, while the bad metal, Kondo insulator and conducting surface state regions of the T vs. P phase diagram are shown in part (b) of the figure. This T vs. P phase diagram is similar to that of SmB_6 .

Magnetic field modulated microwave spectroscopy (MFMMS) measurements were performed on FeSi and reveal a pronounced peak at about 19 K, the onset temperature the metallic surface state. Surprisingly, this peak is similar to that observed at the critical temperature of a superconductor. In contrast, MFMMS measurements on SmB_6 do not show this behavior. We speculate that this may be associated with the condition of the surface of the SmB_6 and plan to make further MFMMS measurements on samples in which the surface has been polished.

Since it is widely believed that SmB_6 is a topological Kondo insulator, it seems reasonable to conclude that FeSi is probably a d -electron version of an f -electron topological Kondo insulator. A manuscript describing these results is in preparation and nearly ready for submitted for publication [2].

Emergent phases generated by tuning competing interactions in URu_2Si_2

We have been involved in a long-term experimental investigation of the emergent electronic states that are unveiled when competing interactions in the “hidden order” (HO) correlated f -electron compound URu_2Si_2 are “tuned” by varying x , P and H . This produces complex temperature T vs. x , P , and H phase diagrams that contain a multitude of correlated electron phases and phenomena. For example, we discovered that the substitution of isoelectronic Fe for Ru in URu_2Si_2 produces a transition from the HO to the AFM phase at $x_c \approx 0.15$, similar to that which occurs under pressure in URu_2Si_2 at $P_c \approx 1.5$ GPa. We proposed that single crystals of $\text{URu}_{2-x}\text{Fe}_x\text{Si}_2$ could provide an opportunity to study the transition from the HO to the AFM phase at ambient pressure with techniques that cannot be readily performed on URu_2Si_2 under pressure (e.g., ARPES, STM, neutron scattering, measurements in high magnetic fields, etc.), providing new information that could provide clues to the identity of the HO phase which has eluded researchers for over 3½ decades. During the past several years, we have synthesized a series of $\text{URu}_{2-x}\text{Fe}_x\text{Si}_2$ single crystals by means of the Czochralski method in a tetra-arc furnace for investigations in our laboratory, laboratories of our collaborators, and national laboratory facilities, with the objective of obtaining information about the identity of the mysterious HO phase. Subsequently, we found that substitution of isoelectronic Os for Ru also induces the HO-AFM transition at $x_c \approx 0.14$.

In one of the most intriguing experiments, the HO and AFM phases in single crystals of $\text{URu}_{2-x}\text{Fe}_x\text{Si}_2$ for various values of x were investigated by means of polarization resolved Raman spectroscopy in collaboration with Girsh Blumberg’s group at Rutgers University [3]. In this work, the energy of a collective mode of pseudovector-like A_{2g} symmetry associated with a “chirality density wave,” identified as a candidate for the HO phase in earlier experiments, was measured as a function of x . With increasing x , the mode energy decreases monotonically in the HO phase, vanishes at x_c where the HO-AFM transition occurs, and then reappears with increasing energy in the AFM phase. The mode’s evolution provides evidence for a unified order parameter for both HO and AFM phases arising from the orbital degrees-of-freedom of the U $5f$ electrons.

In another interesting experiment we carried out at the NHMFL facilities at FSU and LANL, the 3-D T - H - x phase diagram for $\text{URu}_{2-x}\text{Fe}_x\text{Si}_2$ in magnetic fields H up to 45 T was constructed from magnetoresistance data as a function of T , H and x [4]. This work was featured in a NHMFL Highlight.

During the past year, we reported the results of two studies of the transition between the HO and AFM phases in the $\text{URu}_{2-x}\text{M}_x\text{Si}_2$ ($M = \text{Fe, Os}$) series in PNAS. One study involved ARPES measurements on $\text{URu}_{2-x}\text{Fe}_x\text{Si}_2$ single crystals in the HO and AFM phases in collaboration with Prof. Andrés Santander-Syro and his group at CNRS, U. Paris-Sud [page 5, pub. 20]. In another project, the transition from the HO to the AFM phase in the $\text{URu}_{2-x}\text{Os}_x\text{Si}_2$ system was studied under pressure in our laboratory at UCSD. The analysis of the studies of the $\text{URu}_{2-x}\text{M}_x\text{Si}_2$ ($M = \text{Fe, Os}$) systems under pressure indicated that the HO-AFM transition in these systems is driven by the increase of the hybridization of the localized U $5f$ and itinerant electron states which increases for both Fe and Os substitution for Ru and the application of pressure [page 5, pub. 17].

Future work:

The following work on FeSi single crystals is planned for the future:

- Synthesis of larger high quality single crystals of FeSi for ARPES measurements.
- Ultrafast optical spectroscopy measurements on the FeSi with Prof. R. D. Averitt (UCSD).
- Measurements of $\rho(T,P)$ of FeSi to high pressures above 100 GPa using facility we are setting up for performing such measurements on various correlated electron quantum materials.

The following work on the $\text{URu}_{2-x}\text{Fe}_x\text{Si}_2$ ($M = \text{Fe, Os}$) systems is planned for the future:

- Non-linear susceptibility measurements on $\text{URu}_{2-x}\text{Fe}_x\text{Si}_2$ with Prof. A. P. Ramirez (UCSC).
- Angular dependent magnetoresistance measurements on $\text{URu}_{2-x}\text{Fe}_x\text{Si}_2$ compounds as a function of T , H and x in high magnetic fields at the NHMFLs at FSU and LANL.
- Magnetostriction measurements on $\text{URu}_{2-x}\text{Fe}_x\text{Si}_2$ compounds as a function of T , H and x in high magnetic fields at the NHMFLs at FSU and LANL.
- Magnetoresistance measurements in magnetic fields up to $H \approx 45$ T for $\text{URu}_{2-x}\text{Os}_x\text{Si}_2$ to establish the 3-D T - H - x phase diagram and compare it to that of $\text{URu}_{2-x}\text{Fe}_x\text{Si}_2$.

The following work on U-based compounds is planned for the future:

- Search for new correlated $5f$ electron U-based compounds that exhibit emergent phenomena and unconventional superconductivity.
- Measurements of the pressure dependence of the electrical resistivity of correlated $5f$ electron U-based compounds to search for emergent phenomena and unconventional forms of superconductivity at high pressures in the megabar region.

References

1. Yuankan Fang, Sheng Ran, Weiwei Xie, Shen Wang, Ying Shirley Meng, and M. Brian Maple. "Evidence for a conducting surface ground state in high-quality single crystalline FeSi," *Proceedings of the National Academy of Sciences* **115**, 8558 (2018).
2. Alexander Breindel, Yuhang Deng, Camilla Moir, Yuankan Fang, Hongbo Lou, Shubin Li, Qiaoshi Zeng, Lei Shu, Christian T. Wolowiec, Ivan Schuller, Priscila F. S. Rosa, Zachary Fisk, John Singleton, and M. Brian Maple, "High magnetic field and high-pressure transport properties of the conducting surface state of FeSi and its comparison with SmB_6 ," in preparation.
3. H.-H. Kung, S. Ran, N. Kanchanavatee, V. Krapivin, A. Lee, J. A. Mydosh, K. Haule, M. B. Maple, and G. Blumberg, "Analogy between the "hidden order" and the orbital antiferromagnetism in $\text{URu}_{2-x}\text{Fe}_x\text{Si}_2$," *Physical Review Letters* **117**, 227601 (2016).
4. Sheng Ran, Inho Jeon, Naveen Pouse, Alexander J. Breindel, Noravee Kanchanavatee, Kevin Huang, Andrew Gallagher, Kuan-Wen Chen, David Graf, Ryan E. Baumbach, John Singleton, and M. Brian Maple, "Phase diagram of $\text{URu}_{2-x}\text{Fe}_x\text{Si}_2$ in high magnetic fields," *Proceedings of the National Academy of Sciences* **114**, 9826 (2017).

Publications (supported by BES)

1. Z. F. Ding, J. Zhang, C. Tan, K. Huang, I. Lum, O. O. Bernal, P.-C. Ho, D. E. MacLaughlin, M. B. Maple, and L. Shu, "Renormalizations in unconventional superconducting states of $Ce_{1-x}Yb_xCoIn_5$," *Physical Review B* **99**, 035136 (2019). DOI:10.1103/PhysRevB.99.035136
2. Peter Kissin, Sheng Ran, Dylan Lovinger, Verner K. Thorsmolle, Noravee Kanchanavatee, Kevin Huang, M. Brian Maple, and Richard D. Averitt, "Quasiparticle relaxation dynamics in $URu_{2-x}Fe_xSi_2$ single crystals," *Physical Review B* **99**, 165144 (2019). DOI: 10.1103/PhysRevB.99.165144
3. Bin Gao, Tong Chen, David W. Tam, Chien-Lung Huang, Kalyan Sasmal, Devashibhai T. Adroja, Feng Ye, Huibo Cao, Gabriele Sala, Matthew B. Stone, Christopher Baines, Joel A. T. Verezhak, Haoyu Hu, Jae-Ho Chung, Xianghan Xu, Sang-Wook Cheong, Manivannan Nallaiyan, Stefano Spagna, M. Brian Maple, Andriy H. Nevidomskyy, Emilia Morosan, Gang Chen and Pengcheng Dai, "Experimental signatures of a three-dimensional quantum spin liquid in effective spin-1/2 $Ce_2Zr_2O_7$ pyrochlore," *Nature Physics* **15**, 1052 (2019). www.nature.com/naturephysics
4. Tatsuya Yanagisawa, Hiroyuki Hidaka, Hiroshi Amitsuka, Shintaro Nakamura, Satoshi Awaji, Elizabeth L. Green, Sergei Zherlitsyn, Joachim Wosnitza, Duygu Yazici, Benjamin D. White and M. Brian Maple, "Quadrupolar susceptibility and magnetic phase diagram of $PrNi_2Cd_{20}$ with non-Kramers doublet ground state," *Philosophical Magazine* **100**, Issue 10 (Special Issue in Honour of M. Brian Maple), 1282 (2020). DOI: 10.1080/14786435.2019.1709912
5. Nicholas P. Butch, J. A. Rodriguez-Rivera, and M. Brian Maple, "Ungapped magnetic excitations beyond Hidden Order in $URu_{2-x}Re_xSi_2$," *Philosophical Magazine* **100**, Issue 10 (Special Issue in Honour of M. Brian Maple), 1268 (2020). DOI: 10.1080/14786435.2020.1725251
6. K. Götze, M. J. Pearce, P. A. Goddard, M. Jaime, M. B. Maple, K. Sasmal, T. Yanagisawa, A. McCollam, T. Khouri, P.-C. Ho, and J. Singleton, "Unusual phase boundary of the magnetic-field-tuned valence transition in $CeOs_4Sb_{12}$," *Physical Review B* **101**, 075102 (2020). DOI: 10.1103/PhysRevB.101.075102
7. F. Bridges, R. Dudschus, C. Mackeen, T. Keiber, C. H. Booth, and M. B. Maple, "EXAFS investigation of the local structure in $URu_{2-x}Fe_xSi_2$: Evidence for distortions below 100 K," *Physical Review B* **102**, 014109 (2020). DOI: 10.1103/PhysRevB.102.014109
9. S. Zhang, G. Chappell, N. Pouse, R. E. Baumbach, M. B. Maple, L. H. Greene, and W. K. Park, "Origins of gaplike behaviors in URu_2Si_2 : Combined study via quasiparticle scattering spectroscopy and resistivity measurements," *Physical Review B: Rapid Communications* **102**, 081101(R) (2020). DOI: 10.1103/PhysRevB.102.081101
10. B. D. White, R. I. Barabash, O. M. Barabash, I. Jeon, and M. B. Maple, "Magnetocaloric effect near room temperature in quinary and sextenary Heusler alloys," *Journal of Applied Physics* **126**, 165101 (2019). DOI: 10.1063/1.5120819
11. S. Ran, G. M. Schmiedeshoff, N. Pouse, I. Jeon, N. P. Butch, R. B. Adhikari, C. C. Almasan and M. B. Maple, "Rapid suppression of the energy gap and the possibility of a gapless hidden order state in $URu_{2-x}Re_xSi_2$," *Philosophical Magazine* **99**, 1751 (2019). www.pnas.org/cgi/doi/10.1073/pnas.1616542113

12. Yu Song, Weiyi Wang, John S. Van Dyke, Naveen Pouse, Sheng Ran, Duygu Yazici, A. Schneidewind, Petr Cermak, Y. Qui, M. B. Maple, Dirk K. Morr and Pengcheng Dai, "Nature of the spin resonance mode in CeCoIn₅," *Communications Physics* **3**, 98 (2020). <https://doi.org/10.1038/s42005-020-0365-8>
13. A. Slebarski, M. Fijalkowski, P. Zajdel, M. M. Máska, J. Deniszczyk, M. Zubko, O. Pavlosiuk, K. Sasmal, and M. B. Maple, "Enhancing superconductivity of Y₅Rh₆Sn₁₈ by atomic disorder," *Physical Review B* **102**, 054514 (2020). DOI: 10.1103/PhysRevB.102.054514
14. Sooyoung Jang, J. D. Denlinger, J. W. Allen, V. S. Zapf, M. B. Maple, Jae Nyeong Kim, Bo Gyu Jang, and Ji Hoon Shim, "Evolution of the Kondo lattice electronic structure above the transport coherence temperature," *Proceedings of the National Academy of Sciences* **117**, 23467 (2020). <http://www.pnas.org/cgi/doi/10.1073/pnas.2001778117>
15. Andrea Amorese, Martin Sundermann, Brett Leedahl, Andrea Marino, Daisuke Takegami, Hlynur Gretarsson, Andrei Gloskovskii, Christoph Schlueter, Maurits W. Haverkort, Yingkai Huang, Maria Szlawska, Dariusz Kaczorowski, Sheng Ran, M. Brian Maple, Eric D. Bauer, Andreas Leithe-Jasper, Philipp Hansmann, Peter Thalmeier, Liu Hao Tjeng, and Andrea Severing, "Dual nature of 5*f* electrons in the isostructural UM₂Si₂ family: from antiferromagnetic, hidden order to Pauli paramagnetism," *Proceedings of the National Academy of Sciences* **117**, 30220 (2020). <https://doi.org/10.1073/pnas.2005701117>
16. Chunruo Duan, Kalyan Sasmal, M. Brian Maple, Andrey Podlesnyak, Jian-Xin Zhu, Qimiao Si, and Pengcheng Dai, "Incommensurate Spin Fluctuations in the Spin-triplet Superconductor Candidate UTe₂," *Physical Review Letters* **125**, 237003 (2020). <https://doi.org/10.1103/PhysRevLett.125.237003>
17. C. T. Wolowiec, N. Kanchanavatee, K. Huang, S. Ran, A. J. Breindel, N. Pouse, Kalyan Sasmal, R. E. Baumbach, G. Chappell, Peter S. Riseborough, and M. B. Maple, "Isoelectronic perturbations to *f-d*-electron hybridization and the enhancement of hidden order with increasing Os concentration in URu_{2-x}Os_xSi₂," *Proceedings of the National Academy of Sciences* **118**, e2026591118 (2021). <https://doi.org/10.1073/pnas.2026591118>
18. K. Shrestha, S. Zhang, L. H. Greene, Y. Lai, R. E. Baumbach, K. Sasmal, M. B. Maple, and W. K. Park, "Spectroscopic evidence for the direct involvement of local moments in the pairing process of the heavy-fermion superconductor CeCoIn₅," *Physical Review B* **103**, 224515 (2021). DOI: 10.1103/PhysRevB.103.224515
19. D. L. Kunwar, R. B. Adhikari, N. Pouse, M. B. Maple, M. Dzero, and C. C. Almasan, "Quantum criticality in Ce_{1-x}Sm_xCoIn₅," *Physical Review B* **103**, 224519 (2021). DOI: 10.1103/PhysRevB.103.224519
20. E. Frantzeskakis, J. Dai, T. C. Rödel, M. Güttler, C. Bareille, S. Ran, N. Kanchanavatee, K. Huang, N. Pouse, C. T. Wolowiec, E. D. L. Rienks, P. Lejay, F. Fortuna, M. B. Maple, and A. F. Santander-Syro, "From hidden order to antiferromagnetism: electronic structure changes in Fe-doped URu₂Si₂," *Proceedings of the National Academy of Sciences* **118**, e2020750118 (2021). <https://doi.org/10.1073/pnas.2020750118>
21. A. M. Konic, R. B. Adhikari, A. A. Kirmani, A. Breindel, R. Sheng, M. B. Maple, M. Dzero, and C. C. Almasan, "Non-Kramers doublets and quest for the 'hidden-order' state in PrNi₂Cd₂₀ and PrPd₂Cd₂₀," *Physical Review B* (2020). (Submitted). arXiv:2005.09074v1 [cond-mat.str-el] 11 May 2020

Ph.D. THESIS:

Alexander Breindel, Ph.D. Thesis, “High Magnetic Field Investigations of Correlated Electron Quantum Materials,” University of California, San Diego (2021). M. B. Maple, Thesis Advisor.

Spectroscopic investigations of electronic and magnetic materials

Janice L. Musfeldt, Departments of Chemistry and Physics, University of Tennessee

Program Scope

My research group is interested in the behavior of materials under extreme conditions. We are well known for spectroscopic work in high magnetic fields, under pressure, and at small sizes where confinement effects become apparent. This particular program involves the oxides and chalcogenides part of our effort and is inspired by opportunities to explore the properties of quantum materials. Specifically, we reveal energy transfer processes in tunable, high-performance multiferroics, investigate the dynamics and symmetry of van der Waals solids and their single sheet analogs, uncover charge-structure-function relationships in intercalated chalcogenides under compression, and explore the generality of these phenomena and their underlying mechanisms in new settings - such as at ferroelectric and structural domain walls. In addition to advancing the understanding of broken symmetry materials under external stimuli, these systems host properties that can be harnessed in technologies with widespread impact. The development of ultra-low power, logic, and memory devices, multivalued logic for neuromorphic computing, new computing architectures as well as nonreciprocal materials for photonics are most closely related to our efforts. This program builds on our experience with high magnetic field, pressure, and near field spectroscopies, leverages the outstanding facilities at the National High Magnetic Field Laboratory and the light sources at Brookhaven and Lawrence Berkeley National Laboratories, and benefits from the broad expertise of our many long-time collaborators. Our program also supports the interdisciplinary education of a diverse group of graduate students in the area of advanced materials research for future positions in academics, national lab settings, and industry.

Recent Progress

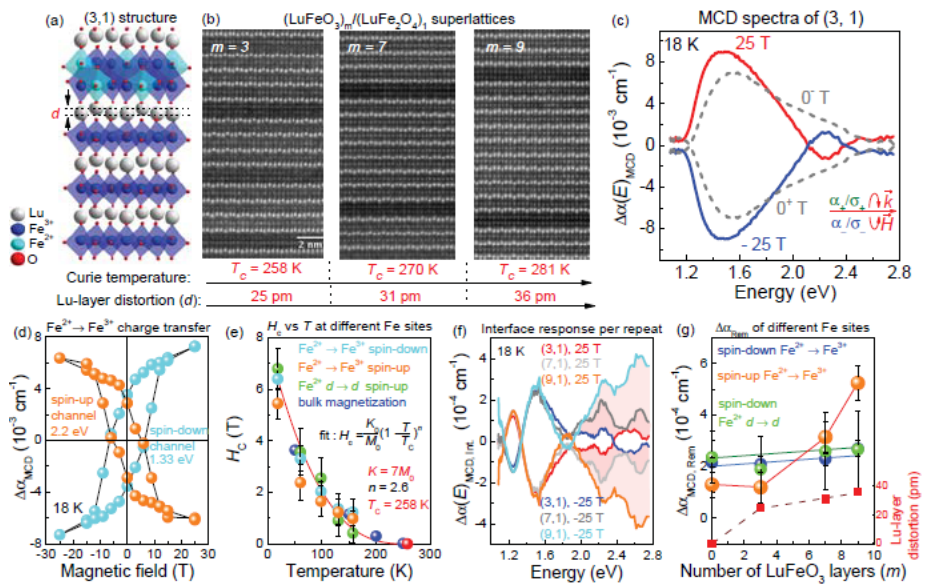
In the past two years, we have made broad progress on a number of fronts, unraveling the site-specific properties of novel oxides and chalcogenides. To focus our efforts, many but not all of our platforms have been magnetoelectric multiferroics – systems that are well known for competing energy scales and complex phase diagrams. Two specific examples of our recent efforts are discussed below.

Site-specific spectroscopic measurement of spin and charge in $(\text{LuFeO}_3)_m/(\text{LuFe}_2\text{O}_4)_1$ multiferroic superlattices

Interface materials offer a means to achieve electrical control of ferrimagnetism at room temperature as was recently demonstrated in $(\text{LuFeO}_3)_m/(\text{LuFe}_2\text{O}_4)_1$ superlattices. A challenge to understanding the inner workings of these complex magnetoelectric multiferroics is the multitude of distinct Fe centers and their associated environments. This is because macroscopic techniques characterize average responses rather than the role of individual iron centers. In this work, we combined optical absorption, magnetic circular dichroism, and first-principles calculations to

uncover the origin of high-temperature magnetism in these superlattices and the charge-ordering pattern in the $m = 3$ member [Fig. 1]. In a significant conceptual advance, we develop a method to extract interface spectra, and we employ this technique to establish how Lu-layer distortion selectively enhances the $\text{Fe}^{2+} \rightarrow \text{Fe}^{3+}$ charge-transfer contribution in the spin-up channel, strengthens the exchange interactions, and increases the Curie temperature. Comparison of predicted and measured spectra also identifies a non-polar self-doped charge ordering arrangement within the LuFe_2O_4 layer in the (3, 1) material, thus resolving controversy regarding the many different isoenergetic charge states. In addition to introducing a remarkably powerful and versatile spectroscopic decomposition technique for revealing microscopic spin and charge character at the interface of a multiferroic superlattice with many different iron centers, this work provides a pathway to link bulk and interface properties of other engineered materials in a site-selective manner.

Fig. 1: (a,b) Structure+STEM images of $(\text{LuFeO}_3)_m/(\text{LuFe}_2\text{O}_4)_1$ superlattices. (c) Magnetic circular dichroism spectra of the $m=3$ member. (d) Optical hysteresis loops. (e) Coercive field vs. temperature. (f) Magnetic circular dichroism of the interface. (g) Remanent dichroism of different Fe-related excitations + Lu-layer distortion vs. number of LuFeO_3 layers.

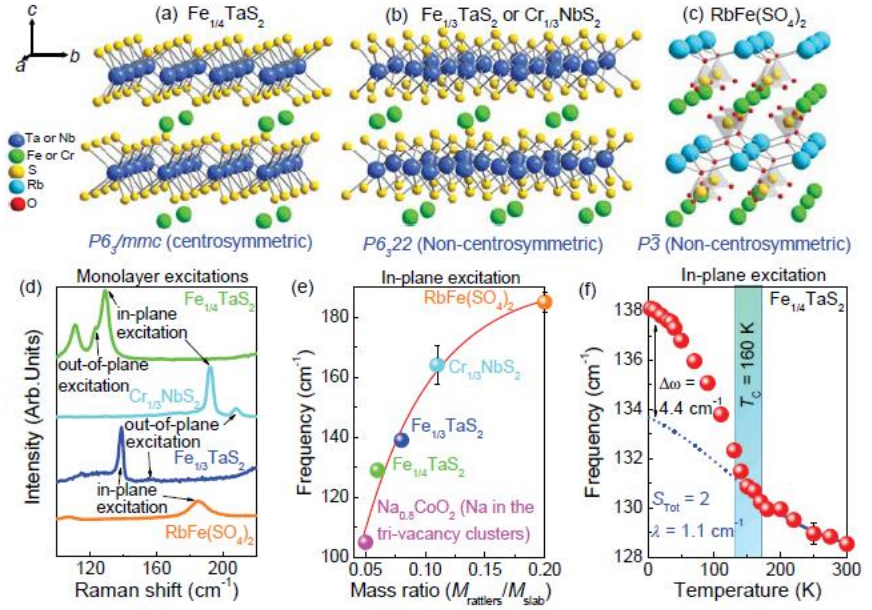


Metal monolayer excitations in intercalated transition metal dichalcogenides

Intercalated van der Waals materials like Fe_xTaS_2 and Cr_xNbS_2 are well known to incorporate atomically thin networks of metal centers between the transition metal dichalcogenide sheets. Different patterns are formed within the gap depending upon the intercalant concentration. When incorporated in this manner, metal monolayers support high temperature magnetic ordering, novel metallicity distinct from that of the parent compound, and superconductivity. In order to explore the properties of the embedded monolayer, we combined Raman scattering spectroscopy with complimentary lattice dynamics calculations to uncover the fundamental excitations of intercalated metal monolayers in the Fe_xTaS_2 ($x = 0, 1/4, \text{ and } 1/3$) family of materials. Extension to related systems including Cr_xNbS_2 ($x = 0, 1/3$) and $\text{RbFe}(\text{SO}_4)_2$ which have comparable metal ordering patterns inside the van der Waals gap [Fig. 2] reveals similar features that we describe as in- and out-of-plane excitations of the embedded metal monolayers. We discuss the frequency, lifetime, and intensity trends as well as spin-phonon coupling in terms of the in-plane metal-metal distance, the size of the van der Waals gap, and the mass ratio between the intercalant and the chalcogenide slab [Fig. 2]. These structure-property relations along with our model for frequency vs. mass ratio effects suggest that external stimuli such as pressure and strain may be able to tune

these excitations. These findings open the door for the creation and control of high sensitivity THz resonators.

Fig. 2: (a-c) Crystal structures of $Fe_{1/4}TaS_2$, $Fe_{1/3}TaS_2$ and $Cr_{1/3}TaS_2$, as well as $RbFe(SO_4)_2$. (d) Close-up view of the Raman-active metal monolayer excitations. Both in- and out-of-plane features are shown. (e) Frequency vs. mass ratio trends. The solid red line is our mass ratio model – developed to describe intercalated chalcogenides. (f) Frequency vs. temperature revealing spin-lattice coupling of the in-plane metal monolayer excitation.



Future Plans

We have several exciting initiatives planned for the upcoming year, the majority of which were motivated by opportunities to reveal new states of matter under external stimuli. These include:

- uncovering the pressure-induced phase transition and phonon softening in ferroelectric h - $Lu_{0.6}Sc_{0.4}FeO_3$,
- exploring the vibrational properties of $CuInP_2S_6$ across the ferroelectric transition,
- revealing the exotic symmetry progression and development of polar metallicity in $NiPS_3$ under pressure,
- unveiling the near field infrared response of ferroelectric domain walls in h - $Lu_{0.6}Sc_{0.4}FeO_3$, and
- illustrating how the insulator-metal transition in $CrSiTe_3$ is triggered by the structural distortion under pressure.

Each of these efforts is of contemporary interest for studies of phase competition under external stimuli and takes advantage of the broad spectroscopic capabilities in our own lab and at various national facilities.

Publications

1. *Spin-lattice and electron-phonon coupling in a 3d/5d hybrid Sr_3NiIrO_6* , K. R. O’Neal, A. Paul, A. al-Wahish, K. D. Hughey, A. L. Blockman, X. Luo, S. -W. Cheong, V. Zapf, C.

- V. Topping, J. Singleton, M. Ozerov, T. Birol, and J. L. Musfeldt, *npj Quant. Mater.* **4**, 48 (2019). NHMFL Science Highlight.
2. *Near-field infrared spectroscopy of single layer MnPS₃*, S. N. Neal, H. -S. Kim, K. A. Smith, A. V. Haglund, D. G. Mandrus, H. A. Bechtel, G. L. Carr, K. Haule, D. H. Vanderbilt, and J. L. Musfeldt, *Phys. Rev. B.* **100**, 075428 (2019).
 3. *Infrared nano-spectroscopy of ferroelastic domain walls in hybrid improper ferroelectric Ca₃Ti₂O₇*, K. A. Smith, E. A. Nowadnick, S. Fan, O. Khatib, S. L. Lim, N. C. Harms, S. Neal, J. K. Kirkland, M. C. Martin, C. J. Won, M. B. Raschke, S. -W. Cheong, C. J. Fennie, G. L. Carr, H. A. Bechtel, and J. L. Musfeldt, *Nature Comm.* **10**, 5235 (2019).
 4. *Realization of the orbital-selective Mott state at the molecular level in Ba₃LaRu₂O₉*, Q. Chen, A. Verrier, D. Ziat, A. J. Clune, R. Rouane, X. Bazier-Matte, G. Wang, S. Calder, K. M. Taddei, C. R. Dela Cruz, A. I. Kolesnikov, J. Ma, J. Cheng, Z. Liu, J. A. Quilliam, J. L. Musfeldt, H. D. Zhou, and A. A. Aczel, *Phys. Rev. Mater.* **4**, 064409 (2020).
 5. *Symmetry crossover in layered MPS₃ complexes (M = Mn, Fe, Ni) via near field infrared spectroscopy*, S. N. Neal, H. -S. Kim, K. R. O'Neal, A. V. Haglund, K. A. Smith, D. G. Mandrus, H. A. Bechtel, G. L. Carr, K. Haule, D. Vanderbilt, and J. L. Musfeldt, *Phys. Rev. B.* **102**, 085408 (2020).
 6. *Piezochromism in the magnetic chalcogenide MnPS₃*, N. C. Harms, H. -S. Kim, A. J. Clune, K. A. Smith, K. R. O'Neal, A. V. Haglund, D. G. Mandrus, Z. Liu, K. Haule, D. Vanderbilt, and J. L. Musfeldt, *npj Quant. Mater.* **5**, 56 (2020).
 7. *Site-specific spectroscopic measurement of spin and charge in (LuFeO₃)_m/(LuFe₂O₄)₁ multiferroic superlattices*, S. Fan, H. Das, A. F. Rebola, K. A. Smith, J. A. Mundy, C. S. Brooks, M. Holtz, D. A. Muller, C. J. Fennie, R. Ramesh, D. G. Schlom, S. A. McGill, and J. L. Musfeldt, *Nature Comm.* **11**, 5582 (2020). NHMFL Highlight, December 2020.
 8. *Fundamental excitations of intercalated metal monolayers in transition metal dichalcogenides*, S. Fan, S. N. Neal, C. J. Won, J. W. Kim, S. Deepak, J. J. Yang, D. G. Mandrus, S. -W. Cheong, J. T. Haraldsen, and J. L. Musfeldt, *Nano Lett.* **21**, 99 (2021).
 9. *Unraveling chemical bonding and Born charge in 1T-HfS₂*, S. N. Neal, S. Li, T. Birol, and J. L. Musfeldt, *npj 2D Materials and Applications*, **5**, 45 (2021).
 10. *Exploring few- and single-layer CrPS₄ with near-field infrared spectroscopy*, S. N. Neal, K. R. O'Neal, A. V. Haglund, D. G. Mandrus, H. A. Bechtel, G. L. Carr, K. Haule, D. Vanderbilt, H. -S. Kim, and J. L. Musfeldt, *2D Materials* **8**, 035020 (2021).
 11. *Revealing pressure-driven structural transitions in hybrid improper ferroelectric Sr₃Sn₂O₇*, K. A. Smith, S. P. Ramkumar, N. C. Harms, A. J. Clune, Xianghan Xu, S. -W. Cheong, Z. Liu, E. A. Nowadnick, J. L. Musfeldt, *Phys. Rev. B* **104**, 064106 (2021). Editor's Choice.

Review Articles

1. *Nanotubes from layered transition metal dichalcogenides*, J. L. Musfeldt, Y. Iwasa, and R. Tenne, *Physics Today* **73**, 42 (2020).
2. *Optical properties of oxide multiferroics*, J. L. Musfeldt, submitted, *Encyclopedia of Applied Physics* (Wiley).

Nanostructure Studies of Correlated Quantum Materials

Douglas Natelson, Dept. of Physics and Astronomy (joint with Electrical & Computer Engineering and Materials Science & Nanoengineering), Rice University

Program Scope

The dynamics of charge and spin in strongly correlated materials can be incredibly rich, as strong interactions between quantum degrees of freedom lead to new, emergent excitations. Nanostructure techniques, originally developed chiefly for conventional metals and semiconductors, can enable previously unachievable measurements on such systems that probe these emergent low-energy current-carrying excitations.

One archetypal correlated quantum material is the so-called quantum critical strange metal. At zero temperature as a function of some tuning parameter such as external magnetic field, pressure, or doping, the ground state of a correlated system can exhibit a second-order quantum phase transition between alternative ground states. For example, in the rare-earth system YbRh_2Si_2 , at low magnetic fields the ground state of the system is Fermi liquid, with conventional, long-lived, electron-like quasiparticles and the local $4f$ moments of the Yb ions ordered antiferromagnetically. In the high field limit, the ground state is instead a lattice of Kondo-screened local moments, with heavy fermion quasiparticles that also act as a Fermi liquid. At intermediate fields and temperatures reaching as high as 25 K, however, the system is a strange metal, a non-Fermi liquid with a linear-in- T resistivity, in which distinct quasiparticles are thought to be poorly defined - “incoherent”. [1]

Making use of epitaxial films of YbRh_2Si_2 grown on Ge substrates by our collaborators (the group of Dr. Prof. Silke Bühler-Paschen at TU Wien) [2], we have made substantial progress in using shot noise to probe the strange metal phase. Charge shot noise is the fluctuation in current through a driven system due to the discrete character of charge carriers. Shot noise is generally compared to the current noise expected for Poissonian arrival of quasiparticles of charge magnitude e , $S_{I,e} = 2eI \coth(eV/2k_B T)$ A^2/Hz , where I is the average current. In a diffusive constriction of length L made from a conventional Fermi liquid, the expected Fano factor, $F \equiv S_I/S_{I,e}$, is $1/3$ when L is less than the inelastic electron-electron scattering length l_{e-e} and the electron-phonon scattering length, l_{e-ph} . When $l_{e-e} < L < l_{e-ph}$, then F is expected to approach $\sqrt{3}/4$, and if L exceeds l_{e-ph} , the noise is strongly suppressed, with $F \rightarrow 0$. [3] Our present experiments involve the lithographic fabrication of a nanoscale YbRh_2Si_2 constriction between thick, highly conductive gold contacts, the measurement of transport properties and shot noise in this system, and the comparison of those data with the Fermi liquid expectations above. No rigorous theoretical calculation yet exists for the noise expected in a quantum critical strange metal, though a lack of well-defined quasiparticles and charge quantization would suppress S_I .

(In addition to these experiments, we are also preparing to perform similar measurements in constrictions of the field-tunable quantum critical strange metal $\text{Sr}_3\text{Ru}_2\text{O}_7$. [4] Separately, we

have also begun studies of angular momentum transport in the unusual correlated paramagnetic insulating phase of VO₂.)

Recent Progress

We have fabricated constrictions (Fig. 1) in YbRh₂Si₂ films (~ 60 nm thick) using a combination of electron beam lithography and plasma-based etching techniques. When working with a material never before patterned into nanostructures, it is important to confirm that the material properties are not altered by the processing techniques. As shown in Fig. 2, the temperature and (in-plane) magnetic field dependences of the resistance in the nanoscale constriction are quantitatively similar to those seen in the unpatterned film.

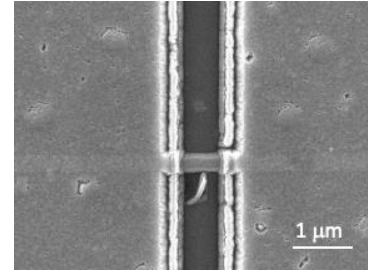


Figure 1. Nanoscale YbRh₂Si₂ constriction fabricated between Au contacts.

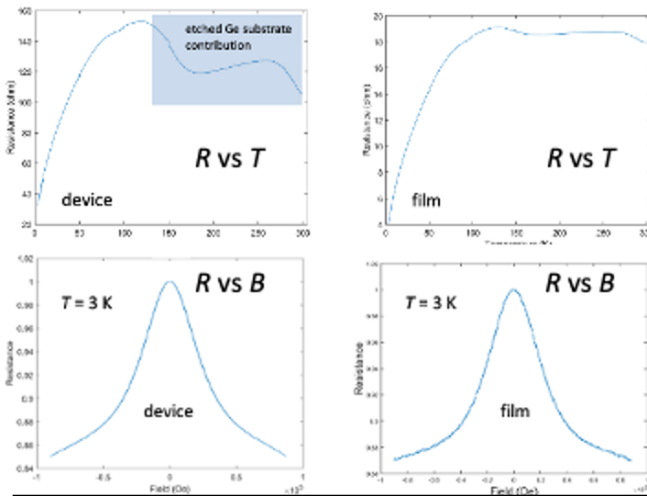


Figure 2. Patterning the material into the nanoconstriction does not alter the resistivity's T or B dependence.

To measure the shot noise in the constrictions, we have mounted the samples on a custom-built probe for a Quantum Design PPMS cryostat and used a standard low-frequency cross-correlation method. At a given temperature, magnetic field, and bias condition, the voltage noise power S_V is measured, using the cross-correlation of two amplifier chains to mitigate amplifier noise. Using careful measurements of the differential resistance dV/dI of the constriction, the current noise is calculated via $S_I = S_V / (dV/dI)^2$ at each bias, for comparison

with the theoretical expectation. The zero-bias voltage noise in all devices measured is consistent with the expectations for Johnson-Nyquist noise ($S_V = 4k_B T (dV/dI)|_{V=0} V^2 / \text{Hz}$) for the measured resistance and cryostat temperature. Acquiring a datapoint at each bias condition requires the averaging of 300 spectra.

Figure 3 shows preliminary results for the zero-field out-of-equilibrium current noise at different temperatures for one such constriction. There is no appreciable change with B . The data are consistent with a Fano factor of 0.15 or less, much lower than the expectations for a conventional Fermi liquid. Quantitatively similar results have been seen in multiple constrictions. In contrast, preliminary measurements performed on a pure Au wire in a nearly identical geometry at 5 K give a Fano factor of 0.28 uncorrected for contact resistance, and 0.33

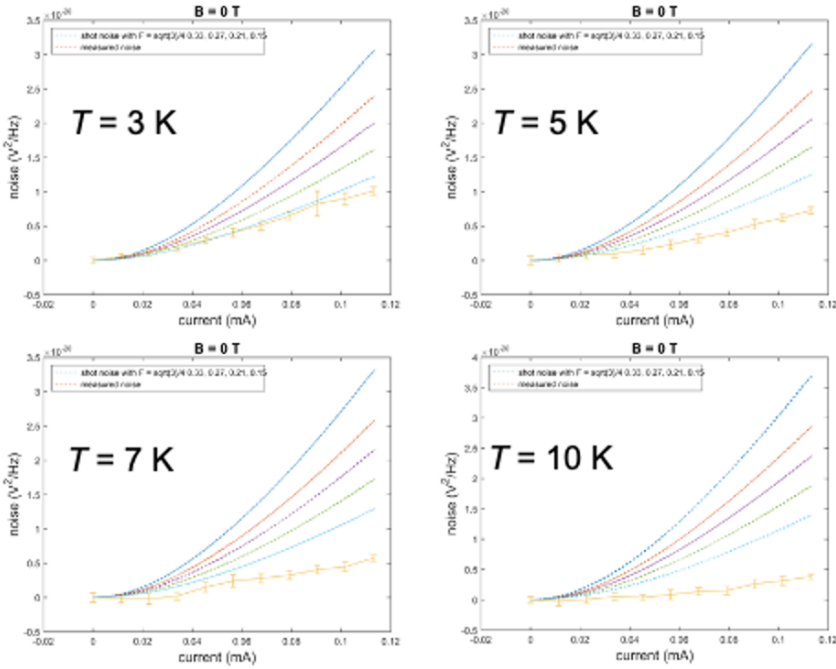


Figure 3. Initial shot noise in YbRh_2Si_2 vs. bias current, compared with expectations for different Fano factors, based on the measured dV/dI . The measured noise is much lower than all diffusive Fermi liquid expectations..

when corrected for contact resistance, as expected for a diffusive Fermi liquid shorter than the electron-phonon scattering length.

It is important to consider whether electron-phonon scattering could be playing a role in suppressing the shot noise in the YbRh_2Si_2 devices. This seems unlikely for multiple reasons. The resistivity of the YbRh_2Si_2 film[2] (and constriction) show the characteristic linear- T response expected from the bulk strange metal,

which is known to be dominated by the quantum critical electron-electron effects. Additionally, the Debye temperature for YbRh_2Si_2 is inferred to be 380 K[5], considerably higher than that of gold (170 K), making it even more likely that phonons would be frozen out at the temperature range of the measurements.

A natural interpretation of the suppressed shot noise would be in terms of the lack of well-defined quasiparticles in the quantum critical regime. In an effective continuum fluid with no discrete charge carriers, one would expect $F \rightarrow 0$. Quantum critical charge fluctuations have already been inferred in this system from the optical conductivity[2]. At present, no theoretical treatment exists of shot noise in a strange metal. We are working with Prof. Qimiao Si as he and a student examine this problem. These data may be the first evidence of charge fractionalization in the strange metal phase.

Beyond these experiments, we have been developing an approach to patterning thin films of another magnetic quantum critical strange metal, $\text{Sr}_3\text{Ru}_2\text{O}_7$, for analogous experiments to test the universality of these observations. This fabrication challenge is considerable, as there is only a narrow region of phase stability for $\text{Sr}_3\text{Ru}_2\text{O}_7$ and standard e-beam lithography can damage the material.

In addition, we have preliminary results looking at spin Seebeck-driven angular momentum transport in the correlated paramagnetic insulating phase of VO_2 .

Future Plans

We will confirm these noise measurement results and work with our collaborators on still lower-temperature measurements in these samples. Collaborating with theorist colleagues we will compare the data with a theoretical treatment of shot noise in the strange metal. To test the universality of these effects, we plan to perform analogous measurements in constrictions fabricated from $\text{Sr}_3\text{Ru}_2\text{O}_7$, with the hope that the field tunability of the quantum criticality in that system will allow direct comparison in one device between Fermi liquid and strange metal noise response. As new samples become available, we will also extend prior examination of noise in cuprate tunneling devices to test for the presence of paired carriers deep into the underdoped pseudogap regime.

Beyond this, we will complete our studies of angular momentum transport in the correlated insulating phase of VO_2 films, and expand those forays to look at angular momentum transport within the Mott insulating cuprate parent compound La_2CuO_4 .

References

- [1] S. Paschen *et al.*, *Nature* **432**, 881–885 (2004). <https://doi.org/10.1038/nature03129>
- [2] L. Prochaska *et al.*, *Science* **367**, 285-288 (2020). <https://doi.org/10.1126/science.aag1595>
- [3] Ya. M. Blanter and M. Büttiker, *Phys. Rep.* **336**, 1-166 (2000). [https://doi.org/10.1016/S0370-1573\(99\)00123-4](https://doi.org/10.1016/S0370-1573(99)00123-4)
- [4] S. A. Grigera *et al.*, *Science* **294**, 329-332 (2001). <https://doi.org/10.1126/science.1063539>
- [5] S. Hartmann *et al.*, *J. Phys.: Conf. Ser.* **150**, 042049 (2009). <https://doi.org/10.1088/1742-6596/150/4/042049>

Publications

1. Mahdiyeh Abbasi *et al.* *ACS Nano* **14**, 17535-17542 (2020). <https://pubs.acs.org/doi/10.1021/acsnano.0c08035>
2. Liyang Chen *et al.*, *APL Materials* **8**, 101103 (2020). <https://doi.org/10.1063/5.0023475>
3. Panpan Zhou *et al.*, *Phys. Rev. B* **101**, 224512 (2020). <https://dx.doi.org/10.1103/PhysRevB.101.224512>
4. Xuanhan Zhao *et al.*, *AIP Adv.* **9**, 105218 (2019). <https://dx.doi.org/10.1063/1.5126129>
5. Panpan Zhou *et al.*, *Nature* **572**, 493-496 (2019). <https://www.nature.com/articles/s41586-019-1486-7>

Probing the Interplay of Topology, Magnetism and Superconductivity in Intrinsic Magnetic and Superconducting Topologic Materials

Ni Ni

Program Scope

The overarching goal of this proposal is to address the grand challenge of basic energy science by discovering new intrinsic magnetic topological materials, and characterizing them through thermodynamic, transport, X-ray, and neutron measurements. Of particular interest in this research is to probe the interplay of band topology, structure, electronic and spin degrees of freedom in these materials through chemical doping, external pressure and uniaxial strains. The proposed research will accelerate the discovery of these materials and advance our understanding of the interplay of the topology and magnetism, potentially enabling us to manipulate the emergent phenomena arising from the interplay.

Recent Progress

During the funding period from 09/01/2020 to 08/31/2021, we have 7 papers published or under review, including Nature, Nature Materials, Physical Review B, etc. In this session, I will report some selected works.

D) The fine control of magnetism and electronic structure is crucial since the interplay between magnetism and band topology can lead to various novel magnetic topological states including axion insulators, magnetic Weyl semimetals and Chern insulators etc. Through crystal growth, transport, thermodynamic, neutron diffraction measurements, we show that with Sb-doping, the newly-discovered intrinsic antiferromagnetic topological insulator MnBi_4Te_7 evolves from antiferro-magnetic to ferromagnetic and then ferromagnetic (Fig. 1)[1]. We attribute this to the formation of $\text{Mn}(\text{Bi},\text{Sb})$ antisites upon doping, which result in additional Mn sublattices that modify the delicate interlayer magnetic interactions and cause the dominant Mn sublattice to go from antiferromagnetic to ferro-magnetic. We further investigate the effect of antisites on the band topology using the first-principles calculations. Without considering antisites, the series evolves from antiferromagnetic topological insulator ($x = 0$) to ferromagnetic axion insulators. In the exaggerated case of 16.7% of periodic antisites, the

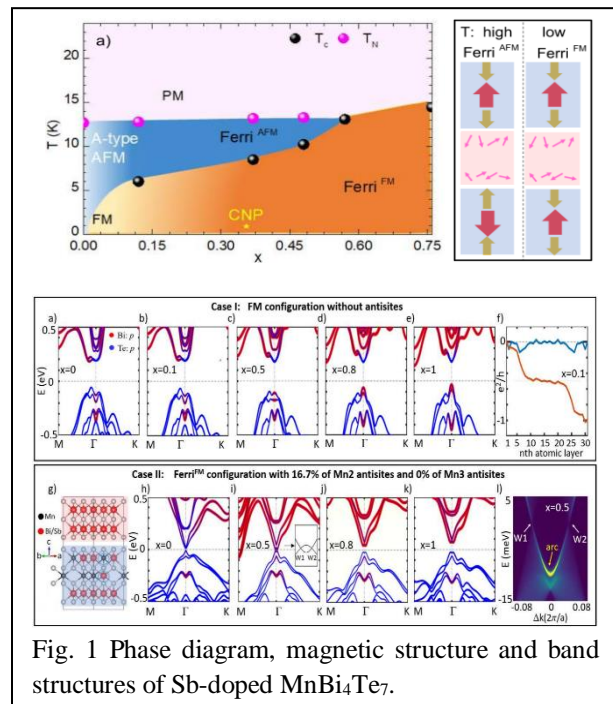
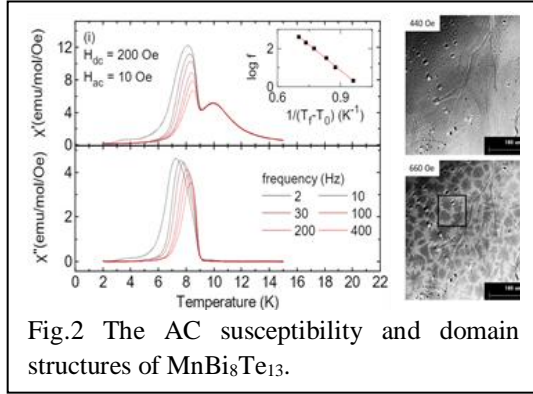


Fig. 1 Phase diagram, magnetic structure and band structures of Sb-doped MnBi_4Te_7 .

band topology is modified and type-I magnetic Weyl semimetal phase can be realized at intermediate dopings. Therefore, this doping series provides a fruitful platform with continuously tunable magnetism and topology for investigating emergent phenomena, including quantum anomalous Hall effect, Fermi arc states, etc.

II) $\text{MnBi}_{2n}\text{Te}_{3n+1}$ is the first intrinsic magnetic topological insulator and is promising to host

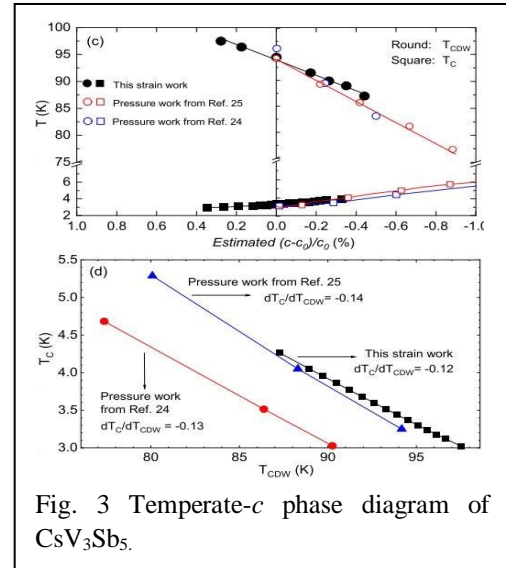


emergent phenomena such as quantum anomalous Hall effect. They can be made ferromagnetic by being a $n \geq 3$ member, or with Sb doping. To pursue high temperature QAHE and other topological phenomena in the MBT device, understanding the magnetic ground state and domain formations is essential. We studied the magnetic dynamics in a few selected FM $\text{MnBi}_{2n}\text{Te}_{3n+1}$ compounds, including $\text{MnBi}_8\text{Te}_{13}$ and Sb doped $\text{MnBi}_{2n}\text{Te}_{3n+1}$ ($n=2, 3$) using AC susceptibility and magnet-optic imaging (Fig. 2) [2].

We observe slow relaxation behavior in all three compounds, suggesting its universality among all ferromagnetic $\text{MnBi}_{2n}\text{Te}_{3n+1}$. We attribute the origin of the relaxation behavior to the irreversible domain movements since they only appear below the saturation fields when ferromagnetic domains form. Furthermore, the very soft ferromagnetic domain nature is revealed by the isotropic dendrite-looking and sea-urchin-shaped domains shown in our magneto-optical imaging measurements. Finally, we ascribe the unusual "double-peak" behavior observed in the AC susceptibility under small DC bias field to the very soft ferromagnetic domain formations.

III) CsV_3Sb_5 was proposed to be a Kagome superconductor with non-trivial topological bands and

CDW. To reveal the interplay of CDW and SC as well as the role of rotational-symmetry-breaking in SC, we used uniaxial strain to tune its ground states [3]. We found that when the uniaxial strain is varied from -0.90% to 0.90% , T_c monotonically increases by $\sim 33\%$ from 3.0 K to 4.0 K while when the uniaxial strain changes from -0.76% to 1.26% , T_{CDW} decreases monotonically by $\sim 10\%$ from 97.5 K to 87.5 K. The opposite response of T_c and T_{CDW} to the uniaxial strain suggests strong competition between these two orders. Comparison with hydrostatic pressure measurements indicate that it is the change in the c -axis that is responsible for these behaviors of the CDW and superconducting transitions, and that the explicit breaking of the sixfold rotational symmetry by strain has a negligible effect. Combined with our first-principles calculations and phenomenological analysis,



we conclude that the enhancement in T_c with decreasing c is caused primarily by the suppression

of T_{CDW} , rather than strain-induced modifications in the bare superconducting parameters. We propose that the sensitivity of T_{CDW} with respect to the changes in the c -axis arises from the impact of the latter on the trilinear coupling between the M_1^+ and L_2^- phonon modes associated with the CDW. Overall, our work reveals that the c -axis lattice parameter, which can be controlled by both pressure and uniaxial strain, is a powerful tuning knob for the phase diagram of CsV_3Sb_5 .

IV) a) In collaboration with Suyang Xu's group at Harvard, we discovered a new-type of Hall effect, the layer-Hall effect in even-layered MnBi_2Te_4 device [4], where electrons from the top and bottom layers spontaneously deflect in opposite directions. Specifically, under no electric field, even-layered MnBi_2Te_4 shows no anomalous Hall effect; However, applying an electric field leads to the surprising emergence of a large layer-polarized AHE arising from the layer-locked Berry curvature, which can be further manipulated by the Axion field $\mathbf{E} \cdot \mathbf{B}$. Our results achieve previously unavailable pathways to detect and manipulate the internal spatial structure of fully-compensated topological AFMs. **b)** In collaboration with Huibo Cao's group at ORNL, we have investigated the sample defects and magnetic structures of $\text{MnBi}_{2n}\text{Te}_{3n+1}$ ($n = 1, 2, 3, 4$) single crystals [5]. We found that a considerable fraction of Bi occupies at the Mn sites in while there is no detectable Mn at the non-magnetic atomic sites within the resolution of neutron diffraction experiments. The defects of Bi at the Mn site naturally explain the continuously reduced saturated magnetic moments from $n = 1$ to $n = 4$. The experimentally estimated critical exponents of all the compounds generally suggest a three-dimensional character of magnetism.

Future Plans

Tuning the magnetic and topological ground state of MBT by magnetic dilution effect. Tuning the magnetic and topological ground state of MBT by hydrostatic pressure. Exploring new synthesis methods to grow MBT with higher magnetic homogeneity. Discovering new intrinsic MBT topological insulators in the 2-2-5 or 3-2-6 ratios. Exploring and charactering new proposed magnetic topological materials. Close collaborations with other groups to investigate the magnetic and topological properties as well as emergent phenomena in devices for materials made in our group.

References

1. Chaowei Hu, et. al, Phys. Rev. B, 104, 054422 (2021)
2. Chaowei Hu, et. al, arXiv: 2106.08969, Journal of Physics D: Applied Physics, resubmitted (2021)
3. Tiema Qian, et. al, arXiv: 2107.04545, Phys. Rev. B , resubmitted (2021)
4. Anyuan Gao, et. al, Nature, 595, 521 (2021)
5. Lei Ding, et. al, Journal of Physics D: Applied Physics, 54, 174003 (2021)

Publications

1. Chaowei Hu, et. al, Phys. Rev. B, 104, 054422 (2021)
2. Chaowei Hu, et. al, arXiv: 2106.08969, Journal of Physics D: Applied Physics, resubmitted (2021)
3. Tiema Qian, et. al, arXiv: 2107.04545, Phys. Rev. B, resubmitted (2021)
4. Anyuan Gao, et. al, Nature, 595, 521 (2021)
5. Lei Ding, et. al, Journal of Physics D: Applied Physics, 54, 174003 (2021),
6. N. Sirica, et. al., arXiv: 2005. 10308, Nature materials, in press (2021)
7. Yujin Cho, et. al., aXriv: 2107.03204 (2021)

Nonlinear charge-spin conversion phenomena in topological insulator/ferromagnet heterostructures

Branislav K. Nikolić¹, Matt F. Doty², Stephanie A. Law², and John O. Xiao¹

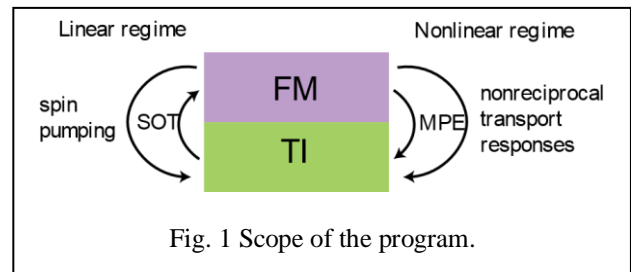
¹ *Department of Physics and Astronomy, University of Delaware, Newark, Delaware, 19716, USA*

² *Department of Materials Science and Engineering, University of Delaware, Newark, Delaware, 19716, USA*

Program Scope

In this program, we investigated charge-spin conversion phenomena in topological insulator/ferromagnet (TI/FM) heterostructures. The scope of the project can be summarized in Fig. 1. To be used for spintronic applications, TIs will be put in contact with a FM. Thus, it is of critical importance to investigate the

magnetic doping and proximity effect on TIs. Experimentally, we found certain sputter-deposited metallic magnetic atoms will diffuse into Bi₂Se₃ and eliminate the topological surface states (TSS). When high-quality Bi₂Se₃ is grown on magnetic insulators (MI), the surface band with spin-momentum locking property still exists, but it is modified at low temperatures due to magnetic proximity effect (MPE). Theoretically, we calculated the influence of proximate Co atoms on the band of Bi₂Se₃. In the linear charge-spin conversion regime, we calibrated the strength of spin-orbit torque (SOT) in Bi₂Se₃/CoFeB heterostructures using both second harmonic Hall voltage and magneto-optical Kerr effect (MOKE) measurements. The inverse process, spin pumping is also modeled through a first-principle approach. In the nonlinear transport regime, we observed a series of second-order spin-to-charge current conversion phenomena, identified their origin, and resolved the peculiar temperature and carrier density dependence.



Recent Progress

1. Modification of TI surface band by magnetic proximity effect

By growing high-quality Bi_2Se_3 on atomically smooth and electrically insulating YIG, TmIG and GGG substrates, we were able to monitor the influence of MPE on TIs through transport measurements. The unusual upturn in resistivity and reduction in carrier density below a threshold temperature of ~ 30 K indicate that the TI energy dispersion as well as Fermi levels are modified by MPE at low temperatures, although a long-range magnetic order does not form in the TI layer. Our first principle calculations also show dramatic change of TI surface band when it is put in contact with just several monolayers of Co atoms [1].

2. SOT and nonlinear Hall effect

Possibly due to the diffusion of Co, Fe, and B atoms into the van-der-Waals-structured TI Bi_2Se_3 [2], the heavily doped Bi_2Se_3 has a relatively small spin Hall angle (~ 0.07) measured by second harmonic Hall voltage and MOKE methods. Besides, we found deposition of just a few atomic layers of Ni will eliminate the TSS. These results suggest magnetic insulators as a better choice for making stable and low-in-carrier-concentration TI/FM heterostructures. At low temperatures, we observed a nonlinear Hall effect (NLHE) which is related to asymmetric magnon scattering processes [3], but the peculiar temperature dependence remains to be answered. We also developed a first-principle approach to model spin pumping phenomenon at the TI/FM interface.

3. Disentangle different UMR mechanisms

The various unidirectional magnetoresistance (UMR) in heavy metal/ferromagnet (HM/FM) and TI/FM heterostructures are illustrated in Fig. 4. We name the magnon-scattering UMR in HM/FM bilayers as Type A MS-UMR. It arises from spin-current-modulated spin-disorder resistivity of the FM layer, and requires the FM to be conductive. It is typically small in magnitude and is suppressed at low temperatures due to reduction in magnon density. However, the MS-UMR in TI/FM

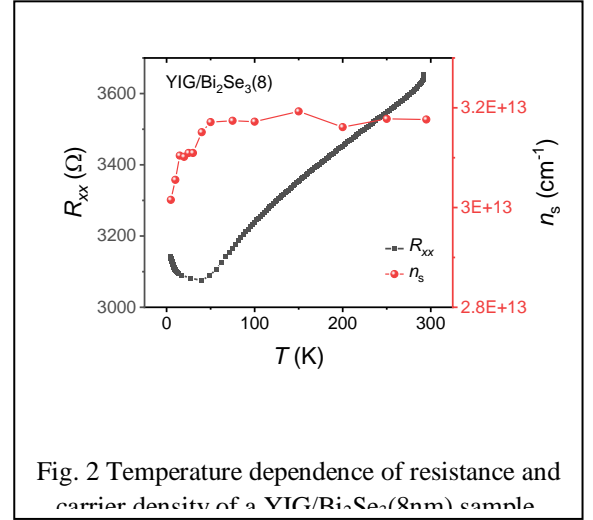


Fig. 2 Temperature dependence of resistance and carrier density of a YIG/ Bi_2Se_3 (8nm) sample

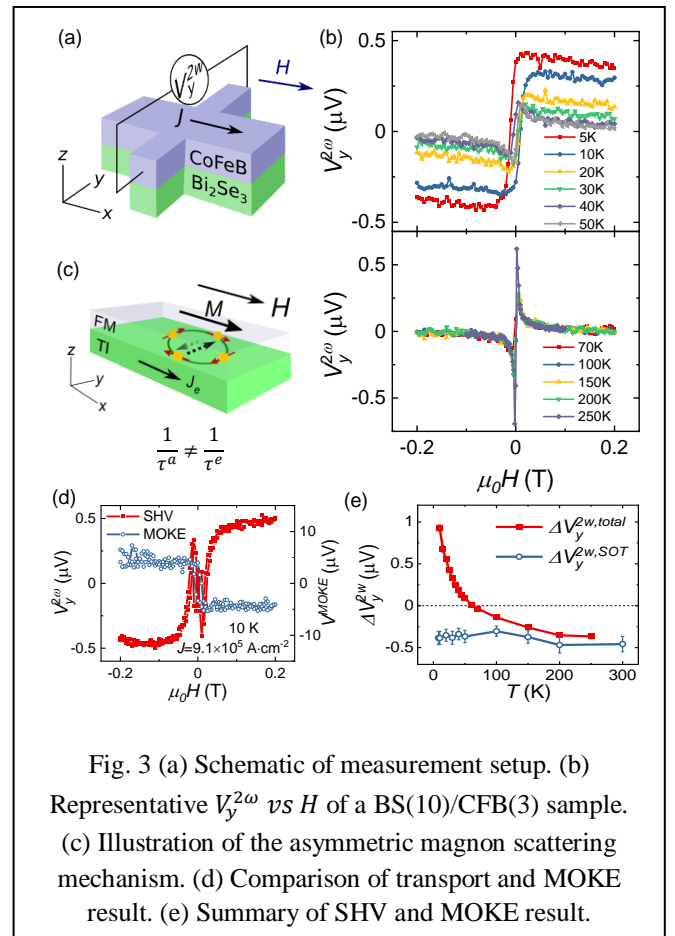
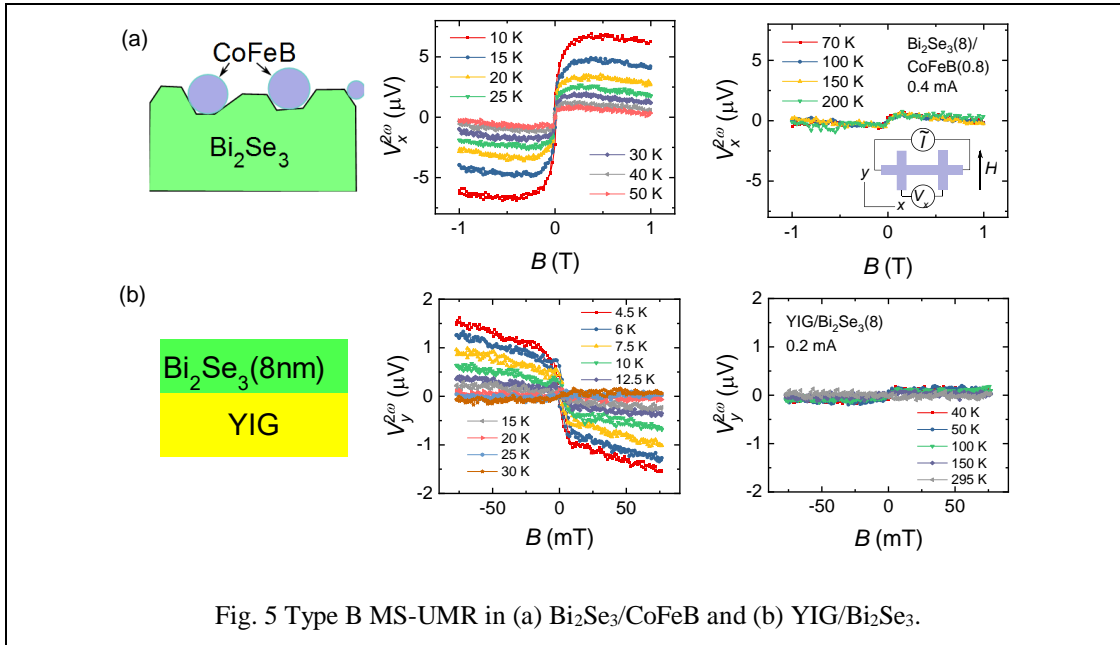
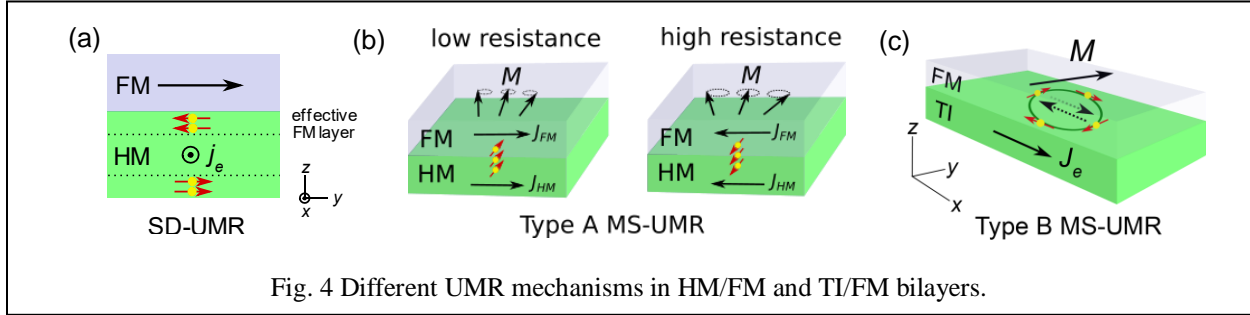


Fig. 3 (a) Schematic of measurement setup. (b) Representative $V_y^{2\omega}$ vs H of a BS(10)/CFB(3) sample. (c) Illustration of the asymmetric magnon scattering mechanism. (d) Comparison of transport and MOKE result. (e) Summary of SHV and MOKE result.

heterostructures is orders of magnitude larger and is enhanced at low temperatures [Fig. 5]. We name the UMR in TI/FM systems as Type B MS-UMR. By utilizing an insulating FM layer, we show that this UMR occurs solely in the TI layer. Its existence is a combined result of spin-momentum locking, magnetic proximity effect and second-order spin-to-charge current conversion, as discussed in the following section.



4. Origin of the UMR and BMR in TI/FM

As shown in Fig. 5(b) and Fig. 6, both the hysteretic UMR and the linear-in-field bilinear magnetoresistance (BMR) in $\text{YIG}/\text{Bi}_2\text{Se}_3$ only appear below ~ 30 K. This coincides with the resistivity upturn and carrier density reduction temperature (Fig. 2), suggesting the role of MPE in these nonreciprocal responses.

For ideal linear TI dispersion, $H = v(k_x\sigma_y - k_y\sigma_x)$, both the first and second spin currents are zero [4]. However, at temperatures below 30 K, MPE modifies the surface band of Bi_2Se_3 and introduces nonlinear (k^2 , k^3 , ...) terms into the dispersion. When an electric field

(current) is applied, the distorted nonlinear surface dispersion together with spin-momentum locking can generate a second-order spin current $j_s^{(2)}(E^2)$ [4]. As illustrated in Fig. 7, when time-reversal symmetry (TRS) is broken by a magnonic reservoir (UMR) or an external magnetic field (BMR), $j_s^{(2)}(E^2)$ is partially converted into a second-order charge current $j_c^{(2)}(E^2)$, giving rise to the UMR or BMR.

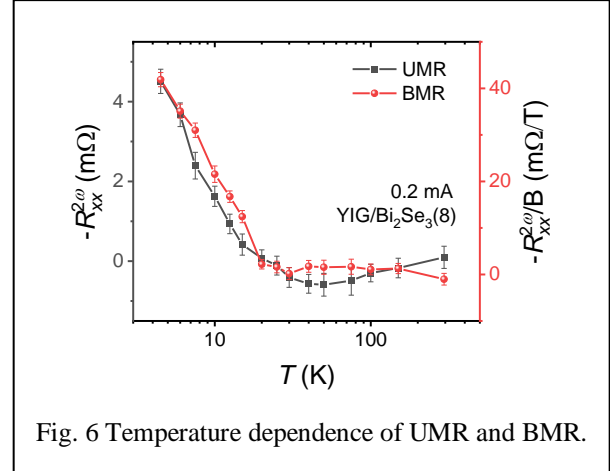


Fig. 6 Temperature dependence of UMR and BMR.

Future Plans

In order to utilize these nonlinear charge-spin conversion effects for spintronic applications, we need to make them observable at room temperature and increase their magnitude. To achieve the first goal, we will grow $(\text{BiSb})_2\text{Te}_3$ on doped TmIG to enhance the MPE and ultimately increase the threshold temperature for the UMR and NLHE. For the second goal, we plan to tune carrier density by changing $(\text{Bi}_x\text{Sb}_{1-x})_2\text{Te}_3$ composition or applying a gate voltage, so the Fermi level can be brought close to the Dirac point.

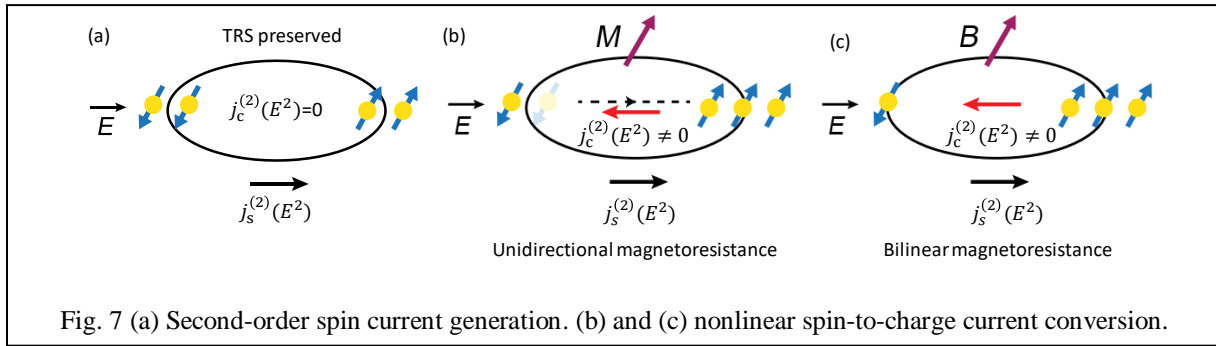


Fig. 7 (a) Second-order spin current generation. (b) and (c) nonlinear spin-to-charge current conversion.

References

- [1] J. M. Marmolejo-Tejada, K. Dolui, P. Lazić, P.-H. Chang, S. Smidstrup, D. Stradi, K. Stokbro, and B. K. Nikolić, *Nano Lett.* **17**, 5626 (2017).
- [2] S.-J. Chang, P.-Y. Chuang, C.-W. Chong, Y. Chen, J.-C. Andrew Huang, P.-W. Chen and Y.-C. Tseng, *RSC Adv.* **8**, 7785 (2018).
- [3] K. Yasuda, A. Tsukazaki, R. Yoshimi, K. S. Takahashi, M. Kawasaki, and Y. Tokura, *Phys. Rev. Lett.* **117**, 127202 (2016).

[4] K. Hamamoto, M. Ezawa, K. W. Kim, T. Morimoto, and N. Nagaosa, *Phys. Rev. B* **95**, 224430 (2017).

Publications in the previous two years

[1] Yang Wang, Vish Mambakkam, Stephanie A. Law, and John. Q. Xiao, “Nonlinear planar Hall effect in magnetic insulator/topological insulator heterostructures” (in preparation).

[2] Yang Wang, Yong Wang, Vish Mambakkam, Saadia Nasir, Zhijie Chen, Kai Liu, Stephanie A. Law, and John. Q. Xiao “Origin of the unidirectional magnetoresistance in topological insulator/ferromagnet heterostructures” (in preparation).

[3] Yang Wang, Xiao Wang, Andy T. Clark, Hang Chen, Xuemei M. Cheng, John W. Freeland, and John Q. Xiao, *Phys. Rev. Materials* **5**, 074409 (2021).

[4] Yang Wang, Yong Wang, Tao Wang, Xinhao Wang, Yusheng Ou, Yi Ji, Matthew F. Doty, Stephanie A. Law, and John Q. Xiao, *Phys. Rev. B* **102**, 125430 (2020).

[5] Kapildeb Dolui, Utkarsh Bajpai, and Branislav K. Nikolić, *Phys. Rev. Materials* **4**, 121201(R) (2020)

Probing novel phenomena in strongly correlated layered materials through van der Waals heterostructures

Claudia Ojeda-Aristizabal, Department of Physics and Astronomy, California State University Long Beach

Program Scope

This program aims to study a variety of materials driven by electronic correlations, spin-orbit coupling and crystal field effects. Examples are spin-orbit driven Mott insulators such as ruthenium chloride (RuCl_3) as well as ferromagnetic insulators presenting two-dimensional magnetism such as VI_3 and $\text{Cr}_x\text{Pt}_{1-x}\text{Te}_2$. Additionally, this program looks to investigate materials beyond those dominated by in-plane strong covalent bonds and van der Waals forces. Molecular solids such as fullerenes and endofullerenes (fullerenes doped with magnetic ions inside) constitute exciting building blocks for novel van der Waals heterostructures. Although fullerenes are fascinating low dimensional materials in their own right, they can thrive exciting properties when combined with layered materials. One of the tasks of this project is to investigate through electronic transport measurements at low temperatures as well as through angle resolved photoemission spectroscopy (ARPES), heterostructures that take advantage of the conducting character of graphene to probe properties of molecular solids as well as more insulating layered materials such as RuCl_3 and VI_3 . ARPES will provide insight on the electronic structure of the ferromagnetic layered materials VI_3 and $\text{Cr}_x\text{Pt}_{1-x}\text{Te}_2$, molecular solids and inform the electronic transport measurements.

Recent Progress

Competition between magnetic order and charge localization in Na_2IrO_3 thin crystal devices

We have performed electronic transport measurements on Na_2IrO_3 thin crystal devices finding that electronic transport is ruled by variable range hopping at temperatures above the magnetic ordering transition known for bulk Na_2IrO_3 (~ 15 K). This observation is supported by ARPES measurements at the high temperature end (290 K) that testify a non-vanishing density of states at the Fermi level as required by Mott's VRH. We have observed that as the system approaches long-range order, it deviates from VRH with no evidence of this mechanism below the ordering temperature. Similarly, we have found that in the presence of an external electric field, transport diverges from VRH, becoming field assisted. Fits of our data to these two mechanisms allow us to deduce the localization length as well as the density of states at the Fermi level in the Na_2IrO_3 thin crystal devices. Our work constitutes a first approach to integrate an exfoliated thin crystal of Na_2IrO_3 into an electronic device, where separate ARPES measurements inform the electronic transport experiments. Using these two complementary and independent experimental techniques on similarly prepared samples can unveil important properties in other insulating 2D-materials.

Topological defects in multilayer graphene probed through strain in the quantum Hall regime

We had the opportunity to perform electronic transport measurements on a multilayer graphene mounted on a sophisticated MEMS (micro-electro mechanical system) actuator device that allowed reversible and controlled uniaxial strain, triggering topological defects on the multilayer graphene. Samples were provided by the Zhou group at the University of Nebraska Lincoln. Although these experiments involve graphene only, it provided an exciting result that helps the understanding of the effect of domain walls in multilayer graphene. During the experiment, domain walls were dynamically created by uniaxial strain applied to the sample using the MEMS actuator while simultaneously measuring electronic transport at low temperatures with an external magnetic field. We observed a strain-induced effect on the quantum Hall effect (QHE) features as well as a discrete modulation of the current across the device that we attribute to a strain-induced tuning of topological line defects in the multilayer graphene. In collaboration with Sinisa Coh at UC Riverside, we simulated numerically the effect of a domain wall in bilayer graphene QHE, finding new QHE plateaus that are absent if no domain walls are included. Our results suggest that while adding regular disorder to multilayer graphene preserves its characteristic QHE features, it is only through the addition of domain walls that the quantization of the resistivity is modified. Our work constitutes a first experimental illustration of the effect of the arrangement of multilayer graphene domain walls in the quantum Hall effect regime, and paves the way for the use of reversible topological defects for electronic applications.

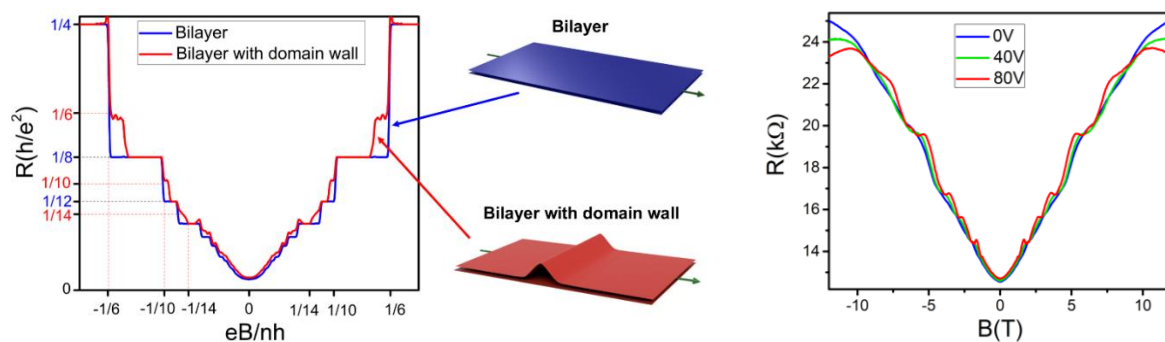


Figure 1: Left: Quantum Hall resistance contrasted with the effect of adding a domain wall. Right: Experimental magnetoresistance with different voltages on the actuator triggering topological defects on the multilayer graphene

Doping dependence of the electronic structure of potassium doped C₆₀ thin films

We have reported in the past the first observation of highly dispersive bands in thin film C₆₀. Our finding, in collaboration with the Lanzara and Zettl groups at UC Berkeley, revealed that in a thin film C₆₀ the electronic structure is not dominated by the electronic interactions within a single molecule. Instead, long range interactions between the molecules in a thin film have a profound effect shaping the electronic structure of this material. Additionally, light polarization studies of the photoemission provided information on the orbital makeup of the C₆₀ band manifolds. Here, we have analyzed the dependence of the photoemission of a C₆₀ thin film upon doping with potassium, finding that K_xC₆₀ is ruled by fundamentally different physics depending on the

stoichiometry. Our in-situ ARPES measurements on a thin film C_{60} as we dope with K, has allowed us to identified in-gap states related to dimer state in K_1C_{60} , and orbital splittings in the LUMO band possibly related to many body effects.

Electronic structure and polarization dependent photoemission of the layered ferromagnet VI_3

VI_3 is a van der Waals layered semiconductor that presents ferromagnetism. This material, made of honeycomb vanadium layers separated by an iodine-iodine van der Waals gap, adds to the family of 2-dimensional materials with the remarkable property of intrinsic ferromagnetism. An important component to unveil the origin of ferromagnetism in 2D materials is the understanding of the electronic structure of these materials. ARPES is an excellent tool to probe the electronic band structure. We have performed, using VI_3 crystals provided by the Kong group at the University of Arizona, a deep study on the linear dichroism dependence of the photoemission that together with first principle calculations, brings light on the properties of the orbitals that play an important role in magnetism. In general, Cr based layered ferromagnets such as CrI_3 yield $S=3/2$ states, as Cr^{3+} has a half-filled t_{2g} level. In VI_3 on the other hand, vanadium has two valence electrons that half fill two of the three degenerate t_{2g} electronic states in the VI_3 octahedra, which leads to $S=1$ states, making VI_3 fundamentally different from CrI_3 . The partial occupancy of the t_{2g} level may be responsible of Jahn-Teller distortions of the VI octahedra [1]. We find through the linear dichroism of VI_3 signature of this effect. VI_3 presents additionally a circular polarization dependence of the photoemission that is currently under analysis. Finally, our photon energy dependent measurements confirms the layered character of VI_3 .

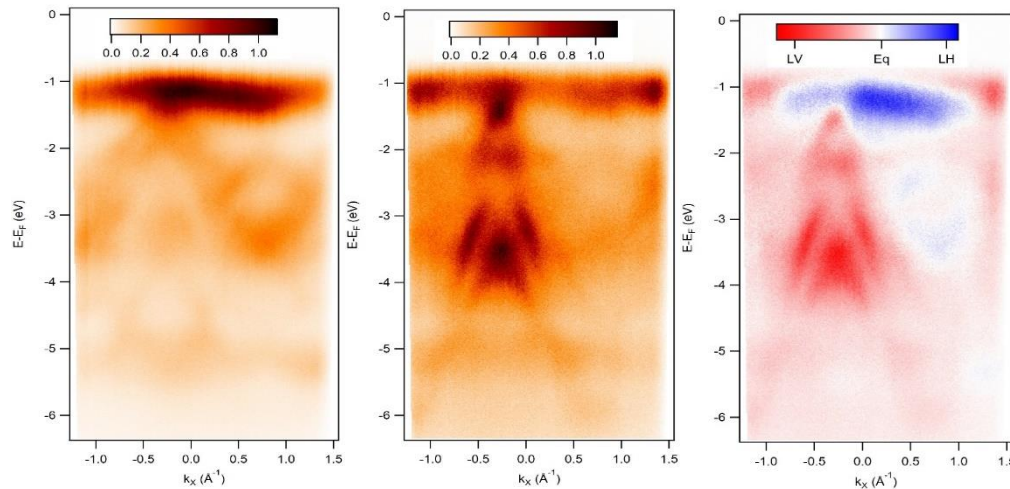


Figure 2: Linear polarization dependent bandstructure of VI_3 using out-of-plane light polarization (left) and in-plane light polarization (center). Right: difference of the two intensities or linear dichroism.

Future Plans

Anomalous Hall effect measurements in devices of $RuCl_3$ and $Cr_xPt_{1-x}Te_2$: we will take advantage of the capabilities in our lab to do guarded measurements, to probe the magnetic ordered states in the Kitaev system $RuCl_3$ and the layered ferromagnet $Cr_xPt_{1-x}Te_2$ through anomalous Hall effect ($Cr_xPt_{1-x}Te_2$ crystals are provided by the Goldberger group at OSU). Nanofabrication techniques will allow us to assess the dependence of the observed anomalous Hall effect on the number of

layers of RuCl₃ or Cr_xPt_{1-x}Te₂, providing information on the evolution of the domain structure in Cr_xPt_{1-x}Te₂ as the number of layers is reduced and the role of interlayer coupling in RuCl₃ on the zig-zag magnetic ordered states.

Electronic transport and ARPES studies of the air-stable layered ferromagnet Cr_xPt_{1-x}Te₂: The layered structure of Cr_xPt_{1-x}Te₂, its metallic character and air-stability make it an ideal material to study through ARPES. We expect the electronic structure of this material to be different from other layered ferromagnets such as Cr₂Ge₂Te₆, as the easy axis of Cr_xPt_{1-x}Te₂ is in-plane in contrast with the out-of-plane easy axis of Cr₂Ge₂Te₆. A study of the effects of the linear polarization of the light should give additional information about the orbital character of the bands in this material.

References

[1] Tai Kong, Karoline Stolze, Erik I. Timmons, Jing Tao, Danrui Ni, Shu Guo, Zoë Yang, Ruslan Prozorov, and Robert J. Cava, “VI3 a new layered ferromagnetic semiconductor” *Adv. Mat.* **31**, 1808074 (2019)

Publications

1. Drew W. Latzke*, C. Ojeda-Aristizabal*, Jonathan Denlinger, Ryan Reno, Alex Zettl and Alessandra Lanzara “Orbital character effects in the photon energy and polarization dependence of pure C60 photoemission” *ACS Nano* **13** (11), 12710 (2019)
2. Drew W. Latzke*, C. Ojeda-Aristizabal*, Sinead M. Griffin, Jonathan Denlinger, Jeffrey B. Neaton, Alex Zettl and Alessandra Lanzara “Observation of highly dispersive bands in pure thin film C60” *Phys. Rev. B* **99**, 045425 (2019)
3. Josue Rodriguez, Gilbert Lopez, Francisco Ramirez, Nicholas P. Breznay, Robert Kealhofer, Vikram Nagarajan, Drew Latzke, Samantha Wilson, Naomy Marrufo, Peter Santiago, Jared Lara, Amirari Diego, Everardo Molina, David Rosser, Hadi Tavassol, Alessandra Lanzara, James G. Analytis and Claudia Ojeda-Aristizabal “Competition between magnetic order and charge localization in Na₂IrO₃ thin crystal devices” *Phys. Rev. B* **101**, 235415 (2020).
4. Paul Anderson, Yifan Huang, Yuanjun Fan, Sara Qubbaj, Sinisa Coh, Qin Zhou and Claudia Ojeda-Aristizabal “Signature of multilayer graphene strain-controlled domain walls in quantum Hall effect” *arXiv* **2012.13153 Under Review** *Phys. Rev. B* (2020)
5. Derek Bergner, Tai Kong, Ping Ai, Daniel Eilbott, Claudia Fatuzzo, Samuel Ciocys, Nicholas Dale, Conrad Stansbury, Ryan Reno, Alessandra Lanzara and Claudia Ojeda-Aristizabal “Polarization dependence of the photoemission of the layered ferromagnetic semiconductor VI3” **In preparation 2021**
6. Ping Ai, Luca Moreschini, Ryo Mori, Drew W. Latzke, Claudia Ojeda-Aristizabal, Jonathan D. Denlinger, Alex Zettl and Alessandra Lanzara “From molecular bands to Dirac fermions in the metal-insulator transition of doped fullerenes” **In preparation 2021**
7. Master thesis dissertations by Josue Rodriguez (2019), Paul Anderson (2019), Sara Qubbaj (2020) and Everardo Molina (2021).

Understanding A Few Spin-Based Fundamental Interactions in Colloidal Organic-Inorganic Hybrid Perovskite Nanostructures by Ultrafast Optical Spectroscopy

Min Ouyang, University of Maryland- College Park

Program Scope

This awarded DOE program is aimed at exploring a few fundamental spin dynamics and structure-spin coupling physics within the quantum confined hybrid nanostructures, including organic-inorganic perovskites. A unique two-prong approach by combining precisely tailored nanoscale materials control with ultrafast optical orientation and manipulation spectroscopic tools is employed in this project.

Recent Progress

We have made substantial progress on two themes so far, including materials development of novel chiral nanostructures and ultrafast optical spin study to understand and manipulate coherent spin dynamics and explore their structure-spin relationship. In particular, we have successfully developed two different synthetic strategies to control both quantum confinement and structural chirality of organic-inorganic perovskite nanostructures: one is the single crystal growth that can be used for mechanical exfoliation to form two-dimensional layered perovskites with different quantum confinements (one example is shown in Figure 1, top left), and the other is the bottom-up synthesis of nanostructures with controllable morphology and structural chirality (one example is shown in Figure 1, top right). Importantly, we have demonstrated that both growth methods can allow introduction of structural chirality during the material synthesis, enabling the chiral perovskite quantum confined nanostructures. These new materials have offered unique condensed matter platform to study chirality dependent spin dynamics. We have also utilized low temperature time-resolved Faraday rotation spectroscopy [1,

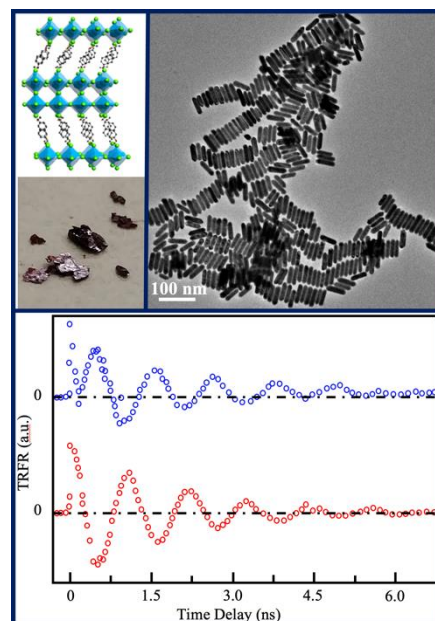


Figure 1. (Top left) Schematics and photo of bulk chiral 2-layer hybrid (*S*-MBA)₂Pb₂I₇ perovskite crystals; (Top right) TEM image of one-dimensional MAPbBr₃ nanorods; (Bottom) Time-resolve Faraday rotation measurement shows chirality-dependent spin polarization in the chiral perovskites nanocubes. Data were acquired at 77K.

2] to study coherent spin dynamics of nanoscale chiral perovskites, and a clear chirality-dependent spin polarization has been observed at 77K (Figure 1, bottom).

In order to explore new chirality-spin coupling through interface, we have developed a new class of nanoscale chiral plasmonic nanostructures and their enabled hybrid metal-semiconductor nanostructures [3-5]. One example of plasmonic Au nanocubes is presented in Figure 2. From the structural view point, metal Au possesses a *fcc* lattice and is in the absence of intrinsic handedness. We have demonstrated that chirality can be induced in such achiral materials through nanoscale enantioselective surface engineering, and a new chiral mechanism by the broken mirror symmetry of high-miller index facets on the surface is proposed (Figure 2, top). We have performed a thorough mechanistic study to substantiate this chiral mechanism by both structural (e.g., middle of Figure 2) and optical characterizations (e.g., bottom of Figure 2). Importantly, our structural and optical simulation based on proposed chiral mechanism have shown excellent agreement with experimental results. Our demonstration and control of surface induced chirality in achiral materials should offer a unique opportunity to explore emerging physics, including interfacial chirality-spin coupling, which is currently under investigation.

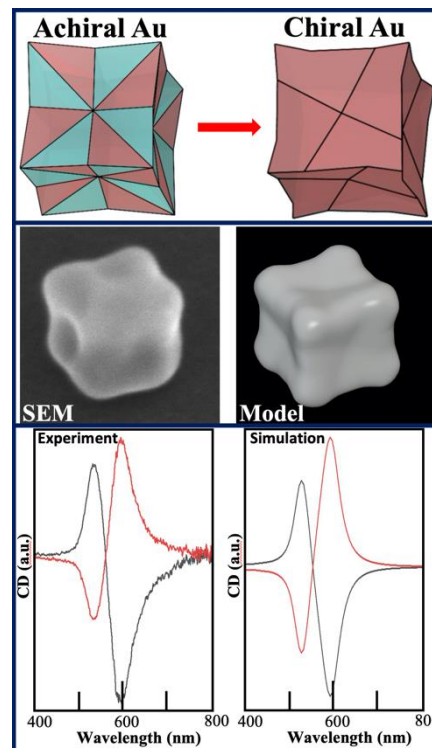


Figure 2. (Top) Proposed chiral mechanism of achiral inorganic lattice by broken mirror symmetry of high-miller index facets on the surface; (Middle) High-resolution SEM image and structural modelling of chiral Au nanocubes; (Bottom) Optical circular dichroism measurement and electromagnetic simulation.

Future Plans

Our progress so far in both material development and ultrafast optical and spin measurements from this project has opened up exciting opportunity for exploring various emerging chirality-spin dependent phenomena. We will continue our work on systematic spin measurement of chiral perovskites to elucidate underlying mechanism of observed chirality induced spin polarization. We will also optimize new class of chiral hybrid metal-semiconductor nanostructures and combine with our ultrafast spin measurements to investigate proximity interactions between spin of semiconductor and chirality of metal. Furthermore, active control of structural chirality in chiral perovskites will be explored with goal to provide a new horizon of spin control at the nanoscale.

References

- [1] J. Zhang, Y. Tang, K. Lee and M. Ouyang, Tailoring light-matter-spin interactions in colloidal hetero-nanostructures, *Nature* **466**, 91 (2010).
- [2] P.P. Wang and M. Ouyang, Uncovering intrinsic spin coherence in colloidal quantum structures by nanoscale spin echo and applications in sensing many-body correlations, *Nature Nano* (under review 2021).
- [3] J. Zhang, Y. Tang, K. Lee and M. Ouyang, Nonepitaxial growth of hybrid core-shell nanostructures with large lattice mismatches, *Science* **327**, 1634 (2010).
- [4] L. Weng, H. Zhang, A. O. Govorov and M. Ouyang, Hierarchical synthesis of non-centrosymmetric hybrid nanostructures and enabled plasmon-driven photocatalysis. *Nat. Commun.* **5**, 4792 (2014).
- [5] K. Lee, J.T. Zhang and M. Ouyang, Injective morphology imprinting synthesis of anisotropic inorganic hybrid nanostructures and enabled applications. *Nature Mater.* (under review 2021).

Publications

1. N. Steinsultz *et al.*, Inherent Plasmonic and Excitonic Couplings in Emerging Nitrogen-Vacancy Centers Based Hybrid Nanostructures. *Nano Lett.* (revision, 2021).
2. Y. Tang *et al.*, Magnetic Core@Metal Shell Nanostructures with Layer-by-Layer Shell Control and Tunable Magnetism. *J.Am.Chem.Soc.* (revision, 2021).
3. K. Lee *et al.*, Injective Morphology Imprinting Synthesis of Anisotropic Inorganic Hybrid Nanostructures and Enabled Applications. *Nature Mater.* (revision, 2021).
4. P.P. Wang *et al.*, Uncovering Intrinsic Spin Coherence in Colloidal Quantum Structures by Nanoscale Spin Echo and Applications in Sensing Many-Body Correlations. *Nature Nano.* (revision, 2021).

Synthesis and Observation of Emergent Phenomena in Epitaxial Heusler Compound Heterostructures

Principal Investigators: Christopher J. Palmstrøm (University of California, Santa Barbara)
Anderson Janotti (University of Delaware)

1. Program Scope

Heusler compounds are an exciting class of ternary compounds that exhibit a wide range of electrical and magnetic properties including materials that can be semiconducting, half-metallic ferromagnets, superconductors, thermoelectrics, and can even host topologically nontrivial ground states¹. The ability to synthesize these materials in thin film form opens up avenues for the realization of multi-functional devices and novel emergent phenomena in engineered heterostructures. Epitaxial thin film growth also allows access to a wide variety of tuning parameters not possible in bulk single crystals: proximity effects in heterostructures, multiple crystallographic faces, thickness and quantum confinement effects, lattice parameters and biaxial strain, and metastable phase growth.

We have further expanded our materials palette to rare-earth monpnictide (RE-V) rock salt compounds that can provide additional functionalities such as extreme magnetoresistance² and potentially topological behavior³. RE-Vs have also been shown to be excellent diffusion barriers stopping interfacial reactions between Heusler compounds and III-V semiconductor substrates, facilitating fabrication of high quality thin films of inter-metallic heterostructures⁴. Combining our molecular beam epitaxy (MBE) synthesis capabilities with angle-resolved photoemission spectroscopy (ARPES), density functional theory (DFT) calculations and low temperature magnetotransport we are investigating electronic structure and material properties in a wide variety of Heusler compounds and RE-Vs.

2. Recent Progress

2.1 Controlling semi-metallicity by dimensional confinement in heteroepitaxial LuSb thin films

Control of heteroepitaxial interfaces plays a crucial role in designing novel devices in the ultra-thin limit and can lead to emergent properties, particularly in semi-metallic systems. We show that polarity mismatch and change in local coordination and bonding across the technologically relevant (001) interface between rock-salt (LuSb) and zinc-blende (GaSb) crystal structure leads to the formation of a two-dimensional bonding induced hole gas (2DHG), which remains tightly bound to the interface. Through a comparison of

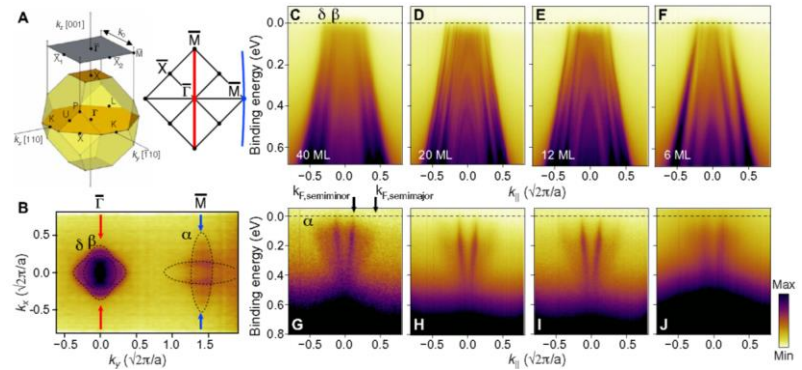


Figure 1: Photoemission spectroscopy of LuSb/GaSb (001) thin films. (A) 3D and surface Brillouin zone of LuSb showing the high-symmetry points. Red and blue lines show the cut directions along which ARPES measurements are taken for (C) to (F) and (G) to (J), respectively. (B) Fermi surface map of bulk LuSb (12 ML) showing both the electron and the hole pockets and the ARPES cut directions. Calculated Fermi surface obtained from DFT using screened hybrid functional (HSE06) is shown by black dotted lines. E-k spectral map at the bulk Γ point (top) along $\bar{M}-\bar{\Gamma}-\bar{M}$ [red line in (A)] of the surface Brillouin zone for thin films of thickness (C) 40 ML, (D) 20 ML, (E) 12 ML, and (F) 6 ML and at the bulk X point (bottom) along $\bar{\Gamma}-\bar{M}-\bar{\Gamma}$ [blue line in (A)] of the surface Brillouin zone for (G) 40-ML-, (H) 20-ML-, (I) 12-ML-, and (J) 6-ML-thick films. All data taken at 70 K and a photon energy of 60 eV.

DFT slab calculations with magneto-transport and ARPES measurements (**Figure 1**) of the Fermi wavevector evolution as function of film thickness we found evidence for charge transfer across the interface, which significantly affects the electronic structure and transport properties in the ultra-thin limit.

2.2 Straining RE-V semimetals

Despite extensive experimental efforts to study RE-Vs' Fermiology, there remains a gap in the understanding of the effects of hydrostatic pressure and biaxial strain on the electronic band structure and magneto-transport properties. To that end we have studied the effect of biaxial strain on LaSb (DFT), GdSb (ARPES+DFT) and hydrostatic pressure on LaAs (DFT).

2.2.1 Engineering carrier compensation and band topology in strained GdSb

We investigated the electronic structures of biaxially strained GdSb (001) films grown on III-V substrates, using epilayers to tune the final lattice parameter from tensile (+2%) to compressive (-2%) strain and 0%. **Figure 2** highlights the ARPES high-symmetry cuts studied, comparing the electron-band dispersion for the compressive and tensile strained film. The in-plane electron pockets ($X_{1,2}$) show an increase of the bandwidth upon compressive strain, and the out-of-plane electron pocket (X_3) is characterized by a highly dispersive band, agreeing with theoretical predictions⁵. The movement of the hole band upwards towards the electron pocket (Figure 2(i)) suggests the band topology is engineered using lattice strain. In addition to modifying the band topology, the compressively strained film is more electron-rich and is further away from exact carrier compensation than the tensile strained film, explaining the lower magnetoresistance seen for compressive strained films than lattice matched films.

2.2.2 Predictions of trivial to nontrivial topology transition in strained LaAs & LaSb

Using DFT calculations with the screened hybrid functional of Heyd, Scuseria, and Ernzerhof (HSE06) we studied the effects of hydrostatic and epitaxial strain on the electronic properties of LaAs and LaSb, respectively. Our HSE06 calculations correct the overestimated RE d -V p band overlap obtained from DFT generalized gradient approximation (GGA) calculations. In LaSb, under 1.6% compressive biaxial strain, the La d band crosses the Sb p band near the Z point in the Brillouin zone, stabilizing a topologically

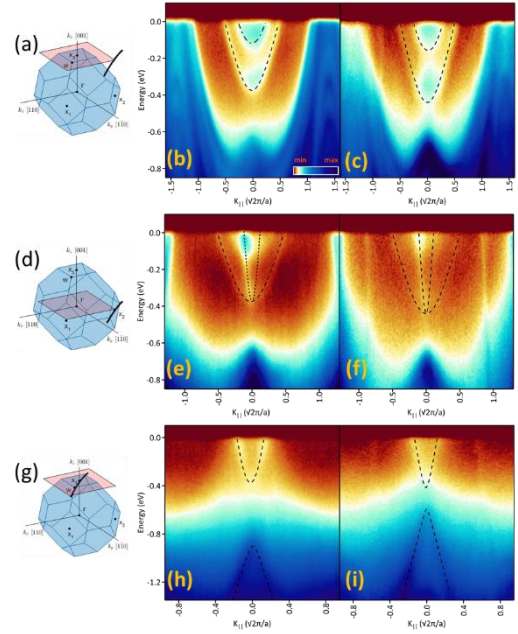


Figure 2: Electron and hole pocket modifications with strain for +2% tensile (left) and -2% compressive (right) biaxial strain. (a), (d), and (g) Schematic of the bulk Brillouin zone projected to the surface Brillouin zone, showing the k_z plane and E-k spectra directions. (a-c)/(d-f) $\bar{\Gamma}$ - \bar{M} - $\bar{\Gamma}$ cut along the in-plane electron pocket $X_{1,2}$ semimajor/semiminor axis, in the bulk X_3/Γ plane, respectively. (g-i) Out-of-plane electron pocket semiminor axis, \bar{M} - $\bar{\Gamma}$ - \bar{M} in bulk X_3 plane.

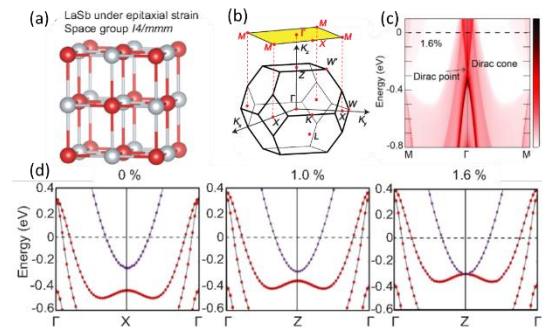


Figure 3: (a) Crystal structure and (b) Brillouin zone of LaSb under compressive epitaxial strain. (c) Electronic band structure of LaSb at 1.6% compressive strain along \bar{M} - $\bar{\Gamma}$ - \bar{M} . (d) Evolution of electronic band structure in the out-of-plane direction along Γ -Z- Γ with compressive strain.

nontrivial phase (Figure 3). In LaAs, the p - d crossing can be induced under hydrostatic pressure, showing a topological phase transition at ~ 7 GPa.

2.3 Modeling the Emergence of Quantum Hall States from Topological Surface States in $\text{Pt}_x\text{Au}_{1-x}\text{LuSb}$

To control the chemical potential and decouple the surface states from the bulk carriers we have synthesized epitaxial thin films of $\text{Pt}_{1-x}\text{Au}_x\text{LuSb}$ with a range of Au compositions, where Au atoms are expected to contribute one extra electron per formula unit compared to Pt. This compensation alloying has allowed us to tune the chemical potential close to the surface Dirac point and to lower the bulk carrier concentration by more than two orders of magnitude (Figure 4). Reduced bulk carrier concentration and surface-bulk coupling combined with lower effective mass of the topological surface states in suitably alloyed $\text{Pt}_{1-x}\text{Au}_x\text{LuSb}$ thin films has led to the observation of quantum Hall states.

The changes in the electronic structure due to substitution alloying of Au is directly observed in ARPES measurements (Figure 5). A comparison between the Fermi levels obtained from ARPES (surface) and Hall measurements (bulk) indicates an upward band-bending (Δ_{bb}) near the sample surface for the alloyed films which is explained by the low bulk carrier concentration. Finally, ARPES measurements reveal a band gap in the topological surface states (TSS) indicative of the formation of massive Dirac fermions due to coupling between the TSS at opposite surfaces in $\text{Pt}_{1-x}\text{Au}_x\text{LuSb}$ thin films.

3. Future Plans

3.1 Searching for native and proximity-induced superconductivity in Heusler thin films

While several Heusler compounds have been found to be superconducting as bulk crystals⁶, to date there are no reports of superconducting thin films. One explanation for this disparity would be the higher disorder present in existing sputtered films⁷. Epitaxial thin-film growth offers a route to study the interplay between structural and chemical order, layer thickness, and superconductivity. Furthermore, by fabricating a heterostructure of a superconductor on a topologically nontrivial Heusler film we can study lateral transport and induced superconductivity. We have begun studying the growth window of the Heusler compound PtLuBi (see poster for preliminary results), which belongs to a new group of superconductors with

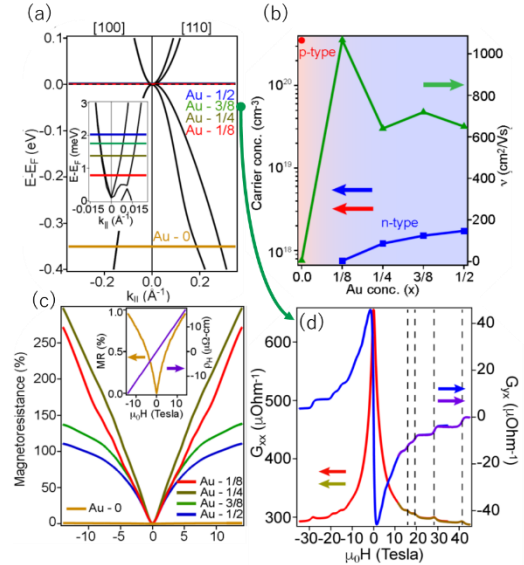


Figure 4: Transport properties of $\text{Pt}_{1-x}\text{Au}_x\text{LuSb}$ thin films*. (a) Fermi level position as function of Au concentration, (b) carrier concentration and mobility estimated from the Hall coefficient, (c) magnetoresistance at 2 K, (d) longitudinal and Hall conductance in $\text{Pt}_{5/8}\text{Au}_{3/8}\text{LuSb}$.

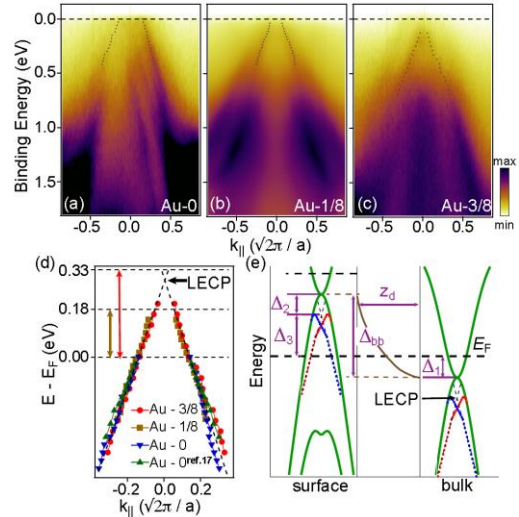


Figure 5: TSS in $\text{Pt}_{1-x}\text{Au}_x\text{LuSb}$ films. ARPES measurements along $\bar{\Gamma}$ - \bar{X} close to the bulk Γ point for (a) PtLuSb (b) $\text{Pt}_{7/8}\text{Au}_{1/8}\text{LuSb}$ (c) $\text{Pt}_{5/8}\text{Au}_{3/8}\text{LuSb}$ (d) Extracted dispersion of the TSS showing the shift in the Fermi level with the addition of gold. (e) Schematic of the upward bandbending Δ_{bb} .

low carrier densities ($<10^{20} \text{ cm}^{-3}$), which could host new mixed pairing states beyond the singlet s wave ($J=0$) and triplet p wave ($J=1$)⁸. In addition to unconventional pairing states, the strong band inversion found in PtLuBi could suggest topological superconducting behavior⁹.

3.2 Emergent topological phases by interfacing/alloying a topological-insulator and a half-metal Heusler

Building upon our previous synthesis efforts we aim to study heterostructures, superlattices and alloys of the topological PtLuSb and the half-metal PtMnSb (see poster for PtMnSb results). PtMnSb is one of the first predicted half-metals with Curie temperature well above room temperature¹⁰. Combining the inversion-broken symmetry of a half-Heusler structure and the large spin-orbit coupling derived from the constituent elements, PtMnSb can be a promising spintronics material with large spin-orbit torque and spin-current transport. In addition to forming a useful epitaxial ferromagnetic contact for spintronic devices, the PtMnSb layer grown on PtLuSb could induce the magnetic proximity effect which triggers a nontrivial gap opening in the surface Dirac dispersion and driving PtLuSb into a Chern insulator (quantized anomalous Hall insulator) phase. By fabricating PtLuSb/PtMnSb superlattices with appropriate periodicity or by forming simple solid solution $\text{PtMn}_{1-x}\text{Lu}_x\text{Sb}$, the band topology and the magnetic properties can be tuned between the two compounds to reach a critical concentration leading the emergence of a Weyl semimetal phase (Figure 6).

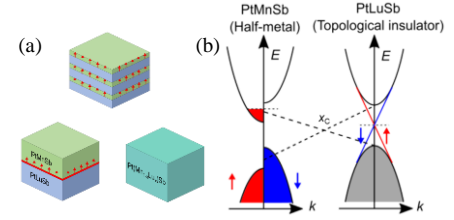


Figure 6: (a) PtMnSb and LuPtSb superlattices and alloys (b) Systematic tuning of the band topology and magnetic properties in $\text{Pt}(\text{Mn}_{1-x}\text{Lu}_x)\text{Sb}$. Possible emergence of a Weyl semimetal phase around the gap closing concentration X_c .

3.3 Exploring new metastable Weyl and nodal line semimetals

We have begun exploring the synthesis conditions and magnetic ordering in Co_2FeSn , a novel metastable nodal line semimetal with a Curie temperature well above room temperature. Co_2FeSn hosts nodal lines $\sim 100 \text{ meV}$ above the Fermi level which should generate record-high intrinsic anomalous Hall conductivity and Nernst conductivity at room temperature.

4. References

- ¹ K. Manna, Y. Sun, L. Muechler, J. Kübler, and C. Felser, *Nat. Rev. Mater.* **3**, 244 (2018).
- ² F.F. Tafti, Q.D. Gibson, S.K. Kushwaha, N. Haldolaarachchige, and R.J. Cava, *Nat. Phys.* **12**, 272 (2016).
- ³ X. Duan, F. Wu, J. Chen, P. Zhang, Y. Liu, H. Yuan, and C. Cao, *Commun. Phys.* **1**, 71 (2018).
- ⁴ C.C. Bomberger, M.R. Lewis, L.R. Vanderhoef, M.F. Doty, and J.M.O. Zide, *J. Vac. Sci. Technol. B, Nanotechnol. Microelectron. Mater. Process. Meas. Phenom.* **35**, 030801 (2017).
- ⁵ X. Duan, F. Wu, J. Chen, P. Zhang, Y. Liu, H. Yuan, and C. Cao, *Commun. Phys.* **1**, 71 (2018).
- ⁶ F.F. Tafti, T. Fujii, A. Juneau-Fecteau, S. René De Cotret, N. Doiron-Leyraud, A. Asamitsu, and L. Taillefer, *Phys. Rev. B* **87**, 184504 (2013).
- ⁷ H. Narita, Y. Niimi, T. Miyawaki, N. Tanaka, and H. Asano, *Jpn. J. Appl. Phys.* **54**, (2015).
- ⁸ M. Meinert, *Phys. Rev. Lett.* **116**, 26 (2016).
- ⁹ B. Roy, S.A.A. Ghorashi, M.S. Foster, and A.H. Nevidomskyy, *Phys. Rev. B* **99**, 1 (2019).
- ¹⁰ R.A. de Groot, F.M. Mueller, P.G. Van Engen, and K.H.J. Buschow, *Phys. Rev. Lett.* **50**, 2024 (1983).
- ¹¹ J. Noky, J. Gooth, C. Felser, and Y. Sun, *Phys. Rev. B* **98**, 241106 (2018).

* The LT magnetotransport measurements were supported by the Office of Naval Research through the Vannevar Bush Faculty Fellowship under the Award No. N00014-15-1-2845

5. Publications

- S. Chatterjee, S. Khalid, H. S. Inbar, T. Guo, Y.-H. Chang, E. Young, A. V. Fedorov, D. Read, A. Janotti, and C. J. Palmstrøm, *Controlling magnetoresistance by tuning semimetallicity through dimensional confinement and heteroepitaxy*, *Sci. Adv.* **7**, 2002.06167eabe8971 (2021). <https://doi.org/10.1126/sciadv.abe8971>
- E. H. Shourov, P. J. Strohbeen, D. X. Du, A. Sharan, F. C. de Lima, F. Rodolakis, J. L. McChesney, V. Yannello, A. Janotti, T. Birol, and J. K. Kawasaki, *Electronic correlations in the semiconducting half-Heusler compound FeVSb*, *Phys. Rev. B* **103**, 045134 (2021). <https://doi.org/10.1103/PhysRevB.103.045134>
- R. Bhandia, B. Cheng, T. L. Brown-Heft, S. Chatterjee, C. J. Palmstrøm, and N. P. Armitage, *THz-range Faraday rotation in the Weyl semimetal candidate Co₂TiGe*, *J. Appl. Phys.* **128**, 244303 (2020). <https://doi.org/10.1063/5.0033536>
- J. B. Pan, J. B. Yu, Y. F. Zhang, S. X. Du, A. Janotti, C. X. Liu, and Q. M. Yan, *Quantum anomalous Hall effect in two-dimensional magnetic insulator heterojunctions*, *npj Comput. Mater.* **6**, 152 (2020). <https://doi.org/10.1038/s41524-020-00419-y>
- S. Khalid and A. Janotti, *Trivial to nontrivial topology transition in rare-earth pnictides with epitaxial strain*, *Phys. Rev. B* **102**, 035151 (2020). <https://doi.org/10.1103/PhysRevB.102.035151>
- W. K. Peria, T. A. Peterson, A. P. McFadden, T. Qu, C. Liu, C. J. Palmstrøm, and P. A. Crowell, *Interplay of large two-magnon ferromagnetic resonance linewidths and low Gilbert damping in Heusler thin films*, *Phys. Rev. B* **101**, 134430 (2020). <https://doi.org/10.1103/PhysRevB.101.134430>
- S. Khalid, A. Sharan, and A. Janotti, *Hybrid functional calculations of electronic structure and carrier densities in rare-earth monpnictides*, *Phys. Rev. B* **101**, 125105 (2020). <https://doi.org/10.1103/PhysRevB.101.125105>

Broken Symmetries for Control of Spin Currents and Spin-Orbit Torques

Daniel C. Ralph, Cornell University

Program Scope

This program is investigating how the production of spin currents and spin-orbit torques can be modified and controlled by utilizing materials with low symmetry. This research has both fundamental and applied objectives. Fundamentally, the combination of low-symmetry materials (e.g., having broken inversion and rotational symmetries), together with the presence of mobile electrons subject to strong spin-orbit and/or exchange coupling, provide the conditions for electron band structures with large Berry curvatures and associated topological states. We are performing experiments to better understand how these effects can influence the production of electrically-driven flows of spin and orbital angular momentum. These fundamental physics questions are directly relevant to the development of magnetic memory and logic applications, because electrically-generated flows of angular momentum within magnetic samples can exert torques to manipulate the magnetic orientation and thereby write information in magnetic devices. We are focused primarily on studying the mechanisms by which low-symmetry materials can generate a particular component of torque (an out-of-plane antidamping torque) that is forbidden in high symmetry materials but which is capable of driving the switching of nanoscale magnetic memories approximately a factor of 100 times more efficiently than conventional spin-orbit torque produced by high-symmetry materials.

Recent Progress

We have experiments in progress studying several different classes of low-symmetry materials, to understand the mechanisms that can produce the strongest electrically-generated spin currents. These include both materials with low crystalline symmetries (including ferroelectrics) and materials in which symmetries are broken by magnetic order (ferromagnets and antiferromagnets). The most promising results to date involve spin generation by antiferromagnets. These results are exciting because they suggest that unconventional components of spin currents and torques can be generated by taking advantage of strong exchange interactions, instead of relatively-weaker spin-orbit interactions that have been the focus of this field before now. Research on electric-field-generated spin currents from antiferromagnets was catalyzed first by predictions for non-collinear chiral antiferromagnets¹⁻³ and promising initial experiments for those materials.^{4,5} Under this program, we have investigated a simpler class of collinear antiferromagnets, motivated by predictions from González-Hernández *et al.*⁶ We have identified the signatures of an antiferromagnetic spin Hall

effect with symmetries that are distinct from other mechanisms of spin-current generation reported in antiferromagnetic or ferromagnetic materials.⁷

The antiferromagnet we have studied is RuO₂ (Fig. 1(a)), a conducting rutile oxide. The Ru atoms at the center and corners of the unit cell have opposite spins, forming a collinear antiferromagnetic (AF) order with the Néel vector (\mathcal{N}) oriented along the [001] or [00 $\bar{1}$] axis. The center and the corner Ru atoms experience

different oxygen environments, which leads to spin-split electrons bands as shown schematically in Fig. 1(b)²³. Due to this spin-split band structure, theory predicts that when an electric field (\vec{E}) is applied it can generate a transverse spin current through an AF spin Hall effect (AF-SHE), even in the absence of any spin-orbit interaction⁶. (Figure 1(c) shows the Fermi surface shifted by an applied field, compared to the $\vec{E} = 0$ Fermi surface in Fig. 1(b), and how this leads to a transverse spin current.) In general, the flow of the spin current from this AF-SHE should have a well-defined angular dependence, with a spin orientation \hat{s} pointing approximately along \mathcal{N} with a spin-flow direction perpendicular to both \vec{E} and \hat{s} . Therefore the direction of the spin and the torque that it can apply to an adjacent magnetic layer can be controlled through the orientation of the Neel vector. The result is fundamentally different from the conventional SHE in heavy metals because it does not require spin-orbit interactions and it is odd under time reversal (\mathcal{T} -odd). Density functional theory calculations performed by our collaborators in the Tsymbal group at Nebraska predict that in a single-domain RuO₂ antiferromagnet the \mathcal{T} -odd spin Hall conductivity should be almost an order of magnitude larger than the conventional \mathcal{T} -even spin Hall conductivity arising from spin-orbit coupling.

We have tested the predictions of this antiferromagnetic spin Hall effect by growing RuO₂ on different crystal facets of TiO₂ substrates to control the orientation of the Néel vector, capping the RuO₂ with

ferromagnetic permalloy, and then measuring the strength of the electric-field-generated spin current through the spin-transfer torque exerted on the permalloy. We have developed a technique to make quantitative measurements of all three vector components of

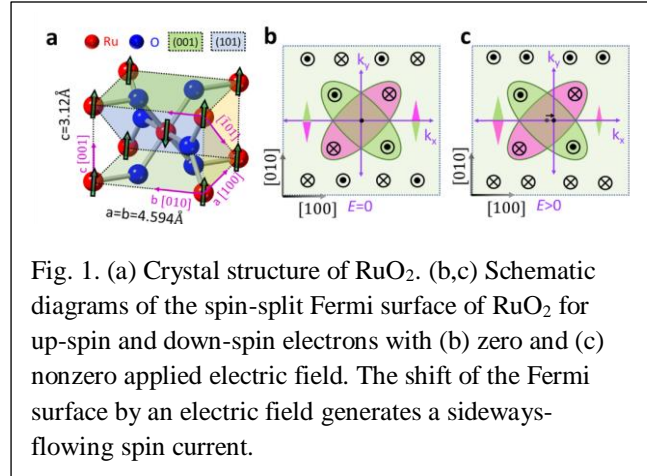


Fig. 1. (a) Crystal structure of RuO₂. (b,c) Schematic diagrams of the spin-split Fermi surface of RuO₂ for up-spin and down-spin electrons with (b) zero and (c) nonzero applied electric field. The shift of the Fermi surface by an electric field generates a sideways-flowing spin current.

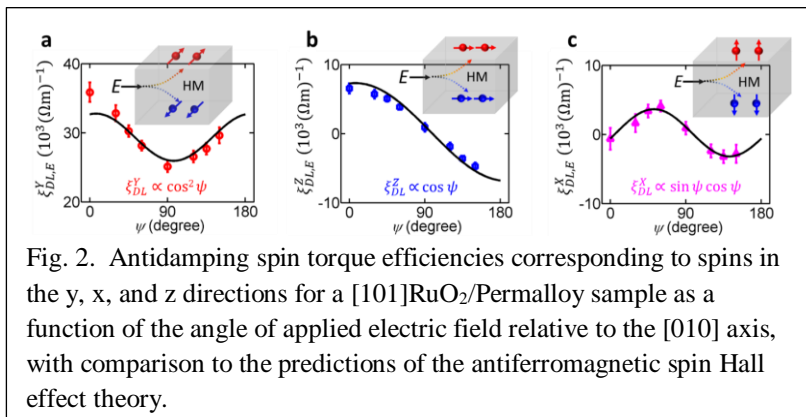


Fig. 2. Antidamping spin torque efficiencies corresponding to spins in the y, x, and z directions for a [101]RuO₂/Permalloy sample as a function of the angle of applied electric field relative to the [010] axis, with comparison to the predictions of the antiferromagnetic spin Hall effect theory.

the spin in the spin current by performing spin-torque ferromagnetic resonance measurements as a function of both the angle of applied magnetic field and the angle of electric field relative to the crystal axes. The results for [101]-oriented RuO₂ are shown in Fig. 2, along with a comparison to the predictions for the AF-SHE. We find excellent agreement, with a spin angle of $44^\circ \pm 5^\circ$ from the out-of-plane direction, close to the optimum angle of 45° for generating maximum out-of-plane antidamping torque.

This result moves forward the field of antiferromagnetic spintronics by demonstrating a new mechanism by which a collinear antiferromagnet can generate a spin current. Our paper also pioneers a new experimental approach for this field by demonstrating that it is possible to measure all components of the resulting spin currents quantitatively.

Future Plans

One of the open questions concerning spin currents generated by antiferromagnets is that theory predicts cancellations between the contributions from different antiferromagnetic domains within the samples. The measured spin currents are much weaker than predicted for single-domain samples, as expected from these predictions. As one next step for our research on antiferromagnets, we are seeking to control the distribution of antiferromagnetic domains, to see if this provides a way to substantially enhance the spin torques that are generated, and in particular whether it can enhance the out-of-plane antidamping spin torque. We are applying large spin currents to the antiferromagnets while heating and then cooling the samples to try to orient their domains, and measuring if this changes the spin currents produced by the antiferromagnets. We are also extending our research to antiferromagnets in addition to RuO₂, guided by the predictions of the Tsymbal group in selecting promising candidate materials.

In addition, we are continuing research on other low-symmetry materials for generating spin currents and out-of-plane antidamping torques, including both materials with low structural symmetries and magnetic moments. The current status of quantitative measurements of out-of-plane antidamping torques is summarized in Table 1. So far the spin Hall conductivities per unit electric field ($\xi_{DL,E}^Z$) of both the collinear (RuO₂) and non-collinear (Mn₃GaN) antiferromagnets are similar to the best results from low-crystal-symmetry materials, even without any control over the antiferromagnetic domains. To be of interest for applications, ratio of the out-of-plane-oriented spin current density to the applied charge current density, $\theta_{SH}^Z = (2e/\hbar)J_s^z/J_e$, must be at least about 0.03-0.05, and the out-of-plane-oriented spin must not be too weak relative to the conventional in-plane spin, $\theta_{SH}^z/\theta_{SH} > 0.16$. The values found for the existing materials need to be improved by about a factor of 2 or three to achieve this goal.

	$\xi_{DL,E}^Z (\Omega m)^{-1}$	θ_{SH}^Z	$\rho (\mu\Omega\text{-cm})$	$\theta_{SH}^z/\theta_{SH} > 0.16?$
Low crystal symmetry				
WTe ₂	3.6×10^3	0.014	380	yes
MoTe ₂	1.4×10^3	0.008	550	yes
(114)MnPd ₃	14×10^3	0.008	60	no
Antiferromagnets				
RuO ₂	6×10^3	0.008	140	yes
Mn ₃ GaN	8.6×10^3	0.019	220	yes

Table 1. Comparison of the out-of-plane antidamping torque efficiency per unit electric field ($\xi_{DL,E}^Z$) and the corresponding spin Hall ratios (θ_{SH}^Z) for materials in which these quantities have been measured.

References

1. J. Železný, Y. Zhang, C. Felser, and B. Yan, “Spin-Polarized Current in Noncollinear Antiferromagnets,” *Phys. Rev. Lett.* **119**, 187204 (2017).
2. Y. Zhang, Y. Sun, H. Yang, J. Železný, S. P. P. Parkin, C. Felser, and B. Yan, Strong anisotropic anomalous Hall effect and spin Hall effect in the chiral antiferromagnetic compounds Mn_3X ($X = Sn, Ga, Ir, Rh, \text{ and } Pt$),” *Phys. Rev. B* **95**, 075128 (2017).
3. Y. Zhang, J. Železný, Y. Sun, J. van den Brink, and B. Yan, “Spin Hall effect emerging from a noncollinear magnetic lattice without spin–orbit coupling,” *New J. Phys.* **20**, 073028 (2018).
4. M. Kimata, H. Chen, K. Kondou, S. Sugimoto, P. K. Muduli, M. Ikhlas, Y. Omori, T. Tomita, A. H. MacDonald, S. Nakatsuji, and Y. Otani, “Magnetic and magnetic inverse spin Hall effects in a non-collinear antiferromagnet,” *Nature* **565**, 627 (2019).
5. J. Holanda H. Saglam, V. Karakas, Z. Zang, Y. Li, R. Divan, Y. Liu, O. Ozatay, V. Novosad, J. E. Pearson, and A. Hoffmann, “Magnetic Damping Modulation in $IrMn_3/Ni_{80}Fe_{20}$ via the Magnetic Spin Hall Effect,” *Phys. Rev. Lett.* **124**, 087204 (2020).
6. T. Nan, C. X. Quintela, J. Irwin, G. Gurung, D. F. Shao, J. Gibbons, N. Campbell, K. Song, S. Y. Choi, L. Guo, R. D. Johnson, P. Manuel, R. V. Chopdekar, I. Hallsteinsen, T. Tybell, P. J. Ryan, J. W. Kim, Y. S. Choi, P. G. Radaelli, D. C. Ralph, E. Y. Tsymbal, M. S. Rzchowski, and C. B. Eom, “Controlling spin current polarization through non-collinear antiferromagnetism,” *Nat. Commun.* **11**, 4671 (2020).
7. A. Bose, N. J. Schreiber, R. Jain, D.-F. Shao, H. P. Nair, J. Sun, X. S. Zhang, D. A. Muller, E. Y. Tsymbal, D. G. Schlom, and D. C. Ralph, “Tilted spin current generated by the collinear antiferromagnet RuO_2 ,” in review at *Nature Electronics*. (arXiv:2108.09150)

Publications resulting from work supported by the DOE grant over the previous two years

1. Gregory M. Stiehl, Ruofan Li, Vishakha Gupta, Ismail El Baggari, Shengwei Jiang, Hongchao Xie, Lena F. Kourkoutis, Kin Fai Mak, Jie Shan, Robert A. Buhrman, and Daniel C. Ralph, “Layer-dependent spin-orbit torques generated by the centrosymmetric transition metal dichalcogenide β -MoTe₂,” *Phys. Rev. B* **100**, 184402 (2019).
2. A. Bose, J. N. Nelson, X. S. Zhang, P. Jadaun, R. Jain, D. G. Schlom, D. C. Ralph, D. A. Muller, K. M. Shen, and R. A. Buhrman, “Effects of Anisotropic Strain on Spin–Orbit Torque Produced by the Dirac Nodal Line Semimetal IrO₂,” *ACS Applied Materials & Interfaces* **12**, 55411 (2020).
3. Ismail El Baggari, Nikhil Sivadas, Gregory M. Stiehl, Jacob Waelder, Daniel C. Ralph, Craig J. Fennie, and Lena F. Kourkoutis, “Direct Visualization of Trimerized States in 1T'-TaTe₂,” *Phys. Rev. Lett.* **125**, 165302 (2020).
4. Vishakha Gupta, Thow Min Cham, Gregory M. Stiehl, Arnab Bose, Joseph A. Mittelstaedt, Kaifei Kang, Shengwei Jiang, Kin Fai Mak, Jie Shan, Robert A. Buhrman, and Daniel C. Ralph, “Manipulation of the van der Waals Magnet Cr₂Ge₂Te₆ by Spin-Orbit Torques,” *Nano Lett.* **20**, 7482–7488 (2020).
5. Xiaoxi Huang, Shehrin Sayed, Joseph Mittelstaedt, Sandhya Susarla, Saba Karimeddiny, Lucas Caretta, Hongrui Zhang, Vladimir A. Stoica, Tanay Gosavi, Farzad Mahfouzi, Qilong Sun, Peter Ercius, Nicholas Kioussis, Sayeef Salahuddin, Daniel C. Ralph, and Ramamoorthy Ramesh, “Novel Spin–Orbit Torque Generation at Room Temperature in an All-Oxide Epitaxial La_{0.7}Sr_{0.3}MnO₃/SrIrO₃ System,” *Adv. Mater.* **33**, 2008269 (2021).
6. S. Karimeddiny and D. C. Ralph, “Resolving Discrepancies in Spin-Torque Ferromagnetic Resonance Measurements: Lineshape vs. Linewidth Analyses,” *Phys Rev. Appl.* **15**, 064017 (2021).
7. Thow Min Cham, Saba Karimeddiny, Vishakha Gupta, Joseph A. Mittelstaedt, and Daniel C. Ralph, “Separation of Artifacts from Spin-Torque Ferromagnetic Resonance Measurements of Spin-Orbit Torque for the Low-Symmetry van der Waals Semi-Metal ZrTe₃,” in review at *Adv. Quantum Technol.*
8. Arnab Bose, Nathaniel J. Schreiber, Rakshit Jain, Ding-Fu Shao, Hari P. Nair, Jiaxin Sun, Xiyue S. Zhang, David A. Muller, Evgeny Y. Tsymbal, Darrell G. Schlom, and Daniel C. Ralph, “Tilted spin current generated by the collinear antiferromagnet RuO₂,” in review at *Nature Electronics*. (arXiv:2108.09150)

Quantum Fluctuations in Narrow Band Systems

Filip Ronning, Eric Bauer, Michihiro Hirata, Roman Movshovich, Priscila Rosa, and Sean Thomas (Los Alamos National Lab)

Program Scope

Coherence and topologically protected modes in quantum matter arise from highly entangled spin, charge, lattice, and orbital degrees of freedom. Narrow band systems, whose renormalized electronic bandwidth is comparable to other relevant energy scales in the material, inherently have stronger interactions and a proliferation of quantum fluctuations. $5f$ -materials possess strong Coulomb repulsion, large spin-orbit coupling, and multiple competing energy scales, which generate coherent narrow bands and topologically non-trivial states of matter. This complexity provides a rich environment for discovering new states of matter, as well as providing representatives that will enable the understanding of quantum matter that also arises in materials more generally. We will address how quantum fluctuations renormalize excitations in topologically trivial and non-trivial matter and will develop conceptual frameworks for understanding and controlling the consequences of quantum fluctuations in classes of electronically correlated systems. In addition, strongly spin-orbit coupled superconductors can be phase sensitive, possess novel excitations, and be highly tunable. Through our subtask we also explore the applicability of strongly spin-orbit coupled superconductors for future quantum information devices.

Recent Progress

Quantum fluctuations in $5f$ electron systems often generate a so-called “dual nature” of simultaneous itinerant and localized electronic behavior. Through non-resonant inelastic X-ray scattering measurements, together with Andrea Severing, we provide evidence for a unified picture of atomic-like $5f^2$ quasi-doublet states and itinerant $5f^3$ states that control the physical properties of tetragonal UM_2Si_2 ($M = Pd, Ni, Ru, Fe$) ranging from antiferromagnetic, hidden order, to Pauli paramagnetism ground states [1]. Similar duality phenomena is found in $4f$ based materials, where magnetism and renormalized bands coexist. A major unsolved issue in condensed matter physics is to understand how such renormalizations occur when including materials specific details. A first step we have taken in that direction is to determine the magnetic exchange interactions starting from first-principles and spectroscopic inputs to a material’s low energy Hamiltonian. Using inelastic neutron scattering we have validated the magnetic exchange interaction derived from first principles in

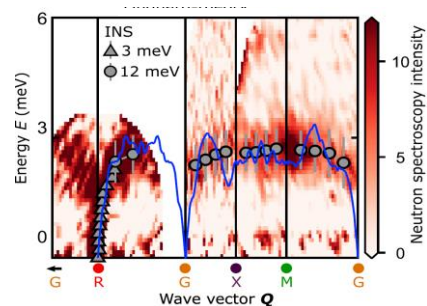


Fig. 1: Spin waves of $CeIn_3$ measured by neutron scattering. Blue line is the theoretical spin wave prediction, which combines a long range RKKY interaction giving steep spin-waves and a short range super-exchange responsible for the ordering at (π, π, π) .

CeIn₃ [2]. This advance enables minimal Kondo lattice models with material specific details to be explored theoretically for the first time. The larger energy in mixed valent materials, such as YbAl₃, has enabled us to also explore the momentum dependence of the renormalization as narrow bands form. Interestingly, our recent neutron scattering measurements with Andy Christianson has found a coupling between an optical phonon of the Al atoms, and the flat bands formed by the Yb electrons. This suggests a novel dynamic $4f/3p$ hybridization enhanced by the beating mode of the light Al atoms [3]. Whether this is unique to YbAl₃ or a more general phenomena needs to be determined. As the quantum fluctuations grow stronger we know that instabilities to other states of matter arise. Our previous work in CeAuSb₂ found the coupling between lattice and f -electrons led to an electronic nematic state coupled with the magnetic order. Our recent subsequent investigations have found that as a multi- \mathbf{Q} state is formed with an applied magnetic field, the f -electron wave function becomes increasingly localized [4]. This work emphasizes the mutual interplay between electron localization and magnetic order.

Magnetic order is also known to generate a Berry curvature, which can cause sizeable effects in transverse response functions. We expect such topological Berry curvature contributions to be

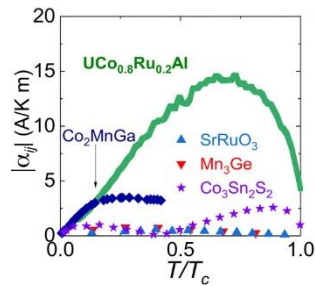


Fig. 2: Anomalous Peltier coefficient versus temperature for various magnetic materials.

maximized in $5f$ electron systems due to the combined large spin-orbit coupling and narrow band widths. With this motivation we explored the ferromagnetic system U(Co,Ru)Al, and indeed, we discovered the largest anomalous Peltier coefficient to date [5]. Through the Mott relation (which connects the Peltier coefficient to the derivative of the Hall conductivity), we expected to further enhance the signals we observed. Instead, by hole doping the system we found a violation of the Mott relation. A possible explanation for this is a non-rigid shift of the Weyl nodes with chemical substitution. Future spectroscopic probes will be required to verify this explanation.

Band inversion yields Berry curvature in metals and topological phases in insulators, but to maximally extract the physics from such materials high purity single crystals are required. We have recently focused on synthesizing clean narrow gap insulators whose resistivity increases many orders of magnitude upon decreasing temperature. These high purity crystals have enabled us to explore the formation of magnetic polarons and colossal negative magnetoresistance in Eu₅In₂Sb₆ and Eu₉InSb₁₁ [6]. We have also found vacancy ordering in the square As net compound R₃Cd₂As₆ ($R = \text{La, Ce}$) [7]. Pnictide square nets are prone to distortions, and indeed, a low temperature structural distortion leads to a net 13 order of magnitude increase in resistance, while DFT calculations incorrectly predict the material to be a metal – a signature that strong correlations are at play. Finally, together with our international collaborations, we have investigated the phase stability of the topological Kondo insulator SmB₆ and its surface state and found that defects can generate metallic islands in the bulk [8].

High purity samples are also key for investigating and exploiting unconventional superconductors. The long mean free path in CeCoIn₅ has enabled us to observe quantum

oscillations in the superconducting state via rotating thermal conductivity measurements. The phase of the oscillations change when entering the regime where magnetism and SC coexist reflecting the change of Fermi surface topology [9]. With such results in mind, together with Bill Halperin, we have zone refined single crystals of the spin-triplet superconductor UCoGe for upcoming studies [10]. Careful investigations into the sample dependence of UTe₂ have also enabled us to identify phase separation as responsible for multiple thermodynamic transitions visible in some samples, while pressure measurements have revealed the unexpected importance of antiferromagnetic fluctuations in this candidate topological superconductor [11].

Future Plans

Understanding how quantum fluctuations give rise to novel correlated electron states of matter is central to our objectives. Hence, we will extend our work on CeIn₃ to include the interactions with excited crystal field states, which become relevant in high magnetic fields and promote changes in the electronic structure. We will perform additional magnetization and neutron scattering measurements to test further theoretical predictions of the exchange interactions based on our microscopic materials Hamiltonians. We will also extend the study on CeIn₃ to include the more complex case of CeRhIn₅. Additionally, we will continue to explore how the enhanced quantum fluctuations in reduced dimensional systems modifies the evolution of narrow band systems. In particular we will examine the quantum criticality using transport, thermodynamic, and strain measurements of quasi 1D systems such as YbFe₅P₃.

Strain can be a powerful tuning parameter in anisotropic systems with small energy scales. We will thus explore the colossal negative magnetoresistance we observed in Eu₅In₂Sb₆ with strain and pressure, and aim to drive the system through a topological phase transition. Similarly, our thermal expansion measurements on UTe₂ and UCoGe suggest that uniaxial strain will significantly tune the ground state of these systems. In our quantum information science subtask we will explore the effects of uniaxial strain both with piezoelectric strain devices as well as FIB microstructured devices. With the latter we will tune the superconducting T_c of a cantilever device in-situ. We will also explore how non-uniform strains can lead to inhomogeneous superconductivity. Thermal transport measurements to mK temperatures will be used to add constraints on the properties of the superconducting order parameter.

References

- [1] “From antiferromagnetic and hidden order to Pauli paramagnetism in UM₂Si₂ compounds with 5f electron duality,” A. Amorese, M. Sundermann, B. Leedahl, A. Marino, D. Takegami, H. Gretarsson, A. Gloskovskii, C. Schlueter, M.W. Haverkort, Y. Huang, M. Szlawska, D. Kaczorowski, S. Ran, M.B. Maple, E.D. Bauer, A. Leithe-Jasper, P. Hansmann, P. Thalmeier, L.H. Tjeng, A. Severing, *Proc. Nat. Acad. Sci.* **117**, 30220 (2020).
- [2] “A microscopic model for correlated electron magnetism,” W. Simeth, Z. Wang, Y. Nomura, A. Podlesnyak, E.D. Bauer, R. Arita, C.D. Batista, F. Ronning, M. Janoschek, *Unpublished*

- [3] “Phonons, Q-dependent Kondo spin fluctuations, and 4f phonon resonance in YbAl₃,” A.D. Christianson, V.R. Fanelli, L. Lindsay, S. Mu, M.C. Rahn, D.G. Mazzone, A.H. Said, F. Ronning, E.D. Bauer, J.M. Lawrence, *Phys. Rev. B*, **102**, 205135 (2020).
- [4] “Spin-texture-driven electrical transport in multi-Q antiferromagnets,” S. Seo, S. Hayami, Y. Su, S.M. Thomas, F. Ronning, E.D. Bauer, J.D. Thompson, S.-Z. Lin, and P.F.S. Rosa, *Commun. Phys.* **4**, 58 (2021)
- [5] “Colossal anomalous Nernst effect in a correlated noncentrosymmetric kagome ferromagnet,” T. Asaba, V. Ivanov, S. M. Thomas, S.Y. Savrasov, J. D. Thompson, E. D. Bauer, F. Ronning, *Science Advances*, **7**, eabf1467 (2021).
- [6] “Narrow-gap semiconducting behavior in antiferromagnetic Eu₁₁InSb₉,” S. S. Fender, S. M. Thomas, F. Ronning, E. D. Bauer, J. D. Thompson, and P. F. S. Rosa, *Phys. Rev. Materials*, **5**, 074603 (2021).
- [7] “Robust narrow-gap semiconducting behavior in square-net material La₃Cd₂As₆,” M. M. Piva, M. C. Rahn, S. M. Thomas, B. L. Scott, P. G. Pagliuso, J. D. Thompson, L. M. Schoop, F. Ronning, and P. F. S. Rosa, *Chemistry of Materials*, **33**, 4122 (2021).
- [8] “Metallic islands in the Kondo insulator SmB₆.” J.C. Souza, P.F.S. Rosa, J. Sichelschmidt, M. Carlone, P.A. Venegas, M.O. Malcolms, P.M. Menegasso, R.R. Urbano, Z. Fisk, and P.G. Pagliuso. *Phys. Rev. Research* **2**, 043181 (2020); “Phase stability in SmB₆,” M.V.A. Crivillero, S. Rossler, H. Borrmann, H. Dawczak-Debicki, P.F.S. Rosa, Z. Fisk, S. Wirth, *Phys. Rev. Materials* **5**, 044204 (2021); “Systematic manipulation of the surface conductivity of SmB₆,” M.V.A. Crivillero, M. Konig, J.C. Souza, P.G. Pagliuso, J. Sichelschmidt, P.F.S. Rosa, Z. Fisk, and S. Wirth, *Phys. Rev. Research* **3**, 023162 (2021).
- [9] “Topology change of the Landau Fermi surface in CeCoIn₅,” S. Lee, D.Y. Kim, E.D. Bauer, S.-Z. Lin, R. Movshovich, *Unpublished*.
- [10] “Electron-beam floating-zone refined UCoGe,” K.E. Avers, M.D. Nguyen, J.W. Scott, A.M. Zimmerman, S.M. Thomas, P.F.S. Rosa, E.D. Bauer, J.D. Thompson, W.P. Halperin, *Phys. Rev. Materials* **5**, 054803 (2021).
- [11] “Evidence for a pressure-induced antiferromagnetic quantum critical point in mixed valence UTe₂,” S.M. Thomas, F.B. Santos, M.H. Christensen, T. Asaba, F. Ronning, J.D. Thompson, E.D. Bauer, R.M. Fernandes, G. Fabbris, P.F.S. Rosa, *Sci. Advances*, **6**, eabc8709 (2020); “Spatially inhomogeneous superconductivity in UTe₂,” S.M. Thomas, C. Stevens, F.B. Santos, S.S. Fender, E.D. Bauer, F. Ronning, J.D. Thompson, A. Huxley, P.F.S. Rosa, *ArXiv:2103.09194*.

Publications (20 out of 51 total publications)

“Spatial control of heavy-fermion superconductivity in CeIrIn₅,” M. D. Bachmann, G. M. Ferguson, F. Theuss, T. Meng, C. Putzke, T. Helm, K. R. Shirer, Y.-S. Li, K. A. Modic, M. Nicklas, M. Koenig, D. Low, S. Ghosh, A.P. Mackenzie, F. Arnold, E. Hassinger, R.D. McDonald, L.E. Winter, E.D. Bauer, F. Ronning, B. J. Ramshaw, K. C. Nowack, P. J. W. Moll, *Science*, **366**, 221 (2019).

“Colossal anomalous Nernst effect in a correlated noncentrosymmetric kagome ferromagnet,” T. Asaba, V. Ivanov, S. M. Thomas, S.Y. Savrasov, J. D. Thompson, E. D. Bauer, F. Ronning, *Science Advances*, **7**, eabf1467 (2021).

“Evidence for a pressure-induced antiferromagnetic quantum critical point in mixed valence UTe₂,” S. M. Thomas, F. B. Santos, M. H. Christensen, T. Asaba, F. Ronning, J. D. Thompson, E. D. Bauer, R. M. Fernandes, G. Fabbris, P. F. S. Rosa, *Science Advances*, **6**, eabc8709 (2020).

“One-component order parameter in URu₂Si₂ uncovered by resonant ultrasound spectroscopy and machine learning,” S. Ghosh, M. Matty, R. Baumbach, E. D. Bauer, K. A. Modic, A. Shekhter, J. A. Mydosh, E. A. Kim, B. J. Ramshaw, *Science Advances* **6**, eaaz4074 (2020).

“Imaging emergent heavy Dirac fermions of a topological Kondo insulator,” H. Pirie, Y. Liu, A. Soumyanarayanan, P. Chen, Y. He, M. M. Yee, P. F. S. Rosa, J. D. Thompson, D.-J. Kim, Z. Fisk, X. Wang, J. Paglione, D. K. Morr, M. H. Hamidian, and J. E. Hoffman, *Nature Physics* **16**, 52-56 (2020).

“From antiferromagnetic and hidden order to Pauli paramagnetism in UM₂Si₂ compounds with 5f electron duality,” A. Amorese, M. Sundermann, B. Leedahl, A. Marino, D. Takegami, H. Gretarsson, A. Gloskovskii, C. Schlueter, M.W. Haverkort, Y. Huang, M. Szlawska, D. Kaczorowski, S. Ran, M.B. Maple, E.D. Bauer, A. Leithe-Jasper, P. Hansmann, P. Thalmeier, L.H. Tjeng, A. Severing, *Proc. Nat. Acad. Sci.* **117**, 30220 (2020).

“Interplay of the spin density wave and a possible Fulde-Ferrell-Larkin-Ovchinnikov state in CeCoIn₅ in rotating magnetic field,” S.-Z. Lin, D.Y. Kim, E.D. Bauer, F. Ronning, J.D. Thompson, R. Movshovich, *Phys. Rev. Letters*, **124**, 217001 (2020).

“Nematic state in CeAuSb₂,” S. Seo, X. Wang, S.M. Thomas, M.C. Rahn, D. Carmo, F. Ronning, E.D. Bauer, R.D. dos Reis, M. Janoschek, J.D. Thompson, R.M. Fernandes and P.F.S. Rosa, *Phys. Rev. X*, **10**, 011035 (2020).

“Non-monotonic pressure dependence of high-field nematicity and magnetism in CeRhIn₅,” T. Helm, A. Grockowiak, F.F. Balakirev, J. Singleton, J.B. Betts, K.R. Shirer, M. König, T. Förster, E.D. Bauer, F. Ronning, S.W. Tozer, P.J.W. Moll, *Nat. Comm.* **11**, 3482 (2020).

“Colossal magnetoresistance in a nonsymmorphic antiferromagnetic insulator,” P. F. S. Rosa, Y. Xu, M.C. Rahn, J. C. Souza, S. K. Kushwaha, L. S. I. Veiga, A. Bombardi, S. M. Thomas, M. Janoschek, E. D. Bauer, M. K. Chan, Z. Wang, J. D. Thompson, P. G. Pagliuso, N. Harrison, B.A. Bernevig, F. Ronning, *npj Quantum Materials*, **5**, 52 (2020).

“Phonons, Q-dependent Kondo spin fluctuations, and 4f phonon resonance in YbAl₃,” A.D. Christianson, V.R. Fanelli, L. Lindsay, S. Mu, M.C. Rahn, D.G. Mazzone, A.H. Said, F. Ronning, E.D. Bauer, J.M. Lawrence, *Phys. Rev. B*, **102**, 205135 (2020).

“Large tunable anomalous Hall effect in kagome antiferromagnet U₃Ru₄Al₁₂,” T. Asaba, Y. Su, M. Janoschek, J. D. Thompson, S. M. Thomas, E. D. Bauer, S.-Z. Lin, F. Ronning, *Phys. Rev. B*, **102**, 035127 (2020).

“Pressure dependence of antiferromagnetic and superconducting phases in U₂Rh_{1-x}Pt_xC₂,” S. Lee, Y. Luo, F. Ronning, N. Wakeham, E.D. Bauer, D.Y. Kim, J.D. Thompson, and T. Park, *Phys. Rev. B*, **102**, 035124 (2020).

“Anomalous Hall effect in the kagome ferrimagnet GdMn₆Sn₆,” T. Asaba, S. M. Thomas, M. Curtis, J. D. Thompson, E. D. Bauer, and F. Ronning, *Phys. Rev. B*, **101**, 174415 (2020).

“Narrow-gap semiconducting behavior in antiferromagnetic Eu₁₁InSb₉,” S. S. Fender, S. M. Thomas, F. Ronning, E. D. Bauer, J. D. Thompson, and P. F. S. Rosa, *Phys. Rev. Materials*, **5**, 074603 (2021).

“Electron-beam floating-zone refined UCoGe,” K.E. Avers, M.D. Nguyen, J.W. Scott, A.M. Zimmerman, S.M. Thomas, P.F.S. Rosa, E.D. Bauer, J.D. Thompson, W.P. Halperin, *Phys. Rev. Materials* **5**, 054803 (2021).

“Machine learning study of magnetism in uranium-based compounds,” A. Ghosh, F. Ronning, S.M. Nakhmanson, J.-X. Zhu, *Phys. Rev. Materials*, **4**, 064414 (2020).

“Robust narrow-gap semiconducting behavior in square-net material La₃Cd₂As₆,” M. M. Piva, M. C. Rahn, S. M. Thomas, B. L. Scott, P. G. Pagliuso, J. D. Thompson, L. M. Schoop, F. Ronning, and P. F. S. Rosa, *Chemistry of Materials*, **33**, 4122 (2021).

“Spin-texture-driven electrical transport in multi-Q antiferromagnets,” S. Seo, S. Hayami, Y. Su, S.M. Thomas, F. Ronning, E.D. Bauer, J.D. Thompson, S.-Z. Lin, and P.F.S. Rosa, *Comm. Phys.* **4**, 58 (2021).

“³³S nuclear magnetic resonance spectra of uranium disulfide β-US₂,” H. Sakai, Y. Tokunaga, Y. Haga, S. Kambe, S. K. Ramakrishna, A. P. Reyes, P. F. S. Rosa, F. Ronning, J. D. Thompson, Z. Fisk, and E. D. Bauer, *JPS Conf. Proc.* **30**, 011169 (2020).

Novel Topological Josephson Junctions Architectures for Fault-Tolerant Qubits and Advanced Sensing

Enrico Rossi, Department of Physics, William & Mary

Javad Shabani, Department of Physics, New York University

Wei Pan, Sandia National Laboratories, Livermore, CA

Program Scope

The overall goal of this, just started, experiment-theory project is to develop two semiconductor-based architectures to realize high quality Josephson junctions (JJs) to be used to: (1) create robust Majorana states; (2) new advanced, high sensitivity, quantum sensors. The motivation for this work is twofold: create devices that can be used to realize topologically protected, and therefore fault tolerant qubits; take advantage of the fact that such devices can be tuned across a topological phase transitions via external electromagnetic fields to create high sensitivity sensors, photo detectors, and bolometers. One architecture comprises planar, 2D, JJs, based on high quality InAs quantum wells proximitized by superconducting Al. The other architecture comprises 1D JJs based on InAs/GaSb double quantum wells. By varying the relative thickness of the InAs and GaSb layer in the semiconductor stack it is possible to vary the gap for the bands of the 2D electron gas. When the thickness of the InAs is larger than a critical value (keeping GaSb's thickness fixed) InAs's electron-like states hybridize with GaSb's hole-like states and a hybridization gap opens. In this situation the conduction and valence bands are inverted. In the "inverted-bands" regime the 2D electron gas (2DEG) is in a quantum spin Hall insulator (QSHI) state characterized by topologically protected helical edges modes. In the presence of superconducting pairing these edge modes form a 1D topological superconducting state that can support Majoranas without the need of an external magnetic field. The ability to realize Majoranas without external magnetic fields would allow a much greater freedom in the layout of networks of topologically protected qubits.

Recent Progress

Josephson Junctions Based on InAs

High quality Al/InAs super-semi heterostructures have been grown via molecular beam epitaxy (Fig. 1). Using these structures JJs with very high transparency have been fabricated [1]. Such junctions are 100 nm long and have a width of 4 μm (Fig. 1). In the presence of an in-plane transverse field (B_y) the JJs are expected to enter a topological phase transition supporting Majoranas. The transition into the topological phase is characterized by the closing and reopening of the superconducting gap and a rapid change of the phase difference between the

superconducting leads [2]. We have recently observed these signatures in some of our devices (Fig.1) [3]. It had been predicted that JJs in the topological phase should exhibit missing odd-Shapiro steps in their voltage-current characteristic when driven by an a.c. current. To test this prediction, in a recent experiment we studied the voltage-current response of Al/InAs JJs when subject to microwave radiation. We found that even when no external magnetic field was present so that the JJs were unquestionably in the topologically trivial regime, the voltage-current characteristic exhibited missing Shapiro steps (Fig.2). We attributed this behavior to the presence of Andreev bound states well separated from the continuum and with a high probability to undergo a Landau-Zener transition when the phase difference between the two superconducting leads is equal to π . Very recently we have started to systematically take measurements of a.c. driven JJs in the presence of an external magnetic field. We find that the frequency of the microwave radiation for which the odd Shapiro steps are missing depends on the strength and direction of the field.

Josephson Junctions Based on InAs/GaSb

InAs/GaSb double quantum wells exhibiting signatures consistent with the presence of inverted-bands have been realized [5]. The structures have a front gate that allows control of the charge density of the 2DEG. By tuning the voltage V_g of such gate, the devices can be tuned into an electron, charge-neutrality, or hole regime (Fig. 3). Recently we have used these structure to realize JJ by depositing superconducting tantalum. We

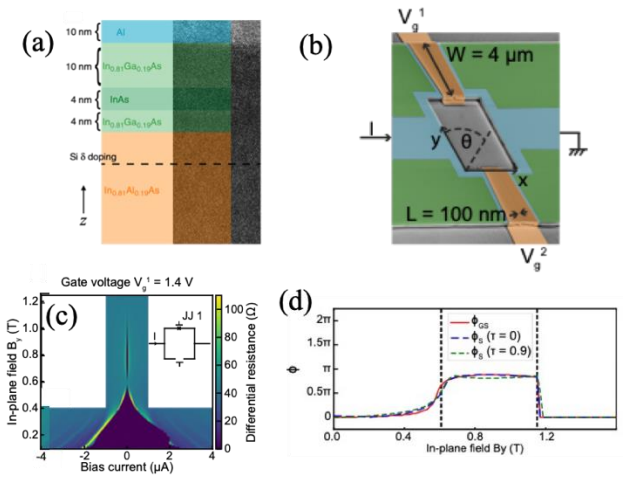


Fig. 1. **Al/InAs Josephson junctions.** (a) Sample stack description superimposed on TEM image. (b) SEM image of a SQUID device formed by two Al/InAs JJs. (c) Closing and re-opening of the superconducting gap as a function of an in-plane field for a Al/InAs JJ. (d) Evolution of the phase across the junction as a function of the in-plane magnetic field.

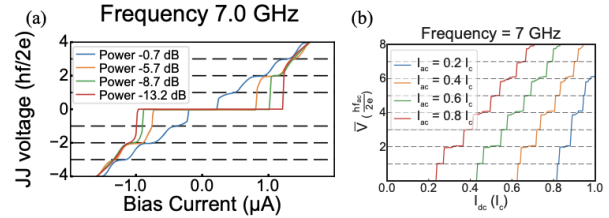


Fig. 2. **Missing Shapiro steps.** (a) Missing odd Shapiro steps in experimentally measured V-I curves for a Al/InAs JJ. (b) Theoretical results for a high transparency JJ with Andreev bound states separated from continuum and large Landau-Zener probability for $\phi=\pi$.

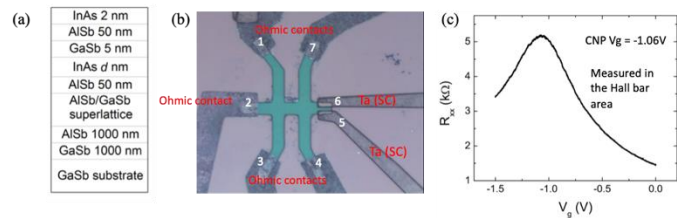


Fig. 3. **InAs/GaSb-based Josephson junctions.** (a) Schematic of the sample stack. (b) Image of a JJ based on InAs/GaSb double quantum well in the inverted-bands regime and superconducting Ta. (c) Longitudinal resistance R_{xx} of the device shown in (b) as a function of the voltage V_g of the front-gate. R_{xx} is maximum at the charge neutrality point (CNP) obtained for $V_g=-1.06$ V.

then measured the dI/dV as a function of V_g and found that it has a dip, with coherence peaks on the side, when the device is tuned at the charge neutrality point (Fig. 4). This is consistent with the expectation that at the charge neutrality point only edge states are present and that superconducting correlations between the edge modes are induced via the proximity effect. By measuring the dI/dV at the charge neutrality point for different values of the temperature we estimate the strength of the induced superconducting gap for the edge modes to be approximately 295 mK (Fig. 4). By following the evolution with temperature of the low energy coherence peaks we also extract the temperature dependence of the induced gap and find it to follow the BCS scaling.

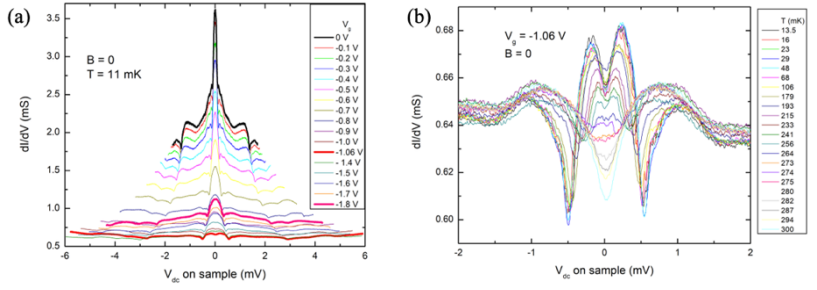


Fig. 4. **InA/GaSb-based Josephson junctions.** (a) dI/dV for the junction shown in Fig. 3 (b), for different values of V_g . (b) dI/dV at different temperatures for $V_g = -1.06$ V when the 2DEG is at the charge neutrality point. We can observe that the two coherence peak closest to $V_{dc}=0$ disappear for $T \sim 295$ mK.

Shapiro Steps in SQUIDs with topological Josephson Junctions

As discussed above, we have shown that missing Shapiro steps in a.c. driven JJs is not a robust signature of the topological character of a JJ. This motivated us to investigate the current-voltage characteristic of SQUIDs formed by one junction robustly in the topologically trivial regime and the junction whose topological phase we want to identify. Compared to a single JJ, a SQUID has several more experimental parameters that can be tuned to affect the V-I characteristic, and therefore a much larger phase-space in which to look for robust signatures associated with the topological phase of the JJ under study. Recently we have performed a systematic theoretical analysis of asymmetric SQUIDs. In particular we have considered SQUIDs in which one JJ is trivial, with low transparency, and the other is topological, and SQUIDs in which both JJs are trivial, but one has a very large transparency, and

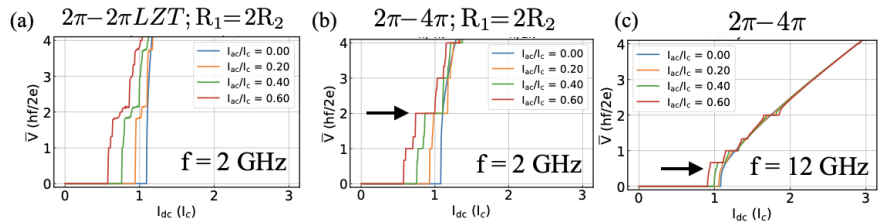


Fig. 5. **Shapiro steps in asymmetric SQUIDs.** (a) V-I characteristic for a SQUID formed by a trivial JJ with low transparency and a JJ with high transparency and a large probability to undergo Landau-Zener transitions for $\phi = \pi$. By tuning the normal resistance of the two junctions to be different the second well defined step “breaks-up” revealing the Landau-Zener origin of the V-I features seemingly due to one of the junctions being in the topological phase. For the case when the junction with high transparency is replaced by a true topological junction (a 4π junction) the second Shapiro step remains well defined even when the normal resistance of the two junctions is set to different values (b). In addition, at high frequencies, fractional $2/3$ and $4/3$ Shapiro steps appear that are not present when both junctions are trivial, (c).

therefore a large probability to undergo Landau-Zener transitions for $\phi=\pi$, transitions that, in the V-I curve of a single junction give rise to behavior that is undistinguishable from the behavior of topological JJ. We find that at low frequencies, when the normal resistance of the two JJs forming the SQUID is the same, the V-I curve of the SQUID with one topological junction is qualitatively the same as the one in which both JJs are trivial. However, when the resistance of the two junctions are different, there are signatures in the V-I curve that allow us to distinguish the two cases (Fig. 5). In addition, we find that at high frequency some of the fractional steps are present only for the case when one of the junctions is topological (Fig. 5).

Future Plans

The unambiguous detection of the topological phase of superconducting devices, and of the zero-energy Majorana modes associated with this phase, has emerged as one of the main challenges toward the realization of topological qubits. Developing theory-experiment protocols to robustly identify the topological phase of Josephson junction, and detect Majoranas, will be one of the focus of our future work. We will therefore continue the work begun to identify reliably the topological phase of JJs based on Al/InAs heterostructures. In parallel, we plan to continue the development and characterization of Josephson junctions based on InAs/GaSb: complete the characterization of Ta/InAs/GaSb junction by studying also the effect of external magnetic fields; develop a comprehensive theoretical description to explain the measurements; fabricate new devices in which Ta is replaced by Al, deposited epitaxially, to further improve the quality of the junctions.

References

- [1] W. Mayer, M. C. Dartiailh, J. Yuan, K. S. Wickramasinghe, E. Rossi, J. Shabani, *Nature Communications*, **11**, 212 (2020).
- [2] ¹ F. Pientka, A. Keselman, E. Berg, A. Yacoby, A. Stern, and B.I. Halperin, *Phys. Rev. X* **7**, 021032 (2017).
- [3] M.C. Dartiailh, W. Mayer, J. Yuan, K.S. Wickramasinghe, A. Matos-Abiague, I. Žutić, and J. Shabani, *PRL* **126**, 036802 (2021)
- [4] M. C. Dartiailh, J. J. Cuzzo, W. Mayer, J. Yuan, K. S. Wickramasinghe, E. Rossi, J. Shabani, *Nature Communications* **12**, 78 (2021)
- [5] Y. Jiang, S. Thapa, G.D. Sanders, C.J. Stanton, Q. Zhang, J. Kono, W.K. Lou, K. Chang, S.D. Hawkins, J.F. Klem, W. Pan, D. Smirnov, and Z. Jiang, *PRB* **95**, 045116 (2017)

Publications

J.J. Cuzzo, W. Pan, J. Shabani, E. Rossi, “DC and AC Response of Asymmetric SQUIDs with Topologically Nontrivial Junctions”, to be submitted.

Exotic Frustration-Induced Phenomena in Artificial Spin Ice

Principal Investigator: Peter Schiffer, Yale University, New Haven, CT 06520

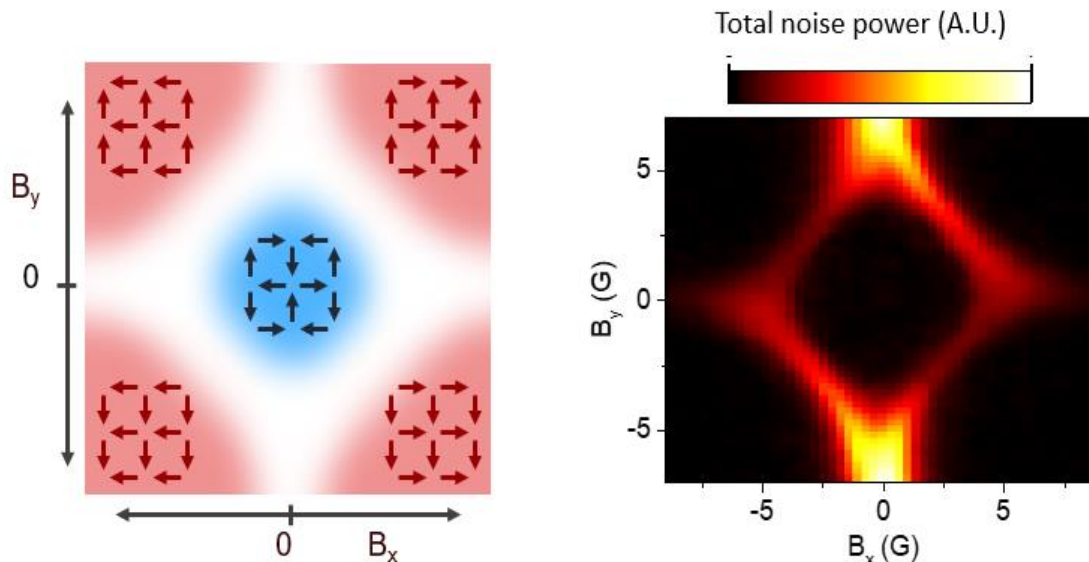
Program Scope

This program encompasses studies of lithographically fabricated “artificial spin ice” arrays of nanometer-scale single-domain ferromagnetic islands in which the array geometry results in frustration of the interactions between the islands. Artificial spin ice offers a wide range of opportunities for studying the mechanism by which nature accommodates frustration. Since the arrays are created lithographically, we can easily vary the array characteristics, including the geometry of the lattice and the level and type of lattice disorder. We can probe the local properties of the arrays by imaging individual moments, and we can also probe thousands of moments simultaneously, allowing us to gain insight into the collective properties of the system and observe novel phenomena that are not accessible in other systems [5].

This research program focuses on the properties of these systems, probing the collective behavior of different geometries, and exploring arrays of more complex nanomagnet shapes.

Recent Progress

The past two years of this program have included several projects within the scope described above. All work has been done in close collaboration with the groups of Chris Leighton at the University of Minnesota and Cristiano Nisoli at Los Alamos National Laboratory, as well as a new collaboration with the group of Scott Crooker at Los Alamos National Laboratory. Much of the work has also involved x-ray magnetic circular dichroism – photoemission electron microscopy (XMCD-PEEM) data-taking at the Advanced Light Source in collaboration with Rajesh Chopdekar. Finally, the work has also included efforts in collaboration with the group of Nitin Samarth at Penn State, who was a co-investigator on previous grants from the Department of Energy. In this abstract, we describe two of the projects, examination of field-induced magnetic monopole plasma regimes in the square ice structure and thermally excited strings in the Santa Fe ice lattice, and we also briefly describe a number of other ongoing studies.

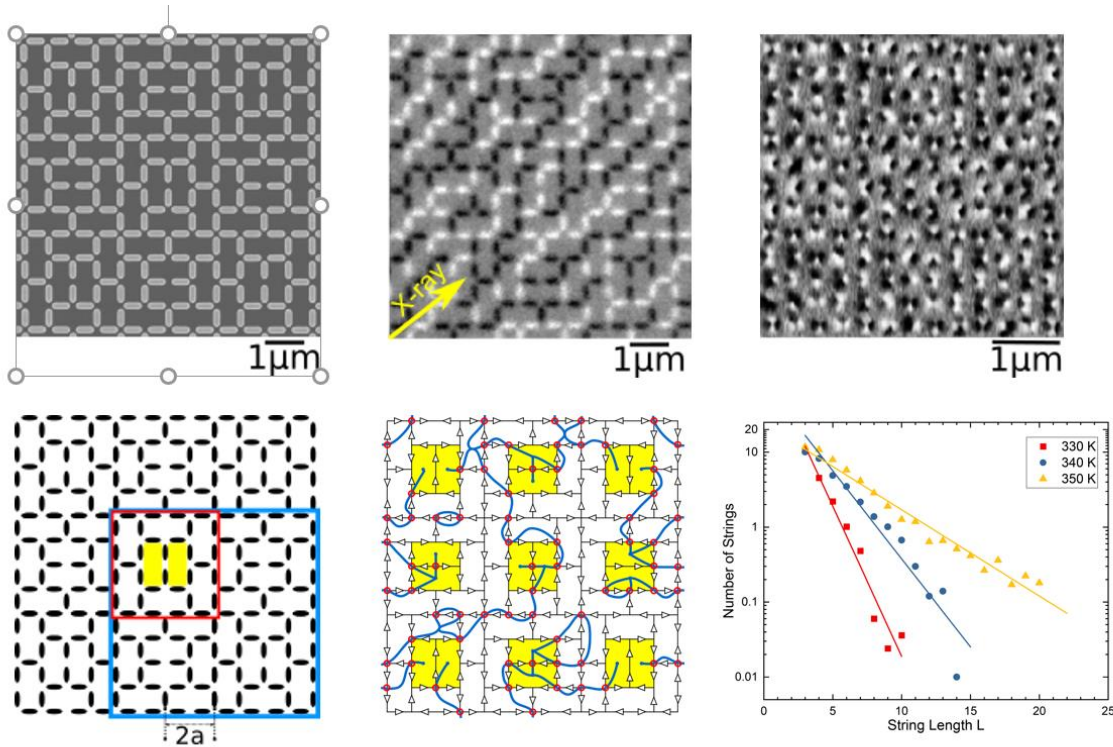


Left: Schematic magnetic field phase diagram for thermally fluctuating square artificial spin ice. The blue central region corresponds to the antiferromagnetic ground state; the corners correspond to the field polarized states; and the white intermediate region is an effective magnetic monopole plasma regime. Right: The measured horizontal magnetic noise power at finite temperature, reflecting the effective magnetic monopole plasma [4].

Magnetic Monopole Plasma in Artificial Square Ice: Much of the physics of artificial spin ice can be understood through the construct of effective magnetic charges at the lattice vertices, i.e., effective magnetic monopoles. We have demonstrated that square artificial spin ice has specific regions of its magnetic phase diagram that correspond to plasma-like regimes containing a high density of mobile monopoles, as shown in the figure above. These regimes result from the magnetic field balancing the local interactions that constrain monopole motion. In collaboration with Scott Crooker at Los Alamos, we probed the spontaneous monopole noise from thermal fluctuations of the moment orientations. This noise, also shown in the figure, reflects the plasma regime in which the monopoles are minimally correlated. These results open the door to more detailed studies of monopole regimes with continuously field-tunable densities, thereby providing a new paradigm for probing the physics of effective magnetic charges in these systems.

String Phase in Santa Fe Artificial Spin Ice: Artificial spin ice arrays can be designed so that the frustration arises from the location of the excitations among the vertices, leading to a range of exotic behavior. We have studied one such vertex-frustrated lattice, dubbed Santa Fe Ice, which is shown in the figure below. We measured both the moment configuration of the nanomagnets, after annealing near the ferromagnetic Curie point and also in a thermally dynamic state. While the Santa Fe Ice lattice structure is complex, our data demonstrate that its disordered magnetic state is naturally described within a framework of emergent strings. We show experimentally that the string length follows a simple Boltzmann distribution with an energy scale that is associated with the system's magnetic interactions and that is consistent with theoretical predictions. The results demonstrate that string descriptions can provide a simplifying description of complex

correlated classical systems with non-trivial frustration, and the findings form the basis for a manuscript currently under review.



Strings in Santa Fe Ice Top (from left to right): Scanning electron microscope image of Santa Fe artificial spin ice made from permalloy islands; XMCD-PEEM image of the moment orientations; and magnetic force microscope image of the moment orientations in a thermally annealed sample. Bottom (from left to right): The lattice structure, showing a unit cell outlined in blue and the different plaquettes of the lattice in red outline and yellow fill; an example of the strings of local excitations, and the distribution of the string lengths at different temperatures from XMCD-PEEM data – the temperature dependence can be directly connected to theoretical expectations [X. Zhang *et al.*, under review].

Other Projects Other projects supported by this program in the past two years include:

1. A completed study of thermalization of permalloy artificial spin ice by high temperature annealing, in which we explored how to optimize annealing and also explored how the thickness of permalloy affects annealing through the Curie temperature [2].
2. Two completed studies of the physics of perpendicular anisotropy artificial spin ice. In these projects, we explored the effects of disorder in the field-induced switching of these moments as well as the impact of a soft magnetic underlayer on moment interactions[3,6].
3. A study of entropy-induced ordering in tetris artificial spin ice, in which we demonstrated a novel form of entropy-induced long range ordering among the moments [Saglam *et al.*, under review].

4. A study of field-induced avalanche statistics in artificial spin ice. We found a close adherence of these avalanches to a one-dimensional random field Ising model, providing a rare and unusually accessible experimental platform for such studies [Bingham *et al.*, under review].

Future Plans

Future plans for this research program include further study of the temperature dependence of the properties of permalloy artificial spin ice, both above and below room temperature, studies of artificial spin ice arrays formed from non-binary moments, and further studies of vertex frustrated lattices in an applied magnetic field.

References and Publications

1. “Field-induced phase coexistence in an artificial spin ice”, Joseph Sklenar, Yuyang Lao, Alan Albrecht, Justin D. Watts, Cristiano Nisoli, Gia-Wei Chern, and Peter Schiffer *Nature Physics* **15**, 191–195 (2019).
2. “Understanding thermal annealing of artificial spin ice”, Xiaoyu Zhang, Yuyang Lao, Joseph Sklenar, Nicholas S. Bingham, Joseph T. Batley, Justin D. Watts, Cristiano Nisoli, Chris Leighton, and Peter Schiffer, *APL Materials* **7**, 111112 – 1 - 5 (2019).
3. “Imaging the stochastic microstructure and dynamic development of correlations in perpendicular artificial spin ice”, Susan Kempinger, Robert D. Fraleigh, Paul E. Lammert, Sheng Zhang, Vincent H. Crespi, Peter Schiffer, and Nitin Samarth, *Physical Review Research* **2**, 012001(R) – 1 - 5 (2020).
4. “Field-Induced Magnetic Monopole Plasma in Artificial Spin Ice”, M. Goryca, X. Zhang, J. Li, A. L. Balk, J. D. Watts, C. Leighton, C. Nisoli, P. Schiffer, and S. A. Crooker, *Physical Review X* **11**, 011042 – 1 - 11 (2021).
5. “Artificial spin ice: Paths forward”, Peter Schiffer and Cristiano Nisoli, *Applied Physics Letters* **118**, 110501 – 1-6 (2021).
6. “Field-tunable interactions and frustration in underlayer-mediated artificial spin ice”, Susan Kempinger, Yu-Sheng Huang, Paul Lammert, Michael Vogel, Axel Hoffmann, Vincent H. Crespi, Peter Schiffer, and Nitin Samarth, *Physical Review Letters* (in press, 2021).

NANOSTRUCTURED MATERIALS: FROM SUPERLATTICES TO QUANTUM DOTS

Ivan K. Schuller, University of California-San Diego

Program Scope

The goals of this project are: (1) to investigate the phenomena arising when magnetic materials are nanostructured in one, two or three dimensions, (2) to explore proximity effects in dissimilar magnetic heterostructures. The comprehensive approach combines preparation of nanostructures using a combination of thin-film growing (sputtering, evaporation and MBE), lithography (electron-beam/optical) and self-assembly techniques, characterization using microscopy (SEM, TEM, scanning probe), high-resolution scattering (light, X-ray, synchrotron and neutron), physical properties measurements (magneto-transport, magnetometry and magneto-optical) and theoretical modeling. Preparation of most unique materials and devices and most structural and physical characterization are performed in the PI's laboratory at UCSD. Additionally, some unique materials are obtained from collaborators at major research institutions and a number of sophisticated structural and magnetic studies at the nanoscale are performed in collaboration at several major facilities of DOE funded national labs.

We aim to investigate general physical phenomena, including the effects of confinement on magnetic properties, a variety of proximity effects in magnetic hybrids, exchange bias, and effects induced by external driving forces such as time varying electric and magnetic fields, light, and other types of excitations. In all cases, a crucial ingredient is confinement of the complex or highly correlated materials at nanoscale, where fundamental changes in their magnetic properties occur. These studies have focused on fluorides, oxides, borides and organics, in addition to many combinations of transition metal elements. We have established a battery of instrumentation and continue expanding our experimental capabilities at UCSD and elsewhere. We have performed experiments at fast time scales to investigate the very unusual dynamics present in many hybrid systems.

Recent Progress

During the current reporting period, we had major advances in several diverse material systems, published extensively in the first-rate refereed literature, and our achievements were recognized by important invitations at international scientific meetings. All this despite major practical limitations imposed by COVID-19. The accomplishments from this research are discussed in detail in a series of published manuscripts. Here we include only brief highlights illustrating our discovery of a novel voltage controlled magnetism in resistive switching systems.

Proximity effects could lead to unusual magnetic phenomena [1] and provide an opportunity to engineer a wide range of functional properties such as magnetization pinning in exchange bias systems [2], giant magnetoresistance [3], anisotropy control in strain tunable heterostructures [4], etc. Typically, proximity effects emerge in artificial multilayers where several magnetic and nonmagnetic materials are placed in direct contact with each other. Such multilayers

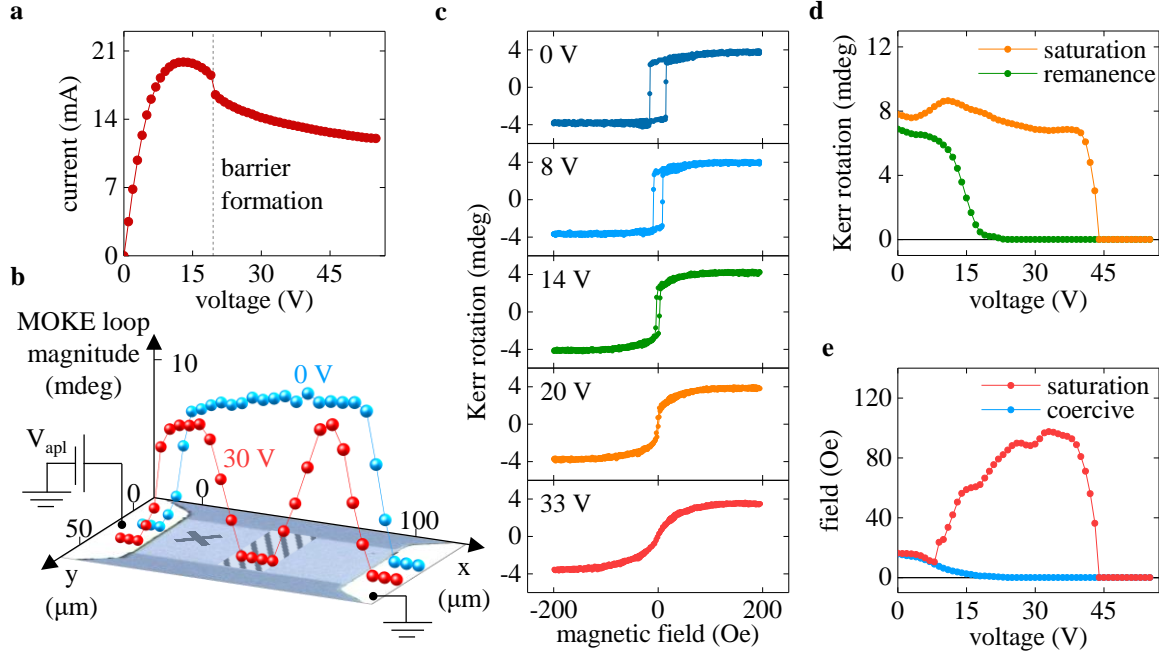


Fig. 1. **a**, I-V curve of an LSMO device showing volatile resistive switching. **b**, Spatial FM mapping: uniform FM state in equilibrium (0 V, blue line) transforms in a state with a PM region in the device center during the resistive switching (30 V, red line). **c**, Voltage evolution of hysteresis loops during the resistive switching. **d**, **e**, Saturation and remanence (**d**) and coercive and saturation fields (**e**) as functions of the applied voltage.

are constructed during the fabrication process, which limits the ability to tune their properties *in-operando*. To overcome this limitation, we explore the interplay between magnetism and resistive switching where the proximity effects arise from an electrically induced phase separation.

Resistive switching is the ability to reversibly change the material’s resistivity by application of voltage. This phenomenon has attracted enormous attention in the past decades because of the possible applications in binary memories for conventional computers and synapse-like memories for hardware level neuromorphic computing [5]. Resistive switching often occurs by the formation of spatially inhomogeneous, yet highly symmetric patterns, such as a longitudinal conducting filaments [6] or transverse insulating barriers [7]. The electrically driven filament/barrier formation locally “injects” a different electronic and magnetic phase into an otherwise homogeneous material. As we demonstrate in this work, the ability to create and tune the local phase separation by inducing resistive switching enables novel approach to electrical control of magnetic properties.

We explored the resistive switching impact on magnetic anisotropy of $\text{La}_{0.7}\text{Sr}_{0.3}\text{MnO}_3$ (LSMO), a material that exhibits a phase transition from a ferromagnetic (FM) metal to a paramagnetic (PM) insulator. Recently, we found that application of a voltage to an LSMO device can trigger the metal-insulator transition resulting in a volatile resistive switching [8], as shown by nonlinearities in the I-V curve (Fig. 1a). At the microscopic level, the metal-to-insulator switching in LSMO occurs by the formation of a transverse insulating barrier that spans across the entire device width and impedes the electric current flow. The insulating barrier formation creates a PM

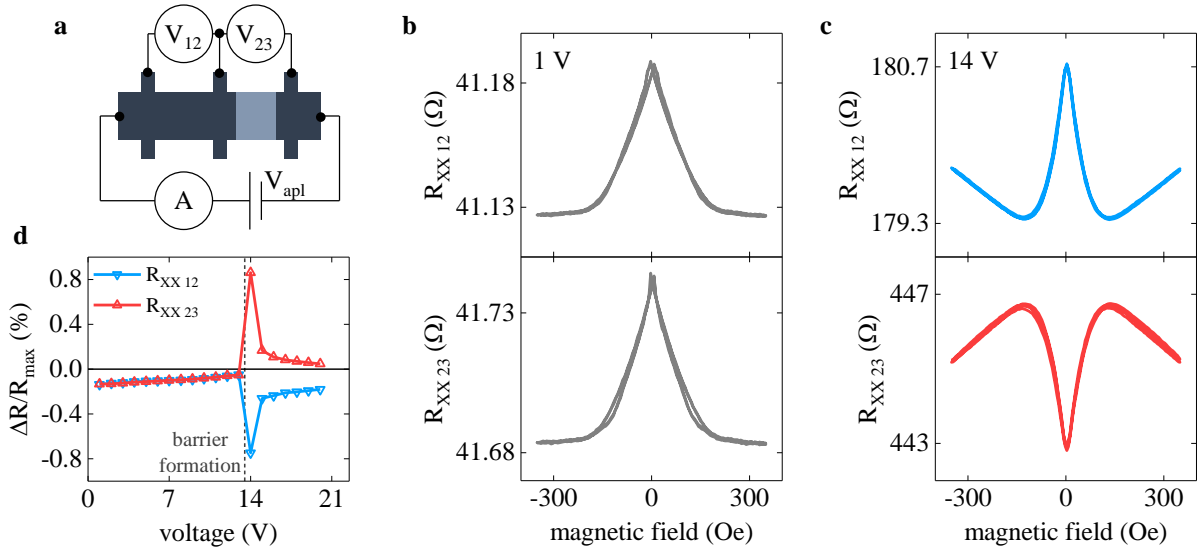


Fig. 2. **a**, Schematic of the Hall bar measurement setup. Blue shaded region indicates the PM barrier that forms during the resistive switching. **b**, **c** Small field magnetoresistance in equilibrium (**b**) and during the resistive switching (**c**). **d**, Voltage dependence of the maximum small field magnetoresistance.

region inside the device enabling local on/off switching of ferromagnetism (Fig. 1b). On the left and right sides of the barrier the device retains a robust FM state. The evolution of magnetic properties in the FM regions surrounding the PM barrier during resistive switching is the primary focus of this work.

Resistive switching in LSMO results in a voltage-controlled magnetic anisotropy (VCMA) effect. As shown in Fig. 1c, when the LSMO device is driven through the resistive switching, the initial square hysteresis loop in the FM regions becomes oblique stretching along the field axis, which indicates easy-to-hard anisotropy axis transition. The anisotropy change occurs without a considerable suppression of the FM state. The saturation signal of the hysteresis loops has a weak dependence on the applied voltage (Fig. 1d, orange line). Only when the applied voltage becomes large enough to drive the material into the PM state, the saturation signal plummets to zero. The remanence, on the other hand, rapidly vanishes as the device undergoes resistive switching (Fig. 1d, green line), suggesting that an internal effective field causes magnetization rotation when the applied field is zero. Fig. 1e compares the coercive field and the field required to achieve saturation. During the resistive switching, the saturation field grows rapidly up to ~ 100 Oe, by a factor of ~ 5 increase compared to its initial zero-voltage value. Such a large increase of saturation field suggests that the applied magnetic field has to overcome a strong opposing internal field that redefines the easy anisotropy axis. The overall impact of the voltage-induced anisotropy in the LSMO devices, i.e., the complete suppression of coercivity and remanence, is qualitatively comparable to the best examples of VCMA in magneto-electric [9] and magneto-ionic [10] devices.

Resistive switching in LSMO produces an anomaly in magneto-transport properties. Using a Hall bar device geometry (Fig. 2a), we probed longitudinal magnetoresistance both in the FM

region and across the PM barrier. In equilibrium, the small-field magnetoresistance (i.e., anisotropic magnetoresistance) with the field parallel to current is negative (resistance decreases in non-zero field) having the magnitude of $\Delta R/R \sim 0.1\%$ (Fig. 2b, top panel). During the switching, the magnetoresistance across the PM barrier becomes positive (resistance increases in non-zero field) as shown in Fig. 1c (bottom panel). The magnetoresistance magnitude both in the FM region and across the PM barrier increases greatly reaching up to $\Delta R/R \sim 1\%$ when the applied voltage induces the PM barrier formation (Fig. 1d). Similar behavior, i.e. a strong magnitude increase and sign change of $\Delta R/R$, was observed in high-field magnetoresistance (i.e., colossal magnetoresistance) in LSMO devices during the resistive switching.

Overall, this work shows that employing resistive switching is a viable strategy to achieve voltage-controlled magnetism. Because resistive switching is a universal phenomenon observed across diverse materials systems, our approach potentially can be extended to a variety of ferromagnetic, ferrimagnetic, and antiferromagnetic materials.

Future Plans

Next year we will concentrate in the following major directions:

1. We will investigate the nanoscale magnetic structures of ferromagnets when they are in proximity to oxides which undergo a Mott transition. State-of-the-art PEEM and NEXAFS experiments will be conducted in collaboration with scientists at major DOE funded facilities.
2. Based on the technical developments of the last year, we will perform acoustoelectric measurements of interesting low dimensional magnetic materials.
3. We will use simultaneous temperature and angular-dependent magnetic and transport measurements in an AFM/FM model system to investigate the effect of the FM texture on the exchange bias.
4. We will explore field-free magnetic state writing/reading and investigate magneto-thermal effects in LSMO during resistive switching. We will study the interplay between magnetism and resistive switching in ferromagnetic and antiferromagnetic materials beyond LSMO.

References

- [1] B. Huang, *et al.*, Nat. Mater. **19**, 1276 (2020).
- [2] J. Nogues, I.K. Schuller, J. Magn. Magn. Mater. **192**, 203 (1999).
- [3] E. Tsymbal, D. Pettifor, Solid State Phys. **56**, 113 (2001).
- [4] M. Liu, N.X. Sun, Phil. Trans. R. Soc. A **372**, 20120439 (2014).
- [5] J. del Valle, *et al.*, J. Appl. Phys. **124**, 211101 (2018).
- [6] S. Kumar, *et al.*, Adv. Mater. **25**, 6128 (2013).
- [7] S. Marinkovic, *et al.*, ACS Nano **14**, 11765 (2020).
- [8] P. Sale, *et al.*, arXiv:2009.07412.
- [9] J. Lou, *et al.*, Adv. Mater. **21**, 4711 (2009).
- [10] U. Bauer, *et al.*, Nat. Mater. **14**, 174 (2015).

Publications

1. *Quantifying Inactive Lithium in Lithium Metal Batteries*, C. Fang, J. Li, M. Zhang, Y. Zhang, F. Yang, J. Z. Lee, M.-H. Lee, J. Alvarado, M.A. Schroeder, Y. Yang, B. Lu, N. Williams, M. Ceja, L. Yang, M. Cai, J. Gu, K. Xu, X. Wang, Y.S. Meng, *Nature* **572**, 511 (2019), DOI: 10.1038/s41586-019-1481-z.
2. *Magnetic-Field Frustration Reveals the Nature of the Metal-Insulator Transition in V_2O_3* , J. Trastoy, A. Camjayi, J. del Valle, Y. Kalcheim, J.P. Crocombette, J.A. Borchers, D.A. Gilbert, J.E. Villegas, D. Ravelosona, M.J. Rozenberg, I.K. Schuller, *Phys. Rev. B* **101**, 245109 (2020), DOI: 10.1103/PhysRevB.101.245109.
3. *Chiral Symmetry and Scale Invariance Breaking in Spin Chains*, F. Torres, M. Kiwi, N.M. Vargas, C. Monton, I.K. Schuller, *AIP Advances* **10**, 025215 (2020), DOI: 10.1063/1.5130190.
4. *Ultradense Arrays of Sub-100 nm Co/CoO Nanodisks for Spintronics Applications*, R. Morales, A. N. Flores, N.M. Vargas, J. Giuliani, I.K. Schuller, C. Monton, *ACS Appl. Nano Mater.* **3**, 4037 (2020), DOI: 10.1021/acsnm.0c00052.
5. *Temperature Trends and Correlation Between SQUID Superparamagnetic Relaxometry and DC-Magnetization on Model Iron-Oxide Nanoparticles*, J.M. Vargas, J. Lawton, N.M. Vargas, I.K. Schuller, N.J. Sowko, M. Zhang, *Appl. Phys.* **127**, 044304 (2020), DOI: 10.1063/1.5131012.
6. *Enhanced positive and negative exchange bias in FeF_2/Ni with dusted interfaces*, I. Montoya, F. Torres, C. Redondo, M. Kiwi, I.K. Schuller, and R. Morales, *Appl. Phys. Lett.* **117**, 092401 (2020), DOI: 10.1063/5.0021267.
7. *Acoustoelectric Drag Current in Vanadium Oxide Films*, P.N. Lapa, G. Kassabian, F. Torres, P. Salev, M.-H. Lee, J. del Valle, I.K. Schuller. *Appl. Phys.* **128**, 155104 (2020), DOI: 10.1063/5.0015215.
8. *Detection of uncompensated magnetization at the interface of an epitaxial antiferromagnetic insulator*, P.N. Lapa, M.-H. Lee, I.V. Roshchin, K.D. Belashchenko, I.K. Schuller. *Phys. Rev. B* **102**, 174406 (2020), DOI: 10.1103/PhysRevB.102.174406.
9. *Hydrostatic pressure mapping of barium titanate phase transitions with quenched $FeRh$* , C. Urban, S.P. Bennett, I.K. Schuller, *Sci. Rep.* **10**, 6312 (2020), DOI: 10.1038/s41598-020-63358-0.
10. *Driving magnetic domains at the nanoscale by interfacial strain-induced proximity*, I. Valmianski, A.F. Rodriguez, J. Rodriguez-Alvarez, M.G. del Muro, C. Wolowiec, F. Kronast, J.G. Ramirez, I.K. Schuller, A. Labarta, X. Batlle, *Nanoscale* **13**, 4985 (2021), DOI: 10.1039/d0nr08253h.
11. *Metal-insulator transition in V_2O_3 with intrinsic defects*, R. Tran, X.-G. Li, S.P. Ong, Y. Kalcheim, I.K. Schuller, *Phys. Rev. B* **103**, 075134 (2021), DOI: 10.1103/PhysRevB.103.075134.

Planar Systems for Quantum Information

PI: Jie Shan (Cornell University)

Co-PIs: Cory R. Dean (Columbia University)

James Hone (Columbia University)

Allan H. MacDonald (University of Texas at Austin)

Kin Fai Mak (Cornell University)

Tony F. Heinz (SLAC National Accelerator Laboratory/Stanford University)

Program Scope

This program aims to develop two-dimensional (2D) moiré materials as a quantum simulator to implement model Hamiltonians and their phase diagrams and dynamics. We will develop advanced methods for material synthesis and 2D assembly, including bulk crystal growth using a flux synthesis method and the creation of tailored 2D heterostructures with on demand control of the rotation angle using dry transfer techniques. We will probe the properties of the resulting 2D heterostructures using a wide variety of electrical and optical methods, including transport, capacitance and optical pump-probe spectroscopy. The experimental research will be pursued in a close feedback loop with predictions and modeling using *ab-initio* and analytical theory.

Recent Progress

The Hubbard model is a simple theoretical model of interacting quantum particles in a lattice. It is thought to capture the essential physics of high-temperature superconductors, magnetic insulators and other complex quantum many-body ground states. The model only has two terms, a kinetic lattice hopping term (t) and an on-site Coulomb repulsion interaction term (U). The Hubbard model on a triangular lattice is particularly rich because geometrical frustration enhances quantum fluctuations and leads to a multitude of closely competing states that challenge theory. A recent theoretical analysis by MacDonald *et al.* has shown that moiré superlattices formed by semiconductor transition metal dichalcogenide (TMD) heterobilayers provide a realization of the triangular-lattice Hubbard model [1]. Unlike graphene systems, in which spin, valley and layer degeneracies are all present, the spin and layer degeneracies in TMD heterobilayers are lifted by the strong spin-orbit interactions and the layer asymmetry, respectively. When the chemical potential is within the topmost valence band, where there is large spin-orbit splitting, holes can be mapped to the single-band Hubbard model with two valley degrees of freedom, which acts as the spin.

Our team studied the phase diagram of aligned WSe₂/WS₂ bilayers in the limit of $U/t \gg 1$ by combining optical spectroscopy and transport measurements. Around half band filling

(corresponding to filling factor of the moiré unit cell $\nu = 1$), the sample resistance increases sharply with decreasing temperature, exhibiting a characteristic insulating behavior. The magnetic susceptibility further indicates that localized moments interact antiferromagnetically. These results are fully consistent with the picture of a Mott insulating state at $\nu = 1$ [Ref. 2]. In addition to the Mott insulating state, we observed an abundance of correlated insulating states at fractional filling factors by a new optical sensing technique (Fig. 1a) [3]. The technique is built on the sensitivity to dielectric environment of the excitons in a single-layer semiconductor (a WSe₂ monolayer) that is placed very close to the sample of interest (WSe₂/WS₂ moiré heterostructure). We proposed charge-ordered states at commensurate filling fractions that range from generalized Wigner crystals to charge density waves (Fig. 1b). The existence of these electron crystal states is indicative of the importance of long-range interactions in addition to the on-site Coulomb repulsion, and that an extended Hubbard model is more appropriate to describe TMD moiré superlattices. Interestingly, some of these states ($\nu = 1/2, 2/5$ and $2/5$ in Fig. 1b) break rotational symmetry. Applying a sensitive optical anisotropy measurement, we found strong electronic anisotropy over a large doping range peaked at $1/2$ filling. Away from $1/2$ filling, we observed additional stripe crystals at commensurate filling (e.g. $2/5$ and $3/5$) and compressible electronic liquid crystal states at incommensurate fillings [4].

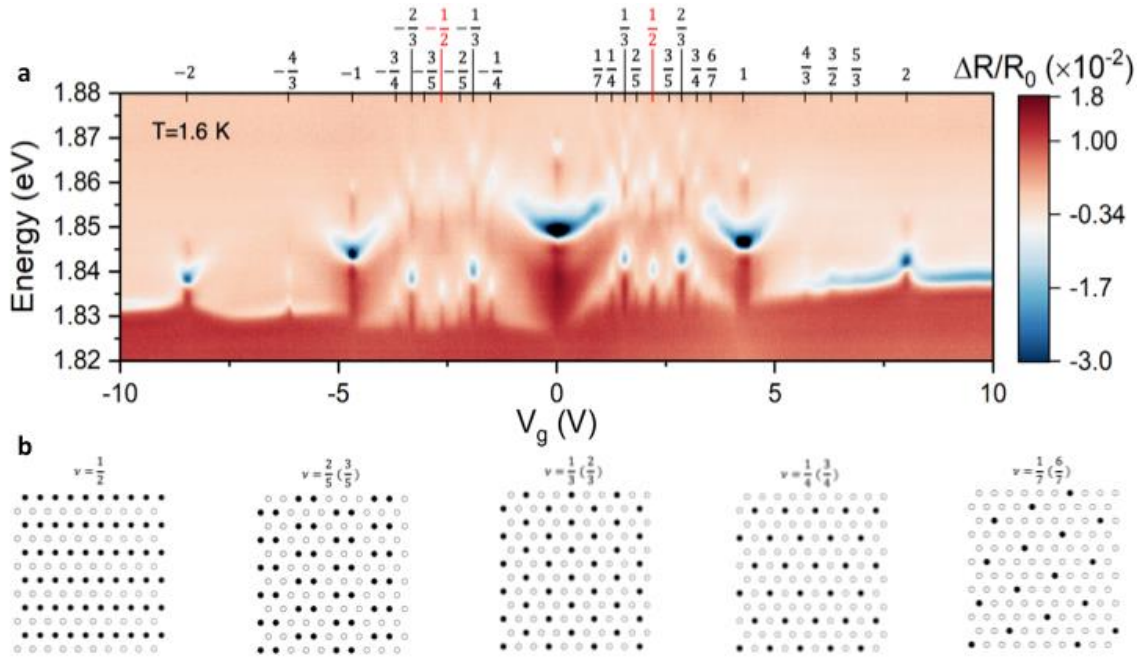


Fig. 1. a, An abundance of insulating states in a WSe₂/WS₂ moiré heterostructure is revealed blueshifts of the 2s exciton resonance, accompanied by an enhancement in the spectral weight. The bottom axis shows the applied gate voltage, which varies the filling factor of the moiré heterostructure. The top axis shows the proposed filling factor for the insulating states. **b**, Proposed charge-order configuration for the observed insulating states at zero temperature on the underlying hexagonal moiré superlattice. Filled and unfilled circles denote occupied and empty sites for state ν , respectively. For state $1 - \nu$, the notation of the occupied and empty sites is switched.

Future Plans

We will investigate the phase diagram of TMD moiré superlattices as a function of effective interaction strength (U/t). An out-of-plane displacement field will be explored to tune U/t . The displacement field controls the potential difference between the two layers and is expected to vary the interlayer tunneling rate and the moiré potential and the bandwidth. In particular, at half band filling the system is a Landau Fermi liquid in the limit of weak interaction. It becomes a Mott insulator in the limit of strong interaction. We will study the metal-to-insulator transition at $\nu = 1$ and explore the phase space in the vicinity of the transition, in which many exotic states have been predicted.

References

1. F. Wu, T. Lovorn, E. Tutuc, A. H. MacDonald, “Hubbard model physics in transition metal dichalcogenide moiré bands,” *Phys. Rev. Lett.* **121**, 026402 (2018).
2. Y. Tang, L. Li, T. Li, Y. Xu, S. Liu, K. Barmak, K. Watanabe, T. Taniguchi, A. H. MacDonald, J. Shan, and K. F. Mak, “Simulation of Hubbard model physics in WSe_2/WS_2 moiré superlattices,” *Nature* **579**, 353-358 (2020).
3. Y. Xu, S. Liu, D. A. Rhodes, K. Watanabe, T. Taniguchi, J. Hone, V. Elser, K. F. Mak, and J. Shan, “Correlated insulating states at fractional fillings of moiré superlattices,” *Nature* **587**, 214–218 (2020).
4. C. Jin, Z. Tao, T. Li, Y. Xu, Y. Tang, J. Zhu, S. Liu, K. Watanabe, T. Taniguchi, J. Hone, L. Fu, J. Shan, and K. F. Mak, “Stripe phases in WSe_2/WS_2 moiré superlattices,” *Nat. Mater.* **20**, 940-944 (2021).

Publications

1. Z. Wang, D. A. Rhodes, K. Watanabe, T. Taniguchi, J. C. Hone, J. Shan, and K. F. Mak, “Evidence of high-temperature exciton condensation in 2D atomic double layers,” *Nature* **574**, 76-80 (2019).
2. A. Mukherjee, K. Shayan, L. Li, J. Shan, K. F. Mak, and A.N. Vamivakas, “Deterministic strain-induced confinement of all optically created charged excitons in CrI_3/WSe_2 heterostructures,” *Nat. Commun.* **11**, 5502 (2020).
3. E. Y. Ma, L. Waldecker, D. Rhodes, J. Hone, K. Watanabe, T. Taniguchi, and T. F. Heinz, “High-resolution optical micro-spectroscopy extending from the near-infrared to the vacuum-ultraviolet,” *Rev. Sci. Instrum.* **91**, 073107 (2020).
4. Y. Tang, L. Li, T. Li, Y. Xu, S. Liu, K. Barmak, K. Watanabe, T. Taniguchi, A. H. MacDonald, J. Shan, and K. F. Mak, “Simulation of Hubbard model physics in WSe_2/WS_2 moiré superlattices,” *Nature* **579**, 353-358 (2020).
5. Y. Xu, S. Liu, D. A. Rhodes, K. Watanabe, T. Taniguchi, J. Hone, V. Elser, K. F. Mak, and J. Shan, “Correlated insulating states at fractional fillings of moiré superlattices,” *Nature* **587**, 214–218 (2020).

6. Y. Zeng and A. H. MacDonald, “Electrically Controlled Two-Dimensional Electron-Hole Fluids,” *Phys Rev B* **102**, 085154 (2020).
7. Y. Tang, J. Gu, S. Liu, K. Watanabe, T. Taniguchi, J. Hone, K. F. Mak, and J. Shan, “Tuning layer-hybridized moiré excitons by the quantum-confined Stark effect,” *Nat. Nanotechnol.* **16**, 52-57 (2021).
8. H. Xie, S. Jiang, D. Rhodes, J. Hone, J. Shan, and K. F. Mak, “Tunable exciton-optomechanical coupling in suspended monolayer MoSe₂,” *Nano Lett.* **21**, 2538–2543 (2021).
9. Y. Xu, C. Horn, J. Zhu, Y. Tang, L. Ma, L. Li, S. Liu, K. Watanabe, T. Taniguchi, J. Hone, J. Shan, and K. F. Mak, “Creation of moiré bands in a monolayer semiconductor by spatially periodic dielectric screening,” *Nat. Mater.* **20**, 645-649 (2021).
10. C. Jin, Z. Tao, T. Li, Y. Xu, Y. Tang, J. Zhu, S. Liu, K. Watanabe, T. Taniguchi, J. Hone, L. Fu, J. Shan, and K. F. Mak, “Stripe phases in WSe₂/WS₂ moiré superlattices,” *Nat. Mater.* **20**, 940-944 (2021).
11. M Angeli and A. H. MacDonald, “ Γ -valley transition-metal-dichalcogenide moiré bands,” *Proc. Natl. Acad. Sci. U. S. A.* **118**, e2021826118 (2021).
12. N. Morales-Durán, P. Potasz, and A. H. MacDonald, “Metal-insulator transition in transition metal dichalcogenide heterobilayer moiré superlattices,” *Phys. Rev. B* **103**, L241110 (2021).
13. T. Li, J. Zhu, Y. Tang, K. Watanabe, T. Taniguchi, V. Elser, J. Shan, and K. F. Mak, “Charge-order-enhanced capacitance in semiconductor moiré superlattices,” *Nat. Nanotechnol.* (2021). doi.org/10.1038/s41565-021-00955-8.
14. E. Liu, E. Barré, J. van Baren, M. Wilson, T. Taniguchi, K. Watanabe, Y. Cui, N. M. Gabor, T. F. Heinz, Y. Chang, and C. H. Lui, “Signature of moiré trions in a WSe₂/MoSe₂ heterobilayer,” *Nature* **594**, 46–50 (2021).

Program Title: Correlated States of Two-dimensional Electron Systems in AlAs Quantum Wells

Principal Investigator: M. Shayegan

Mailing Address: Department of Electrical Engineering, Princeton University, Princeton, NJ, 08544

E-mail: shayegan@princeton.edu

Program Scope

Two-dimensional (2D) carrier systems confined to modulation-doped semiconductor heterostructures provide a nearly ideal testing ground for exploring new physical phenomena. At low temperatures and in the presence of a strong magnetic field, these systems exhibit fascinating, often unexpected, many-body states, arising from the strong electron-electron interaction. Examples include the fractional quantum Hall liquid, the Wigner solid, and the newly discovered striped and bubble phases in the higher Landau levels.

Much of the work on clean 2D systems has been performed on 2D electrons in a remotely-doped *GaAs* quantum well. The goal of this project is to study the physics of 2D electrons confined to a remotely-doped *AlAs* quantum well. The 2D electrons in *AlAs* have parameters that are very different from those of the commonly-studied, *GaAs* 2D electrons: they have a much larger, anisotropic effective mass, a much larger effective Landé *g*-factor, and they occupy multiple conduction band valleys. Moreover, through varying the *AlAs* quantum well width, and also by applying uniaxial, in-plane strain, one can control the electron occupation in the different valleys. Demonstration of such control in *AlAs* quantum wells provided the first example of using the valley degree of freedom to change the electronic properties of an electron system and to make a functional device, and paved the way for the emerging field of “valleytronics.”

We have had a very recent breakthrough in making *AlAs* quantum well samples with unprecedented quality. Through a systematic purification of the Al source material, we were able to optimize the growth conditions for *AlAs* quantum wells, and broke the world record (by a factor of eight) for the mobility of 2D electrons confined to these wells. The extremely high quality of these new samples, combined with the tunable valley degree of freedom, renders the *AlAs* 2D electron system a unique platform for studies of interaction-induced phenomena. Exploring such phenomena is the main goal of this research. For example, what role does the valley/spin degrees of freedom and effective mass anisotropy play in the competition between different correlated phases at high magnetic fields, namely the fractional quantum Hall liquid state and broken-symmetry states such as the Wigner crystal and stripe phases?

Moreover, the effective mass of electrons is about seven times larger in *AlAs* compared to *GaAs*, effectively making the *AlAs* 2D electrons much more dilute and therefore more interacting, even in the absence of a magnetic field. The parameter r_s , defined as the ratio of the Coulomb to kinetic (Fermi) energy, can indeed reach ~ 50 in our new *AlAs* samples (at a density of $\sim 1 \times 10^{10} \text{ cm}^{-2}$) while still maintaining high enough quality to exhibit quantum Hall effect. These are prime samples to potentially exhibit the long-anticipated (since 1929) Bloch/Stoner spin and/or valley ferromagnetism of itinerant electrons.

In our project we study *AlAs* quantum well structures grown via state-of-the-art molecular beam epitaxy (MBE), and use low-temperature magneto-transport measurements to explore their

novel physics. For sample fabrication, we collaborate closely with Dr. Loren Pfeiffer at Princeton University who is a world expert in MBE, and Prof. Roland Winkler at the Univ. of Northern Illinois, who has expertise in calculating the energy band structure and Landau levels in various 2D systems. We also have a strong collaboration with Dr. Lloyd Engel at the National High Magnetic Laboratory in Tallahassee, FL, on high-frequency (microwave) measurements on 2D carrier systems at high magnetic fields.

Recent Progress

We briefly describe here one of our major, recent accomplishments, namely our observation of spontaneous ferromagnetism, for both the spin and valley degrees of freedom, in dilute, interacting, AIAs 2D electron systems [12, 16].

In a seminal work in 1929 Felix Bloch predicted that as the electron density is lowered in an ensemble of electrons, the exchange energy gained by aligning the electron spins should exceed the enhancement in the kinetic (Fermi) energy, leading to a (Bloch) ferromagnetic transition. At even lower densities, another transition to a (Wigner) solid, an ordered array of electrons, should occur. Experimental access to these regimes, however, has been limited because of the absence of a material platform that supports an electron system with very high quality (low disorder) and low density simultaneously.

In our study we explored the ground states of interacting electrons in an exceptionally clean, 2D electron system confined to a modulation-doped AIAs quantum well [12, 16]. Our findings are highlighted in Fig. 1. The large electron effective mass in this system allows us to reach very large values of the interaction parameter r_s . As we lower the electron density via back-gate bias, we find a sequence of phases, qualitatively consistent with the above scenario: a paramagnetic phase at large densities, a spontaneous transition to a ferromagnetic state when r_s surpasses ~ 35 , and then a phase with strongly nonlinear current-voltage characteristics, suggestive of a pinned Wigner solid, when r_s exceeds ~ 38 . However, our sample makes a transition to an insulating state at $r_s \sim 27$, preceding the onset of the spontaneous spin ferromagnetism, implying that besides interaction, the role of disorder must also be taken into account in understanding the different phases of a realistic dilute electron system [12].

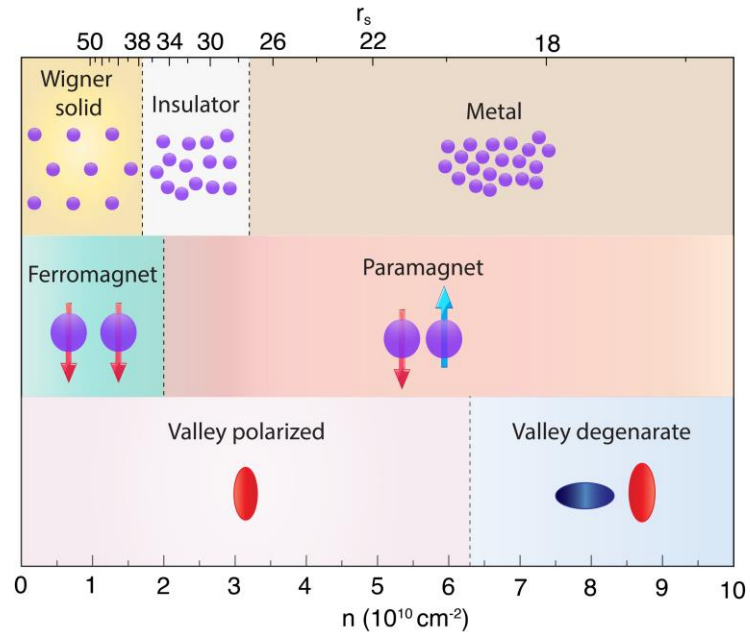


Fig. 1 Summary of various man-body states of AIAs 2D electrons observed in our studies.

A very exciting surprise in our study has been that, before the 2D electron system makes the transition to a fully-spin-polarized state at $r_s \sim 35$, it reveals a sudden “valley-polarization” transition at higher densities ($r_s \sim 21$) [16]. The data and its description are summarized in Fig. 2. Note that this transition is akin to the spin-polarization transition, except that here we see a transition in the valley degree of freedom. It is also noteworthy that the phenomenon and data demonstrate a quintessential example of a “valleytronic” field-effect type device: as we tune the density with a gate, we see a large change in the conductance of the device resulting from a change in the valley occupation.

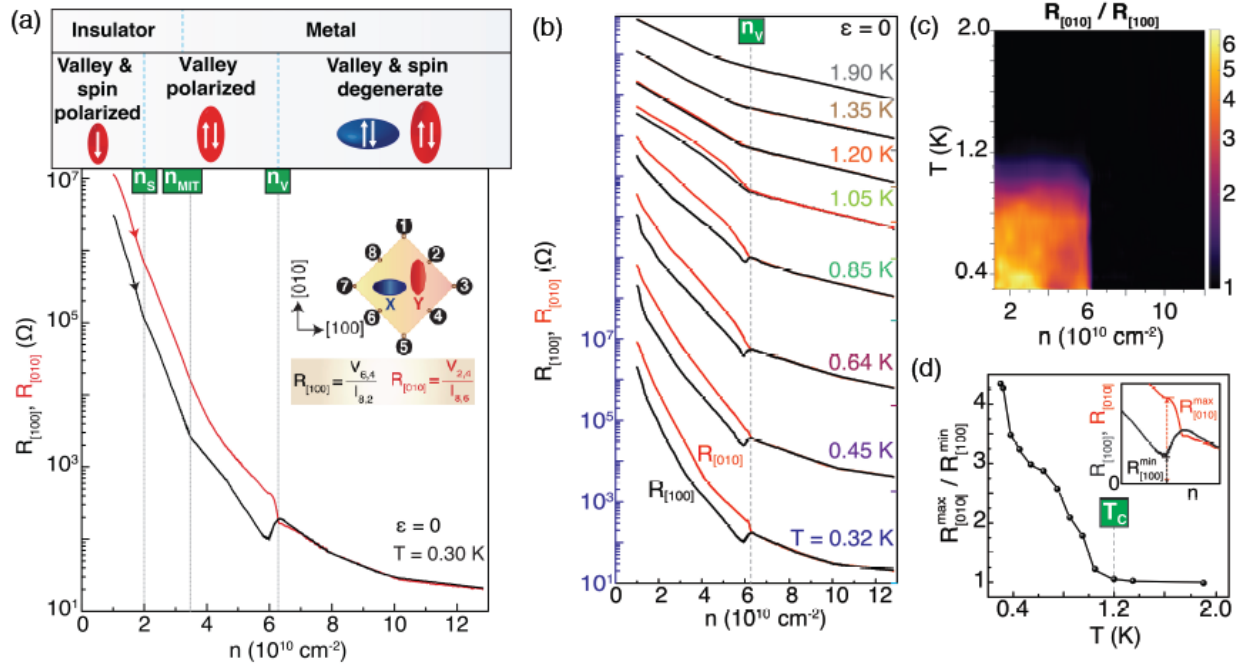


Fig. 2 Signatures of a spontaneous valley polarization in a valley-degenerate 2D electron system at low densities. (a) Resistances along [100] and [010] directions plotted as a function of density; see the inset for the sample geometry. X and Y valleys are degenerate at high densities and the 2D electron system is isotropic. However, as the density is lowered below $n = 6.3 \times 10^{10} \text{ cm}^{-2}$, $R_{[100]}$ and $R_{[010]}$ suddenly split, signaling a spontaneous lifting of the valley degeneracy, i.e., a **spontaneous** valley polarization. The upper panel illustrates the spin and valley configurations as a function of density. The density $n = 6.3 \times 10^{10} \text{ cm}^{-2}$ corresponds to $r_s = 21$, where r_s is the ratio of Coulomb to kinetic (Fermi) energies. (b) Temperature dependence of $R_{[100]}$ and $R_{[010]}$, and (c) resistance anisotropy ($R_{[010]}/R_{[100]}$), as a function of density and temperature, exhibiting the disappearance of the spontaneous valley polarization above $T = 1.2 \text{ K}$. (d) Anisotropy vs. T at $n = 6.0 \times 10^{10} \text{ cm}^{-2}$ where we observe a minimum in $R_{[100]}$.

Future plans

We plan to continue our studies of 2D electrons in AIAs quantum wells. One problem of interest is the insulating phase we observe at extremely low densities, when r_s exceeds ~ 38 . This phase exhibits a strongly nonlinear current-voltage characteristics, suggestive of a pinned Wigner solid. Of particular interest is that transport is anisotropic with resistances and the de-pinning thresholds both being significantly larger along [010] compared to [100]. We believe these

features are signatures of an *anisotropic* pinned Wigner solid. We plan to study in detail the properties of this unusual state of matter.

Publications acknowledging DOE support; since 2019:

1. Jing Xu, Meng K. Ma, Maksim Sultanov, Zhi-Li Xiao, Yong-Lei Wang, Dafei Jin, Yang-Yang Lyu, Wei Zhang, Loren N. Pfeiffer, Ken W. West, Kirk W. Baldwin, Mansour Shayegan, and Wai-Kwong Kwok, “Negative Longitudinal Magnetoresistance in GaAs Quantum Wells,” *Nature Communications* **10**, 287 (2019).
2. Yoon Jang Chung, K. W. Baldwin, K. W. West, N. Haug, J. van de Wetering, M. Shayegan, and L. N. Pfeiffer, “Spatial Mapping of Local Density Variations in GaAs Two-dimensional Electron Systems Using Photoluminescence,” *Nano Letters* **19**, 1908 (2019).
3. A. T. Hatke, H. Deng, Yang Liu, L. W. Engel, ^[1]L. N. Pfeiffer, K. W. West, K. W. Baldwin, M. Shayegan, “Wigner Solid Pinning Modes Tuned by Fractional Quantum Hall States of a Nearby Layer,” *Science Advances* **5**, eaao2848 (2019).
4. H. Deng, L.N. Pfeiffer, K.W. West, K.W. Baldwin, and M. Shayegan, “Probing the Melting of a Two-dimensional Quantum Wigner Crystal via its Screening Efficiency,” *Phys. Rev. Lett.* **122**, 116601 (2019). [**Editor’s Suggestion**]
5. Md. Shafayat Hossain, Meng K. Ma, M. A. Mueed, D. Kamburov, L. N. Pfeiffer, K. W. West, K. W. Baldwin, R. Winkler, and M. Shayegan, “Geometric Resonance of Four-flux Composite Fermions,” *Phys. Rev. B (Rapid Communications)* **100**, 041112(R) (2019).
6. Yoon Jang Chung, K. A. Villegas Rosales, K. W. Baldwin, K. W. West, M. Shayegan, and L. N. Pfeiffer, “Working Principles of Doping-well Structures for High-mobility Two-dimensional Electron Systems,” *Phys. Rev. Materials* **4**, 044003 (2020).
7. M. Shayegan, “Probing Composite Fermions Near Half-filled Landau Levels,” Review article in *Fractional Quantum Hall Effects: New Developments*, edited by B. I. Halperin and J. K. Jain (World Scientific, 2020), pp. 133-181. (<https://doi.org/10.1142/11751>)
8. Meng K. Ma, K. A. Villegas Rosales, H. Deng, Y. J. Chung, L. N. Pfeiffer, K. W. West, K. W. Baldwin, and M. Shayegan, “Thermal and Quantum Melting Phase Diagrams for a Magnetic-field-induced Wigner Solid,” *Phys. Rev. Lett.* **125**, 036601 (2020).
9. Yoon Jang Chung, K. W. Baldwin, K. W. West, M. Shayegan, L. N. Pfeiffer, S. Yuan, and Yang Liu, “Heterostructure Design to Achieve High-quality, High-density, GaAs 2D Electron System with *g*-factor Tending to Zero,” *Appl. Phys. Lett.* **117**, 022102 (2020).
10. Md. Shafayat Hossain, M. A. Mueed, M. K. Ma, K. A. V. Rosales, Y. J. Chung, L. N. Pfeiffer, K. W. West, K. W. Baldwin, and M. Shayegan, “Precise Experimental Test of the Luttinger Theorem and Particle-hole Symmetry for a Strongly Correlated Fermionic System,” *Phys. Rev. Lett.* **125**, 046601 (2020). [**Editor’s Suggestion.**]
11. M. Lupatini, P. Knueppel, S. Faelt, R. Winkler, M. Shayegan, A. Imamoglu, and W. Wegscheider, “Spin Reversal of a Quantum Hall Ferromagnet at a Landau Level Crossing,” *Phys. Rev. Lett.* **125**, 067404 (2020).
12. Md. S. Hossain, K. A. Villegas-Rosales, M. K. Ma, Y. J. Chung, L. N. Pfeiffer, K. W. West, K. W. Baldwin, and M. Shayegan, “Observation of Spontaneous Ferromagnetism in a Two-Dimensional Electron System,” *Proc. National Acad. Sciences (PNAS)* **117**, 32244 (2020).

See **Commentary:** Kyung-Su Kim and Steven A. Kivelson, “Discovery of an Insulating Ferromagnetic Phase of Electrons in Two Dimensions,” *PNAS* **118** (2) e2023964118 (2021); <https://doi.org/10.1073/pnas.2023964118>

13. Md. Shafayat Hossain, Tongzhou Zhao, Songyang Pu, M. A. Mueed, M. K. Ma, K. A. V. Rosales, Y. J. Chung, L. N. Pfeiffer, K. W. West, K. W. Baldwin, J. K. Jain, and M. Shayegan, “Bloch Ferromagnetism of Composite Fermions,” *Nature Physics* **17**, 48 (2021).
See **Commentary**: “The Observation of Bloch Ferromagnetism in Composite Fermions,” by Ingrid Fadelli (Phys.org); <https://phys.org/news/2020-09-bloch-ferromagnetism-composite-fermions.html>.
14. K. A. Villegas Rosales, S. K. Singh, Meng K. Ma, Shafayat M. Hossain, Y. J. Chung, L. N. Pfeiffer, K. W. West, K. W. Baldwin, and M. Shayegan, “Competition between Fractional Quantum Hall Liquid and Wigner Solid at Small Fillings: Role of Layer Thickness and Landau level Mixing,” *Phys. Rev. Research* **3**, 013181 (2021).
15. Yoon Jang Chung, K. A. Villegas-Rosales, K. W. Baldwin, P. T. Madathil, K. W. West, M. Shayegan, and L. N. Pfeiffer, “Ultra-high-quality Two-dimensional Electron Systems,” *Nature Materials* **20**, 632 (2021).
16. Md. S. Hossain, M. K. Ma, K. A. Villegas-Rosales, Y. J. Chung, L. N. Pfeiffer, K. W. West, K. W. Baldwin, and M. Shayegan, “Spontaneous Valley Polarization of Itinerant Electrons,” *Phys. Rev. Lett.* **127**, 116601 (2021).
17. K. A. Villegas Rosales, S. K. Singh, H. Deng, Y. J. Chung, L. N. Pfeiffer, K. W. West, K. W. Baldwin, and M. Shayegan, “Melting Phase Diagram of Bubble Phases in High Landau Levels,” *Phys. Rev. B* **xxx**, xxxx (2021); in press.

Magneto-optical Study of Correlated Electron Materials in High Magnetic Fields

Principal Investigator: Dmitry Smirnov¹; Co-PI: Zhigang Jiang²

¹ National High Magnetic Field Laboratory, Tallahassee, FL 32310

² Georgia Institute of Technology, Atlanta, GA 30332

Program Scope

This program is focused on studying electronic structure, low-energy excitations, and many-body effects in novel electronic materials via magneto-optical spectroscopy. Our research interest spans over two broad and interconnected areas: (i) properties of Dirac and Weyl fermions in topological materials, and (ii) atomically thin materials with the valley degree of freedom and strong spin-orbit coupling.

Recent Progress

Unraveling Topological Phases in Narrow-Gap Topological Materials: Case Study of ZrTe₅

For materials near the phase boundary between a normal insulator (NI) and topological insulator (TI), their band topology depends on the band alignment, with the inverted (normal) band corresponding to the TI (NI) phase. For narrow-gap van der Waals materials, we demonstrate that the band inversion can manifest itself as a second extremum (bandgap) in the layer stacking direction, leading to characteristic features in the magneto-infrared spectroscopy and magneto-transport measurements. Using transition-metal pentatelluride ZrTe₅ as an example, we show that the band anisotropy results in a slow dispersion in the layer stacking direction, along with an additional set of optical transitions [1] or quantum oscillations [2] from the (second) bandgap slightly away from the Brillouin zone center. The rising interest in ZrTe₅ is due to the theoretical prediction of a room-temperature quantum spin Hall insulator phase in its monolayer limit [3]. However, because of the delicate dependence of its band topology on the lattice constants [3, 4], there has not yet been a consensus on the bulk topological phase of ZrTe₅ from experiments [5, 6]. Our work coherently identifies ZrTe₅ as a TI at liquid helium temperature and provides a new perspective in determining band inversion in narrow-gap topological materials.

(i) Accurately determine the anisotropic band parameters via magneto-infrared spectroscopy

The low-energy electronic structure of narrow-gap materials usually exhibits mixing characters of both linear band (LB, $E \propto k$, where k is the wave vector) and parabolic band (PB, $E \propto k^2$), if higher-order terms are neglected. Via combining Faraday and Voigt geometry measurements (Figs. 1(a-c)), we show that the LB and PB components in ZrTe₅ can be extracted by carefully tracking the magnetic field dependence of the inter-Landau-level (inter-LL) transitions (Figs. 1(d-f)). This allows us to reconstruct the 3D electronic structure $E(\vec{k})$ of ZrTe₅ with great energy resolution, using the dispersion relation $E = \pm \sqrt{\hbar^2 v_F^2 k^2 + (M - \mathfrak{B}k^2)^2}$, where the Fermi velocity $\vec{v}_F = (v_{F_x}, v_{F_y}, v_{F_z})$ describes the LB dispersion, the band inversion parameter $\vec{\mathfrak{B}} = (\mathfrak{B}_x, \mathfrak{B}_y, \mathfrak{B}_z)$ characterizes the PB component, and $\Delta = 2M$ is the bandgap.

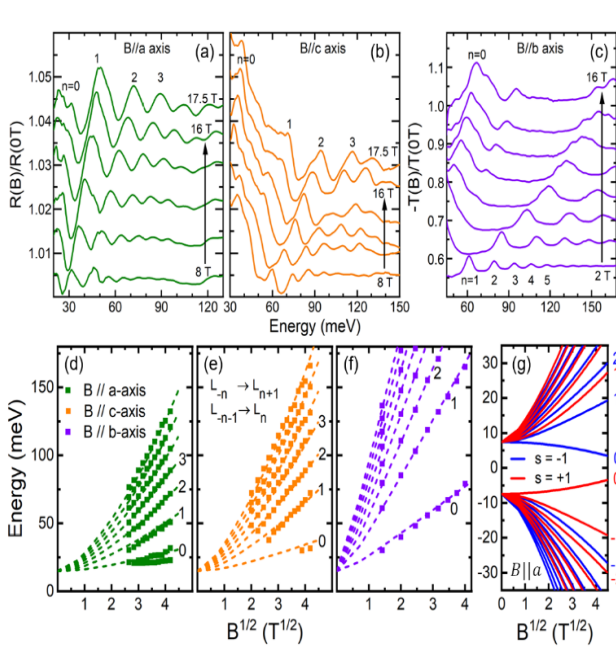


Figure 1: (a-c) Normalized magneto-infrared spectra of ZrTe_5 with the magnetic field applied along three principal crystal axes. To optimize the signal, the spectra with $B||a$ axis (a) and $B||c$ axis (b) are measured in Voigt reflection, while those with $B||b$ axis (c) are measured in Faraday transmission. (d-f) Magnetic field dependence of the extracted LL transition energies from (a-c) for $B||a$ axis (a), $B||c$ axis (b), and $B||b$ axis (c), with the symbol size indicating the upper bound of errors in energy positions. The dash lines are best fits to the data. When splitting occurs, the fit goes through the average energy of the two branches. (g) Representative Landau fan diagram for the case of $B||a$ axis.

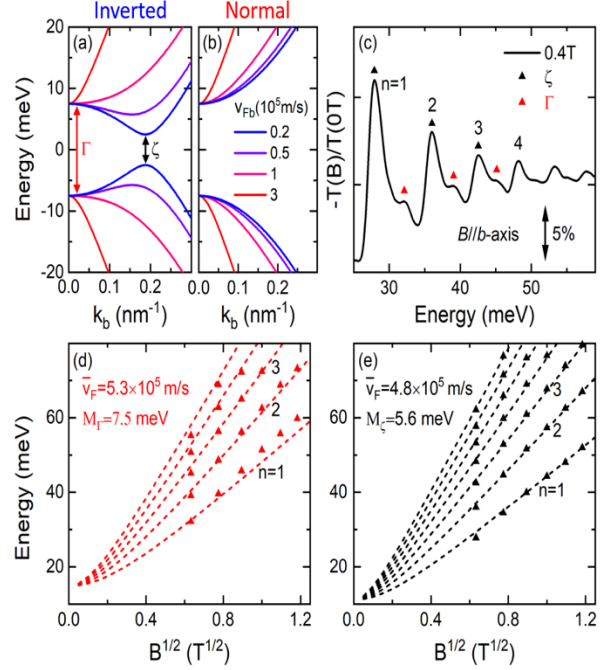


Figure 2: (a,b) Zero-field band structures of ZrTe_5 , calculated in the TI (a) and NI (b) phases with different Fermi velocities v_{Fb} (red arrow) and Γ is sufficiently small. (c) Normalized magneto-transmission spectrum, $-T(B)/T(0T)$, of ZrTe_5 measured at $B||b$ axis. The up triangles label the energy positions of the LL transitions from ζ (black) and Γ (red) points. (d,e) Best fits to the magnetic field dependence of the LL transitions from Γ (d) and ζ (e) points using the simple massive Dirac fermion model.

(ii) Demonstrate the second bandgap at ζ point

From the above measurements (Fig. 1), we find that the Fermi velocity along the b axis (the layer stacking direction of ZrTe_5) is an order of magnitude smaller than those for in-plane axes. As a result, the b -direction low-energy dispersion is dominated by the PB component. In Figs. 2(a,b), we plot the band dispersion along the b axis with different v_{Fb} values for an inverted and normal band, respectively. For the inverted band (Fig. 2(a)), the electronic structures exhibit a local extremum not only at Γ point but also at ζ point when v_{Fb} is sufficiently small. On the contrary, such extremum (bandgap) at ζ point never occurs in the normal band case (Fig. 3(b)) regardless of the magnitude of v_{Fb} . Therefore, the presence of a second extremum at ζ point signifies band inversion in ZrTe_5 and provide a smoking gun evidence for the TI phase. Practically, this direct approach does not require any quantitative analysis, but solid proof of the second extremum. Experimentally, since each local extremum in electronic structure carries a large density of states (DOS), it can host a set of LL transitions under a magnetic field. This is indeed the case observed in our experiment when the magnetic field is applied in the b direction (when $B||b$ axis), as shown

in Fig. 2(c). In Figs. 2(d,e), we plot the magnetic field dependence of the two sets of LL transitions and extract energy gaps $\Delta_\Gamma = 15$ meV and $\Delta_\zeta = 11.2$ meV, respectively.

(iii) Magneto-transport evidence of the second bandgap

Combining theoretical model calculation with high-field magneto-transport measurements, we demonstrate an alternative way to distinguish the TI phase from the NI phase in van der Waals narrow-gap materials. The smoking gun evidences are: (1) the four-fold splitting of the non-zero LLs, and (2) an anomalous $n = 0$ peak in the extreme quantum limit.

In Fig. 3(a), we plot the k_z (the layer stacking direction) dispersion of the normal (red) and inverted (blue) bands. As one can see, although only one energy extremum occurs at Γ point in the normal band case, a second extremum appears at ζ point for the inverted band. Figure 3(b) shows the k_z dispersion of the low-lying electron LLs at $B = 10$ T and applied along the z direction. Two energy extrema at Γ and ζ points are preserved for the inverted band but only one for the normal band at Γ point. When considering a nonzero PB component $\mathfrak{B} \neq 0$, the $n > 0$ LLs split into two sub-levels even without the introduction of the Zeeman effect, and the splitting energy increases with larger $|\mathfrak{B}|$. The Zeeman effect can change the energy separation of the two sub-LLs, but no additional splittings are expected. Since each energy extremum produces a divergent contribution in DOS, calculated at the Fermi energy as a function of magnetic field (Fig. 3(c)), a total of four

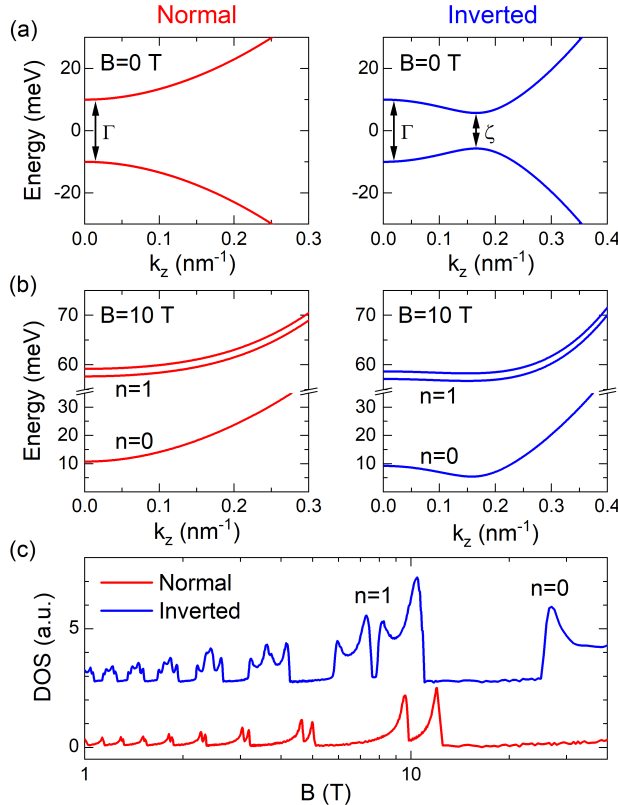


Figure 3: (a) Side-by-side comparison of the zero-field dispersion of the normal (red) and inverted (blue) bands. (b) Dispersion of the low-lying electron LLs of the normal and inverted bands in (a) at $B = 10$ T. (c) Calculated DOS oscillations as a function of magnetic field.

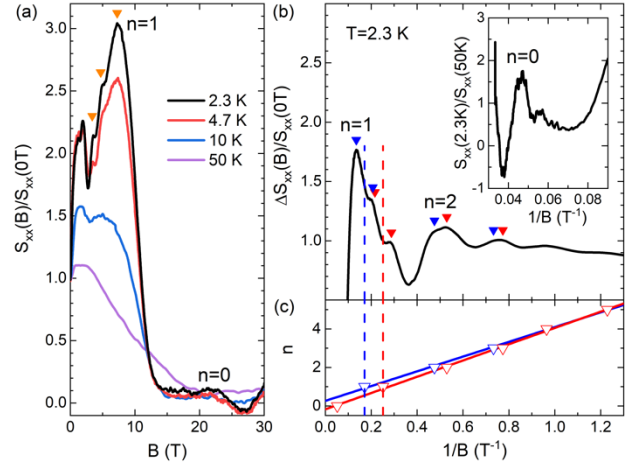


Figure 4: (a) Normalized magneto-thermopower, $S_{xx}(B)/S_{xx}(0)$, measured at different temperatures. The three orange down-triangles indicate the splitting of the $n=1$ peak. (b) Oscillatory component $\Delta S_{xx}(B)/S_{xx}(0)$ as a function of $1/B$ at 2.3 K, obtained by subtracting a linear background from $S_{xx}(B)/S_{xx}(0)$ peak obtained by reference to the high-temperature data at 50 K, $S_{xx}(B)/S_{xx}(0)$. (c) Landau fan diagram of the magneto-thermopower oscillations at 2.3 K. The peak features in (b) are separated into two groups depending on the splitting mechanism and labeled by the red and blue down-triangles, respectively. The dash lines indicate the average positions of additional splittings in the $n=1$ LL, and the solid lines are linear fits to the data of each group.

DOS peaks appear within each $n > 0$ LL for the inverted band while only two peaks for the normal band. The $n = 0$ LL, however, needs a separate discussion. First, it does not split under a magnetic field. Second, for a finite number of electrons, the Fermi level is always above the global minimum of the $n = 0$ LL regardless of the magnitude of B , which is at Γ point for the normal band and ζ point for the inverted band. Therefore, no DOS peak is expected in the $n = 0$ LL of the normal band, whereas one peak for the inverted band (Fig. 3(c)) when the Fermi level is aligned with the Γ point extremum.

Experimentally, we confirm our model predictions using magneto-transport (including magneto-thermopower) measurements on ZrTe₅. Figure 4 summarizes our results of the high-field magneto-thermopower measurements. Both the anomalous $n = 0$ peak and the multiple-fold (at least three-fold) splitting of the $n = 1$ LL are observed. Our work establishes an effective strategy for identifying the band inversion as well as the associated topological phases for future topological materials research.

Future Plans

Probing energy, symmetry and dispersion of low-lying excitations and studying topological phase transitions in novel electronic materials via magneto-optical spectroscopy is a longstanding goal of this program. One of the near-future goals is to provide experimental evidence of the role of Weyl cones tilting on the magnetic field response of realistic Weyl semimetals following theoretical predictions developed in Ref. [7]. We will continue magneto-spectroscopy studies of exotic optically excited states and many-body effects in atomically thin 2D systems with strong spin-orbit coupling and their parent van der Waals crystals. In the next funding period, we also plan to add a new dimension to our arsenal of experimental tools – optical spectroscopy at high pressure, and to enlarge the scope of the project to include layered spin-orbit coupled quantum magnets.

References

1. Y. Jiang et al., Unraveling the Topological Phase of ZrTe₅ via Magnetoinfrared Spectroscopy. *Physical Review Letters* **125**, 046403 (2020).
2. J. Wang et al., Magneto-transport evidence for strong topological insulator phase in ZrTe₅. Under review (2021).
3. H. Weng, X. Dai, Z. Fang, Transition-Metal Pentatelluride ZrTe₅ and HfTe₅: A Paradigm for Large-Gap Quantum Spin Hall Insulators. *Physical Review X* **4**, 011002 (2014).
4. Z. Fan, Q.-F. Liang, Y. B. Chen, S.-H. Yao, J. Zhou, Transition between strong and weak topological insulator in ZrTe₅ and HfTe₅. *Scientific Reports* **7**, 45667 (2017).
5. Q. Li et al., Chiral magnetic effect in ZrTe₅. *Nature Physics* **12**, 550-554 (2016).
6. T. Liang et al., Anomalous Hall effect in ZrTe₅. *Nature Physics* **14**, 451-455 (2018).
7. L. Zhang, Y. Jiang, D. Smirnov, Z. Jiang, Landau quantization in tilted Weyl semimetals with broken symmetry. *J. Appl. Phys.* **129**, 105107 (2021).

Publications

- [1] Zhang L, Jiang Y, Smirnov D, Jiang Z. Landau quantization in tilted Weyl semimetals with broken symmetry. *Journal of Applied Physics*. **129**, 105107 (2021).
- [2] Y. Jiang, J. Wang, T. Zhao, Z. L. Dun, Q. Huang, X. S. Wu, M. Mourigal, H. D. Zhou, W. Pan, M. Ozerov, D. Smirnov and Z. Jiang, Unraveling the Topological Phase of ZrTe₅ via Magneto-infrared Spectroscopy. *Physical Review Letters*. **125**, 046403 (2020).
- [3] Y. Jiang, M. M. Asmar, X. Han, M. Ozerov, D. Smirnov, M. Salehi, S. Oh, Z. Jiang, W.-K. Tse and L. Wu, Electron–Hole Asymmetry of Surface States in Topological Insulator Sb₂Te₃ Thin Films Revealed by Magneto-Infrared Spectroscopy. *Nano Letters*. **20**, 4588 (2020).
- [4] Z. Lu, D. Rhodes, Z. Li, D. Van Tuan, Y. Jiang, J. Ludwig, Z. Jiang, Z. Lian, S.-F. Shi, J. Hone, H. Dery and D. Smirnov, Magnetic field mixing and splitting of bright and dark excitons in monolayer MoSe₂. *2d Materials*. *2d Materials* **7**, 015017 (2020).
- [5] S. Suchalkin, M. Ermolaev, T. Valla, G. Kipshidze, D. Smirnov, S. Moon, M. Ozerov, Z. Jiang, Y. Jiang, S. P. Svensson, W. L. Sarney and G. Belenky, Dirac energy spectrum and inverted bandgap in metamorphic InAsSb/InSb superlattices. *Applied Physics Letters* **116**, 032101 (2020).
- [6] Y. Shao, A. N. Rudenko, J. Hu, Z. Sun, Y. Zhu, S. Moon, A. J. Millis, S. Yuan, A. I. Lichtenstein, D. Smirnov, Z. Q. Mao, M. I. Katsnelson and D. N. Basov, Electronic correlations in nodal-line semimetals. *Nature Physics* **16**, 636 (2020).
- [7] T. Wang, Z. Li, Z. Lu, Y. Li, S. Miao, Z. Lian, Y. Meng, M. Blei, T. Taniguchi, K. Watanabe, S. Tongay, W. Yao, D. Smirnov, C. Zhang and S.-F. Shi, Observation of Quantized Exciton Energies in Monolayer WSe₂ under a Strong Magnetic Field. *Physical Review X* **10**, 021024 (2020).
- [8] T. M. Wang, S. N. Miao, Z. P. Li, Y. Z. Meng, Z. G. Lu, Z. Lian, M. Blei, T. Taniguchi, K. Watanabe, S. Tongay, D. Smirnov and S. F. Shi, Giant Valley-Zeeman Splitting from Spin-Singlet and Spin-Triplet Interlayer Excitons in WSe₂/MoSe₂ Heterostructure. *Nano Letters*. **20**, 694-700 (2020).
- [9] M. K. Hudait, M. Clavel, P. S. Goley, Y. Xie, J. J. Heremans, Y. Jiang, Z. Jiang, D. Smirnov, G. D. Sanders and C. J. Stanton, Structural, morphological and magnetotransport properties of composite semiconducting and semimetallic InAs/GaSb superlattice structure. *Materials Advances*, **1** (5), 1099 (2020).

Title: ER46317: “Spin-Polarized Scanning Tunneling Microscopy Studies of Magnetic, Electronic, and Spintronic Phenomena in Nitride Systems”

PI: Arthur R. Smith

**Address: Ohio University
Nanoscale & Quantum Phenomena Institute
Department of Physics & Astronomy
Athens, OH 45701**

E-mail: smitha2@ohio.edu

1. Program Scope

The scope of this project is to investigate the structural, electronic, and spin properties of nitride-related material systems, in particular magnetic nitrides, magnetic gallium nitrides, and related elemental magnetic materials. The project seeks to explore, image, and even manipulate the ferromagnetic, antiferromagnetic, and ferrimagnetic structures of these material systems. An important goal is to develop these materials as advanced spintronic systems which may have future energy-related applications. In order to probe these systems, this project makes use of scanning tunneling microscopy (STM) and especially spin-polarized STM (SP-STM). The latter is a powerful technique which can provide spin information on surfaces with atomic-scale resolution. Combining ultra-high vacuum SP-STM together with *in-situ* molecular beam epitaxial growth, diverse nitride-related material systems can be explored in a pristine state.

2. Recent Progress

Investigations of the electronic and magnetic properties of manganese-based spintronic structures on wurtzite GaN(0001) surfaces

In our work reported in 2018, we showed the formation of a room-temperature ferromagnetic monolayer material, MnGaN-2D grown on GaN(0001) surface [1]. This work followed from earlier work in which we focused on the detailed atomic-scale structural properties together with first-principles calculations including structural models of the surface structures seen using STM [2,3]. The MnGaN-2D material was prepared using molecular beam epitaxy and involves the deposition of only one-third monolayer of Mn at around 200 degrees C on top of the 1×1 Ga adlayer resulting in the spontaneous formation of MnGaN-2D. Using spin polarized STM, we demonstrated the existence of ferromagnetic domains. Using tunneling spectroscopy, we also showed the presence of two sharp surface state peaks, one for filled states and one for empty states. Comparing to the results from first-principles calculations via our collaborators in Argentina, we showed that these surface states are highly spin-split and spin-polarized. We also demonstrated magnetic hysteresis behavior of the magnetic domains using an applied magnetic field.

Strain effect on electronic properties and perpendicular magnetic anisotropy

In the recent 2 years, we have published 2 additional papers closely related to this project with a 4th in progress. In our 2020 paper, we demonstrated that the same MnGaN-2D surface is not only ferromagnetic but is also has high perpendicular magnetic anisotropy (PMA) as well as a high magnetic moment. But even more interesting behavior is found, namely that this material has

inverse magneto-strictive behavior, which we showed as variations in the energy of the filled-states Mn DOS peak in dI/dV spectroscopy and then via our theoretical collaborators, found that this can be explained as a consequence of lattice strain. The lattice strain calculations considered both isotropic and anisotropic strain models, with different results for each case.

Noncollinear magnetic configurations and substrate-mediated interactions

Our 2021 paper focused on the spin properties of Mn monomers, dimers, and trimers on the same GaN(000 $\bar{1}$) surface. A comparison was made between experimental atomic resolution STM measurements and theoretical calculations in the case of the Mn trimer units which occur in a 3×3 surface lattice (see Fig. 1 at right). With high resolution STM, intra-trimer resolution is seen which agrees ideally with the theoretical result.

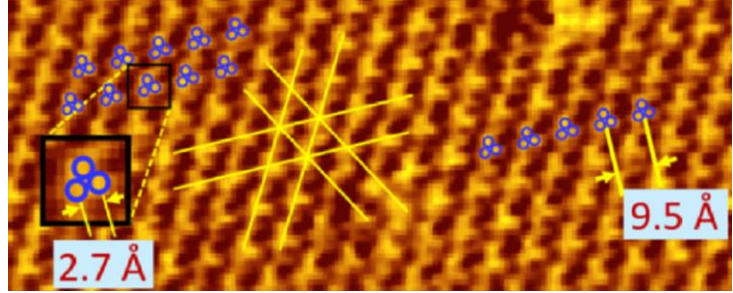


Fig. 1. Mn 3×3 trimer lattice structure on GaN(000 $\bar{1}$). Image in derivative mode with $V_s = -1.21$ V, $I_t = 63$ pA.

The spin structure of the trimers is found theoretically to be antiferromagnetic as opposed to the ferromagnetism of the MnGaN-2D structure in its $\sqrt{3} \times \sqrt{3}$ reconstruction. Our recent publication explores the intra-trimer spin coupling and finds that the 3 spins within the trimer are *in-plane* with the GaN surface and that the 3 spins are at 120° angles to each other. The theoretical investigation exploring the magnetic anisotropy and spin-orbit coupling for isolated Mn monomers and dimers revealed a magnetic anisotropy energy 4 orders of magnitude smaller than the direct exchange coupling energy between neighboring Mn adatoms. Nevertheless, the calculations show that there exist indirect, trimer-trimer interactions leading to an ordered state. To explore this more deeply, our paper reports on the investigation of the long-range coupling between 2 Mn spins placed at a variable distance d_{ij} apart on the GaN surface and mediated by interaction via the two-dimensional GaN surface states. These results are then analyzed as a function of distance, and the results are examined and discussed in terms of a Ruderman-Kittel-Kasuya-Yosida (RKKY)-type interaction.

Surface exchange coupling effect

Work in progress investigates what happens when we deposit an additional layer of Mn atoms on top of the ferromagnetic MnGaN-2D surface. We explore this with high resolution STM and theoretical calculations. The STM images (as seen in Fig. 2) reveal an ordered array of hexagonal protrusions having two rotational orientations offset by $\sim 21^\circ$. We also observe domain boundaries separating different regions of hexagonal domains. These boundaries are bright in empty states images.

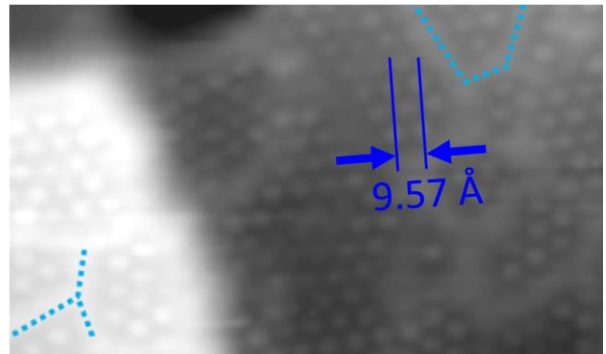


Fig. 2 Mn/MnGaN-2D hexagonal adatom domains separated by domain boundaries. $V_s = +1.75$ V, $I_t = 100$ pA.

We have investigated the magnetic properties of these bilayer surfaces using SQUID magnetometry to find out if the antiferromagnetic Mn atoms on top couple to, or affect somehow, the ferromagnetic MnGaN-2D layer underneath. The results are the focus of our present work and

point to a possible spin compensation effect. Certainly, the results imply that the MnGaN-2D layer remains intact after the Mn deposition.

3. Future Plans

The project presented here is one central line of research of this DOE-supported project which has focused on manganese on gallium nitride spintronic systems. At the same time, over the past several years we have also carried out a variety of different projects including investigating the structural, electronic, and magnetic properties of the Fe/CrN surface/interface, the magnetostrictive $D0_3$ -Fe₃Ga(001) surface, the nitrogen-induced reconstructions of Cr(001) surfaces, and the bilayer $L1_0$ -MnGa/ η - \perp -Mn₃N₂ interface. What is next is that first, we would like to continue to develop and improve our technical capabilities using spin polarized STM to better explore the structural, electronic, and magnetic properties of the nitride surfaces and interfaces down to the atomic scale. This would include being able to resolve some of the antiferromagnetic spin structures presented in section 2, including the spin structure of the 3×3 trimers and the compensated spin structure at and around the Mn adatoms on MnGaN-2D. Ultimately, we hope to be able to resolve, at the atomic scale and as a function of position, the full electronic spectra of magnetic structures such as these, including with spin polarized STM tips down to as low as 1 K with our current low temperature STM system and over a range from 4K – 100K with our variable temperature STM system.

4. References

- [1] A Two-Dimensional Manganese Gallium Nitride Surface Structure Showing Ferromagnetism at Room Temperature, Yingqiao Ma, Abhijit V. Chinchore, Arthur R. Smith, María Andrea Barral, and Valeria Ferrari, *Nano Letters* **18**, 158 (2018).
- [2] Manganese 3×3 and $rt3 \times rt3$ -R30° Structures and Structural Phase Transition on w-GaN(000-1) Studied by Scanning Tunneling Microscopy and First-principles Theory, Abhijit V. Chinchore, Kangkang Wang, Meng Shi, Andrada Mandru, Yinghao Liu, Muhammad Haider, Arthur R. Smith, Valeria Ferrari, Maria Andrea Barral, and Pablo Ordejon, *Physical Review B* **87**, 165426 (2013).
- [3] Atomic Layer Structure of Manganese Atoms on Wurtzite Gallium Nitride (000-1), Abhijit Chinchore, Kangkang Wang, Wenzhi Lin, Jeongihm Pak, and Arthur R. Smith, *Applied Physics Letters* **93**(18), 181908 (2008).

5. Publications of DOE sponsored research (2019-2021)

Papers listed below are shown in reverse chronological order, with the numbering defined based on paper #1 = A.R. Smith's first paper. Full publication list can be seen at:

<http://www.phy.ohiou.edu/~asmith/publist.html>.

104. Investigating the Magnetic and Atomic Interface Configuration for a Model Ferromagnetic/Antiferromagnetic Bilayer, Khan Alam, Rodrigo Ponce-Perez, Kai Sun, Andrew Foley, Noboru Takeuchi, and Arthur R. Smith, Accepted, *Journal of Vacuum Science & Technology A* (2021).
103. Noncollinear magnetic configurations and substrate-mediated interactions in Mn trimers on the GaN(000-1) surface, Diego Hunt, María Andrea Barral, Arthur R. Smith, and Valeria Ferrari, *Physical Review B* **103**, 094418 (2021).
102. Surface structures of magnetostrictive $D0_3$ -Fe₃Ga(001), Ricardo Ruvalcaba, Joseph P. Corbett, Andrada-Oana Mandru, Noboru Takeuchi, Arthur R. Smith, and Jonathan Guerrero-Sanchez, *Applied Surface Science* **553**, 149488 (2021).
101. Local strain-dependent electronic structure and perpendicular magnetic anisotropy of a MnGaN 2D magnetic monolayer, Yingqiao Ma, Diego Hunt, Kengyuan Meng, Tyler Erickson, Fengyuan Yang, María Andrea Barral, Valeria Ferrari, and Arthur R. Smith, *Physical Review Materials* **4**, 064006 (2020).
100. Exchange Bias and Exchange Spring Effects in Fe/CrN Bilayers, Khan Alam, Keng-Yuan Meng, Rodrigo Ponce-Perez, Gregorio H. Cocolletzi, Noboru Takeuchi, Andrew Foley, Fengyuan Yang, and Arthur R. Smith, *Journal of Physics D: Applied Physics* **53**, 125001 (2020).
99. Nitrogen-induced reconstructions on the Cr (001) surface, Emiliano Ventura-Macias*, J. Guerrero-Sánchez, Joseph P. Corbett, Arthur R. Smith, and Noboru Takeuchi, *Applied Surface Science* **484**, 578 (2019).
98. Dislocation Structures, Interfacing, and Magnetism in the L1₀-MnGa on η - \perp -Mn₃N₂ bilayer, J. P. Corbett, J. Guerrero-Sanchez, J. C. Gallagher, A.-O. Mandru, A. L. Richard, D. C. Ingram, F. Yang, N. Takeuchi, and A. R. Smith, *Journal of Vacuum Science & Technology A* **37**, 031102 (2019).

DE-SC0021281: Exploring Nontrivial Topological Superconductivity in 2M WS₂ for Topological Quantum Computation

Jifa Tian¹, John Ackerman², TeYu Chien¹, Brian Leonard³, Jinke Tang¹,

¹Department of Physics & Astronomy, University of Wyoming, Laramie, WY 82071, USA

²Department of Chemical Engineering, University of Wyoming, Laramie, WY 82071, USA

³Department of Chemistry, University of Wyoming, Laramie, WY 82071, USA

Program Scope

This collaborative project aims to: (1) establish the layer-dependence of superconductivity in the newly discovered intrinsic topological superconductor (TSC) 2M WS₂; and (2) identify its clear signatures of Majorana zero modes (MZMs). These aims will be achieved by growing high-quality pure and magnetic-ion doped 2M WS₂ single crystals and preparing their thin layers down to the 2D limit for various measurements, including transport measurements (charge, thermal and spin), scanning tunneling microscopy and spectroscopy (STM/S), and angle-resolved photoemission spectroscopy (ARPES). The project is in collaboration with three national laboratories, including Sandia National Labs (SNL), Argonne National Laboratory (ANL) and Lawrence Berkeley National Lab (LBNL).

Recent Progress

Developed new methods to grow 2M WS₂ bulk crystals.

One of the primary tasks of this project is to obtain pure and large size 2M phase single crystals. In the past year, we have developed new methods to grow pure 2M phase WS₂ single crystals and tried to understand the corresponding reaction pathway.

1) *Obtained pure phase 2M WS₂ single crystals.*

The pure 2M phase WS₂ single crystals have been achieved by two growth methods. The first method is to grow K_{0.7}WS₂ crystals using a direct combination of the elements (with precursors of S, W powder, and K turnings) followed by heating in a thermal gradient at elevated temperatures. Then, the 2M WS₂ crystals can be obtained by deintercalation K ions from the K_{0.7}WS₂ crystals. The second growth method is to first grow Na_xWS₂ crystals by replacing the precursor K with sodium (Na) followed by the growth condition similar to that of growth method one. After the deintercalation of Na ions, we are able to get pure 2M phase WS₂ samples. With the two growth methods, we will have a better understanding of the reaction pathway.

2) *Obtained 1-2 mm sized high-quality 2M WS₂ single crystals.*

We have found that the reaction proceeds through an intercalated hexagonal (2H) WS₂ phase at low temperatures and needs to be annealed at 800-850 °C to achieve the 2M crystal structure. At these temperatures, potassium thermally deintercalates and the structure reverts to the 2H phase. By fine-tuning the synthesis temperature and cooling rate, we can reduce this thermal deintercalation and produce large crystals of the K_xWS₂ phase with the correct 2M crystal structure. So far, we have successfully grown 1-2 mm sized 2M WS₂ crystals.

Identified superconductivity with unconventional pairing symmetry in 2M WS₂ nanolayers

1) Confirmed the diamagnetism below T_C by magnetization measurements.

We have confirmed the Meissner effect of the 2M WS₂ bulk crystals by magnetization measurements using the Physical Property Measurement System. These measurements were performed under both zero-field-cooled condition (ZFC) and field-cooled condition (FC). The Meissner effect was successfully observed with negative magnetization below the superconducting transition temperature T_C, being a clear signature of diamagnetism. The transition temperature determined from this measurement is ~ 6.9 K, which is slightly lower than the reported bulk value. We speculate that the reduced T_C is because the measured bulk sample entirely is not a single crystal but made of a lot of small single crystals.

2) Identified superconductivity in 2M WS₂ thin layers by electrical transport measurements.

Identifying the layer dependence of superconductivity in 2M WS₂ is one focus of the project. Here, the main challenge is that different from other 2H phase 2D materials, the 2M phase WS₂ is extremely difficult to be exfoliated down to the atomic layers. We have successfully developed techniques to obtain 3.5 nm-thick 2M WS₂ layers. We further developed nanofabrication techniques (in collaboration with SNL) to make Hall bar devices on these 2M WS₂ thin layers ranging from 40 to 3.5 nm. Surprisingly, we found that the T_C only varies from 8.75 K to 7.4 K as the thickness decreases from 40 to 3.5 nm.

3) Confirmed the non-conventional pairing symmetry in 2M WS₂ thin layers.

Understanding the pairing symmetry in 2M WS₂ is the key to identifying its non-trivial topological properties. By studying the relationship between the upper critical magnetic field $\mu_0 H_{C2}$ and the corresponding critical temperature T_C, we have found that our data deviates from the standard spin-singlet behavior, suggesting a possible different pairing symmetry (such as the topological superconducting states) of the observed superconductivity in 2M-WS₂. We further analyzed our data using the one-band Werthamer Helfand and Hohenberg (WHH) model, which can perfectly fit our results. To further clarify the possible unconventional superconductivity, more detailed studies have been planned, such as the angle and temperature dependences of the upper critical field $\mu_0 H_{C2}$.

4) Determined superconducting gap of 2M WS₂ thin layers by LTSTM at 4.2 K.

We have successfully measured the dI/dV spectra on the 2M WS₂ thin layers at low temperatures. At 4.2 K, a clear superconducting gap can be observed in the 2M WS₂ thin layers through dI/dV measurements by STM. The superconducting gap is consistent with what has been reported in the literature. This observation provides us strong confidence in the planned experiments – determining T_C as the function of the thickness of the 2M WS₂ flakes.

5) Observed Moiré patterns in 2M WS₂ thin layers by STM.

We have also identified two distinct Moiré patterns. One exhibits as line patterns with a periodicity of ~10 nm and with the same orientation along the “a” axis of the single crystal 2M WS₂. We believed that this moiré pattern might be caused by twisting the first layer 2M WS₂ with respect to the second layer by a certain angle. The second exhibits a hexagonal pattern with a periodicity of ~10 nm. With atomic resolution images taken on top of the layer exhibiting the hexagonal moiré pattern and the layer underneath it, we identified that it is a moiré pattern caused by 1T (top layer)

and 1T' (bottom layer) phase of WS₂. This observation inspired us to further explore the influence of the moiré pattern on superconductivity and topological superconductivity.

Future Plans

In the next period, we plan to focus on the following aims:

- 1) We will continue to develop techniques to grow even larger size 2M WS₂ single crystals, and focus on doping these crystals with alkali metals.
- 2) We will further study the superconductivity on larger size bulk pure and/or alkali metal ions doped 2M WS₂ crystals by electrical transport measurements. On the other hand, we will measure the electrical properties of 2M WS₂ nanolayers down to the monolayer limit. This will allow us to complete the layer dependence of superconductivity in 2M WS₂.
- 3) We plan to perform the ARPES and STM/S measurements on thinner 2M WS₂ flakes. In particular, with these thin flakes, we will identify the thickness dependences of the superconductivity gap size and transition temperature. Furthermore, by applying magnetic fields, low-temperature STM in ANL will be used to study the MZMs.
- 4) We will carry out thermal conductivity and thermal Hall effect measurements on the bulk 2M WS₂ single crystals.

Publications

(I) Exclusively funded by this grant;

1. Samarawickrama, P.; Dulal, R.; Fu, Z.; Erugu, U.; Wang, W.; Ackerman, J.; Leonard, B.; Tang, J.; Chien, T.; Tian, J. Two-Dimensional 2M-WS₂ Nanolayers for Superconductivity. *ACS Omega* **2021**, 6, (4), 2966-2972.

(II) Jointly funded by this grant and other grants with leading intellectual contribution from this grant;

2. Fu, Z.; Hill, J. W.; Parkinson, B.; Hill, C. M.; Tian, J., Layer and Material Type Dependent Photoresponse of WSe₂/WS₂ Vertical Heterostructures. Submitted.

(II) Jointly funded by this grant and other grants with relatively minor intellectual contribution from this grant;

3. Ding, J.; Liu, C.; Kalappattil, V.; Zhang, Y.; Mosendz, O.; Erugu, U.; Yu, R.; Tian, J.; DeMann, A.; Field, S. B.; Yang, X.; Ding, H.; Tang, J.; Terris, B.; Fert, A.; Chen, H.; Wu, M. Switching of a Magnet by Spin-Orbit Torque from a Topological Dirac Semimetal. *Adv. Mater.* **2021**, 33, (23), 2005909.
4. Tian, J.; Şahin, C.; Miotkowski, I.; Flatté, M. E.; Chen, Y. P. Opposite current-induced spin polarizations in bulk-metallic Bi₂Se₃ and bulk-insulating Bi₂Te₂Se topological insulator thin flakes. *Physical Review B* **2021**, 103, (3), 035412.
5. Tian, J.; Jauregui, L. A.; Wilen, C. D.; Rigosi, A. F.; Newell, D. B.; McDermott, R.; Chen, Y. P., A Josephson Junction with h-BN Tunnel Barrier: Observation of Low Critical Current Noise. *J. Phys.: Condens. Matter* In revision.

6. Zhang, Y.; Kalappattil, V.; Liu, C.; Zhang, S. S.-L.; Ding, J.; Erugu, U.; Tian, J.; Tang, J.; Wu, M., Large Magneto-Electric Resistance in the Topological Dirac Semimetal α Sn. 2021; p arXiv:2107.03472. Submitted.

Magneto-electronic phenomena due to quantum magnetization fluctuations

Sergei Urazhdin, Emory University

Program Scope

The goal of the current program has been to elucidate the purely quantum aspects of magnetism and magneto-electronic phenomena such as spin transfer (ST), i.e. the aspects that cannot be described in terms of the classical vector of magnetization and/or semiclassical magnetic dynamics described by spin waves. Experimental measurements have focused on thin ferromagnetic (F) films. They utilized anomalous Hall effect and/or anomalous magnetoresistance effects to detect the magnetization states, at frequencies extending from dc to the microwave range to characterize resonant magnetization dynamics. Since very little theoretical work has explored these effects, and in conjunction with the COVID-related shutdown of experimental labs, the project has also included simulations and conceptual development based on non-classical models of magnetic systems and of their interaction with spin-polarized transport electrons. In the process of analyzing dc magneto-electronic signals, the project has also uncovered hitherto unexplored non-equilibrium current-induced phonon states in nanostructures, which resulted in two publications on this subject.

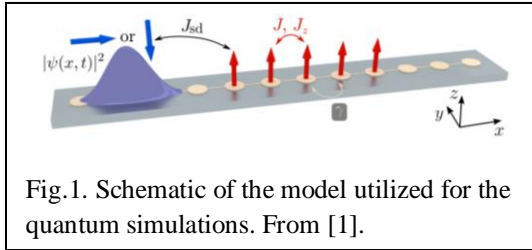


Fig.1. Schematic of the model utilized for the quantum simulations. From [1].

Recent Progress

One-dimensional (1d) tight-binding model of ST was developed. It included a chain of exchange-coupled quantum spins-1/2 interacting with a propagating electronic wave packet via s-d exchange interaction

[Fig.1]. This model theoretically addressed one of the central questions posed by the project, namely the role of the quasiparticle energy and momentum conservation in ST. Simulations showed that the energies and the momenta of magnons generated by ST are determined by these conservation

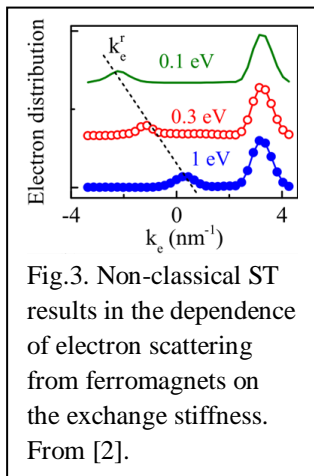


Fig.3. Non-classical ST results in the dependence of electron scattering from ferromagnets on the exchange stiffness. From [2].

laws neglected in semiclassical models [Fig.2], and therefore the semiclassical approximation is not sufficient to determine the frequency and the amplitude of ST-induced magnetization dynamics. One of several significant consequences is the dependence of ST and electron scattering by F on their exchange stiffness [Fig.3], which does not appear in the semiclassical models of ST.

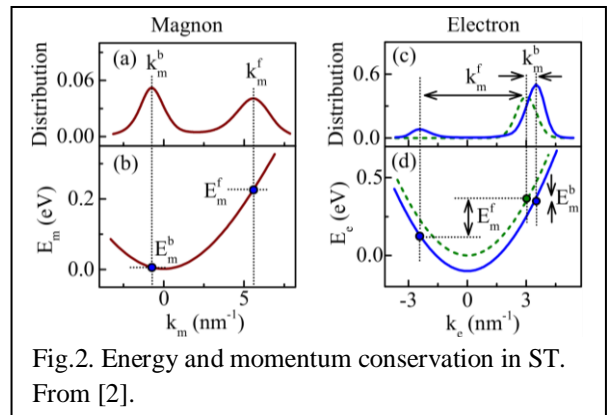


Fig.2. Energy and momentum conservation in ST. From [2].

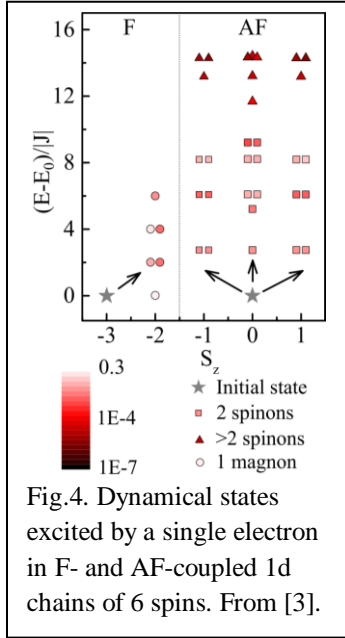


Fig.4. Dynamical states excited by a single electron in F- and AF-coupled 1d chains of 6 spins. From [3].

Analysis of antiferromagnets (AFs) predicted even larger non-classical ST effects. Spin angular momentum conservation dictates that a single electron can excite only one-magnon states in F, e.g. 6 such states for a chain of 6 atoms in Fig.4. On the other hand, a multitude of spin-conserving many-quasiparticle excitations are possible in AFs due to the existence of excitations with different spins [Fig.4]. Only a small fraction of these excitations are semiclassical. As a consequence, semiclassical approximation vastly under-estimates ST effects, as illustrated in Fig.5 by the comparison of the fully quantum [solid curves] vs semi-classical [dashed] predictions for an AF-coupled chain as a function of the AF ordering stabilized by a staggered field, for two spin

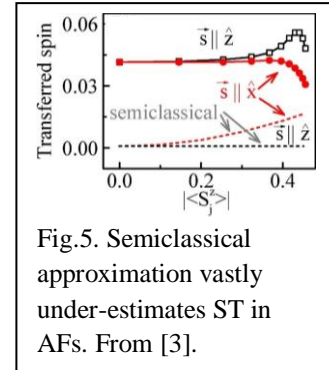


Fig.5. Semiclassical approximation vastly under-estimates ST in AFs. From [3].

polarizations of the scattered electron.

Measurements. One of the salient features of non-classical magnetization states is the modulation

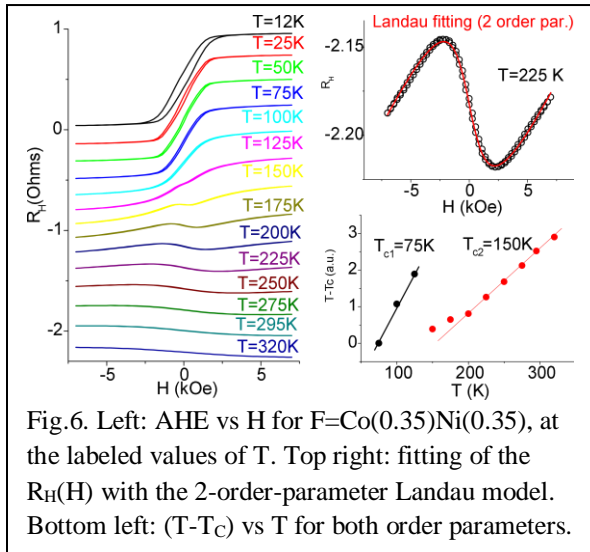


Fig.6. Left: AHE vs H for F=Co(0.35)Ni(0.35), at the labeled values of T. Top right: fitting of the $R_H(H)$ with the 2-order-parameter Landau model. Bottom left: $(T-T_C)$ vs T for both order parameters.

of the expectation value of magnetization due to the quantum interference between the spin wavefunction components. The experimental measurements focused on thin F films where the Curie temperature T_C is suppressed due to the finite size effects. The magnitude of magnetization varies from zero above T_C to a large saturation value sufficiently below T_C , and may thus be expected to be easily

modulated by external perturbations, if non-classical ST effects are indeed significant.

Figure 6 shows the dependences of anomalous Hall effect (AHE) resistance R_H on field H for a representative Ta(3)Pt(3)Cu(0.5)Co(0.35)Ni(0.35)Ta(3) structure, at temperatures T ranging from 12K to 320K. Here, number are thicknesses in nanometers. The dependence is almost linear at high T, as expected for

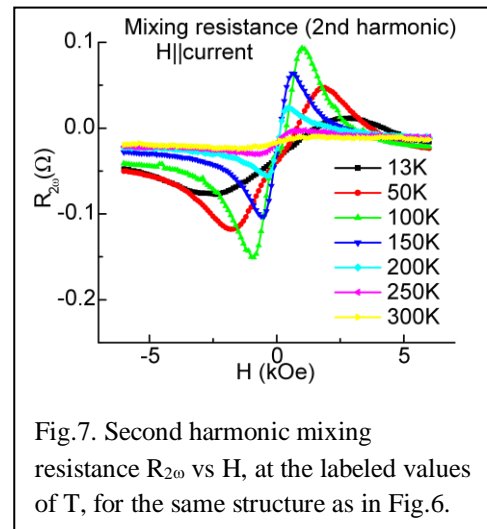


Fig.7. Second harmonic mixing resistance $R_{2\omega}$ vs H, at the labeled values of T, for the same structure as in Fig.6.

the paramagnetic state. At smaller T, the curves become nonlinear, and a hysteresis emerges at $T < 50\text{K}$, as expected for the ferromagnetic state below the Curie temperature T_C . All of the data are well fitted by the Landau theory of magnetism (top right panel), but the fitting requires two order parameters, with different transition temperatures (bottom right panel) $T_{c1}=75\text{K}$ and $T_{c2}=150\text{K}$. T_{c1} is the Curie temperature for the onset of ferromagnetism, but there is no spontaneous magnetism below T_{c2} , because the corresponding amplitude vanishes above T_{c2} .

The significance of non-classical ST effects is demonstrated by the second harmonic mixing resistance $R_{2\omega}$ measured on the film patterned into a micron-scale Hall bar, Fig.7, with \mathbf{H} oriented in-plane parallel to the current I applied to the bar. The mixing signal originates from the current-induced oscillation of magnetization, consistent with the effects of damping-like spin torque. However, large signals persist far above the Curie temperature, where according to Fig.6 the magnetization is very small at the characteristic applied fields. This demonstrates that injection of spin current substantially modulates the magnetization. This is expected for non-classical ST effects, but not from the classical spin torque.

The existence of two order parameters and the observed non-classical ST effects can be interpreted in terms of the correlated hole states that likely become dominant in ultrathin films due to the band narrowing with decreased atomic coordination. The ansatz

$|\psi_{S\uparrow}\rangle = \frac{1}{\sqrt{2}}(|\uparrow, \uparrow\rangle(|L, -L\rangle - |-L, L\rangle)$, $|\psi_{S0}\rangle = \frac{1}{2}(|\uparrow, \downarrow\rangle + |\downarrow, \uparrow\rangle)(|L, -L\rangle - |-L, L\rangle)$, $|\psi_{S\downarrow}\rangle = \frac{1}{\sqrt{2}}|\downarrow, \downarrow\rangle(|L, -L\rangle - |-L, L\rangle)$ describes two-hole correlations minimizing the kinetic and the Coulomb energy of holes at the neighboring atomic sites, and can be interpreted as a spin triplon. A similar ansatz can be written for the orbital triplon. The two observed phase transitions correspond to the condensation of the two types of triplons, while the non-classical ST effects - as Larmor precession of spin triplons injected due to the spin Hall effect.

Future Plans

It is planned to explore the correlated-electron physics and the interplay between spin and orbital electron degrees of freedom, by utilizing the following approaches.

Ferromagnetic heterostructures with different ferromagnetic and non-magnetic materials will be explored by the same magnetoelectronic techniques as described above to test the role of electron doping on the magnetic properties. Among the proposed ferromagnets will be alloys of Fe with Co (including FeCoB extensively used in applications), and Fe with Ni whose relative elemental concentrations will be varied to test the effects of d-level filling. The proposed nonmagnetic layers interfacing with F will include nonmagnetic 3d, 4d, and 5 d transition metals, with the column varied (e.g. from Ti to Zn for 3d) to test the effects of the electron filling on correlations, and the row varied to explore the effects of spin-orbit variations that increase from 3d to 5d.

Dynamical measurements of magnetic resonance will be performed to establish the g-factors, which will provide direct evidence for orbital magnetism (g-factor =1 for pure orbital

magnetism, $g > 2$ for the predominantly spin magnetism, with some orbital contribution in late transitional metals). Since the relative roles of orbital vs spin magnetism are dependent on the external field, the standard approach to magnetic resonance measurements, which utilizes a field sweep at a fixed frequency, will not be useful. Instead, an approach based on frequency sweep at a fixed field will be developed, which will require analysis and optimization of frequency-dependent signal transmission.

To elucidate the microscopic origins of the observed phenomena, field- and temperature-dependent magneto-optical Kerr effect (MOKE) measurements will be performed by utilizing a custom variable-temperature MOKE system developed over the current project period. Preliminary measurements show that MOKE is completely insensitive to the orbital magnetism, but exhibits a surprising decrease of response at large fields (see Fig.8), which is likely associated with the reduction of spin magnetization due to the spin-orbit interaction with the orbital magnetization.

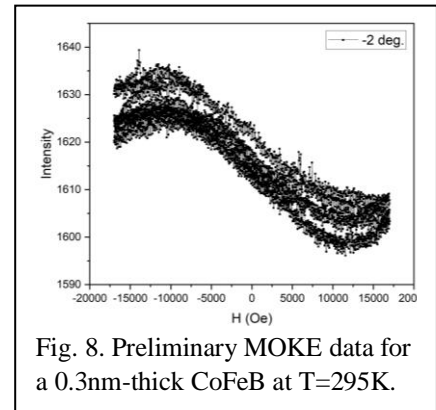


Fig. 8. Preliminary MOKE data for a 0.3nm-thick CoFeB at T=295K.

A microscopic two-orbital Hubbard model for the proposed phenomena will be developed and analyzed numerically and/or analytically. Because of the large size of Hilbert space, simulations will be limited to 2-4 sites, which may be sufficient to capture the essence of the observed phenomena. For larger systems, the possibility to develop a two-particle mean-field model, similar to BCS, will be also explored.

Beyond orbital/spin ferromagnetism, the proposed correlated-electron picture suggests a broad range of novel phenomena in thin transition-metal films. The planned research will focus on two materials: β -Ta and Mn. The d-shell of Mn is half-filled. According to the Mott criterion, it is expected to become an insulator for sufficiently small hopping, which can be achieved when the thickness of the film is sufficiently small.

β -Ta is known as a “strange” metal due to its resistivity decrease with T. The hypothesis to be tested is that its electronic properties can be approximated as a glassy state of nonlocal j-singlets. If the effective crystalline field of interfaces in thin films becomes dominant, this state is expected to transform into an antiferromagnetic order with perpendicular anisotropy, which is expected to become manifested as exchange bias in bilayers with ferromagnets.

References

- [1] P. Mondal et al, PRB **99**, 094431 (2019).
- [2] A. Mitrofanov and S. Urazhdin, Phys. Rev. B **102**, 184402 (2020).
- [3] A. Mitrofanov and S. Urazhdin, “Non-classical spin transfer effects in an antiferromagnet”, Phys. Rev. Lett. **126**, 037203 (2021).

Publications

1. G. Chen and S. Urazhdin, “Transport and relaxation of current-generated nonequilibrium phonons from nonlocal electronic measurements”, arXiv:2107.04634 (2021).
2. D. Ksenzov et al. “Nanoscale transient gratings of magnetization excited and probed by femtosecond extreme ultraviolet pulses”, Nano Letters 21, 2905 (2021)
3. N. Tramsen, A. Mitrofanov and S. Urazhdin, “Effects of the dynamical magnetization state on spin transfer”, Phys. Rev. B, 103, 134415 (2021)
4. A. Mitrofanov and S. Urazhdin, “Non-classical spin transfer effects in an antiferromagnet”, Phys. Rev. Lett.126, 037203 (2021)
5. A. Mitrofanov and S. Urazhdin, “Energy and momentum conservation in spin transfer”, Phys. Rev. B 102, 184402 (2020)
6. G.X. Chen, D. Collette, S. Urazhdin “Experimental demonstration and analysis of random field effects in ferromagnet/antiferromagnet bilayers”, Phys. Rev. B 101, 144427 (2020)
7. G.X. Chen, R. Freeman, A. Zholud, S. Urazhdin “Observation of anomalous non-Ohmic transport in current-driven nanostructures”, Phys. Rev. X 10, 011064 (2020).

Van der Waals Heterostructures: Novel Materials and Emerging Phenomena

Feng Wang, Michael Crommie, Steven G. Louie, Zi Q. Qiu, Mike Zaletel, Alex Zettl

Materials Science Division, LBNL

Program Scope

This program aims to exploit extraordinary new scientific opportunities enabled by designing van der Waals (vdW) heterostructures that allow creation of novel functional materials with unprecedented flexibility and control. We will explore a variety of quantum phenomena in these systems, ranging from 2D magnetism and spin liquids to moiré physics and exciton Bose-Einstein condensates in van der Waals heterostructures. The proposed objectives will be achieved by an integrated team effort combining materials development, advanced experimental characterization, and state-of-the-art theoretical calculations.

Recent Progress: Observation and Imaging of Wigner Crystals in WS₂/WSe₂ moiré heterostructures

Moiré superlattices offer a general and powerful way to engineer correlated electronic states in van der Waals heterostructures. Consider a simplified but highly informative toy model: a 2D electron gas in a periodic potential of periodicity L . The periodic potential leads to the formation a set of minibands in the electron bandstructure. The on-site Coulomb potential U and the electronic bandwidth W of the lowest electronic miniband can be estimated as $U \sim \frac{e^2}{\epsilon L}$ and $W \sim \frac{\hbar^2 k^2}{2m_e^*} \sim \frac{\hbar^2}{2m_e^* L^2}$, and the ratio U/W scales linearly with $m_e^* L$. Here ϵ is the effective dielectric constant and m_e^* the electron effective mass. Strong correlation (with $U/W > 1$) can be readily achieved with sufficiently large $m_e^* L$, for example, with a moiré superlattice ($L \sim 10\text{nm}$) and an effective mass $m_e^* > 0.1m_0$ for $\epsilon \sim 10$. The design criteria of large $m_e^* L$ can be satisfied in many moiré heterostructures. One successful instance is the ABC trilayer graphene/boron nitride moiré

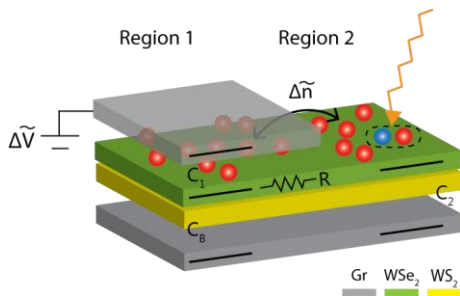


Fig. 1. Optically detected resistance and capacitance (ODRC) technique. The speed and magnitude of the charge redistribution is measured optically, which can be used to determine the RC constant and the quantum capacitance.

superlattice, which exhibits tunable Mott insulator, superconductor, and correlated Chern insulator states [1, 2, 3]. TMDC heterostructures represent another intriguing platform: the large effective mass ($m_e^* \sim 0.5m_0$) of TMDCs can lead to particularly strong correlation effects, and the strong light-matter interaction in TMDCs can enable optical detection and manipulation of the correlated quantum states of matter.

In a collaborative research led by Wang, Zettl, and Crommie, we observed for the first time

the Mott insulator and Wigner crystal states in a semiconducting WSe_2/WS_2 moiré superlattice. [4] Taking advantage of TMDCs' strong light-matter interactions, we developed a novel spectroscopy technique that enables optical detection of quantum capacitance and electrical resistance (ODRC) of the moiré heterostructure. Figure 1 illustrates this ODRC technique, where the dynamic change of charge distribution induced by a local gate is detected by spatially and temporally resolved spectroscopy. This ODRC technique avoids complications from bad electrical contact typical of TMDC moiré superlattices.

Using the ODRC technique, we show that the WS_2/WSe_2 moiré superlattice exhibit a pronounced resistance peak the hole filling factor $\nu = 1$ (i.e. 1 hole per superlattice unit cell, SUC) (Fig. 2a, 2b). This is a hallmark of the Mott insulating state, which persists exist up to 45 K in WSe_2/WS_2 moiré superlattices.

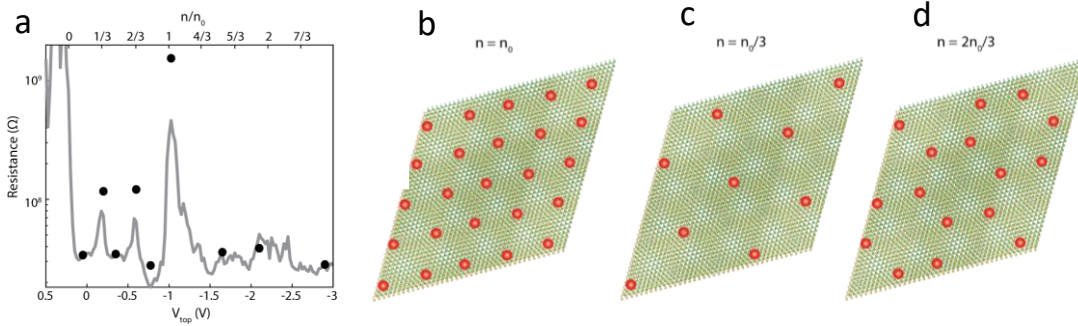


Fig. 2. Mott and Wigner crystal states. (a) Resistance as a function of hole doping in the WS_2/WSe_2 moiré heterostructure. The pronounced resistance peak at $\nu=1$ is from the Mott insulator state. The resistance peaks at $\nu= 1/3$ and $2/3$ are attributed to generalized Wigner crystal states. (b) Illustration of the Mott insulator state. (c) and (d) Illustrations of the $\nu= 1/3$ and $2/3$ Wigner crystal states, respectively.

Surprisingly, we also observe additional Wigner transitions at fractional filling factors $\nu = 1/3$ and $2/3$. (Fig. 1b) Such insulating state at fractional fillings of the lattice sites cannot be described by a Mott insulator or Hubbard model with only on-site repulsion energy. We attribute these insulating states at $\nu = 1/3$ and $\nu = 2/3$ generalized Wigner crystal states in the TMDC moiré superlattice. Figure 2c and 2d illustrate the real-space configurations of such Wigner crystal states, where holes try to avoid not only double-occupation in one site, but also simultaneous occupation of adjacent sites. The emergence of these zero-field Wigner crystal states suggests strong inter-site (long-range) interactions in the TMDC moiré superlattice, confirming the very strong correlation in the system.

To conclusively demonstrate the Wigner crystal states, it is desirable to directly image the correlated electron lattice directly. However, such direct observation of the 2D Wigner crystal lattice have proved a daunting challenge ever since the Wigner crystal was first proposed nearly 90 years ago. Scanning tunneling microscopy (STM) in principle has sufficient spatial resolution

to image a Wigner crystal, but conventional STM measurements can potentially alter fragile Wigner crystal states in the process of measurement.

In another collaborative effort lead by Crommie and Wang, we developed a novel non-invasive STM spectroscopy technique for imaging delicate electron lattices. In this new technique, we employ a monolayer graphene in close proximity to the WSe_2/WS_2 moiré superlattice as a sensing layer, where the local STM tunneling current into the graphene sensing layer is modulated by the underlying electron lattice of the Wigner crystal in the WSe_2/WS_2 heterostructure. Figure 3a illustrates the mechanism of this new non-invasive STS spectroscopy.

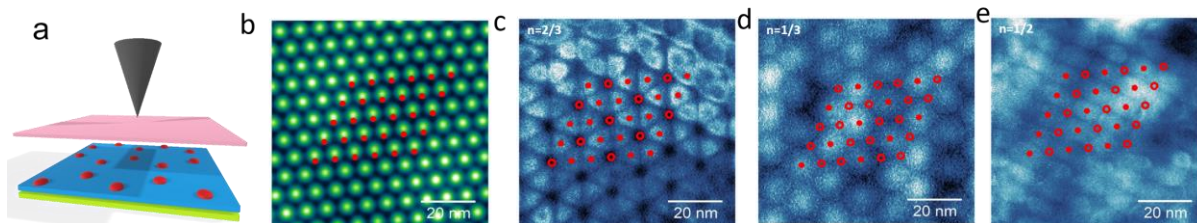


Fig. 3. (a) A monolayer graphene near the WS_2/WSe_2 moiré superlattice acts as a sensing layer for noninvasive STS of the Wigner crystal states. (b) STM topography image of the WSe_2/WS_2 moiré superlattice. Solid red dots show moiré sites that can host electrons. (c,d,e) Differential conductivity maps for Wigner crystal states having $\nu = 2/3$, $\nu = 1/3$, and $\nu = 1/2$, respectively. Solid red dots show locations of electrons, while hollow circles represent electron-empty sites.

Using this new Our measurement directly visualizes different lattice configurations associated with Wigner crystal states at fractional electron fillings of $\nu = 1/3$, $1/2$, and $2/3$ (Fig. 3c-e). [5] The $\nu=1/3$ and $\nu=2/3$ Wigner crystals are observed to exhibit a triangle and a honeycomb lattice, respectively, in order to minimize nearest-neighbor occupations. The $\nu = 1/2$ state, on the other hand, spontaneously breaks the original C_3 symmetry and forms a stripe structure in real space. Our study lays a solid foundation toward the fundamental understanding of rich Wigner crystal states in WSe_2/WS_2 moiré heterostructures. Furthermore, this new STM technique is generally applicable to imaging novel correlated electron lattices in different van der Waals moiré heterostructures.

Future Plans

We propose to further explore novel strongly correlated electron phases in 2D TMD Moiré superlattices.

(1) We will use the novel non-invasive STS technique to quantitative understand the different Wigner crystal phases in different TMD moiré heterostructures. In addition to the more robust $1/3$, $2/3$, and $1/2$ fillings, we will image Wigner crystals at other fractional fillings. We will examine the effect of atomic defects on the local Wigner crystal structures. We will investigate how the rotational symmetry gets broken in some of the Wigner crystal states and their coupling

to local strain. Furthermore, we will examine the real-space evolution of the metal-insulator phase transition when charge carrier are doped into the Wigner crystal states.

(2) We will explore other novel correlated phases that can emerge in the TMD moire superlattices, such as exciton insulators and correlated Chern insulators, by combining electrical transport, optical spectroscopy, scanning probe spectroscopy, and advanced theoretical calculations.

References

1. Chen, G., Jiang, L., Wu, S. *et al.* Evidence of a gate-tunable Mott insulator in a trilayer graphene moiré superlattice. *Nat. Phys.* 15, 237–241 (2019). <https://doi.org/10.1038/s41567-018-0387-2>
2. Chen, G., Sharpe, A.L., Gallagher, P. *et al.* Signatures of tunable superconductivity in a trilayer graphene moiré superlattice. *Nature* 572, 215–219 (2019). <https://doi.org/10.1038/s41586-019-1393-y>
3. Chen, G., Sharpe, A.L., Fox, E.J. *et al.* Tunable correlated Chern insulator and ferromagnetism in a moiré superlattice. *Nature* 579, 56–61 (2020). <https://doi.org/10.1038/s41586-020-2049-7>
4. Regan, E.C., Wang, D., Jin, C. *et al.* Mott and generalized Wigner crystal states in WSe₂/WS₂ moiré superlattices. *Nature* 579, 359–363 (2020). <https://doi.org/10.1038/s41586-020-2092-4>
5. H. Li*, S. Li*, *et al.* “Imaging Two-dimensional Generalized Wigner Crystals,” To appear on *Nature*.

Publications

1. Brian Shevitski, Søren Ulstrup, Roland J. Koch, Hui Cai, Sefaattin Tongay, Luca Moreschini, Chris Jozwiak, Aaron Bostwick, Alex Zettl, Eli Rotenberg, and Shaul Aloni. Tunable electronic structure in gallium chalcogenide van der Waals compounds Phys.Rev.B 100, 165112 (2019) doi:10.1103/PhysRevB.100.165112
2. Wu Shi, Salman Kahn, Lili Jiang, Sheng-Yu Wang, Hsin-Zon Tsai, Dillon Wong, Takashi Taniguchi, Kenji Watanabe, Feng Wang, Michael F. Crommie & Alex Zettl Reversible writing of high-mobility and high-carrier-density doping patterns in two-dimensional van der Waals heterostructures. Nature Electronics (2020) doi: 10.1038/s41928-019-0351-x
3. Amin Azizi, Mehmet Dogan, Jeffrey D. Cain, Rahmatollah Eskandari, Xuanze Yu, Emily C. Glazer, Marvin L. Cohen, and Alex Zettl Frustration and Atomic Ordering in a Monolayer Semiconductor Alloy. Phys. Rev. Lett. 124, 096101 (2020) doi: 10.1103/PhysRevLett.124.096101
4. Emma C. Regan, Danqing Wang, Chenhao Jin, M. Iqbal Bakti Utama, Beini Gao, Xin Wei, Sihan Zhao, Wenyu Zhao, Kentaro Yumigeta, Mark Blei, Johan Carlstroem, Kenji Watanabe, Takashi Taniguchi, Sefaattin Tongay, Michael Crommie, Alex Zettl, Feng Wang Mott and generalized Wigner crystal states in WSe₂/WS₂ moiré superlattices. Nature 579, 359-363 (2020) doi: 10.1038/s41586-020-2092-4
5. N. Gao, S. -G. Je, M. -Y. Im, J. W. Choi, M. Yang, Q. Li, T. Y. Wang, S. Lee, H. -S. Han, K. -S. Lee, W. Chao, C. Hwang, J. Li, and Z. Q. Qiu, “Creation and annihilation of topological meron pairs in a continuous ferromagnetic film”, Nat. Commun. 10, 5603 (2019).
6. Yi Chen, Wei Ruan, Meng Wu, Shujie Tang, Hyejin Ryu, Hsin-Zon Tsai, Ryan Lee, Salman Kahn, Franklin Liou, Caihong Jia, Oliver R. Albertini, Hongyu Xiong, Tao Jia, Zhi Liu, Jonathan A. Sobota, Amy Y. Liu, Joel E. Moore, Zhi-Xun Shen, Steven G. Louie, Sung-Kwan Mo, and Michael F. Crommie. “Strong Correlations and Orbital Texture in Single-Layer 1T-TaSe₂”, *Nature Physics* **16**, 218 (2020).
7. Q. Li, M. Yang, C. Klewe, P. Shafer, A. T. N'Diaye, D. Hou, T. Y. Wang, N. Gao, E. Saitoh, C. Hwang, R. J. Hicken, J. Li, E. Arenholz, and Z. Q. Qiu, “Coherent ac spin current transmission across an antiferromagnetic CoO insulator”, Nat. Commun. 10, 5265 (2019).
8. Q. Li, M. Yang, A. T. N'Diaye, C. Klewe, P. Shafer, N. Gao, T. Y. Wang, E. Arenholz, Xixiang Zhang, C. Hwang, J. Li, and Z. Q. Qiu, “Chirality switching of antiferromagnetic spiral wall and its consequence on magnetic anisotropy”, Phys. Rev. Mat. 3, 114415 (2019).
9. E. Gaufres, F. Fossard, V. Gosselin, L. Sponza, F. Ducastelle, Z. L. Li, S. G. Louie, R. Martel, M. Cote, and A. Loiseau, “Momentum-Resolved Dielectric Response of Free-Standing Mono-, Bi-, and Trilayer Black Phosphorus,” Nano Lett. 19, 8303 (2019).
10. Mengmeng Yang, Qian Li, Rajesh V. Chopdekar, Camelia Stan, Stefano Cabrini, Jun Woo Choi, Sheng Wang, Tianye Wang, Nan Gao, Andreas Scholl, Nobumichi Tamura, Chanyong Hwang, Feng Wang, Ziqiang Qiu, Highly enhanced curie temperature in ga-implanted fe₃gete₂ van der waals material, *ADVANCED QUANTUM TECHNOLOGIES*, n/a(n/a), 2000017 doi:10.1002/qute.202000017

11. Nanoscale Conductivity Imaging of Correlated Electronic States in WSe₂/WS₂ Moiré Superlattices, Zhaodong Chu, Emma C. Regan, Xuejian Ma, Danqing Wang, Zifan Xu, M. Iqbal Bakti Utama, Kentaro Yumigeta, Mark Blei, Kenji Watanabe, Takashi Taniguchi, Sefaattin Tongay, Feng Wang, and Keji Lai, *Phys. Rev. Lett.* 125, 186803 (2020)
12. Nick Bultinck, Eslam Khalaf, Shang Liu, Shubhayu Chatterjee, Ashvin Vishwanath, and Michael P. Zaletel, Ground State and Hidden Symmetry of Magic-Angle Graphene at Even Integer Filling. *Phys. Rev. X* 10, 031034 (2020)
13. Shubhayu Chatterjee, Nick Bultinck, Michael P Zaletel, Symmetry breaking and skyrmionic transport in twisted bilayer graphene. *Phys. Rev. B* 101, 165141 (2020)
14. Nick Bultinck, Shubhayu Chatterjee, and Michael P. Zaletel, Mechanism for Anomalous Hall Ferromagnetism in Twisted Bilayer Graphene, *Physical Review Letters* 124, 166601 (2020)
15. Hongyuan Li*, Shaowei Li*, Mit H. Naik, Jingxu Xie, Xinyu Li, Emma Regan, Danqing Wang, Wenyu Zhao, Kentaro Yumigeta, Mark Blei, Takashi Taniguchi, Kenji Watanabe, Sefaattin Tongay, Alex Zettl, Steven G. Louie, Michael F. Crommie and Feng Wang. Imaging local discharge cascades for correlated electrons in WS₂/WSe₂ moiré superlattices. *Nature Physics* (2021). <https://doi.org/10.1038/s41567-021-01324-x>
16. Hongyuan Li*, Shaowei Li*, Mit H. Naik*, Jingxu Xie, Xinyu Li, Jiayin Wang, Emma Regan, Danqing Wang, Wenyu Zhao, Sihan Zhao, Salman Kahn, Kentaro Yumigeta, Mark Blei, Takashi Taniguchi, Kenji Watanabe, Sefaattin Tongay, Alex Zettl, Steven G. Louie, Feng Wang, and Michael F. Crommie. Imaging moiré flat bands in three-dimensional reconstructed WSe₂/WS₂ superlattices. *Nature Materials* 20, 945–950 (2021). <https://doi.org/10.1038/s41563-021-00923-6>
17. Zhaodong Chu*, Emma C. Regan*, Xuejian Ma, Danqing Wang, Zifan Xu, M. Iqbal Bakti Utama, Kentaro Yumigeta, Mark Blei, Kenji Watanabe, Takashi Taniguchi, Sefaattin Tongay, Feng Wang, and Keji Lai. Nanoscale conductivity imaging of correlated electronic states in WSe₂/WS₂ moiré superlattices. *Physical Review Letters* 125, 186803 (2020). <https://journals.aps.org/prl/abstract/10.1103/PhysRevLett.125.186803>
18. M. Yang, Q. Li, R. V. Chopdekar, C. Stan, S. Cabrini, J. W. Choi, S. Wang, T. Y. Wang, N. Gao, A. Scholl, N. Tamura, C. Hwang, F. Wang, and Z. Q. Qiu, “Highly enhanced Curie temperature in Ga-implanted Fe₃GeTe₂ van der Waals material”, *Adv. Quan. Tech.*, 202000017 (2020).
19. Christoph Klewe, Qian Li, Mengmeng Yang, Alpha T. N’Diaye, David M. Burn, Thorsten Hesjedal, Adriana I. Figueroa, Chanyong Hwang, Jia Li, Robert J. Hicken, Pádraic Shafer, Elke Arenholz, Gerrit van der Laan & Ziqiang Qiu, “Element- and Time-Resolved Measurements of Spin Dynamics Using X-ray Detected Ferromagnetic Resonance”, *Synchrotron Radiation News* 33, 12 (2020).
20. Senfu Zhang, Junwei Zhang, Yan Wen, Yong Peng, Ziqiang Qiu, Takao Matsumoto, and Xixiang Zhang, “Deformation of Neel-type skyrmions revealed by Lorentz transmission electron microscopy”, *Appl. Phys. Lett.* 116, 142402 (2020).
21. Maciej Dabrowski, Takafumi Nakano, David M. Burn, Andreas Frisk, David G. Newman, Christoph Klewe, Qian Li, Mengmeng Yang, Pádraic Shafer, Elke Arenholz, Thorsten Hesjedal, Gerrit van der Laan, Zi Q. Qiu, and Robert J. Hicken, “Coherent transfer of spin angular momentum by evanescent spin waves within antiferromagnetic NiO”, *Phys. Rev. Lett.* 124, 217201 (2020).
22. M. Yang, Q. Li, D. Hou, P. Shafer, A. T. N’Diaye, C. Klewe, T. Y. Wang, Xixiang Zhang, C. Hwang and Z. Q. Qiu, “Independence of spin current on Néel vector orientation in antiferromagnet CoO”, *Phys. Rev. B* 101, 224418 (2020).

23. Yu Yang, Jianhui Liang, Qian Li, Gong Chen, Chao Zhou, Jia Xu, Lu Sun, Mengmeng Yang, Alpha T. N'Diaye, Ziqiang Qiu, and Yizheng Wu, “Antiferromagnetic domain switching modulated by an ultrathin Co interlayer in the Fe/Co/CoO/MgO(001) system”, *Phys. Rev. B* 102, 024434 (2020).
24. M. Yang, Q. Li, R. V. Chopdekar, R. Dhall, J. Turner, J. D. Carlstroem, C. Ophus, C. Klewe, P. Shafer, A. T. N'Diaye, J. W. Choi, G. Chen, Y. Z. Wu, C. Hwang, F. Wang, and Z. Q. Qiu, “Coupling induced skyrmions in van der Waals ferromagnet Fe₃GeTe₂”, *Sci. Adv.* (2020).
25. Wei Ruan, Yi Chen, Shujie Tang, Jinwoong Hwang, Hsin-Zon Tsai, Ryan L. Lee, Meng Wu, Hyejin Ryu, Salman Kahn, Franklin Liou, Caihong Jia, Andrew Aikawa, Choongyu Hwang, Feng Wang, Yongseong Choi, Steven G. Louie, Patrick A. Lee, Zhi-Xun Shen, Sung-Kwan Mo, and Michael F. Crommie. “Evidence for quantum spin liquid behaviour in single-layer 1T-TaSe₂ from scanning tunnelling microscopy”, *Nature Physics* (2021). <https://doi.org/10.1038/s41567-021-01321-0>

Designing Metastability: Coercing Materials to Phase Boundaries

T. Zac Ward, Oak Ridge National Laboratory

Program Scope

The research in this project aims to understand and, ultimately, predictively design materials' behaviors in close proximity to electronic and magnetic phase boundaries in strongly correlated electron systems. Transition metal oxides often possess metastable and non-equilibrium states which can interact across multiple length scales to give highly desirable emergent properties, ranging from metal-insulator transitions to superconductivity to multiferroicity. Due to the strong coupling between the spin, charge, orbital, and lattice parameters in these materials, even small changes to the underlying crystal lattice structure and composition can have a dramatic impact on the emergence of macroscopic phenomena. Effective control over the crystal lattice not only facilitates the understanding of multiple interactions in strongly correlated systems but can also be used to create new phases and functionalities. Central to our effort are the ability to control structural lattice symmetries through strain doping and the ability to probe spin and exchange coupling symmetry breaking by creating crystals with high compositional complexity. These approaches are making it possible to gain insight into how local environments can lead to emergent meso- and macroscopic responses as we move through phase boundaries. The specific aims of this research are: (1) to design new metastable ferroic states, (2) to understand local inhomogeneity's role in the formation of macroscopic functional phases, and (3) to identify relevant differences between the effects of the strong and weak disorder limits. Continuous manipulation of order parameters provides fundamental insights into correlation effects while opening new phase spaces to functionalization. The ability to make fine adjustments to individual parameters allows us to home in on metastable degeneracies at phase boundaries.

Recent Progress

The preliminary studies in this project relied on manipulation of lattice symmetry by placing low concentrations of helium atoms interstitially in correlated systems^{1,2}; we have found that this approach to symmetry modification allows continuous and iterative manipulation of phase dynamics that can be applied to control magnetic anisotropy energies³, bandgaps⁴, and morphotropic multiferroic phases⁵. Building off of these results, we have begun to develop a novel means of controlling symmetry and distortions through the inherent effects of chemical pressure exerted by compositional disorder on ordered single crystal lattices. We have done this by refining the synthesis of configurationally complex single crystals and have demonstrated the first examples of heteroepitaxial growth of perovskite (ABO_3)⁶⁻⁸, Ruddlesden-Popper (A_2BO_4)⁹, and spinel (AB_2O_4)¹⁰ films where one or more of the cation sublattices host 5 or more elements. This approach gives a means of not only controlling gross crystallographic atomic positional symmetries but also the means to break specific parameter symmetries on positionally ordered

lattices. From this, we have been able to interrogate the role of local spin, charge, and exchange discontinuities on the emergence of macroscopic magnetic and electronic phases in several strongly correlated systems.

Compositionally complex single crystals

Configurational disorder can have a dominating role in the formation of macroscopic functional responses in strongly correlated quantum materials. However, traditional enthalpy-driven synthesis approaches often create materials that possess unintended secondary crystal phase formations or defects which generate extrinsic contributions when more than a few elements are combined. This limits our ability to cover a continuously tunable parameter phase space that can be simply modelled using only intrinsic parameter variables. We have developed entropy-assisted synthesis to create single-crystal epitaxial ABO_3 perovskite thin films which can be made to host 5 or more cations on either the A -site or B -site sublattices (**Fig 1**). Manipulating A -site cation radius variance makes it possible to directly shift electron-phonon interactions and to indirectly influence B -site sublattice charge state, coordination, orbital population, and/or bond symmetries⁶. We found that adjusting the complexity of the constituent B -site elements in transition metal oxides provides a more direct route to accessing the local spin and exchange coupling parameters. As example, we find that PLD-grown $\text{La}(\text{Cr}_{0.2}\text{Mn}_{0.2}\text{Fe}_{0.2}\text{Co}_{0.2}\text{Ni}_{0.2})\text{O}_3$ films possess exceptional crystallinity, smooth film surfaces, and uniform mixing of the $3d$ transition-

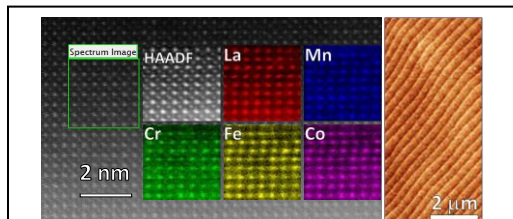
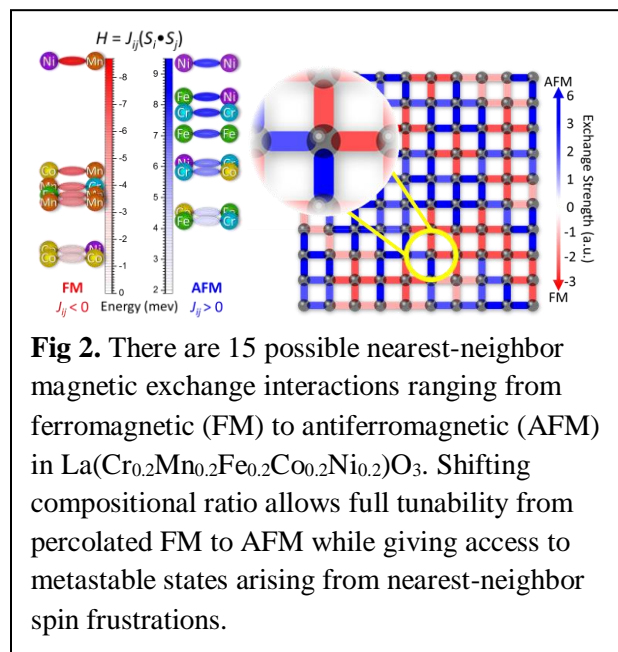


Fig 1. STEM-EELS and AFM of single crystal $\text{La}(\text{Cr}_{0.2}\text{Mn}_{0.2}\text{Fe}_{0.2}\text{Co}_{0.2}\text{Ni}_{0.2})\text{O}_3$ ABO_3 perovskite films show chaotic mixing of B -site cations on a positionally uniform crystal lattice.



metal cations throughout the B -site sublattice; these new materials behave fundamentally differently than would be expected from a simple sum of the ternary parent compounds^{7,8}. Magnetometry and neutron experiments show that these compositionally disordered materials have strong magnetic anisotropy and can paradoxically contain long-range magnetic order. This work suggests a new approach to design magnetic responses by tailoring combinations of B -site stoichiometries, in which the disordered spin and exchange coupling parameters might be continuously manipulated by adjusting cation ratios (**Fig 2**).

Future Plans

Frustration and degeneracy are critical in the formation of dynamic and metastable states. In magnetic systems, degeneracy-driven metastability can be accessed by manipulating the underlying spin states of the constituent elements and nearest neighbor magnetic exchange interactions. We are following up on initial results showing the stabilization of extraordinarily complex spin and exchange environments through cation composition (**Fig 3**).

Maximizing the number of populated microstates through increasing parameter disorder on a positionally ordered lattice provides new opportunities to create highly tunable states and never before possible functionalities—exemplified by the observation of controllable exchange bias responses. Importantly, this is the first ever example of exchange bias effects in a 3D monolithic single crystal.

Frustration has been explored extensively on triangular lattices, where dynamic magnetic behaviors such as spin liquids can be attributed to degenerate ground states relying on geometric frustration. In magnetically complex entropy-stabilized oxides such as those described above, we are working to understand if it is possible to replace geometric frustration by exchange frustration controlled by modifying the variance of exchange couplings populating a square lattice. Additionally, we are working with theory collaborators to explore how our new ability to shift local variances in spin and coupling types while maintaining position symmetries may lead to experimental testbeds for exploration of novel Griffiths phases or quantum many-body systems with tunable critical behaviors.

References

1. Guo, H. *et al.* Strain Doping: Reversible Single-Axis Control of a Complex Oxide Lattice via Helium Implantation. *Phys. Rev. Lett.* **114**, 256801 (2015).
2. Herklotz, A. *et al.* Controlling Octahedral Rotations in a Perovskite via Strain Doping. *Sci. Rep.* **6**, 26491 (2016).
3. Herklotz, A. *et al.* Designing Magnetic Anisotropy through Strain Doping. *Adv. Sci.* **5**, 1800356 (2018).

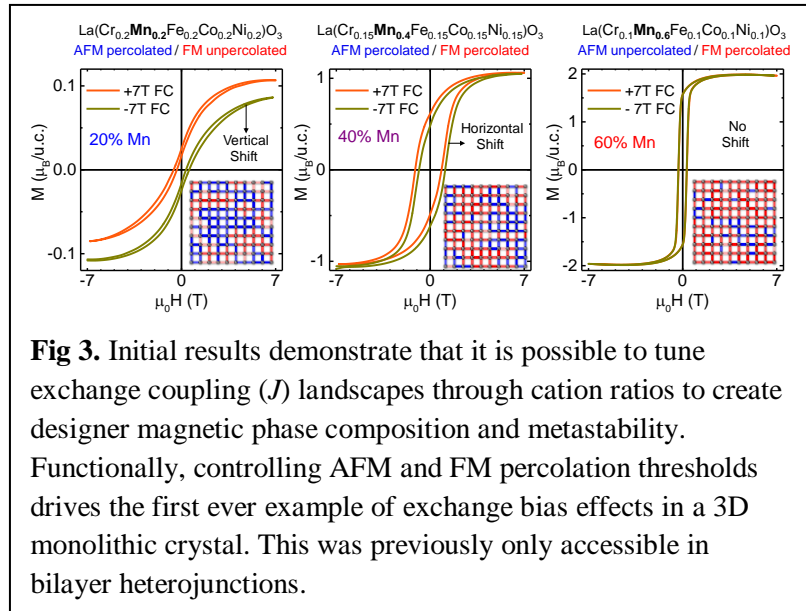


Fig 3. Initial results demonstrate that it is possible to tune exchange coupling (J) landscapes through cation ratios to create designer magnetic phase composition and metastability. Functionally, controlling AFM and FM percolation thresholds drives the first ever example of exchange bias effects in a 3D monolithic crystal. This was previously only accessible in bilayer heterojunctions.

4. Herklotz, A. *et al.* Symmetry driven control of optical properties in WO₃ films. *APL Mater.* **5**, 066106 (2017).
5. Herklotz, A. *et al.* Designing Morphotropic Phase Composition in BiFeO₃. *Nano Lett.* **19**, 1033–1038 (2019).
6. Sharma, Y. *et al.* Single-crystal high entropy perovskite oxide epitaxial films. *Phys. Rev. Mater.* **2**, 060404(R) (2018).
7. Sharma, Y. *et al.* Magnetic anisotropy in single-crystal high-entropy perovskite oxide La(Cr_{0.2}Mn_{0.2}Fe_{0.2}Co_{0.2}Ni_{0.2})O₃ films. *Phys. Rev. Mater.* **4**, 014404 (2020).
8. Brahlek, M. *et al.* Unexpected crystalline homogeneity from the disordered bond network in La(Cr_{0.2}Mn_{0.2}Fe_{0.2}Co_{0.2}Ni_{0.2})O₃. *Phys. Rev. Mater.* **4**, 054407 (2020).
9. Zhang, W. *et al.* Applying Configurational Complexity to the 2D Ruddlesden–Popper Crystal Structure. *ACS Nano* **14**, 13030–13037 (2020).
10. Sharma, Y. *et al.* Magnetism in configurationally complex single crystal spinel films. *Rev.* (2020).

Publications (FY20 & FY21)

1. A.R. Mazza, E. Skoropata, J.M. Lapano, J. Zhang, Y. Sharma, B.L. Musico, V. Keppens, Z. Gai, M. Brahlek, A. Moreo, D.A. Gilbert, E. Dagotto, T.Z. Ward, *Charge Doping Effects on Magnetic Properties of Single Crystal La_{1-x}Sr_x(Cr_{0.2}Mn_{0.2}Fe_{0.2}Co_{0.2}Ni_{0.2})O₃ (0 ≤ x ≤ 0.5) High Entropy Perovskite Oxides*, Physical Review B **X**, XXX (2021) In-press.
2. W. Zhang, A.R. Mazza, E. Skoropata, D. Mukherjee, B. Musico, J. Zhang, V. Keppens, L. Zhang, K. Kisslinger, E. Stavitski, M. Brahlek, J. Freeland, P. Lu, T.Z. Ward, *Applying Configurational Complexity to the 2D Ruddlesden-Popper Crystal Structure*, ACS Nano **14**, 13030 (2020).
3. Y. Sharma, A.R. Mazza, B.L. Musico, E. Skoropata, R. Nepal, R. Jin, A.V. Ievlev, L. Collins, Z. Gai, A. Chen, M. Brahlek, V. Keppens, T.Z. Ward, *Magnetic Texture in Insulating Single Crystal High Entropy Oxide Spinel Films*, ACS Applied Materials & Interfaces **13**, 17971 (2021).
4. Y. Sharma, Q. Zheng, A.R. Mazza, E. Skoropata, T. Heitmann, Z. Gai, B. Musico, P.F. Miceli, B.C. Sales, V. Keppens, M. Brahlek, T.Z. Ward, *Magnetic anisotropy in single-crystal high-entropy perovskite oxide La(Cr_{0.2}Mn_{0.2}Fe_{0.2}Co_{0.2}Ni_{0.2})O₃ films*, Physical Review Materials **4**, 014404 (2020).
5. Y. Sharma, R. Agarwal, L. Collins, Q. Zheng, A.V. Ievlev, R.P. Hermann, V.R. Cooper, S. KC, I.N. Ivanov, R.S. Katiyar, S.V. Kalinin, H.N. Lee, S. Hong, T.Z. Ward, *Self-Assembled Room Temperature Multiferroic BiFeO₃-LiFe₅O₈ Nanocomposites*, Advanced Functional Materials **30**, 1906849 (2020).
6. G. Eres, S. Lee, J. Nichols, C. Sohn, J.M. Ok, A.R. Mazza, C. Liu, G. Duscher, H.N. Lee, D.E. McNally, X. Lu, M. Radovic, T. Schmitt, *Versatile Tunability of the Metal Insulator Transition in (TiO₂)_m/(VO₂)_m Superlattices*, Advanced Functional Materials **30**, 2004914 (2020).

7. B. Musicó, Q. Wright, C. Delzer, T.Z. Ward, C.J. Rawn, D. Mandrus, V. Keppens, *Synthesis method comparison of compositionally complex rare-earth based Ruddlesden–Popper $n=1$ T' -type cuprates*, Journal of the American Ceramic Society **104**, 3750 (2021).
8. E. Skoropata, A.R. Mazza, A. Herklotz, J.M. Ok, G. Eres, M. Brahlek, T.R. Charlton, H.N. Lee, T.Z. Ward, *Post-synthesis control of Berry phase-driven magnetotransport in $SrRuO_3$ films*, Physical Review B **103**, 085121 (2021).
9. T. Feng, Y. Wang, A. Herklotz, M.F. Chisholm, T.Z. Ward, P.C. Snijders, S.T. Pantelides, *Determination of rutile transition metal oxide (110) surface terminations by scanning tunneling microscopy contrast reversal*, Physical Review B **103**, 035409 (2021).
10. J.M. Lapano, L. Nuckols, A.R. Mazza, Y.-Y. Pai, J. Zhang, B. Lawrie, R.G. Moore, G. Eres, H.N. Lee, M.-H. Du, T.Z. Ward, J.S. Lee, W.J. Weber, Y. Zhang, M. Brahlek, *Adsorption-controlled growth of $MnTe(Bi_2Te_3)_n$ by molecular beam epitaxy exhibiting stoichiometry-controlled magnetism*, Physical Review Materials **4**, 111201(R) (2020).
11. Y. Sharma, E. Skoropata, B. Paudel, K.-T. Kang, D. Yarotski, T.Z. Ward, A. Chen, *Epitaxial Stabilization of Single Crystal Multiferroic $YCrO_3$ Thin Films*, Nanomaterials **10**, 2085 (2020).
12. J.M. Lapano, A.R. Mazza, H. Li, D. Mukherjee, E. Skoropata, J.-M. OK, H. Miao, R.G. Moore, T.Z. Ward, G. Eres, H.N. Lee, M. Brahlek, *Strong spin-dephasing in a topological insulator- paramagnet heterostructure*, APL Materials **8**, 091113 (2020).
13. M. Brahlek, A.R. Mazza, K.C. Pitike, E. Skoropata, J. Lapano, G. Eres, V.R. Cooper, T.Z. Ward, *Unexpected crystalline homogeneity from the disordered bond network in $La(Cr_{0.2}Mn_{0.2}Fe_{0.2}Co_{0.2}Ni_{0.2})O_3$ films*, Physical Review Materials **4**, 054407 (2020) (**Editor's Suggestion**).
14. B. Musicó, D. Gilbert, T.Z. Ward, K. Page, E. George, J. Yan, D. Mandrus, V. Keppens, *The emergent field of High Entropy Oxides: Design, prospects, challenges, and opportunities for tailoring material properties*, APL Materials **8**, 040912 (2020) (**Featured Article**)
15. B. Musicó, Q. Wright, T.Z. Ward, A. Grutter, E. Arenholz, D. Gilbert, D. Mandrus, V. Keppens, *Tunable magnetic ordering through cation selection in entropic spinel*, Physical Review Materials **3**, 104416 (2019).
16. Y. Sharma, M.V. Holt, N. Laanait, X. Gao, I. Ivanov, L. Collins, C. Sohn, Z. Liao, E. Skoropata, S.V. Kalinin, N. Balke, G. Eres, T.Z. Ward, H.N. Lee, *Competing phases in epitaxial vanadium dioxide at nanoscale*, APL Materials **7**, 081127 (2019).
17. W.L. Boldman, C. Zhang, T.Z. Ward, D.P. Briggs, B.R. Srijanto, P. Brisk, P.D. Rack, *Programmable Electrofluidics for Ionic Liquid based Neuromorphic Platform*, Micromachines **10**, 478 (2019).
18. M. Brahlek, G. Rimal, J.M. Ok, D. Mukherjee, A.R. Mazza, Q. Lu, H.N. Lee, T.Z. Ward, R.R. Unocic, G. Eres, S. Oh, *Growth of metallic delafossite $PdCoO_2$ by molecular beam epitaxy*, Physical Review Materials **3**, 093401 (2019).
19. A. Herklotz, S.F. Rus, C. Sohn, S. KC, V.R. Cooper, E.J Guo, T.Z. Ward, *Optical response of $BiFeO_3$ films subjected to uniaxial strain*, Physical Review Materials **3**, 094410 (2019).

Topological Surface and Bulk States in Dirac Semimetal α -Sn Thin Films

Mingzhong Wu, Department of Physics, Colorado State University

Program Scope

This program will advance the fundamental understanding of topological surface and bulk states in TDS α -Sn thin films and pave the way to new technology. The program consists of six focus topics: (1) film growth, (2) Fermi level tuning, (3) BMER effects, (4) quantum oscillations, (5) negative magnetoresistance, and (6) magnetization manipulation. Our recent work shows that Sn films grown on Si substrates exhibit pure α phase only when the thicknesses are no larger than 6 nm. Under Topic (1), we aim to overcome this thickness limitation through several strategies that include growth at lower temperatures, post-cooling, and metallic capping. Under Topic (2), we will investigate how to tune the Fermi level via doping, metallic capping, and voltage gating. Our preliminary data indicate the existence of the BMER effect in TDS α -Sn thin films. Under Topic (3), we will fully examine this effect through field angle-dependent, second-harmonic resistance measurements. The goals of Topics (4) and (5) are to demonstrate the TSS-associated quantum oscillations and the negative magnetoresistance associated with a topological Dirac-to-Weyl phase transition, respectively. This will be done through the measurements of resistance as a function of a magnetic field at low temperatures. Topic (6) aims to establish the high potential of TDS α -Sn thin films for spintronics applications through two model experiments: SOT-induced magnetization switching in small ferromagnetic islands and SOT-driven domain wall motion in narrow ferromagnetic strips, both with strong perpendicular magnetic anisotropy.

Recent Progress

The major achievements since the last PI meeting include the following three works.

(1) Large damping enhancement in Dirac-semimetal – ferromagnetic-metal layered structures caused by topological surface states. We observed damping enhancement in a ferromagnetic NiFe thin film due to an adjacent α -Sn thin film.¹ Ferromagnetic resonance studies show that an α -Sn film separated from a NiFe film by an ultrathin Ag spacer can cause an extra damping in the NiFe film that is three times bigger than the intrinsic damping of the NiFe film. Such an extra damping is absent in structures where the α -Sn film interfaces directly with a NiFe film, or is replaced by a β -Sn film. The data suggest that the extra damping is associated with topologically nontrivial surface states in the topological Dirac semimetal phase of the α -Sn film. This work suggests that, like topological insulators, topological Dirac semimetal α -Sn may have promising applications in spintronics. Figure 1 shows the

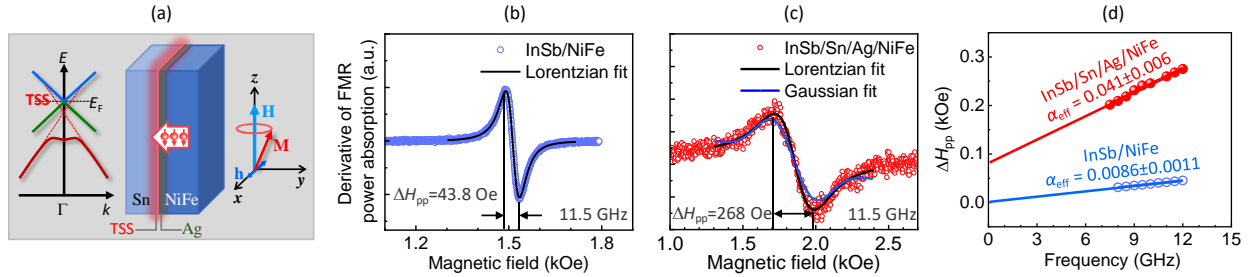


Figure 1. Topological surface states-enhanced spin pumping in α -Sn/NiFe structures. (a) Conceptual diagram. (b) FMR profile of InSb/NiFe(20nm). (c) FMR profile of InSb/ α -Sn(6nm)/Ag(2nm)/NiFe(20nm). (d) FMR linewidth as a function of frequency for the two samples.

ferromagnetic resonance (FMR) representative data. We can see that the FMR peak in (c) is significantly broader than that in (b). We can also see from (d) that the sample with α -Sn has a notably larger damping than that without α -Sn.

(2) Switching of a magnet by spin-orbit torque from a topological Dirac semimetal.

Recent experiments show that topological surface states (TSS) in topological insulators (TI) can be exploited to manipulate magnetic ordering in ferromagnets. In principle, TSS should also exist for other topological materials, but it remains unexplored whether such states can also be utilized to manipulate ferromagnets. We recently demonstrated current-induced magnetization switching enabled by TSS in a non-TI topological material, namely, a topological Dirac semimetal α -Sn.² Our experiments used an α -Sn/Ag/CoFeB tri-layer structure. The magnetization in the CoFeB layer can be switched by a charge current at room temperature, without an external magnetic field. The data show that the switching is driven by the TSS of the α -Sn layer, rather than spin-orbit coupling in the bulk of the α -Sn layer or current-produced heating. The switching efficiency is as high as in TI systems. This shows that the topological Dirac semimetal α -Sn is as promising as TI materials in terms of spintronic applications. Figure 2 gives representative data. The hysteresis loops in (b) and (c) show field- and pure current-induced magnetization switching responses, respectively, in the tri-layered depicted in (a).

(3) Large Magneto-Electric Resistance in the Topological Dirac Semimetal α -Sn. The spin-momentum locking of surface states in topological quantum materials can produce a resistance that scales linearly with magnetic and electric fields. Such a bilinear magneto-electric

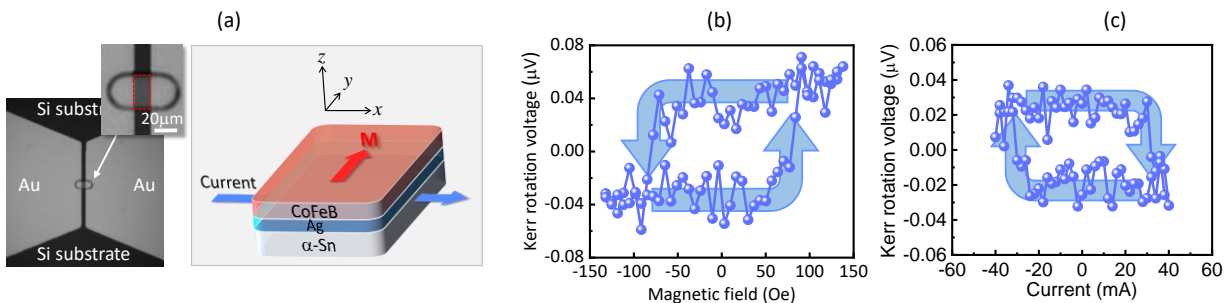


Figure 2. Magnetization switching in a Si/ α -Sn(6nm)/Ag(2nm)/CoFeB(2nm) structure. (a) Experimental configuration. (b) Field-induced switching measured by a magneto-optical Kerr effect (MOKE) technique. (c) Field-free, current-induced switching measured by the MOKE technique.

resistance (BMER) effect offers a completely new approach for magnetic storage and magnetic field sensing applications. The effects demonstrated so far, however, are relatively weak or for low temperatures. Strong room-temperature BMER effects have now been found in topological Dirac semimetal α -Sn thin films. The epitaxial α -Sn films were grown by sputtering on silicon substrates. They showed BMER responses that are 10^6 times larger than previously reported at room temperature and also larger than that previously reported at low temperatures. These results represent a major advance toward realistic BMER applications. The data also made possible the first characterization of the three-dimensional, Fermi-level spin texture of topological surface states in α -Sn. We are currently carrying out some control measurements to further support our conclusions and also advance our understanding on the physical mechanisms underlying the strong effect we observed.

Future Plans

Our major plans for the next one-year period include: (1) finalizing of our study on the bilinear magneto-electric resistance effect in topological Dirac semimetal α -Sn thin films, (2) characterization of spin-orbit coupling in topological surface states in α -Sn thin films through comprehensive spin-torque ferromagnetic resonance measurements, and (3) exploration of quantum oscillations and negative magnetoresistance in α -Sn thin films.

References

¹ “Large damping enhancement in Dirac-semimetal – ferromagnetic-metal layered structures caused by topological surface states,” Jinjun Ding, Chuanpu Liu, Yuejie Zhang, Vijaysankar Kalappattil, Rui Yu, Uppalaiah Erugu, Jinke Tang, Haifeng Ding, Hua Chen, and Mingzhong Wu, *Advanced Functional Materials*, 2008411 (2021). DOI: 10.1002/adfm.202008411

² “Switching of a magnet by spin-orbit torque from a topological Dirac semimetal,” Jinjun Ding, Chuanpu Liu, Vijaysankar Kalappattil, Yuejie Zhang, Oleksandr Mosendz, Uppalaiah Erugu, Rui Yu, Jifa Tian, August DeMann, Stuart B. Field, Xiaofei Yang, Haifeng Ding, Jinke Tang, Bruce Terris, Albert Fert, Hua Chen, and Mingzhong Wu, *Advanced Materials* 2021, 2005909 (2021). <https://doi.org/10.1002/adma.202005909>

Publications

2-year list of publications supported by BES (since August 2019)

“Switching of a magnet by spin-orbit torque from a topological Dirac semimetal,” Jinjun Ding, Chuanpu Liu, Vijaysankar Kalappattil, Yuejie Zhang, Oleksandr Mosendz, Uppalaiah Erugu, Rui Yu, Jifa Tian, August DeMann, Stuart B. Field, Xiaofei Yang, Haifeng Ding, Jinke Tang, Bruce Terris, Albert Fert, Hua Chen, and Mingzhong Wu, *Advanced Materials* 2021, 2005909 (2021). <https://doi.org/10.1002/adma.202005909>

“Large damping enhancement in Dirac-semimetal – ferromagnetic-metal layered structures caused by topological surface states,” Jinjun Ding, Chuanpu Liu, Yuejie Zhang, Vijaysankar Kalappattil, Rui Yu, Uppalaiah Erugu, Jinke Tang, Haifeng Ding, Hua Chen, and Mingzhong Wu, *Advanced Functional Materials*, 2008411 (2021). DOI: 10.1002/adfm.202008411

“Topological Hall effects in a topological insulator interfaced with a magnetic insulator,” Peng Li, Jinjun Ding, Steve S.-L. Zhang, James Kally, Timothy Pillsbury, Olle G. Heinonen, Gaurab Rimal, Chong Bi, August DeMann, Stuart B. Field, Weigang Wang, Jinke Tang, Jidong Samuel Jiang, Axel Hoffmann, Nitin Samarth, and Mingzhong Wu, *Nano Letters*, <https://dx.doi.org/10.1021/acs.nanolett.0c03195> (2020).

“Changes of magnetism in a magnetic insulator due to proximity to a topological insulator,” Tao Liu, James Kally, Timothy Pillsbury, Chuanpu Liu, Houchen Chang, Jinjun Ding, Yang Chen, Maria Hilse, Roman Engel-Herbert, Anthony Richardella, Nitin Samarth, and Mingzhong Wu, *Physical Review Letters* 125, 017204 (2020). <https://doi.org/10.1103/PhysRevLett.125.017204>

“Chiral spin-wave velocities induced by all-garnet interfacial Dzyaloshinskii-Moriya interaction in ultrathin yttrium iron garnet films,” Hanchen Wang, Jilei Chen, Tao Liu, Jianyu Zhang, Korbinian Baumgaertl, Chenyang Guo, Yuehui Li, Chuanpu Liu, Ping Che, Sa Tu, Song Liu, Peng Gao, Xiufeng Han, Dapeng Yu, Mingzhong Wu, Dirk Grundler, and Haiming Yu, *Physical Review Letters* 124, 027203 (2020).

“Magnetization switching utilizing topological surface states,” Peng Li, James Kally, Steven S.-L. Zhang, Timothy Pillsbury, Jinjun Ding, Gyorgy Csaba, Junjia Ding, Sam Jiang, Yunzhi Liu, Robert Sinclair, Chong Bi, August DeMann, Gaurab Rimal, Wei Zhang, Stuart B. Field, Jinke Tang, Weigang Wang, Olle G. Heinonen, Valentine Novosad, Axel Hoffmann, Nitin Samarth, and Mingzhong Wu, *Science Advances* 5, eaaw3415 (2019).

Non-volatile active control of spin transport using interfaces with molecular ferroelectrics

Xiaoshan Xu

Department of Physics and Astronomy, University of Nebraska-Lincoln

Program Scope

The overarching goal of this project is to realize the non-volatile electric-field control of spin transport across interfaces [1] and in spin-orbit coupled materials, which is crucial for the operations in spin-based circuitry. Particularly, this project exploits non-volatile control using interfaces with ferroelectrics in both spin-polarized charge current and in non-magnetic spin-orbit coupled materials, especially the recently discovered molecular ferroelectrics that have large polarizations and small switching fields [2]. The specific aims are 1: elucidate the effect of polarization on the spin transport through the ferromagnet/molecular ferroelectrics interfaces [3]; 2: gain fundamental understanding on the effect of polarization on the charge/spin conversion in spin-orbit coupled materials at the interfaces with molecular ferroelectrics. 3: characterize spin transport in crystalline molecular ferroelectrics.

Recent Progress (*Persistent Opto-ferroelectric Control of Molecular Ferroelectrics Based on Proton Metastable States*)

Previously, we have demonstrated the ferroelectric control of spin transport employing the electrostatic effect (energy landscape change) due to the polarization reversal in a magnetic tunneling junction using proton-transfer type molecular ferroelectrics as the tunneling barrier. Molecular ferroelectric materials are more suitable for realizing this effect because of the weak structural coupling at the organic/inorganic interfaces and the small dielectric constant of organic materials that enable a large depolarization field and large electric potential shift and maximize the electrostatic effect. Another advantage of the molecular ferroelectrics is the potentially large optical control of ferroelectricity due to the strong electron-proton coupling and the proton-transfer origin of polarization switching. The recent progress of our work demonstrates that in addition to the electric control of ferroelectric properties, molecular ferroelectrics exhibit persistent photo-response in their ferroelectric properties, suggesting opto-ferroelectric tunability.

Persistent photo-response relies on metastable states and photoexcitation to them. The bistable polarization states in ferroelectric materials offer natural candidates for ionic metastable states. However, photoexcitation to these states is unlikely due to the indirect photon-ion interactions. As illustrated in Figure 1a, according to the Frank-Condon principle, photoexcitation mostly starts with electronic excitation in a “vertical” fashion in femtoseconds without changing the vibrational states of the ions (or nuclei). The excited electronic states modify the potential energy landscape of the ions and change the vibrational eigenstates. The ions acquire energy indirectly, in the form of only a few vibrational energy quanta (phonons) by transitioning to the modified eigenstates in picoseconds. Whether the vibrational energy acquired by ions in the Frank-Condon process can promote them to the metastable states depends on the distortion of the ionic potential energy caused by the electronic excited states and the mass of the ions. In this regard, the proton-transfer type molecular ferroelectrics is promising given the strong electron-proton coupling and the small mass of proton.

A prototypical example of proton-transfer type molecular ferroelectrics is croconic acid (CA), which consists of stacked herringbone layers, as shown in Figure 1b. While these layers are held together by the van der Waals interactions, the molecules within a layer are connected by the (ridge

and plane) hydrogen bonds (H-bond). As depicted in Figure 1c, the protons in the hydrogen bonds have two energy minima resulting from the double-well potentials. CA crystals exhibit spontaneous polarization due to the ordering of proton positions on the same side of the double wells with a Curie temperature higher than 400 K. Polarization switching of CA corresponds to the collective transfer of protons to the other wells, or transition between two tautomers. The large spontaneous polarization ($\approx 20 \mu\text{C}/\text{cm}^2$) originates from both the ordered protons and the distorted π electronic cloud. The electronic excitation is expected to have a significant impact on the proton potential well. The vibrational energy quantum can be estimated as $\sim 0.1 \text{ eV}$, which is comparable to the hydrogen-bond energy. Therefore, the electronic excited states are likely to transfer protons to the other well as a metastable state.

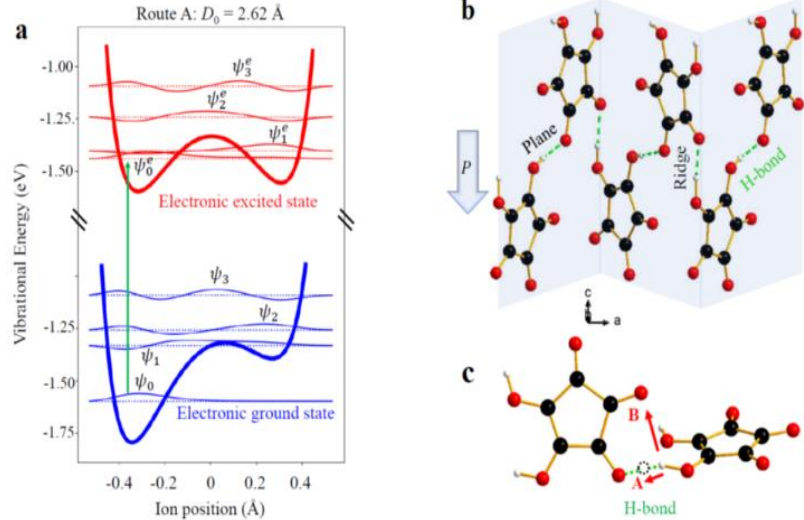


Figure 1. Illustration of proton transfer process and the structure of croconic acid. (a) Simulated potential energy landscapes (thick lines) and the vibrational eigenstates (thin lines) of protons in croconic acid hydrogen bonds with the electronic ground state and the excited state respectively. The eigenstate wave functions are plotted on the dashed baselines indicating the energies of the eigenstates. The vertical arrow connects the initial and final states for the possible proton transfer after the “vertical” electronic excitation. (b) Fragment of a herring-bone layer of the croconic acid crystal structure. (c) Two croconic acid molecules connected by a ridge hydrogen bond. The dashed circle indicates the other energy minimum position of the proton. The arrows indicate the two potential proton transfer routes.

is expected to have a significant impact on the proton potential well. The vibrational energy quantum can be estimated as $\sim 0.1 \text{ eV}$, which is comparable to the hydrogen-bond energy. Therefore, the electronic excited states are likely to transfer protons to the other well as a metastable state.

Positive photostriction is expected for CA crystals, because photoexcitation reduces the order of the positions of protons and molecules which are otherwise tightly packed. We studied the photostriction and its timescale of polycrystalline CA films using the time-resolved x-ray diffraction (XRD), as depicted in Figure 2a. The results are plotted in Figure 2b and 2c as a function of time. Starting at zero time in Figure 2b, the film sample was photoexcited. All lattice constants increase, consistent with the expected positive photostriction. At about 300 s, while the lattice expansion continues, the rate of lattice expansion reduces; this trend remains for the rest of the measurement with the photoexcitation. Figure 2c displays the lattice change after the photoexcitation is stopped at zero time. The lattice constants decrease slowly until they relax back to approximately the original values before the photoexcitation. Interestingly, there appears to be two timescales including a fast one and a slow one on the order of 10^2 s and 10^3 s respectively.

To check the impact of temperature increase (due to the light absorption) to the lattice expansion, we measured the thermal expansion of the CA films directly. As shown in Figure 2d, the thermal expansion coefficients are 50, 80, and 27 ppm/K along the a , b , and c axes, respectively, with a large anisotropy. The anisotropy of the thermal expansion is consistent with the crystal structural anisotropy of CA and previous measurements: the largest expansion is along the b axis which is the direction along which the herringbone layers are held together by the van der Waals

interaction. The large difference in anisotropy between Figure 2b and Figure 2d suggests that the impact of thermal expansion to the observed photostriction is minimal.

The transfer of protons to the metastable states may also manifest in the ferroelectric properties of the CA films, since the proton displacements generate local electric dipole moments. To reveal the photoinduced modification of polarization, we studied the ferroelectric switching behavior of the photoexcited CA films using piezoresponse force microscopy (PFM). As depicted in Figure 3a, using the PFM, the time evolution of piezoresponse of the CA grains were measured. Clear butterfly-type hysteresis loops have been observed, indicative of polarization switchability. The coercive voltage is about 6 V, in agreement with our previous results measured on films grown under similar conditions [4]. Interestingly, the piezoresponse hysteresis loops, after photoexcitation, show dramatic asymmetry in Figure 3b. The hysteresis loops are shifted to the right immediately after stopping the photoexcitation; correspondingly, the piezoresponses for the positively and negatively poled states at zero bias show large contrasts (> 2). The voltage shift of the hysteresis loop in Figure 3b indicates the existence of an internal bias field. The asymmetry slowly decays overtime after the photoexcitation is turned off and the hysteresis loop becomes symmetric after about 1 hour. To analyze the time evolution of the asymmetry, we plotted the internal bias as a function of time after the photoexcitation in Figure 3c; a fit assuming exponential decay results in a time constant of 1513 s, consistent with the timescale of the slow process observed in photostriction.

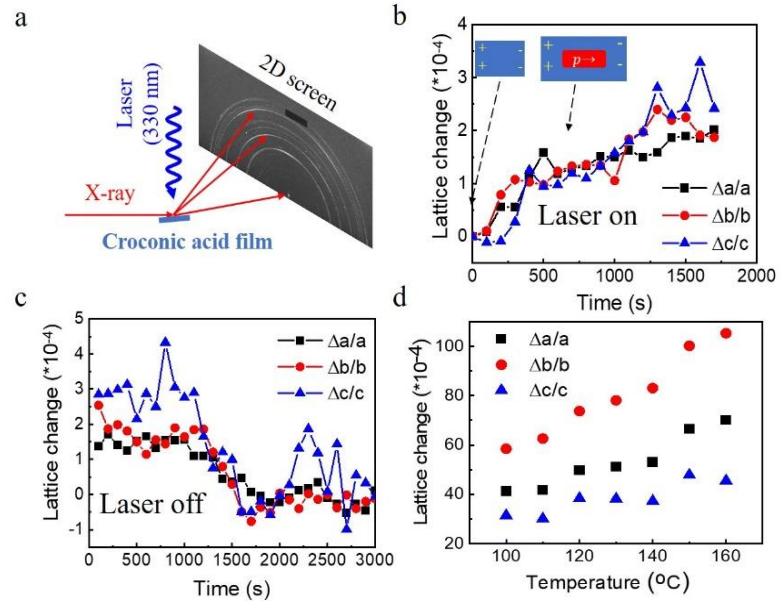


Figure 2. Photostriction in croconic acid thin film and its relaxation. (a) Experimental setup for time-resolved synchrotron x-ray diffraction. (b) Time-resolved lattice distortion along three axes under photoexcitation starting at zero time. (c) Lattice relaxation after the laser is turned off at zero time. (d) Lattice change due to the thermal expansion with a large anisotropy with respect to the room-temperature values.

the piezoresponse force microscopy (PFM). As depicted in Figure 3a, using the PFM, the time evolution of piezoresponse of the CA grains were measured. Clear butterfly-type hysteresis loops have been observed, indicative of polarization switchability. The coercive voltage is about 6 V, in agreement with our previous results measured on films grown under similar conditions [4]. Interestingly, the piezoresponse hysteresis loops, after photoexcitation, show dramatic asymmetry in Figure 3b. The hysteresis loops are shifted to the right immediately after stopping the photoexcitation; correspondingly, the piezoresponses for the positively and negatively poled states at zero bias show large contrasts (> 2). The voltage shift of the hysteresis loop in Figure 3b indicates the existence of an internal bias field. The asymmetry slowly decays overtime

after the photoexcitation is turned off and the hysteresis loop becomes symmetric after about 1 hour. To analyze the time evolution of the asymmetry, we plotted the internal bias as a function of time after the photoexcitation in Figure 3c; a fit assuming exponential decay results in a time constant of 1513 s, consistent with the timescale of the slow process observed in photostriction.

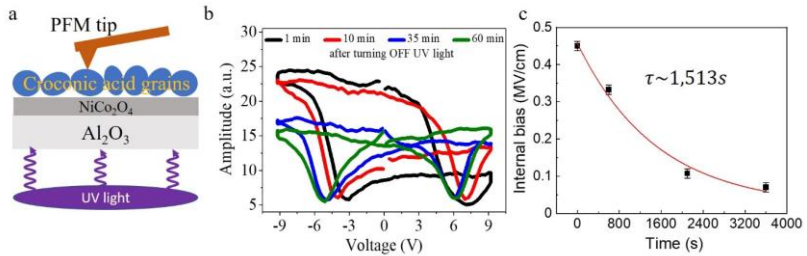


Figure 3. Effect of photoexcitation on the piezoresponse of croconic acid grains. (a) Schematic diagram of the internal bias study via piezoresponse force microscope (PFM) under the illumination. (b) Hysteric piezoresponse amplitude at different time after photoexcitation stops, showing shape distortions and shifts of the response along the voltage axis. (c) Internal bias from (b) as a function of relaxation time and the corresponding fit assuming exponential decay. The error bar is 0.0125 MV/cm.

Combining the results from the measurement of photostriction and the measurement of photo-induced changes in piezoresponses, there appears to be two metastable states of different time scales. The 10^2 s timescale was observed in photostriction but not in change of piezoresponse in the polarization switching processes, suggesting that the energy scale of this metastable state is comparable or less than that of the ferroelectric domain walls. This is consistent with the metastable states resulting from proton transfer along the hydrogen bonds, indicated as route A in Figure 1c; the configuration can be viewed as the reversed single-molecule ferroelectric domain. We call this domain-like metastable state. The 10^3 s timescale was observed in both measurements, suggesting a different metastable state. The longer timescale of this metastable state is consistent with a larger energy scale than that of the domain walls since the polarization switching process cannot remove this metastable state. We propose that this metastable state results from proton transfer to another nearby oxygen site, indicated as route B in Figure 1c. Also depicted in Figure 1c is the slight bending (155 degree) of hydrogen bond toward the other oxygen along the route B in the crystal structure, suggesting sizable attractive force. In this metastable state, with the broken hydrogen bond, the hydrogen is bonded to only one oxygen site, generating an interstitial/vacancy defect. We call this defect-like metastable state. The proton is further away from the originally bonded oxygen site, making it more difficult to return to the ground state, consistent with the internal bias field that cannot be removed by the polarization switching process. Another possible origin for the internal bias is the charge carriers in trap states, which can be ruled out according to our photoconductivity measurements.

Future Plans

1. Study the persistent opto-ferroelectric control on charge and spin transport properties. The effect of photoconductivity can be separated according to the time scale.
2. Extend the study of persistent photo-response to other molecular ferroelectrics such as methyl benzimidazol (MBI) and 3-hydroxyphenalenone (3-HPLN). These molecular ferroelectrics have smaller polarization due to smaller density of H-bonds, while the electron-proton coupling is similar to that of the croconic acid, which suggests the possibility of persistent photo-response.

References

- [1] X. Xu, *A Brief Review of Ferroelectric Control of Magnetoresistance in Organic Spin Valves*, *J. Mater.* **4**, 1 (2018).
- [2] S. Horiuchi, Y. Tokunaga, G. Giovannetti, S. Picozzi, H. Itoh, R. Shimano, R. Kumai, and Y. Tokura, *Above-Room-Temperature Ferroelectricity in a Single-Component Molecular Crystal*, *Nature* **463**, 789 (2010).
- [3] Y. Yin, Y. Yin, X. Jiang, M. A. Koten, J. E. Shield, X. Chen, Y. Yun, A. T. N'Diaye, X. Hong, and X. Xu, *Spin Rectification and Electrically Controlled Spin Transport in Molecular-Ferroelectrics-Based Spin Valves*, *Phys. Rev. Appl.* **13**, 064011 (2020).
- [4] X. Jiang, H. Lu, Y. Yin, X. Zhang, X. Wang, L. Yu, Z. Ahmadi, P. S. P. S. Costa, A. D. A. D. Dichiara, X. Cheng, A. Gruverman, A. Enders, and X. Xu, *Room Temperature Ferroelectricity in Continuous Croconic Acid Thin Films*, *Appl. Phys. Lett.* **109**, 102902 (2016).

Publications

Y. Yin, Y. Yin, X. Jiang, M. A. Koton, J. E. Shield, X. Chen, Y. Yun, A. T. N'Diaye, X. Hong, and X. Xu, *Spin Rectification and Electrically Controlled Spin Transport in Molecular-Ferroelectrics-Based Spin Valves*, Phys. Rev. Appl. **13**, 064011 (2020).

Project Title: Sub-Nanosecond Switching of Antiferromagnets Driven by Interfacial Spin-Orbit Torque

Principle Investigator: Fengyuan Yang

Mailing Address: Department of Physics, The Ohio State University, Columbus, OH 43210

Program Scope:

The goal of this project is to investigate fast spin-orbit torque (SOT) switching of antiferromagnets (AFM) enabled by their interface with heavy metals (HM) or topological insulators (TI) driven by electrical pulses with duration down to 0.3 nanosecond. Compared to ferromagnets (FM), AFMs offer numerous advantages such as low damping loss, robustness against stray magnetic field, ultrafast picosecond speed, terahertz dynamics, and abundance for spintronics. Recent breakthroughs in electrical switching of AFMs have led to the emergence of antiferromagnetic spintronics as one of the most exciting frontiers in condensed matter physics. SOT has become the preferred choice for controlling both FMs and AFMs with high scalability and novel functionalities. Given the infancy of the new field of antiferromagnetic spintronics, the electrical switching of AFMs at fast time scales (\sim ns) has been essentially unexplored, which is needed for the understanding of ultrafast AFM spin dynamics and the development of high-speed AFM spintronic devices. This project has the following aims to uncover the fast switching behaviors of AFM spins and the underlying mechanisms: (1) achieve spin-orbit torque switching of AFM insulators (e.g., Fe_2O_3 and NiO) and semiconductor (MnTe) enabled by an adjacent TI layer (e.g., Bi_2Se_3); (2) probe electrical switching in HM/AFM and TI/AFM bilayers using pulses with duration ranging from quasi-DC to 0.3 ns and understand the time-energy scales of fast AFM switching.

This research project focuses on AFM insulators and semiconductor with high Néel temperatures and moderate anisotropies, which ensure AFM stability and allow for electrical switching at room temperature. TIs can provide high charge-to-spin conversion efficiency and giant SOT due to the surface spin-momentum locking. This project will demonstrate electrical switching of AFMs by an adjacent TI with high charge-to-spin conversion efficiency.

Recent Progress

1. Tunable topological Hall effects in noncollinear antiferromagnet $\text{Mn}_3\text{Sn}/\text{Pt}$ bilayers

Non-collinear AFM intermetallics attract significant interests recently because of the theoretical prediction and experimental conformation of anomalous Hall effect (AHE) in these AFMs with a Kagome lattice of Mn (Fig. 1a) arising from the topological band structure and momentum space Berry curvature. Interestingly, noncollinear AFMs such as Mn_3Sn and Mn_3Ge have been predicted to be magnetic Weyl semimetals. In addition, it is expected that heavy metals, such as Pt, with large spin-orbit coupling can induce a sizable interfacial Dzyaloshinskii-Moriya interaction (DMI) in Pt/AFM bilayers,

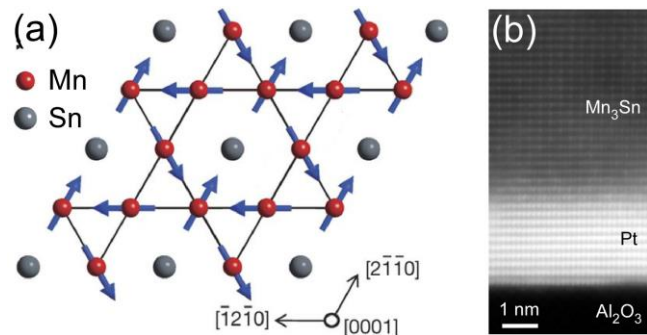


Figure 1. (a) Schematic of a - b plane of hexagonal Mn_3Sn with noncollinear AFM spins on Mn.¹ (b) STEM image of a Mn_3Sn (45 nm)/Pt(3 nm) bilayer on Al_2O_3 (0001).

leading to the formation of AFM topological spin textures. The investigation of AFM topological spin textures in these HM/AFM bilayers will provide an alternative angle for probing the topological spin and band structures in these intriguing materials.

Under the primary support of this DOE grant, we investigated the existence of AFM topological spin textures in Mn₃Sn/Pt bilayers via the detection of topological Hall effect (THE) as well as the presence of out-of-plane AHE. For the epitaxial growth of Mn₃Sn (0001) films, we first grow a thin Pt at a substrate temperature of 260°C as an epitaxial buffer layer on Al₂O₃ (0001) substrate, followed by the in-situ growth of Mn₃Sn at 210°C on Pt by off-axis sputtering. The hexagonal Mn₃Sn (0001) plane is well matched (~1% lattice mismatch) to the FCC Pt(111) plane. X-ray diffraction and scanning transmission electron microscopy (STEM) imaging (Fig. 1b) confirm the good crystalline quality of the Mn₃Sn epitaxial films.

Figure 2a shows a schematic of Hall measurement on a Mn₃Sn(5 nm)/Pt(1.5 nm) bilayer with an out-of-plane magnetic field. Figures 2b and 2c show the longitudinal magnetoresistance $MR = \rho_{xx}/\rho_0$ (ρ_0 is the zero-field resistivity) and the Hall resistivity (ρ_{xy}), respectively, as a function of the out-of-plane field, $H \parallel \text{Mn}_3\text{Sn}[0001]$. The ordinary Hall effect (OHE) contribution, ρ_{OHE} , with a linear field dependence has been subtracted in Fig. 2c. At $T = 300\text{K}$, a large anomalous Hall resistivity $\rho_{\text{AHE}} = 43 \text{ n}\Omega \text{ cm}$ is observed. The non-ferromagnetic origin of the AHE is confirmed by the longitudinal MR as shown in Fig. 2b, which is non-hysteretic with a magnitude of only <0.05% up to 14 T.

Surprisingly, as temperature increases, the magnitude of ρ_{AHE} decreases and changes sign at ~330 K (Fig. 2c), while the longitudinal MR has essentially no change (Fig. 2b). Because the observed AHE in Mn₃Sn is not ferromagnetic in origin, we fit the ρ_{AHE} loops using the Langevin equation as shown in Fig. 2c, which is subtracted from ρ_{xy} to obtain an additional Hall signal (other than OHE and AHE) in Fig. 2d. In general, $\rho_{xy} = \rho_{\text{OHE}} + \rho_{\text{AHE}} + \rho_{\text{THE}}$ where the last term

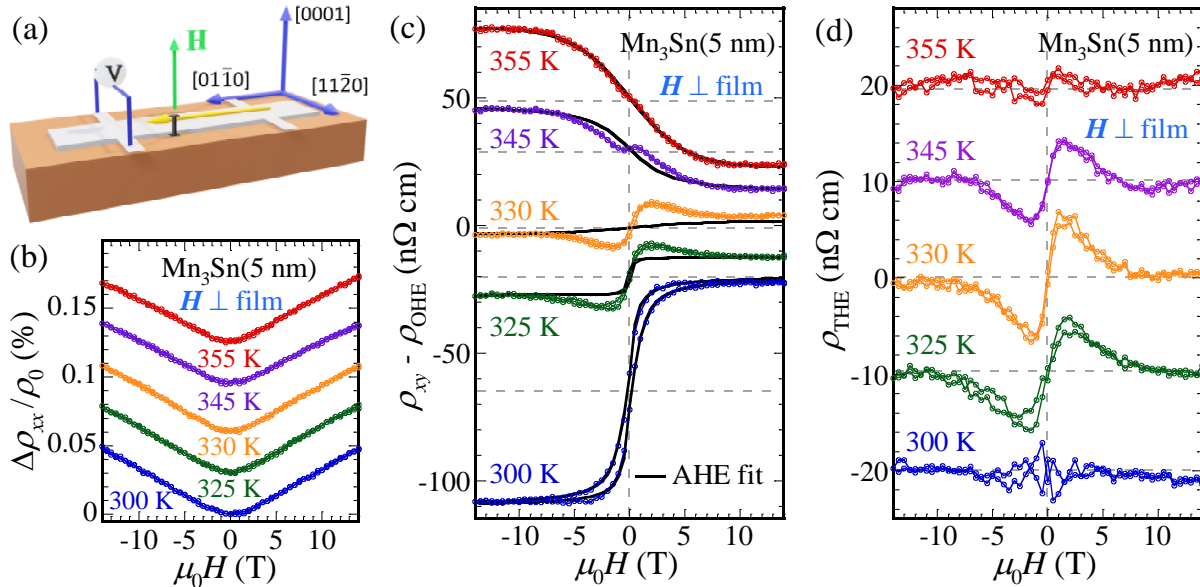


Figure 2. (a) Schematic of Hall measurement on a Mn₃Sn(5 nm)/Pt(1.5 nm) bilayer with an out-of-plane field. (b) Longitudinal magnetoresistance $\Delta\rho_{xx}/\rho_0$ at $T = 300$ to 355 K . (c) Hall resistivity $\rho_{xy} - \rho_{\text{OHE}}$ measured from 300 to 355 K , where the black curve is the fitting for ρ_{AHE} with Langevin function. (d) ρ_{THE} after subtraction of the fitting curve for ρ_{AHE} in (c) at each temperature.

arises from the topological Hall effect typically attributed to the formation of topological spin textures. The maximum magnitude of ρ_{THE} occurs near the temperature where ρ_{AHE} reserves its sign, which is similar to the previous reports of SrRuO₃/SrIrO₃ bilayers.

To further exclude the possibility of spurious signals, we measure the longitudinal and Hall resistivities of the Mn₃Sn(5 nm)/Pt(1.5 nm) bilayer with an in-plane field $H \parallel \text{Mn}_3\text{Sn}[11\bar{2}0]$. Non-zero in-plane ρ_{AHE} is detected; however, the magnitude of in-plane ρ_{AHE} is approximately an order of magnitude smaller than that of out-of-plane ρ_{AHE} . The Hall resistivity after subtracting the fitted ρ_{AHE} contribution shows no detectable topological Hall signal.

Next, we perform similar measurements on different Mn₃Sn thicknesses ranging from 3 to 15 nm, all of which exhibit topological Hall peaks in an out-of-plane field. The magnitude of ρ_{THE} decreases from 5 nm to 15 nm and vanishes at 45 nm Mn₃Sn. This agrees with the behavior expected from the interfacial DMI due to broken inversion symmetry at the Mn₃Sn/Pt interface. However, the values of ρ_{THE} for the 3 and 4 nm samples are smaller than that of the 5 nm sample, which may be due to the lower quality of the Mn₃Sn film at thickness below 5 nm.

Figure 3 summarizes the field-temperature phase diagrams of ρ_{THE} for the 3, 5, 10, and 15 nm Mn₃Sn films for both the decreasing and increasing field branches of the hysteresis loops, indicating the phase space of topological spin textures. As the thickness of Mn₃Sn increases, the temperature range of ρ_{THE} increases from 210-225 K for the 3 nm Mn₃Sn to 345-365 K for the 15 nm Mn₃Sn. Previously, the THE in Mn₃Sn was observed only at $T < 50$ K, where the triangular spin state transitions into a glassy ferromagnetic state. For the triangular spin state of Mn₃Sn, the small intrinsic DMI vector is perpendicular to the in-plane (0001). Thus, it is predicted that the spin chirality of Mn₃Sn is small. However, heavy metal like Pt provides a strong interfacial DMI in Mn₃Sn/Pt bilayers, which can generate topological spin

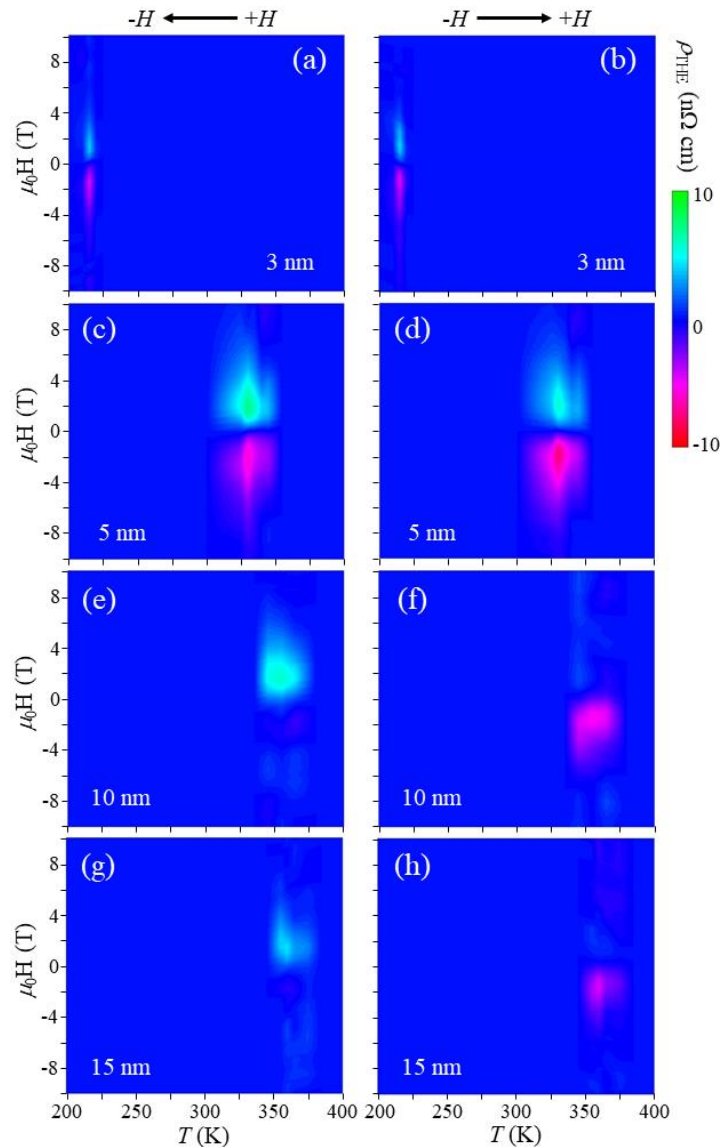


Figure 3. (a) to (h) H - T phase diagrams of topological Hall resistivity for Mn₃Sn(t)/Pt(1.5 nm)/Al₂O₃(0001) with $t = 3, 5, 10$ and 15 nm. The plots on the left have the field sweeping from positive to negative field, and the plots on the right have the field sweeping in the opposite direction.

textures in Mn_3Sn . The emergence of topological spin textures in frustrated triangular AFMs with DMI has been theoretically predicted by Monte-Carlo simulations. The observation of topological Hall effect offers evidence for the existence of chiral spin textures in the $\text{Mn}_3\text{Sn}/\text{Pt}$ bilayers.

Recently, it is proposed that the THE-like signal observed in some systems could be due to the superposition of different AHE contributions with opposite signs. However, it is not likely to be the case here. AHE sign change occurs in our 5 nm Mn_3Sn sample with both out-of-plane and in-plane fields. If the THE-like signal is originated from the superposition of two opposite AHE signals, it should appear in both field orientations. We only detect THE when the field is out-of-plane, which is consistent with the prediction that the interfacial DMI tilts the noncollinear spins towards out-of-plane, resulting to non-zero topological charges. This work was published in *APL Materials*² in May 2021.

2. *Third Harmonic Characterization of Antiferromagnetic Heterostructures*

Electrical switching of AFMs is an exciting recent development in spintronics, which promises active antiferromagnetic devices with high speed and low energy cost. In this emerging field, there is an active debate about the mechanisms of current-driven switching of AFMs. Harmonic characterization is a powerful tool to quantify current-induced spin-orbit torques and spin Seebeck effect in HM/FM systems. However, the harmonic measurement technique has never been verified in AFM heterostructures. Under the primary support of this DOE grant, we perform harmonic measurements in $\text{Pt}/\alpha\text{-Fe}_2\text{O}_3$ bilayers, which are explained by our modeling of higher-order harmonic voltages. As compared with FM heterostructures where all current-induced effects appear in the second harmonic signals, the damping-like torque and thermally-induced magnetoelastic effect contributions in $\text{Pt}/\alpha\text{-Fe}_2\text{O}_3$ emerge in the third harmonic voltage. Our results provide a new path to probe the current-induced magnetization dynamics in antiferromagnets, promoting the application of antiferromagnetic spintronic devices. This work is currently under review.³

Future Plans

To investigate fast spin-orbit torque switching of AFM spins in HM/AFM and TI/AFM heterostructures using nanosecond electrical pulses, we have recently implemented experimental apparatus in the PI's lab that include an electrical pulser down to 300 ps, a 6 GHz oscilloscope, fast switch boxes, other electronic meters, and computer control programs. We have grown high quality AFM epitaxial films such as $\alpha\text{-Fe}_2\text{O}_3$, NiO, LaFeO_3 , and MnTe using off-axis sputtering and molecular-beam epitaxy. For the coming year, this DOE project will focus on electrical switching of HM/AFM bilayers using pulses with duration ranging from ms to sub-ns, as well as characterization of the AFM characteristics, such as anisotropy and spin configuration, and their dependence on AFM film thickness, crystal orientation, and external magnetic field.

References:

1. S. Nakatsuji, N. Kiyohara, and T. Higo, "Large anomalous Hall effect in a non-collinear antiferromagnet at room temperature," *Nature* **527**, 212 (2015).
2. Y. Cheng, S. S. Yu, M. L. Zhu, J. Hwang, and F. Y. Yang, "Tunable topological Hall effects in noncollinear antiferromagnet $\text{Mn}_3\text{Sn}/\text{Pt}$ bilayers," *APL Mater.* **9**, 051121 (2021).
3. Y. Cheng, E. Cogulu, R. D. Resnick, J. J. Michel, N. N. Statuto, A. D. Kent, and F. Y. Yang, "Third Harmonic Characterization of Antiferromagnetic Heterostructures," Under review.

Publications supported by this DOE grant (2019 – 2021)

1. Y. Cheng, E. Cogulu, R. D. Resnick, J. J. Michel, N. N. Statuto, A. D. Kent, and F. Y. Yang, “Third Harmonic Characterization of Antiferromagnetic Heterostructures,” Under review.
2. Y. Cheng, S. S. Yu, M. L. Zhu, J. Hwang, and F. Y. Yang, “Tunable topological Hall effects in noncollinear antiferromagnet Mn_3Sn/Pt bilayers,” *APL Mater.* **9**, 051121 (2021).
3. X. Kuang, S. Wu, Q. J. Ze, L. Yue, Y. Jin, S. M. Montgomery, F. Y. Yang, H. J. Qi, and R. K. Zhao, “Magnetic Dynamic Polymers for Modular Assembling and Reconfigurable Morphing Architectures,” *Adv. Mater.* **33**, 2102113 (2021).
4. G. Z. Wu, Y. Cheng, S. D. Guo, F. Y. Yang, D. V. Pelekhov, and P. Chris Hammel, “Nanoscale imaging of Gilbert damping using signal amplitude mapping,” *Appl. Phys. Lett.* **118**, 042403 (2021).
5. A. J. Lee, S. D. Guo, A. S. Ahmed, and F. Y. Yang, “Crystal orientation dependence of interfacial magnetic anisotropy at heavy-metal/magnetic-garnet interfaces,” *Phys. Rev. B* **102**, 174434 (2020).
6. Y. Cheng, A. J. Lee, G. Z. Wu, D. V. Pelekhov, P. C. Hammel, and F. Y. Yang, “Nonlocal Uniform-Mode Ferromagnetic Resonance Spin Pumping,” *Nano Lett.* **20**, 7257 (2020).
7. S. Wu, C. M. Hamel, Q. J. Ze, F. Y. Yang, H. J. Qi, R. K. Zhao, “Evolutionary Algorithm Guided Voxel-Encoding Printing of Functional Hard-Magnetic Soft Active Materials,” *Adv. Intell. Syst.* **2**, 2000060 (2020).
8. A. J. Lee, A. S. Ahmed, B. A. McCullian, S. D. Guo, M. L. Zhu, S. S. Yu, P. M. Woodward, J. Hwang, P. C. Hammel, and F. Y. Yang, “Interfacial Rashba Effect-Induced Anisotropy in Nonmagnetic-Material/Ferrimagnetic-Insulator Bilayers,” *Phys. Rev. Lett.* **124**, 257202 (2020). (Editor’s Suggestion)
9. B. A. Noesges, T. C. Zhu, J. J. Repicky, S. S. Yu, F. Y. Yang, J. A. Gupta, R. K. Kawakami and L. J. Brillson, “Chemical migration and dipole formation at van der Waals interfaces between magnetic transition metal chalcogenides and topological insulators,” *Phys. Rev. Mater.* **4**, 054001 (2020).
10. K. Alam, K.-Y. Meng, R. Ponce-Pérez, G. H Cocolletzi, N. Takeuchi, A. Foley, F. Y. Yang, and A. R. Smith, “Exchange Bias and Exchange Spring Effects in Fe/CrN Bilayers,” *J. Phys. D: Appl. Phys.* **53**, 125001 (2020).
11. Y. Cheng, S. S. Yu, A. S. Ahmed, M. L. Zhu, J. Hwang, and F. Y. Yang, “Electrical Switching of Tri-State Antiferromagnetic Néel Order in α - Fe_2O_3 Epitaxial Films,” *Phys. Rev. Lett.* **124**, 027202 (2020).
12. Q. J. Ze, X. Kuang, S. Wu, J. Wong, S. M. Montgomery, R. D. Zhang, J. M. Kovitz, F. Y. Yang, H. J. Qi, and R. K. Zhao, “Magnetic Shape Memory Polymers with Integrated Multifunctional Shape Manipulation,” *Adv. Mater.* **32**, 1906657 (2020).
13. Y. Cheng, S. S. Yu, A. S. Ahmed, M. L. Zhu, Y. Rao, M. Ghazisaeidi, J. Hwang, and F. Y. Yang, “Anisotropic magnetoresistance and nontrivial spin Hall magnetoresistance in Pt/ α - Fe_2O_3 bilayers,” *Phys. Rev. B Rapid Comm.* **100**, 220408(R) (2019).
14. Y. Cheng, S. S. Yu, M. L. Zhu, J. Hwang, and F. Y. Yang, “Evidence of the Topological Hall Effect in Pt/Antiferromagnetic Insulator Bilayers,” *Phys. Rev. Lett.* **123**, 237206 (2019).
15. S. Wu, Q. J. Ze, R. D. Zhang, N. Hu, Y. Cheng, F. Y. Yang, and R. K. Zhao, “Symmetry-Breaking Actuation Mechanism for Soft Robotics and Active Metamaterials,” *ACS Appl.*

- Mater. Interfaces* **11**, 41649 (2019).
16. J. S. Jamison, Z. H. Yang, B. L. Giles, J. T. Brangham, G. Z. Wu, P. C. Hammel, F. Y. Yang, and R. C. Myer, “Long lifetime of thermally-excited magnons in bulk yttrium iron garnet,” *Phys. Rev. B* **100**, 134402 (2019).
 17. H. L. Wang, K. Y. Meng, P. X. Zhang, J. T. Hou, J. Finley, J. H. Han, F. Y. Yang, and L. Q. Liu, “Large spin-orbit torque observed in epitaxial SrIrO₃ thin films,” *Appl. Phys. Lett.* **114**, 232406 (2019).
 18. A. J. Lee, A. S. Ahmed, S. D. Guo, B. D. Esser, D. W. McComb, F. Y. Yang, “Epitaxial Co₅₀Fe₅₀(110)/Pt(111) Films on MgAl₂O₄(001) and its Enhancement of Perpendicular Magnetic Anisotropy,” *J. Appl. Phys.* **125**, 183903 (2019).
 19. K.-Y. Meng, A. S. Ahmed, M. Baćani, A.-O. Mandru, X. Zhao, N. Bagués, B. D. Esser, J. Flores, D. W. McComb, H. J. Hug, and F. Y. Yang, “Observation of Nanoscale Skyrmions in SrIrO₃/SrRuO₃ Bilayers,” *Nano Lett.* **19**, 3169 (2019).
 20. Y. Cheng, R. Zarzuela, J. T. Brangham, A. J. Lee, S. White, P. C. Hammel, Y. Tserkovnyak, F. Y. Yang, “Non-sinusoidal angular dependence of FMR-driven spin current across an antiferromagnet in Y₃Fe₅O₁₂/NiO/Pt trilayers,” *Phys. Rev. B Rapid Comm* **99**, 060405 (2019).

Quantum Hall Systems In and Out of Equilibrium

Michael Zudov, University of Minnesota – Twin Cities

Program Scope

This program studies quantum transport phenomena in semiconductor nanostructures focusing on the roles of microwave radiation, dc electric field, in-plane magnetic field, carrier density, and disorder. The research expands upon the area originated by the discoveries of integer and fractional quantum Hall effects [1], followed by discoveries of other phenomena, such as quantum Hall stripes (QHSs) and bubbles [2], microwave-induced resistance oscillations and zero-resistance states [3], etc. The proposal is aimed to address issues of contemporary interest related to both nonequilibrium and equilibrium physics in quantum Hall systems.

Recent Progress

Two-dimensional electrons in GaAs quantum wells can support a variety of phases when subjected to quantizing magnetic fields and low temperatures. At half-integer filling factors ($\nu = i/2$, $i = \text{odd integer}$), these states include composite fermion metals ($i = 1, 3$) [4], quantum Hall insulators ($i = 5, 7$) [5], and quantum Hall stripe (QHS) phases ($i = 9, 11, \dots$) [2]. The QHS phases can be viewed as unidirectional charge density waves, composed of parallel strips with alternating integer filling factors $\nu = (i \pm 1)/2$. The QHSs exhibit very large resistance anisotropies and are usually aligned along $\langle 110 \rangle$ axis of GaAs.

The generic QHS features are a maximum (minimum) in a longitudinal resistance R_{xx} (R_{yy}), which develop at temperatures $T \lesssim 0.1$ K, and a nonquantized Hall resistance R_H . More precisely, the QHSs form when partial filling factor ν^* falls in the range of $0.4 \lesssim \nu^* \lesssim 0.6$. The resistance

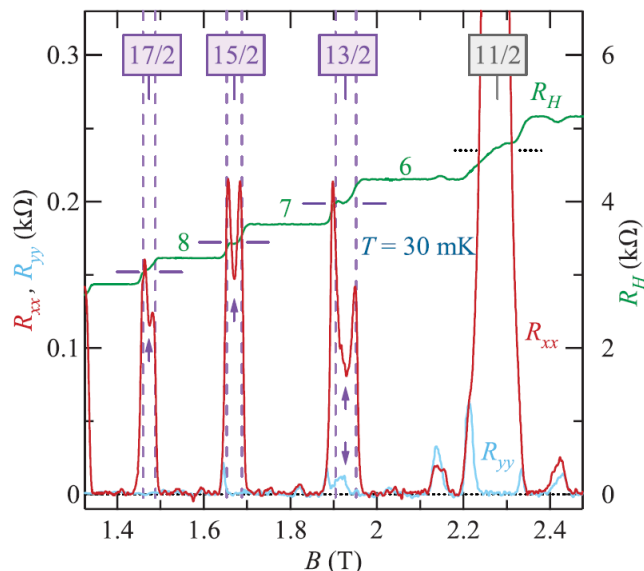


FIG. 1. Longitudinal resistances R_{xx} , R_{yy} (left axis) and Hall resistance R_H (right axis) as a function of perpendicular magnetic field B measured at $T = 30$ mK. At filling factor $\nu = 11/2$, one observes the QHS phase characterized by the R_{xx} maximum, the R_{yy} minimum, and the featureless R_H . At $\nu = 13/2$, $15/2$, and $17/2$ the data reveal ANSs, characterized by the R_{xx} minima, the R_{yy} maxima (here, resolved only at $13/2$), and the plateau-like features in R_H , with values close to $2R_K/13$, $2R_K/15$, $2R_K/17$, where $R_K \equiv h/e^2$ is the von Klitzing constant. All of our samples are 4×4 mm squares fabricated from 29-30 nm wide GaAs/Al_{0.24}Ga_{0.76}As quantum wells. The density is $n_e \approx 3.0 \times 10^{11} \text{ cm}^{-2}$, the mobility is $\mu \gtrsim 2 \times 10^7 \text{ cm}^2 \text{ V}^{-1}$.

anisotropy ratio R_{xx}/R_{yy} achieves a single maximal value $R_{xx}/R_{yy} \gg 1$ at $\delta\nu \equiv \nu^* - 0.5 \approx 0$ and quickly drops to $R_{xx}/R_{yy} \approx 1$ at $\delta\nu \approx \pm 0.1$. This drop occurs due to a monotonic decrease (increase) of the R_{xx} (R_{yy}) with $|\delta\nu|$.

In our recent study [6], we reported on anomalous nematic states (ANSs) which are distinguished from the QHS phases by the *opposite* dependencies of the R_{xx} and the R_{yy} on the detuning from half-filling $|\delta\nu|$ and on the temperature T . In particular, unlike the QHS phases characterized by a maximum (minimum) in the R_{xx} (R_{yy}) at $\delta\nu \approx 0$, the ANSs are marked by a minimum (maximum) in the R_{xx} (R_{yy}) and exhibit much smaller anisotropy ratio $R_{xx}/R_{yy} > 1$ [see Fig. 1(a)]. In addition, the Hall resistance R_H near $\nu = i/2$ develops plateau-like features with the values close to $R_H = 2R_K/i$, where $R_K = h/e^2$ is the von Klitzing constant [see Fig. 1(b)]. As shown in Fig. 1(a), a small detuning of $|\delta\nu| \approx 0.08$ transforms the ANSs into the QHSs phases (cf. vertical dashed lines), reflecting tight competition between these ground states.

As illustrated in Fig. 2, the ANSs emerge from the QHSs upon further cooling. Indeed, at $T = 135$ mK, one finds the QHS phase at $\nu = 13/2$ and the isotropic liquid phases at $\nu = 11/2$ and $15/2$. At $T = 100$ mK, the QHS phase at $\nu = 13/2$ is replaced by the ANS and the QHS phases emerge at both $\nu = 11/2$ and $15/2$. At $T = 60$ mK, the QHS yields to the ANS also at $\nu = 15/2$, but persists at $\nu = 11/2$. Upon further cooling, the ANSs at $\nu = 13/2$ and $\nu = 15/2$ become more pronounced, whereas the QHS phase at $\nu = 11/2$ remains the ground state. Further studies are needed to understand why the ANSs are favored at $\nu = 13/2$ and $\nu = 15/2$, but not at $\nu = 11/2$.

We have also investigated the response of the ANSs to the in-plane components of the magnetic field $B_{\parallel} = B_x$ and $B_{\parallel} = B_y$ [7]. We have found that the immediate effects of B_{\parallel} are to transform the minimum (maximum) in the R_{xx} (R_{yy}) at half-filling into a maximum (minimum), to eliminate the plateau in the R_H , and to restore the anisotropy ratio R_{xx}/R_{yy} to values consistent with the QHS phases. Remarkably, the ANSs respond to B_{\parallel} in essentially the same manner when B_{\parallel} is applied along either the x or the y direction; in both cases the revived QHS phase is aligned along

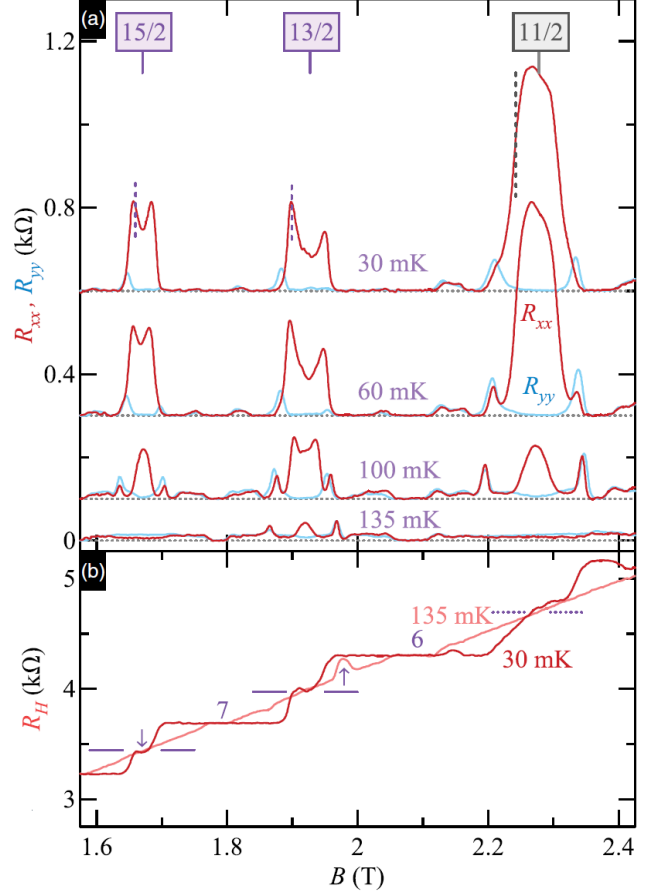


FIG. 2. (a) Longitudinal resistances R_{xx} (dark line) and R_{yy} (light line) as a function of magnetic field B at $T \approx 135$ mK (bottom), $T \approx 100$ mK (offset by 0.1 kΩ), $T \approx 60$ mK (offset by 0.3 kΩ), and $T \approx 30$ mK (offset by 0.6 kΩ). (b) Hall resistance R_H versus B at $T \approx 30$ mK (dark line) and at $T \approx 135$ mK (light line). Solid (dotted) horizontal lines next to the R_H are drawn at $2R_K/13$, $2R_K/15$ ($2R_K/11$).

its native $\langle 110 \rangle$ direction. This is in contrast with the effect of B_{\parallel} on the QHS phases which respond very differently to B_x and B_y , whereas persisting to much higher B_{\parallel} [8,9].

The effect of $B_{\parallel} = B_y$ on the ANS is illustrated in Fig. 3. The evolution of the R_{xx} in the QHS phase at $\nu = 11/2$ with B_y is consistent with previous studies [9,10]; upon tilting, the R_{xx} decreases, as the QHS phase starts to reorient perpendicular to B_y . In contrast, the R_{xx} in the ANS at $\nu = 13/2$ grows with the tilt angle, the characteristic minimum quickly disappears, and the Hall plateau with $R_H \approx 2R_K/13$ is destroyed. As shown in Fig. 4, the QHS phase at $\nu = 11/2$ reorients twice under B_y , as previously reported [9]. At $\nu = 13/2$, the immediate effect of B_y is to *increase* (*decrease*) the R_{xx} (R_{yy}) to a value consistent with the QHS phases. As a result, R_{xx}/R_{yy} grows from ≈ 10 at $B_y = 0$ to ≈ 300 . The effect of $B_{\parallel} = B_x$ on the ANS is qualitatively the same [7].

Distinct effects of B_y on the ANS and on the QHS phase are further highlighted by opposite dependencies on the detuning from half-filling $|\delta\nu|$. Near $\nu = 13/2$, the response of the ANS to B_y is the strongest at $\delta\nu = 0$ resulting in the disappearance of the R_{xx} minimum and the restoration of a single maximum. This is in contrast to the QHS phase at $\nu = 11/2$, at which the response to B_y is the strongest away from half-filling (cf. two deep R_{xx} minima). Finally, (a) since B_{\parallel} , regardless of its orientation, causes a transition from the ANS to the QHS phase aligned along its native direction and (b) since B_y (B_x) should raise (lower) the energy of the QHS phase with the native orientation, we conclude that B_{\parallel} raises the energy of the ANS above its value at $B_{\parallel} = 0$. In summary, the ANSs yield to the QHS phases (i) with increasing T [6], (ii) with increasing detuning from half-filling $|\delta\nu|$ [6], and (iii) under modest in-plane magnetic field $B_{\parallel} = B_x$ or $B_{\parallel} = B_y$ [7].

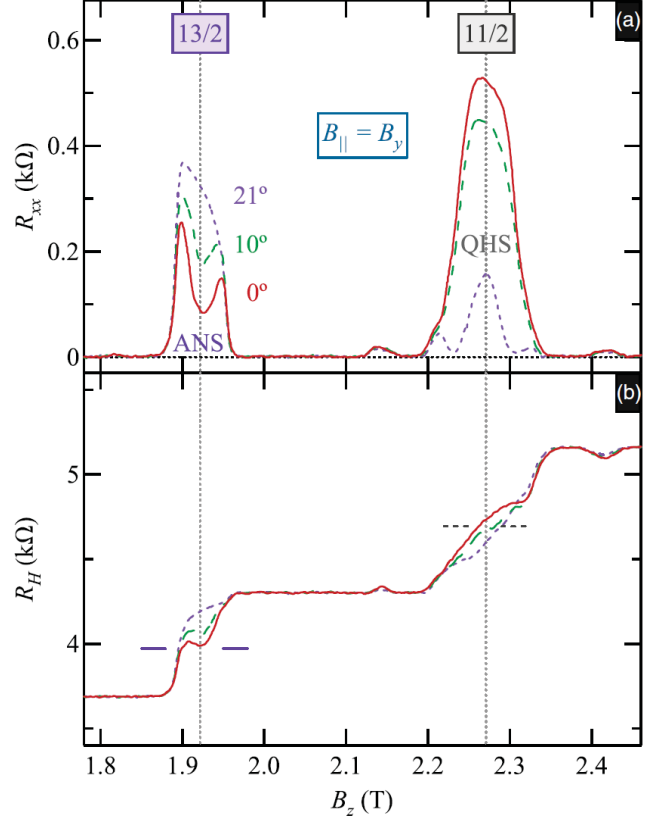


FIG. 3. (a) Longitudinal resistances R_{xx} and (b) Hall resistance R_H as a function of magnetic field B_z under $B_{\parallel} = B_y$ at $\theta = 0$ degrees (solid line), 10 degrees (dashed line), and 21 degrees (dotted line). Solid (dashed) horizontal lines next to are drawn at $2R_K/13$ ($2R_K/11$).

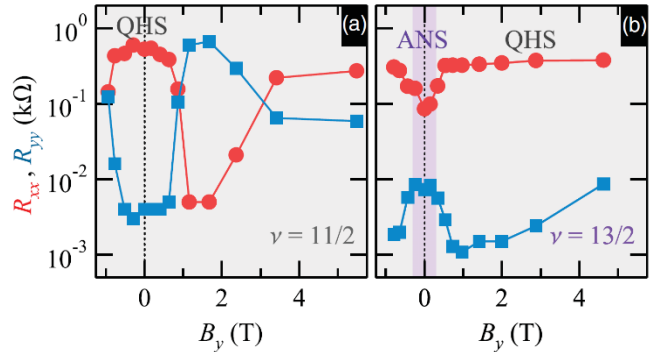


FIG. 4. (a) R_{xx} (circles), R_{yy} (squares) as a function of $B_{\parallel} = B_y$ at $\nu = 11/2$. (b) Same as (a) but at $\nu = 13/2$.

Future Plans

We plan to study the role of density on the QHSs reorientation under B_{\parallel} applied perpendicular to the native QHSs. This study should provide an insight on possible coupling between B_{\parallel} -induced and native symmetry-breaking potentials [9]. We also plan to investigate the ANSs can be realized in lower density samples with higher carrier mobility. In the area of non-equilibrium transport, we will study microwave-induced resistance oscillations (MIROs) in a tunable-density GaAs quantum well in the regime when the second subband is populated. In particular, we will look for changes in the amplitude, the quantum lifetime, and the effective mass.

References

- [1] K. von Klitzing, G. Dorda, and M. Pepper, Phys. Rev. Lett. **45**, 494 (1980); D.C. Tsui, H. L. Stormer, and A. C. Gossard, Phys. Rev. Lett. **48**, 1559 (1982).
- [2] A. A. Koulakov, M. M. Fogler, and B. I. Shklovskii, Phys. Rev. Lett. **76**, 499 (1996); M. P. Lilly, K. B. Cooper, J. P. Eisenstein, L. N. Pfeiffer, and K. W. West, Phys. Rev. Lett. **82**, 394 (1999); R. R. Du, D. C. Tsui, H. L. Stormer, L. N. Pfeiffer, K. W. Baldwin, and K. W. West, Solid State Commun. **109**, 389 (1999).
- [3] M. A. Zudov, R. R. Du, J. A. Simmons, and J. L. Reno, **64**, Phys. Rev. B 201311(R) (2001); R. G. Mani, J. H. Smet, K. von Klitzing, V. Narayanamurti, W. B. Johnson, and V. Umansky, Nature (London) **420**, 646 (2002); M. A. Zudov, R. R. Du, L. N. Pfeiffer, and K. W. West, Phys. Rev. Lett. **90**, 46807 (2003).
- [4] J. K. Jain, Phys. Rev. Lett. **63**, 199 (1989).
- [5] R. Willett, J. P. Eisenstein, H. L. Stormer, D. C. Tsui, A. C. Gossard, and J. H. English, Phys. Rev. Lett. **59**, 1776 (1987); W. Pan, J.-S. Xia, V. Shvarts, D. E. Adams, H. L. Stormer, D. C. Tsui, L. N. Pfeiffer, K. W. Baldwin, and K. W. West, Phys. Rev. Lett. **83**, 3530 (1999).
- [6] X. Fu, Q. Shi, M. A. Zudov, G. C. Gardner, J. D. Watson, M. J. Manfra, K. W. Baldwin, L. N. Pfeiffer, and K. W. West, Phys. Rev. Lett. **124**, 067601 (2020)
- [7] X. Fu, Q. Shi, M. A. Zudov, G. C. Gardner, J. D. Watson, M. J. Manfra, K. W. Baldwin, L. N. Pfeiffer, and K. W. West, Phys. Rev. B Lett. **104**, L081301 (2021)
- [8] W. Pan, R. R. Du, H. L. Stormer, D. C. Tsui, L. N. Pfeiffer, K. W. Baldwin, and K. W. West, Phys. Rev. Lett. **83**, 820 (1999); M. P. Lilly, K. B. Cooper, J. P. Eisenstein, L. N. Pfeiffer, and K. W. West, Phys. Rev. Lett. **83**, 824 (1999)
- [9] Q. Shi, M. A. Zudov, J. D. Watson, G. C. Gardner, and M. J. Manfra, Phys. Rev. B **93**, 121411(R) (2016).
- [10] Q. Shi, M. A. Zudov, J. D. Watson, G. C. Gardner, and M. J. Manfra, Phys. Rev. B **93**, 121404(R) (2016).

Publications (2019-2021)

1. X. Fu, Q. Shi, M. A. Zudov, G. C. Gardner, J. D. Watson, M. J. Manfra, K. W. Baldwin, L. N. Pfeiffer, and K. W. West, “Anomalous nematic state to stripe phase transition driven by in-plane magnetic fields”, *Physical Review B Lett.* **104**, L081301 (2021)
2. X. Fu, Yi Huang, B. I. Shklovskii, M. A. Zudov, G. C. Gardner, and M. J. Manfra, “Hidden quantum Hall stripes in $\text{Al}_x\text{Ga}_{1-x}\text{As}/\text{Al}_{0.24}\text{Ga}_{0.76}\text{As}$ quantum wells”, *Physical Review Letters* **125**, 236803 (2020) [Editors’ Suggestion]
3. Yi Huang, M. Sammon, M. A. Zudov, and B. I. Shklovskii, “Isotropically conducting (hidden) quantum Hall stripe phases in a two-dimensional electron gas”, *Physical Review B – Rapid Communications* **101**, 161302(R) (2020)
4. O. E. Raichev and M. A. Zudov, “Effect of Berry phase on nonlinear response of two-dimensional fermions”, *Physical Review Research – Rapid Communications* **2**, 022011(R) (2020)
5. X. Fu, Q. Shi, M. A. Zudov, G. C. Gardner, J. D. Watson, M. J. Manfra, K. W. Baldwin, L. N. Pfeiffer, and K. W. West, “Anomalous nematic states in high half-filled Landau levels”, *Physical Review Letters* **124**, 067601 (2020)
6. M. Sammon, X. Fu, Yi Huang, M. A. Zudov, B. I. Shklovskii, G.C. Gardner, J.D. Watson, M. J. Manfra, K. W. Baldwin, L. N. Pfeiffer, and K. W. West, “Resistivity anisotropy of quantum Hall stripe phases”, *Physical Review B – Rapid Communications* **100**, 241303(R) (2019)
7. X. Fu, Q. Shi, M. A. Zudov, G. C. Gardner, J. D. Watson, and M. J. Manfra, “Two- and three-electron bubbles in $\text{Al}_x\text{Ga}_{1-x}\text{As}/\text{Al}_{0.24}\text{Ga}_{0.76}\text{As}$ quantum wells”, *Physical Review B – Rapid Communications* **99**, 151402(R) (2019) [Editors’ Suggestion]

Author Index

Ackerman, John.....	381	Ghimire, Nirmal	104
Ahn, Charles	43	Goertzen, Renee Michelle.....	69
Analytis, James	151	Gu, Genda	122
Andrei, Eva Y.	29	Halperin, W. P.....	238
Ashoori, Raymond.....	157, 161	Harrison, Neil.....	242
Awschalom, David	3	Heinz, Tony F.....	363
Balicas, Luis.....	166	Hellman, Frances	48
Basov, Dimitri N.	173	Hersam, Mark.....	3
Bauer, Eric	344	Hilton, David J.	13
Bhattacharya, Anand	82	Hirata, Michihiro	344
Birgeneau, Robert.....	151	Hoffmann, Axel.....	248
Bisogni, Valentina.....	177	Hone, James	34, 363
Bockrath, Marc.....	284	Hsieh, David.....	119
Bokor, Jeff	48	Hu, Jin	252
Bougher, Cortney	182	Hunt, Benjamin	258
Brahlek, Matt	289	Hwang, Harold Y.....	78
Bud'ko, Sergey	189	Jaime, Marcelo	242
Butov, Leonid.....	184	Janotti, Anderson.....	334
Canfield, Paul.....	189	Jarillo-Herrero, Pablo	161
Cha, Judy J.	195	Jiang, Sam	82
Chakhalian, Jak	200	Jiang, Zhigang	372
Chan, Moses H. W.	204	Johnston, David C.....	91
Chan, Mun	242	Kaminski, Adam.....	189
Chang, Cui-Zu.....	204	Kapitulnik, Aharon	228
Checkelsky, Joseph	161, 209	Ke, Liqin	91
Chien, TeYu.....	111, 381	Kevan, Steve	48
Cohen, Marvin	136	Kidd, T.	263
Crommie, Michael.....	136, 390	Kim, Philip	267
Crooker, Scott	242	Kivelson, Steven A.	228
Dahnovsky, Yuri	111	Kono, Junichiro	272
Dean, Cory R.....	34, 213, 363	Koshelev, A. E.....	278
Dessau, Dan	61	Kwok, W.-K.	278
Doty, Matt F.....	322	Lanzara, Alessandra.....	136, 151
Engel, Lloyd W.	213	Lau, Chun Ning (Jeanie).....	284
Eom, Chang-Beom	217	Law, Stephanie A.	322
Eres, Gyula.....	289	Lee, Dunghai	151
Finkelstein, Gleb	223	Lee, Ho Nyung	289
Fischer, Peter.....	48	Lee, Minhyea.....	295
Fisher, Ian R.....	228	Leonard, Brian.....	381
Fong, Dillon	82	Li, Lu	128
Freedman, Danna	3	Li, Qi.....	298
Frolov, Sergey M.....	234	Li, Qiang	122
Fu, Liang	161	Li, Yi.....	248
Furukawa, Yuji.....	189	Liu, Chao-Xing.....	204
Geballe, Theodore H.	228	Liu, Jian.....	55
Gedik, Nuh.....	161	Liu, Mengkun	122

Long, Jeffrey	3	Roy, Sujoy.....	48
Louie, Steven	136, 390	Salahuddin, Sayeef	48
Lukashev, P.....	263	Sales, Brian C.....	98
MacDonald, Allan H.	363	Schiffer, Peter.....	354
Madhavan, Vidya	302	Schleife, Andre.....	248
Mak, Kin Fai	38, 363	Schuller, Ivan K.....	358
Mandrus, David.....	98	Shabani, Javad.....	350
Manfra, Michael J.....	10	Shan, Jie	363
Maple, M. Brian	303	Shand, P.	263
May, Andrew F.	98	Shayegan, Monsour	367
McGuire, Michael A.....	98	Singleton, John	242
McQueeney, Robert J.....	91	Smirnov, Dmitry.....	372
Miao, Hu	289	Smith, Arthur R.	377
Mitchell, John F.	104	Stollenwerk, A.....	263
Moler, Kathryn A.	228	Strauss, L.....	263
Moore, Joel	151	Tanatar, Makariy	189
Morosan, Emilia.....	63	Tang, Jinke	111, 381
Movshovich, Roman.....	344	Thomas, Sean	344
Musfeldt, Janice L.	310	Tian, Jifa	111, 381
Natelson, Douglas	314	Ueland, Ben G.	91
Ni, Ni	318	Urazhdin, Sergei.....	385
Nikolić, Branislav K.....	322	Vaknin, David	91
Novosad, Valentine	248, 278	Valla, Tonic.....	122
Ojeda-Aristizabal, Claudia.....	327	Vlasko-Vlasov, V.	278
Ong, N. Phuan.....	133	Walker, Fred.....	43
Orenstein, Joseph	151	Wang, Feng	136, 390
Orth, Peter P.....	91	Wang, Linlin	189
Ouyang, Min	331	Wang, Lin-Wang	48
Paglione, Johnpierre	73	Ward, T. Zac.....	289, 397
Palmstrøm, Christopher J.....	334	Wasielewski, Michael.....	3
Pan, Wei.....	350	Welp, U.	278
Perakis, Ilias E.....	13	Wu, Mingzhong.....	402
Pfaff, Wolfgang.....	248	Xiao, John Q.....	322
Phelan, Daniel	104	Xiao, Z.-L.....	278
Plisch, Monica.....	69	Xu, Xiaoshan.....	406
Prozorov, Ruslan	189	Yan, Jiaqiang.....	98
Qiu, Zi Q.	390	Yang, Fengyuan.....	411
Raghu, S.....	78	Yi, Ming	108
Ralph, Daniel C.	339	Yin, Weiguo	122
Ramesh, R.....	151	Young, Andrea	25
Ramshaw, Brad	70	Zaletel, Mike	390
Rondinelli, James	3	Zettl, Alex	136, 390
Ronning, Filip	344	Zhou, Haidong.....	55
Rosa, Priscila.....	242, 344	Zudov, Michael	417
Rosenbaum, Thomas F.	19	Zuo, Jian-Min	248
Rossi, Enrico	350		

Participant List

Name	Organization	Email
Ahn, Charles	Yale University	charles.ahn@yale.edu
Andrei, Eva	Rutgers	eandrei@physics.rutgers.edu
Ashoori, Raymond	Massachusetts Institute of Technology	ashoori@mit.edu
Balicas, Luis	Maglab / FSU	balicas@magnet.fsu.edu
Basov, Dmitri	Columbia	db3056@columbia.edu
Bhattacharya, Anand	Argonne National Laboratory	anand@anl.gov
Bisogni, Valentina	Brookhaven National Laboratory	bisogni@bnl.gov
Bockrath, Marc	The Ohio State University	bockrath.31@osu.edu
Bougher, Cortney	American Physical Society	bougher@aps.org
Bud'ko, Sergey	Ames Laboratory	budko@ameslab.gov
Butov, Leonid	University of California, San Diego	lvbutov@physics.ucsd.edu
Cantoni, Claudia	Department of Energy	claudia.cantoni@science.doe.gov
Cha, Judy	Yale University	judy.cha@yale.edu
Chakhalian, Jak	Rutgers university	jak.chakhalian@rutgers.edu
Chang, Cui-Zu	Penn State	cxc955@psu.edu
Checkelsky, Joseph	Massachusetts Institute of Technology	checkelsky@mit.edu
Chen, Shawn	Department of Energy	shawn.chen@science.doe.gov
Chien, TeYu	University of Wyoming	tchien@uwyo.edu
Csathy, Gabor	Purdue University	gcsathy@purdue.edu
Dessau, Dan	University of Colorado	dessau@Colorado.edu
Engel, Lloyd	Florida State University	engel@magnet.fsu.edu
Eom, Chang-Beom	University of Wisconsin, Madison	eom@engr.wisc.edu
Fecko, Chris	Department of Energy	christopher.fecko@science.doe.gov
Finkelstein, Gleb	Duke University	gleb@phy.duke.edu
Fisher, Ian	SLAC & Stanford University	irfisher@stanford.edu
Freedman, Danna	Massachusetts Institute of Technology	danna@mit.edu
Frolov, Sergey	University of Pittsburgh	frolovsm@pitt.edu
Graf, Matthias	Department of Energy	matthias.graf@science.doe.gov
Halperin, Bill	Northwestern University	w-halperin@northwestern.edu
Harrison, Neil	Los Alamos National Laboratory	nharrison@lanl.gov
Hellman, Frances	UC Berkeley/Lawrence Berkeley National Lab	fhellman@berkeley.edu
Hoffmann, Axel	University of Illinois, Urbana-Champaign	axelh@illinois.edu
Hone, James	Columbia University	jh2228@columbia.edu
Hsieh, David	California Institute of Technology	dhsieh@caltech.edu
Hu, Jin	University of Arkansas	jinhu@uark.edu
Hunt, Benjamin	Carnegie Mellon University	bmhunt@andrew.cmu.edu
Hwang, Harold	SLAC National Accelerator Laboratory	hyhwang@stanford.edu
Jiang, Zhigang	Georgia Institute of Technology	zhigang.jiang@physics.gatech.edu
Kerch, Helen	Department of Energy	helenkmd@gmail.com
Kidd, Timothy	University of Northern Iowa	tim.kidd@uni.edu
Kim, Philip	Harvard University	pkim@physics.harvard.edu
Kono, Junichiro	Rice University	kono@rice.edu

Kwok, Wai-Kwong	Argonne National Laboratory	wkwok@anl.gov
Lau, Jeanie	The Ohio State University	lau.232@osu.edu
Lee, Ho Nyung	Oak Ridge National Laboratory	hnlee@ornl.gov
Lee, Minhyea	University of Colorado, Boulder	minhyea.lee@colorado.edu
Li, Lu	University of Michigan	luli@umich.edu
Li, Qi	Penn State University	qil1@psu.edu
Li, Qiang	Brookhaven National Laboratory	qiangli@bnl.gov
Madhavan, Vidya	University of Illinois, Urbana-Champaign	vm1@illinois.edu
Mak, Kin Fai	Cornell University	km627@cornell.edu
Manfra, Michael	Purdue University	mmanfra@purdue.edu
Maple, M. Brian	University of California, San Diego	mbmaple@ucsd.edu
McGuire, Michael	Oak Ridge National Laboratory	mcguirema@ornl.gov
McQueeney, Robert	Ames Laboratory	mcqueeney@ameslab.gov
Mitchell, John	Argonne National Laboratory	mitchell@anl.gov
Morosan, Emilia	Rice University	emorosan@rice.edu
Musfeldt, Janice	University of Tennessee	musfeldt@utk.edu
Natelson, Douglas	Rice University	natelson@rice.edu
Ni, Ni	University of California, Los Angeles	nini@physics.ucla.edu
Ojeda-Aristizabal, Claudia	California State University, Long Beach	claudia.ojeda-aristizabal@csulb.edu
Ong, Nai-Phuan	Princeton University	npo@princeton.edu
Orenstein, Joseph	Lawrence Berkeley National Laboratory	jworenstein@lbl.gov
Ouyang, Min	University of Maryland, College Park	mouyang@umd.edu
Paglione, Johnpierre	University of Maryland	paglione@umd.edu
Palmstrøm, Chris	University of California, Santa Barbara	cjpalm@ucsb.edu
Pechan, Mick	Department of Energy	michael.pechan@science.doe.gov
Perakis, Ilias	University of Alabama, Birmingham	iperakis@uab.edu
Phelan, Daniel	Argonne National Laboratory	dphelan@anl.gov
Plisch, Monica	American Physical Society	plisch@aps.org
Ralph, Dan	Cornell University	dcr14@cornell.edu
Ramirez, Arthur	University of California, Santa Cruz	apr@ucsc.edu
Ramshaw, Brad	Cornell University	bradramshaw@cornell.edu
Roizen, Jennifer	Department of Energy	jennifer.roizen@science.doe.gov
Ronning, Filip	Los Alamos National Laboratory	fronning@lanl.gov
Rosenbaum, Thomas	California Institute of Technology	tfr@caltech.edu
Rossi, Enrico	College of William & Mary	erossi@wm.edu
Schiffer, Peter	Yale University	peter.schiffer@yale.edu
Schuller, Ivan	University of California, San Diego	ischuller@ucsd.edu
Schwartz, Andrew	Department of Energy	andrew.schwartz@science.doe.gov
Sefat, Athena	Department of Energy	athena.sefat@science.doe.gov
Shan, Jie	Cornell University	jie.shan@cornell.edu
Shayegan, Mansour	Princeton University	shayegan@princeton.edu
Smirnov, Dmitry	National High Magnetic Field Laboratory	smirnov@magnet.fsu.edu
Smith, Arthur	Ohio University	smitha2@ohio.edu

Thiyagarajan, Pappannan	Department of Energy	p.thiyagarajan@science.doe.gov
Tian, Jifa	University of Wyoming	jtian@uwyo.edu
Urazhdin, Sergei	Emory University	surazhd@emory.edu
Wang, Feng	Lawrence Berkeley National Laboratory	fengwang76@berkeley.edu
Ward, Zac	Oak Ridge National Laboratory	wardtz@ornl.gov
Wu, Mingzhong	Colorado State University	mwu@colostate.edu
Xiao, John	University of Delaware	jqx@udel.edu
Xu, Xiaoshan	University of Nebraska, Lincoln	xiaoshan.xu@unl.edu
Yang, Fengyuan	The Ohio State University	yang.1006@osu.edu
Yi, Ming	Rice University	mingyi@rice.edu
Young, Andrea	University of California, Santa Barbara	andrea@physics.ucsb.edu
Zettl, Alex	University of California, Berkeley	azettl@berkeley.edu
Zhou, Haidong	University of Tennessee	hzhou10@utk.edu
Zhu, Jane	Department of Energy	jane.zhu@science.doe.gov
Zudov, Michael	University of Minnesota	zudov001@umn.edu